PIERS 2009 Beijing

Progress In Electromagnetics Research Symposium

Abstracts

March 23–27, 2009
Beijing, China

www.emacademy.org
www.piers.org

PIERS 2009 Beijing Abstracts

Published by

The Electromagnetics Academy
777 Concord Avenue, Suite 207
Cambridge, MA 02138

www.emacademy.org
www.piers.org

ISSN: 1559-9450
ISBN: 978-1-934142-07-3

Progress in Electromagnetics Research Symposium
March 23–27, 2009
Beijing, CHINA

PIERS 2009 BEIJING ORGANIZATION

PIERS Founding Chair

J. A. Kong, MIT, USA

PIERS Chair

L. Tsang, University of Washington, USA

PIERS 2009 Beijing General Chair

B. Ning, Beijing Jiaotong University, CHINA

PIERS 2009 Beijing Organization Committee Chair

T. Q. Zheng, Beijing Jiaotong University, CHINA

PIERS 2009 Beijing International Advisory Committee

S. Barmada	L. C. Botten	C.-H. Chan	W.-C. Chew
C-K. Chou	H.-T. Chuah	S.-T. Chun	N. Engheta
Z.-H. Feng	J.-M. R. Fournier	A. K. Fung	Z.-H. Gu
L. Gurel	T. M. Habashy	M. Hallikainen	Y. Hara
H.-C. Huang	A. Ishimaru	E. Jakeman	J.-S. Jiang
K. Kobayashi	Z. Lemnios	L.-W. Li	X.-W. Li
I. V. Lindell	S.-G. Liu	K.-M. Luk	S. Mano
G. D. McNeal	Y. Miyazaki	P. Pampaloni	A. Priou
K. Senne	R. Shin	M. Tateiba	L. Tsang
J. Wu	K. Yasumoto	H.-J. Yin	W.-X. Zhang

PIERS 2009 Beijing Technical Program Committee

S. J. Anderson	A. Baghai-Wadji	G. Berginc	W.-M. Boerner
H. Braunisch	C.-T. Chan	H.-S. Chen	K.-S. Chen
T.-J. Cui	Y. Du	T. Endo	A. Elsherbeni
H. C. Fernandes	S. He	W. Hong	Y.-Q. Jin
F. Li	L.-J. Li	Q.-H. Liu	S. Lucyszyn
A. Massa	E. L. Miller	M. Moghaddam	Z.-P. Nie
M. Oristaglio	J. Pribetich	G. S. N. Raju	R. Ramer
L.-X. Ran	C. M. Rappaport	C. Seo	X.-Q. Sheng
J.-C. Shi	A. Sihvola	M.-S. Tong	D.-P. Tsai
J. Vrba	M. Y. Xia	G. Xie	S.-J. Xu
C. Wang	B.-I. Wu	D.-Z. Zhang	L.-X. Zhang
X.-M. Zhang	Y.-H. Zhang	J. Zhou	

PIERS 2009 Beijing Organization Committee

J. J. Bao	H.-S. Chen	Y. Du	Y. Fan
J. Fang	W. Feng	H. Huang	J. T. Huangfu
C. Z. Jia	Q. Jiang	X. D. Jiang	Z.-Y. Li
D.-W. Liu	R. F. Liu	R. C. Qiu	H. G. Wang
Y. Wang	B. I. Wu	P.-L. Xie	L. Ye
L. Y. Yu	X. M. Zhang		

PIERS 2009 BEIJING SESSION ORGANIZERS

Y. N. Barabanenkov	W.-M. Boerner	H. Chen	K.-S. Chen
M. Chen	C-K. Chou	H.-R. Chuang	T. J. Cui
Y. Du	H. T. Ewe	D. Felbacq	E. Gescheidtová
L. Giuliani	S. Gonzalez-Garcia	F. Güneş	S. He
J. Hu	W. Hu	K. Iwatsuki	T. J. Jackson
G. V. Jandieri	K. Kobayashi	Y.-C. Lan	J. Li
L.-W. Li	D. Lippens	J. T. Lue	E. Marx
J. Miao	H. Misawa	Y. Miyazaki	M. R. Murphy
T. Nakamura	C. Ninagawa	Y. Okuno	M. Oristaglio
A. V. Osipov	K. Ouchi	G. W. Pan	D. K. Panda
J. Qiu	I. M. Reid	I. V. Shadrivov	Y. V. Shestopalov
J. Shi	X. Song	S. Tjuatja	D. P. Tsai
J. Wang	B.-I. Wu	C.-J. Wu	C.-Q. Wu
Z.-S. Wu	G. Xiao	G. Xie	T. Yamasaki
J. Yang	T.-J. Yang	T.-S. Yeo	H. O. Zhang
H. Zhang	Q. Zhang	J. Zhou	X. Zhou

PIERS 2009 BEIJING EXHIBITOR

- ☐ FEKO (www.feko.info)
- ☐ ATK National Capital Region (www.magictoolsuite.com / www.lspsuite.com)
- ☐ Beijing Land High Tech Co., Ltd. (www.landhightech.com)

PIERS 2009 BEIJING SPONSORSHIP

- ☐ Beijing Jiaotong University
- ☐ Zhejiang University
- ☐ National Natural Science Foundation of China
- ☐ The Electromagnetics Academy at Zhejiang University
- ☐ MIT Center for Electromagnetic Theory and Applications/Research Laboratory of Electronics
- ☐ The Electromagnetics Academy

PIERS 2009 SESSIONS

Session 1P1
Microwave/Terahertz Photonics Technologies and Their Applications

Plasmon-resonant Microchip Emitters and Their Applications to Terahertz Spectroscopy

T. Otsuji[1], **Y. Tsuda**[1], **T. Komori**[1], **T. Nishimura**[1], **A. El Fatimy**[1], **Y. M. Meziani**[1], **T. Suemitsu**[1], **and E. Sano**[2]

[1]Research Institute of Electrical Communication, Tohoku University, Japan
[2]Research Center for Integrated Quantum Electronics, Hokkaido University, Japan

Abstract— Development of compact, tunable and coherent sources operating at terahertz (THz) frequencies is one of the hottest issues of the modern ultrafast electronics [1]. Two dimensional (2D) plasmons in submicron transistors have attracted much attention due to their nature of promoting emission/detection of THz electromagnetic radiation [2, 3]. This paper reviews recent advances in emission of THz radiation from our original dual-grating gate high-electron mobility transistors (HEMT's) originated from two-dimensional plasmons [4–9]. The dual grating gates can alternately modulate the 2D electron densities to periodically distribute the plasmonic cavities along the channel, acting as an antenna [4]. The first sample was fabricated with standard GaAs-based heterostructure material systems, succeeding in emission of broadband (0.5 to 6.5 THz) radiation even at room temperature from self-oscillating 2D plasmons under the DC-biased conditions [7, 9]. When the 2D plasmons are optically excited by a femtosecond laser, emission with sharp peaks reflecting coherent 2D plasmon modes is clearly observed in their relaxation processes [5, 6]. Photomixing operation: difference THz frequency generation from the photomixed dual-CW laser irradiation, is also expected [4]. The second sample was fabricated in a double-decked (DD-) HEMT structure in which the grating-gate metal layer was replaced with the semiconducting upper-deck 2D electron layer, resulting in enhancement of emission by one order of magnitude [8]. Currently maximum available THz output power is estimated to be on the order of 10 μW from a single die active area of $75 \times 75\,\mu m^2$ with an excellent power conversion efficiency of 10^{-3} [9]. The fabricated DD-HEMT is introduced to the Fourier-transform infrared spectroscopy (FTIR) as a microchip THz source. Water-vapor absorption spectrum is successfully observed at 300 K [10], which is proven to the standard data provided by NASA. To the best of the author's knowledge, this is the first-time demonstration of THz spectroscopy utilizing room-temperature operating THz solid-state micro-light.

ACKNOWLEDGMENT

The author would like to acknowledge Profs. W. Knap, V. V. Popov, V. Ryzhii, Drs. F. Teppe, D. Coquillat, A. Satou, M. C. Haibo, T. Komori for their contributions. They also thank Prof. M. Dyakonov and M. S. Shur for valuable discussion. This work was supported in part by the SCOPE, MIC, Japan, and the grant-in-aid for basic research (S), JSPS, Japan.

REFERENCES

1. Tonouchi, M., *Nature Photon.*, Vol. 1, 97–105, 2007.
2. Dyakonov, M. and M. Shur, *Phys. Rev. Lett.*, Vol. 71, 2465, 1993.
3. Dyakonov, M. and M. Shur, *IEEE Trans. Electron Devices*, Vol. 43, 380, 1996.
4. Otsuji, T., et al., *Opt. Express*, Vol. 14, 4815, 2006.
5. Otsuji, T., et al., *Applied Physics Letters*, Vol. 89, 263502, 2006.
6. Otsuji, T., et al., *Solid State Electronics*, Vol. 51, 1319, 2007.
7. Meziani, Y. M., et al., *Applied Physics Letters*, Vol. 92, 201108, 2008.
8. Nishimura, T., et al., *Device Research Conf.*, 263, 2008.
9. Otsuji, T., et al., *J. Phys. Cond. Matt.*, Vol. 20, 384206, 2008.
10. Otsuji, T., et al., *Lester Eastman Conf.*, 2008.

Terahertz Quantum-cascade Laser and Its Applicability to Ultra-high Bit-rate Wireless Access System

I. Hosako
National Institute of Information and Communications Technology, Japan

Abstract— It is well known that there is no small and reliable oscillator technology in the terahertz frequency bands. The non-availability of semiconductor devices in the terahertz frequency region is known as "THz-Gap". However, with the availability of small semiconductor oscillators in the terahertz frequency region, it would be possible to realize ultra-short-range wireless access, with data transfer rates greater than 10 Gbps, even though, there is a large atmospheric attenuation in the terahertz frequency range.

In recent years, there has been a rapid progress in the development of semiconductor devices in the terahertz frequency range, and the THz-Gap is shrinking. A 100-Gbps Ethernet is developed and is being standardized for use in optical networks. In addition, millimeter wave communications with a rate of 10 Gbps (@125 GHz) have been achieved in wireless networks. With this background, the IEEE 802.15 Terahertz Interest Group (IGthz) explored the feasibility of terahertz frequency bands for wireless communications in January, 2008. In the IGthz, the basic principle and economical feasibility of the THz wireless were discussed.

The terahertz quantum cascade laser (THz-QCL) is a newly developed semiconductor laser that operates in the frequency range from 1 to 5 THz with milliwatt-class output power. After initial developments by R. Kolher et al., in 2002 [1], THz-QCLs with an output power of a few hundred milliwatts and a maximum operating temperature of 178 K [2] have been achieved. Further, electronic semiconductors operating at room temperature at frequencies lesser than 1 THz have also been fabricated [3]. The output power of these electronic semiconductor devices very is small, i.e., it is of the order of few tens of milliwatts and microwatts at 300 GHz. Therefore, the availability of the semiconductor oscillator technology is different in each frequency band. In this study, we focus on a dynamic behavior and possible modulation frequency of the THz-QCL and its possible application to wireless access systems.

ACKNOWLEDGMENT

I would like to thank members of our research; Prof. K. Hirakawa of University of Tokyo, Dr. N. Sekine, Dr. Y. Kasai, and Dr. H. Yasuda of NICT for their cooperation, fruitful discussions, and efforts.

REFERENCES

1. Köhler, R., A. Tredicucci, F. Beltram, H. E. Beere, E. H. Linfield, A. G. Davies, D. A. Ritchie, R. C. Iotti, and F. Rossi, *Nature*, Vol. 417, 156–159, London, 2002.
2. Belkin, M., J. Fan, S. Hormoz, F. Capasso, S. Khanna, M. Lachab, A. Davies, and E. Linfield, *Optics Express*, Vol. 16, No. 5, 3242–3248, 2008.
3. Orihashi, N., S. Suzuki, and M. Asada, *Appl. Phys. Lett.*, Vol. 87, 233501, 2005.

High-power RF Photodiodes and Their Applications

Tadao Nagatsuma
Graduate School of Engineering Science, Osaka University
1-3 Machikaneyama, Toyonaka, Osaka 560-8531, Japan

Abstract— Research on exploring millimeter-waves (MMWs) and terahertz (THz) waves, which cover the frequency range from 30 GHz to 10 THz, has lately become very active, since nature of these electromagnetic waves is suited to spectroscopic sensing as well as to ultra-broadband wireless communications. One of the obstacles to develop applications of MMWs and THz waves is a lack of solid-sate signal sources, rather than detectors, as the frequency band in this region is often referred to as "terahertz gap". For the generation of MMWs and THz waves, photonic techniques are considered to be superior to conventional techniques based on electronic devices with respect to wide frequency bandwidth, tunability, and stability. Moreover, the use of optical fiber cables enables us to distribute high-frequency RF signals over long distances. In this scheme, optical-to-electrical (O-E) converters and/or photodiodes, which operate at long optical wavelengths (1.3–1.55 μm), play a key role, and high-output-current operation is required in addition to high-frequency operation for practical applications.

This paper reviews recent progress in the high-power RF photodiodes such as Uni-Traveling-Carrier-Photodiodes (UTC-PDs), which operate at these frequencies. Several approaches to increasing both the bandwidth and output power of photodiodes are discussed, and recent promising applications to broadband wireless communications and spectroscopic sensing are described.

High-speed and Precise Lightwave Modulation for Millimeter- or Micro-wave Generation

Tetsuya Kawanishi[1], **Takahide Sakamoto**[1], **Akito Chiba**[1], **Daiki Nanbu**[2]
Hiroyuki Toda[2], **Hiroshi Murata**[3], **and Akira Enokihara**[4]

[1]National Institute of Information and Communications Technology
4-2-1 Nukui-Kita, Koganei, Tokyo 184-9795, Japan
[2]Faculty of Science and Engineering, Doshisha University
1-3 Tatara-Miyakodani, Kyotanabe, Kyoto 610-0321, Japan
[3]Graduate School of Engineering Science, Osaka University
1-3 Machikaneyama, Toyonaka, Osaka 560-8531, Japan
[4]Graduate School of Engineering, University of Hyogo
2167 Shosha, Himeji, Hyogo 671-2280, Japan

Abstract— LiNbO3 Mach-Zehnder (MZ) optical intensity modulators have been widely used in optical communication systems. The important figures, which specify the performance of the modulators, are frequency response bandwidth, halfwave voltage, chirp parameter and extinction ratio. The chirp parameter can be less than 0.2 by using x-cut LiNbO3 modulators. A typical extinction ratio of an MZ modulator is less than 35 dB. These figures are good enough for digital transmission, however, more precise lightwave modulation would be required for analog applications, such as two-tone lightwave signal generations in photonic local oscillator system for radio astronomy. The chirp parameter depends on imbalance in electric field of the modulating signal, while the extinction ratio depends on the MZ waveguide structure. These two parameters are limited by fabrication errors in the waveguide structures and electrodes. Recently, we proposed high extinction ratio and low chirp optical intensity modulation technique using an integrated Mach-Zehnder (MZ) LiNbO3 modulator with active trimmers [1, 2], where imbalance in the MZ structure in the modulator can be compensated. This technique is useful to generate two-tone signals with high carrier suppression ratio. For such a precise lightwave modulation, performance estimation and characterization methods would be very important. In this paper, we investigate two-tone lightwave signal generation using high extinction ratio and low chirp optical intensity modulation, and discuss characterization of generated signal and modulators. The extinction ratio can be larger than 70 dB, and the chirp parameter can be less than 0.01 [1, 2]. By using this technique, we can achieve very pure two tone lightwave generation, which would be useful for radio astronomy, advanced measurement, etc.

REFERENCES

1. Toda, H., et al., MWP, B4P-E, 2007.
2. Kawanishi, T., et al., CLEO, CFA1, 2008.

Photonic Integration with Si-wire Waveguides for Photonic Networks

Hirohito Yamada[1] and Tao Chu[2]

[1]Department of Electrical and Communication Engineering
Graduate School of Engineering, Tohoku University, Japan
[2]Nano Electronics Research Labs., NEC Corp., Japan

Abstract— Micro-photonic devices based on Si-wire waveguides are attractive for realizing photonic integrated circuits using optical interconnection with the Si-wire waveguides, since the waveguide can be bent with extremely small curvature. We have demonstrated various micro-photonic devices with the waveguides. In this paper, we describe optical ring resonators, optical multiplexer/demultiplexers and optical switches.

Optical ring resonators are one of the most attractive applications of the Si-wire waveguides, since they can have very wide free-spectral ranges (FSRs) due to those small ring radiuses of several micrometers. The ring resonators are expected to be used in constructing many novel devices, such as tunable lasers, optical delay lines and optical filters for use in photonic networks. We demonstrate optical filters using ring resonators with Si-wire waveguides. Obtained FSR of the single ring resonator was about 380 GHz which is more than one order of magnitude larger than the FSR obtained by ring resonators with silica based waveguides.

Optical add/drop multiplexers (OADMs) are indispensable devices in wavelength division multiplexing (WDM) network for dropping out or adding in light signals with specific wavelengths. In this paper we demonstrate a Mach-Zehnder interferometer (MZI) type ROADM in which Bragg-grating reflectors are formed on both the MZI branches. The Bragg gratings were formed by making small fins at a period of 370 nm on the sidewalls of the 500-μm-long waveguides. The device was 700-μm-long which is more than one order of magnitude smaller than conventional OADMs made of silica waveguides.

Finally, we describe ultra small optical switches based on Si-wire waveguides. We fabricated MZI-type 1×2 optical switches composed by Y-splitters and 3-dB directional couplers. The switches were controlled with thin-film heaters formed over the MZI branches. The footprint of the 1×2 optical switches were 85×30 μm which is more than two orders of magnitude smaller than conventional optical switches made of silica waveguides. We also describe 1×4 and 4×4 optical switches made by the 1×2 switches and demonstrate their fundamental switching characteristics.

Technical Trends in Millimeter-wave Band Radio-On-Fiber Access System

Tomohiro Taniguchi, **Naoya Sakurai**, **Hideaki Kimura**, **and Kiyomi Kumozaki**
NTT Access Network Service Systems Laboratories, NTT Corporation, Japan

Abstract— In recent years, fiber-to-the-home (FTTH) customers are increasing explosively in Japan, Korea, and certain other countries, and this means that optical fibers is becoming the most popular communication infrastructure in access networks. On the other hand, there is wide-spread use of wireless networks, such as wireless LAN or WiMAX, and bit rates of the wireless systems are approaching 100 Mb/s and more. As hybrid architecture of fiber optics and wireless systems, Radio On Fiber (ROF) system is known. Radio On Fiber (ROF) is optical analog transmission technique of RF signals, that utilizes broad band and low loss characteristics of optical fiber. With ROF access systems, since base stations are needed only to perform an optical-electrical conversion, configurations of base stations can be simplified and independent of modulation format and protocol. From these advantages, ROF is expected as useful solution to realize future flexible and high capacity access networks.

This paper reviews technical trends in ROF access systems, focusing especially on millimeter-wave band systems. In the millimeter-wave band, wide band spectrum can be used for transmission (for example, several GHz bandwidth is available in 60 GHz band), therefore, Gb/s class bit-rate is realized. On the other hand, due to its very high frequency, comparing to micro-wave band systems, there are difficulties in signal generation, up-conversion/down-conversion, modulation/demodulation, and transmission. In ROF systems, these problems are solved effectively with optical domain techniques.

In addition, this paper describes our proposal based on optical heterodyne technique for 60 GHz band ROF access system. The points of the proposal are achievement of adequate optical link budget and simple system configuration, therefore, high quality transmission can be realized with low cost. As a proof of concept, full duplex 1.0 Gb/s transmission experiment over 60 GHz ROF is demonstrated. Further, future perspective for higher bit-rate employing the optical heterodyne technique is discussed.

Radio on Fiber Technologies and Their Application toward Universal Platform for Heterogeneous Wireless Services

Katsutoshi Tsukamoto, **Takuya Yamagami**, **Takeshi Higashino**, **and Shozo Komaki**
Division of Electrical, Electronic and Information Engineering
Graduate School of Engineering, Osaka University, Japan

Abstract— To realize user-centric and flexible wireless services, the network platforms for heterogeneous wireless require improvements in radio frequency utilization, dead zone reduction, traffic dispersion in urban area, and universal service abilities in rural area with a low population. Radio on Fiber (RoF) technologies arisen from the combination of optical fiber and radio communication technologies are able to transparently transmit various types of radio services, and realize a effective universal network platform for wireless communications and broadcastings. To realize the universal network for heterogeneous wireless services, we have proposed Software Definable Radio Networks (SDRN), where RoF networks are used as a universal entrance network among various types of radio access points and IP core network. The first part of this paper describes the concept of SDRN, and the role of RoF as a universal platform for heterogeneous wireless services. In the second part, especially, the paper proposes a new types of distributed antenna architecture by use of RoF, and shows some theoretical and experimental results for the effect in MIMO-SDMA capability improvement.

Experimental Demonstration of a Radio on Free Space Optics System for Ubiquitous Wireless

Kamugisha Kazaura[1], **Toshiji Suzuki**[2], **Kazuhiko Wakamori**[2], **Mitsuji Matsumoto**[3], **Takeshi Higashino**[4], **Katsutoshi Tsukamoto**[4], **and Shozo Komaki**[4]

[1]Research Institute for Science and Engineering (RISE), Waseda University, Japan
[2]Global Information and Telecommunication Institute (GITI)
Waseda University, Japan
[3]Graduate School of Global Information and Telecommunication Studies (GITS)
Waseda University, Japan
[4]Department of Electrical, Electronic and Information Engineering
Graduate School of Engineering, Osaka University, Japan

Abstract— One of the ultimate goals in next generation network design is to achieve an ubiquitous environment enabling connectivity between any wireless access system with optical fiber core network. Radio on Fiber (RoF) technology has been applied to realize a universal platform for transparently carrying various types of wireless services. By applying free-space optical (FSO) communication techniques with RoF, this concept can be extended to free space channels. This paper describes a development project of DWDM Radio on Free-Space Optics (RoFSO) system, which can realize a universal platform to quickly and effectively provide ubiquitous wireless services to underserved areas left out due prohibitive costs associated with laying optical fiber cables. In order to realize the RoFSO system, we developed an all-optical connection between free-space and optical fiber links by directly coupling the free-space propagated beam to a single mode fiber without any conversion of the transmitted light signal. Furthermore, we have demonstrated this system by conducting field experiments of transmission of various kinds of wireless services; for example, 3GPP, WLAN, terrestrial digital television broadcasting etc.; over extended durations using this RoFSO system. The obtained results indicate satisfactory performance and potential of the RoFSO system. As a result, we show the possibility to utilize the RoFSO system for optical and radio frequency signals transmission not only for optical fiber transmission but also over a free-space channel.

Radio on Leaky Coaxial Cable (RoLCX) System and Its Applications

T. Higashino, **K. Tsukamoto**, **and S. Komaki**
Division of Electric, Electronic and Information Engineering, Osaka University, Japan

Abstract— In the next generation radio access network, different kind of radio service coexists and they are mutually connected via the IP-based network. In this paper, radio on leaky coaxial cable (RoLCX) system is introduced as a wideband universal antenna toward heterogeneous radio access networks. It could be strong candidate of common antenna to construct heterogeneous radio space by virtue of its large bandwidth as well as coaxial cables.

Some applications such as remote antenna, wireless positioning, spatially delivery functions are also proposed. The purpose of first application is to expand a service area enabling to use radio service. Since the remote LCX antenna enables us to reduce the distance between transceiver compared to an omni antenna, transmission power reduction is obtained. In 2nd application, while an omni antenna can detect distance between transceiver, 2-dimensional relative location by using LCX based on impulse response between transceiver can be achieved because it depends on the position of wireless terminal at the area which is constructed by the LCX antenna. Time difference of arrival (TDOA) is applied to positioning method. The last is a kind of interference suppression method by using a characteristic of a slot array antenna. It suppresses interference radio signals for partial space in order to coexist different kind of radio service provided by the same RF channel.

Exploring Sub-THz Waves for Communications, Imaging, and Gas Sensing

Yuichi Kado[1] **and Tadao Nagatsuma**[1,2]

[1]NTT Microsystem Integration Laboratories, NTT Corporation
3-1, Morinosato Wakamiya, Atsugi, Kanagawa 243-0198, Japan
[2]Graduate School of Engineering Science, Osaka University
3-1 Machikaneyama, Toyonaka, Osaka 565-8650, Japan

Abstract— The development of technology that applies terahertz (THz) waves to industry is expected to play an important role in the creation of new industrial fields that meet such social needs. The THz region of the electromagnetic spectrum runs from 0.1–10 THz, which corresponds to the wavelength region from 30 µm–3 mm.

Exploiting the features of THz waves, we are researching application fields that can respond to social needs with a focus on communications, imaging, and gas sensing.

In the field of communications, there is a great demand for large-capacity wireless links with bit rates in excess of 10 Gbit/s and for expansion of radio spectrum resources. The paper will describe ultra-high-speed wireless technology at the 10 Gbit/s level with a carrier frequency in the 120-GHz band.

In addition, concerns are growing about the earthquake resistance of concrete structures. There has consequently been a focus on the detection of 0.2–0.3 mm cracks on the surface layer of buildings as a basic element in the diagnosis of concrete structures. In this regard, the paper will describe imaging technology using sub-THz waves that can detect cracks on the surface of concrete even through wallpaper or tile and display them on a display screen.

Next, in rescue efforts at sites affected by fires or other natural disasters, there is a need for technology that can remotely sense the concentration of harmful gases. The paper describes sensing technology that makes use of the fact that the intrinsic absorption of toxic gas lies in the sub-THz range.

Real-time Visualization of W-band Millimeter Wave by Live Electro-optic Imaging

Kiyotaka Sasagawa[1, 2], **Atsushi Kanno**[1], **and Masahiro Tsuchiya**[1]

[1]National Institute of Information and Communications Technology, Japan
[2]Graduate School of Materials Science, Nara Institute of Science and Technology, Japan

Abstract— Live electro-optic imaging (LEI) is a scheme for the real-time visualization of RF electric field distributions, which has been recently developed by the authors (http://lei-camera.nict.go.jp/) and enables intuitive grasps of RF circuit functions. In this paper, the successful extension of its operation frequency up to 100 GHz in W-band is described. Indeed, it has resulted in observations of some features of traveling millimeter waves, which could lead to new schemes of effective diagnoses for millimeter-wave circuits.

LEI is based on ultra-fast and ultra-parallel nature of photonics technologies, where RF electric near-field distributions are converted instantaneously to 10,000 channel optical signals via an electro-optic crystal plate with the Pockels effect. Simultaneously, the frequency of the optical signal modulation is down-converted by photonic heterodyning to what is within the operation speed of a high speed image sensor with a large degree of parallelism (10,000). Electric field intensity and phase distribution images are displayed on a computer screen through some digital signal processing after the photo-detection. Thus, the time needed for image acquisition of electric near-field is drastically reduced and real-time RF electric near-field imaging has been realized. The resolution and the frame rate are 100×100 pixels and 30 frames/sec at highest, respectively.

The extension of frequencies of electric fields to be observed has been brought about by the newly developed technique: a millimeter-wave two-tone photonic signal generation, which is at a wavelength detectable with the Si-based image sensor and works as a local oscillator source in the system. Some advanced techniques of optical modulator operations and optical frequency conversions are key issues for the photonic signal generators.

Session 1P2a
Tunable and Nonlinear Metamaterials

New Guided Nonlinear Waves in Tuneable Gyrotropic Metamaterial Structures

A. D. Boardman, **P. Egan**, **R. C. Mitchell-Thomas**, **and Y. G. Rapoport**
Joule Physics Laboratory, University of Salford, Salford, UK

Abstract— The literature is alive with papers [1] devoted to the creation of electromagnetic metamaterials and there appears to be a particular desire to create photonic applications that will operate at THz frequencies and beyond. These are extremely important ranges medically and it is imperative to study structures that sustain both guided and surface waves in the nonlinear regime and to offer the possibility of extra tunability through the addition of a gyromagnetic environment. In particular, a magneto-optic influence is required that will take advantage of the types of nanostructured metaparticles that are coming into existence. If the nonlinearity is strong, the shape of the modal fields of nonlinear guided waves changes significantly with power, as demonstrated in the widely cited papers by Boardman and Egan [2, 3]. For this regime, the first-order coupled-mode approach is quite inadequate. This is the situation that will be considered here, and will require exact solutions of the nonlinear equations that deploy the special boundary conditions that metamaterials can offer. The background dielectric tensor of the metamaterial will be assumed to be centrosymmetric and the nonlinearity will be unsaturated, gaining its form from a third-order polarization. It is straightforward to include this type of nonlinearity into the permeability as well with a suitable modification of the effective nonlinear coefficient. Hence a quadratic dependence of the nonlinear refractive index is adopted and waves that are at the fundamental frequency ω and also at the harmonic frequency 3ω, assumed to be a, poorly phase-matched, small effect. The possibility that the nonlinearity will saturate and the role of any absorption process will be addressed elsewhere. This Kerr regime will be examined through an investigation of TE waves in a nonlinear slab guide that has linear bounding material that could be gyrotropic. Both the relative permittivity and the relative permeability are less that zero and, hence, are in the negative phase frequency range of operation. The damping is not considered here on the grounds that this is assumed to be an active medium, for which the loss is, at least, minimized to have a very small influence on the final outcomes. It is shown that unique, exact, nonlinear surface waves exist because of the metamaterial properties, and a unique concentration of guided energy is created that is a direct consequence of the power flow coupling to the new boundary conditions. Finally, it is shown that this form of nonlinear tunability of negative phase metamaterials is considerably extended when gyrotropic boundaries [4] are added to the system. The conclusion is that modern metamaterials are going to have a positive impact upon magneto-optic recording processes, some of which will be highlighted here.

REFERENCES

1. Boardman, A. D., N. King, and L. Velasco, "Negative refraction in perspective," *Electromagnetics*, Vol. 25, 1, 2005.
2. Boardman, A. D. and P. Egan, "Optically nonlinear-waves in thin-films," *IEEE J. Quant. Elec.*, Vol. 22, 319–324, 1986.
3. Boardman, A. D. and P. Egan, "S-polarised waves in a thin dielectric film asymmetrically bounded by optically nonlinear media," *IEEE J. Quant. Elec.*, Vol. 10, 1701, 1985.
4. Boardman, A. D., N. King, Y. Rapoport, and L. Velasco, "Gyrotropic impact upon negatively refracting surfaces," *New Journal of Physics*, Vol. 7, 191, 2005.

Dissipative Breathers in rf SQUID Metamaterials

G. P. Tsironis[1], **N. Lazarides**[1, 2], **and M. Eleftheriou**[1, 3]

[1]Department of Physics, University of Crete, and Institute of Electronic Structure and Laser Foundation for Research and Technology-Hellas, P. O. Box 2208, Heraklion 71003, Greece
[2]Department of Electrical Engineering, Technological Educational Institute of Crete P. O. Box 140, Stavromenos, Heraklion 71500, Crete, Greece
[3]Department of Music Technology and Acoustics, Technological Educational Institute of Crete E. Daskalaki, Perivolia, Rethymno 74100, Crete, Greece

Abstract— The development of artificially structured, composite materials (metamaterials) have substantially extended the range of possible electromagnetic response that can be obtained by naturally occuring materials. For example, some magnetic metamaterials (MMs) exhibit significant magnetic properties at Terahertz and optical frequencies, as well as negative magnetic response at far-infrared frequencies. It has been recently suggested that rf SQUID (i.e., superconducting quantum interference device) arrays in an alternating magnetic field can operate as nonlinear MMs in microwaves [1], leading to negative magnetic response above the resonance frequency of its constituent elements. The nonlinearity, which is intrinsic to each rf SQUID due to the presence of the Josephson junction, provides the possibility of tuning the magnetic permeability of the MM by varying the applied flux.

Moreover, the combined effects of nonlinearity and discreteness may lead in the generation of nonlinear excitations of the form of dissipative discrete breathers (DDBs), i.e., spatially localized, time-periodic, and stable excitations, whose dynamics is governed by power balance between losses and external driving field. The existence and stability of DDBs in rf SQUID arrays is investigated numerically. We analyze several DDB excitations, both in one and two dimensions, which are linearly stable up to relatively large coupling parameters. We find that DDBs may locally alter the magnetic response of the array from paramagnetic to diamagnetic (or vice versa), and that they are not destroyed by increasing the dimensionality [2].

Those DDB excitation exhibit some similarities with those appearing in other systems whose elements are coupled magnetically, which are usually referred to as magneto-inductive systems. For instance, DDBs may appear in MMs comprised of nonlinear split-ring resonators [3–5]. However, there are distinct differences between DDB excitations in those systems, due to the different form of the nonlinear on-site potential. Given that both nonlinear systems have been constructed in the laboratory [6, 7], our theoretical predictions are experimentally testable.

REFERENCES

1. Lazarides, N. and G. P. Tsironis, *Appl. Phys. Lett.*, Vol. 90, 163501, 2007.
2. Lazarides, N., G. P. Tsironis, and M. Eleftheriou, *Nonlinear Phenomena in Complex Systems*, arXiv:0712.0719.
3. Lazarides, N., M. Eleftheriou, and G. P. Tsironis, *Phys. Rev. Lett.*, Vol. 97, 157406, 2006.
4. Eleftheriou, M., N. Lazarides, and G. P. Tsironis, *Phys. Rev. E*, Vol. 77, 036608, 2008.
5. Lazarides, N., G. P. Tsironis, and Yu. S. Kivshar, *Phys. Rev. E*, Vol. 77, 065601 (R), 2008.
6. Shadrivov, I. V., A. B. Kozyrev, D. W. van der Weide, and Yu. S. Kivshar, arXiv:0805.0028.
7. Kirtley, J. R., et al., *Phys. Rev. B*, Vol. 72, 214521, 2005.

Tunable Dynamic Capacitance Arising from Coulomb Blockade in a 2D Nanoclusters Assembly

F. Peschaud, **D. Crété**, **P. Seneor**, **and F. Nguyen Van Dau**
Unité Mixte de Physique CNRS/Thales, Palaiseau, France

Abstract— Radio-frequency devices such as voltage controlled oscillators or mixers are present in a wide variety of applications from general public electronics or telecoms to military radars. They mainly rely on variable capacitors to tune their operating frequency. In the quest for performance and low power consumption, downscaling has been the main answer from the CMOS industry. However, this option will tackle its limits reaching the nanometer scale. Hence, alternative ways such as the Micro ElectroMechanical Systems and their nanometer-sized equivalent have been sought for. We show how Coulomb blockade of electrons in a dispersive set of clusters embedded in the dielectric of a capacitor can be used to design a voltage tunable variable capacitor.

A layer of nanoparticles is embedded in a thin capacitor in tunnelling range from the first electrode. Typical sizes of clusters range from 1 nm to 8 nm which gives rise to a Coulomb blockade transport regime as the electrostatic charging energy is higher than the thermal fluctuation. The first insulating layer is supposed to be thin enough to make tunnel phenomenon possible on the contrary to the second one which is too thick and prevents tunnelling. The whole structure is biased via a DC source controlling the onset of Coulomb blockade according to their position in the size distribution. A complementary small AC signal that leads to a charging-discharging process of the clusters modifies the total dynamic capacitance of the system.

The multi-layer system is grown by sputtering. After a first dielectric layer on top of a metal electrode, the three-dimensional growing process allows to obtain a self-assembled two dimensional plane of metallic clusters presenting a gaussian distribution. Then a second dielectric layer is grown that covers the entire assembly.

We will present the model, numerical simulations and validating experiences using insulating materials such as alumina or MgO.

Continuously Tunable Effective Properties of Metamaterials Controlled by Varactor Diodes

L. Liu, **S. Matitsine**, **P. K. Tan**, **and C. B. Tang**
Temasek Laboratories, National University of Singapore, Singapore 117508, Singapore

Abstract— Microwave properties of composites or Metamaterials with embedded long conductive fibers have attracted much attention recently due to various promising applications, such as frequency selective or impedance matching layers, smart materials, or meta-materials [1]. Band stop properties at microwave frequency can be obtained from composites that contain single or multi-layer half-wavelength conductive fibers distributed on planar surfaces. Both randomly and periodically distributed fibers in composites were investigated. Cluster effect due to the overlapping of fibers was proposed to explain the dispersive microwave properties of composites with randomly distributed fibers [2]. The main limitation of such composites is that such structures are not tunable or re-deployable. Once they are fabricated, the properties of the composites, such as working frequency and bandwidth, etc, cannot be modified to meet changes in operational requirement. Electromagnetic smart screen with conductive fiber array and pin diodes was investigated. Transmission coefficient was simulated using finite element method (FEM) with validation by free space measurement. Tunable properties are obtained through controlling the on/off state of the microwave diodes [3].

In this study, we proposed Metamaterials with periodic distributed long conductive fiber controlled by varactor diodes. The impedance and circuit parameters of the varactors were measurement with impedance analyzer. The tunable effective permittivity was investigated using vector network analyzer and free space measurement as well as finite element calculation. The pattern design was optimized numerical through parametric study. It is found that the effective properties of such Metamaterials can be continuously adjusted within certain frequency band. The potential applications include in hybrid radomes, band-stop filters, subreflector and circuit analog absorbers for radar cross section reduction (RCSR) and many other civilian and military applications.

REFERENCES

1. Liu, L., S. Matitsine, Y. B. Gan, and K. N. Rozanov, *J. Appl. Phys.*, Vol. 98, 063512, 2005.
2. Liu, L., S. Matitsine, Y. B. Gan, and K. N. Rozanov, *J. Phys. D: Appl. Phys.*, Vol. 40, 7534, 2007.
3. Liu, L., S. Matitsine, and P. K. Tan, *Micro. & Optic. Tech. Lett.*, Vol. 50, No. 6, 1510, 2008.

Ultra-thin Strip Line Metamaterial Absorber

Ruifeng Huang, **Zheng-Wen Li**, **Lingbing Kong**, **and Serguei Matitsine**
Temasek Laboratories, National University of Singapore, Singapore 117508, Singapore

Abstract— Short strip pairs (SSPs) show strong magnetic responses, just as the split-ring resonators (SRRs), at the free space wavelengths much larger than the distance between the two short strips. Compared with the SRRs, the SSPs have the advantages of easy fabrication and simple experimental characterization. In this paper, it is shown that the SSPs can be used in the design of metamaterial absorbers. Due to the image effects of the backing metallic surface, only one of the two short strips in the SSP is needed. For simplicity, the short strips stretch into infinity in the polarization direction of the magnetic field components of the incident waves, as shown in Figure 1. Only normal incidence is considered. With the periodic characteristic of the structure taken into account, the computational model of the original structure is shown in Figure 2. It can be seen that the computational model actually is an ideal short-ended parallel plate discontinuous waveguide. Mode matching method is used to efficiently solve the electromagnetic response of the strip line metamaterial absorber based on the model in Figure 2. To optimize the physical dimensions of the absorber and the electromagnetic properties of the substrate, genetic algorithm is used. A few examples of the optimized strip line metamaterial absorbers are presented. For the metamaterial absorber consisting of dielectric substrate with frequency-independent permittivity and with the substrate thickness of about $1/66\lambda$ at the center frequency of 9 GHz, the optimized result shows 10 dB absorption bandwidth of around 0.54 GHz. The thickness to bandwidth ratio of the metamaterial absorber is smaller than that of the physically realizable homogenous dielectric absorbers with frequency-independent permittivity.

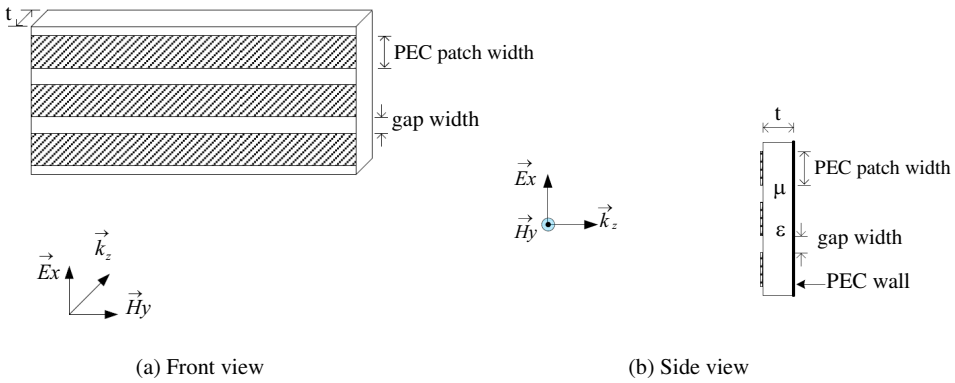

Figure 1: The strip line metamaterial absorber under consideration.

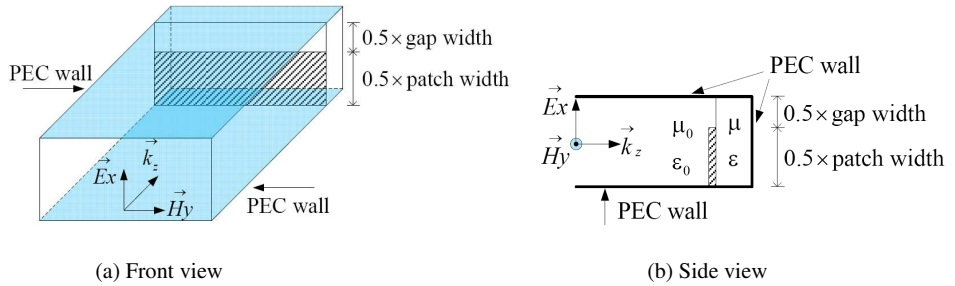

Figure 2: The computational model of the metamaterial absorber in Figure 1.

Tunable Effective Permittivity of Carbon Nanotube Composites and Applications as EM Smart Materials

L. Liu, L. B. Kong, and S. Matitsine
Temasek Laboratories, National University of Singapore, 117508, Singapore

Abstract— Carbon nanotubes (CNTs) have been developed in the last decade. Due to their fibrous shape, CNTs may allow high permittivity and frequency dispersion to be obtained in composites with low concentrations [1]. The significant difference is that CNTs are nanoscaled particles whose diameter is several orders of magnitude smaller than that of carbon fibers (typically about 10 μm). It is well known that the nanosized particles usually display distinct properties from microsized particles of the same composition, which is the primary reason for the great attention currently given to the high frequency performance of CNTs composites. In addition, the use of CNTs with nanoscaled dimension may avoid the drawbacks of composites filled with short CF, such as anisotropic properties due to orientation of included fibers and bonding problems with the holding matrix.

Composites with CNTs as inclusions were prepared and the dielectric properties under bias voltages were studied. It was found that the composites with weight concentrations of CNTs above 6 wt% exhibited tunable dielectric characteristics under external applied bias voltage, with real part decreasing while imaginary part increasing with increasing applied voltage [2]. The tunable properties may be understood from the percolation threshold point of view. The tunable permittivity of the CNTs composites may have potential applications in electromagnetic smart materials and structures. Smart materials normally use pin diodes to realize on-off switch. One of the drawbacks of pin diodes is their relatively weak tolerance to high current or power, which is usually encountered in practical applications. A possible solution is to use a small piece of CNT composite with higher power handling capability to replace pin diode.

REFERENCES

1. Liu, L., S. Matitsine, Y. B. Gan, L. F. Chen, L. B. Kong, and K. N. Rozanov, *J. Appl. Phys.*, Vol. 101, 094106, 2007.
2. Liu, L., L. B. Kong, and S. Matitsine, *Appl. Phys. Lett.*, Vol. 93, 113106, 2008.

Session 1P2b
Backward Emitted Cherenkov Radiation in Left-Handed Material

Cherenkov Radiation in a Waveguide Partially Loaded with Anisotropic Double-negative Metamaterials

Zhaoyun Duan[1], **Bae-Ian Wu**[2], **Jie Lu**[2], **and Min Chen**[3]

[1]Vacuum Electronics National Lab, School of Physical Electronics
University of Electronic Science and Technology of China, Chengdu 610054, China
[2]Research Laboratory of Electronics, Massachusetts Institute of Technology
Cambridge, MA 02139, USA
[3]Department of Physics, Massachusetts Institute of Technology
Cambridge, MA 02139, USA

Abstract— Currently, a DNM is composite medium with different materials such as the metallic strips for the SRRs and rods/dielectric materials for holding the strips. Therefore, the DNMs are in essence anisotropic rather than isotropic. A charged particle in a waveguide fully filled with such an anisotropic DNM will lose energy by polarization radiation in addition to Cherenkov radiation (CR). The polarization losses are actually responsible for the greater part of the energy loss and the particle is quickly brought to stop. Hence, it might be better to leave a vacuum channel in the center to allow the particle to pass. As a result, the polarization losses can be avoided. In this paper, a general CR theory in anisotropic DNMs is presented, especially for the case of an empty waveguide partially filled with anisotropic DNMs. The theory presented here provides a theoretical basis for possible experiments and potential applications. As an example, we discuss the physical properties of CR and the potential applications such as particle detectors and high-power sources.

ACKNOWLEDGMENT

This work was supported by the Office of Naval Research under Contract N00014-06-1-0001, the Department of the Air Force under Air Force Contract F19628-00-C-0002, National Natural Science Foundation of China (Grant Nos. 60601007, 60532010 and 60531020), Youth Science and Technology Foundation of UESTC (Grant No. JX05018) and Chinese Scholarship Council.

Experimental Verification of Negative Index Metamaterial for Cerenkov Radiation

Sheng Xi[1, 3], **Hongsheng Chen**[1, 3], **Tao Jiang**[1], **Lixin Ran**[2], **Jiangtao Huangfu**[2], **Bae-Ian Wu**[3], **Jin Au Kong**[1, 3], **and Min Chen**[4]

[1]The Electromagnetics Academy at Zhejiang University
Zhejiang University, Hangzhou 310027, China
[2]Department of Information and Electronic Engineering, Zhejiang University
Hangzhou 310027, China
[3]Research Laboratory of Electronics, Massachusetts Institute of Technology
Cambridge, Massachusetts 02139-4307, USA
[4]Department of Physics, Massachusetts Institute of Technology
Cambridge, Massachusetts 02139-4307, USA

Abstract— Previous theoretical work [1] showed that Reversed Cerenkov can be observed in negative index metamaterials for transverse magnetic (TM) electromagnetic waves. We have fabricated metamaterial that has negative permittivity in two dimensions and negative permeability in the third dimension [2] and experimentally verify the negative refraction behavior of it. This TM metamaterial shows a pass band between about 8.5 GHz and 9.5 GHz. Through the prism experiment in which a beam is normally incident on to the prism composed of such metamaterial, we measure the refraction angle for the waves emitting from the hypotenuse, and negative refraction is observed between 8.5 GHz and 9.5 GHz.

REFERENCES

1. Lu, J., T. M. Grzegorczyk, Y. Zhang, J. Pacheco, Jr., B.-I. Wu, J. A. Kong, and M. Chen, "Cerenkov radiation in materials with negative permittivity and permeability," *Optics Express*, Vol. 11, No. 7, 723, 2003.
2. Wu, B.-I., J. Lu, J. A. Kong, and M. Chen, "Left-handed metamaterial design for Čerenkov radiation," *J. Appl. Phys.*, Vol. 102, 114907, 2007.

Review of Cherenkov Radiation in Double-negative Metamaterials

Zhaoyun Duan[1], **Bae-Ian Wu**[2], **and Min Chen**[3]

[1]Vacuum Electronics National Lab, School of Physical Electronics
University of Electronic Science and Technology of China, Chengdu 610054, China
[2]Research Laboratory of Electronics, Massachusetts Institute of Technology
Cambridge, MA 02139, USA
[3]Department of Physics, Massachusetts Institute of Technology
Cambridge, MA 02139, USA

Abstract— In this paper, we briefly review the research progress in Cherenkov radiation in double-negative metamaterials (DNMs) since the first experimental verification of the DNMs was reported in 2001, from the theoretical research, numerical simulation to experimental design. And then we pursue on discussing the potential applications to particle detectors and high-power microwave or millimeter wave devices, including oscillators and amplifiers. At last, we conclude the challenges and benefits from the use of the novel artificial materials.

ACKNOWLEDGMENT

This work was supported by the Office of Naval Research under Contract N00014-06-1-0001, the Department of the Air Force under Air Force Contract F19628-00-C-0002, National Natural Science Foundation of China (Grant Nos. 60601007, 60532010 and 60531020), Youth Science and Technology Foundation of UESTC (Grant No. JX05018) and Chinese Scholarship Council.

Session 1P3
Radar Investigation of the Atmosphere from the Ground to 110 km

Introduction to the Re-locatable Atmospheric Observatory in China

Xiong Hu and Jiancun Gong
Center for Space Science and Applied Research, Chinese Academy of Sciences
Beijing 100190, China

Abstract— The atmospheric environment in the near space (20–100 km) plays a significant role in the energy and momentum coupling between the upper atmospheric space weather and the lower atmospheric meteorology. In order to exploring the near space atmosphere, a Re-locatable Atmospheric Observatory (RAO) has been being developed in China. In this RAO, there are a Sodium wind/temperature lidar for measuring the atmospheric wind, temperature and Sodium density profiles of the Sodium layer within 75–110 km, and a mobile Doppler wind lidar for measuring the atmospheric wind profile from the near earth surface up to 40 km, and a mobile FP wind interferometer for measuring the horizontal winds near mesopause region, and an all-sky airglow imager for exploring the gravity waves over the mesopause region, and a Medium-Frequency (MF) partial reflection radar for measuring the horizontal atmospheric wind and electron density of the mesosphere and lower thermosphere within 60–100 km for day time and 80–100 km for nighttime, and a meteor radar for measuring the horizontal winds and meteor flux within 70–110 km. Besides the above ground-based instruments, the stratospheric balloon dropsonde technique for measuring the atmospheric wind, temperature, humidity and pressure profiles below the height of the stratospheric balloon, and the GPS rocketsonde exploring the atmospheric wind and temperature within 20–60 km are developed. All of the ground-based instruments are designed for re-locatable so that the observatory can be moved to a new site for new observations within a short time. This RAO will operate routinely in 2010 and provide abundant data for the researches of the atmospheric structure and dynamics in China, which will help to promote the empirical and physical model of the near space atmosphere and knowledge of the dynamical coupling among the atmospheric layers.

Gravity Wave Observations in the Tropical Mesosphere

Robert A. Vincent, **Sujata Kovalam**, **and Iain M. Reid**
School of Chemistry and Physics, University of Adelaide, Adelaide, SA 5005, Australia

Abstract— In January and February 2006 a major field campaign (TWP-ICE) was undertaken in Darwin (12S, 131E), Australia. As part of this campaign a meteor radar operating at 33 MHz and a 54-MHz boundary layer (BL) radar were installed in Darwin to study atmospheric motions during TWP-ICE. The high temporal and spatial resolutions of the radars were used to study gravity wave (GW) motions and compare with predictions made by a high-resolution numerical model. The model is initiated by latent heat release measurements derived from weather radars located in the Darwin area. Output from the numerical model is then tested against gravity wave measurements made with the BL and meteor radars. For the meteor radar comparisons GW ray tracing techniques were used to investigate propagation of waves from the troposphere to the mesopause region at 85–92 Km. We show that there is large temporal variation in wave activity due to the presence of a strong two-day wave as well as diurnal and semidiurnal tides. Despite these variations there is good agreement between the mesospheric wave activity predicted by the model/ray tracing results and the GW flux observations made with the meteor radar.

Ground Based Radar for Observations of the Atmosphere

Iain Reid[1, 2]

[1]ATRAD Pty Ltd, 1/26 Stirling Street, Thebarton 5031, Australia
[2]School of Chemistry and Physics University of Adelaide, Adelaide 5005, Australia

Abstract— Radar can be used to make measurements of the dynamics, structure and temperature of the atmosphere by detecting irregularities in refractive index due to variations in humidity and temperature in the lower atmosphere (*0–20* km), and due to variations due to fluctuations in electron density in the Mesosphere Lower Thermosphere (*MLT*) region of the upper atmosphere (*50–110* km). *MF* and *HF* radars have been used to routinely investigate the *MLT* for over 50 years. They remain one of the few radar types to reliably provide measurements of the winds and structure of the atmosphere in the region between *50* and *80* km. Wind Profiling Radars operating in the *VHF* band have been used for about *25* years to investigate the Stratosphere Troposphere (*ST*) region, but only routinely in the last *15* years. Considerable development has occurred within the past decade and a number of rocket launch sites now utilize Wind Profilers for launch support. They are also becoming increasingly common for airport operations. A variant of the wind profiling radar, the MST or Mesosphere Stratosphere Troposphere radar can be used with high transmitter powers to investigate the *60* to *80* km height region of the atmosphere, but generally only during daylight hours and with intermittent height and time coverage. Radars operating in the *VHF* and *UHF* bands are now commonly used in Boundary Layer (*BL*) studies and in forecast meteorology. Most recently, the meteor radar technique has been re-birthed in the form of all-sky interferometric radars operating in the *30* to *60* MHz band. These particular radars are being exploited for the measurement of temperature in the *MLT-region* of the atmosphere and for meteor radiant studies. Here we briefly describe some recent developments in each of these types of radar.

Meteor Radar Observations at Adelaide, Darwin and Davis Station

Daniel McIntosh[2], **Iain Reid**[1, 2], **Robert Vincent**[2], **Andrew Klekociuk**[3], **and Damian Murphy**[3]

[1]ATRAD Pty Ltd., 1/26 Stirling Street, Thebarton 5031, Australia
[2]School of Chemistry & Physics, University of Adelaide, Adelaide 5005, Australia
[3]Australian Antarctic Division, Channel Highway Kingston, Tasmania 7050, Australia

Abstract— Recently, the meteor radar technique has been re-birthed in the form of all-sky interferometric radars operating in the 30 to 60 MHz band. A great many of these radars are now installed in all latitude ranges. They radars are being exploited for the measurement of temperature and winds in the MLT-region of the atmosphere and for meteor radiant studies. In this paper, we focus on measurements of winds and temperatures using meteor radars located at Darwin (12°S), Adelaide (35°S) and Davis Station (69°S). We compare dual frequency meteor radar operation at Adelaide and Davis Station, and consider single frequency operation at Darwin. Using various pressure models to determine the temperature from the diffusion of the meteor trails indicates a significant difference in values determined using very similar radars using the same analysis schemes and operating at frequencies near 33 and 55 MHz. The reasons for this difference are explored. The results compared with a variety of other estimates of temperature derived from AURA and SABER satellite measurements, from rotational temperature measurements derived from observation of the OH nightglow and from rocket climatologies. Wind velocities measured with the meteor radars and collocated MF radars at Adelaide and Davis Station give particular insight into the particular strengths and weaknesses of each technique. There is a tendency for the MF radar wind speeds to be underestimates of the meteor radar derived wind speeds. There is good agreement in wind direction. Finally, we also briefly consider the sampling issues associated with the meteor radar technique.

Meteor Radar Observations at Hainan Island

Jiankui Shi[1] **and Iain Reid**[2, 3]

[1]Center for Space Science and Applied Research, Chinese Academy of Sciences
P. O. Box 8701, Beijing 100080, China
[2]ATRAD Pty Ltd., 1/26 Stirling Street, Thebarton 5031, Australia
[3]School of Chemistry & Physics, University of Adelaide, Adelaide 5005, Australia

Abstract— Recently, a new high power (20 KW) all sky 38.9 MHz meteor radar has been installed at Fuke, on Hainan Island (19.5°N, 109.1°E), China. This radar regularly obtains count rates in excess of 30,000 per day, making it one of the most capable all sky meteor radars in the world. A similar but lower power (12 KW) radar is operated at Darwin (12°S, 131°E), Australia. In this paper, we describe the Hainan Island radar and its performance, and compare the wind measurements obtained with it with those from the Darwin radar.

On the Diffusion of Meteor Trails

Joel Younger[1], **Iain Reid**[1,2], **Robert Vincent**[1], **and Damian Murphy**[3]
[1]School of Chemistry and Physics, University of Adelaide, Adelaide 5005, Australia
[2]ATRAD Pty Ltd., 1/26 Stirling Street, Thebarton 5031, Australia
[3]Australian Antarctic Division, Channel Highway, Kingston, Tasmania 7050, Australia

Abstract— The diffusion of meteor trails has recently been exploited to estimate temperatures in the 80–100 km region of the atmosphere. More recent modeling work suggests that meteoric dust laid down by the trails themselves will affect the diffusion of the trails. Naturally, this will lead to incorrect temperatures being determined. In this work, we model the diffusion of the trail and confirm a difference in the diffusion of observed meteor trails when sorted by echo strength. We also demonstrate a difference when echoes are sorted by height and by radar frequency. These observational results are in agreement with our simple model.

An Investigation on Properties of Ionospheric Es in Hainan Region

Jiankui Shi and Guojun Wang
State Key Laboratory of Space Weather, Center for Space Science and Applied Research
Chinese Academy of Sciences, Beijing 100190, China

Abstract— In this study, using the DPS-4 digisonde data obtained in Hainan ionosphere observation station from March 2002 to February 2008, diurnal, seasonal and annual occurrence variations of the observed Sporadic E (Es) and its responding to the SSN are studied. The main results are as: The diurnal characteristic of h/c type Es had a single peak which was different from the double peak of the Es over Cachoeira Paulista, and the Es-q had two peaks (one in the morning and the other in the evening) which was also different from the Es-q occurrence (mainly in daytime) over Fortaleza, Brazil. The frequent season was spring, summer, summer and autumn for the f/l, h/c, q and r type Es, respectively. For the annual occurrence rate, the highest was f/l type Es, while the lowest was r type Es. The f/l and q type Es showed a clear increase with SSN and had a positive correlation with SSN during equinoxes and winter, while during summer the each type of Es showed no correlation with SSN. The mechanisms of the Es are also discussed.

Observation of Dynamics in the Mesosphere and Lower Thermosphere with the MU Radar Ultra-multichannel Meteor Observation and Optical Instruments

Takuji Nakamura[1], **Masaki Tsutsumi**[2], **Takuya D. Kawahara**[3], **Kazuo Shiokawa**[4], **and William E. Ward**[5]

[1]Research Institute for Sustainable Humanosphere
Kyoto University, Uji, Kyoto 611-0011, Japan
[2]National Institute of Polar Research, Tokyo, Japan
[3]Faculty of Engineering, Shinshu University, Nagano, Japan
[4]STE laboratory, Nagoya University, Toyokawa, Aichi, Japan
[5]University of New Brunswick, Fredericton, NB, Canada

Abstract— The MU radar meteor echo observation with 1 MW transmission power at 46.5 MHz and large array antenna (8300 m^2) has been used to derive precise horizontal wind velocities in the MLT region (80–100 Km). A new receiving system with a 29 digital quadrature detection was attached to the MU radar in 2004. We have applied the new MU radar system for meteor echo observation. Coherently integrated 25 channel receiving signals improved the SNR of meteor echoes significantly, and meteor echo number became as large as 50,000 per a day, which is about five times of previous meteor observations with the MU radar. The high-rate meteor echoes were utilized to detect horizontal distribution of wind velocity field of about 50 Km scale. The limited area for determining wind velocity significantly changed the characteristics of wind velocity variation within the field of view (FOV) of 300–400 Km, and enabled to detect wind perturbations due to horizontally propagating waves such as gravity waves. The comparison with the airglow imaging by OMTI (Optical mesosphere thermosphere imagers) has shown that similar wave structures were observed both the radar and the imager, suggesting capability of simultaneous observation of an identical wave. A sodium temperature lidar has also been extensively operated since August 2007 in order to derive atmospheric stability of the background of the wave propagation. Combined airglow, radar and lidar observations have shown the details of a shear instability and a related mixing event at the MLT region.

A campaign observation with the MU radar, Na lidar and airglow instruments has been carried out between August and November 2008. A new Michelson interferometer imager (MIADI: Michelson interferometer for airglow dynamics imaging) for Doppler velocity mapping, as well as an additional all-sky imager with about 50 Km distance for triangulation of airglow height structure has joined the campaign as well as the above mentioned instruments. Initial results of the campaign will also be reported in the paper.

Study of Ionospheric Irregularity in the Midlatitude E-region with Portable Radar and Other Instruments

Mamoru Yamamoto
Research Institute for Sustainable Humanosphere (RISH), Kyoto University, Japan

Abstract— We have been studying field-aligned irregularities (FAIs) in the mid-latitude ionosphere with variety of instruments. Portable VHF radar is a powerful tool for the study especially when it is used with other instruments like sounding rockets or the MU radar. SEEK-1 and -2 were both observation campaigns with sounding rockets that aimed to investigate structures of sporadic-E layers and associated FAIs. Portable VHF radars were used to monitor to determine the launch condition of the rockets, and gave important information of FAIs, i.e., echo structures and/or drift velocity of ionospheric plasma. We also conducted observations campaigns called FERIX-1 and -2 to study coupling processes between F-region and E-region ionosphere through the geomagnetic field line. In these observations, F-region FAIs were observed by the MU radar while portable VHF radar was used to measure E-region FAIs on the same field line. Radar imaging technique was utilized to show small structures in the FAIs. In all these studies the portable VHF radar played a key role. We would review these observations, and show results from them.

Comparison of Simultaneous Wind Measurements Using Colocated All-sky Meteor Radar and MF Spaced Antenna Radar Systems

Jinsong Chen, **Lei Zhao**, **Zhenwei Zhao**, **and Jian Wu**
China Research Institute of Radio Propagation, Qingdao 266107, China

Abstract— An all-sky meteor radar and a MF spaced antenna radar have been installed to measure winds in the mesosphere and lower thermosphere (MLT) over Kunming (103.7°E, 25.6°N), China in 2007 by CRIRP (China Research Institute of Radio Propagation), and that provide us an opportunity to carry out a comparison study of winds measured by two different techniques. The first method involves the determination of winds using meteor drifts, and the second method used to determine winds was the spaced antenna technique. The two radar systems are independent, the all-sky meteor radar operating at 37.5 MHz and MF radar at 2.138 MHz. The spatial separation of the two radars is approximately 200 m. Simultaneous data obtained from September 20 to 30, 2008, are presented here, and this paper will describe a preliminary comparative result derived by these two radars. Several possible reasons for those discrepancies are discussed also.

Session 1P4a
Wave Propagation in Random Media

Imaging and Communication through Random Multiple Scattering Media

Akira Ishimaru, **Sermsak Jaruwatanadilok**, **and Yasuo Kuga**
Department of Electrical Engineering, University of Washington
Seattle, WA 98195, USA

Abstract— Imaging through random multiple scattering environments is important in medical detection in biological media and in imaging of hidden objects in obscuring environments. The key questions are how the resolutions in lateral and longitudinal directions are affected by the random medium. In recent years there has been increasing interest in using correlation and signal processing techniques to distinguish images from clutter. This paper discusses several imaging techniques applied to objects in random media. They include angular and frequency correlation techniques and ordinary beam forming, Capon's method and MUSIC (Multiple Signal Classification). Time-space MUSIC applied to a random medium is discussed showing the effects of the random medium on lateral and longitudinal resolutions and multiple targets. Communication channel capacity is greatly affected by the intervening multiple scattering medium. This paper discusses the effects of random media on MIMO channel capacity in terms of the antenna gain characteristics, stochastic Green's functions, and mutual coherence functions (MCF). MCF for random distributions of scatterers is given in terms of the optical depth, albedo, and the phase functions of scatterers. MCF for a turbulent medium is given in terms of power spectrum such as Kolmogorov and the structure constant. Channel capacity is formulated in terms of transmitted power, eigenvalues of channel correlation matrix, normalization factor, and signal-to-noise ratio. As an example, the channel capacities for a 60-GHz channel through rain are calculated in terms of rain rate, numbers of transmitter and receiver antennas, noise power, and signal-to-noise ratio. These formulations for imaging and communication in a complex random environment combine the existing imaging and communication in deterministic media and propagation in multiple scattering random media and lead to better understanding of the physical processes of realistic imaging and communication.

Peculiarities of the Spatial Spectrum of Scattered Electromagnetic Waves by Anisotropic Collisional Magnetized Turbulent Plasma Layer

G. V. Jandieri[1], A. Ishimaru[2], V. G. Jandieri[3], A. G. Khantadze[4], N. Kh. Gomidze[1], K. V. Kotetishvili[1], T. N. Bzhalava[1], Sh. V. Dekanosidze[1], and I. S. Surmanidze[1]

[1]Physics Department, Georgian Technical University, Tbilisi, Georgia
[2]Department of Electrical Engineering, University of Washington
FT-10 Seattle, Washington 98195, USA
[3]Department of Electrical and Computer Engineering, Kumamoto University, Japan
[4]Physics Department, Faculty of Exact and Natural Sciences
Tbilisi State University, Tbilisi, Georgia

Abstract— In the last years scintillation has found many applications in Radio-astronomy, Space-based radar systems and the diverse phenomena observed have provided a powerful stimulus to theoretical developments. The ionospheric scintillation study comes from its significant impact on satellite radio communications. Scintillation in phase is, for example, observed in interferometric observations when small-scale ionospheric irregularities cause phase difference in the signals received between the different interferometer elements. Power spectral studies of amplitude and phase scintillations is used to obtain information about the power spectrum of ionospheric irregularities, which give rise to a variety of scintillation phenomena, as well as the irregularity drift speeds transverse to the signal path. It has been established that the absorption of HF electromagnetic waves caused due to particles collision in turbulent magnetized plasma leads to a substantial distortion of an angular distribution of the scattered field.

The present paper reports the results of an analysis of statistical characteristics (correlation, structure functions, scintillation coefficients) of the spatial spectrum of multiply scattered electromagnetic waves by turbulent anisotropic collision magnetized ionospheric plasma layer which is related to fluctuations in the radio refractive index in the F-region are investigated analytically and numerically for both power-law and anisotropic Gaussian correlation functions of electron density fluctuations using complex geometrical optics approximation and smooth perturbation method. Frequency fluctuations of scattered radiowaves being the natural factor limiting accuracy of measurement of radial speed of space vehicles in a turbulent layer is considered. Analytical expression for polarization angle caused by ordinary and extraordinary waves is obtained and is shown strong dependence on a spectral index. The influence of the distance, both from the emitter to the upper boundary of anisotropic turbulent plasma layer, and from lower boundary to the receiver, the factor of anisotropy and the angle of inclination of irregularities with respect to geomagnetic field on the statistical characteristics of multiply scattered radiation are studied for F-region of the ionosphere.

Propagation and Localization of Random Cylindrical Waves in Two-dimensional Random Medium

Rui Ding and Ya-Qiu Jin
Key Laboratory of Wave Scattering and Remote Sensing Information (MOE)
Fudan University, Shanghai 200433, China

Abstract— A stochastic functional approach is developed to study propagation and localization of random cylindrical waves in two-dimensional (2D) homogeneous and isotropic random medium. The random wave is expressed in terms of Hankel functions with stochastic linear coefficients, and the random medium is derived as a Fourier integral form with a narrow band spectrum centered at $2k$, where k is wave number.

It is demonstrated that the random cylindrical wave exists as a stochastic angular mode because of the rotational symmetry of the medium. The asymptotic wave solution for different angular quantum numbers, while demonstrating different phase properties, has the same amplitude exponential factor $\exp(\gamma kr)/\sqrt{kr}$, $\gamma = \alpha + i\beta$, where the average exponential coefficient γ is given in terms of the spectral density of the random medium. This exponential behavior due to α in the amplitude indicates the localized nature arising from the multiple Bragg scattering in random medium. For a narrowband medium with the variance σ^2 and the spectral bandwidth $\delta = k\Delta$, γ is found to be proportional to $k\sigma^2/\sqrt{\Delta}$, as a comparison of $k\sigma^2/\Delta$ in 1D case. Numerical simulations show the difference between the waves in random and non-random media, and well match analytic results.

Effect of Rainfall on Millimeter Wavelength Radio in Gough and Marion Islands

P. A. Owolawi, **T. J. Afullo**, **and S. B. Malinga**
University of KwaZulu-Natal Durban, P. O. Box 4000, South Africa

Abstract— With increasing spectrum occupancy and demand of high bandwidth for evolution of complex radio access network, the needs to explore the blessing of millimetric wave band become imperative. The advantages of the band are: large spectrum availability, high frequency reused potential, small antenna and equipment size.

Due to the biological diversity and environmental uniqueness of both islands which make them a main attraction for both tourists as well as scientific researchers, need for data transfer, video and voice communication has become inevitable. The millimeter wave spectrum at 30–300 GHz may be of great interest in these islands and also to service providers and systems designers because of the wide bandwidths available for communications at these frequencies. Such wide bandwidths are valuable in supporting applications such as high speed data transmission and video distribution.

A millimeter wavelength radio system is largely influenced by attenuation due to rainfall rate. In order to predict reliable rain attenuation for both islands, it is therefore essential to determine characteristics of rainfall rate at the location of interest which is geographically dependent. In this paper, new-hybrid approach is attempted to convert the rainfall from five-minute integration time to one-minute integration time for the calculation of rain attenuation. The paper also includes Cumulative distributions, seasonal variability, and worst month of rainfall rate for the islands. Consequently, new rain climatic zones are suggested and the relationship between average year (AY) and average worst month (AWM) are obtained.

Comparison between Mixing and Pure Walfisch-Ikegami Path Loss Models for Cellular Mobile Communication Network

Supachai Phaiboon[1] **and Pisit Phokharatkul**[2]

[1]Electrical Engineering Department, Faculty of Engineering
Mahidol University, Salaya, Nakhorn Pathom 73170, Thailand
[2]Computer Engineering Department, Faculty of Engineering
Mahidol University, Salaya, Nakhorn Pathom 73170, Thailand

Abstract— This paper presents a method to apply the popular Walfisch- Ikegami model. We classified 2D aerial images taken from the actual areas into small grids of sub-areas to determine the environment category of each grid area and then provided suitable path loss models for those grids including the Walfisch-Ikegami model. This make prediction provides high accuracy for overall area. We performed measurements at a frequency of 800 GHz in band of a cellular mobile CDMA 2000. The equipment for propagation measurement consisted of a fixed transmitter and a portable spectrum. The fixed transmitter consisted of a signal generator (with 18 dBm power output) and a horn antenna. We used a half wave dipole antenna for signal strength measurement via a recorder and then plotted path loss contour on the aerial images of 5 different areas namely, den-urban, urban, first sub-urban, second sub-urban, and forest areas. Comparison between the proposed method and the conventional Walfisch-Ikegami model provide a good agreement.

REFERENCES

1. Walfisch, J. and H. L. Bertoni, "A theoretical model of UHF propagation in urban environments," *IEEE Trans. Antennas and Propag.*, Vol. 36, 1788-96, 1988.
2. Ikegami, F., T. Takeuchi, and S. Yoshida, "Theoretical prediction of mean field strength for urban environments," *IEEE Trans. Antennas and Propag.*, Vol. 39, 1991.
3. Oda, Y., K. Tsunekawa, and M. Hata, "Advanced LOS path loss model in microwave mobile communications," *IEEE Trans. Veh. Technol.*, Vol. 49, 2121–25, 2000.
4. Chang, P.-R. and W.-H. Yang, "Environment-adaptation mobile radio propagation prediction using radial basis function neural networks," *IEEE Trans. Veh. Technol.*, Vol. 46, 155–60, 1997.
5. Torrico, S. A., H. L. Bertoni, and R. H. Lan, "Modeling tree effects on path loss in a residential environment," *IEEE Trans. Antennas and Propag.*, Vol. 46, 870–80, 1998.
6. Cheon, C., G. Liang, and H. L. Bertoni, "Simulating radio channel statistics for different building environments," *IEEE J. Select. Areas Commun.*, Vol. 19, 2191-200, 2001.
7. Petrus, P., J. H. Reed, and T. S. Rappaport, "Geometrical-based statistical macrocell channel model for mobile environments," *IEEE Trans. Commun.*, Vol. 50, 2002.
8. Piazzi, L. and H. L. Bertoni, "Effect of terrain on path loss in urban environments for wireless applications," *IEEE Trans. Antennas and Propag.*, Vol. 46, 1138–47, 1998.
9. Tarng, J. H. and K. M. Ju, "A novel 3-D scattering model of 1.8 GHz radio propagation in microcellular urban environment," *IEEE Trans. Electromag Compat.*, Vol. 41, 100–6, 1999.
10. Weissberger, M., R. Meidenbauer, H. Fugging, and S. Marcus, "Radio wave propagation: A handbook of practical techniques for computing basic transmission loss and field strength," *ECAC*, Annapolis, Maryland, 369, 1982
11. Weissber, M. A., "An initial critical summary of predicting the attenuation of radio waves by trees," ESD-TR-81-101, EMC Analysis Center, Annapolis MD.
12. Perkins, T. C., "Remote sensing image classification and fusion for terrain reconstruction," B.S.E.E. University of Louisville, 1999.
13. Wnukowicz, K. and W. Skarbek, "Color temperature estimation algorithm for digital images properties and convergence," *Opto-electronics Review*, Vol. 11, No. 3, 193–96, 2003.
14. Phokharatkul, P., S. Chaisriya, S. Somkuarnpanit, S. Phaiboon, and C. Kimpan, "Developing the color temperature histogram method for improving the content-based image retrieval," *Trans. Eng. Comp. and Technol.*, Vol. 8, 270–74, 2005.

Session 1P4b
EM Theory, Moving Media, Relativity, Field Quantization

Variation of Gravitational Mass in Electromagnetic Field

Z.-H. Weng[1] and Y. Weng[2]

[1]School of Physics and Mechanical & Electrical Engineering
Xiamen University, Xiamen 361005, China
[2]College of Chemistry & Chemical Engineering
Xiamen University, Xiamen 361005, China

Abstract— The equality of the inertial and gravitational masses is being doubted all the time. And the equality of masses remains as puzzling as ever. However, the existing theories do not explain why the gravitational mass has to equal the inertial mass, and then do not offer compelling reason for this empirical fact. The paper attempts to reason out why there exists the equality of masses in most cases, even in the electromagnetic field.

The equality of masses has not been validated in the electromagnetic field. Some experiments for the equality of masses have been performed. But all of these verifications are solely constrained to be in the range of weak gravitational strength, and have not been validated in the strong gravity nor in the electromagnetic field. So this puzzle of the equality of masses remains unclear and has not satisfied results. The paper carries out the gravitational mass will be varied in the strong strength by capture or release the energy density of the electromagnetic field.

The electromagnetic field can be described with quaternions. In the treatise on electromagnetic field theory, the quaternion was first used by J. C. Maxwell to demonstrate the electromagnetic field. The gravitational field and electromagnetic field both can be illustrated by the quaternion, but they are quite different from each other. We add another four-dimensional basis vector to the ordinary four-dimensional basis vector to include the feature of gravitational and electromagnetic fields.

The gravitational mass changes with the electromagnetic strength, and has a small deviation from the inertial mass. The variation of gravitational mass has a limited effect on the motion of the large-mass particle, because the variation of gravitational mass is quite small. Therefore the equality of masses is believed to be correct in most cases. However, when there exists a very strong electromagnetic strength, the variation of gravitational mass can become very huge, and then has an impact on the motion of the low-mass charged particle obviously.

ACKNOWLEDGMENT

The author is grateful for the financial support from the National Natural Science Foundation of China under grant number 60677039.

Observation of a Non-conventional Influence of Earth's Motion on the Velocity of Photons, and Calculation of the Velocity of Our Galaxy

Héctor A. Múnera[1, 2], Daniel Hernández-Deckers[2, 3], Germán Arenas[2], Edgar Alfonso[2], and Iván López[1]

[1]International Center for Physics (Centro Internacional de Física, CIF), Bogotá, Colombia
[2]Department of Physics, Universidad Nacional de Colombia, Bogotá, Colombia
[3]Max Planck Research Centre, Hamburg, Germany

Abstract— We operated a stationary Michelson-Morley interferometer during two consecutive years (2003–2005) in Bogotá, Colombia. An interferometer of equal 2.044 m long arms was placed on top of a massive 13,000 kg concrete table, pneumatically damped to avoid external vibration. The interference fringes were produced using a stable green light laser (YAG doubled), and the interference pattern (IP) was continuously observed by a video camera, on top of the name table, that was sampled every minute, for a total of 1,440 patterns per day. Every datum was stored in a computer standing outside the table to avoid unwarranted vibration. We used 20 sets of data, each one extending over several days, around the middle of each month.

The pixel-positions of 2 or 3 dark fringes were determined in every IP, and the average displacement relative to the position of a reference IP, typically at midnight, was plotted as a function of civil local time. There are striking 24-hour periodicities, and the fringe-shift amplitude is very significant. Of course, a large part of this periodic variation is due to the periodic 24 hour environmental variation of temperature, humidity and pressure. After subtracting these unwanted effects, there is still a 24-hr periodic residual that is no longer correlated to the environmental variables. The amplitude of the residual varies from month to month, but is around 4 fringes, i.e., 2 wavelengths.

There is a significant correlation between the daily fringe-shift residuals for each month and the motion of the earth orbiting the sun, which hints to a possible dependence of the velocity of light in our terrestrial laboratory and the velocity of the earth. Of course, such result is contrary to current theory. As a working hypothesis, a simple classical pre-relativistic model was adopted: the velocity of light is constant relative to a preferred frame of reference.

Our data was used to calculate the velocity of the sun relative to such frame, by finding the velocity vector maximizing the correlation R between the 12 average monthly sets of data and the predictions of our model. A maximum average $R = 0.71$ (std. dev. 0.15) obtains for solar motion $V = 365\,\mathrm{km/s}$, $R.A. = 81^\circ = 5\mathrm{h}\text{-}24\mathrm{m}$, Dec $= +79^\circ$ towards the northern apex, or in galactic coordinates $(l,\, b) = (134^\circ,\, 23^\circ)$. For comparison, earth's velocity with respect to the CMB is $V = 365 \pm 18\,\mathrm{km/s}$, $(l,\, b) = (265^\circ,\, 48^\circ)$. It is a remarkable coincidence that we obtained the same speed.

Motion of our sun with respect to the centroid of our local group (LG) is the vector sum of (a) solar orbit around the center of our galaxy, (b) peculiar motion with respect to previous orbit, and (c) motion of our galaxy towards LG, yielding a net solar motion $V = 264\,\mathrm{km/s}$, in direction $(l,\, b) = (92.23^\circ,\, -1.67^\circ)$, and thence a velocity of our LG with respect to the preferred frame $V = 269\,\mathrm{km/s}$, $(l,\, b) = (185^\circ,\, +33^\circ)$. For comparison, the LG moves with respect to the CMB in direction $(l,\, b) = (77^\circ,\, +30^\circ)$. It appears that our velocity is approximately at right angles (108°) with respect of the motion of the LG relative to the CMB. It is rather surprising that an optical experiment on the earth can detect the right order of magnitude of the speed of our galaxy.

Determination of Speeds of Light in Vacuum for Different Galilean Reference Systems

Namik Yener
Technical Education Faculty, Kocaeli University
Umuttepe Campus, Izmit, Kocaeli 41380, Turkey

Abstract— Having established in a previous article that the postulate of the constancy of speed light of Special Relativity Theory is false in general, we investigate a procedure to determine the different speeds of light in vacuum for different Galilean reference frames attached to a particular electromagnetic system. As it was done in the previous paper, we consider a modified Lorentz transformation incorporating different speeds of light for different inertial frames, and based on it we examine two media that are observed from the two reference systems, to be simple and lossy. In other words, we consider an electromagnetic system that consists of a rest frame (to be denoted by K), constituted by a simple medium but with loss, and a frame (to be denoted by K') in uniform rectilinear motion with respect to the first, wherein another simple, lossy medium fills the half space such that the interface of the two media is an infinite plane, perpendicular to the direction of motion of K'. The electromagnetic fields are derived for the electromagnetic system in hand and using the boundary conditions on the plane interface of the two media, a relation is derived, using which together with a relationship obtained in above mentioned paper, we obtain the speeds of light in vacuum for the two inertial reference frames. The speeds found, are functions of the material properties of the two media such as conductivity, magnetic permeability, dielectric permittivity, frequency, and the relative speeds of the reference frames. This result suggests that speed of light in vacuum for a particular inertial reference frame is merely a constant and the expectation that it be independent of material properties of the media, frequency, and the relative speeds of the reference frames is not necessarily true, at least where Special Relativity Theory fails to account for the loss in the system. The results of this work are a direct consequence of the above mentioned paper in which Special Relativity Theory is negated.

Tunable TE/TM Wave Splitter Using Symmetric Gyrotropic Slab

Hui Huang[1, 2], **Yu Fan**[1], **Bae-Ian Wu**[2], **and Jin Au Kong**[2]

[1]School of Electrical Engineering, Beijing Jiaotong University, Beijing 100044, China
[2]Research Laboratory of Electronics, Massachusetts Institute of Technology
Cambridge, MA 02139, USA

Abstract— A TE/TM wave splitter composed of a gyrotropic slab is proposed. We demonstrate theoretically that, when the working frequency is chosen to be within one of the two ranges, total reflection occurs at the boundary of a slab of gyrotropic medium for either TE or TM component of the incident waves. Tuning can be done by choosing the working frequency band or adjusting the applied magnetic field. Furthermore, within the TE-stop or TM-stop frequency region, if the incident angle is selected appropriately, the other polarized component of the wave is totally transmitted. And we also show that when the slab is thicker, there are more possibilities to satisfy the full-pass condition. Finite-element method simulations verified the theoretical results.

Session 1P5
Extended/Unconventionl Electromagnetic Theory, EHD (Elecrohydrodynamics)/EMHD (Electromagnetohydrodynamics), Electrobiology

A New Algorithm for Electrical Impedance Tomography Inverse Problem

T. Kříž and J. Dědková
Department of Theoretical and Experimental Electrical Engineering
Brno University of Technology
Kolejní 2906/4, Brno 612 00, Czech Republic

Abstract— This paper proposes new techniques to solve the electrical impedance tomography (EIT) inverse problem. Usually, a set of voltage measurements is acquired from the boundaries of an investigated volume, whilst this is subjected to a sequence of low-frequency current patterns. In principle, measuring both the amplitude and the phase angle of the voltage can result in images of the electric conductivity and permittivity (impedivity) in the interior of a body. Alternating current patterns are preferred to DC to avoid polarization effects. In the usual frequency range (below 1 MHz) the field can be considered a steady current field, which is governed by the Laplace equation. It is well known that while the forward problem is well-posed, the inverse problem is nonlinear and highly ill-posed. The recently described methods are based on deterministic or stochastic approach to solve mainly 2D problems. The aim of this paper is to present new way for a successful image reconstruction to obtain highquality reconstruction in EIT 2D problems. Numerical results of the reconstruction based on new methods are presented and compared.

REFERENCES

1. Cheney, M., D. Isaacson, and J. C. Newell, "Electrical impedance tomography," *SIAM Rev.*, Vol. 41, No. 1, 85–101, 1999.
2. Olmi, R., M. Bini, and S. Priori, "A genetic algorithm approach to image reconstruction in electrical impedance tomography," *IEEE Trans. Evol. Comp.*, Vol. 4, 83–88, 2000.
3. Borsic, A., "Regularization methods for imaging from electrical measurement," Ph.D. Thesis, Oxford Brookes University, 2002.
4. Burger, M., "A level set method for inverse problems," *Inverse Problems*, Vol. 17, 1327–1356, 2001.

FEM Analysis of HF Magnetic Field Deformation Near Conductive Samples

J. Dědková, **T. Kříž**, **and M. Steinbauer**
Department of Theoretical and Experimental Electrical Engineering
Brno University of Technology, Kolejní 2906/4, Brno 61200, Czech Republic

Abstract— The aim of this paper is to present an effective way for numerical simulations and measurement problems of high-frequency magnetic fields deformation in the surround conducting samples of selected shapes. We consider both the magnetic conductive and electrical conductive materials. There are shown the physical, mathematical and numerical models for the simulation of deformation HF field. There is providing influences of sample dimensions, material properties, working frequency to results of numerical simulation. For the special cases these numerical results are compared with analytical results.

REFERENCES

1. Dědek, L. and J. Dědková, *Elektromagnetismus*, skripta VUT, VUTIUM, Brno, 2000.
2. Mayer, D. and B. Ulrych, Základy numerického řešení elektrických a magnetických polí, Praha, SNTL, 1988.
3. Barglik, J., I. Doležel, M. Škopek, P. Šolín, and B. Ulrych, "3D integral model of eddy currents and losses in thin nonmagnetic structures in linear media," *Proceedings of IC CEM'2002*, 8–11, IV, Bournemouth, GB, 2002.

Utilization of Faraday Mirror in Fiber Optic Current Sensors and Experiments

P. Drexler, **P. Fiala**, **and R. Kadlec**
Department of Theoretical and Experimental Electrical Engineering
Brno University of Technology, Kolejní 2, Brno 612 00, Czech Republic

Abstract— This paper proposes novel techniques to measure of a pulsed magnetic field. Fiber optic sensors dispose of some advantages in the field of electrical current and magnetic field measurement, like large bandwidth, linearity, and light transmission possibilities. Although they suffer from some parasitic phenomenons, the crucial issue is the presence of induced and the latent linear birefringence, which is imposed by the fiber manufacture imperfections as well as a mechanical stress by the fiber bending. In order to the linear birefringence compensation a promising method was chosen for the pulsed current sensor design. The method employs an orthogonal polarization conjugation by the back direction propagation of the light wave in the fiber. The Jones calculus analysis presents its propriety. An experimental fiber optic current sensor has been designed and realized. The advantage of the proposed method was proved considering to the sensitivity improvement. There are presented some experiments with these measurement methods.

REFERENCES

1. Drexler, P. and P. Fiala, "Methods for HP EM pulse measurement," *IEEE Sensors Journal*, Vol. 7, No. 7, 1006–1011, ISSN: 1530-437X, 2007.
2. Fiala, P. and P. Drexler, "Sensors and methods for electromagnetic pulse identification," *Sensors & Transducers*, Vol. 74, No. 12, 844–854, ISSN:1726-5479, 2006.
3. Cowan, M. and R. B. Spileman, *Magnetocumulative Generators*, Springer Verlag, ISBN 0-387-98786-x, 2001.
4. *Proceedings, 13-th IEEE International Pulsed Power Conference, IEEE*, ISBN 0-7803-7122-4, USA, 2001.
5. *Proceedings, 12-th IEEE International Pulsed Power Conference, IEEE*, ISBN 0-7803-5498-2, California, USA, June 27–30, 1999.
6. *Proceedings, 11-th IEEE International Pulsed Power Conference, IEEE*, ISBN 0-7803-4213-5, Maryland, USA, June 29–July 2, 1997.
7. Barker, R. J. and E. Schamiloglu, *High-Power Microwave Sources and Technologies*, John Wiley and Sons, ISBN 0-7803-6006-0, 2001.
8. Barker, R, J., *High-Power Microwave Sources and Technologies, IEEE*, ISBN 0-7803-6006-0, 2001.

Change Detection in the Video Sequences with Small Density of Information

P. Fiala, **T. Jirků**, **and R. Kubásek**
Department of Theoretical and Experimental Electrical Engineering
Brno University of Technology, Kolejní 2906/4, Brno 61200, Czech Republic

Abstract— This article deals with the principles of basic detection methods usable for the specific dynamical objects in the image data. These methods are designed in accordance with passive location, where there is no interaction between the sensor and the tracked object. The methods become even more significant in, for instance, the applications of microscopic-size objects detection (material particles) or particles groups detection in the field of plasma research using commercial devices only.

REFERENCES

1. Gonzales, C. G., R. E. Woods, and S. L. Eddins, *Digital Image Processing Using MATLAB*, Pearson Prentice Hall, New Jersey, 2004.
2. Fiala, P., T. Jirku, R. Kubasek, P. Drexler, and P. Konas, "A passive optical location with limited range," *PIERS Online*, Vol. 2, No. 6, 685–688, 2006.
3. Dostál, V., "Dynamic image processing," The Bachelor's thesis, DTEEE FEEC BUT, 2007.
4. Daniel, M., "A passive optical location," The Bachelor's thesis, DTEEE FEEC BUT, 2007.
5. Suchardal, J., "A dynamic object image processing," The Bachelor's thesis, DTEEE FEEC BUT, 2007.
6. Andrews, A. P. and M. S. Grewal, *Kalman Filtering: Theory and Pratice Using MATLAB*, Second Edition, John Wiley & sons, Inc., 2001.
7. Marshall, D., Online Course Notes, http://www.cs.cf.ac.uk/Dave/Multimedia/BSC_MM_CALLER.html.
8. Smith, S. W., *The Scientist and Engineer's Guide to Digital Signal Processing*, Second Edition, California Technical Publishing, San Diego, California, 1999.
9. MATLAB Help.

A Numerical Model of Relativistic Pulsed Power Generator

P. Fiala and T. Jirku
DTEEE FEEC BUT
Kolejní 2906/4, Brno 61200, Czech Republic

Abstract— This paper proposes the numerical model of a relativistic generator. The generator conception is based on the Cherenkov electromagnetic radiation used on vacuum diode. This work solves an elektromagnetic field analysis and a particles moving in basic parts of the diode construction and tests the design like a numerical tool and compares the results with the experimental diode design. The verification of the pulsed power generator was done. There were built a numerical model and parts of generator like an analytical model. There were tested the generator parameters and numerical results were verified by the experimental tests. The final generator test proved its function and rightness of the applied numerical model.

REFERENCES

1. Drexler, P. and P. Fiala, "Methods for HP EM pulse measurement," *IEEE Sensors Journal*, Vol. 7, No. 7, 1006–1011, 2007.
2. Fiala, P. and P. Drexler, "Sensors and methods for electromagnetic pulse identification," *Sensors & Transducers*, Vol. 74, No. 12, 844–854, 2006.
3. Fiala, P., "Finite element method analysis of electromagnetic field inside pulsed power generator," *2-nd European Symposium on Non-lethal Weapons*, May 13–14, 52-1–52-11, DWS Werbeagentur und Verlag GmbH, Karlsruhe, Ettlingen, Germany, May 13–15, 2003.
4. *2-nd European Symposium on Non-lethal Weapons*, Ettlingen, SRN, May 13–14, 2003.
5. *3-rd European Symposium on Non-lethal Weapons*, Ettlingen, SRN, May 12–14, 2005.
6. *4-th European Symposium on Non-lethal Weapons*, Ettlingen, SRN, May 14–16, 2007.

Tuned Structures for Special THz Applications

P. Fiala, **E. Gescheidtová**, **and T. Jirku**
Brno, FEEC BUT, UTEE, Kolejní 2906/4, Brno 612 00, Czech Republic

Abstract— The aim of this paper is to present a new research in the special structures used for THz applications. The practical application is focused on an impedance matching of the basic THz structure for the wave transformation. The element produced by nanotechnology was numerically modeled and the analysis of obtained results was used for the following change of the design. The final design was prepared for the mid-infrared and long-infrared wavelength applications. According to the result interpretation was prepared the basic design for experimental manufactures of the first prototype these nanostructure elements.

REFERENCES

1. Caloz, C. and T. Itoh, "Application of the transmission line theory of left-handed (LH) materials to the realization of a microstrip 'LH line'," *IEEE Antennas and Propagation Society International Symposium 2002*, Vol. 2, 16–21, June 2002.
2. Lai, A., C. Caloz, and T. Itoh, "Composite right/left-handed transmission line metamaterials," *IEEE Microwave Magazine*, 2004.
3. Baccarelli, P., et al., "Fundamental modal properties of surface waves on metamaterial grounded slabs," *IEEE Trans. on MTT*, Vol. 53, No. 4, April 2005.

Improving of Ray-tracing Method for Numerical Modeling of Lighting Systems

R. Kadlec, **E. Kroutilová**, **and P. Fiala**
Department of Theoretical and Experimental Electrical Engineering
Faculty of Electrical Engineering and Communication
Brno University of Technology, Kolejní 2906/4, Brno 61200, Czech Republic

Abstract— This paper deals with the possibilities of applying numerical modeling in the process of calculation of illumination. Within the description of these possibilities, the basic principles of the most widely applied numerical methods are presented, and the resulting overview is complemented with an evaluation of the main advantages and drawbacks to the application of the discussed methods as theoretical introduction. For the selected method of ray-tracing, a numerical model was prepared using the MatLab program, and the results were experimentally verified by measurement.

Ray-tracing is a realistic imaging technique of monitoring a ray. This method is based on a global illumination model, where we imagine the scene as a set of objects and sources of light. Rays, which propagate between the sources of light and the scene, are determined by the direction, color, and intensity.

Acquired experimental results are portrayed and compared with the results of numerical modelling. Based on the obtained data, the conclusion to the paper then presents an evaluation of the ray-tracing method applicability for the numerical modeling of lighting systems and an evaluation was performed of the advantages and drawbacks to the method.

Today, there are strict requirements placed on the illumination of interiors and exteriors; for example, the ambient light level must fulfill the limits stipulated by the respective hygiene authorities. In this respect, it is important to mention the fact that illumination designs will be further facilitated by improvements introduced into program design methods. The present study deals with the numerical modeling of lighting systems applying a concrete numerical modeling technique.

REFERENCES

1. Kadlec, R., *Nové směry výpočt ˚u v osvětlovací technice*, [s.l.], 2005, 57 s., 1 CD-ROM. VUT v Brně, Supervisor of bachelor thesis Ing. Eva Kadlecová, Ph.D., 2005.
2. Kadlecová, E. and P. Fiala, "New directions in modeling the lighting systems," *Radioengineering*, Vol. 13, No. 4. 75–80, ISSN: 1210-2512, 2004.
3. Kazda, I., *Numerické modelování metodou konečných prvk ˚u*, Publishing ČVUT, Praha, 1995.
4. Zemčík, P., *Počítačová grafika* [online], [cit. 2005-04-03], Available from WWW: http://www.fit.vutbr.cz/study/courses/POG, 2005.
5. Rektorys, K., *Přehled užité matematiky 1*, Prometheus, Praha, ISBN 80-7196-180-9 (1. part), 2000.
6. Šula, O., *Příručka osvětlovací techniky*, SNTL, Praha, ISBN 04-534-79, 1979.

Segmentation of NMR Slices and 3D Modeling of Temporomandibular Joint

J. Mikulka[1], **E. Gescheidtova**[1], **and K. Bartusek**[2]

[1]Department of Theoretical and Experimental Electrical Engineering
Brno University of Technology
Kolejni 4, Brno 612 00, Czech Republic
[2]Institute of Scientific Instruments, Academy of Sciences of the Czech Republic
Kralovopolska 147, Brno 612 64, Czech Republic

Abstract— NMR images serve the purpose of following the development and quantitative measurement of tissues. Segmentation can be applied to images and subsequent evaluation of the parameters of individual regions such as circuit, area or volume in case images from several slices are available. The paper describes the pre-processing and subsequent segmentation of NMR images of the human head in the region of temporomandibular joint in several slices. Image obtained by means of the tomograph used are of very low resolution and contrast, and their processing may prove to be difficult. A suitable algorithm was found, which consists in pre-processing the image by a smoothing filter, sharpening, and the four-phase level set segmentation. This method segments the image on the basis of the intensity of regions and is thus suitable for processing the above-mentioned NMR images, in which there are no sharp edges. The method also has some filtering capability. The length of contour or the area of segmented regions can be minimized. It is described by partial differential equations that have been transformed into corresponding difference equations, which are solved numerically. In the next stage, segmented slices of temporomandibular joint will be used to create a multidimensional model. A spatial model gives a better idea of the situation, structure and properties of tissues in the scanned part of patient's body. Multidimensional modeling mainly represents a change in describing input NMR data. The segmented regions need to be transformed from discrete to vector description, i.e., the outer geometry of objects needs to be described mathematically. The paper describes the creation procedure of the three-dimensional model of temporomandibular joint with view to "Marching cubes" method.

REFERENCES

1. Aubert, G. and P. Kornprobst, *Mathematical Problems in Image Processing*, Springer, ISBN 0-387-32200-0, New York, 2006.
2. Vese, L. and F. Chan, "A multiphase level set framework for image segmentation using the Mumford and Shah model," www.math.ucla.edu/ lvese/PAPERS/IJCV2002.pdf.
3. Chan, F. and J. Shen, "Image processing and analysis: Variational, PDE, wavelet and stochastic methods," *SIAM 2005*, ISBN 0-89871-589-X, Philadelphia, 2005.
4. Kršek, P., "Problematika 3D modelování tkání z medicínských obrazových dat," *Neurologie pro praxi*, roč 6, č. 3, 149–153, ISSN 1335-9592, Olomouc, CZ, 2005.

Session 1P6
Electromagnetic Wave Applications in Material Processing and Characterization

Absorbing Properties of Frequency Selective Surface Absorbers on a Lossy Dielectric Slab

Huiling Zhao, **Guobing Wan**, **and Wei Wan**
Northwestern Polytechnical University, Xi'an, Shaanxi 710072, China

Abstract— Radar absorbing materials (RAM) are often used to reduce the radar cross section (RCS) of a target. In order to obtain a broadband and low RCS, multilayered structures were preferred. This will result in thick RAM and increase the weight of the target. Frequency selective surface (FSS) absorber can be a substitute for traditional RAM. This structure utilize both the frequency selective character of FSS and absorber property of lossy dielectric layer. In this paper, electromagnetic scattering by patch array on a PEC backed lossy dielectric slab was studied. The current distribution on infinite patch array were expressed by the current on single periodic element patch according to Floquet's theorem. After giving pertinent dyadic Green's function, the subdomain rooftop basis functions and a Galerkin's procedure were employed to develop a impedance matrix for the current calculation. Each matrix elements were obtained through several two dimensional fast Fourier transform and the patch currents were solved through L. U. method. Computation of the radiation by the patch currents then provided a solution for the scattered field. The calculated results were compared with experimental data and the results show that they are in good agreement. Absorbing properties were discussed through changing the incidence angle, periodicity, patch dimension, thickness and permittivity of the dielectric slab.

Direct Measurements of the *c*-axis Polarization in Orthorhombic $HoMnO_3$ Multiferroic Thin Films

T. H. Lin[1], **C. C. Hsieh**[1], **C. W. Luo**[1], **K. H. Wu**[1], **T. M. Uen**[1], **J. Y. Juang**[1], **and J.-Y. Lin**[2]

[1]Department of Electrophysics, National Chiao Tung University, Hsinchu, Taiwan
[2]Institute of Physics, National Chiao Tung University, Hsinchu, Taiwan

Abstract— We had made *c*-axis oriented orthorhombic $HoMnO_3$ mulitiferroic thin films on Nb-doped $SrTiO_3$ (001) substrates by pulsed laser deposition. The films displayed an antiferromagnetic (AFM) magnetic transition around 40 K with an apparent incommensurate to commensurate (ICM-CM) transition at 30 K. The dielectric constant of the films shows anomalies around 30 K and reaches a maximum value around 13 K. Nonetheless, direct measurements of the temperature dependence of electric polarization indicate that significant polarization emerges only after the ICM-CM transition occurred. The results clearly demonstrate the magnetism-induced ferroelectricity in this E-type AFM perovskite.

On Measurements of Reflection Coefficient of RF Absorbing Materials for Anechoic Chambers

N. P. Balabukha, **V. S. Solosin**, **and A. S. Zubov**
Institute for Theoretical and Applied Electromagnetics, RAS, Russia

Abstract— The measurement of RF absorbing materials reflection coefficient for pyramidal, honeycomb and other similar materials used in anechoic chambers is characterized by certain specific features. In this case, measurement results significantly depend on the parameters of a measurement setup contrary to the similar measurements for the materials with plane boundary surfaces. The reason is that the absorbers have predominantly diffuse component of reflection, especially in the high frequency range. Indeed, if the given component is the only one then the accepted power is proportional to the sector width. Hence, the measurement results depend on the antenna radiation pattern width, the distance from the sample and the size of the sample as follows from the analysis of the measurement data for different commercial absorbers.

Thus, it is important to have the parameter that characterizes the properties of the absorber regardless parameters of a measurement setup.

Let us define the diffuse reflection coefficient R_{diff} by formula

$$|R|^2_{diff} = \frac{P_{diff}}{P_{inc}}, \tag{1}$$

where P_{diff} is a total power reflected by the radio absorbing material, excluding the power, reflected in the mirrored direction and the direction of diffraction lobes, and P_{inc} is the power of the incident wave.

When receiving and transmitting antennas are the same, the relation between the diffuse reflection coefficient and the average power P^{rec}_{av}, which is accepted by a receiving-transmitting system, is defined by formula

$$|R|^2_{diff} = \frac{P^{rec}_{av}}{P_{inc}} \frac{S_{eff}\pi}{\lambda^2} \tag{2}$$

where S_{eff} is the illuminated part of the anechoic chamber back wall.

According to the authors' investigation, the value of R_{diff} calculated by the formula (2) practically does not depend on the parameters of the measurement setup. It is important that the value R_{diff} defined by the formula (1) has a simple relation with anechoic chamber reflectivity level

$$K_{AEC} = |R|^2_{diff} \frac{10S_{eff}}{\pi L^2} \tag{3}$$

where L is the distance between the quite zone and the back wall of anechoic chambers. For many typical cases $K_{AEC} \approx |R|^2_{diff}$.

Thus, the value of R_{diff} proves to be independent on parameters of a measurement setup and directly related to the expected reflectivity level in the quite zone of the anechoic chamber.

REFERENCES

1. Balabukha, N. P., V. S. Solosin, and A. S. Zubov, *Compact Ranges for Scattering Measurement*, Nauka, Moscow, 2008.
2. DeWitt, B. T. and W. D. Burnside, "Electromagnetic scattering by pyramidal and wedge absorber," *IEEE Transactions on Antennas and Propagation*, Vol. 36, No. 7, 971–984, 1988.

Multiple-scale Patterning of Self-assembled Monolayers via Controlled RF-plasma Flow

Meng-Hsien Lin and Shangjr Gwo
Institute of Nanoengineering and Microsystems and Department of Physics
National Tsing-Hua University, Hsinchu 30013, Taiwan

Abstract— Integration of individual nanoscale objects into functional structures represents a key challenge for emerging fields of nanotechnology. Especially for the interfacing of nanoscopic devices with the macroscopic world, a large number of hierarchical and multilength-scale organization steps based on patterning and controlled assembly are required to implement practical nanodevice applications. Recently, soft lithographic approaches such as microcontact printing, replica molding, and nanoimprint have been developed to overcome this difficulty. The main concerns of soft lithography are durability of stamp, uniformity of large-area processing, and possibility of hierarchical structures. To enhance the applicability of soft lithography, we present here our recent results based on local chemical modification of organosilane monolayers using controlled low-power RF plasma flow. Using this technique, we have realized the controlled flow of low-power RF plasma within the designated areas of organosilane organosilane self-assembled monolayer (SAM) surfaces. Furthermore, we have successfully applied this method to multiple length scales ranging from full-wafer to sub-micron scale. The optimized patterning resolution can reach the precision of a few nanometers.

A Scanning Quasi-optical Microwave Applicator for Advanced Materials Processing

T. H. Chang[1], **W. Y. Chiang**[1], **L. R. Barnett**[1, 2], **H. Y. Chang**[2], **S. Y. Cheng**[2], **and K. R. Chu**[1]

[1]Department of Physics, National Tsing Hua University, Hsinchu 300, Taiwan
[2]Material Research Laboratories, Industrial Technology Research Institute Chutung 310, Taiwan

Abstract— A microwave applicator featuring a quasi-optical processing chamber and scanning capability is proposed and demonstrated for the purpose of rapid, position-selective processing of materials to meet the needs of emerging technologies. The focusing ability and high-frequency compatibility of the quasi-optical structure make it possible to produce extremely intense radiation at a focal spot where multi-layer complex materials can be rapidly treated at a differential temperature. As a further advantage, the open space between the mirrors permits continuous scanning of materials, thereby achieving a high degree of uniformity over a large area.

Microwave heating brings about numerous advantages over furnace heating, such as rapid heating rate, volumetric or localized treatment, and energy savings. Existing microwave applicators [1] invariably employ an enclosed cavity as the processing chamber. In an enclosed cavity, the intensity of the rf field is generally low for rapid materials treatment and the size of the treated material is limited by the size of the cavity. On the other hand, technologies of the future, such as flexible electronic modules embedded in textiles, [2–5] often come with the critical demand for new materials and consequently more complex processing techniques. For example, to form multi-layer materials in which a function layer is to be densified at a high temperature and joined tightly with organic substrate of low melting temperature, a steep temperature gradient must be created and maintained throughout the procedure by means of rapid and selective heating of a highly absorbing layer. This is beyond the capability of the conventional microwave applicator in which a typical procedure can take up several tens of minutes of processing time. High-speed microwave applicators of entirely different designs are thus required to provide a heating rate orders of magnitude beyond the state-of-the art.

Here we report the concept and experimental demonstration of a novel applicator which completely eliminates the constraints of the conventional microwave applicator. This is accomplished with a two-mirror quasi-optical (QO) resonator. The QO resonator operates on the same principles as the laser resonator and has been commonly used in a variety of microwave systems. By trapping and focusing an electromagnetic wave to a spot of the dimensions of one wavelength, it produces the maximum possible radiation intensity at a given incident power level.

REFERENCES

1. Link, G., L. Feher, M. Thumm, H. J. Ritzhaupt-Kleissl, R. Bohme, and A. Weisenburger, *IEEE Trans. Plasma Sci.*, Vol. 27, 547, 1999.
2. Service, R. F., *Science*, Vol. 301, 909, 2003.
3. Miyake, S., *IEEE Trans. Plasma Sci.*, Vol. 31, 1010, 2003.
4. Roy, R., D. Agrawal, J. Cheng, and S. Gedevanishvili, *Nature*, Vol. 399, 668, 1999.
5. Copty, A., F. Sakran, M. Golosovsky, and D. Davidov, *Appl. Phys. Lett.*, Vol. 84, 5109, 1999.

Waveform Parameter Estimation and Dispersive Material Characterization

Qingsheng Zeng[1] **and Gilles Y. Delisle**[2]

[1]Communications Research Centre Canada, Government of Canada
Ottawa, Ontario, Canada
[2]Technology Integration Center, Technopôle Defense & Security
Quebec City, Quebec, Canada

Abstract— The reflection of short duration electromagnetic pulses from dielectric media is of interest in diverse technological applications, e.g., geophysics, material science and biomedical engineering. In this paper, the time domain pulse reflection from a dispersive lossy dielectric half space is investigated. The properties of a half space are described in frequency domain by the Debye and Cole-Cole models, respectively. The two models are commonly used to capture the relaxation-based dispersive properties. First, transient reflected pulses are analyzed and waveform parameters are estimated for both horizontal and vertical polarizations. Then, based on the estimation, the relationships between the waveform parameters of reflected pulses and the properties of dispersive material as well as incident angles are discussed. Meanwhile, the results obtained with the Debye model are compared to those obtained with the Cole-Cole model. The application of these results to material characterization and diagnosis is explored. A practical example is demonstrated, which is meaningful and useful in microelectronics and material science, and validates the correctness and effectiveness of this work. Our technique is based on the numerical inversion of the Laplace transform, leads to good accuracy, and has a simple algorithm, short calculation time, small required memory size, readily controlled error and wide range of applicability.

The Fabrication of Bucky-Paper and It's Dielectric Constants Measurement Study in Microwave Frequency

H. Y. Miao[1] and J. T. Lue[2]

[1]Department of Electrical Engineering, Tunghai University, Taichung, Taiwan
[2]Departments of Physics, National Tsing Hua University, Hsin Chu, Taiwan

Abstract— By well-disperse suspension and filtrating, single-wall, multi-wall carbon nanotubes (CNTs) and mix of them with different weight percentage were made as a sheet-like, A4 size thin film material. That is so called Bucky-Paper (B. P.). B. P. presents the properties such as semimetals examined by Hall Effect; light-weight and special electrical, mechanical properties could be adjustable by varying different weight percentage of single-wall and multi-wall CNTs.

The property of dielectric constants of B. P. is derived by parallel plate dielectric resonator rod method and effective medium approximation combining electromagnetic theory with experiments. Same as the behavior of traditional semimetal material, B. P. presents high level of dielectric property. The real and the imaginary part behave in an adverse tendency when frequency increasing, but they both present great vibration in low frequency and get saturation in high frequency, the critical point is at 3 MHz around. It is expected that B. P. will make a prospect feature in application of electromagnetic field.

The Electro-magnetic Properties of Co and Fe Films Percept from the Coexistence of Ferromagnetic and Microstrip Resonance for a T-type Microstrip

Yi-Chen Yeh[1] and Juh Tzeng Lue[2]

[1]Institute of Photonics Technologies, National Tsing Hua University, Hsin Chu, Taiwan
[2]Department of Physics, National Tsing Hua University, Hsin Chu, Taiwan

Abstract— The large demand in communication and video applications intrigues us an impetus to develop the design of monolithic microwave micro-strip circuits for the use of filters and resonators. Microwave techniques allow high sensitivity measurement of the dependence of the conductivity of thin magnetic films on frequencies, temperatures and magnetic fields. A permissive investigation on the resonance frequency tunable by magnetic or electric fields for filters is desired. Ferromagnetic resonance for magnetic thin films is found to be coexisted with the transmission resonance of a T-type microwave micro-strip at certain applied magnetic fields. The frequency dependence of conductivity, the magnetization, and the magnetic anisotropy of magnetic films can be eventually solved from the measured resonance frequency and quality Q factors of the resonance spectra. Equivalent resistances (R), inductances (L), and capacitances (C) corresponding to the displayed transmission S_{21} spectra are simulated to comply with proper values. With this equivalent circuit, an accurate determination of the magnetic properties can be closely scrutinized.

A Versatile Route to the Controlled Synthesis of Gold Nanostructures

R. S. Liu[1], **H. M. Chen**[1], **and D. P. Tsai**[2]

[1]Department of Chemistry, National Taiwan University, Taipei 106, Taiwan
[2]Department of Physics, National Taiwan University, Taipei 106, Taiwan

Abstract— In present study, we demonstrate a versatile route to the controlled synthesis of gold nanoparticles that could significantly alter the resulting products with desired shapes. To achieve controlled fabrication of nanomaterials, fundamental aspects of synthetic conditions need to be investigated, which include amount of growth solution, introduction of foreign ions, and reaction temperature. A mechanism corresponding to the fabrication of these multi-shaped gold nanostructures is also proposed. The current synthetic approach and mechanism for the generation of multi-shaped gold nanostructures may offer great opportunities for the design of novel materials with improved optical and structural properties.

Biomagnetic Applications Using High-transition-temperature Superconducting Quantum Interference Devices: Status and Perspectives

Hong-Chang Yang[1] and Herng-Er Horng[2]

[1]Department of Physics, National Taiwan University, Taipei 106, Taiwan
[2]Institute of Electro-Optical Science and Technology
National Normal Taiwan University, Taipei 116, Taiwan

Abstract— After the discovery of high-T_c superconductivity, tremendous efforts have been put into developing technologies of high-transition-temperature (high-T_c) superconducting quantum interference devices (SQUIDs) and biomagnetic applications. In this paper, we address the current status, challenges and perspectives of high-T_c SQUID-based biomagnetism. The emphasis is specially focused on magnetocardiography (MCG), magnetically labeled immunoassays (MLIs) and nuclear magnetic resonance and imaging (NMR/MRI). The status of high-T_c SQUIDs MCG and the challenges encountered are addressed. In MLIs we report and discuss the metrologies using remanence, magnetic relaxation, and magneto-immunoassay reduction (IMR) measurements. In addition, IMR without bound free separation showing both high sensitivity and specificity is addressed for assaying biological targets. In low field NMR/MRI we report the metrology to achieve high spectral resolution and high signal-to-noise ratio by using high pre-polarization and flux coupling. We demonstrate the proton-phosphate J-coupling in trimethyl phosphate in none shot and observe the proton-phosphate coupling $J_3[H,\ P] = (10.94 \pm 0.08)$ Hz in microtela magnetic field.

Silicon Quantum Dots Solar Cells

Shu-Fen Hu[1], **Chun Chi Huang**[2], **Chang Hsueh Li**[2], **Ting-Wei Liao**[2], **and Chao-Yuan Huang**[1]

[1]Department of Physics, National Taiwan Normal University, Taiwan
[2]Institute of Electro-Optical Science and Technology
National Taiwan Normal University, Taiwan

Abstract— A device is composed of triple quantum dots sandwiched between electrodes and is highly sensitive to the surrounding electrostatic environment. We show that the photoelectric effect resulting from the capture of photo-excited carriers by quantum dots produces a detectable change in the sourcedrain resistance of the transistor. Current-voltage characteristics measured at room temperature as a function of source-drain bias for sample device 1 under dark and various intensities of 580 nm illumination. The photocurrent increased rapidly as the illumination intensity increased. The dark current shows quasilinear characteristics. The photo currents were measured under various illuminations. Dramatically an increase in the measured current is observed across the entire bias range. Moreover, the measured current under manually chopped visual illumination, where the illumination was switched on and off at every 5 seconds intervals during the bias sweep. The observed I-V characteristics clearly exhibit almost complete recovery of the device after illumination is removed. We have demonstrated photoconductive detectors can inherently be quite efficient, since the photo carriers are produced by band-to-band absorption in indirect band gap semiconductor.

Wave Fields in X-ray Fabry-Perot Resonators

S.-Y. Chen[1], **M.-S. Chiu**[1], **Y.-Y. Chang**[1], **M.-T. Tang**[1], **Yu. P. Stetsko**[2], **H.-H. Wu**[1]
Y.-R. Lee[1], **M. Yabashi**[3], **B.-Y. Shew**[2], **and S.-L. Chang**[1]

[1]Department of Physics, National Tsing Hua University, Hsinchu 300, Taiwan R.O.C.
[2]National Synchrotron Radiation Research Center, Hsinchu 300, Taiwan R.O.C.
[3]Spring-8/RIKEN Mikazuki, Hyogo 679-5148, Japan

Abstract— Very recently cavity resonant interference patterns have been observed for X-rays at 14.4388 keV, using (12 4 0) back diffraction in monolithic silicon multi-plate Fabry-Perot type resonators with synchrotron radiation of ultra-high energy resolution. The (12 4 0) atomic planes act as reflecting mirrors for X-rays to produce successive reflections back and forth between two adjacent crystal plates. Since the formation of X-ray wavefields inside the cavity and within the crystal plate is essential for realization of cavity resonance in the X-ray regime, it is interesting to investigate the distribution of X-ray wave fields inside the crystal devices.

Because of the involvement of X-ray diffraction from perfect silicon single crystals, the dynamical theory of X-ray diffraction, dealing with the interaction of diffracted EM waves in periodic crystal lattices, is employed to calculate the intensities of X-ray wavefields, the dispersion surface of wavevector versus angle of incidence, excitation of mode of wave-propagation, and the intensity distributions of transmitted and back-reflected beams. Usually, for a conventional Bragg diffraction, the dynamical theory gives the solutions to Maxwell equations, the Bloch functions, from a complex linear eigen-value equation and appropriate boundary conditions. Due to the nature of back diffraction, the eigen-value equation, involving second-order terms, is no longer linear. A Cartesian coordinate representation for X-ray polarization based on the dynamical theory is then adopted to solve the second-order eigen-value equation and perform the calculation. It is found that standing-wave patterns and reflection phases are functions of energy and angular position. In other words, standing waves can be tuned by slightly varying the photon energy, as well as the angular positions of the incident beam relative to the crystal plates. Some of the experimental results regarding X-ray cavity resonance will be briefly mentioned.

Session 1P7
Electromagnetic Field in Materials and EM Field Dispersion in Cloaks and Photonic Crystals

Global and Local Field EM Modeling for PHC Dispersion and Metamaterial Cloak Design

Ganquan Xie, **Jianhua Li**, **Feng Xie**, **and Lee Xie**
GL Geophysical Laboratory, USA

Abstract— The Global and Local Field (GL) has been proposed by authors since 2003 and 2005. In this paper, we propose a GL transform modeling for metamaterials. The GL modeling is based on electromagnetic integral equation, magnetic and electric differential integral equations. The integral and differential integral equations reserved same form under coordinate transformation. The cloak strategy is a special coordinate transform in our integral and differential integral equations. In our paper "GL METHOD AND ITS ADVANTAGES FOR RESOLVING HISTORICAL DIFFICULTIES" in PIER 63, 2006, the integral Equations (1) and (2) in page 143 have same form under various coordinate transformation. The Equation (1) has the following form in the sphere coordinate system

$$\begin{bmatrix} E(r,\theta,\phi) \\ H(r,\theta,\phi) \end{bmatrix} = \begin{bmatrix} E_b(r,\theta,\phi) \\ H_b(r,\theta,\phi) \end{bmatrix} + \int_{\Omega} \begin{bmatrix} E_b^J(r,\theta,\phi,r'\theta'\phi') & H_b^J(r,\theta,\phi,r'\theta'\phi') \\ E_b^M(r,\theta,\phi,r'\theta'\phi') & H_b^M(r,\theta,\phi,r'\theta'\phi') \end{bmatrix} [D] \begin{bmatrix} E(r',\theta,'\phi') \\ H(r',\theta',\phi') \end{bmatrix} r'^2 \sin\theta' dr' d\theta' d\phi',$$

The $[D]$ is 6×6 materials variation matrix, for isotropic materials, $[D]$ is diagonal matrix with diagonal element of the variance materials, $(\sigma+i\omega\varepsilon)-(\sigma+i\omega\varepsilon)_b$ and $-i\omega(\mu-\mu_b)$, for diagonal anisotropic material, $[D]$ is diagonal matrix with anisotropic diagonal element of the variance materials, $(\sigma+i\omega\varepsilon)_r-(\sigma+i\omega\varepsilon)_b$, $-i\omega(\mu_r-\mu_{r,b})$, $(\sigma+i\omega\varepsilon)_\theta-(\sigma+i\omega\varepsilon)_{\theta,b}$, $-i\omega(\mu_\theta-\mu_{\theta,b})$, $(\sigma+i\omega\varepsilon)_\phi-(\sigma+i\omega\varepsilon)_{\phi,b}$, $-i\omega(\mu_\phi-\mu_{\phi,b})$. In cloak transform, for diagonal anisotropic material, $[D]$ is diagonal matrix with anisotropic diagonal element of the variance materials, $\frac{R_2}{R_2-R_1}\frac{(r'-R_1)^2}{r'^2}(\sigma+i\omega\varepsilon)_{r,b}-(\sigma+i\omega\varepsilon)_{r,b}$, $-i\omega(\frac{R_2}{R_2-R_1}\frac{(r'-R_1)^2}{r'^2}\mu_r-\mu_{r,b})$, $\frac{R_2}{R_2-R_1}(\sigma+i\omega\varepsilon)_\theta-(\sigma+i\omega\varepsilon)_{\theta,b}$, $-i\omega(\frac{R_2}{R_2-R_1}\mu_\theta-\mu_{\theta,b})$ etc.. In non orthogonal coordinate transform and some anisotropic materials the variation materials matrix is 6×6 full matrix. The $E_b^J(r,\theta,\phi,r'\theta'\phi')$, $H_b^J(r,\theta,\phi,r'\theta'\phi')$, $E_b^M(r,\theta,\phi,r'\theta'\phi')$, and $H_b^M(r,\theta,\phi,r'\theta'\phi')$ are Green tensor in the sphere coordinate system, and EM field are vector in the sphere coordinate. Our GL transform is not only for simulating the cloaking strategy, but also it has more border applications for simulating nanometer materials, dispersion engineering of the photonic crystals, biophysical materials, Space sciences, Earth sciences, Earthquake simulation, geophysical exploration etc.. The Global and Local field transform modeling combines the analytic and numerical consistent together. GL transform method does not need to solve large matrix and do not need artificial boundary and absorption condition on it to truncate the infinite domain. GL transform has more advantages to challenge FEM and FD method and Born approximation. GL transform modeling can be useful to use various coordinate transform to discover new metamaterials structure and properties which is not found in nature.

Highly Birefringent Bragg Fiber with a Fiber Core of 2-dimension Elliptical-hole Photonic Crystal Structure

Jin-Jei Wu[1], **Tzong-Jer Yang**[1], **Kun-Lin Liao**[1], **Daru Chen**[2], **and Linfang Shen**[3]

[1]Department of Electrical Engineering, Chung Hua University
Hsinchu 30012, Taiwan, R.O.C.
[2]Center for Optical and Electromagnetic Research, Zhejiang University
Hangzhou 310058, China
[3]Department of Information Science and Electronic Engineering, Zhejiang University
Hangzhou 310058, China

Abstract— A novel highly birefringent Bragg fiber with a fiber core of 2-dimension (2-D) elliptical-hole photonic crystal structure is proposed. Elliptical air holes are introduced into the fiber core to form a normal 2-D photonic crystal structure with a hole pitch (center-to-center distance between the air holes) much smaller that the operation wavelength of the Bragg fiber. The elliptical-hole photonic crystal structure tends to act as an anisotropic medium with different effective indices for transmission light of differently polarization, which inevitably results to high birefringence (up to the order of magnitude of 0.01) of the Bragg fiber. The fiber core of the 2-D elliptical-hole photonic crystal structure is surrounded by a multilayer cladding which is formed by the suitable designed periodic alternating layers of high/low refractive indices in the radial direction. The proposed Bragg fiber possesses different band-gaps for differently polarized mode, which indicates in some wavelength regions the proposed Bragg fiber can only support one polarized mode transmission. Besides the periodic alternating layers of high/low refractive indices, the bandwidth of the band-gap is also dependent on the effective index of the fiber core, which can controlled by the area of the elliptical air holes. In addition, we have also found some phenomenon about the confinement loss of the proposed highly birefringent Bragg fiber.

Tunable Y-shaped Waveguides in Two-dimensional Photonic Crystals

Chung-Jen Hsu and Chin-Ping Yu
Department of Photonics, National Sun Yat-Sen University, Kaohsiung, Taiwan 804, R.O.C.

Abstract— Photonic crystals (PCs) are periodic dielectric structures that possess the ability to control the propagation of light for the existence of photonic band gaps (PBGs). By introducing a line defect in two-dimensional (2-D) PCs, one can cause dispersion curves in the PBGs. As the effective index of PCs is decreased, the original dispersion curve will be shifted toward upper frequencies and a mode gap between the two curves will appear within the same PBG. If the frequency of light falls within this mode-gap range, light can only propagate on the original waveguide and is forbidden on the one with a smaller refractive index. We use the mode-gap effect to design a new type of tunable Y-shaped waveguide in the 2-D silica PCs composed of air holes infiltrated with polyaniline type electrorheological fluids in triangular lattices. The refractive index of the silica is $n_s = 1.5$ and the indium-tin oxide (ITO) electrodes are attached on the top and bottom in the specific region. The refractive index of the electrorheological fluids is $n = 4.848$ and can be alternated to be $n = 4.393$ by applying the external electric field. To investigate the propagation characteristics of the Y-shaped waveguide structures, two numerical methods are utilized: the plane wave expansion (PWE) method and the finite-difference time-domain (FDTD) method. The PWE method is adopted for the analysis of the dispersion relation of the guided modes on the Y-shaped waveguide and the mode-gap range which is from 0.231 to 0.241 can be obtained. To obtain the transmission properties, a TM input light is launched into the input of the Y-shaped waveguide and the FDTD method is utilized to find out the light propagation characteristics of the 2-D Y-shaped waveguides. By varying the applied electric field, the refractive index of the electrorheological fluids can be rapidly changed and the mode-gap effect can be induced in the Y-shaped waveguide. The light propagation in each arm of the Y-shaped waveguide can then be controlled by selectively applying the external electric field. These results are useful for further designs of optical switching devices.

A Novel Fiber Sensor Based on a Bragg Fiber with a Defect Layer

Kun-Lin Liao[1], **Jin-Jei Wu**[1], **Tzong-Jer Yang**[1], **Daru Chen**[2], **and Linfang Shen**[3]

[1]Department of Electrical Engineering, Chung Hua University
Hsinchu 30012, Taiwan, R.O.C.
[2]Center for Optical and Electromagnetic Research, Zhejiang University
Hangzhou 310058, China
[3]Department of Information Science and Electronic Engineering, Zhejiang University
Hangzhou 310058, China

Abstract— A novel fiber sensor based on a Bragg fiber with a defect layer is proposed. The Bragg fiber consists of a hollow core and a multilayer cladding which is formed by the suitable designed periodic alternating layers of high/low refractive indices in the radial direction. A defect layer is introduced in the multilayer cladding resulting to the resonant operation of some wavelengths. For these resonant wavelengths inside the band-gap of the Bragg fiber, large confinement loss occurs due to coupling between the core mode and the defect mode. The refractive index and thickness of the defect layer determines both the number and the location of the resonant wavelengths inside the band-gap of the Bragg fiber, which indicates a segment of the Bragg fiber with a defect layer can be used as a fiber sensor with applications of refractive index sensing or strain sensing when the defect layer is used as the sensitive region. We will show the relationship between the resonant wavelengths and the refractive index/thickness of the defect layer. Besides the defect layer, our simulated results have also shown that the resonant wavelengths of the Bragg fiber with a fixed defect layer is also dependent on the refractive index of the fiber core of the Bragg fiber, which indicates the refractive index of the medium filled in the hollow fiber core can be detected by measuring the transmission spectrum of the proposed fiber sensor.

Embedded 3-D Integrated Inductor for Voltage-controlled SAW Oscillator

Yao-Huang Kao[1] **and Way-Yu Chen**[2]
[1]Department of Communication Engineering
Chung-Hua University, Hsin-Chu, Taiwan
[2]Institute of Communication Engineering
National Chiao-Tung University, Hsin-Chu 30050, Taiwan

Abstract— VCSO has a crucial application in timing synchronization, such as clock recovery due to its high frequency stability. Low jitter performance is important for high quality service. In this study an integrated VCSO with Pierce configuration was developed as shown in Fig. 1. Except for the SAW resonator, a phase shift with π-type LC circuit was embedded to achieve the Barkhausen's oscillation condition. A 3-D inductor as shown in Fig. 2 was constructed by the standard CMOS process to save the chip area. Its rf behavior was first calculated by the EM simulator. The related lumped model as shown in Fig. 3 was then extracted. For a 14 nH inductance, the area was reduced 1/16 as compared to that by conventional one-layer winding. Under 0.18 µm TSMC CMOS process the values of the equivalent circuit were listed in the following Table 1. With such a small inductor and two shunted capacitors, an oscillator with high Q saw resonator at 622 MHz was easily obtained. The phase noise of VCSO at 1 MHz offset is −162.5 dBc/Hz. The measured RMS jitter is 880 fs and peak-to-peak jitter is 6.22 ps. The tuning range was about 140 KHz. The power consumption is 22.45 mW. The clock recovery using this high quality oscillator was also studied. With the half-rate phase detector, the oscillator was applied to high speed data rate at 1.244 GBit/s.

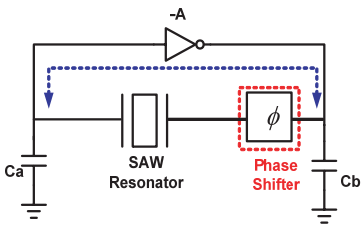

Figure 1: Block diagram of VCSO.

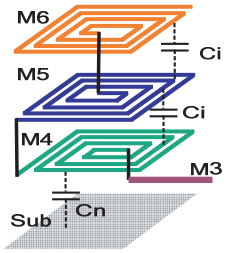

Figure 2: 3-D inductor.

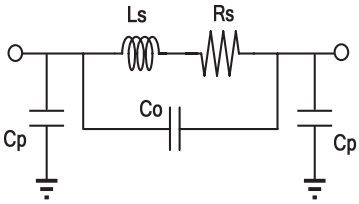

Figure 3: Equivalent lumped circuit of 3-D inductor.

Table 1: Summary of element values of 3-D inductor.

Ls	Rs	C0	Cp
14.302 nH	30.54 Ω	0.026 pF	0.51 fF

A Novel Band-rejection Filter Based on a Bragg Fiber of Transversal Resonant Structure

Daru Chen[1], **Tzong-Jer Yang**[2], **Jin-Jei Wu**[2], **and Linfang Shen**[3]

[1]Center for Optical and Electromagnetic Research, Zhejiang University
Hangzhou 310058, China
[2]Department of Electrical Engineering, Chung Hua University
Hsinchu 30012, Taiwan, R.O.C.
[3]Department of Information Science and Electronic Engineering, Zhejiang University
Hangzhou 310058, China

Abstract— A novel band-rejection fiber filter based on a Bragg fiber of transversal resonant structure is proposed. A hollow core of radius r is surrounded by a multilayer cladding with the suitable designed alternating layers of high/low refractive indices. Among the N periodic two-layer structures in the radial direction of the Bragg fiber, a defect layer is introduced in the certain two-layer structure with the resonant operation of some wavelengths. For these resonant wavelengths inside the band-gap of the Bragg fiber, large confinement loss occurs due to coupling between the core mode and the defect mode. Hence, a segment of the Bragg fiber of transversal resonant structure can be used as a band-rejection fiber filter. The characteristics are mainly determined by nature of the defect layer. The possible other applications also will be discussed.

Calculation of Effective Microwave Surface Impedance in the Superconducting Film Layered Structure

Chien-Jang Wu[1], **C.-C. Liu**[2], **and Yang-Hua Chang**[3]

[1]Institute of Electro-optical Science and Technology
National Taiwan Normal University, Taipei 11677, Taiwan
[2]Graduate School of Engineering Science and Technology
National Yunlin University of Science and Technology, Douliou, Yunlin 64002, Taiwan
[3]Department and Graduate School of Electronic Engineering
National Yunlin University of Science and Technology, Douliou, Yunlin 64002, Taiwan

Abstract— Microwave surface impedances of the superconducting films in layered structures have been calculated. We first consider a superconducting bilayer structure consisting of a high-temperature superconductor and a nearly ferroelectric superconductor. Effective microwave surface impedances are analyzed in the forward and reverse incidence in this bilayer. The anomalous resonant peak height in the effective surface resistance is found to be decreased in the forward case, while it is enhanced in the reverse incidence. This bilayer makes it possible to design a superconducting Fabry-Perot resonator at microwave frequency. Next, we calculate the effective microwave surface impedance for superlattice made of a nearly ferroelectric superconductor and a dielectric as well. The strong dependence of surface resistance on the frequency, the number of periods, and the thickness of the superconductor layer will be numerically illustrated. The results indicate that such a superconducting superlattice could work as a frequency-selective filter in the microwave regime.

Higher Order Finite-difference Frequency-domain Analysis of Two-dimensional Photonic Crystals with Arbitrary Shapes

Yen-Chung Chiang
National Chung Hsing University, Taiwan

Abstract— A higher order finite-difference frequency-domain method is proposed for the analysis of the band diagrams of two-dimensional photonic crystals. This improved formulation is based on Taylor series expansion, local coordinate transformation, boundary condition matching, and the generalized Douglas scheme. The fourth-order convergence can be achieved with little additional computational cost compared with that of a second-order scheme. This proposed scheme can deal with piecewise homogeneous structures with slanted dielectric interfaces.

Band Structure Analysis of Liquid-crystal Photonic Crystal Fibers

Chia-Lung Kao and Chin-Ping Yu
Institute of Electro-Optical Engineering and Department of Photonics
National Sun Yat-Sen University, Kaohsiung, Taiwan 804, R.O.C.

Abstract— Recently, many optical devices based on the nematic liquid crystals (LCs) have been proposed for the tunable optical properties of the LCs. By adjusting the external electric field or the operation temperature, the refractive index of the LCs can be varied to modify the performance of the optical devices. Liquid-crystal photonic crystal fibers (LCPCFs) with LCs filled in the air holes of PCFs also attract a lot of interest for their tunable PBG effects resulting from the LCs. In order to develop more useful devices based on the LCPCFs, it is essential to understand the propagation properties of a LCPCF, especially the band structures. To analyze the band structures of the LCPCFs, we use the finite-difference frequency-domain method and consider only the unit cell in the PC cladding associated with the periodic boundary condition. The relative permittivity of the LCs is expressed in a tensor form for the anisotropic properties. By varying the value of the propagation constant β, the frequencies of the existing hybrid modes on the PC cladding can be found and the gap maps of the PC cladding with the LC molecules aligned at variant directions can be successfully obtained. Several band gaps in the gap maps can be found and these band gaps must extend bellow the core line to support guided modes in the core. From our calculated results, we can observe that the alignment of the LC molecules indeed has a great influence on the band structures of the LCPCFs. The transmission spectrum of a LCPCF could be dramatically varied by applying the external electric field to rotate the LCs. To design optical devices based on the LCPCFs, one should carefully figure out the corresponding band structures and our method is shown to be helpful in designing the related devices.

Poled Thick-film Polymer Electro-optic Modulation Using Rotational Deformation Configuration

Wen-Kai Kuo and Yu-Chuan Tung
Institute of Electro-Optical and Material Science, National Formosa University
64 Wenhua Rd., Huwei, Yunlin 63208, Taiwan, R.O.C.

Abstract— In this paper, we propose the experimental results of electro-optic polymer modulation using a rotational deformation configuration, then, the results for the conventional compressed/stretched deformation configuration is compared. The experimental results show that, the modulation index of the former is almost two times than that of the latter.

For most polymer EO modulation configurations, the compressed/stretched deformation (CSD) of the index ellipsoid is used to measure the EO coefficient [1], or study orientational relaxation dynamics [2]. In this paper, the rotational deformation (RD) of the index ellipsoid, which was proposed in our previous study, is applied to the EO polymer modulation [3] and because two refractive indexes, n_o and n_e, of the EO polymer are very close, the expected modulation index of the RD configuration has a much better performance than that of the CSD configuration.

In the experiment, the sample EO polymer is the often-used guest-host system DRl/PMMA, i.e., a mixture of azo dye 4-[ethyl(2-hydroxy-ethyl)amino]-6 nitroazo-benzene (DRl) and the amorphous polymer poly(methy1 methacrylate) (PMMA). Under the condition that the heating temperature was 120°C and poling voltage was 800 V, the sample showed the best r_{33} value of approximately 11 pm/V.

REFERENCES

1. Teng, C. C. and H. T. Man, "Simple reflection technique for measuring the electro-optic coefficient of poled polymer," *App. Phys. Lett.*, Vol. 56, 1734–1736, 1990.
2. Michelotti, F., E. Toussaere, R. Levenson, J. Liang, and J. Zyss, "Study of the orientational relaxation dynamics in a nonlinear optical copolymer by mean of pole and probe technique," *J. Appl. Phys.*, Vol. 80, 1773–1778, 1996.
3. Kuo, W. K., et al., "Two-dimensional electric-field vector measurement by a $LiTaO_3$ electro-optic probe tip," *App. Opt.*, Vol. 39, 4985–4993, 2000.

Wave Propagation in General Bi-isotropic Media

Heng-Tung Hsu and Song-Tsuen Peng
Department of Communications Engineering, Communications Research Center
Yuan Ze University, 135 Yuan-Tung Road, Chung-Li, Taiwan 32003, R.O.C.

Abstract— The wave phenomena associated with the class of bi-isotropic (BI) materials had attracted great interests for over two decades due to their extra medium parameter which gives additional freedom in designing various microwave devices. Promising applications in antennas including the polarization rotating lenses and the compact microstrip antennas as well as microwave devices and radar engineering are all based on BI materials. In this paper, we present a new approach to the propagation of uniform plane wave in BI media. While the case of normal incidence is the main focus in this paper, the same approach can be applied for the oblique incidence case as well. Firstly, we employ the technique of Scalarization to simplify the Maxwell equations in vector form to become a set of scalar ones, and then introduce the concept of perturbation analysis to exhibit the effect of the bi-isotropy on the wave characteristics in general. The method of analysis is based on the development of the dispersion relation of a BI medium, so that the result obtained are cast in a concise form and will appear as an extension of well known ones of isotropic media. In particular, the familiar technique of equivalent circuit is developed to enhance the understanding of the wave phenomena associated with BI media.

Design and Implementation of High-speed Laser Diode Driver Circuitry for High-speed Data Recording

Heng-Shou Hsu
Department of Electronic Engineering, Feng-Chia University
100 Wenhwa Road, Seatwen, Taichung 40724, Taiwan, R.O.C.

Abstract— This paper proposed the design and implementation of high speed Laser-Diode Driver (LDD) circuitry suitable for high speed CD/DVD data recording and optical data transmission. As for the case in high speed (X16 for DVD and X48 for CD) data recording, the Laser Diode requires to transmit data pulse with rising/falling time shorter than 0.8 ns. Besides, the current which drives Laser Diode should be at the level up to 300 mA. With such tough requirements necessary to meet, some performance degradation due to inductor-induced bouncing and electromagnetic interference (EMI) noise must be carefully considered. This paper proposed novel high speed Laser-Diode-Driver circuitry implemented by 0.35 μm 5 v CMOS process. With the help of novel circuit structures and circuit design technique, the proposed LDD driver possess the advantages of shorter rising/falling time (< 0.5 ns) which can meet the need for high speed data recording, less overshoot/undershoot of output driving current to cope with the inductor-induced bouncing problems, and adjustable output driving current level to solve electromagnetic interference noise. The circuits were implemented in a 5 v 0.35 μm CMOS process. Simulation results have successfully demonstrate the novel Laser-diode driver is suitable for high speed data recording and has wide application on optical data transmission.

ACKNOWLEDGMENT

This Work is supported by National Science Council of Taiwan, R.O.C. under contract Number: NSC97-2221-E-035-086.

Session 1P8
Poster Session 1

Aspects Regarding the Adapting and Optimization of Mixed Drying Systems Microwave-hot Air for the Processing of Agricultural Seeds

V. D. Soproni, **F. I. Hathazi**, **M. N. Arion**, **C. O. Molnar**, **and L. Bandici**
Faculty of Electrical Engineering and Information Science, University of Oradea
1 Univrsity St., Oradea 410087, Romania

Abstract— Microwave system developed and presented in this paper is designed for drying and treatment against agricultural pests for storage seeds. Precursory storage stage of cereal seeds, which ensures them a high quality and which is done with this microwave system is drying by using mixed microwave — hot air and radiation through selective eradication of insects and pathogenic factors existing in the seed bed. Has been in this case the treatment in the microwave field of agricultural products moving through applicator on a tape Conveyors, transparent to microwaves, made from a special textile material so as allow the air spurt which will blow at the bottom of equipment to dry the product. Drying equipment uses microwave guides to carry energy from microwaves generator (in our case magnetron) to applicator where are placed the absorbed microwave products. Microwave applicators used in the case of our systems are the wave guides, which usually are continuing and may be a single volume cavity or more cavities lowest in series by passing Conveyors. The wave guides system is usually made of wave guides in which the load is displaced by a band Conveyors exposed to microwave radiation. Most of the microwaves energy is coupled with the task dielectric acquiring energy and the rest is absorbed by the tasks at the entry and exit ends of the dryer. Such applicator can function without charge (empty) without damaging the microwave generator.

A optimized technique for drying in microwave field has been designed by combining technology with volume drying in microwave and conventional drying by convection. Thus, products sensitive to high temperatures and fast (as is the case of agricultural seed) can be processed through such innovations, ensuring the preservation or even improving the agricultural products harvested.

Artificial drying of cereal seed is made in drying systems, by using combined microwave — hot air spurt. The method use the microwave for bringing the water from the inside of the seeds to migrate to the surface wherefrom with the hot air spurt in the pre-heat sector of the dryer is accomplish the seeds perspiration during the drying to obtain the vaporization and water disposal and in the next sector following occurs cooling with the atmospheric air of the seeds. Reduction of the moisture contains is carried out at temperatures of heat agent up to 40°C for seed (so as not to affect germination) and give up 50°C to those intended for consumption. In wheat, for example, if it passes 50°C gluten loses its elasticity being affected the line up bread. Core of the seeds can not be totally dry while the environmental air contains moisture. The microwave energy absorbed by 0.25 W/g seeds moist can be used for the drying seed. The level of energy for drying seeds as food and forage food must not exceed 0.75 W/g. Applications that use an energy absorbed 0.25 W/g lead to an increase in germination over 92% of dry seeds in the microwave field. It recommends the use of energy levels less than 0.25 W/g in order to improve germination values.

A Passive Optical Location Implemented on the One-board Computer

P. Fiala, **T. Jirků**, **and R. Kubásek**
Department of Theoretical and Experimental Electrical Engineering
Brno University of Technology, Kolejní 2906/4, Brno 61200, Czech Republic

Abstract— There is a research of the plasma in our department. We have developed the method to detect micro-particles or their groups in the video-record of the plasma. These particles are very small compared to the image frame size, their velocity is relatively high and their trajectory is not linear. We have tested this method in the MATLAB environment and these tests were successful. The method implementation is done on the commercial devices only. We have used a CMOS camera sensor and the microprocessor with the ARM architecture for the data processing. As testing video sequence the record of the birds in countryside was chosen, because the birds have similar movements like the particles and also they are very small compared to the image size and the device function was tested. This article shows the results of these tests.

REFERENCES

1. Fiala, P., T. Jirku, R. Kubasek, P. Drexler, and P. Konas, "A passive optical location with limited range," *PIERS Online*, Vol. 2, No. 6, 685–688, 2006.
2. Dostál, V., "Dynamic image processing," The Bachelor's thesis, DTEEE FEEC BUT, 2007.
3. Daniel, M., "A passive optical location," The Bachelor's thesis, DTEEE FEEC BUT, 2007.
4. Suchardal, J., "A dynamic object image processing," The Bachelor's thesis, DTEEE FEEC BUT, 2007.
5. http://www.cs.cf.ac.uk/Dave/Multimedia/BSC_MM_CALLER.html.
6. Smith, S. W., *The Scientist and Engineer's Guide to Digital Signal Processing*, Second Edition, California Technical Publishing, San Diego, California, 1999.
7. http://www.st.com/stonline/products/promlit/pdf/flvs67241106.pdf.
8. http://www.freescale.com/files/32bit/doc/ref_manual/MCIMX31RM.pdf?fpsp=1&WT_TYPE=Reference%20Manuals&WT_VENDOR=FREESCALE&WT_FILE_FORMAT=pdf&WT_ASSET=Documentation.
9. Louis, D., P. Mejzlík, and M. Virius, *Jazyky C a C++ Podle Normy ANSI/ISO : Kompletní Kapesní Průvodce*, Grada Publishing, 1. vyd. Praha, 644 s, 1999.

The Meaning of the Lightspeed on the Basis of Its Determinations

S. L. Vesely[1] and A. A. Vesely[2]

[1]I.T.B.-C.N.R., Italy
[2]Via L. Anelli 13, Milano 20122, Italy

Abstract— In this paper, we shall examine in some depth the classical measurements of the speed of light carried out by Rømer, Bradley, Fizeau-Cornu, and Foucault, seeking a meaning for the constant c of electromagnetic waves propagation in a vacuum that is useful for telecommunications. Resting upon the two latter methods, we propose that the value c is considered a conversion factor between time and length, similar to parallel-to-serial data conversions.

The term "velocity" may occur in physics with different meanings, and two of them concern this topic. On the one hand, talking, for example, about the average velocity through a displacement, e.g., by car along a tract of highway, the term refers to kinematic values that may be read on the tachometers of the relevant vehicles. On the other hand, talking about the diffusion velocity of a liquid into another the same term carries an interpretation of convection and mixing phenomena in accordance with the kinetic theory of gases. Although tachometers may deliver a vehicle's relative speed according to different technologies, their calibration on a given length per unit of time is consistent with their usage. Sticking to the same conventions for explaining diffusion phenomena might be a matter of convenience.

Classical electromagnetism introduces c essentially as a conversion factor for capacitors' capacitance when translating between emu and esu conventions. However, it is well known how relations with optics let Maxwell confer to c the allegedly more fundamental meaning of speed of light (i.e., $c = \lambda\nu$). More precisely, he interpreted light as an isotropic propagation of small elastic perturbations in the ether medium. Thus, at least originally, c was the characteristic diffusion constant for ether. The second postulate of special relativity holds something different, that is that electromagnetic radiation propagates through a vacuum with speed c, which is both a characteristic of light and a kinematic property of its motion. The speed is a characteristic of the light alone because vacuum has no corresponding physical characteristics, and is also a kinematic trait because relativity adopts a kind of extension $x \to \mathbf{r}$ of the Cartesian plane (x, t) along with the concept of inertial observer endowed with a reference frame for times and lengths. Considering c a transmission factor in absence of any media, and taking into account the accruing experimental evidence in favor of fast and slow light phenomena in the matter, it is natural to ask why in developing frequency and time division multiplexers it is still a conceptual must to relate the numerical values of the transmission speed with the measuring rods and spring driven clocks.

The two classical astronomical methods for measuring c, mentioned above, are fully framed in the Newtonian picture (except for light), while the so-called earth-bound techniques of Fizeau and Foucault convert lengths to time intervals (i.e., $L = cT$) and vice-versa by means of stroboscopic rotation. Even if a stroboscope is a mechanical device, the relationship between time and length on which it works may be profitably extended to electrical relays in order to supply a linear conversion from time to length units, enjoying the precision that electronics has achieved meanwhile. Indeed, we suggest herein to consider c a conversion factor, as it used to be.

In conclusion, in our opinion the idea that signals have typical velocities that telecommunications should care about is reminiscent of the attempts at mechanical interpretations of electromagnetism, and it cannot but elude synchronization problems related to phase tracking of guided waves as well as receptions of signals radiated by moving bodies.

Lateral Displacements of an Electromagnetic Beam Transmitted and Reflected from a Gyrotropic Slab

Hui Huang[1, 2], **Yu Fan**[1], **Bae-Ian Wu**[2], **and Jin Au Kong**[2]

[1]School of Electrical Engineering, Beijing Jiaotong University, Beijing 100044, China
[2]Research Laboratory of Electronics, Massachusetts Institute of Technology
Cambridge, MA 02139, USA

Abstract— It is known that for a gyrotropic medium in the Voigt configuration, waves can be decoupled into TE and TM modes. A detailed study on the lateral displacements of an electromagnetic beam reflected and transmitted from a gyrotropic slab in Voigt configuration is presented, for both TM and TE waves. Using the stationary phase approach, analytic expressions for lateral displacements of the reflected and transmitted waves from a symmetric gyrotropic slab are obtained, and we also give examples for both cases. It is found that the lateral displacements for TM and TE waves have different characteristics. Only the TM mode is affected by the gyrotropy. Due to the external magnetic field, the lateral displacement of a TM wave transmitted from a gyrotropic slab is not the same as the reflected one, even when the configuration is symmetric and the media are lossless. We also discuss the phenomena when the incident angle is near the Brewster angle.

Electromagnetic Interference Modeling Research on the Electrical Machine and Converter Systems

Lingyun Wang, **Ruifang Liu**, **and Hui Huang**
School of Electrical Engineering, Beijing Jiaotong University, Beijing, China

Abstract— Electrical machine and converter systems are widely used in renewable energy power generation system and speed regulation of motors. With the applications of power electronic devices in a variety of equipments and systems, the electromagnetic interference (EMI) is attracting more and more attentions. Modeling to the EMI of the system is the fundamental of forecasting and removing the EMI. In the electrical machine and converter systems, compared with the radiated EMI, conducted EMI is the main problem in the system. Based on this, considered the EMI in the switching devices and the electrical machines, this paper discussed and analyzed the conducted EMI modeling methods and technology widely used today in the electrical machinery and converter system. Time domain and frequency domain modeling methods are analyzed respectively.

In detail, considered the influence of the turning-on and off of the switching devices, the high-frequency parasitic parameters of the electrical machine, and the ground current on the system, the paper discusses and analyzes the modeling technology of sub-systems. Firstly, in the converter system, the EMI pulses produced by the switching devices has a great influence on electrical machines, causing the problems such as the insulation of electrical machines, shaft voltages, bearing currents and so on. So the paper discusses the modeling methods in the converter system. Secondly, in the electrical machinery system, since the high-frequency parasitic parameters of the electrical machine can't be ignored, the model of the electrical machine is presented. Thirdly, because of the effects of distribution parameters existed in cable, voltage reflection will be occurred at machine terminals, the paper discusses the modeling technology of the system. On top of that, the paper also analyzes the modeling methods of the ground loop in the system. Finally, the current status of conducted EMI modeling research of the electrical machine and converter systems is presented.

Transient Field Distribution in a Transformer Affected by Variably Loaded Secondaries

Gerd Mrozynski[1], **Eckhard Baum**[2], **and Otto Erb**[2]

[1]Institute of Electromagnetic Theory, University of Paderborn
Warburger Str. 100, D-33098 Paderborn, Germany
[2]Fundamentals of Electrical Engineering, University of Applied Sciences Fulda
P. O. Box 2254, D-36039 Fulda, Germany

Abstract— Ring core transformers are analyzed by using a two dimensional axisymmetric model. The primary and secondaries are foil windings surrounding a core with finite permeability. The secondaries are positioned between core and primary winding. They can either be short circuited or connected to a resistive load. The current in the primary is constant up to the switching point at $t = 0$. At this moment it is abruptly forced to zero hereby causing transient fields in the other windings. The spatial distribution and temporal devolution of these fields is affected by the loading of the secondaries.

The scope of the paper is to analyze the current density distribution and the total current in the secondaries and the primary as a function of time. To achieve this the spatial distribution of the magnetic field for $t < 0$ is expressed by a sum of spatial eigenfunctions each of them decaying with a particular time constant in $t > 0$. Because of spatial continuity requirements the time constants in adjacent regions with different material properties must be identical.

The transformer analysis can easily be modified to become applicable for coils. Also the switching process may be modified: instead of changing source voltage or current material parameters as for instance conductivity can be switched in the framework of the developed formulas.

To verify the results the energy stored in the magnetic field before switching is compared with the energy consumed in the windings after switching, the latter being computed with the help of Poyntings theorem.

Research on Arch Method for Testing the Absorbing Capability of Absorbing Materials

Gai Tao and Qun Wang
College of Material Science and Engineering, Beijing University of Technology
Beijing 100024, China

Abstract— First, the paper introduces the principle, the instrument and the visual compiler of the arch method test system. Considering the mixed coupling between antennas, the general field strength of the receiving antenna can be described by the sum between the field strength of the mixed coupling antennas and the field strength of reflecting field strength as follows:

$$E_t = E_p + E_c = |E_p| \cdot e^{j(\theta+\omega t)} + |E_c| \cdot e^{j(\psi+\omega t)} \tag{1}$$

When absorbing wave material is on the plate, the general field strength will be changed and will be described as follows:

$$E'_t = E'_p + E_c = |A \cdot E_p| \cdot e^{j(\theta+\alpha+\omega t)} + |E_c| \cdot e^{j(\psi+\omega t)} \tag{2}$$

Ideally the mixed coupling of antennas is ignored, but in fact the error witch it comes into being is involved in the exactitude of the test system. The visual compiler is based on VEE program (Visual Engineering Environment program). VEE program is supported by Agilent Company and fulfilled the auto test technology. With VEE program we can compile the program to connect the instrument and the computer independently.

Second, estimated that the error of the test system due to the mixed coupling between antennas with moving the plate up and down.

Last, showed that the reflectivity of some microwave absorbing material when the angle of incidence is 10°, 20° and 30° respective. Ideally the arch method will be used to test the absorbing capacity of the absorbing wave material with any angles of incidence affective, but the right testing radius is not easy to carry out and the paper adopts three different angles of incidence to test.

Progress in Studies of Transients Analysis Method of Multiconductor Transmission Lines

Chaoqun Jiao and Yi Sun
School of Electrical Engineering, Beijing Jiaotong University
No. 3 Shangyuan Residence, Haidian District, Beijing 100044, China

Abstract— Throughing read a lot of literature, the progress in Studies of transients analysis method of multiconductor transmission lines (MTLs) is presented in this paper. These methods mainly include Bergeron's method, the finite difference time domain (FDTD) method and the time domain finite element (TDFE) method. Then, the disadvantage and advantage of these methods are pointed out through one example. Finally, with different situation, it is suggested that which method is chosen to resolve the pratical problem.

Introduction: The MTLs structure is capable of guiding wave whose frequencies rabge from dc to where the line cross-sectional dimensions become a significant fraction of a wavelengh. There are many applictions for this wave-guiding structure. The fault, lightning and switching operation in a three-phase substation all cause very intense wave processes of voltage and current distributed along the busbars and the power lines. Because the frequency spectrum of the transient process is very wide and the electromagnetic field at the high frequency domain is radiated from the busbars and the power lines, therefore, the switching transient is a very important problem.

In order to research this problem, in general, the method of moment (MoM) may be used. But it is too difficult to use for a complex configuration and is only valid in the fiequency domain and for the linear problem. Another approach is to model the busbars and the power lines as the MTLs. In this approach, firstly, the wave processes of voltage and current distributed along the busbars and the power lines are calculated, and then, the electromagnetic fields at arbitrary points in the substation and in neighborhood are directly evaluated through the known voltage and current distributed along the MTLs. Therefore, it is a key to develop an effective algorithm for calculating the wave processes of voltage and current distributed along the MTLs with branches.

Presented Methods: There are many methods to analyze the MTLs, in general, they may be classified into two classes. One is the fiequency domain method, and another is the time-domain method.The first method is very conventional and simple, but it is limited in the linear problem and is not adaptable in transient analysis. The second one can be used to deal with not only the linear problem but also the nonlinear problem. However, for the fiequency-dependent parameter problem, it is difficult. Some special methods have been developed to overcome the shortcoming of above two methods. In fact, in order to analyze the wave processes, the time-domain method is always recommended. Bergron's method is a time-domain method, which has been widely used to calculate the wave processes in the power system and has been implemented in EMTP code [1, 2]. But only the voltage and current at some specified nodes can be calculated by this method, it is not effective for the calculation of whole wave processes of voltage and current distributed along the MTLs. For this case, the problem can be solved by FDTD [3]. Professor C. R. Paul proposed an iterative algorithm for the lossy MTLs with arbitrary loads [4]. Dr. Lu Tiebing and Qi Lei improved and complemented the Paul's method [5–8]. Because of Gibbs effect of the FDTD method, Park and Liu Lei developed the TDFE method [9, 10].

Comparation of These Method and Suggestion: The disadvantage and advantage of these methods are pointed out through one example in [4]. The process and result of test will be developed in the extended paper.

Conclusion: The progress in Studies of transients analysis method of multiconductor transmission lines (MTLs) is presented in this paper. The disadvantage and advantage of these methods are pointed out. It is suggested that which method is chosen to resolve the pratical problem.

REFERENCES

1. Dommel, H. W., "Digital computer solution of electromagnetic transients in single- and multiphase networks," *IEEE Trans. on Power Appa-ratus and Systems*, Vol. 88, No. 2, 734–741, 1969.
2. Dommel, H. W. and I. I. Dommel, "Transients program," *User's Manual*, February 1982.
3. Tesche, F. M., M. V. Ianoz, and T. Karlsson, *EMC Analysis Methods and Computation Models*, John Wiley & Sons Press, New York, 1996.

4. Paul, C. R., *Analysis of Multicodutor Transmission Lines*, John Wiley & Sons Press, New York, 1994.
5. Lu, T., X. Cui, and L. Li, "Transient analysis of aerial multiconductor transmission lines with branch [J]," *IEEE Transactions on Magnetics*, Vol. 37, No. 5, 3298–3302, 2001.
6. Lu, T., X. Cui, and H. Yin, "Time-domain analysis of transient electromagnetic field generated aerial busbars above lossy soil [J]," *IEEE Transactions on Magnetics*, Vol. 38, No. 2, 773–776, 2002.
7. Qi, L., X. Cui, and T. Lu, "Transient plane wave coupling to overhead line above a multi-layer soil," *2005 IEEE Intemational Symposium on Microwave, Antenna, Propagation and EMC Technologies for Wireless Communications Proeedings*, 851–854, 2005.
8. Qi, L., X. Cui, and L. Li, "Transient plane wave coupling to overhead line above a multi-layer soil," *15th Conference on the Computation of Electromagnetic Fields*, Shenyang, Liaoning, China, June 2005.
9. Park, S. and S. J., "Transmission line analysis of MRSM cell [J]," *IEEE Transactions on Magnetis*, Vol. 40, No. 4, 2089–2091, 2004.
10. Liu, L., X. Cui, and L. Qi, "Transients analysis of transmission line by time domain finite element metho [J]," *Proceedings of the Chinese Society of Electrical Engineering*, Vol. 28, No. 3, 112–118, 2008 (in Chinese).

Efficient Calculation of Vehicular Antennas' Radiation Patterns

Xiao-Fei Xu, **Xiang-Yu Cao**, **and Jia-Jun Ma**
Telecommunication Engineering Institute, AFEU
Xi'an 710077, China

Abstract— The wire antennas mounted on the metal carrier are concerned by people for a long time. They are applied on large aircraft, ships as small as cell phones, and other mobile communications devices. The problem of wire antennas mounted on all types of carriers is analyzed accurately by the moment method based on integral equation. However, when calculating the large carrier such as vehicular antennas, the traditional method of moment will consume a very long time. To improve the algorithm and accelerate the speed of calculation, multilevel fast multipole algorithm (MLFMA) is adopted. MLFMA is the multilevel application of FMM and can speed up the matrix-vector multiplication, which reduces the computational complexity, both memory requirement and CPU time, to $O(N \log N)$ for an N-unknown problem. In this paper, the problem of vehicular antennas is analyzed and calculated efficiently by the method, and the calculated results agree well with the simulation results of Ansoft HFSS, which indicates that the analytical expressions derived in this paper are correct. The method has a certain significance for the rapid analysis and the calculation of the vehicular antennas' performance.

ACKNOWLEDGMENT

The project is supported by Natural Science Foundation of China (Program No. 60671001) and Doctor Innovative Fund of the Telecommunication Engineering College, AFEU (200706).

Analysis of Vehicular Wire Antennas Using MoM

Xiao-Fei Xu, **Xiang-Yu Cao**, **and Tao Liu**
Telecommunication Engineering Institute, AFEU
Xi'an 710077, China

Abstract— In this paper, the problem of connection between wire antennas and conductors is analyzed in detail by the moment method. The surface-wire structure is divided into three parts: the wire antenna, the connection part and the conductor. Then three types of basis functions are introduced respectively for surface-wire structure. In testing procedure, Garlerkin's method is used and the singular integral is treated analytically. Finally, the matrix equation is derived.

Firstly, In order to prove the method presented in this paper, one classical example is analyzed and calculated. One monopole is attached to the center of a metallic plane, the size of metallic plane is 2 m × 2 m and the length of the monopole is 0.2 m, the operation frequency of the monopole is 375 MHz. Then the far-field characteristic of radiation is computed. The calculated results agree well with the simulation results of Ansoft HFSS, which indicates that the analytical expressions derived in this paper are correct.

Secondly, the problem of vehicular wire antenna is analyzed with the method. One monopole is attached to the top surface of a car, the length of monopole is 0.25 m, the operation frequency of the monopole is 300 MHz, the length of the car is 3 m, the width of the car is 1.6 m and the height of the car is 1.5 m. The calculated results also agree well with the simulation results of Ansoft HFSS, the patterns of power radiation are given in three directions. It is proved that the method is theoretical correct which gives high calculation accuracy and can be used as a guidance for the installation and disposition of vehicular wire antennas.

ACKNOWLEDGMENT

The project is supported by natural science foundation of China (Program No. 60671001) and doctor innovative fund of the telecommunication engineering college, AFEU.

Inverse Problem of Multiple Objects Buried in a Half-space

W. Chien[1], **C. H. Sun**[2], **C. C. Chiu**[2], **and W. C. Chuang**[2]

[1]Electronic Engineering Department, De Lin Institute of Technology, Tu-Cheng, Taipei, Taiwan, R.O.C.
[2]Electrical Engineering Department, Tamkang University, Tamsui, Taiwan, R.O.C.

Abstract— Electromagnetic imaging of buried multiple dielectric cylinders by using genetic algorithm has been presented. The unknown amount and distribution of dielectric cylinders are buried in one half-space and illuminated by transverse magnetic (TM) polarization plane wave from the other half-space. Based on the boundary condition and the measured scattered field, we have derived a set of nonlinear integral equations, and the imaging problem is reformulated into an optimization problem. In particular, by taking account into the complete nonlinear formulations, the amount and distribution of the dielectric cylinders could be highly-contrasted and complicated. In inverse algorithm, the improved steady state genetic algorithm is employed to search for the global extreme solution of objective function. Numerical results have demonstrated that the powerful performance of the inverse algorithm. Numerical results show that satisfactory reconstruction has been obtained.

Simulations on the Whole Structure of Microwave Radiometer Calibration Load by FDTD Method

Ming Jin, **Ming Bai**, **and Jungang Miao**
Electromagnetics laboratory, School of Electronic Information and Engineering
Beijing University of Aeronautics and Astronautics, Beijing 100191, China

Abstract— The emissivity of the microwave radiometer calibration load is designed to be close to ideal blackbody, which is important to calibrate the linearity and sensitivity of a microwave radiometer by providing a standard brightness temperature in the microwave region. The load emissivity is expected to be close to 1, and required to be determined precisely. Under thermal equilibrium, according to Kirchhoff's law, the emissivity of an object is equal to its absorptivity. The emissivity can be obtained from its reflectivity, which is the method commonly used both in the measurement and simulation.

The microwave radiometer calibration load is usually in shape of coated pyramid arrays, the direct simulation of which is quite difficult due to its large electric size. In order to perform parametric optimizations on such load, taking into account of its periodical structure, a coated pyramid unit can be simulated using the Finite-Difference Time-Domain (FDTD) method under the periodic boundary condition for infinite arrays, so that the amount of calculation is acceptable. However, the detailed scattering from a size-limited microwave radiometer calibration load should be calculated to obtain the emissivity, i.e., the simulation on the whole load structure is needed. In this work, the full-space scattering field patterns for load illuminated by a plane wave and a Gaussian beam are respectively obtained through the FDTD simulation on the whole structure. The coating material is described as Lorentz dispersion medium and simulated by means of second-order difference in the FDTD method. Simulation results of an actual coated pyramid array at several frequency points (10.65 GHz, 18.7 GHz, 23.8 GHz) are obtained. The evaluation of the microwave radiometer calibration load emissivity from the FDTD calculation results is provided and the related issues are discussed.

Convergence Analysis of Electric/Magnetic Current Sampling for Antenna Design in the Presence of Electrically Large and Complex Structures

Heng-Tung Hsu, **Fang-Yao Kuo**, **and Hsi-Tseng Chou**
Department of Communications Engineering, Communications Research Center
Yuan Ze University, 135 Yuan-Tung Road, Chung-Li 32003, Taiwan, R.O.C.

Abstract— Designing antennas in the presence of electrically large and complex structures such as cars or aircrafts has become an important issue for next generation communication systems. Based on the principle of equivalence, the hybridization approach that integrates the high frequency (HF) and low frequency (LF) techniques has shown its superiority in terms of its computing efficiency. In such approach, discrete samplings of continuous electric or magnetic field components resulted from LF sub-domain are required to be converted to the excitation current sources for the HF sub-domain. Thus, the overall accuracy of the calculation results will strongly depend on the similarities between the sampled and original filed distributions with both the magnitude and phase involved. In this paper, the convergence analysis of electric and magnetic current sampling is performed. Impact of the different sampling profiles on the overall accuracy is also investigated through numerical examples. Results revealed that sampling profiles may closely be related to the field distributions of the antenna types.

Forward Modeling of High Frequency Magnetotelluric Using Finite Element Method

Jing-Tian Tang[1], **Xiao Xiao**[1], **Ye Wang**[1], **Ji-Feng Zhang**[1], **and Chaozhuang Xi**[2]

[1]School of Info-physics and Geomatics Engineering, Central South University
Changsha 410083, China
[2]School of Geosciences and Environmental Engineering, Central South University
Changsha, Hunan 410083, China

Abstract— With the development of geophysical prospecting in 1000 meters below surface, the High-Frequency Magnetotelluric (HMT) method is applied more and more extensively in our country. The required frequency range is from 10 Hz to 100 KHz. In this paper, the author studies numerical modeling of the high-frequency Magnetotelluric method. First of all, the paper derives the finite element equation of HMT method from Maxwell equations using generalized variational principles, and produced the bilinear interpolation and double quadratic interpolation finite element program, calculated and verified the layered model. And then, the author researches the typically rift valley model, through accuracy analysis of the simulation results, comes to some meaningful conclusions.

A Three Dimensional FEM-BEM Approach for the Simulation of Magnetic Force Microscopes

T. Preisner and W. Mathis
Leibniz Universität Hannover, Germany

Abstract— In recent years a rapid miniaturization of integrated devices and data storage media is noticeable. In this regard high resolution measurement techniques have been developed, which fulfill the increasing requirements for device error analysis. One of these highly sensitive measuring instruments is the Magnetic Force Microscope (MFM), which reveals the magnetic properties of an arbitrary sample. During the measurement process a micro-mechanical cantilever, which holds a magnetic coated tip underneath, is moved over a magnetic field inducing sample surface. Due to the magnetic interactions attractive or repulsing forces act on the cantilever and cause a deflection, which can be detected by a reflected laser beam focused onto a photodetector. Thereby it is possible to image the magnetic domain structures and hence to draw conclusions about the sample magnetizations or currents. Due to different error sources, as for instance a tip asymmetry or a heterogeneous tip coating as well as occurring difficulties in the investigation of soft magnetic sample materials, it is useful to support the laboratory measurements with theoretical considerations.

In this work a three dimensional numerical MFM model will be presented. Due to the immense differences in size between the single components inside the microscope, which are most extensive between the apex radius of the magnetic coated tip and the length of the cantilever (10 nm versus 200 µm), the FEM cannot conveniently be applied for the discretization of the whole considered calculation domain. Therefore, for this multiscale problem the considered domain is enclosed with boundary elements. This FEM-BEM coupling is necessary for a precise and efficient calculation of the magnetic interaction fields. In order to simulate an overall MFM scanning process and the involved cantilever deflection, it is essential to compute the resulting forces acting on the cantilever. For this purpose two methods are implemented and compared with each other; the Virtual Work Principle (VWP) and the integration over the divergence of the Maxwell Stress Tensor (MST). Both are applicable for the total force calculation of a body. However, in the case of permanent magnetic materials the local force distributions strongly differ from each other [1, 2]. Considering a following structural analysis of the cantilever deflection appropriate physical local forces on the magnetic coated tip are required. For this reason the VWP is furthermore implemented in such a manner as reported in [1, 2] in order to obtain the applicable local interaction forces between the tip and the magnetic inducing sample.

REFERENCES

1. De Medeiros, L. H., G. Reyne, G. Meunier, and J. P. Yonnet, "Distribution of electromagnetic force in permanent magnets," *IEEE Trans. Magn.*, Vol. 34, No. 5, 3012–3015, 1998.
2. De Medeiros, L. H., G. Reyne, and G. Meunier, "About the distribution of forces in permanent magnets," *IEEE Trans. Magn.*, Vol. 35, No. 3, 3345–3348, 1999.

A General ADE-FDTD Algorithm for the Simulation of Different Dispersive Materials

A. A. Al-Jabr[1] and M. A. Alsunaidi[2]

[1]Jubail Industrial College, Saudi Arabia
[2]King Fahd University of Petroleum & Minerals, Saudi Arabia

Abstract— A number of FDTD-based algorithms for the analysis of dispersive materials have been already proposed. When the problem space involves materials having different types of dispersion with or without multi-poles, the solution algorithms become complicated. The existing algorithms require a separate formulation for each dispersion type. For example, a dispersion model like the Lorentz-Drude with six poles will require long derivations and many values to be stored in memory. In this work, a general algorithm is proposed that will remove this complication; only one algorithm can be used for all dispersion types.

Starting with the most general form of dispersion, the Lorentzian form, the polarization field in the frequency domain can be written as

$$P(\omega) = \frac{a}{b + jc\omega - d\omega^2} E(\omega) \tag{1}$$

Shifting to the time domain through inverse Fourier transform gives

$$bP(t) + cP'(t) + dP''(t) = aE(t) \tag{2}$$

The key step towards the formulation of a consistent and general FDTD algorithm is approximating the time derivatives in Equation (2) at time instant $n-1$. Thus, one obtains the following update equation.

$$P^n = \frac{4d - 2b\Delta t^2}{2d + c\Delta t} P^{n-1} + \frac{-2d + c\Delta t}{2d + c\Delta t} P^{n-2} + \frac{2a\Delta t^2}{2d + c\Delta t} E^{n-2} \tag{3}$$

which can be written in the form

$$P^n = C_1 P^{n-1} + C_2 P^{n-2} + C_3 E^{n-1} \tag{4}$$

The constants C_1, C_2 and C_3 can be found for any form of dispersion relation (see table below). In the case of multi-pole dispersion, the same relation is written for each pole with appropriate constants. The update equation for the electric field intensity is given by

$$E^n = \frac{D^n - \sum_i^N P_i^n}{\varepsilon_o \varepsilon_\infty} \tag{5}$$

where D is the flux density and N is the number of poles. Several numerical experiments have shown that, while keeping the same level of accuracy, the proposed ADE-FDTD algorithm provides savings in both memory and computational requirements compared to other established methods.

Dispersion term in frequency domain	C_1	C_2	C_3
Lorentz Pole $P(\omega) = \frac{a}{b + jc\omega - d\omega^2} E(\omega)$	$\frac{4d - 2b\Delta t^2}{2d + c\Delta t}$	$\frac{-2d + c\Delta t}{2d + c\Delta t}$	$\frac{2a\Delta t^2}{2d + c\Delta t}$
Drude Pole $P(\omega) = \frac{a}{jc\omega - d\omega^2} E(\omega)$	$\frac{4d}{2d + c\Delta t}$	$\frac{-2d + c\Delta t}{2d + c\Delta t}$	$\frac{2a\Delta t^2}{2d + c\Delta t}$
Debye term $P(\omega) = \frac{a}{b + jc\omega} E(\omega)$	$\frac{-2b\Delta t}{c}$	1	$\frac{2a\Delta t}{c}$

ACKNOWLEDGMENT

The authors would like to acknowledge the support of King Fahd University of Petroleum & Minerals.

Analysis of Antennas and Scatterers with Nonlinear Loads: A MoM-AOM Approach

S. M. Azimi[1], **H. R. Karami**[2],
S. Rajabi[2], **A. Kalantarnia**[2], **and S. M. M. Moosavi**[1]
[1]Hamedan University of Technology, Iran
[2]Amirkabir University of Technology, Iran

Abstract— A frequency-domain spectral balance technique is utilized in this paper to analyze the non-linearly loaded wire antenna located over a lossy dielectric half-space. The technique involves two stages. First, the problem is transformed to a nonlinear microwave equivalent circuit with the circuit parameters of antenna extracted by the method of moment (MoM) solution of the electric field integral equation [1]. Then, the arithmetic operator method (AOM) [2] is applied to solve the nonlinear microwave equivalent circuit. The main feature of the proposed technique is its efficiency in analyzing the transient response of the antenna with strong nonlinear loads over a lossy dielectric half-space. The technique works purely in the frequency domain, so the effects of lossy dielectric half-space can be considered properly by using method of moment in conjunction with Sommerfeld asymptotic method. The AOM is now used to the analysis of a centre nonlinearly loaded thin wire scatterer illuminated by Gaussian pulse. It is well known that the frequency domain behavior of scatterer excited by a Gaussian pulse can be represented by the Norton equivalent circuit obtained by the use of MOM. Applying the kirchhoffs circuit law to Norton equivalent circuit gives

$$I_{NL} = Y_{in} V_L - I_{SC} \tag{1}$$

where V_L is the terminal voltage, and the current of nonlinear subcircuits is I_{NL} corresponding to nonlinear load part. I_{SC} is the short circuit current of the antenna input and Y_{in} is the input admittance of the antenna for different frequency components, both being defined as a function of the frequency. Using the AOM transform matrix [2], T_V, the current-voltage nonlinear relationship can be represented in the frequency domain as

$$-I_{NL} = \sum_{n=0}^{N} a_n T_V^{n-1} V_L \tag{2}$$

One can substitute (2) into (1) and obtains V_L by an iterative numerical method such as Newton-Raphson method. The other parameters can be easily calculated by using V_L. In order to evaluate the performance of the proposed method, the midpoint transient current of the nonlinearly loaded antenna oriented at an angle of 45 degree over a lossy dielectric half-space with length of 1 m and radius of 6.74 mm, excited by a Gaussian pulse voltage source at its midpoint is shown in Fig. 1. The *i-v* characteristic of nonlinear load used in this example is similar to [3].

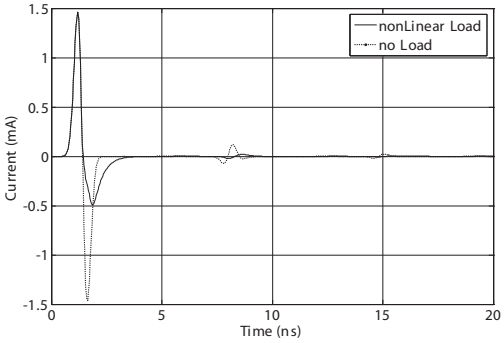

Figure 1: The midpoint transient current of the nonlinearly loaded antenna oriented at an angle of 45 degree over a lossy dielectric half-space with $L = 1$ m, $a = 6.74$ mm, excited by a Gaussian pulse voltage source at its midpoint.

REFERENCES

1. Liu, T. K. and F. M. Tesche, "Analysis of antennas and scatterers with nonlinear loads," *IEEE Trans. Antennas Propagat.*, Vol. 24, 131–139, Mar. 1976.
2. Chang, C. R. and M. B. Steer, "Frequency-domain nonlinear microwave circuit simulation using the arithmetic operator method," *IEEE Trans. Microwave Theory Tech.*, Vol. 38, 1139–1143, 1990.
3. Landt, J. A., E. K. Miller, and F. J. Deadrick, "Time domain modeling of nonlinear loads," *IEEE Trans. Antennas Propagat.*, Vol. 31, 121–126, Jan. 1983.

A New Broadband Triangular Microstrip Antenna Using Slots and Integrated Reactive Loading Optimized by Genetic Algorithm and Method of Moment (GA/MOM)

M. Kiani, **A. Keshtkar**, **A. Kalantarnia**, **and H. R. Karami**
Amirkabir University of Technology, Iran

Abstract— A new broadband triangular microstrip antenna for Digital Communication System (DCS) is presented. Triangular patch fed by coaxial probe and substrate parameters is designed for integrating antenna and microwave circuit. Suggested Antenna in this Paper uses mixture techniques of slot and integrated reactive loading. Pair of slots on the patch is presented for exciting TM_{10} and TM_{20} by suitable ratio and increases the bandwidth. Also influence of integrated reactive loading is decreasing reactance of probe and helps for bandwidth improvement. Using both techniques can enhance antenna bandwidth. Moreover slots increase effective current path and decrease antenna size. Design of suggested antenna consists of parameters including dimension of patch, slot and integrated reactive loading. More than twenty variables without having exact influences of them in this antenna are main reasons for using reliable and powerful optimization method. So optimization code is written by binary genetic algorithm method and is attached to full wave moment method. Because of much time and calculation between MOM and GA code a Model Based Parameter Estimation technique (MBPE) is used. This technique is important for speed up the simulation software in frequency band. MBPE technique simulate the problem in few point and produces a continuous antenna parameter (i.e., S_{11}) for calculating fitness function needed by optimization code. Achieved bandwidth from optimized antenna is about 6.94% in 1800 MHz center frequency. This value is 3.8 times of simple triangular patch and 1.3 times the triangular patch antenna using slots reported until now. In fact the idea of using mixture method of using slot and integrated reactive loading linked to GA optimization can improve antenna bandwidth as 1.64%.

FDTD Analysis of a Nonlinear Transmission Line

J. Dědková and T. Kříž
Department of Theoretical and Experimental Electrical Engineering
Brno University of Technology, Kolejní 2906/4, Brno 612 00, Czech Republic

Abstract— The paper describes a new effective approach to simulation of voltage and current distributions along the nonlinear transmission line (NTL). Numerical results of the transmission line simulations based on Finite Difference Time Domain (FDTD) method are presented. There are several possibilities how to simulate the voltage and current distributions along the single or multiconductor linear transmission line. The aim of our investigation was to find an effective algorithm for numerical simulation of the current and voltage wave propagation on NTL. The best solution was obtained by using so-called leapfrog method, when the spatial and temporal derivatives were replaced by the combination of both central and forward differences. This modification of FDTD was discussed and it was applied first to the numerical simulation of electromagnetic wave propagations in a free space. The new algorithm based on FDTD was programmed in Matlab language. Some illustrative examples are solved and obtained numerical results are presented.

REFERENCES

1. Griffith, J. R. and M. S. Nakhla, "Time-domain analysis of lossy coupled transmission lines," *IEEE Transaction on Microwave Theory and Techniques*, Vol. 38, No. 10, Oct. 1990.
2. Orel, T. and J. Valsa, "An efficient numerical calculation of the convolution integral as an interface between the models of a linear transmission line and its nonlinear terminations," *21st Seminar on Fundamentals of Electrotechnics and Circuit Theory*, Gliwice, 1998.
3. Dědková, J. and L. Brančík, "Laplace transform and FDTD approach applied to MTL simulation," *PIERS Online*, Vol. 4, No. 1, 16–20, Mar. 2008.
4. Sullivan, D. M., *Electromagnetic Simulation Using the FDTD Method*, IEEE Press, New York, 2000.

Combined RKDG and LDG Method for the Simulation of the Bipolar Charge Transport in Solid Dielectrics

Jihuan Tian, **Jun Zou**, **and Jiansheng Yuan**
Department of Electrical Engineering, Tsinghua University, Beijing 100084, China

Abstract— The space charge dynamics plays an important role on the degradation and the breakdown of solid dielectrics under high voltage due to the intensification of the local electric field. The transport of different species of space charges under the electric field can be described by a set of convection-reaction equations coupled with the Poisson's equation as follows:

$$\begin{aligned} \frac{\partial n_a}{\partial t} + \frac{\partial f_a}{\partial x} &= S_a \text{ (convection} - \text{reaction equation)}, \\ \frac{\partial E}{\partial x} &= \frac{\rho_{\text{all}}}{\varepsilon_0 \varepsilon_r} \text{ (Poisson}'\text{s equation)}, \\ \text{where } f_a &= \pm \mu_a n_a E \text{ } (a \text{ represents the carrier types}). \end{aligned} \tag{1}$$

Thus, to obtain the time-dependent space charge distribution, the two types of equations should be calculated alternately.

The previous work used the QUICKEST method with a flux limiter to solve the convection-reaction equation. However, it cannot accurately calculate the space charge profile with very steep wavefront or shocks, due to the wide stencil adopted for the interpolation of the numerical flux and the split treatment of the originally coupled convection and reaction terms. In this paper, the Runge-Kutta discontinuous Galerkin method is applied to solve the convection-reaction equations, in which the high-order piecewise continuous Legendre polynomials are chosen as the basis functions to expand the space charge profile, and a special Runge-Kutta method combined with a slope limiter is used for the time discretization, which is able to ensure the numerical stability. The convection and the reaction terms can be handled simultaneously by the RKDG method without the split procedure, and the high-order accuracy can be obtained without incorporating a wide stencil, which is more suitable for shock capturing than the QUICKEST method.

In the solution of the Poisson's equation, to cooperate with the RKDG method, the local discontinuous Galerkin method (LDG) is adopted instead of the conventional boundary element method (BEM). In the LDG method, the basis function is also the piecewise continuous Legendre polynomial. Therefore, the integrals in the weak formulation of the convection-reaction equations obtained from the RKDG method can be given analytically. Thus, the Gauss-Legendre quadrature, which requires the evaluation of the integrands at the Gauss points, is avoided, so that higher efficiency can be achieved compared with the combined RKDG and BEM method.

The combined RKDG and LDG method has been verified by the simulation of the space charge transport in a low-density polyethylene sample under high dc voltage. The results show that the method has a better performance of shock capturing over the QUICKEST method, and is more efficient than the combined RKDG and BEM method.

Continuous Tabu Search for the Corona Loss Calculation of the Double-circuit High Voltage dc Transmission Lines

Jihuan Tian[1], **Yafei Ji**[2], **Jun Zou**[1], **and Jiansheng Yuan**[1]

[1]The State Key Lab of Power System, Department of Electrical Engineering
Tsinghua University, Beijing 100084, China
[2]Power System Research Department, China Electric Power Research Institute
Beijing 100192, China

Abstract— The experience for the construction and the operation of double-circuit high voltage dc (HVDC) transmission lines is still limited in the world. The corona loss, which is caused by the flow of ions in the space around the conductors, is one of the important factors that should be considered for the sake of economy in the operation of the lines.

To obtain the corona loss, the distribution of ions should be calculated. In the previous work, the Deutsch assumption was adopted, which assumes that the ions do not affect the direction of the space-charge-free electric field. Consequently, the coupled continuity equation and the Poisson's equation, which describe the distribution of the ions in the steady state, are simplified to a two-point boundary value problem (TBVP) of the ordinary differential equations (ODE). The TBVP is established on the space-charge-free electric flux lines. The ODEs for the electric flux lines that connect two conductors are as follows:

$$\begin{aligned}
&\frac{d\Phi}{d\varphi} = \xi \\
&\frac{d\xi}{d\varphi} = -\frac{\rho_+ - \rho_-}{\varepsilon_0 E'^2} && \text{at} \quad \varphi = U_+ : \Phi = U_+,\ \xi = \frac{U_0}{U_+} \\
&\frac{d\rho_+}{d\varphi} = \frac{1}{\varepsilon_0 \xi E'^2}\left[\rho_+^2 - \rho_+\rho_-\left(1 - \frac{\varepsilon_0 R_i}{\mu_+ e}\right)\right] && \text{at} \quad \varphi = U_- : \Phi = U_-,\ \xi = \frac{U_0}{U_-}. \qquad (1) \\
&\frac{d\rho_-}{d\varphi} = \frac{1}{\varepsilon_0 \xi E'^2}\left[\rho_+\rho_-\left(1 - \frac{\varepsilon_0 R_i}{\mu_- e}\right) - \rho_-^2\right]
\end{aligned}$$

This TBVP is then converted to an equivalent optimization problem by the shooting method. However, the conventional deterministic optimization methods are usually unable to get the solution of the optimization problem, due to the lack of approaches for choosing proper initial values for the concentration of the ions on the conductor surfaces.

In this paper, the continuous Tabu search, which is a heuristic global optimization method, is adopted to solve the optimization problem. It can provide the result in the global optimization sense, without relying on the initial values. In the evaluation of the objective function, the numerical integration applied to the ODEs is simplified by using Haar wavelets, in which the ODEs are transformed into algebraic equations and the integral operator is replaced by an operational matrix. Compared to the conventional Runge-Kutta integration method, the solution of the TBVP with Haar wavelets is more efficient and suitable for solving the ion distribution with abrupt variations.

The proposed method is verified by comparing it with the empirical formulas of the corona loss for the single-circuit bipolar lines. With this new method, it is found that for the vertically arranged double-circuit lines, the corona loss can be much smaller than the single-circuit lines by reducing the vertical inter-spacing between the two circuits, which implies that the construction of the double-circuit HVDC transmission lines can be more economical.

Measurement and Interpretation of Radar Cross Section Data in an Educational Setting: A Comparison between Simulations and Experiments

M. A. Alves[1], **I. M. Martins**[2, 3], **A. C. Coelho**[2],
L. C. Folgueras[1], **and M. C. Rezende**[1]

[1]Instituto de Aeronáutica e Espaço, Divisão de Materiais, CTA, São José dos Campos, SP, Brazil
[2]Instituto Tecnológico de Aeronáutica, CTA, São José dos Campos, SP, Brazil
[3]Universidade de Taubaté, Taubaté, SP, Brazil

Abstract— Radar technology is ubiquitous in modern society. Its application spectrum is very wide and new civilian and military uses for radar are currently being developed. Radars can be used in rather mundane situations such as speed detectors or they can be carried on spacecraft to the far reaches of the Solar System to map the surfaces of unexplored bodies. Although contact with radar technologies happens on a daily basis, few undergraduate students have a good grasp of the basics of radar operation and interpretation of radar data. This is understandable given that the mathematics and physics involved in the explanation of this type of phenomenon is very complicated. In order to improve the understanding of radar technology and especially the interpretation of radar cross section (RCS) data by undergraduate students, we developed a study where the RCS of objects having simple and complex geometries were obtained using a simulation software tool and a radar training system. This training system consisted of inverse synthetic aperture radar designed to operate at close range in an academic laboratory or classroom environment. Both simulations and measurements were made at 9.4 GHz (X band). The radar operated in a monostatic configuration, and vertically polarized electromagnetic waves illuminated the study objects; these conditions were also used by the simulation software. The comparison of results obtained by both methods served to demonstrate the advantage of using simulations and experimental data to interpret RCS data. Moreover, the simulations provided the students with a wealth of visual information and the radar operation allowed the students valuable hands-on experience with rather sophisticated equipment. Thus, simulations and measurements, in this type of setting, supplemented each other and their simultaneous use proved to be a powerful educational tool.

Single- and Multi-layer Microwave Absorbing Material Based on Conducting Polyaniline and Polyurethane Polymers for Operation in the X-band

L. C. Folgueras[1], **M. A. Alves**[1], **I. M. Martin**[2, 3], **and M. C. Rezende**[1]

[1]Instituto de Aeronáutica e Espaço, Divisão de Materiais, CTA, São José dos Campos, SP, Brazil
[2]Instituto Tecnológico de Aeronáutica, CTA, São José dos Campos, SP, Brazil
[3]Universidade de Taubaté, Taubaté, SP, Brazil

Abstract— The presence of spurious electromagnetic radiation at microwave frequencies in the environment has become an ever-growing problem, with the potential to affect deleteriously the proper functioning of many types of sensitive electronic equipment. Many technologies have been developed to minimize this type of interference: from shielding in the form of bulky metallic boxes to thin films and paints that absorb the incident electromagnetic radiation. In this work, absorbent materials were produced in the form of single- and multi-layer flexible sheets containing the conducting polymer polyaniline dispersed in a polyurethane matrix. The flexible sheets consisted of 1, 2, 3 and 4 layers of absorbing materials, each having different electromagnetic properties. The absorbing materials thus produced are flexible and lightweight and can serve as an alternative to microwave absorbers produced with more traditional and heavier components such as ferrites. Individual and combined electromagnetic properties of these materials were analyzed using the waveguide technique in the frequency range of 8 to 12 GHz (X-Band). The absorption of the incident electromagnetic radiation was measured for all materials as function of the wavelength. From the measurements of the scattering parameters, the complex permeability and permittivity were also obtained as a function of the wavelength of the materials. The multi-layer materials exhibited characteristics of broadband absorbers in the frequency range studied. The measured absorption of these materials was compared with absorption values derived from analytical calculations. The good agreement between these set of values demonstrate that the techniques used for the characterization of the materials is valid.

Identification for Wiener Model Based on Improved PSO

Y.-H. Chen and W.-X. Lin
Faculty of Information Science and Technology, Ningbo University, Ningbo, China

Abstract— This paper studies in identification for a class of nonlinear systems described by Wiener model based on improved PSO (Particle Swarm Optimization). The nonlinear system identification problem is equivalent to the nonlinear minimization problem with the estimated parameters as the optimized variables subjected to different constraints. PSO is a parallel algorithm based on swarm intelligence which is used to obtain the optimal solution to the minimization problem (i.e., the optimal estimation of Wiener model parameters). It is also an efficient stochastic global optimization technique, where each particle represents a solution to the problem being optimized. It can find the optimal regions of complex search spaces through the interaction of individuals in a population of particles. However, the standard PSO (SPSO) has some defects such as poor global search ability, not fast enough to be convergent and so on. In order to overcome these defects, an improved PSO (IPSO) is proposed which sets inertial weight according to the optimal damping ratio. Simultaneously, convergency analysis from control theory is carried out and a range of inertia weight which is a crucial parameter to keep balance between exploration and exploitation is given in convergence. A numerical simulation of a Wiener model identification applying the improved PSO algorithm is provided to verify the effectiveness. The result shows that IPSO achieves better performance in identification for Wiener model.

A Circular Multi-conductor Transmission Line Model for Simulation of Very Fast Transient in Circular Windings

Y. Yang and Z. J. Wang
State Key Lab. of Power Systems, Department of Electrical Engineering
Tsinghua University, China

Abstract— While modeling the windings under high frequency conditions, the turn-to-turn model based on multi-conductor-transmission-line (MTL) is usually used so that the wave propagation in the turns could be well considered. To use that method the circular coils should approximate to a group of parallel straight lines with the same line length. However, in a large power transformer the difference of the turn lengths at inner diameter and outer diameter may be large, say from 15% to 20%. When all turn lengths are assumed to be the same, the coefficient matrices of the MTL equation are not real unit length parameters. Also, it is hard to explain if the assumption of same turn-length could cause inaccuracy in MTL model or not.

In this paper a circular MTL (CMTL) model is developed on cylindrical coordinate for modeling wide frequency transient response in core-type transformer windings. As the insulation distances between turns are very small compared with the wavelength and the turn-length and the resistive losses are very small, so that the tangential components of electrical strength and magnetic strength can be ignored in the process of mathematical development. Hence the equations of voltage and current distribution along the coil can be obtained as follows:

$$\frac{\partial u}{\partial \theta} = \frac{\partial}{\partial t}\int_1^2 (rB_z dr - rB_r dz) = \frac{1}{d\theta}\frac{\partial}{\partial t}\int_1^2 (B_z ds_z - B_r ds_r) = \frac{\partial \phi}{\partial t} = -L_\theta \frac{\partial i}{\partial t}$$

$$\frac{\partial i}{\partial \theta} = \frac{\partial}{\partial t}\oint (-rD_z dr + rD_r dz) = -\frac{1}{d\theta}\frac{\partial}{\partial t}\oint (D_z ds_z - D_r ds_r) = -\frac{\partial q}{\partial t} = -C_\theta \frac{\partial u}{\partial t}$$

The electrical and magnetic coupling effects between turns are represented respectively by the capacitance and inductance matrixes. Different from the straight MTL model, the equations of the CMTL model are built in the cylindrical coordinate system, where the parameter matrixes per radian are calculated. In this way, all lines are measured with the same 'length' starting at 0 radian and end at 2π radian.

Based on the proposed model, the characteristics of the travelling wave in the winding are discussed in details and some interesting conclusions are obtained. Firstly, since the transient wave has the same line velocity, so that the travelling time on each turn of different radius will be different. This will cause the coupling of the travelling voltages and currents in each turns more complicated. Secondly, ignoring the electromagnetic wave inside the conductor at high frequency region, the capacitance and inductance matrix have a simple relationship of $[L][C] = [C][L] = \mu\varepsilon$ [1] in MTL model, but there is no such relationship in CMTL model. Thirdly, CMTL model can be equivalently transformed to MTL model where all lines have the same length, while the coefficient matrixes should be calculated in the original circular system.

A New Wideband Vertical Transition between Coplanar Waveguide and Coplanar Stripline

Daqun Yu[1] **and Ruiping Zhu**[1, 2]

[1]Nanjing Research Institute of Electronics Technology
Nanjing 210013, China
[2]China National Key Laboratory of Antenna and Microwave Technology
Nanjing 210013, China

Abstract— A new wideband vertical transition between coplanar waveguide (CPW) and coplanar stripline (CPS) is proposed and analyzed in this paper. It functions as an unbalanced-to-balanced (balun) transformer as well. This new transition utilizes CPW-slotline mode conversion phenomenon to convert CPW mode to CPS mode. Ansoft HFSS is employed to analyze this vertical transition which is based on thin-membrane structure and a very wide transition bandwidth is observed.

A Novel Configuration of Temperature Compensation in Rectangular Waveguide Resonant Cavities

Xiao-Dan Pan and Qiang Sui
Communication University of China, Beijing, China

Abstract— In this paper, the frequency shift of rectangular waveguide resonant cavity caused by temperature change is discussed. Analytical results in different situations are presented in the paper. A metal cylinder is applied in rectangular waveguide. By changing some parameters, such as the diameter and the depth of the metal cylinder inserted into the resonant cavity, a perfect temperature compensation performance can be achieved.

A novel temperature compensation method is proposed, in which SCM (Single Chip Microcomputer) is used to control the depth of the metal cylinder inserted into a resonant cavity in order to adjust resonant frequency which is caused by temperature change. A frequency compensation system which is based on the SCM and digital monobus technology is designed. This system is studied mainly by using AT89C51 single chip, 1-wire digital temperature transducer DS18B20, LCD, L297, L298 and linear-stepping motor. Taking temperature as the parameter, it can communicate with the single chip and control the linear-stepping motor to impel the metal cylinder up and down, so that the frequency shift can be compensated. In this system, the change of the temperature in the cavity is transformed into the change of electric current and then into the change of voltage by using the temperature sensor. The change of voltage is input into the A/D conversion units and the output is dealt with by SCM. Under the control of the SCM, the metal cylinder is droved by linear-stepping motor to change the depth inserted into the resonant cavity. At the same time, the real time temperature in the cavity can also be displayed on the LCD under the control of SCM.

The proposed method is applied on a rectangular waveguide cavity, which is equipped with the proposed temperature-compensation system. Experiment verification of the rectangular waveguide has been carried out, and the results of simulation and measurement are given in this paper. The results demonstrate that by using the temperature-compensation system, the resonant frequency remain approximately unchanged.

Universal Electronically Tunable Current-mode Filter Using CCCIIs

H.-P. Chen and P.-L. Chu
Department of Electronic Engineering, De-Lin Institute of Technology, Taiwan, R.O.C.

Abstract— A novel universal electronically tunable current-mode filter with three inputs and three outputs using three multiple-output current-controlled conveyors (MO-CCCIIs) and two grounded capacitors is proposed. The proposed configuration can be used as either a single-input three-output or three-input single-output. It can simultaneously realize all five different generic filtering signals: lowpass, bandpass, highpass, bandreject and allpass, unlike the previously reported works. It still maintains the following advantages: (i) the employment two grounded capacitors ideal for integrated circuit implementation, (ii) high output impedance good for cascadability for the current-mode circuits, (iii) no need to impose component choice, (iv) no need to employ inverting-type current input signals, and (v) low active and passive sensitivity performances. H-Spice simulations with TSMC 0.35 µm process and ±1.65 V supply voltages are included and confirm the theoretical predictions.

Planar Fresnel Zone Lens Antenna

Cheng-Hung Lin[1], **Guan-Yu Chen**[2], **Jwo-Shiun Sun**[2], **Kwong-Kau Tiong**[1], **Yu-Hsiang Chen**[1], **Tsan-Hsuan Peng**[1], **and Y. D. Chen**[3]

[1]Department of Electrical Engineering, National Taiwan Ocean University, Taiwan
[2]Department of Electronic Engineering, National Taipei University of Technology, Taiwan
[3]Antenna and EMC Laboratory, HTC, Taiwan

Abstract— The Fresnel zone plate is a planar device that produces lens-like focusing and imaging of electromagnetic waves. In this design, we want to develop a planar Fresnel zone antenna with high gain and low side-lobe planar focusing antenna. Based on Fresnel diffraction theory and simulate the EM wave analysis, and measured the radiation pattern. The characteristics of pattern radiation of gain, efficiency, and low side-lobe by measured data. These effects are produced by diffraction, rather than refraction. The zone plate transforms a normally incident plane wave into a converging wave, concentrating the radiation field in a small region about a point that has all the characteristics usually associated with the focal point of a metal lens, as shown in Figure 1 [1].

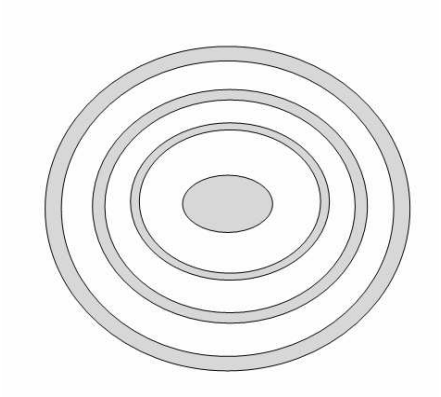

Figure 1: The fresnel zone plate antenna structure.

REFERENCES

1. Hristov, H. D., *Fresnel Zones in Wireless Links, Zone Plate Lenses and Antennas*, Artech House, 2000.

Cylindrical DR Antenna Design

Cheng-Hung Lin[1], **Guan-Yu Chen**[2], **Jwo-Shiun Sun**[2], **Kwong-Kau Tiong**[1], **Tsan-Hsuan Peng**[1], **Yu-Hsiang Chen**[1], **and Y. D. Chen**[3]

[1]Department of Electrical Engineering, National Taiwan Ocean University, Taiwan
[2]Department of Electronic Engineering, National Taipei University of Technology, Taiwan
[3]Antenna and EMC Laboratory, HTC, Taiwan

Abstract— Dielectric resonator antennas (DRA) are attractive as alternative to patch antennas because of their small size and wideband bandwidth. This DRA is positioned over a feeding pad in a conducting ground plane in a way that excites the ***HEM*** mode. The DRA offer advantages such as low cost, ease of manufacture, wider bandwidth, and high radiation efficiency. This design presents an examination of DRA (Fig. 1) operated at C band frequencies. A parametric study is performed to optimize the antenna performance and a prototype for microwave and WLAN application has been designed and measured.

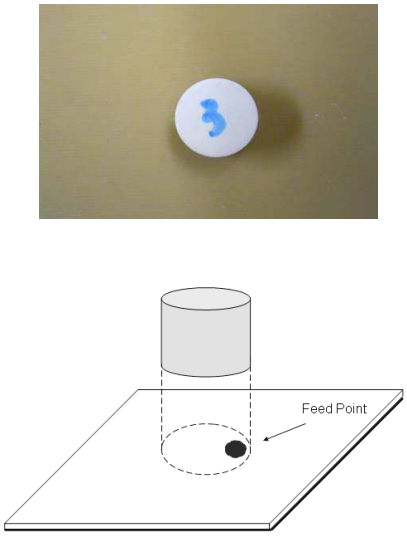

Figure 1: The proposed DR antenna structure.

Antenna Pattern Measurement

Guan-Yu Chen[1], **Jwo-Shiun Sun**[1], **Kekun Chang**[1], **and Y. D. Chen**[2]

[1]Department of Electronic Engineering, National Taipei University of Technology, Taiwan
[2]Antenna and EMC Laboratory, HTC Corporation, Taiwan

Abstract— Wireless systems, especially require antennas and wireless system integration and requirements. They include operation near the human body effect, operation in a multi path and fading environment, extremely small antenna size, receiver diversity, multi frequency operation, radiation pattern performance and adaptive antenna techniques. Unique quality factors, in contrast to the classical ones, are also introduced such as parameters of total radiation efficiency, mean effective gain and correlation coefficience. A measurement method [1, 2] is described for analying the pattern averaged gain (PAG) mean effective gain (MEG) of antenna in 3D far field chamber environment. By using (1) and (2) the expression for the PAG and MEG can be calculate [1, 2]. And the mean incident power ratio P_V/P_H represents the cross polarization power ratio (XPR), by using (3). Based on response of mobile antenna, the 3D measured results of PAG, MEG, and XPR are measured.

$$G_e = \frac{P_{rec}}{P_V + P_H} \tag{1}$$

$$\begin{aligned} P_{rec} &= \int_0^{2\pi}\int_0^{\pi} \{P_1 G_\theta(\theta,\phi)P_\theta(\theta,\phi) + P_2 G_\phi(\theta,\phi)P_\phi(\theta,\phi)\}\sin\theta d\theta d\phi \\ G_e &= \int_0^{2\pi}\int_0^{\pi} \left\{\frac{XPR}{1+XPR}G_\theta(\theta,\phi)P_\theta(\theta,\phi) + \frac{1}{1+XPR}G_\phi(\theta,\phi)P_\phi(\theta,\phi)\right\}\sin\theta d\theta d\phi \end{aligned} \tag{2}$$

$$XPR = \frac{P_V}{P_H} \tag{3}$$

REFERENCES

1. Taga, T., "Analysis for mean effective gain of mobile antennas in land mobile radio environments," *IEEE Transaction on Vehicular Technology*, Vol. 39, 117–131, 1990.
2. Douglas, M. G., M. Okoniewski, and M. A. Stuchly, "A planar diversity antenna for handheld PCS devices," *IEEE Transaction on Vehicular Technology*, Vol. 47, 747–754, 1998.

Simulation of Induction Cookers with Different Structure and Material Parameters by the Finite Element Software

Li Hao, **Yueqin Dun**, **and Jiansheng Yuan**
State Key Lab of Power Systems, Tsinghua University, Beijing 100084, China

Abstract— An induction cooker is usually made up of a flat-type spiral coil, on which the pan to be heated is placed. Beneath the coil a ferrite disc is placed to obtain strong magnetic field. The basic principle of induction cooking is electromagnetic induction law and the eddy current loss. The eddy current loss is of non-linear relationships with the electrical and structure parameters. Generally, it is not easy to obtain the quantitative influence with the eddy current loss by the parameters. We must employ the software for electromagnetic field numerical calculation to simulate the induction cookers.

The coupling between the coil and the pan is modeled as the series connection of an inductor and a resistor, based on the transformer analogy. The value of the equivalent inductor and resistor can be obtained by the electromagnetic field analysis on induction cooker. And then the power and the efficiency of induction cooker can be calculated by the circuit analysis method.

In this paper, the electric power and the efficiency of induction cookers, concerning with different electrical and structure parameter, are simulated by the finite element software. The parameters include the frequency of exciting current, different material and thickness of the pan, different height between the coil and the bottom of the pan, as well as different material and thickness of the ferrite disc. Meanwhile, the effect of adjusting some parameters has been measured. The experimental and the computational results are in good agreement.

By the simulation, the efficiency of induction cookers against the frequency of exciting current, the permeability and the conductivity of the pan, and the thickness of the pan is obtained. The parameters which may provide the highest efficiency are suggested. The electromagnetic environment is also analyzed around the cookers, based on the electromagnetic field restriction standard.

Measurement and Analysis of Radiated Electromagnetic Fields around the Pulsed Power Supplies

Ronggang Cao[1], **Jihuan Tian**[1], **Peizhu Liu**[2], **Jun Li**[2], **and Jiansheng Yuan**[1]

[1]State Key Lab of Power Systems, Tsinghua University, Beijing 100084, China
[2]Beijing Institute of Special Electromechanical Technology, Beijing 100012, China

Abstract— The pulsed power supply generates great current pulse that would reach several hundreds thousands amperes. Thereby, the measurement of the spatial and temporal distributions of the radiated electromagnetic fields could be useful to analyze the electromagnetic interference to the electronic apparatuses around the power supply. Two types of pulsed power supplies are focused. They all use capacities as their energy storage modules, while one type of supply uses trigatron switches (the spark gap switch with three electrodes), and the other uses SCR (Silicon Controlled Rectifier). The main pulse current of the first supply lasts several milliseconds, and the current peak can reach up to 40,000 amperes. The second also lasts several milliseconds, and the current peak reaches up to 500,000 amperes. Several B-dot loop probes, D-dot probes and a digital oscilloscope, with enough sampling rate and memory depth, are used to measure the magnetic field and the electric field around the supplies separately. The magnetic field near the switches of the two types of supplies is focused especially. By the measurement of the radiated magnetic field around the supplies, we get the spatial and temporal distributions of magnetic field. The probe proofreading certification experiment is also developed to verify the probe coefficients. With the corrected experimental data, we get the waveforms of magnetic field in time domain. The electric field around the supplies is very small.

The different characteristics of the electromagnetic filed between the two types of supplies will be discussed in the full paper. The comparisons between the two pulsed power supply, using trigatron switches and SCR respectively, have been made, and the results show that the radiation magnetic field of the pulsed power supply using spark gap switches has the spectrum that could reach up to 10 MHz, while the spectrum of the supply using SCR is less than 100 kHz.

Numerical Study of IEEE 802.15.4 Performance

Shuai Fang[1], **Lu Rong**[2], **Qiang Xu**[1], **and Yang Du**[1]

[1]The Electromagnetics Academy at Zhejiang University, Zhejiang University
Hangzhou 310058, China
[2]Shanghai Research Center for Wireless Communications
Shanghai 200050, China

Abstract— IEEE 802.15^{TM} working group has designed the IEEE 802.15.4 standards to target the low-rate wireless personal area network (LR-WPAN) which is characterized by low complexity, low cost and low power. The IEEE 802.15.4 standards specify operations of the physical layer (PHY) and medium access control (MAC) sublayer. These standards are to ensure acceptable system performance in terms of network PHY collisions, MAC collisions, throughput, average transmission delay and energy efficiency. Yet there are a number of factors that may affect the system performance, including beacon order (BO), backoff exponent (BE), contention window (CW), existence of hidden terminal problem, and existence of acknowledgement (ACK) mechanism. Understanding the impacts of these factors is of great importance in system design to improve performance. These impacts are examined numerically via network simulator (NS2) in the current work, which leads to some nontrivial findings.

Analysis of Performance of Unsaturated Slotted IEEE 802.15.4 Medium Access Layer

Shuai Fang[1], **Lu Rong**[2], **Qiang Xu**[1], **and Yang Du**[1]

[1]The Electromagnetics Academy at Zhejiang University, Zhejiang University
Hangzhou 310058, China
[2]Shanghai Research Center for Wireless Communications
Shanghai 200050, China

Abstract— In this paper, we analyze the performance of unsaturated slotted medium access layer (MAC) as specified by the IEEE 802.15.4 standard. The analytical tool that we use to model the behavior of uplink transmission of a standard compliant device is the Markov chain model, a general framework that also used by some other researchers (e.g., Bianchi, Pollin, Misic). Yet we deviate from their approaches essentially in one way or another. We consider different types of traffic, including saturated and unsaturated, with the source process being Poisson. In the unsaturated case, the idle time is allowed to be random to reflect the realistic scenario. We discard the assumption about independent carrier sensing probabilities among devices, except for the first transmission attempt. When retransmission is required due to collision, there are conditions under which independence of carrier sensing may or may not hold. Such conditions are explicitly identified and incorporated in our model. The effect of beacon order (BO) is also included. Validity of our model is verified by good agreement between model predictions and numerical simulations via Network Simulation (NS2) of key model parameters and of system performance descriptors such as throughput.

Energy-efficient Scheme for IEEE 802.15.4 Compliant Device

Qiang Xu[1], **Lu Rong**[2], **Shuai Fang**[1], **and Yang Du**[1]

[1]The Electromagnetics Academy at Zhejiang University, Zhejiang University
Hangzhou 310058, China
[2]Shanghai Research Center for Wireless Communications
Shanghai 200050, China

Abstract— Low-rate personal area network (LR-WPAN) specified by the IEEE 802.15.4 standards is characterized by low complexity, low cost and low power. It holds great potential in many fields, such as telemetry, patient monitoring, and industrial automated control. Yet one of the most important determining factors is the power consumption, since most standards compliant devices are believed to be battery-powered.

In this paper, we analyze power consumption of the sleep mode, specifically, the indirect mode in downlink transmission and the direct mode in uplink transmission. Analysis by other researchers and by our own indicates that overhearing presents a significant problem in energy waste and should be avoided. Yet unlike the case of IEEE 802.11 wireless local area network (WLAN) where RTS/CTS mechanism is specifically adopted to this end, LR-WPAN is designed to operate without RTS/CTS to reduce system complexity. To attack the overhearing problem, we propose a sleep mechanism in the backoff stage in uplink transmission. The efficiency of such mechanism is evaluated analytically using the system model that we have recently developed and is verified numerically via network simulator (NS2).

Throughput Analysis of Delayed Acknowledgement over 802.15.3 WPAN with Hybrid ARQ Retransmission

R. F. Lin[1], **L. Rong**[2], **Q. Xu**[1], **and Y. Du**[1]

[1]The Electromagnetics Academy at Zhejiang University, Zhejiang University
Hangzhou 310058, China
[2]Shanghai Research Center for Wireless Communications
Shanghai 200050, China

Abstract— The EU IST project My personal Adaptive Global NET (MAGNET) project aims at user-centric service provision, with an emphasis on personalisation, adaptation, interoperability, personal networking and interconnecting heterogeneous networks. It strives to provide users secure and seamless communications. Yet it is a challenging task to maintain a guaranteed QoS for all in-session traffic flows when a moving cluster of a personal network (PN) causes the micro- or macro-mobility handoff. The primary QoS parameters of concern are end-to-end packet delay and packet loss. The high data rate (HDR) services of MAGNET project to large degree belong to the QoS sensitive streaming multimedia traffic, thus require a handoff delay under 100 ms according to the ETSI QoS specification.

In this paper, we propose a handoff scheme that incorporates two mechanisms: 1) make-before-break to realize soft handoff; 2) SIP, since its operation is transparent to the underlying network, thus well suitable for interconnecting heterogeneous networks, and in the meanwhile it is heavily deployed in the 3GPP standards.

However, there are still other issues to be considered. For instance, in the old SIP handoff scheme, it will send a new INVITE to establish connection after obtaining the new IP address, which causes packet loss and considerable re-connection delay. To deal with this issue, we propose to use the INVITE/JOIN mechanism. The associated potential redundancy at both the mobile host (MH) and corresponding host (CH) is also well taken care of. Finally we present some numerical results to demonstrate the effectiveness of our approach.

Comparative Study of MAC Scheduling Schemes for IEEE 802.15.3

GuangDi Yang[1], **Lu Rong**[2], **Dingyuan Tu**[2], **Rufeng Lin**[1], **and Yang Du**[1]

[1]The Electromagnetics Academy at Zhejiang University, Zhejiang University
Hangzhou 310058, China
[2]Shanghai Research Center for Wireless Communication
Shanghai 200050, China

Abstract— In this paper we examine the performance of a variety of HDR MAC scheduling schemes using numerical simulations, with a focus on channel aware schemes. The performance determinant factors, such as traffic characteristics, terminal mobility, and channel conditions, are included in this study in order to ensure the results more relevant to realistic wireless personal area network (WPAN) scenarios.

The scheduling algorithms under consideration are 1) SRPT; 2) the exponential rule (EXP); 3) the modified largest weighted delay first rule (M-LWDF); 4) the proportionally fair rule (PROP-FAIR); and 5) the maximum rate rule (MAX-RATE). We find that under good channel conditions and light network load, the EXP and M-LWDF algorithms tend to have better performance in terms of average throughput and job failure than others; on the other hand, under heavy traffic conditions, these two schedulers suffer from a drastic performance degradation, since none of them gives sufficient consideration for the cases of packet loss or timeout. SRPT rule appears to have the minimal system response time in this case. In addition, because of its non-preemptive characteristic, SRPT is fairly robust among these schedulers against adverse channel conditions and heavy traffic load. However, since SRPT prefers small packets to large ones, it is unsuitable for cases where large packets are important.

Our findings shed light on the features of the prevailing scheduling algorithms and their suitability in WPAN flow scheduling, and are useful in designing new scheduling algorithms.

On the Convergency Properties of Translational Addition Theorems

W. Z. Yan[1], **H. Wu**[1], **Y. Du**[1], **Q. W. Xiao**[1], **D. W. Liu**[1], **and J. A. Kong**[1, 2]

[1]The Electromagnetics Academy at Zhejiang University, Zhejiang University
Hangzhou 310058, China
[2]Department of Electrical Engineering and Computer Science
Massachusetts Institute of Technology, Cambridge, MA02139, USA

Abstract— Translational addition theorems are powerful analytic tools to translate a multipole expansion of an electromagnetic field from one to another coordinate system and are of considerable importance for a wide range of electromagnetic scattering problems. For instance, to study the multiple volumes scattering behavior, a coupled linear system may be used, where the electromagnetic fields are expanded in terms of vector spherical harmonics, which may need to be translated from the center of a scatterer to that of another. The convergence property of translational addition theorem thus bears its influence on the convergence of the linear system.

In this paper we review several efficient methods for calculating both scalar and vector translation additional coefficients and check the convergence properties of translational addition theorem from a numerical point of view. As expected the convergence behavior depends on the configuration and the harmonic function. For the extreme cases there may only need a few addition terms to guarantee convergence on one hand and a few hundred terms on the other hand. The latter case indicates that caution may need to be taken against common engineering practice where several tens of terms are commonly used. We illustrate such effect through multiple-sphere scattering problems.

SIP-based Mobility Management in HDR System

Bing Zhao[1], **Lu Rong**[2], **Peng Qiao**[1], **and Yang Du**[1]

[1]The Electromagnetics Academy at Zhejiang University
Zhejiang University, Hangzhou 310058, China
[2]Shanghai Research Center for Wireless Communications, Shanghai 200050, China

Abstract— The EU IST project My personal Adaptive Global NET (MAGNET) project aims at user-centric service provision, with an emphasis on personalisation, adaptation, interoperability, personal networking and interconnecting heterogeneous networks. It strives to provide users secure and seamless communications. Yet it is a challenging task to maintain a guaranteed QoS for all in-session traffic flows when a moving cluster of a personal network (PN) causes the micro- or macro-mobility handoff. The primary QoS parameters of concern are end-to-end packet delay and packet loss. The high data rate (HDR) services of MAGNET project to large degree belong to the QoS sensitive streaming multimedia traffic, thus require a handoff delay under 100 ms according to the ETSI QoS specification.

In this paper, we propose a handoff scheme that incorporates two mechanisms: 1) make-before-break to realize soft handoff; 2) SIP, since its operation is transparent to the underlying network, thus well suitable for interconnecting heterogeneous networks, and in the meanwhile it is heavily deployed in the 3GPP standards.

However, there are still other issues to be considered. For instance, in the old SIP handoff scheme, it will send a new INVITE to establish connection after obtaining the new IP address, which causes packet loss and considerable re-connection delay. To deal with this issue, we propose to use the INVITE/JOIN mechanism. The associated potential redundancy at both the mobile host (MH) and corresponding host (CH) is also well taken care of. Finally we present some numerical results to demonstrate the effectiveness of our approach.

Diffraction Grating of Azo Dye Doped Liquid Crystals

Shuan-Yu Huang[1] **and Chie-Tong Kuo**[2]

[1]Department of Optometry, Chung Shan Medical University
No. 110, Sec. 1, Jianguo N. Rd., Taichung 402, Taiwan
[2]Department of Physics and Center for Nanoscience and Nanotechnology
National Sun Yat-sen University, Kaohsiung 804, Taiwan, R.O.C.

Abstract— Diffraction properties of azo dye doped liquid crystals with a periodic electrode are studied. With an external voltage of $\sim 5.0\,\mathrm{V}$, the first order diffraction can reach to a maximum value in this experiment. The polarization state of the first order is also discussed, and it shows $+1$ and -1 diffraction orders are antisymmetrical. The intensity of diffraction can be improved with appropriate amount of azo dye.

EM Inverse Scattering Versus Compressive Sensing: A New Perspective to an Old Discussion

Lianlin Li, **Wenji Zhang**, **Yin Xiang**, **and Fang Li**
Institute of Electronics, Chinese Academics of Sciences, Beijing, China

Abstract— Recently, Compressive Sensing (CS) proposed by Donoho, Candes, Romberg and Tao et al. is a revolutionary signal sensing theory, consequently, become a very attractive and promising field, by which the data can be sampled much less than one required by Nyquist principle.

From the Nyquist's viewpoint, the solution to the considered problem is non-unique if the measured data are under-sampled; however, from the CS's viewpoint, the solution to the same problem can be unique only if the measure matrix satisfies the so-called restricted isometry principle (RIP) (see Appendix). In this presentation, within the framework of CS, the unique solution to the problem of diffraction tomography is reconsidered, by which the optimal sampled data related to the unknown object(s) is constructed. In addition, the well-known migration algorithm(s) is/and also checked, from which the sample data also can be much smaller than one required by Nyquist principle.

Appendix: The Restricted Isometry Principle (RIP)

Considering the complex matrix Φ with size of n by m ($n << m$), let $T \subset J$ be a set of indices, where the set $J = \{1, 2, \ldots, m\}$ indexes all columns of Φ; T identifies an indexed subset of columns in Φ, and Φ_T represents the submatrix Φ for which only these columns are retained. Consider $\Phi_T c = \sum_{j \in T} c_j f_j$, where f_j represents the jth column of Φ, and the c_j are the arbitary complex numbers. Candes and Tao define the S-restricted isometry constants δ_S to be the smallest quantity such that Φ_T obeys $(1 - \delta_S) \|c\|_{l_2}^2 \leq \|\Phi_T c\|_{l_2}^2 \leq (1 + \delta_S) \|c\|_{l_2}^2$ for all subsets $T \subset J$ of cardinality $|T| \leq S$ and all complex coefficients $\{c_j\}_{j \in T}$.

Session 2A1
Plasmonics Nanophotonics: Theory

Dirac Spactra in Plamonic Systems: Honeycomb and Triangular Lattices

Dezhuan Han and C. T. Chan
The Hong Kong University of Science and Technology
Clear Water Bay, Kowloon, Hong Kong, China

Abstract— Recently, graphene has received considerable interest because of the existence of Dirac points that offer remarkable electronic properties due to the specific topology of the band dispersion. The Dirac spectra in two dimensional (2D) photonic crystals (PCs) for electromagnetic waves have also been identified and the Dirac-point-derived edge states are found to exhibit novel transportation properties when time-reversal symmetry breaking is introduced. Although both graphene and 2D PCs support Dirac dispersions, the Dirac spectrum in graphene is derived directly from the nearest-neighbor hopping of bound electron states in a honeycomb lattice, while that in 2D PCs is a consequence of the coupling of scattering photons. In this work, we study theoretically the plasmonic band structures of metal nanospheres arranged in honeycomb and triangular lattices. The plasmonic lattice is an open system that supports both guided modes and leaky modes, and in this context, it bears similarity to both electronic systems and PCs. On the other hand, unlike the Dirac dispersions found in graphene and 2D PCs, which are for "scalar waves" only, the plasmonic systems require vector wave description. Our results reveal the honeycomb plasmonic lattice possesses Dirac points for out-of-plane and in-plane modes that bear respectively scalar wave and vector wave characteristics. We also found guided edge states when an edge is present in semi-infinite (finite) systems. The conditions for the existence of Dirac-point-derived edge states in honeycomb plasmonic lattices are derived analytically. The difference between honeycomb and triangular lattices is discussed.

Hybrid Plasmonic Excitation Induced Optical Rotation at Near-IR Wavelength

Tao Li, **Hui Liu**, **Shu-Ming Wang**, **and Shi-Ning Zhu**
National Laboratory of Solid State Microstructures
Nanjing University, Nanjing 210093, China

Abstract— Since the pioneering work of extraordinary optical transmission (EOT) [1], the interaction between the light and surface plasmon in metallic micro/nano structures has arrested a growing attention of researches. However, most of these works are focused on the enhanced intensity of transmitted light. On the other hand, polarization property is another important feature of the optics. Although some research noticed effect using metamaterial to manipulate the polarization of the electromagnetic waves, their studies either acquired complex nanostructures [2] or performed at microwave region [3]. So in this study [4], we make a detailed investigation on the polarized optical transmission properties through an L-shaped hole array in silver film at near-IR wavelength. Besides the enhanced transmission due to the combined plasmonic excitations, strong optical rotation was definitely observed at specific polarized incidences. After elaborate analyses, two eigenmodes were clearly characterized as the results of the hybrid localized plasmon resonances. Any polarization states from the incidences will degenerate into these two eigenstates after transmissions, suggesting a practical method to manipulate the polarization of light. Our result demonstrates the giant rotation rate achieved by the nanothin sample, indicating potential applications in the micro-optical devices.

REFERENCES

1. Ebbesen, T. W., H. J. Lezec, H. F. Ghaemi, T. Thio, and P. A. Wolff, *Nature*, Vol. 391, 667, London, 1998.
2. Theil, M., M. Decker, M. Deubel, M. Wegener, S. Linden, and G. von Fremann, *Adv. Mater.*, Vol. 19, 207, 2007.
3. Hao, J. M., Y. Yuan, L. X. Ran, T. Jiang, J. A. Kong, C. T. Chan, and L. Zhou, *Phys. Rev. Lett.*, Vol. 99, 063908, 2007.
4. Li, T., H. Liu, S. M. Wang, X. G. Yin, F. M. Wang, S. N. Zhu, and X. Zhang, *Appl. Phys. Lett.*, Vol. 93, 021110, 2008.

Tunable Plasmonic Metamaterials for Subwavelength Focusing

Xueqin Huang, **Shiyi Xiao**, **and Lei Zhou**
Surface Physics Laboratory (State Key Laboratory) and Physics Department
Fudan University, Shanghai 200433, China

Abstract— We show that a metallic plate with subwavelength fractal-shaped slits supports surface plasmon polaritons with plasmon frequencies *tuned efficiently* by the geometry of the fractal structure. We derive effective-medium models to describe such *tunable* plasmonic metamaterials (TPM), and found that the latter can mimic plasmonic metals in frequency regimes beyond the (*fixed*) plasmon frequencies of natural metals (gold, silver, etc.). As one application of our TPM, we show that one can use it to focus light sources with subwavelength imaging abilities and enhanced field strengths. Finite-difference-time-domain (FDTD) simulations are performed to design realistic TPM's and verify all predicted phenomena.

Local Transmission Amplification for Resonant Tunneling Effects Caused by Surface Plasmon Excitations

Peng-Hsiao Lee and Yung-Chiang Lan
Institute of Electro-optical Science and Engineering
National Cheng Kung University, Taiwan, R.O.C.

Abstract— Surface plasmons (SPs) are the coherent fluctuations of the electron charges at the metal-dielectric interface. The phenomenon of resonant tunneling through thin metal films with periodic grooves is attributed to excitation of standing waves of coupled SP modes in the grooves on two opposite surfaces. The tunneling frequencies and transmission powers can be modulated by changing relative permittivity filling in the grooves, which results from the change in characteristics of coupled SPs of the metal-insulator-metal structure.

In this work, enhancement of the local transmission power in the main groove for resonant tunneling by adjusting relative permittivity filling in the side grooves is proposed and studied via computer simulation. The simulated structure is shown in Fig. 1. A p-polarized plane wave is normally incident into a silver film with periodic grooves on film's both surfaces. The finite-difference time-domain (FDTD) method with the Drude dispersion model is utilized in this simulation.

Figure 2 presents the local output-power amplification in the main groove as a function of relative permittivity filling in the side grooves. Our simulation results exhibit that the local output power is increased as relative permittivity in the side grooves increases and approximates to a saturated value finally. The increase in distance between two adjacent grooves also increases the output power enhancement. The observed local power enhancement is attributed to reflection of power from the side grooves that re-entering the main groove and tunneling to the other side. These phenomena will be useful for designing new plasmonics devices.

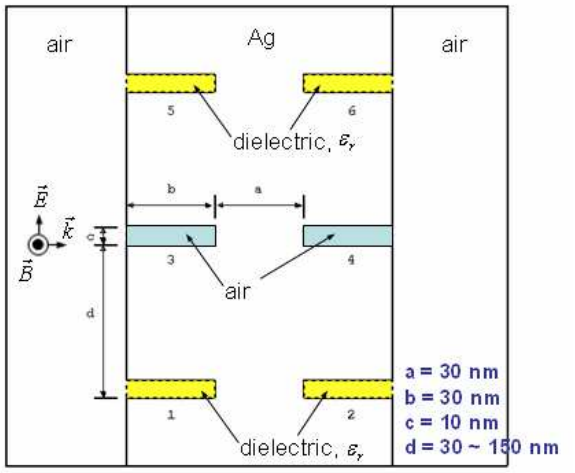

Figure 1: Simulated structure.

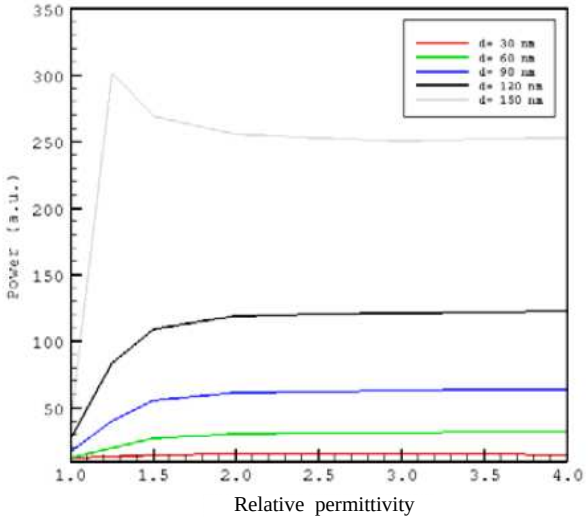

Figure 2: Local power amplification as a function of relative permittivity filling in the side grooves.

Enhanced Spontaneous Emission by Gold Nanodimer

Mao-Kuen Kuo[1], **J.-H. Chen**[1], **and Jiunn-Woei Liaw**[2]

[1]Institute of Applied Mechanics, National Taiwan University
1, Sec. 4, Roosevelt Rd., Taipei 106, Taiwan, R.O.C.
[2]Department of Mechanical Engineering, Chang Gung University
259 Wen-Hwa 1st Rd., Kwei-Shan, Tao-Yuan 333, Taiwan, R.O.C.

Abstract— The enhancement of a single emitter's spontaneous emission by a gold nanodimer (a pair of nanoparticles) is studied by using multiple multi-pole (MMP) method. A simple two-stage model of the spontaneous emission is used for analysis, including the excitation and the following emission stages. The emitter is assumed located within the gap of the nanodimer. For the first stage, the amplification of local-field intensity is calculated by a model of an incident plane wave irradiating upon the nanodimer. Further, for the emission stage, the normalized nonradiative and the radiative decay rates of an electric dipole (the excited emitter) in the presence of the nanodimer are also studied, and then the quantum yield of the system in terms of both decay rates is obtained. The results indicate that the overall effect of gold nanodimer on the spontaneous emission depends on the gap and the radius of the nanodimer, as well as the absorption and emission spectra of the specific emitter. In addition, the life time of the emission is dramatically reduced by the nanodimer, due to the energy transfer between the dipole and the nanodimer.

Optical Force Modeling by the Boundary Element Method

J. J. Xiao and C. T. Chan
Department of Physics, The Hong Kong University of Science and Technology
Clear Water Bay, Kowloon, Hong Kong, China

Abstract— Optical manipulation has been an area of active research in the past few decades. However, theoretical studies come across various challenges in providing accurate electromagnetic computational approaches for efficient modeling of such systems. In this context, we develop and implement a numerical scheme to compute optical forces in complex structures based on the Maxwell stress tensor and boundary integral equations. The equations are numerically solved using the boundary element method. Within the framework of this method, the objects can be of arbitrary shape with sizes that are either larger, comparable, or much less smaller than the wavelength concerned. The constituent components can be either dielectric or metallic. As concrete examples, we first demonstrate the efficiency of this method by calculating the optical scattering and radiation pressures exerted on 2D objects under the illumination of both plane wave and cylindrical Gaussian beams. The results are validated by comparing to analytical Mie scattering results on circular cylinders. We then applied the method to study the geometric resonance enhancement of optical forces and the effect of surface roughness on such enhancement. Furthermore, we take advantages of this approach to modeling whispering gallery resonant force in the presence of a substrate.

Surface Plasmon Waves of Curved Metal-dielectric Interfaces

Po-Tsang Wu and Jiunn-Woei Liaw
Department of Mechanical Engineering, Chang Gung University
259 Wen-Hwa 1st Rd., Kwei-Shan, Tao-Yuan 333, Taiwan

Abstract— In this paper, the dispersion relations of surface plasmon wave (SPW) along convex or concave metal-dielectric interfaces of different radius of curvature are discussed. For a given frequency, the characteristic equation of SPW in terms of Bessel and Hankel functions is solved numerically to obtain the unknown complex order, which is the product of the radius of curvature and the wavenumber. Two metals (Au, Ag) and different dielectric media (air, water, glass) are studied. Our results indicate that the phase velocity of SPW along a convex interface is always less than that of SPW along a planar, whereas the phase velocity of a concave case is always faster than that of a planar one. For both cases, the attenuation constants are larger than a planar one, due to the radial radiation of the energy into the surrounding medium, except the dissipation in the metal.

Subwavelength Photonics beyond the Diffraction Limit and Photolithography Application

K. R. Chen[1,2,3], W. H. Chu[1,4], H. C. Fang[1,4], C. P. Liu[1,4], C. H. Huang[1,3], H. C. Chui[1,3], C. H. Chuang[1,5], Y. L. Lo[1,5], C. Y. Lin[1,2], S. J. Chang[1,6], F. Y. Hung[1,7], K. J. Chen[1,6], Z. S. Hu[1,7], H. H. Hwuang[1,8], Andy Y.-G. Fuh[1,2,3], J. S. Hong[1,2], H. Y. Lin[1,9], C. C. Liao[1,5], and Y. C. Chen[1,2]

[1]Subwavelength Research Center, National Cheng Kung University
1 University Road, Tainan 70101, Taiwan, R.O.C.
[2]Department of Physics, National Cheng Kung University
1 University Road, Tainan 70101, Taiwan, R.O.C.
[3]Institute of Electro-optical Science and Engineering, National Cheng Kung University
1 University Road, Tainan 70101, Taiwan, R.O.C.
[4]Department of Materials Science and Engineering, National Cheng Kung University
1 University Road, Tainan 70101, Taiwan, R.O.C.
[5]Department of Mechanical Engineering, National Cheng Kung University
1 University Road, Tainan 70101, Taiwan, R.O.C.
[6]Department of Electrical Engineering, National Cheng Kung University
1 University Road, Tainan 70101, Taiwan, R.O.C.
[7]Institute of Nanotechnology and Microsystems Engineering, National Cheng Kung University
1 University Road, Tainan 70101, Taiwan, R.O.C.
[8]Department of Hydraulic and Ocean Engineering, National Cheng Kung University
1 University Road, Tainan 70101, Taiwan, R.O.C.
[9]Institute of Biomedical Engineering, National Cheng Kung University
1 University Road, Tainan 70101, Taiwan, R.O.C.

Abstract— Diffraction limits the behaviour of light in any optical system and sets the smallest achievable line width at half the wavelength, which is the ultimate manipulability and resolution of numerous diagnostic and fabrication instruments. The diffraction limit was the inspiration for Heisenberg's quantum uncertainty principle that is a foundation of modern science; in fact, they can be deduced from each other. We note that the wave function within a slit whose width is smaller than half the wavelength is not considered in either of the above theories. Thus, herein we demonstrate that by utilising a new metallic subwavelength aperture as the lens to preserve, generate and squeeze the sub-limit wave functions an incident light can be focused to a single-line width beyond the diffraction limit. The fields focused by the lens with the focusing aperture beyond the limit (FAB; i.e., "fabulous") are verified to be radiative with a momentum capable of propagating to the far zone as concerned by the limit and in sharp contrast to the evanescent near-field that cannot propagate in free space, such as occurs in a super lens. The light focusing process of the FAB lens, besides being of academic interest, is expected to open up a wide range of application possibilities. For example, this removes the limit on lithography that is the key issue preventing the semiconductor industry from progressing according to Moore's Law and also what limits the imaging and manipulation of biomoleculars with propagating light, especially in the harmless visible range.

Survey the Absorption of Plasmonic Energy in Metal Nanostructures

Sheng Chung Chen[1] and Din Ping Tsai[2]

[1]Department of Optoelectronic Engineering, Far East University Tainan, Taiwan, R.O.C.
[2]Department of Physics, Center of Nanostorage Research
National Taiwan University, Taipei, Taiwan, R.O.C.

Abstract— Metallic nanostructures can absorb optical energy, and the absorbed energy is consumed by collective motion of free electrons, that is the generation of surface plasmons. More and more applications are developed and proposed based on such mechanism. For example, surface plasmon resonance (SPR) on a metallic thin film coated on a glass prism, it has been implemented to biosensors [1]. For discrete nanostructures, dipole nanoantenna is one of well known applications of optical energy receiver [2], and it could be a fundamental device for interfacing light to nanoscale elements. Recently, a new application of metamaterial is proposed that it can be used as a bio-detector. A novel structure named as "planar wallpaper group metamaterial" is constructed, and it has different resonant frequencies which coincide with those of vitamin H. This match could form the basis of a bio-detector [3]. Besides, the well known extraordinary optical properties of nanostructures, such as Surface Enhanced Raman Scattering (SERS), subwavelength transmission, negative refraction, are all correlated with the process of absorption and consumption of the incident optical energies. During the consumption, the energy could radiate away from nanostructures but the intensity, frequency, and direction of the re-emit light might be different from the incident light.

Plasmonic energy emphasizes the absorbed optical energy which is exhausted by collective motion of free electrons. We will base on the analyses of such collective motion and further to study that, besides the re-emit light, whether the plasmonic energy could be transferred to another type of energy, for example, electricity or heat.

ACKNOWLEDGMENT

This research is supported by the National Science Council of Taiwan, R.O.C. through the grant number NSC 97-2120-M-002-013-.

REFERENCES

1. Homola, J., *Surface Plasmon Resonance Based Sensors*, Springer, 2006.
2. Mühlschlegel, P., H.-J. Eisler, O. J. F. Martin, B. Hecht, and D. W. Pohl, *Science*, Vol. 308, 1607, 2005.
3. Bingham, C. M., et al., *Optics Express*, Vol. 16, 18565–18575, 2008.

Electromagnetic Field Enhancement and Magnetooptical Effects in Plasmonic Heterostructures

V. I. Belotelov[1, 2], **D. A. Bykov**[3], **L. L. Doskolovich**[3], **A. N. Kalish**[1, 2], **and A. K. Zvezdin**[1]

[1]A. M. Prokhorov General Physics Institute, Russia
[2]M. V. Lomonosov Moscow State University, Russia
[3]Image Processing Systems Institute RAS, 151, Molodog. St., Samara 443001, Russia

Abstract— Optical properties of plasmonic heterostructures, i.e., metal-dielectric periodically nanostructured materials (metallic gratings, perforated films) which can sustain the propagation of the surface plasmon-polariton waves, are shown to have some peculiarities leading to new optical effects like the effect of the extraordinary optical transmission and magnetooptical Faraday effect [1, 2]. Moreover, such systems have some other interesting properties.

In this work, we consider a bilayer system of the periodically perforated with the holes arrays metallic layer (silver or gold) and a dielectric layer magnetized either in longitudinal or polar configurations (bismuth iron garnet). By varying the thickness of the dielectric layer it is possible to achieve quasi-waveguiding conditions. Magnetooptical effect determined by the relative intensity change while passing between magnetized and demagnetized states of the magnetic layer is found. It is quadratic in magnetization and shown to be related to the quasi-waveguiding in the magnetic layer. This effect can be attributed to the class of so-called orientational magnetooptical effects observed earlier for uniform magnetic films [3]. However, orientational effects in nanostructured media is several times or even an order of magnitude lager then that for the smooth films.

The other very important phenomenon related to the excitation of surface plasmon-polaritons is related to the electromagnetic field enhancement in the vicinity of the metal-dielectric interface. For example, the increase of the field intensity leads to the growth of some nonlinear effects. In this work, we investigate another very interesting consequence of the field enhancement. This is the increase of the local stationary magnetic field appearing due to the inverse Faraday effect while the heterostructure is illuminated by the circular polarized light. We show that the stationary magnetic field can be made an order of magnitude lager being compared to the uniform non-plasmonic case. Such increase of the magnetic field implies possibility of much more efficient remagnetization process and consequently writing magnetic bits at record-breaking subpicosecond time scale.

ACKNOWLEDGMENT

Work is supported by RFBR (07-02-01445, 07-02-92183, 08-02-00717, 07-07-91580), Russian foundation "Dynasty", and "Progetto Lagrange-Fondazione CRT".

REFERENCES

1. Ebbesen, T. W., H. J. Lezec, H. F. Ghaemi, T. Thio, and P. A. Wolff, *Nature*, Vol. 391, 667, 1998.
2. Belotelov, V. I., L. L. Doskolovich, and A. K. Zvezdin, *Phys. Rev. Lett.*, Vol. 98, 77401, 2007.
3. Krinchik, G. S. and E. A. Gan'shina, *Zh. Eksp. Teor. Fiz.*, Vol. 65, 1970, 1973.

Session 2A2
Modeling, Characterization and Measurement for Microwave and Millimeter Wave Applications

Fast Algorithms of Full Vector Wave Propagation between Parallel and Tilted Planes

Ming Bai, **Ming Jin**, **Shan Yang**, **and Jungang Miao**
Electromagnetics Laboratory, School of Electronic Information and Engineering
Beijing University of Aeronautics and Astronautics, Beijing 100191, China

Abstract— The propagation of electromagnetic wave in a homogenous linear medium has always been a fundamental problem. The solutions of the wave diffraction have been extensively studied with the scalar and the vector diffraction theories. The Rayleigh-Sommerfeld (RS) theory is most widely applied, which is well-known to produce the accurate solutions for both near-field and far-field diffraction. The calculation for scalar wave propagation between parallel planes requires a two dimensional RS diffraction integral to be solved. The numerical calculation of the integrals can be time assuming for large plane area. However, it is realized that the mathematical nature of the scalar RS integral is a two dimensional convolution, which can be calculated with Fourier transform and inverse Fourier transform, therefore the whole integral calculation can be significantly accelerated utilizing the FFT techniques. The Fresnel and Fraunhofer approximations are no longer necessary in case of numerical evaluation of the beam propagation either close the optical axis or not. The angular spectrum treatment of the plane waves is proved as another equivalent solution for RS integral via spatial frequency domain, and a suitable method for wave propagation between tilted planes, which is also capable of being calculated with FFT techniques.

The calculation of scalar wave propagation between parallel or tilted planes has been studied and implemented using FFT method. The vector wave propagation calculation is more required for accurate and intensive wave analysis. In this work, we present algorithms for full vector wave diffraction calculation based on vectorial version of RS integrals, preserving advantage of the FFT technique for fast calculations. The calculation of the vectorial diffraction between parallel or tilted planes is carried out using fast convolution for RS integrals and the angular spectrum transform respectively, both implemented with FFT method. The backward wave diffraction based on the RS integral is also studied and implemented for further extensive application of the algorithm.

Design of Quasi-optical Multiplexer and Calibration System for FY-4 Microwave Meteorological Satellite

Jungang Miao[1], **Zheng Lou**[1], **Ming Bai**[1], **Chongbin Yao**[2], **Shili Yu**[2], **and Gaofeng Liu**[2]

[1]Electromagnetics Laboratory, Beihang University, Beijing 100191, China
[2]Shanghai Academy of Spaceflight Technology, Shanghai 201109, China

Abstract— The FengYun-4 (FY-4) is China's second-generation geosynchronous meteorological satellite currently under development. It includes one optical series and one microwave series. The major payload of the microwave FY-4 is a millimeter/sub-millimeter sounder (MSS) designed to observe the atmospheric temperature and humidity profiles and monitor hazardous weather events such as intense precipitation. The MSS operates in seven frequency channels, with two temperature sounding channels (118 and 424 GHz), two humidity sounding channels (183 and 380 GHz), and three dual-polarization window channels (150, 220, and 340 GHz). The front end of the MSS consists of a Cassegrain antenna system (with a 3-meter diameter parabolic main reflector), a quasi-optical multiplexer (QOM), and a calibration system. The QOM allows different frequency and polarization channels to share a single antenna aperture, while the calibration system enables receiver input switching between target scenes, a hot calibration load, and a cold-sky mirror.

This talk describes a candidate design for realizing the QOM and calibration system for the FY-4's MSS payload. Both of the two components are designed based on the theory of quasi-optics. To ensure the optics function properly, the two components are designed as a unified system, with the output of the calibration system being the input of the multiplexer. The multiplexer layout adopted a two-panel design that hosts ten quasi-optical channels (with feed-horns and receiver modules) within an enclosure of $540 \times 540 \times 166$ mm. The calibration system employs two calibration mirrors to reduce interference between different calibration sources and a conical-shaped calibration load which is found to exhibit better emissivity than the conventional pyramidal absorbers. Performances of the design are assessed and some of the fabrication issues are also discussed.

General Dispersion for Conditional and Unconditional FDTD Algorithms

George Pan
Department of Electrical Engineering, Arizona State University
Tempe, AZ 85287-7206, USA

Abstract— Numerical dispersion is one of the most important properties of the finite-difference time-domain (FDTD) method, which affects accuracy of the solutions. That is, the propagation velocity of the numerical solution differs from its physical value. A way to investigate numerical dispersion of a particular FDTD scheme is to work on the plane waves in a homogeneous lossless medium by solving the dispersion relation for the numerical phase velocity or magnitude of the numerical wavenumber. Such a way allows investigating the numerical phase velocity and its anisotropy in an inexpensive manner, bypassing sources, physical, and computational boundaries. Namely, one may only consider the finite-differences to characterize and compare FDTD schemes before programming and computing. The dispersion analysis for the FDTD method in the frame of plane waves has been presented for different 2-D and 3-D FDTD schemes, conditionally and unconditionally stable. We have found that a number of conditionally and unconditionally stable FDTD algorithms on the staggered rectangular grid are subject to the same and quite simple dispersion equation.

In this talk, we present a general numerical dispersion equation which is applicable to all known conditionally and unconditionally stable FDTD algorithms on staggered rectangular grid, including Yee's FDTD, wavelet-based FDTD, extended curl FDTD, alternating direction implicit (ADI)-FDTD, Crank-Nicholson (CN)-FDTD, Crank-Nich olson split-step (CNSS)-FDTD, and their modifications of higher order spatial stencils. The real part of the complex eigenvalue of the total amplification matrix defines and distinguishes the dispersion relation for each individual scheme. Easy-to-check conditions are provided, under which the numerical dispersion of a particular time-domain scheme is governed by the proposed dispersion equation. These conditions are on the amplification matrix eigenvalues. The proposed dispersion equation includes each considered dispersion relation as a special case, and presents itself a general governing equation to estimate 3-D numerical dispersion of the aforementioned schemes in the frame of plane waves. It is observed that FDTD2, FDTD3 and SBTD spatial discretiations combined with the CN temporal discretization reduce anisotropy of the numerical phase velocity significantly. However, limited gain on numerical dispersion can be achieved if these higher order spatial discretizaations are combined with the ADI-FDTD and CNSS-FDTD temporal discreatization. While the T-FDTD is useful for narrow band signals owing to its high isotropy, the SBTD is more powerful to reduce the numerical dispersion for wide band signals.

Perfect Plane Wave Injection for Crank-Nicholson Time Domain Method

Zhenyu Huang, **George Pan**, **and Rodolfo Diaz**
Department of Electrical Engineering, Arizona State University
Tempe, AZ 85287-7206, USA

Abstract— In the finite-difference time-domain (FDTD) method, the total-field/scattered field formulation (TFSF) is a popular method for electromagnetic scattering problems. Based on the equivalence principle, this method divides the whole computational domain into two regions: the total field and scattered field regions. The incident field, which usually comes from the 1-D auxiliary simulation, is applied to the interface between the two regions. Ideally, there are the total fields in the inner region, while there are only scattered fields back from the scatters in the outer region. In practice, however, the TFSF method suffers from the field leakage in the scatted region, especially for the case with oblique incident fields. A lot of work in reducing the leakage error has been done in the past decade. Recently, Tan has developed a novel 1-D multipoint auxiliary source propagator for TFSF method.

Based on the modified 1-D multipoint auxiliary source propagator, a novel method of perfect plane wave injection for Crank-Nicholson time domain (CNTD) is presented in this talk. By projecting the 2-D dispersion equation onto 1-D case, the identical dispersion relation can be realized between 1-D case and 2-D case, which leads to a perfect plane wave injection at an angle forming an integer grid cell ratio. Several numerical experiments are implemented, which show the leakage errors are on the order of the finite precision (-300 dB for double precision) when Δt is around the Courant-Friedrich-Levy (CFL) limit. Beyond the CFL limit, the leakage error is still kept low even though it deteriorates with the increment of time step.

Multi-reflector Antenna System Analysis by Multiresolution MoM and Diffracted Gaussian Beams

Le Wang[1], **Jun-Gang Miao**[2], **and George Pan**[1]

[1]Arizona State University, Tempe, AZ 85287, USA
[2]Beijing University of Aeronautics and Astronautics, Beijing 100083, USA

Abstract— Reflector antennas are widely used and many methods are introduced to calculate them. These methods are mainly separated into two kinds: geometrical optics (GO) based method and Physical optics (PO) based method. As for GO, it does not account for the effect of edge diffraction. The geometrical theory of diffraction (GTD) is an extension to GO which includes diffraction but fails at caustics; this can be overcome by use of uniform of diffraction (UTD). However, the method cannot easily be applied to multi-reflector systems because of its non-modularity due to multiple diffraction and caustics. Physical optics coupled with the physical theory of diffraction (PTD) is an accurate and modular method for analyzing reflector antenna but is very expensive in terms of computation time and storage for electrically large multi-reflector systems. Gaussian beam optics has been successfully applied to the design of reflector antenna. But it does not account for beam distortion and assumes negligible field at all reflector edges.

In this talk, we present a hybrid edge diffraction of Gaussian beam and the method of moments (MoM). The hybrid method employs the triangular patch based MoM, which is equivalent to the RWG basis but possesses the multi-resolution analysis (MRA). The MRA has greatly improved the matrix condition number, and hence achieves high accuracy for the intermediate results. The Gaussian beam expansion and diffraction are applied to the secondary reflector. As a result, the fast speed of the Gaussian beam expansion is preserved. In the mean time, higher precision of the final results are accomplished. Numerical examples and comparisons are provided.

High Precision Characterization of Complex Permittivity in Broadband

Zhonghai Guo, George Pan, and Rudolph Diaz
Department of Electrical Engineering, Arizona State University
Tempe, AZ 85287-7206, USA

Abstract— Complex permittivity of dielectrics plays important roles in the modeling, design, fabrication and testing of antennas; microwave and millimeter wave circuits and high speed digital systems. Accordingly, extensive research has been conducted in the past decades. To date, the popular measurement techniques in the RF and microwave region are cavity resonator, transmission line, free space and open-ended coaxial probe, among others. Each method has its unique pros and cons. For instance, the advantage of high Q resonant method is its high accuracy; but the measurement can only be performed at a single frequency for each laboratory setup. Recently, a broadband split cylinder resonant technique is reported, which is nondestructive. Nevertheless, the method is quite complicated in terms of apparatus and operations. Transmission line technique, as a non-destructive approach, seems to be simple for broadband characterization. However, it lacks precision. The free-space technique may suffer from electromagnetic interference; while the open-end coaxial probe method may not be suitable for extremely low-loss materials.

We present a new broadband and high accuracy nondestructive method for determination of the permittivity and loss tangent of low loss dielectrics, using printed circuit board (PCB) circular disks. Because it utilizes multiple resonances, this method is in high precision and broadband (500 MHz–12 GHz), covering the UHF, GSM 850/1800, 802.11b/g, WiMax, WLAN and UWB bands. The method is simple and accurate based on closed form analytic expressions of cylindrical symmetry, taking into account of disk rim fringing fields and radiation loss, in addition to the ohmic loss. Numerical results are conducted for popular PCB material, FR4, and the self consistent Kramers-Kronig relation is verified.

Session 2A3
Synthetic Aperture Radar and Its Applications 1

MIMO Radar Wide Band Array Range-Angle Imaging

Changzheng Ma[1, 2], **Tat Soon Yeo**[1], **Junjie Feng**[2], **and Hwee Siang Tan**[1]

[1]Department of Electrical and Computer Engineering
National University of Singapore, Singapore
[2]School of Electric and Information, Zhongyuan University of Technology, China

Abstract— Multiple-Input Multiple-Output radar are used in long distance surveillance. In order to increase the range resolution while increasing the angular resolution, the aperture of the virtual array may be larger than the range resolution, then the antenna array is a wide band array. In this paper we discuss the wide band array signal processing and show that long time coherent integration can improve the performance of target separation.

Development of Circularly Polarized Synthetic Aperture Radar Onboard Microsatellite (μSAT CP-SAR)

J. T. Sri Sumantyo[1], **H. Wakabayashi**[2], **A. Iwasaki**[3], **F. Takahashi**[4, 6], **H. Ohmae**[5], **H. Watanabe**[6], **R. Tateishi**[1], **F. Nishio**[1], **M. Baharuddin**[1], **and P. Rizki Akbar**[1]

[1]Center for Environmental Remote Sensing, Chiba University, Japan
[2]Faculty of Engineering, Nihon University, Japan
[3]Department of Aeronautics and Astronautics, Tokyo University, Japan
[4]Japan Aerospace Exploration Agency (JAXA), Japan
[5]Sentencia Corporation, Japan
[6]National Institute for Environmental Studies (NIES), Japan

Abstract— Synthetic Aperture Radar (SAR) is a multipurpose sensor that can be operated in all-weather and day-night time. Recently, the SAR sensor is operated in linear polarization (HH, VV and its combination) with limited retrieved information. The characteristic of the conventional SAR sensor is bulky, high power, sensitive to Faraday rotation effect etc. Recently, we are developing the *Circularly Polarized Synthetic Aperture Radar* (*CP-SAR*) *onboard Microsatellite* (μSAT CP-SAR) to retrieve the physical information of Earth surface, especially to monitor the cryosphere, global vegetation and disaster area in the future. In this research, the CP-SAR sensor is developed to radiate and receive circularly polarized wave. The sensor is designed as a low cost, simple, light, strong, low power, low profile configuration to transmit and receive left-handed circular polarization (LHCP) and right-handed circular polarization (RHCP), where the transmission (Tx) and reception (Rx) are working in RHCP and RCHP+LCHP, respectively. Then these circularly polarized waves are employed to generate the *axial ratio image* (ARI). This sensor is not depending to the platform posture, and it is available to avoid the effect of Faraday rotation during the propagation in ionosphere. Therefore, the high precision and low noise image is expected to be obtained by the CP-SAR. This satellite platform is composed by RCHP and LHCP antennas for CP-SAR sensor subsystem, telemetry subsystem that constructed by S band telemetry and X band transponder to transmit CP-SAR signal to ground station, and some altitude controller subsystem. This satellite planned to be launched in 2014 with altitude between 500 km and 700 km. This sensor is operated with center frequency on L band (1.27 GHz) and 10 MHz of chirp pulse bandwidth. The gain in main beam is set higher than 30 dBic to obtain received signal higher than -20 dB (equivalent backscattered noise level). The axial ratio is set lower than 3 dB to obtained ideal circular polarization. The antenna size (inflatable antenna) is 4 m and 8 m for range and azimuth directions, respectively. The center of off-nadir angle and swap width are set 29° and 50 km, respectively. The ARI is expected to retrieve various physical information of Earth surface accurately and high precision. i.e., up-lift and subsidence, biomass, vegetation height and age, soil and snow physical characteristics based on the relationship between axial ratio and each characteristic. In the near future, CP-SAR is expected to improve the characteristics of conventional SAR system, especially to extract some new physical information on the Earth surface.

Efficient Interpolation for Range-cell Migration Correction of RADARSAT-1 Data

C. Bhattacharya
DEAL (DRDO), India

Abstract— RADARSAT-I platform is not yaw steered, and has large squint of -1.6° in the antenna beam radiation. This causes phase of the range-compressed data to migrate over a large number of range-cells. In the range-Doppler algorithm and in its variations, secondary range compression (SRC) is utilized to change the rate of transmitted chirp signal to compensate for range curvature produced by this large squint [1]. Range-walk in the Doppler spectrum is compensated by interpolation in the range direction and re-indexing of data.

In the traditional interpretation of range-Doppler algorithm, range migration of Doppler spectrum is estimated for variation of absolute Doppler frequency. This is true for continuous variation of phase of the range-migrated data. On the other hand, Doppler spectrum is centered on the fractional Doppler centroid in the digital processing domain causing ambiguity in the estimation of range migration. Secondly, computation of range migration for each sample of Doppler spectrum over the interpolated range is hugely expensive in terms of computation efficiency, and requires a large number of memory call operations. Besides, choice of the interpolation kernel is crucial as traditional *sinc* interpolation produces ringing in results and erroneous interpolation.

In this paper, our objective is to demonstrate efficient solution for digital interpolation of RADARSAT-I data in the range-Doppler domain. We show explicit analytical relationship for range migration of Doppler spectrum around fractional Doppler centroid to facilitate estimation of rangewalk in the digital domain. Secondly, we propose polyphase interpolation in range; this has twofold advantages. Polyphase interpolation is parallel, and is therefore faster for large kernel of interpolation. We implement data re-indexing in the Doppler domain for each phase of interpolation, making the correction for range-cell migration highly efficient in terms of computation load. Thirdly, we use spline interpolation kernel that provides smooth interpolation of the Doppler spectrum.

Analytical derivations and validation of results for point targets as obtained from RADARSAT-I raw data are shown in the paper. The results demonstrate the efficiency of the proposed method.

REFERENCES

1. Jin, M. Y. and C. Wu, "A SAR correlation algorithm which accommodates large-range migration," *IEEE Trans. Geoscience and Remote Sensing*, Vol. 22, No. 6, 592–597, Nov. 1984.

A Novel Three-Dimensional Microwave Imaging Mode and Experiment: Bistatic Circular Synthetic Aperture Radar

W. X. Tan[1, 2, 3], **Y. P. Wang**[1, 2], **W. Hong**[1, 2], **Y. Lin**[1, 2, 3], **and Y. R. Wu**[1, 2]

[1]National Key Laboratory of Microwave Imaging Technology, China
[2]Institute of Electronics, Chinese Academy of Sciences, China
[3]Graduate University of Chinese Academy of Sciences, China

Abstract— Circular Synthetic Aperture Radar (CSAR) has been developed as a new SAR imaging mode for its capability of Three-Dimensional (3D) resolution and high resolution on the plane which is parallel to the track plane. However, the conventional CSAR imaging system could only acquire the backscattering information of the targets in the illuminated area. In this paper, a new 3-D imaging method — Bistatic Circular Synthetic Aperture Radar (BiCSAR) is proposed. The corresponding imaging geometry and signal models are introduced firstly. Then the restriction, 3-D imaging capabilities, imaging algorithm and so on are analyzed and presented. Finally, the simulation and experiment of BiCSAR are made to demonstrate the capability of 3-D resolution, obtaining the non-backscattering information and improving the radar system parameter NEσ°.

Bistatic Circular Synthetic Aperture Radar (BiCSAR) imaging technique is a combination of Bisatic SAR (BiSAR) and Circular Synthetic Aperture Radar (CSAR) and has the capabilities of resolving the targets distributed in the three-dimensional (3D) space. In addition, it can obtain the non-backscattering information of the illuminated area with the bistatic flight. Last but not the least, the echoed data could be received passively and the radar system parameter NEσ° can be improved through reducing the transmitting distance of the electromagnetic wave. In order to demonstrate the detailed effects and the performances of the BiCSAR, we investigate BiCSAR through the following aspects.

First, we propose the concept of BiCSAR and point out the similarities and differences among the CSAR and BiSAR imaging modes. A particular imaging geometry is given and the signal model based on BiCSAR is presented.

Next, we give the restrictions for BiCSAR 3-D imaging and analyze the 3-D resolution capability theoretically. In addition, the influence of BiCSAR on radar system parameter NEσ° is discussed, and an imaging algorithm is utilized to reconstruct the 3-D image of the target area.

Finally, the simulation is made to demonstrate the efficiency of the algorithm. Furthermore, an experiment of BiCSAR is carried out in the microwave anechoic chamber at Ka band. The experimental system is mainly consisting of Vector Network Analyzer (VNA) and two wave-guide antennas. Eight metallic spheres of diameter 3 cm placed on the rotating platform which rotates in circular flight path with equal angle interval. The transmission and reception of microwave signals is performed for each rotation angle.

In this paper, the concept BiCSAR is proposed and introduced. Then the feasibility of BiCSAR for 3-D imaging is verified both numerically and experimentally. Finally, the experiment results in anechoic chamber are provided to illustrate the validity of BiCSAR and the algorithm.

Non Stationary Bistatic Synthetic Aperture Radar Processing: Assessment of Frequency Domain Processing from Simulated and Real Signals

Hubert M. J. Cantalloube
Office National d'Études et Recherches Aérospatiales, France

Abstract— Bistatic synthetic aperture radar (SAR) imaging from very asymmetric configuration is a promising technique for both military and civilian issues.

Indeed, an illuminating radar standing off at a safe distance may be combined with a low cost, possibly unmanned air vehicle using a passive radar receiver operating at closer range. Practical civilian application could be high resolution remote sensing of dangerous disaster areas (fire, chemical or radioactive hazard) with small unmanned air-crafts. Military application could be SAR imaging in the forward direction for a missile guidance without signalling the sensor by its transmitted radiation.

However, such configurations are strongly non-stationary in the sense that the transmitter to receiver distance and relative orientation varies. This severely harden the task of frequency domain processing and especially its motion compensation.

Here we test frequency domain processing and motion compensation for both simulated and real (acquisitions scheduled for mid-October 2008) signal for an asymmetric configuration with a large freighter aircraft (Transall) flying at 5000 feet/165 knots illuminating at 90° from track and as a receiver a small touring motor-glider (simulating an unmanned aircraft) flying at 3000 feet/85 knots with antenna squinted 60° from track and flying with an heading separated by 30° from that of the illuminating aircraft.

The SAR processor may provide self-testing before image synthesis and forecast phase errors in the resulting image depending on terrain elevation features. Error maps provided may be used for illustrating the motion compensation and the frequency domain processing in a didactic way.

Issues such as sensitivity to elevation and clock drifting will also be addressed.

Coded Frequency Shifting Transponder Observation and Identification in Imaging SAR Signal

H. M. J. Cantalloube
Office National d'Études et Recherches Aérospatiales, France

Abstract— Frequency shifting coded transponders are routinely used by almost any aircraft. This transponder when receiving a radar pulse from a traffic control (ATC) radar, transmits a frequency shifted pulse on which information is coded (12 bits of status/identification and the barometric altitude). The transmitted pulse is received by a secondary radar antenna and the coded information is displayed beside the radar plot on the ATC display screen.

Such a status/identification and radar cross section (RCS) enhancement capability may be adapted to air-to-ground applications for both civilian and military application, especially with foliage penetrating wavelengths.

For example, fire fighting vehicles and even individual firemen could carry a transponder such that repeated synthetic aperture radar (SAR) scanning of a forest fire area could indicate their position, identification and status (fuel, water, oxygen levels, health/fatigue condition...).

In military applications, the system may be used for friend or foe identification, and soldier status such as fuel/ammunition levels, idle/engaged/wounded/captured/dead status and so on.

We propose here a scheme using frequency transposition of half the SAR bandwidth in order to simplify transponder design (by minimising transmit to receive coupling) and allowing to keep the SAR waveform unchanged (and processing is made from existing imaging and autofocus software).

The transponder transmits the signal received from, e.g., the lower half of the SAR bandwidth, shifts it to the higher half and modulate it with a slow binary (0 and 1) sequence. Slow meaning, e.g., 1/10 of the SAR repetition frequency (PRF). The binary sequence is chosen in a way that it conveys the payload data (identification/status) and has some constraints (payload decoding should be tolerant to loss of signal due to transient foliage masking and the sequence should be relatively even in 0/1 local frequency).

On the processing side, the transponder echoes are severely range shifted and azimuth defocused in the normally processed image, however they are correctly localised and focused (with higher azimuth side lobes containing the code) on an auxiliary SAR image obtained with changed processor parameters. Once detected, the echo signal of the transponder is isolated from the raw radar signal using a narrow Doppler and range filter centred at the transponder ground position. (such a filter is routinely used in phase tracking type of autofocus). Transponder signal modulation is eventually extracted and the payload data is recovered.

The concept is illustrated using real airborne SAR signal at L-band into which transponder simulated echoes have been added.

Study on Absolute Calibration Coefficient Improvement for ALOS PALSAR Data after Initial Calibration Check

K. Nakamura, **S. Kodama**, **Y. Takeyama**, **and M. Matsuoka**
National Institute of Advanced Industrial Science and Technology, Japan

Abstract— The Advanced Land Observing Satellite (ALOS) was launched by Japanese Aero space Exploration Agency (JAXA) in 2006, which has the Phased Array type L-band Synthetic Aperture Radar (PALSAR) and follows the Japanese Earth Resources Satellite-1 (JERS-1). Although three years have passed from the start of ALOS PALSAR observation, the PALSAR is known as the greatly stable operation. However, we have been continuously monitored the gain for the future sustain able operation in order to the PALSAR sensor variations across the ages.

National Institute of Advanced Industrial Science and Technology (AIST) has been studying the remote-sensing based natural resource survey and one of the research targets is the soil moisture estimation under vegetation and forest. In order to better estimate soil moisture and above ground biomass, we need and carry out the maintenance of calibration coefficient quality and its improvement. To achieve this goal, we kicked off the PALSAR calibration and validation (Cal/Val) campaign of AIST. We has been promoting joint activities for the PALSAR calibration observation and the AIST Cal/Val campaign was launched under cooperation with four universities working together, Earth Remote Sensing Data Analysis Center (ERSDAC), and JAXA Calibration and Validation Science Team (CVST). Our campaign is planned in accordance with the ALOS systematic observation strategy. We calculated calibration coefficients, using two and/or three meters triangle side trihedral corner reflectors for like-polarization calibration for twelve times from November 2007 to August 2008, which were compared with the theoretical radar cross section of corner reflector with calibrated Single looked Complex (SLC) data from ERSDAC. As the result of that comparison with using the integral method [1], the mean of the difference values and the standard deviation are -0.18 dB and 0.52 dB, respectively.

We especially focus on cross-polarization calibration based on ground truth because that calibration depends only on computationally approach using Quegan method [2]. We therefore have been developing a prototype of rotatable dihedral corner reflector, and carrying out the trial observations in this year. The first version prototype is made of punching aluminum (ϕ5 and 8 mm pitch) square plate of two meters on a side, which were installed three times from June to August 2008: one observation was intended for cross-polarization and others were for like-polarization. By comparison with theoretical results, the mean of differences and the standard deviation are -2.40 dB and 0.28 dB, respectively. Because the dihedral corner reflector should be installed with high precision, the disagreement of setting angles of the corner reflector might be remained.

REFERENCES

1. Gray, A. L., P. W. Vachon, et al., "Synthtetic aperture radar calibration using reference reflectors," *IEEE Trans. Geosci. and Remote Sens.*, Vol. 28, No. 3, 374–383, 1990.
2. Quegan, S., "A unified algorithm for phase and cross-talk calibration of polarimetric data — Theory and observations," *IEEE Trans. Geosci. and Remote Sens.*, Vol. 32, No. 1, 89–99, 1994.

New Approach to Extraction of Linear Features in a SAR Image

Si Chen, **Weijie Zhang**, **and Jian Yang**
Department of Electronic Engineering, Tsinghua University, Beijing 100084, China

Abstract— Automatic extraction of linear features, such as roads, water channels, railways, bridges, and airport runways, has been one of the most important applications of SAR images. It can be used in target detecting, map updating, scene matching, and kinds of military tasks.

The traditional framework can be found in [1]. It consists of 1) detecting the pixels which potentially belong to roads from the whole image, 2) forming road segments based on the detected pixels, and 3) connecting as well as selecting the road segments to obtain the road network. Another effective framework models the problem as a tracking process [2].

Some good results have been obtained under the frameworks mentioned above. However, there are still problems, most of which are caused by the pixel-detecting stage. Some special detectors have been developed to improve the performance, but all of them are restricted to certain assumptions. For example, it was assumed in [3] that roads are dark elongated areas with bright lateral edges. Thresholds are necessary in these detectors, too. Therefore, the results by these methods may be very good for some images and may be rather bad for some others. Too many false points of a road make the following steps harder, while the missed ones become lots of gaps so that more additional treatments are necessary.

Due to the complexity of scenes and poor quality of SAR images, roads may appear differently even in one image. They can be dark or bright, several pixels wide or zero pixel wide (just edge), and not consecutive visually. Thus, it is really hard to say if a single pixel belongs to or not belongs to the road network. However, it is comparatively easy to say if a segment of line, as a whole, comparing with its neighbourhood, belongs to or not belongs to the road network, since it must show higher consistency along the line and higher contrast vertically, simultaneously.

In this paper, we propose a new approach to extraction of linear features in SAR images. First, an original SAR image is divided into 8×8 blocks. In each block, we have 36 (directions) $\times$ 12 (offsets) different segments of lines. The extraction of linear features is equivalent to a selection from all the segments in all the blocks. A local processing method within each block is proposed to give each segment a measurement on its "linear probability". This process consists of two steps, firstly on directions and secondly on offsets. No threshold is necessary in both the steps. A global fuzzy method is then used to take into account a priori knowledge and optimize the network topology. Finally, a threshold is used to select the most likely segments, followed by a post processing stage. Experiments on SAR images validate the effectiveness of the proposed approach.

ACKNOWLEDGMENT

This work was supported by the National Natural Science Foudation of China (40871157).

REFERENCES

1. Tupin, F., H. Maitre, J.-F. Mangin, J.-M. Nicolas, and E. Pechersky, "Detection of linear features in SAR images: Application to road network extraction," *IEEE Trans. Geosci. Remote Sens.*, Vol. 36, No. 2, 434–453, Mar. 1998.
2. Chen, Y., Y. Gu, J. Gu, and J. Yang, "Particle filter based road detection in SAR image," *Proc. MAPE*, Vol. 1, 301–305, Beijing, China, Aug. 8–12, 2005.
3. Negri, M., P. Gamba, G. Lisini, and F. Tupin, "Junction-aware extraction and regularization of urban road networks in high-resolution SAR images," *IEEE Trans. Geosci. Remote Sens.*, Vol. 44, No. 10, 2962–2971, Oct. 2006.

Session 2A4
Signal Processing for Communication Systems & Cognitive Radar 1

Robust Adaptive Beamforming under Quadratic Constraint

Xin Song, **Jinkuan Wang**, **and Yinghua Han**
School of Computer Engineering, Northeastern University at Qinhuangdao
Qinhuangdao 066004, China

Abstract— Adaptive beamforming has received considerable attention in the past decades due to its wide applications in the fields of radar, sonar, seismology, radio astronomy, and wireless communications. One of the main problems that occur in practical adaptive array processing is the mismatches between the presumed and actual signal steering vectors. The performance of adaptive beamforming methods is known to degrade severely in the presence of such slight signal steering vector mismatches that may occur due to signal pointing errors, imperfect array calibration, source local scattering, wavefront distortions, etc. Similar types of performance degradation can take place because of the small training sample size. Quadratic constraints on the weight vector of an adaptive linearly constrained minimum power beamformer can improve robustness to the signal steering vector mismatches.

In this paper, based on explicit modeling of uncertainties in the desired signal array response and data covariance matrix, we propose robust adaptive beamforming algorithm under a quadratic inequality constraint. To improve robustness, the weight vector is optimized to involve minimization of the output power function subject to the norm of error between the actual and assumed array beampatterns. We can show that the proposed algorithm belongs to the class of diagonal loading approaches, but the diagonal loading term can be precisely calculated based on the given level of uncertainties in the signal array response and data covariance matrix. Our proposed robust adaptive beamforming algorithm provides a significantly improved robustness against the signal steering vector mismatches and small training sample size, enhances the array system performance under random perturbations in sensor parameters and makes the mean output array SINR consistently close to the optimal one. Computer simulation results validate substantial performance improvement of our proposed algorithm as compared with the existing adaptive beamforming algorithms.

User Selection for the Capacity Maximum in Multiuser MIMO System

Zhibin Xie, **Jinkuan Wang**, **Xin Song**, **and Jing Gao**
School of Information Science & Engineering, Northeastern University, China

Abstract— Multi-use multiple-input multiple-output (MU-MIMO) wireless communication system can provide potential significant capacity performance and has been paid considerable attention in recent years. In multi-user MIMO scenarios, several co-channel users with multiple antennas aim to communicate with a base station in the same frequency and time slots. In this case, it is necessary to design transmission schemes that are able to precancel the multi-user interference (MUI) at the end of users. To mitigate the MUI caused by the spatial multiplexing in a multi-user downlink system, several precoding schemes have been introduced in the form of transmit processing algorithms. However, the multi-user spatial multiplexing system has no special strategies for the computational cost and worst channel-case user. In this paper, we propose a decreasing user selection scheduling for the multi-user MIMO spatial multiplexing scheme with a large number of users. In each iterative course, the user which has worst channel station is dropped, and the sum rate capacity of MU-MIMO system is not less than a threshold. Therefore, the base station may select a subset of users to serve so as to maximize the total throughput. In particular, to reduce the complexity, we propose a low complexity suboptimal selection algorithm to maximize the capacity of system. Compared with the traditional algorithm, when the sum rate capacity of all users is not far more than the upper bound of the MU-MIMO system, the proposed scheme attains good capacity performance, has lower complexity, and is suitable for real-time communication. Simulation results show that the proposed multi-user selection method is able to achieve good performance.

Peak-to-average Power Ratio Reduction Based on Cyclic Iteration Partial Transmit Sequence

Jing Gao, **Jinkuan Wang**, **and Zhibin Xie**
School of Information Science & Engineering
Northeastern University, Shenyang 110004, China

Abstract— Partial transmit sequence is an efficient algorithm to solve the problem of high peak-to-average power ratio (PAPR) in orthogonal frequency division multiplexing (OFDM), but its exhaustive search of phase factors results in high computational complexity. A PTS algorithm based on cyclic iteration (C-IPTS) is proposed to solve this problem. In the proposed algorithm, the phase factor achieved by the previous iteration is set as the initial phase factor of the current search, thus the search is more close to the optimal phase factor after repetition, as a result, the PAPR performance is eliminated effectively. Moreover, the effect of initial phase factor is decreased significantly. Simulation shows that C-IPTS algorithm can achieve good PAPR reduction with low computational complexity.

A Simple DOA Estimation Employing Second-order Statistics for Distributed Source

Y. H. Han, **J. K. Wang**, **Q. Zhao**, **and X. Song**
Northeastern University at Qinhuangdao, Northeastern University, China

Abstract— In array processing it is commonly assumed that the received signals originate from far-field point sources and give rise to perfectly planar wavefronts which impinge on the array from discrete and fixed directions of arrive (DOAs). However, in many practical applications such as radar, sonar and mobile communications, the sensor array often receives sources which have been reflected by a number of scatters. The scattered signals are received from a narrow angular region, an alternative signal model can be derived which is called distributed source model.

Recently, distributed source localization has been a focus of intensive research. An interesting alternative is to use the beamforming methods. The generalized beamformer is presented. The resulting method maintains a distortionless response to a hypothetical source in a mean-power sense. However, the algorithm need to the prior knowledge about the shape of the angular signal intensity. And in peak-finding searching, it needs compute the integral steering vector, which has large computational cost. Another subspace-based algorithm TLS-ESPRIT approach is employed to estimate the central DOA based on Taylor series expansion, when angular spread is not large. However, the subspace-based algorithm needs eigenvalue decomposition, which is computationally intensive. In addition, the performance of this algorithm is unsatisfactory when angular spread is large.

In this paper, we propose an algorithm for the central DOA estimation of a coherently distributed source based on second-order statistics. The integral steering vector for distributed source can be deduced to be Schur-Hadamard product comprising the steering vector for point source and a real vector. And then a second-order statistics is proposed based on the Schur-Hadamard product. So a closed-form solution to the central DOA estimation can be derived. The proposed algorithm needs not any peak-finding searching and eigenvalue decomposition or singular value decomposition, which significantly reduces the computational complexity. In addition, the proposed second-order statistics algorithm has a substantially better estimation performance even at low SNR. The explanation of this fact is that the second-order statistics algorithm has weaken the inflection of noise. Furthermore, our proposed algorithm yields the better performance especially at large angular spread compared with subspace-method TLS-ESPRIT estimators.

Bragg Grating Vibration Sensor Array Based on Wavelet Filtering

Zhaoxia Wu, **Dongmei Yan**, **Lina Fan**, **and Jinkuan Wang**
Department of Automation, Northeast University at Qinhuangdao, Qinhuangdao 066004, China

Abstract— A vibrating acceleration measuring system with distributed Fiber Bragg Grating is presented in this paper. The continuous wave modulation frequency and wavelength division multiplex technology are used in this system. The wavelet filter is designed to improve imbalanced and nonlinear optical signal efficiently and the optical wavelength absolute code is completed. The changes of environment and changes of power intensity do not influence the measurement are discussed. This system has some advantages such as simple structure, high scan frequency, high resolution and good linearity.

Distributed Sensor Positioning System Using Virtual Trajectories

Zhigang Liu and Jinkuan Wang

Northeastern University, China

Abstract— Sensor cooperative localization has attracted significant research effort in recent years. Many approaches have been proposed. The majority of them assume that a small fraction of the nodes have a prior knowledge of their locations. The location discovery problem can be usually split into two stages: distance estimation and position computation. The first phase is to estimate the distance between two nodes based on methods such as Received Signal Strength (RSS) Indicator, Time of Arrival (ToA), and Time Difference of arrival (TDoA). The second phase is to compute the node location based on the ranging measurements. Some proposals have an optional third phase, which is to refine the position utilizing the local or global information. Other methods have a preprocessing phase, which is to reduce the fluctuation of the original RSS data using Grey Prediction (GP) and Unscented Kalman Filter (UKF).

Conventional two-step localization processes have been studied extensively. However, these methods have the disadvantage of making a premature decision on an intermediate measurement, discarding useful information. By introducing the virtual trajectory, we propose a direct approach to the location discovery problem in this paper. This trajectory consists of static location-aware sensors that are randomly deployed, and is highly nonlinear. Therefore, utilizing a Cascade Unscented Kalman Filter (CUKF) algorithm, we let each location-unaware sensor discover its position by following this virtual trajectory. This method has the advantage of making a mature decision on an immediate measurement. In addition, this algorithm has several favorable features such as high scalability, robustness to measurement error, etc. The effectiveness and advantages have been showed through Monte Carlo simulation results.

Dynamic Load Balancing Based-on Packet Loss Rate Prediction

Cai Ling, **Jinkuan Wang**, **and Cuirong Wang**
School of Information Science & Engineering, Northeastern University, China

Abstract— When there are multiple paths across a network it is common for network operators to use some form of load balancing. Load-balancing allows more flexible and efficient forwarding of packet proportion on each path, and thereby extends the performance and reliability of a network. A major challenge in load balancing is how to cope with dynamic and unpredictable changes in network. If a load balancing algorithm is not prepared for them, it may cause network links and routers to be unnecessarily overloaded. Overloaded links and routers can cause long delay, high packet loss rates, reduced network throughput and even router crashes. As motivation, in this paper we propose a new, lightweight method based on the concept of packet loss rate prediction (PLRP) that can generate accurate forecasts for every path packet loss rate dynamically. This prediction information is then used as an input to adjust the forwarding proportion for next prediction period. Our prediction method is based on Support Vector Regression modeling that uses a combination of prior packet forwarding proportion and measurements of loss rate of each path. To evaluate the effect of packet loss rate of each path on load balancing in regards to a wide spectrum of application, we introduce a new packet forwarding scheme based on path gain, which means the penalization function for the path based on the prediction loss rate. Using a combination of analysis and trace-driven simulations in ns2, we show that the dynamic load balancing algorithm based on PLRP attains significantly better performance than other load balancing mechanisms, such as ECMP.

Detection of a Dim Point Target Using Dynamic Programming Approach

Lina Fan, **Jinkuan Wang**, **and Dongmei Shu**
School of Information Science & Engineering, Northeastern University, China

Abstract— The detection and tracking of dim point targets is the key technology to enhance the ability of guidance system. In most cases, the signal to noise ratio (SNR), the clutter conditions and the maneuvers of the target cause the detection behind. The target detection in image sequences is part of multidimensional signal detection. Because point target is far away from the interceptor, its size is a scale of pixel in the image. Dim point target from an image sequence has been merged into the clutter. So the image has a low SNR and the detection of the dim point target under the low conditions becomes the sticking point.

We introduce a novel tracking system based on dynamic programming algorithm(DPA). This algorithm can detect the dim point targets under the condition of low SNR. With the theory of step optimization of dynamic programming we can decompose target trace searching problem into grading optimization. The dynamic programming technique can detect the trace of the point target which is moving with straight line and reduce the calculation amount. In this paper the DPA was selected and meliorated. The improved DPA has merits of simple and high efficiency and enhances the probability of detection. It is based on the assumption that the some information of the target has been known. With the result of simulation test, it can be shown that the introduced algorithm can effectively detect moving point target trajectory in image sequences than previously developed algorithm.

A Concurrent Ant Colony Optimization Multipath Forwarding Algorithm in IP Networks

Laiquan Han, **Jinkuan Wang**, **and Cuirong Wang**
School of Information Science & Engineering, Northeastern University, China

Abstract— The rapid development of communication technology and programming router in the last few years have given rise to a strong research interest in Concurrent Multi-Path (CMP). At the same time, much of the researches of ant colony optimization (ACO) focus on wireless networks such as MANET (Mobile Ad-hoc Networks) and WSN (Wireless Sensor Networks), on the other hand, there are little researches about ACO on wired networks such as Internet. Combining with the advantages of CMP and ACO while based on the disadvantages of conventional single-path OSPF (Open Shortest Path First), ECMP (Equal Cost MultiPath) and random CMP, this paper proposes a novel CMP forwarding algorithm aimed to increase the scalability and decrease the route overhead to existing ant-based routing algorithm. The proposed algorithm, which is called Concurrent ACO CMP Forward (CACF), makes full use of the positive pheromone feedback of forward ants and backward ants to update the state of different paths. Forward ants probe the current condition of the networks and backward ants update the routing information of each path and adjust forwarding granularity for different availability bandwidth. CACF can adapt to the changing of link performance dynamically and utilize multiple paths to transmit simultaneously. We validate CACF algorithm through three methods: (i) theoretical analysis; (ii) NS2 simulation driven by real-world traffic traces and networks topologies; and (iii) wide-area experimentation in PlanetLab. Results prove that CACF algorithm reduces the degradation of performance of different paths, obtains significant performances of throughput, end-to-end delay and jitter, and it is easily deployed into the programming router.

On Nonlinear Iterative Partial Transmit Sequence for PAPR Reduction in OFDM Systems

J. Gao, **J. K. Wang**, **and Z. B. Xie**
School of Information Science & Engineering
Northeastern University, Shenyang 110004, China

Abstract— Orthogonal frequency division multiplexing (OFDM) has become a promising candidate for high performance wireless communications. However, OFDM systems exists a prohibitively large peak-to-average power ratio (PAPR) of the transmitted signal, which can lead to unwanted saturation in the power amplifier. A number of approaches have been proposed to deal with the PAPR problem, including clipping, coding and multiple signal representation techniques such as partial transmit sequence (PTS) and selected mapping (SLM). Among these, PTS is the most attractive algorithm to reduce the PAPR, but the considerable computational complexity for the required exhaustive search is a potential problem for practical implementation. To reduce the search complexity, iterative PTS (IPTS) algorithm was presented by Cimini and Sollenberger's as a sub-optimum technique, which achieved significant reduction in search complexity at the expense of certain PAPR performance degradation. In this paper, we propose a nonlinear iterative PTS (N-IPTS) algorithm to further address the complexity issue. Firstly, we use IPTS algorithm repeatedly, and in every cycle, the phase factor achieved by the previous iteration is set as the initial phase factor of the current search, which enables us to (i) make the search solution more close to the optimal phase factor (ii) eliminate the effect of initial phase factor effectively. Moreover, the solution of IPTS is always updated in the direction of improvements and hence is quickly trapped in a local optimum. Therefore, rather than the linear search of IPTS, we adopt the Metroplis criterion to avoid the search being trapped in local optimum phase factor, thus obtain better PAPR performance. Simulation results show that the proposed N-IPTS algorithm yields the best performance-complexity tradeoff for moderate PAPR reduction compared with the conventional PTS algorithms.

A Concentric Data Aggregation Model in Wireless Sensor Network

Cong Wang[1] and Cuirong Wang[2]

[1]Northeastern University, Shenyang 110004, China
[2]Northeastern University at Qinhuangdao, Qinhuangdao 066004, China

Abstract— The wireless sensor network(WSN) is composed of a collection of sensor nodes. Sensor nodes are small energy constrained devices, so the main focus is to be as energy effective as possible. The focus should be on minimizing the transmitting and receiving of data, because these are expensive operations. If the base station does not need access to individual sensor readings, in-network data aggregation offers an alternative that significantly reduces the energy consumption when collecting data. The PEGASIS (Power-Efficient GAthering in Sensor Information Systems) protocol is a chain-based protocol, which presents twice or more performance in comparison with the LEACH (Low Energy Adaptive Clustering Hierarchy) protocol in data gathering. The PEGASIS protocol, however, has a critical problem that the redundant transmission of the data is occurred. The cause of this problem is that there is no consideration of the base station's location when one of nodes is selected as the head node. In this paper, a concentric data aggregation model is proposed to solve the problem. The main idea of the concentric data aggregation model is to consider the location of the base station, and divide the whole WSN into several concentric and hierarchical zones refer to the location of the base station, each zone is also divided into some areas, nodes in every area are organized as PEGASIS. Data collected by sensor nodes goes through proper areas belong to different level zones towards the base station and aggregated in each hop, the last area's head node which is one of the nearest nodes of the base station transmits the aggregated data to the base station. As simulation results, the concentric data aggregation model performs better than the current PEGASIS in transmission delay and energy efficiency.

Session 2A5
RF Exposure Safety Issues

Measurement of the Dielectric Properties of Thin Disks Using a Resonant Cavity at Microwave Frequencies

Q. Balzano, **V. Hodzic**, **R. W. Gammon**, **and C. C. Davis**
ECE Dept., University of Maryland, College Park, MD 20742, USA

Abstract— The complex dielectric properties of small samples placed in a large cylindrical cavity [1] can be evaluated conveniently from the measurements of frequency and Q before and after the insertion of the sample. The sample, a disk of material or biological preparation (e.g., cells+ medium) should be very thin ($\ll 1\,\mathrm{mm}$), located in the center of the cavity, have axial symmetry and a radius much smaller than the cavity's. In these conditions, we can expect that the distribution of electric and magnetic field lines is not altered substantially by the sample from that established by the dielectric support components in the cavity. The thin layer sample provides a dielectric path to the E field lines in parallel to those in the dielectric materials of the support system, specifically a shelf and a holding dish. The following model can be used to evaluate the average complex dielectric constant of the sample.

The Q of a cavity is the ratio of the RF energy stored to the energy dissipated during one cycle of the fields [2]. Call Q_o the cavity quality factor with no sample. The supporting shelf, the holding dish are placed in the cavity in order to evaluate Q_o. The cavity resonates at the angular frequency ω_o. In this condition all the input RF power at ω_o is absorbed by the dielectric components. With the additional sample, the cavity resonates at angular frequency ω_L lower than ω_o and has a (lower) $Q = Q_L < Q_o$.

By definition of the quality factor we have:

$$Q_o = \omega_o \left|V_o\right|^2 F / \left(\left|V_o\right|^2 / R_o\right) = \omega_o F / \left(1/R_o\right) \quad \text{and} \tag{1}$$

$$Q_L = \omega_L \left|V_L\right|^2 F / \left(\left|V_L\right|^2 / R_L\right) = \omega_L F / \left(1/R_L\right), \tag{2}$$

where $|V_o|^2/R_o$ and $|V_L|^2/R_L$ represent the power lost in the cavity in the two different conditions and F is a dimensionless geometrical factor that relates the stored electric energy to the geometry of the cavity and its load. Let $1/R_B$ represents the additional RF loss in the sample. Now, $1/R_L = 1/R_o + 1/R_B$, with $1/R_B$ giving the energy dissipation in the sample caused by the same geometrical cavity field lines that produced $1/R_o$. In addition, we have:

$$\omega_L = \omega_0/\sqrt{1+\varepsilon_{rb}} \quad \varepsilon_{rb} = 4t/d\left(\varepsilon_b - 1\right) F \tag{3}$$

where ε_b is the relative dielectric permittivity of the sample, $2t$ its thickness and d the height of the cylindrical cavity. From the above equations is possible to extract the relation between the Q degradation and the frequency shift with the dissipation factor and the dielectric constant of the sample.

The results of a series of measurements of plant DNA will be presented to the show the effectiveness of the proposed method.

REFERENCES

1. Balzano, Q., et al., "A doubly resonant cavity for the detection of RF demodulation in living cells," *Bioelectromagnetics*, Vol. 29, 81–91, 2008, published on line on Sept. 26, 2007.
2. Harrington, R. F., *Time-Harmonic Electromagnetic Fields*, Chapter 5, Sections 5.4, 210–216, McGraw-Hill, New York, 1961.

Coaxial Artefact Standard for Specific Absorption Rate 100 kHz to 400 MHz

B. G. Loader, **A. G. Gregory**, **and Daniel Bownds**
National Physical Laboratory, UK

Abstract— To avoid biological effects, it is necessary to limit the heating of tissues caused by exposure to electromagnetic fields (EMF), and this is related to the specific absorption rate (SAR) of energy (units Wkg^{-1}). SAR forms the basic restriction of the International Commission on Non-Ionizing Radiation Protection (ICNIRP) for human exposure to EMF (100 kHz to 10 GHz), and European Directive EC/40/2004 will make these limits mandatory for workers. This will have an impact on industries using high power RF processing, plastic welding and Magnetic Resonance Imaging (MRI). Measuring the electric field distribution in a liquid phantom placed next to a transmitter allows the SAR to be determined. For these measurements, the sensitivity of the electric field probe in the liquid must be calibrated.

This paper presents a new artefact for the calibration of electric field probes in liquids for the frequency range 100 kHz to 400 MHz that has been developed at the National Physical Laboratory. It also gives the formulation of phantom materials to simulate the electrical properties of head and body tissues at 30 MHz, 150 MHz and 300 MHz. The calibration system, shown in Fig. 1, is a short-circuited coaxial transmission line in which the liquid forms part of the inner conductor.

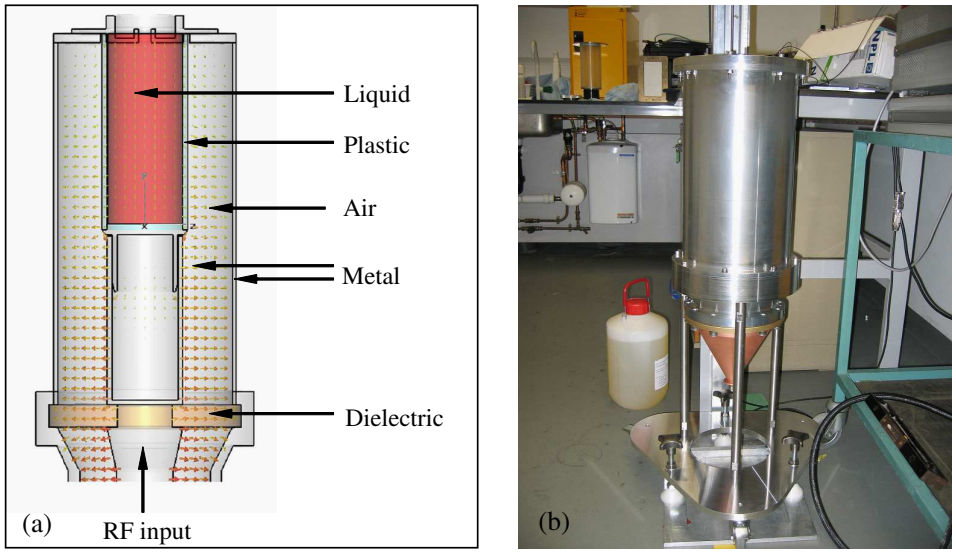

Figure 1: (a) Cross-section through system showing computed electric field distribution, and (b) photograph of the actual system.

This arrangement gives a good input match for the system, high efficiency, and results in a uniform field distribution in the liquid, thus limiting thermal gradients. A thermometer measures the rate of temperature rise in the liquid due to the applied RF power, and the liquid density and specific heat capacity are used to calculate the SAR level. Substituting an electric field probe for the thermometer allows its sensitivity to be calibrated (Eq. (1)).

$$\mathrm{SAR} = \frac{E^2\sigma}{\rho} = k\left(\frac{dT}{dt}\right) \tag{1}$$

By limiting the thermal gradients in the liquid, the temperature increases at a constant rate over many minutes, and this improves the accuracy of the calibration. The system is being used to provide traceability for SAR measurements in phantoms used to assess patient exposure during magnetic resonance imaging (MRI).

Can Magnetic rf-fields Effect Biochemical Reactions?

J. Boiden Pedersen[1] **and N. N. Lukzen**[2]

[1]University of Southern Denmark, IFK, DK-5230 Odense M, Denmark
[2]International Tomography Center, SB RAS, Novosibirsk 630090, Russia

Abstract— There is still some discussion on whether magnetic fields and especially rf-fields can influence biochemical and biological reactions and whether such effects can be measured and conceivable be hazardous to human health.

Using numerical and analytic solutions of the relevant model equations for the radical pair mechanism (RPM) we are currently studying possible effect. The RPM is a well established mechanism for magnetic field effects on chemical reactions and it has been used to obtain detailed information on the intermediate radical pair step in such reactions. The good agreement between experimental and theoretical results proves that such model calculations can be used to provide reliable estimates of the effects; In most cases, the calculated results are more accurate than experimental measurements, which in most cases, are extremely difficult to carry out. This procedure has allowed us to study a large range of systems and types of reactions.

Our results for the influence of rf-fields, radiated from mobile phones, on biochemical reactions are divided into four different types of reactions.

1. Reactions in liquids, where the radicals are free to diffuse apart. Such reactions show no measurable effect of the weak rf-field radiated by mobile phones.
2. Reactions on membranes are characterized by a very slow diffusion and a reencounter probability equal to one in the absence of scavengers. These characteristics give rize to a very large effect of magnetic fields. However, there are several conditions that must be satisfied in order to have an effect of a rf-field. The frequency of the field, i.e., 900 MHz or 1800 MHz, must be in resonance with an electron spin transition. This requires that the radicals have very large hyperfine constant, much larger than the most common values. Another condition is that the lifetime of the radical pair must be long, i.e., scavenging must be slow. No reaction satisfying both conditions is known.
3. Reactions of types 1 or 2 may show an enlarged effect if the reaction scheme includes chain reactions. An important example is the lipid peroxidation which is described by a complicated set of reaction steps that include chain reactions. This leads to bifurcations and under some conditions the reaction explodes. We are trying determine if and how the trigger point dependens on magnetic fields.
4. Enzyme reactions or electron transfer reactions often involves radicals in fixed spatial positions and metal radical ions with large hyperfine constants. Such reactions have the potential to be affected by magnetic fields. The phosphorylation by ATP synthase has been been observed to have a very large isotope effect [1]. Our calculations [2] support the proposed reaction scheme [1] and show that a strong dependence on a static magnetic field may be expected. We find no effect of rf-fields from mobile phones since the power radiated from the phone is too small. However, for larger (10 times or more) we see an effect on the rate of ATP production when the frequency is close to 1000 MHz.

It should be noted that our previous results were obtained for cw rf-fields. At present we are developing a new calculation scheme that allow us to study the effect of pulsed fields. The results of these attempts will be presented.

REFERENCES

1. Buchachenko, A. L., et al., *Proc. Nat. Acad. Sci.*, Vol. 48, 886–894, CCB, USA, 2005.
2. Buchachenko, A. L., N. N. Lukzen, and J. Boiden Pedersen, *Chem. Phys. Lett.*, Vol. 417, 311–13, 2007.

Effect of Passive RF-exposure from Mobile Phones on the SAR and Absorbed Power of Passengers in an Elevator at 900 MHz

Ally. Y. Simba[1], **Takashi Hikage**[2], **Soichi Watanabe**[1], **and Toshio Nojima**[2]

[1]National Institute of Information and Communications Technology, Tokyo, Japan
[2]Graduate School of Information Science and Technology
Hokkaido University, Sapporo, Japan

Abstract— With a rapid increase in the use of mobile communications devices such as mobile phones in various environments, a public concern on the safety of the RF-fields emitted by these devices has been growing. One of the questions being raised is whether or not the public exposure limits can be exceeded by simultaneously operation of many mobile phones inside semi-enclosed environments such as elevators, cars, train carriages and other vehicles. This anxiety is based on the fact that with small or no escape route for the electromagnetic energy, all energy emitted by mobile phones is absorbed by the passengers. Another concern of the use of mobile phones in these environments is the effect of passive RF-exposure, a case in which a non-user passenger is subjected to RF-radiation from other passengers using mobile phone in these environments.

There have been several attempts to quantitatively study the effect of the RF-radiation in these environments for many user situations. However, most of the previous investigations used theoretical approach. One short coming of the theoretical investigations for this problem is the fact that it is difficult predict amount of energy absorbed by individual passenger, as a result the assumptions are made that the power absorbed by each passenger is the equal. A numerical investigation of many passengers modeled as a realistic human model can predict amount of energy absorbed by each passenger, however, one of the main obstacle of numerical investigation is the large amount of computer resources required for simulation.

Based on the above facts, the paper presents the numerical investigations of the effect of simultaneous operation of many mobile phones inside a completely covered elevator on the specific absorption rate (SAR) and absorbed power of mobile phone users and a non-user passenger at 900 MHz. We placed up to 24 passengers in the elevator and calculate the specific absorption rate (SAR) and power absorbed by each passenger using non-uniform mesh FDTD technique running on the SX-8R NEC super computer. 23 of the passengers are using mobile phones. One passenger is without phone and is used to study the passive RF-exposure.

We used a 3-y old Japanese child model to represent the passengers. Due to its small weight, the child model gives a whole-body averaged (WBA) SAR 5 times larger than that obtained in an adult model. The worst case scenario considered in this work includes: 1) antenna maximum output power of 250 mW, 2) completely covered elevator, and 3) passenger positions giving maximum passive exposure to the non-user passenger. Under these conditions, the maximum values of the peak 10-g SAR, WBA-SAR and absorbed power of the passenger not using mobile phone are 0.45 W/kg, 30 mW/kg and 415 mW, respectively.

Effects of Losses Due to Human Phantoms on 3-dimensional Electromagnetic Field Distribution in Elevators

Y. Kawamaura[1], **T. Hikage**[1], **T. Nojima**[1], **A. Simba**[2], **and S. Watanabe**[2]

[1]Hokkaido University, Japan
[2]National Institute of Information and Communications Technology, Japan

Abstract— The purpose of this study is to estimate the Electromagnetic field (EMF) distributions emitted by Cellular radios in environments surrounded by conductive surfaces, e.g., elevators. In this paper, we discuss the EMF absorption effects due to lossy materials being present in elevators using precise numerical analysis based on the FDTD method. Furthermore, measured results are compared with analytical results to confirm if the computation method is accurate. Then, the computation method is used in order to obtain 3-dimensional spatial electric field distributions throughout the inner space of the elevator. Finally, field histograms and cumulative ratios are derived from the spatial distributions to estimate the percentage of the area having the same strength. These methods are useful for carrying out a complete estimation in the whole area. Here, the relative field strength, normalized to a certain reference level, is adopted. The elevator model's dimensions are 1.4 m × 1.35 m × 2.3 m (Length × Width × Height). We use a half-wavelength dipole antenna to represent a cellular radio operating in the 800 MHz, 1.5 GHz and 2 GHz bands. The antenna is set 1.15 m from the floor. As an example, the estimation result for the absorbing effects due to a simplified rectangular phantom is shown in Figure 1. In this case, a dipole antenna is set 0.08 m × 0.08 m (Length × Width) from a corner of the elevator. A simplified rectangular phantom that has homogeneous electric parameters is applied in the analysis. The phantom sizes are 0.05 m × 0.4 m × 0.4 m (Phantom 1) and 0.1 m × 0.4 m × 1.8 m (Phantom 2), respectively. Phantom 2 is more developed and is considered to be the average height and weight of male adults. The relative electric field strength normalized to a field strength with cumulative ratio is approximately 100% in an analysis without the phantom. These results suggest that a small phantom results in a decrease of about 10 dB of the field strength in the elevator. Also, with the Phantom which has almost the same volume as male adults, the field strength decreases by about 18 dB compared with the case when no phantom is present.

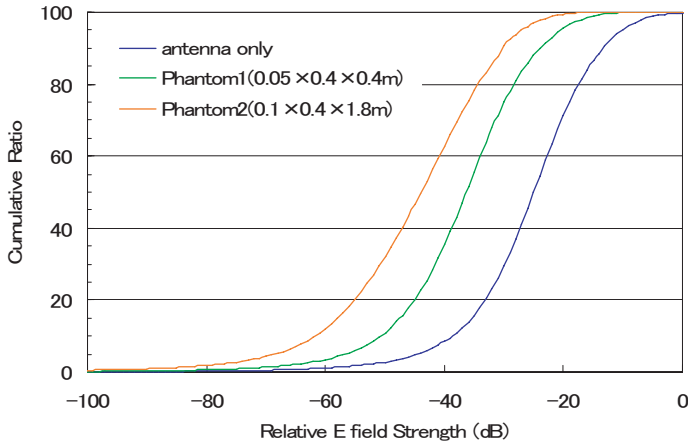

Figure 1: Absorption effects due to lossy phantom in elevator.

Temperature Rise in the MRI Head Models Exposed to Commercial Mobile Phones

Jafar Keshvari

Corporate Development Office, Nokia Corporation Itämerenkatu 11-13
Helsinki 00180, Finland

Abstract— The physiological adverse health effects to humans through electromagnetic-wave exposure are induced by temperature increases although the safety standards at the moment are regulated in terms of the local peak specific absorption rate (SAR). The temperature rise the Magnetic Resonance Imaging MRI based adult and child head models following exposure to two commercially available mobile phones are calculated. Also the temperature rise in child and adult head models were compared. Four (MRI) based head models; one female, one adult, two child head models aged 3 and 5 years were used. The finite-difference time-domain method (FDTD) was employed for calculating the temperature. The results show that the temperature rise in the brain region remains below 0.15°C.

Mobile Phone Base Stations and Sleep Quality — Results from an Experimental Study

Heidi Danker-Hopfe[1], **Cornelia Sauter**[1], **Christian Bornkessel**[2], **and Hans Dorn**[1]

[1]Dept. of Psychiatry and Psychotherapy
Charité — Universitaetsmedizin Berlin, Berlin, Germany
[2]IMST GmbH, Kamp Lintfort, Germany

Abstract—

Introduction: There is some evidence that sleep parameters, brain activity during wake (EEG) and the processing of intellectual information are influenced by exposure to mobile phone electromagnetic fields, i.e., at field intensities below accepted limit values. For residents living close to mobile phone base stations, the subjective perception of a disturbed sleep is among the most often mentioned complaints attributed to the EMF (electromagnetic field) exposure. Since epidemiological studies have shown contradictory results, the aim of the present study is to analyse the impact of electromagnetic fields of mobile phone base stations on sleep of residents in an experimental setting using a double-blind, sham-controlled, balanced randomized cross-over design.

Methods: Study participants were recruited from sites, where 1) no mobile phone service was available, 2) only weak fields from other RF-sources (TV etc.) were present, and 3) there was no emotional EMF-discussion in the run-up to the study. Data acquisition comprised individual measurement of EMF-exposure (performed by IMST GmbH, Kamp Lintfort, Germany), questionnaires to characterize the sample (with regard to clinically relevant sleep disorders (LISST), overall sleep quality (PSQI), excessive daytime sleepiness (ESS), Zung scales to assess anxiety and depression (SAS and SDS), attitude towards mobile phone communication and personality traits (NEO-FFI)), and subjective (morning and evening protocols) and objective (derived from frontal EEG and EOG recordings performed in an ambulant setting at home) sleep data. For each participant subjective and objective sleep data were recorded for twelve nights. Exposure was realized by an experimental base station working constantly with a well defined emission. The base station was manipulated to ensure blinding.

Results: Altogether 397 subjects ($>$ 17 years) from 10 villages in various parts of Germany participated in the study. The number of inhabitants of the villages varied from 125 to 652, the total number was 2856 ($>$ 17 years: 2329). That is 17.1% of the eligible inhabitants participated in the study (50.9% females in the sample out of 48.5% eligible females). The mean age of participants was 45.0 ± 14.2 years, the range was 18 to 81 years. Males were slightly, but not significantly older than females (46.3 ± 14.2 years vs. 43.8 ± 14.2 years). 21 subjects (5.3%) had to drop out of the study before the end due to illness (own or of relatives) or job-related reasons.

Analysis of the questionnaires to characterize the sample showed that study participants are representative of general population based samples. There was no indication of an increased prevalence of depression, anxiety, special personality traits, extreme morning-evening types. Furthermore the attitude towards mobile communication in the sample was equivalent to results from representative population surveys.

The results of the present study do not provide evidence for short-term physiological effects from electromagnetic fields emitted by mobile phone base stations on objective and subjective sleep quality in a broad representative population sample. However, concerns about possible health risks resulting specifically from mobile phone base stations were associated with a significant deterioration of sleep quality in the sham condition.

ACKNOWLEDGMENT

This study was funded by the Federal Agency of Radiation Protection, Project Nr. M8837.

"Non-Thermal" RF Bioeffects: Real or Artifact?

C.-K. Chou[1], **J. A. Elder**[1], **and A. W. Guy**[2]

[1]Corporate EME Research Lab, Motorola, Fort Lauderdale, FL, USA
[2]Department of Bioengineering, University of Washington, Seattle, WA, USA

Abstract— RF safety concerns started in the 1950s with exposure to radar, then expanded to radio and TV broadcasting in the 1960s, microwave ovens in 1970s, police radar in 1980s and mobile phones and other wireless communication devices in the last 15 years. These concerns can be addressed by the weight of scientific evidence in approximately 2000 peer-reviewed articles in the WHO database relating to RF bioeffects that includes more than 600 peer-reviewed papers on mobile telephony exposure. The extensive RF database with effects at high and low RF exposure levels has been reviewed by both the International Commission on Non-Ionizing Radiation Protection (ICNIRP) and International Committee on Electromagnetic Safety (ICES) of IEEE to develop exposure limits to protect against established adverse health effects. More than 40 countries have adopted ICNIRP or ICES limits. Since the early 1990s, world wide organizations have spent and committed about half a billon US dollars on RF safety research on wireless communications alone. However, reports of effects at low exposure levels continue to raise public concern about the safety of long-term exposure at current RF exposure limits. Because there is no known mechanism to explain any observed effect at low exposure levels, the changes have been called "non-thermal effects" by some researchers. The problem in confirming that the effect is indeed "non-thermal," and not due to an experimental artifact or a small change in temperature, contributes greatly to the controversy about bioeffects of RF exposure. Labeling a biological effect "non-thermal" implies that the effect is due to a "yet-to-be-discovered" mechanism other than a temperature increase. The objective of this presentation is to show the importance of properly conducted and thorough scientific research in identifying a weak thermal effect or experimental artifact as an explanation for a number of biological changes reported as "non-thermal" effects of low level RF exposure.

In the 1960s, a Soviet study reported a non-thermal effect of microwave exposure on action potentials of isolated nerves. When the nerves were exposed in a temperature-controlled waveguide, no effect on action potentials was found other than a thermal effect, even if the nerves were exposed to very high intensity pulsed fields with peak SAR up to 220,000 W/kg. US researchers in 1965 reported behavioral effects in rats at a low power density (1 mW/cm^2); however, a more thorough dosimetry evaluation showed the effect was due to a poorly designed exposure system. The SAR was found as high as 185 W/kg in the hind legs when the rat's tongue touched the water bottle and the legs and tail were in contact with the metal ground plane. Without this detailed dosimetry data, the behavioral effect was misinterpreted as evidence of a non-thermal RF effect. In the late 1970s, an RF effect on tumor cells was almost reported as non-thermal, until it was realized that the effect was due to the significant temperature gradient at the monolayer at the bottom of the cell culture container. More recently in 2006, de Pomerai et al. reported that their earlier published paper claiming that SARs of 0.004–0.04 W/kg induced a non-thermal heat shock response in nematodes was incorrect because detailed dosimetry showed that a small temperature rise explained the effect. In 2007, Tattersall et al. reported that the effects of low intensity RF fields on electrical activity in rat brain slices published in 2001 were due to heating at the electrodes. Other effects labeled as "non-thermal" that have been identified to be due to experimental artifacts or temperature changes will be discussed. Researchers must be responsible for including detailed and accurate dosimetry as an integral part of their biological studies to make their efforts useful for the understanding of RF bioeffects. At this time, the existence of "non-thermal" RF effects that could be associated with potential adverse health effects is not proven.

Why Do People Still Worry about Radiofrequency Safety in 2008?

David Black
University of Auckland, New Zealand

Abstract— The recent rollout of third generation mobile telephone technology has seen resurgence in public concern about radio frequency safety in some parts of the world. The biological and medical science regarding radio frequency safety is well established, mature, consistent and coherent. Standards are in place throughout the world which are also coherent and in the most part are soundly based on the science. The position generally taken by competent authorities goes so far as to say that no adverse health effects at all are expected to arise from compliant use of radiofrequency energy.

Despite this, during the last year public concern seems to be escalating in some countries, including New Zealand. This anxiety appears to be particularly centred around mobile telephones and their base stations. This paper analyses the sources of information frequently used by people with ongoing concerns, the ways in which this information is interpreted and translated to anxiety and the role of researchers, regulators and the media in perpetuating such concerns.

There is no doubt that, particularly having regard to the rapidly expanding nature of radiofrequency based communications technology, ongoing searches for knowledge and understanding are both worthwhile and inevitable. Nevertheless, it would seem that a side-effect of this process is escalation and perpetuation of non- scientifically based ideas at the expense of public confidence in the health protection afforded by modern and thoroughly researched standards. The media and politicians are often held responsible for this, but it is questionable whether they doing any more than should be expected of them. If so, who, if anybody, is to blame?

Session 2A6
Novel Computation Techniques in Microwaves

Particle Swarm Intelligence Applied to Design Microwave Amplifier for the Maximum Gain Constrained by the Minimum Noise over the Available Bandwidth

Salih Demirel, Filiz Güneş, and Ufuk Özkaya
Electronics and Communication Engineering Department, Yıldız Technical University
Beşiktaş, Istanbul, Turkey

Abstract— Nowadays, microwave amplifier design is doubtlessly one of the major interests of microwave engineering. Considering all the stringent requirements which include high gain, low input VSWR together with the low-power consumption from the low-battery, the wideband miniature LNA design is one of the biggest challenges to UWB transceiver integrations. In order to meet these stringent requirements, first of all, the fast and low-noise, high quality transistors are needed, which is of course the matter of the available technology. Traditionally, wideband microwave amplifiers relied on transistors realized with composite semiconductors, e.g., GaAs, because of the intrinsic superior frequency characteristics of such devices. The second level of the challenge is the accurate analysis performance capabilities of the chosen transistor in order to obtain the feasible design target space, and then is to design the microwave amplifier subject to the feasible design target space. Otherwise is to utilize the device either under its potential performance or for unrealizable requirements. This device characterisation problem is solved point on the rigorous mathematical bases throughout the operation domain within the physical limitations of the employed device. Thus, combining this performance characterisation with the ANN or /SVRM model of the device, the compatible (Noise Figure F, Input VSWR V_i, Gain G_T) triplets together with their source Z_S, and load Z_L terminations can be obtained as the functions of the operation variables V_{DS}, I_{DS}, f of the device. Originalities of this work can be ordered as follows: (i) Exploiting the performance characterisation of a chosen high technology transistor, the compatible triplet of (Minimum Noise Figure $F_{\min}(f)$, input VSWR $V_i = \text{const.}$, the Maximum gain $G_{T\max}(f)$) is chosen over a predetermined bandwidth B as the design target; (ii) This design target is achieved only gain optimisation of the two simple matching circuits at front and back-ends; (iii) Particle Swarm Optimisation (PSO)algorithm is employed as a simple and efficient optimisation tool. Due to the superior intrinsic frequency features of the device, a flat gain characteristic is obtained under the available minimum noise and input VSWR along a maximum operation bandwidth. Moreover, the resulted amplifier circuit is a feasible circuit that can be realized by microstrip technology. A typical design example is given synthesized, target, simulated with the resulted, characteristics. Finally, the complete analysis of the whole system is done using the optimized parameters and the resulted performance are compared with the results of a Professional soft packet and shown that all of them are agreed well.

Support Vector Synthesis Formulation of RF/Microwave Transmission Lines

Nurhan Türker Tokan and Filiz Güneş
Department of Electronics and Communication Engineering
Electrical and Electronics Engineering Faculty, Yıldız Technical University
Istanbul 34349, Turkey

Abstract— As it is well known, by offering the unique solution based on the structural risk optimization process, Support Vector Machines (SVMs) have verified their improved generalization performance over other classical optimization techniques in the wide range of applications. This is mainly because firstly, SVM solves a convex constrained quadratic optimization problem, whose error surface is free of local minima and has a unique global optimum; secondly, SVM approach is based on structural risk minimization (SRM) principle instead of empirical risk minimization (ERM) which is used in ANN approach. SRM principle implements well trade-off between the model's complexity and its generalization ability. Furthermore, SVM is based on small sample statistical learning theory, whose optimum solution is based on limited samples instead of infinite sample that ensures enormous computational advantages.

Here, we introduce a general approach to synthesis formulation of the RF/microwave transmission lines to be used in the microwave integrated circuits (MICs): Support Vector Regression (SVR) formulation based upon their electromagnetic analysis. For this purpose, firstly we define analysis and synthesis sides of the problem in the terms of the generalized structure of a transmission line as the black-box representation. In these representations, one-to-one mappings are implicitly assumed between the input and output pairs. Therefore, secondly, according to the given synthesis definition, rearranging the input-output components of the analysis data, we have the synthesis data to be inputted to the SVR to obtain its corresponding support vector (SV) expansion.

In this work, we apply our approach "Support Vector synthesis formulation" to two types of the transmission lines: (i) Conductor-backed coplanar waveguides with upper shielding; (ii) Microstrip lines. "Support Vector synthesis formulation" is made for the first type of the transmission lines based on its the rigorous electromagnetic analysis, while for the second one, firstly the coarse analysis model is employed, then "knowledge based SV" expansion is generated using its "fine model". Thus we demonstrated the basic method in the first example, while in the second one "knowledge loading" to the SVs is given.

Particle Swarm Intelligence Applied to Determination of the Feasible Design Target for Low-noise Amplifier

Ufuk Özkaya, Filiz Günes, and Salih Demirel
Department of Electronics and Communication Engineering, Yıldız Technical University
İstanbul, Turkey

Abstract— In this work, the feasible design target space (FDTS) for a microwave transistor is determined for use in the front-end as a low-noise amplifier employing a global optimum searcher. The feasible design space (FDTS) is generated from the performance (Noise F, Input VSWR V_i, transducer Gain G_T) triplets and their source Z_S and load Z_L terminations. Here, the passive (Z_S, Z_L) termination pair is the simultaneous solution of the nonlinear performance F, V_i, G_T equations of the transistor subject to the physical realization conditions. The physical realization conditions are $F \geq F_{\min}$, $V_i \geq 1$, $G_{T\min} < G_T \leq G_{T\max}$, $\Re e\{Z_{in}\} > 0$, $\Re e\{Z_{out}\} > 0$ for the solution passive (Z_S, Z_L) termination pair. In order to determine the design target space of a microwave transistor at a certain operation (V_{DS}, I_{DS}, f) condition, the problem can be considered into two parts: In the first part, upper limitation of the gain $G_{T\max}$ should be determined with its $Z_{S\max}$, $Z_{L\max}$ termination couple. This problem can be described as a mathematically constrained maximization to find out the maximum value of $G_T(R_S, X_S, R_L, X_L)$ for the passive Z_S and Z_L terminations satisfying the stability conditions subject to the constraints of $\Phi_1 = F_{req} - F(R_S, X_S) = 0$ and $\Phi_2 = V_{ireq} - V_i(R_S, X_S, R_L, X_L) = 0$, where $F(R_S, X_S)$ and $V_i(R_S, X_S, R_L, X_L)$ are noise and input VSWR performance measure functions of the transistor at the chosen operation condition and F_{req} and V_{ireq} are the required noise and input VSWR values; respectively. In the second part of the FDTS problem, the passive (Z_S, Z_L) termination pair is determined for the required gain $G_{T\min} < G_T \leq G_{T\max}$ constrained by the required noise, $F_{req} \geq F_{\min}$ and input VSWR, $V_{ireq} \geq 1$. For the optimization process, cost functions can be expressed suitable for these objectives and then particle swarm intelligence is applied as a simple, fast and efficient tool. The results are compared to the corresponding ones obtained from the performance characterization theory [1]. Excellent agreement are resulted, thus, we present a simple and efficient approach to be used during the design process of a low-noise amplifier, to determine the FDTS at a chosen operation point of the device without having need for more complicated knowledge and software.

REFERENCES

1. Güneş, F., M. Güneş, and M. Fidan, "Performance characterisation of a microwave transistor," *IEE Proceedings — Circuits, Devices and Systems*, Vol. 141, No. 5, 337–344, Oct. 1994.

Synthesis of Multi-beam Uniform Linear Antenna Arrays Using Psearch Algorithm

Fikret Tokan and Filiz Güneş
Department of Electronics and Communication Engineering
Electrical and Electronics Engineering Faculty, Yıldız Technical University
Istanbul 34349, Turkey

Abstract— Nowadays, multiple-beam antenna arrays have received significant attention of the researchers, since their syntheses reduce space and cost and they find a wide-range of application in microwave technology such as communication and radar. The way changing the radiation pattern for an antenna array on a ready printed board is to change the feeding conditions. Here the main idea is to get result with the optimum cost [1]. Based upon this idea, in the last years there has been a great interest in the design and applications of multi-beam antenna arrays in the form of the re-configurable arrays using optimization algorithms, particularly derivative-free, evolutionary algorithms such as bees algorithm [2], particle swarm optimization (PSO) [3], genetic algorithms [4].

In this work, design of a reconfigurable multi-beam antenna array is carried out: Two types of radiation patterns — pencil beam and flat-top — are synthesized using the 20 element; uniform, linear array feeding a 5-bit digital attenuator in steps of 1/32. We achieve the flat-top radiation pattern requirements by using additionally a 6-bit digital phase shifter in the steps of 5.625°. In the optimization process, pattern search (PSearch) is implemented successfully. Psearch is a direct method for searching minima of a function which is not necessarily differentiable, stochastic, or even continuous. Furthermore, a fixed dynamic range ratio (DRR) value is kept in the synthesis of excitation amplitudes in order to minimize the effects of coupling between the neighboring array elements. In addition to these two types of radiation patterns, a difference pattern can also be obtained by only exciting with the 180° phase uniformly to the half of array elements in symmetrical positions in the pencil-beam distribution. Besides, "Thinning" process can be applied to each of the feeding arrangement, thus two more different radiation patterns are obtained. All of these patterns can be controlled under the established objectives with a single optimization procedure.

A sensitivity analysis is also performed to verify that optimized designs could be successfully applied in real-world scenarios. Finally many typical worked examples will be presented for the above-mentioned design approaches.

REFERENCES

1. Bucci, O. M., G. Mazzarella, and G. Panariello, "Reconfigurable arrays by phase only control," *IEEE Transactions on Antennas and Propagation*, Vol. 39, No. 7, 919–925, 1991.
2. Guney, K. and M. Onay, "Bees algorithm for design of dual-beam linear antenna arrays with digital attenuators and digital phase shifters," *International Journal of RF and Microwave Computer-Aided Engineering*, Vol. 18, No. 4, 337–347, 2008.
3. Gies, D. and Y. Rahmat-Samii, "Particle swarm optimization for reconfigurable phase-differentiated array design," *Microwave and Optical Technology Letters*, Vol. 38, No. 3, 168–175, 2003.
4. Mahanti, G. K. and A. Chakrabarty, "Phase-only and amplitude-phase synthesis of dual-pattern linear antenna arrays using floating-point genetic algorithms," *Progress In Electromagnetics Research*, PIER 68, 247–259, 2007.

Design of a Broadband Microwave Amplifier Using Fuzzy Logic Performance Data Sheets with a Artificial Immune System

Yavuz Cengiz[1], **Fırat Yücel**[2], **and Filiz Güneş**[3]

[1]Department of Electronics and Communication Engineering,
Süleyman Demirel University, Isparta, Turkey
[2]International Computing Institute, Ege University, İzmir, Turkey
[3]Department of Electronics and Communication Engineering,
Yıldız Technical University, Istanbul, Turkey

Abstract— Optimization is one of the fundamental processes frequently encountered in the engineering problems and is highly nonlinear in terms of the descriptive parameters of the system. An optimization process generally contains two fundamental problems:

(i) The first is to form a feasible Design Space which is defined in terms of the design variables and targets;
(ii) The second is that the global minimum of the error (objective) function governing the optimization must be obtained with respect to the design variables within the feasible design space.

For optimization of a microwave amplifier, design variables are generally the matching circuit parameters whose lower and upper limits are very often determined by the technology to be utilized in the realization stage of the design. Nevertheless, design targets are still one of the main problems of the amplifier optimization. Generally, the optimization is focused on the transducer power gain (G_T) over a frequency band of operation without controlling the other performance criteria such as the noise (F), the input standing wave ratio (V_i). Certainly, within the optimization process one can easily embed the desired performance goals without knowing the physical limits and/or compromise relations among F, V_i and G_T appropriately. Unfortunately this process often fails to attain the desired goals. However, the Fuzzy Logic Performance Data Sheets (FLPDS) of the transistor overcomes all the above-mentioned handicaps and embeds the compatible (F, V_i, G_T) triplets with their source (Z_S) and load (Z_L) terminations together over a predetermined frequency band of operation, which is given in the accompanied paper [1]. So optimization of a microwave amplifier is a multi-objective design problem with a mix of equality and inequality constraints.

The Artificial Immune Optimization algorithm with the binary mode is utilized in the multi-objective optimization process for the global minimum of the objective function which is expressed as a function only gain of a matching circuit, in the negative exponential form to ensure the rapid convergence. Here optimization of a microwave amplifier with the different type matching circuits is given as a worked example and its resulted performance ingredients are compared with the design targets.

REFERENCES

1. Güneş, F. and C. Tepe, "Identification of a microwave transistor using 'Neural performance data sheets'," submitted in the *Progress In Electromagnetics Research Symposium 2003*, Hawai, 2003.

Design of a Patch Antenna with Integration Cellular Automata and Genetic Algorithm

Y. Cengiz[1] **and H. Tokat**[2]

[1]Suleyman Demirel University, Isparta, Turkey
[2] Turk Telekom, Isparta, Turkey

Abstract— Microstrip patch antennas are used in many communication systems as they are low-weight, low-cost and as they have multi band properties and effective performances. Especially microstrip antennas gain importance because they have a great range of usage area such as, GSM, space vehicles, planes, radars, satellite communication in many millitary services and their production is easy with printed circuit technology [1].

At the antenna design, small changes affects the performance of the antenna. While optimizing the shape, the probality of the finding best configuration is very low, because of possible wide range geometries. If the geometry can be determined by formulations, then optimized geometry range can be more computable.

Cellular Automata is a geometri determination method which has a system with simple rules and becomes from stages affecting by themselves mentioned at 1982 by Stephen Wolfram. Through this method, beginning from a black box, it is possible to reach the whole different rules that models the system.

REFERENCES

1. Yazgan, E., "Mikroşerit antenler," *Elektrik Mühendisliği Dergisi*, September 1987.

Neural Network Based Target Recognition

S. Makal and A. Kizilay
Electronics and Communications Engineering
Yildiz Technical University, Turkey

Abstract— In this paper, a neural network solution is proposed for identification of cylindrical targets located above the perfectly conducting (PEC) flat surface. A set of features are derived from scattered fields calculated by using the image technique formulation and Moment Method (MoM). In this simulation problem, 100 field values are obtained at a given scattering angle for each of the ten targets by changing the starting frequency 1 GHz to 10 GHz. Thus, there are 1000 samples for the dataset used for neural network. An RBF (Radial Basis Function) network, the two layer feed-forward neural network using radial basis functions, utilizes the feature set for target identification. Such a network is characterized by a set of inputs and a set of outputs. The input layer of the RBF is designed to have three neurons including the frequency, the real and the imaginary parts of the scattered field and the output layer has two neurons corresponding to the radius and the height.

This work aims to find the heights measured from the surface and radiuses of the targets from the scattered field values. Thus, it is shown that electric field features for a target can be extracted from its radar returns that are independent of such radar parameters as target range, loss, antenna gain, etc. They are determined only by the frequencies, the scattering angles and the fields. These results are very useful in practical applications especially relating to target recognition.

A 5 GHz LNA Design Using Neural Smith Chart

M. Fatih Çağlar[1] and Filiz Güneş[2]

[1]Department of Electronics and Communication Engineering
Süleyman Demirel University, Isparta, Turkey
[2]Department of Electronics and Communication Engineering
Yıldız Technical University, Beşiktaş, Istanbul

Abstract— In wireless communications, receivers need to be able to detect and amplify incoming low-power signals without adding much noise. Therefore, a Low Noise Amplifier (LNA) is often used as the first stage of these receivers. As the usage of wireless communication in 2.4 GHz band grows, it causes uncontrolled occupancy by users in that band. Since it is an unregulated frequency, the 2.4 GHz band also suffers from enormous interference effects generated by devices like microwave ovens and 2.4 GHz transmitters that will reduce performance especially in wireless local area networks (WLANs). On the other hand, the 5 GHz band provides lots of unlicensed spectrum and it has less interference. Recently, many researchers have been focused on the 5 GHz standard in the design of wireless transceivers which should be used in 802.11a, HiperLAN2 and HiSWANa applications. The Smith chart was originally intended to be a graphical aid for eliminating the drudgery of computation with complex numbers in microwave engineering. A great deal of knowledge can be acquired from a Smith chart e.g., standing wave ratio, single and double stub tunings and much more. Also, it is very useful in conveying input impedance variations along a transmission line as the observation point moves away from the load. Although Smith charts are valuable and contain significant amount of information, inaccurate observations can lead to erroneous results and frustration. In this work, an Artificial Neural Network (ANN) model of the Smith chart is proposed for an alternative solution to impedance matching of a LNA design which has been entitled "Neural Smith Chart" shortly. The feed-forward Multilayer Perceptron (MLP) type of neural network is utilized with the two hidden layers, three inputs and twenty-three outputs. Real and imaginary part of source impedance, physical length and characteristic impedance of the transmission line, operation frequency are inputted to this network, while the magnitude and the phase of the output reflection coefficient, real and imaginary part of output impedance, single stub matching lengths and reactance, double stub matching lengths, position lengths and VSWR are taken as the outputs. This work presents the design of a single-stage, low noise, stable and matched amplifier. The amplifier is designed around the Agilent ATF-551M4 low noise enhancement mode pseudomorphic HEMT (EpHEMT). At 5 GHz and biased at 2 V and 20 mA, simulation results show that the amplifier provides 13.00 dB transducer gain, 0.77 dB noise figure, 5 dB and 77 dB input and output return loss, respectively. The input and the output impedance matching circuits are performed using Neural Smith chart outputs and MATLAB® RF Toolbox simulation solutions for comparison. Neural Smith chart gives satisfying results at 5 GHz which are 12.81 dB transducer gain, 0.76 dB noise figure, 4.7 dB and 28 dB input and output return loss, respectively.

Session 2A7
Electromagnetic Field Modeling and Inversion and Applications 1

Effect of Edge-preserving Parameters on GPR Reconstruction

Hui Zhou[1,3], **Zhaolei Wang**[2], **Dongling Qiu**[3], **and Guofa Li**[1,3]

[1]State Key Laboratory of Petroleum Resources and Prospecting
Key Laboratory of Geophysical Prospecting, CNPC, China
[2]Oriental Geophysical Corporation, Zhuozhou, Hebei, China
[3]China University of Petroleum Beijing, Beijing 102249, China

Abstract— The key of the application of regularization is to construct a regularization operator and to determine regularization parameters. A simple and well-known regularization method is to suppose the model is globally smooth. However, realistic geological model consists of not only smooth regions, but also evident boundaries that are important characteristics of the model. These boundaries need be preserved in order to obtain high-resolution reconstruction images with a clear background and boundaries. However, it is difficult to preserve the boundaries and to avoid excessive smooth in the effective application of the regularization method. Conventional smooth method cannot overcome the conflict of suppressing noise and preserving edges since the noise and the edges are both high frequency components of a reconstructed image. Conventional smooth method deals with the noise and boundaries equally. As a result, the noise is weakened, and the boundaries are blurred. Contrarily, the boundaries are reserved, the ability to resist noise is lowered. In practical reconstructions it is necessary to tradeoff the edge preservation and noise suppression.

In this paper we use the edge-preserving method to reconstruct the subsurface. We try to investigate the relation between the regularization parameters and the error of data by theoretical analysis and numerical calculation, and to find a rule to determine the edge preserving parameters reasonably and efficiently.

By theoretical analysis we find that χ, which is one of two regularization parameters, should be selected to let the gradient (be protected) of the actual model be located in the right section of a potential function, and to let the gradient (be smoothed) created by error and noise be located in the left section.

In addition, two-dimensional numerical reconstruction examples are conducted from synthetic ground-penetrating radar data. For each reconstruction example using a data set with a certain signal to noise ratio (SNR), a best regularization parameter pair θ and χ is obtained. θ is another regularization parameter. By fitting two lines of θ-SNR and χ-E_N/E_S (the ratio of noise to signal), two graphs of θ-SNR and χ-E_N/E_S are obtained and they are shown in Figure 1. It shows that θ-SNR and χ-E_N/E_S are nearly linear. As a result it is possible to determine θ and χ by SNR.

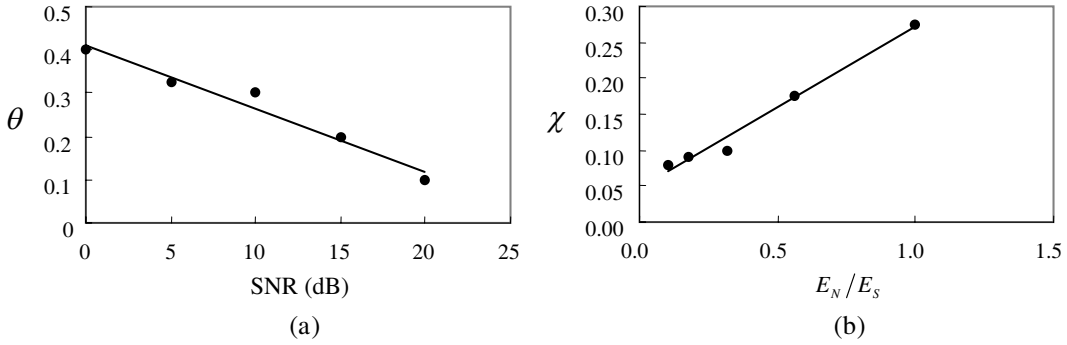

Figure 1: The relation of (a) auxiliary parameter θ and SNR, and (b) regularization parameter χ and E_N/E_S.

Use GL TM Model Inversion to Detect the Dielectric Parameter

Jianhua Li[1, 2], **Ganquan Xie**[1], **Lee Xie**[1], **Chien-Chuang Lin**[2], **and Michael Oristaglio**[3]

[1]GL Geophysical Laboratory, USA
[2]Da Yeh University, Taiwan
[3]Schlumberger Research, USA

Abstract— In this paper, we present an Advanced Global Integral and Local differential Control Source Magenetotelluric inversion, shortly call AGILD CSMT, for Earthquake and geophysical imaging. The MT data in the Wenchuan Earthquake area and Long Men mountain crack layers is measured by us and Chengdu Technology University during the risk aftershock period. For compensating the lack of the MT data, the control source MT data in the low frequency in some locations are measured. The low frequency band is from 0.01 to 100 Hz. A low frequency CSMT AGILD is developed that the shallow-deep layer is chosen to match the corresponding higher-lower frequency. Suppose that the resistivity can be measured in the surface, the AGILD inversion is performed to search the variance resistivity in the k layered 3D-2D sub domain if the variance resistivity in the above $k-1$ layered subdomains is determined. Our Global and Local EM field modeling is used in the AGILD CSMT 3D FML inversion. Because the GL modeling does not need to solve big matrix equation and the variance of the resistivity is changed in 3D layered subdomain only, the ADILD CSMT LMF inversion is fast and high resolution and can be extended to 3D ocean CSMT inversion with the controlled EM sources is located in ocean bed surface.

A Model for the Lower Atmospheric Electric Field Due to Thunder Cloud Charge Distribution

S. S. De, **B. Bandyopadhyay**, **Suman Paul**, **M. De**, **and D. K. Haldar**
Centre of Advanced Study in Radiophysics & Electronics, University of Calcutta, India

Abstract— The distribution of electric charges in the electrified cloud introduce important effects in the ionosphere and into the region between the ionosphere and the earth. The electrical properties of the medium changes greatly between thundercloud altitudes and the magnetosphere. Various models are there to examine the electrical coupling between the earth's upper and lower atmospheric regions. The main sources of electric current in these regions are thunderstorms which are distributed statistically in geographic areas.

A model for the penetration of DC thundercloud electric field at these regions has been presented here. The model deals with the electromagnetic responses of the atmosphere which are simulated through Maxwell's equations together with a time varying source charge distribution.

The modified ellipsoidal-Gaussian profile has been taken for the charge distribution of the electrified cloud. The conductivity profile of the medium is taken to be isotropic below 70 Km height and anisotropic above 70 Km. The earth's surface has been considered to be perfectly conductor.

A general form of equation representing the thundercloud electric field component is deduced. The solution is appropriate to study the electric field variation in the atmosphere.

Electrified clouds and lightning play important role in the global electric circuit. The vertical component of the electric field would relate the global electric circuit while the radial component would show the electrical coupling between the lower ionosphere and the ionized earth environment. The role of such thundercloud electric field may be made useful to investigate the formation of field-aligned irregularities in the upper atmosphere.

ACKNOWLEDGMENT

This work is funded by Indian Space Research Organization (ISRO) through S K Mitra Centre for Research in Space Environment, University of Calcutta, Kolkata, India.

Loss Mapped Perfectly Matched Layer (LMPML) Absorbing Boundary Conditions for Truncation of FDTD Lattices

Roman Trogan and Carey M. Rappaport
Northeastern University, Boston, MA 02115, USA

Abstract— Loss Mapped Perfectly Matched Layer (LMPML) ABC is presented here as a new approach for memory storage and operation count efficient ABC formulation. The derivation of this method starts similarly as other approaches with the frequency domain definition of original PML method. Unlike other approaches, the LMPML does not immediately Fourier transformation the equation to the time domain. Instead the LMPML manipulates the frequency-domain PML formulation by introducing two auxiliary variables $\tilde{E}$ and $\tilde{H}$. These variables are calculated in a very efficient way inside ABC layer. While these are not real electric and magnetic fields components, their usage is allowed in the region outside main computational grid. The basic relationship between these auxiliary variables and real electric and magnetic fields is defined by:

$$\frac{\partial \tilde{F}_b}{\partial n} \equiv \frac{1}{1 - jS_n} \frac{\partial F_b}{\partial n} \tag{1}$$

with F being electric or magnetic field at the spatial point (n, s, b), with unit vectors $\hat{n} \times \hat{s} = \hat{b}$, and spatially-dependent loss $S_n = \sigma_{PML}/\omega\varepsilon$ for the PML at $n = n_{PML}$. The method then derives a new relationship between auxiliary and real electromagnetic fields for the time domain:

$$\frac{\partial F_b}{\partial t} = \left(\frac{\partial}{\partial t} + \frac{1}{\tau(n)}\right) \tilde{F}_b - \int dn \tilde{F}_b \frac{\partial \left(1/\tau(n)\right)}{\partial n}; \quad \text{where} \;\; \tau(n) \equiv \frac{\varepsilon}{\sigma_{PML}} \tag{2}$$

Using both time and frequency domain relationships between the auxiliary and real fields of the same type (electric or magnetic), a new relationship between the different auxiliary fields inside the LMPML can be specified. This is achieved by replacing the space derivative term of the time-harmonic Maxwell's curl equations for the PML media, transforming the new equation into the time domain, and finally replacing the time derivative term of the remaining real electromagnetic field. In two dimensions (TM_b or TE_b the resulting relationship will have the form:

$$\frac{1}{p}\left(\frac{\partial \tilde{F}_{1s}}{\partial n} - \frac{\partial \tilde{F}_{1n}}{\partial s}\right) = \left(\frac{\partial}{\partial t} + \frac{1}{\tau(n)}\right) \tilde{F}_{2b} - \int dn \tilde{F}_{2b} \frac{\partial \left(1/\tau(n)\right)}{\partial n} \tag{3}$$

with $\tilde{F}_{1s}$ being $\tilde{H}_s$ (or $\tilde{E}_s$), $\tilde{F}_{2b}$ being $\tilde{E}_b$ (or $\tilde{H}_b$), and p being $\tilde{H}_s$ (or -μ).

The LMPML formulation presented here was implemented and fully tested for the two-dimensional case. The theoretical discussion also applies to the three-dimensional case. The method shows an improvement in the memory storage saving and operation count compared to the regular split PML formulation, and seems to be competitive with other PML methods. The method is expected to have a significant memory saving and operation count advantage over all known methods for the lossy medium case.

Retrieval of Atmospheric Temperature and Moisture Profiles from Combined High Spatial Imager and Hyperspectral Infrared Sounder Measurements

Jun Li, **Jinlong Li**, **Elisabeth Weisz**, **and Chian-Yi Liu**
Cooperative Institute for Meteorological Satellite Studies
Space Science and Engineering Center, University of Wisconsin-Madison
1225 West Dayton Street, Madison, WI 53706, USA

Abstract— Hyperspectral infrared (IR) sounders such as Atmospheric InfraRed Sounder (AIRS) onboard the NASA's Earth Observing System (EOS) Aqua platform and Infrared Atmospheric Sounding Interferometer (IASI) onboard the Europe's Metop-A satellite, provide unique capability of deriving global atmospheric temperature and moisture profiles with high vertical resolution and accuracy. The high spatial resolution imagers such as Moderate Resolution Imaging Spectroradiometer (MODIS onboard Terra and Aqua platforms) and Advanced Very High Resolution Radiometer (AVHRR, onboard NOAA satellites and Metop-A) provide abundant surface and cloud information with IR sounder sub-pixel. Combination of collocated imager and IR sounder measurements provides unique capability of sounding the atmospheric in cloudy skies. This presentation summarised the algorithm of synergistic use of high spatial imager and high spectral sounder radiance measurements for the retrieval of atmospheric temperature and moisture profiles as well as the cloud-top properties. MODIS/AIRS and AVHRR/IASI are used for algorithm evaluation and sounding retrieval demonstration.

Improvements in a Boundary Element Model for Eddy Current Nondestructive Testing of Cracks

Theodoros Theodoulidis
University of Western Macedonia, Greece

Abstract— In eddy current nondestructive testing a probe coil is used to induce eddy currents in conductive structures and to detect and quantify flaws in these structures by monitoring its impedance changes. From the modeling point of view, a typical problem is the calculation of the coil impedance when this is located above a planar conductor that contains a flaw either in the form of a narrow crack or in the form of a volumetric loss of material, both of which can be surface or subsurface.

Existing models that utilize integral approaches comprise either boundary element or volume element schemes for discretizing the crack area. Especially for fatigue cracks, which are very narrow, only the crack surface needs to be discretized and so boundary elements are better adapted. These models originate from similar ones in the field of geo-electromagnetic induction and are limited to the quasistatic domain since for eddy current frequencies the displacement current is negligible.

In this work, we improvise on two aspects of a boundary element model that has been shown to be very efficient in simulating real inspections [1]. First, we analytically evaluate the Green's functions Sommerfeld-type integrals in the spatial domain by using the Generalized Pencil of Function (GPOF) method instead of attempting to compute them in the spectral domain, and further apply Taylor expansions so that the computation becomes independent from numerical integrations [2]. As a result, the moment matrix fill-time is considerably reduced. Although this approach that actually constitutes the complex image method is common knowledge in the field of wave propagation and especially microstrip design, it has not been used at eddy current frequencies so far.

Regarding the second improvement, we reduce the calculation speed of the incident field (i.e., unperturbed by the crack) either by using again GPOF or by introducing domain truncation [3]. The former is possible because the expression of the incident eddy current field from the usual pancaketype excitation coil has the form of a Sommerfeld-type integral. However, for alternative coil shapes like the rectangular one or for the general case of arbitrary coil shape and orientation, the incident eddy current field is given by a 2D-inverse Fourier expression. In this case, when GPOF is precluded, we can speed up the calculation by recasting the problem in a domain of finite extent. As a result, the 2D-Fourier integral is transformed to a 2D-Fourier summation which can be computed more rapidly and efficiently. Domain truncation is feasible at eddy current frequencies since the medium is lossy and the excitation coil field has a finite extent usually of the order of a few coil sizes. Truncated domain solution can yield results that are numerically as close to the infinite domain solution as desired by adjusting the location of the imposed boundaries to make them more remote from the field source. Both magnetic and electric insulation boundaries are possible.

The net result from these improvements is the rapid calculation of the eddy current crack signal which is very useful for crack shape inversions. We compare theoretical results to published experimental measurements for verification purposes and also compare them to previous calculations in order to demonstrate the considerable reduction in computation time.

REFERENCES

1. Bowler, J. R., "Eddy-current interaction with an ideal crack. I. The forward problem," *J. Appl. Phys.*, Vol. 75, No. 12, 8128–8137, 1994.
2. Alatan, L., M. I. Aksun, K. Mahadevan, and M. T. Birand, "Analytical evaluation of the MoM matrix elements," *IEEE Trans. Microwave Theory Tech.*, Vol. 44, No. 4, 519–525, 1996.
3. Theodoulidis, T. P. and J. R. Bowler, "Eddy current coil interaction with a right-angled conductive wedge," *Proc. R. Soc. A*, Vol. 461, 3123–3139, 2005.

Multi-parameter Inversion of Electrical Array Lateral-logging by Using the Neural Networks

Yueqin Dun, **Jihuan Tian**, **and Jiansheng Yuan**
Department of Electrical Engineering, Tsinghua University, Beijing 100084, China

Abstract— To judge which layer or what depth of the earth is of petroleum or gas, a measurement sonde is put into a borehole and moved down to measure the physical characteristics of the soil, which is called logging. Extracting the electrical and the structure parameters of the soil from the measured data, which is an inversion problem, is the most important objective of logging. The principal parameters need to be inversed involve the resistivity of the mud (Rm) in the borehole, the resistivity of invasion (Rxo) surrounding the borehole, the resistivity of the true formation (Rt), and the diameter of the invasion (Di).

The inversion of the parameters is a nonlinear and multi-solution problem. The linearization methods are often used to solve the problems, such as the damped least-square method, which gets a convergent solution by an iterative process with suitable initial parameters. The linearization methods may converge to a local optimal solution if the initial parameters deviate far from the real solution. And the forward problem must be calculated for many times during the iterative process. Therefore, the solution based on the conventional iterative algorithms is time-consuming and unstable.

To avoid the defects of the iterative algorithms, the back propagation (BP) neural network is applied to inverse the parameters in this paper. The targets and training samples are setup based on the characteristics of the electrical array lateral-logging. By the array logging sonde, a total of six apparent resistivity (Ra) responses are measured, among which the shallowest apparent resistivity (Ra0) is most sensitive to the mud in the borehole and can be used to estimate Rm, and the other five responses, Ra1 to Ra5, are all sensitive to the formation parameters. Therefore, two sets of supervised neural networks with three layers are built to inverse the parameters. One is single target that is Rm, and the other is multi-targets that are Di, Rxo, and Rt. The transfer function between the input layer and the hidden layer is "tansig", between the hidden layer and the output layer is "purelin", and the Levenberg-Marquardt optimization function "trainlm" is adopted as the training function. Before training, the representative and proper sample data according to the practical engineering logging are prepared by the forward problem solution, which are taken as the inputs and the targets of the neural nets. To get a better and stable net, the data are standardized so that they have means of zero and standard deviations of 1. After training the nets by the models or samples, they can converge rapidly, and the target parameters can be inversed accurately.

The BP neural network doesn't need any initial parameters, so that it can reach to the global optimal solution if the number of samples is great enough. Once the neural network has been trained successfully, it can be used without any iterative calculation, and it only needs 0.3 second to provide the Rm for 400 logging points by the neural network presented in this paper.

A Pore-scale Network Flow Model for Two Phase Flow

Koukung Alex Chang
Department of Applied Mathematics
National Pingtung University of Education, Taiwan

Abstract— A pore-scale network flow model is one that discretizes the void space of a porous medium into a collection of pores within an interconnected network. This research presents a reactive transport pore-scale network flow model as well as a computational algorithm to study the genesis of the gaseous phase from the liquid phase. This model can also be used to study the influence of CO_2 sequestration to the environments.

It is believed that the carbon dioxide's emission into the atmosphere is one reason to cause the global warming. Sequestration of CO_2 in deep saline aquifers is a strategy to reduce atmospheric CO_2 emissions and has appeared as a reasonable choice. The maximum CO_2 storage capacity in worldwide is approximately in the range 10,000 to 200,000 Gt CO_2. This amount of carbon dioxide is about hundreds to thousands of years of global CO_2 emissions.

Because the solubility of carbon dioxide in the water varies with the pressure and temperature, the gaseous phase may be generated while the carbon dioxide saturated fluids flow through various depths. This phenomenon may jeopardize the underground environments. Therefore the decision carrying out CO_2 sequestration relies on some geochemical simulations to demonstrate long-term residence of CO_2 underground even though it is such large amount potential capacity for subsurface CO_2 storage. These simulations depend on adequate models to understand the mechanisms that govern the chemical reaction, transport and transformation of the injected CO_2 over different length and time scales.

The model presented here contains two parts: one describes fluid transport equations which follow mass conservation law; the other one is reactive equations which represent phase equilateral conditions. Combining these two parts, this model forms a nonlinear system which contains six unknowns as well as six equations. The challenge of this model is that the mass conservation equations and the phase equilateral conditions should be solved simultaneously and the algorithm must be very flexible to allow for the spontaneous creation and extension the gas phase.

The Pore-Scale Network Flow Model will be developed to AGILD flow electric coupled model for Taiwan's water environment.

A Pore-scale Network Flow and DC GILD Coupled Modeling for Prediction of the Earthquake

Koukung Alex Chang[1] **and Ganquan Xie**[2]
[1]Department of Applied Mathematics
National Pingtung University of Education, Taiwan
[2]GL Geophysical Laboratory, USA

Abstract— In observing before Wenchuan Earthquake and Tang Shan Earthquake, the changing of the underground water have important signification. In this paper, we present a pore-scale network flow and DC GILD coupled modeling for prediction of the earthquake. A pore-scale network flow model is one that discretizes the void space of a porous medium into a collection of pores within an interconnected network. This research presents a reactive transport pore-scale network flow model as well as a computational algorithm to study the genesis of the gaseous phase from the liquid phase. Before earthquake, the metal, pressure, water table and Co2 in ground water should be changed. According to these changing records, we develop Pore-Scale Network Flow and DC GILD Coupled Modeling to simulate the two phase flow and electric conductivity and electric potential that will be useful for predict earthquake and, in particular, useful for prediction and remediation of the water environment.

Experimental Study on the Role of Water in the TIR Anomaly before Earthquake

Shanjun Liu[1,2], **Qunlong Chen**[1], **Guoliang Li**[1], **and Lixin Wu**[2]

[1]College of Resources and Environment
Hebei Polytechnic University, Tangshan 063000, China
[2]Institute for GIS/RS/GPS & Digital Mine Research
Northeastern University, Shenyang 110004, China

Abstract— TIR anomaly before tectonic earthquake is becoming a research hotspot for seismology and remote sensing. Past study showed the thermal infrared (TIR) anomaly precursors appear before violent earthquake, and the anomaly appeared mostly in the water area of earth surface. To study the mechanisms of Infrared anomaly some physical simulation experiments of rock fracture were carried out. The experimental results showed that the TIR anomaly precursors appeared before the fracture of rock samples. There were two kinds of TIR anomaly as precursors of rock fracturing and failure: IRR image anomaly and IRR temperature curve anomaly, which are prospectively used as the monitoring index of remote sensing for rock fracturing phenomenon. The results of the simulation experiments indicated that TIR remote sensing will be prospectively applied to monitor the earthquake precursors. However, the IRR feature of hydrous rock was rarely researched in past simulation experiment.

In this paper, a contrastive infrared radiation imaging detection experiment of dry rock and wet rock in uniaxially compressing process is carried out. The types of rock include sandstone, marble and granite diorite. A high-capability infrared thermal imager is used to detect the infrared radiation from rock samples.

The experimental results show that: 1) along with load applying, the IR radiation temperatures of two type of rocks increase. But in the same circumstances, the increment of IR radiation temperature of wet rock increases greater than the dry rock. For example, the infrared radiation temperature of wet sandstone increases averagely about 1 K, meanwhile the that of dry sandstone increases averagely about 0.2 K; 2) AIRT (average infrared radiation temperature)-time curve of the wet rock keeps accordant variation with the load-time curve, whereas dry rock does not, which seems that the relationship of wet rock between stress and IR radiation temperature is closer than that of dry rock. The result indicates that infrared detection technique was better used to monitor the stress change of the wet rock than dry rock.

In the basis of the experimental result analysis the thermomechanical coupling effects for dry rock and wet rock are discussed, and some views are also put forward to explain the experimental phenomenon and the TIR anomaly before earthquake.

Session 2A8
Poster Session 2

A Novel RSW Antenna

Kai Ma[1], **Di Wu**[1], **and Seo Kazuyuki**[2]

[1]Jiangsu Key Laboratory of Wireless Communications
Nanjing University of Posts & Telecommunications, Nanjing 210003, China
[2]Development 2nd Dept., Nippon Pillar Packing Co. Ltd.
Sanda, Hyogo 669-1333, Japan

Abstract— In this paper, a novel design of reduced-surface wave (RSW) antenna that have minimum surface-wave excitation and radiation at the horizon is presented. The antenna is a rectangular patch which is a classic rectangular patch and has its inner edge shorted by a rectangular conducting wall. Different from other RSW antenna, the upper substrate of the antenna is air substrate. The feed network is achieved by using H-sharp aperture-coupled configuration. These patch designs excite very little surface-wave power, and thus have better radiation characteristics when mounted on finite-size ground planes.

An Improvement to Decrease the Effect of Handset Internal Components on a Dual Band PIFA Performance

M. Pasandehmanesh, **D. Arefan**, **and M. A. Ebrahimi-Ganjeh**
Electrical Engineering Department, Sadjad Institute of Higher Education, Iran

Abstract— This paper presents a dual band planar inverted-F antenna (PIFA) which has been designed to get less effect of handset internal components than previous ones in 900 and 1800 MHz. The applied technique based on decreasing the space between radiation and ground plane in some parts of the antenna. Two shapes of a handset ground plane, as well as the antenna alone are examined. VSWR and radiation pattern of the antenna has been computed, and compared in each case. All numerical simulations are performed using the Ansoft HFSS software.

A Sample:

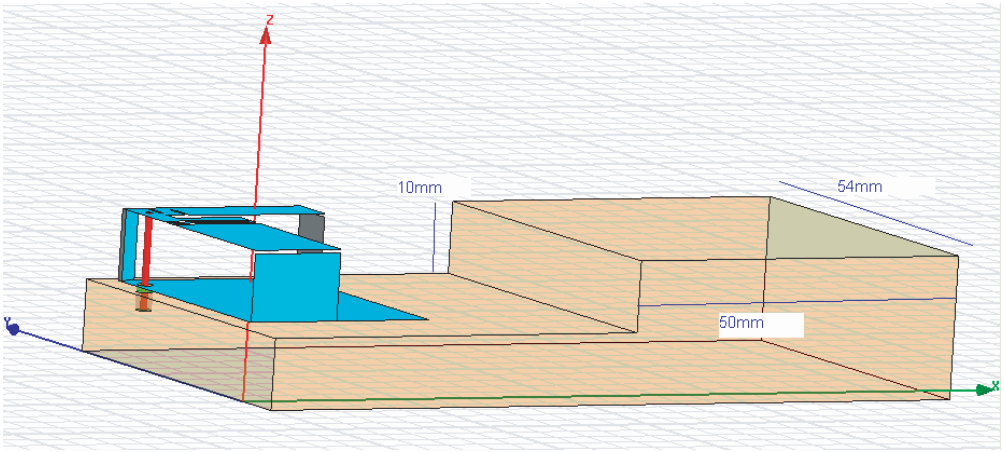

Figure 1: The Antenna in top of a handset ground plane. The effect of an inner grounded battery has been considered.

Low-profile Array Antenna for UHF RFID Tag on Metallic Objects

Horng-Dean Chen and Yu-Hung Tsao
National Kaohsiung Normal University, Taiwan

Abstract— The use of radio frequency identification (RFID) systems in recent years has increased noticeably. At present, the desirable frequency band for RFID application is UHF band (860–960 MHz) owing to forceful demands for long reading distance, high data rate, and small antenna size. Tag antenna is one of the essential components for RFID system. In many applications, tag antenna of very low profile and metal proximity use is desirable. Recently several designs based on PIFA or microstrip patch antennas have been proposed for metal objects. Although all of the related antennas give good reading-range performance for RFID application, they use a high profile structure (substrate thickness ≥ 3 mm). However, it should be noted that microstrip antenna having a lower profile structure exhibit a lower antenna gain. To improve the characteristics of low-profile antenna, array antenna is well-known candidate. So far, little research has been done on the RFID development in tag array antenna.

In this paper, a two-element shorted microstrip array for UHF band RFID tag mountable on metallic objects, as shown in Fig. 1, is proposed. The proposed antenna used the meandered quarter-wavelength microstrip lines as impedance transformer to achieve conjugate impedance matching between the radiating patches and microchip. Moreover, the microstrip lines are also used as phase-reverse device that makes the surface currents of two radiating patch in phase and can thus achieve the enhanced antenna gain. Fig. 2 shows the simulated and measured return loss. The measured result agrees well with the simulated one. The effects of the spacing (d) between the two radiating patches on RFID tag read range were also investigated. Details of the proposed designs and obtained experimental results will be presented.

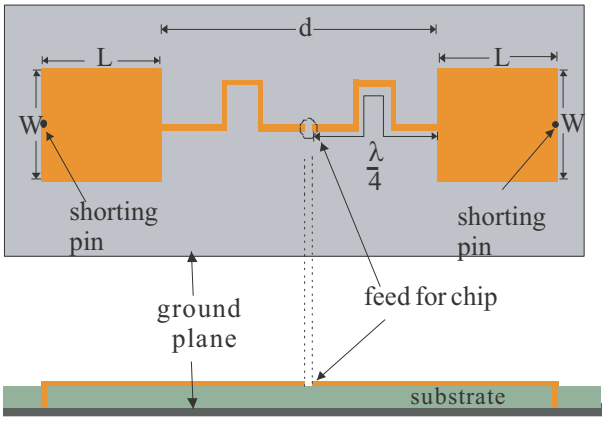

Figure 1.

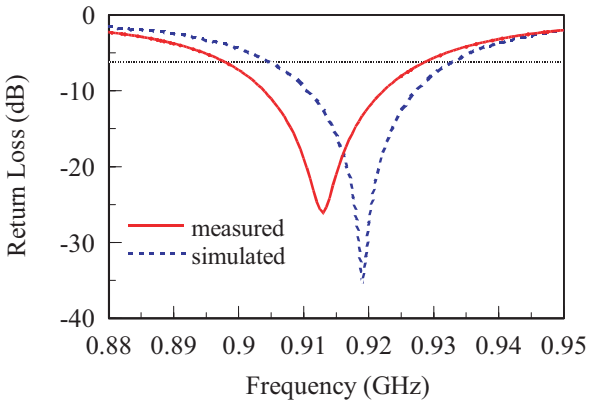

Figure 2.

Design of Thin-membrane Printed Dipole

Daqun Yu[1] **and Ruiping Zhu**[1, 2]

[1]Nanjing Research Institute of Electronics Technology, Nanjing 210013, China
[2]China National Key Laboratory of Antenna and Microwave Technology
Nanjing 210013, China

Abstract— Future space-based radar and spaceborne SAR require very large aperture and high-gain phased array antennas. Membrane-based deployable antennas provide a means to reduce mass, stowage volume, and overall cost of radar antenna system. JPL has developed some array antennas which are based on thin-membrane structure, and the elements of these antennas are microstrip antenna. But there are some distinct disadvantages associated with these thin-membrane microstrip antennas, as shown in Section 1 of this paper. As an improved antenna element, a novel printed dipole which based on thin-membrane structure is presented in this paper. This thin-membrane printed dipole is center fed by parallel-strip (PS), which is transformed from coplanar waveguide (CPW) by using a vertical transition balun. This vertical transition between CPW and PS has a wide frequency band due to the two waveguide structures have little or no variation of their characteristic impedance with respect to frequency and can meet the design requirement of thin-membrane printed dipole. The use of CPW in the feed network make this printed dipole easily integration with T/R modules. The whole thin-membrane printed dipole with vertical transition balun is simulated by means of Ansoft HFSS. From the simulation result, it is know that this printed dipole has wide bandwidth of 190 MHz (15.2%) and good radiation characteristic with low cross-polarization (< -30 dB). The thin-membrane printed dipole is a very useful antenna element for future large aperture, lightweight, deployable and high-gain phased array application.

CPW-fed Compact Planar UWB Antenna with Circular Disc and Spiral Split Ring Resonators

Li-Ming Si, **Hou-Jun Sun**, **Yong Yuan**, **and Xin Lv**
Department of Electronic Engineering, School of Information Science and Technology
Beijing Institute of Technology, Beijing 100081, China

Abstract— This paper presents a novel compact-size (the diameter of the radiating element is only 0.05λ at the lower end of the operating band, 1.2 GHz) coplanar waveguide (CPW)-fed planar antenna with 10 dB return loss (VSWR < 2) bandwidth from 1.2 to 25 GHz, 182%, for ultra-wideband (UWB) communications. The proposed antenna consists of a circular disc and a spiral split ring resonator displayed on an inexpensive FR4_expoxy substrate. This UWB printed monopole antenna adopts CPW-fed and two tapered transmission lines for improving broadband impedance matching in the required band. Numerical simulations using finite element method (FEM) show that the radiation patterns over the mostly operation band are omni-directional in H-plane and symmetrical in E-plane, with an average gain of 4.5 dB.

Design and Fabrication of Wide Band Printed Multi-ring Fractal Antenna for Commercial Applications

M. Kazerooni and A. Cheldavi
College of Electrical Engineering, Iran University of Science and Technology (IUST)
Narmak, Tehran, Iran

Abstract— This paper presents a wideband printed multiring fractal antenna. The ground plane is only under part of the feed line. Good performance of S-parameters is obtained. This optimized fractal antenna has the potential of operating in several of the currently broad band commercial existing systems such as, Bluetooth and GSM.

In our work, a simple structure of printed multiple elliptic ring fractal antennas has investigated and also demonstrated. A significant matched bandwidth compared to the conventional multiple ring monopole antenna has obtained. Many possibilities of improved design have been investigated by varying the width of the rings. On the other hand, this type of structure can achieve larger matched bandwidth in comparison to conventional multiple ring monopole antennas. Simulation and experimental results confirm that this type of antenna can achieve better performance than the conventional multiple ring monopole antennas, and obtain ultra wide bandwidth of more than 14 GHz under −10 dB. By tuning of elliptic ring partial ground size the optimum operation is obtained. The gap between antenna and ground plane is the key point for impedance matching performance of radiation pattern and S parameters. On the other hand, a novel wide-band fractal patch antenna is designed, measured and analyzed. Based on these concepts, a compact printed fractal antenna has constructed with the aid of an electromagnetic (EM) simulator using Ansoft HFSS (a full wave simulator). The impedance antenna structure bandwidth of the proposed antenna could reach 64%, which has rarely been reported for patch antennas. All results and performance are validated and confirmed experimentally.

Analysis of the Multi Surface Current Distributed within in a Broadband Printed Monopole Antenna

Sung-Keun Jeon[1], **Nam Kim**[2], **Seung-Woo Lee**[2], **and Liu-Yu Lin**[1]

[1]Department Bio and Information Technology, Chungbuk National University, Korea
[2]Division of Information and Communication Eng., Chungbuk National University, Korea

Abstract— In this paper, we proposed a novel broadband printed monopole antenna for PCS/IMT-2000/WLAN terminals by widening current flow. To compensate narrow bandwidth characteristics which is one of disadvantages of general printed monopole antenna, we add the patch of diamond shape and induce the current in various directions for acquiring broadband characteristics. And frequency characteristics is optimized with various design parameters. The bandwidth of the realized antenna is 1.66∼3.04 GHz (58.72%) below the return loss of −10 dB which contain the required bandwidth of PCS/IMT-2000/WLAN band.

Divided Two-arms Spiral Slot Antenna fed by Coplanar Waveguide Using the Different Magnetic Phase Different

S. W. Park[1], **N. Kim**[1], **S. Y. Rhee**[2], **and S. W. Lee**[1]

[1]Chungbuk National University, Korea
[2]Chonnam National University, Korea

Abstract— In this paper, we proposed a divided two-arms spiral slot antenna fed by coplanar waveguide using the magnetic flow at slots. This antenna has characteristics of which one is to short-circuit at the end of the slot and another is to turn spirals separately. To reduce the offset of magnetic flow, two spiral slots are fed by 180° phase difference. Because we proposed a printed two-arms spiral slot antenna without a balun circuit, antenna size become smaller substantially. And frequency characteristics are optimized with various design parameters. The bandwidth of the realized antenna is 2.7 GHz ∼ 12 GHz below the return loss of −10 dB.

Design of Multi-Band Dual-Polarized Two-Port E-shape Microstrip Antenna

A. M. El-Teger[1] and A. M. Abdin[2]

[1]Electronics Department, M. T. C., Cairo, Egypt
[2]Department of Communications and Electronics, Shorouk Academy, Cairo, Egypt

Abstract— With the increased development of wireless communications, compact, multi-frequency and multi-polarization planar antennas become highly desirable. Such antennas would greatly simplify the installation of multi-band systems and provide a much more aesthetic appearance. There are various techniques to achieve multi-band operation from various types of microstrip antennas. In this paper, a novel compact size E-shape microstrip patch antenna is designed, analyzed, and fabricated for multi-band dual-polarized wireless applications. It has two ports excited with stripline feed mechanism.

The physical parameters of the novel structure as well as its partial ground plane are analyzed, and optimized using the commercial electromagnetic simulation tool, IE3D by Zeland. Return loss at both ports (S_{11}, S_{22}), voltage standing wave ratio (VSWR), isolation between both ports (S_{21}), and radiation pattern are carried out. Furthermore, polarization, gain and efficiency are investigated to fulfill the requirements of the targeted communication system. In addition, these results are compared to that obtained from the FEM-based software, HFSS by ANSOFT.

The optimized antenna is fabricated using photolithographic technique on RT/Duroid 6010 substrate with ($\varepsilon_r = 10.5$ and $h = 1.25\,\text{mm}$).

Measurements show that at 5 GHz: $S_{11} = -17\,\text{dB}$, $S_{22} = -20\,\text{dB}$, and $S_{21} = -27\,\text{dB}$ with impedance bandwidth of 20%. In addition, the antenna exhibits $S_{11} = -26\,\text{dB}$, $S_{22} = -21\,\text{dB}$, and $S_{21} = -12\,\text{dB}$ at 9.7 GHz with bandwidth of 8%, and $S_{11} = -30\,\text{dB}$, $S_{22} = -21\,\text{dB}$, and $S_{21} = -18\,\text{dB}$ at 20 GHz with bandwidth of 7%.

Measurements are in good agreement with simulated results, which validates the design strategy. Therefore, the proposed antenna is very promising for various communication systems.

A Circularly Polarized Dual-frequency Square Patch Antenna for TT&C Satellite Applications

A. M. El-Tager[1], **M. A. Eleiwa**[1], **and M. I. Salama**[2]

[1]Electronics Department, M. T. C., Cairo, Egypt
[2]Egyptian Armed Forces, Cairo, Egypt

Abstract— In many applications, operation in two or more discrete bands with an arbitrary separation of bands is desirable especially for telemetry, tracking and command (TT&C) antennas for satellite aircrafts. On the other hand, to overcome the noise due to spinning of satellite aircrafts, Circular polarization is required in order not to be affected by that rotation. In this paper, a circularly polarized, dual-frequency square patch is designed with probe feeding mechanism to operate as the TT&C antenna for satellite aircrafts. This antenna is optimized, fabricated and measured to verify its operation and show its advantages over other published antennas for this specific application.

An initial design is carried out based on theoretical equations. The patch is fed by a probe at an optimized position and perturbed by a rectangular slot to achieve circular polarization. Furthermore, a 3D EM model is created using HFSS which is based on finite element method. In addition, two rectangular slots are added and optimized to obtain the required dual-frequency of operation, namely 2.25 GHz and 3 GHz. Sensitivity analysis and several optimizations are performed to obtain the optimum values of the antenna physical parameters.

The proposed antenna is fabricated using low loss Teflon microstrip substrate with $\varepsilon_r = 2.2$ and 1.6 mm height. Finally, the fabricated antenna is measured suing HP8510c VNA achieving S_{11} of -24 dB at 2.25 GHz and -21.5 dB at 3 GHz. The measured impedance bandwidth is about 30 MHz at f_1 and 100 MHz at f_2, which are sufficient for both uplink and downlink operation. Measurements are in great agreement with simulations, which verifies the design procedure. Therefore, the proposed structure is very promising in TT&C satellite applications.

Design and Experiment of a Loop Rectenna for RFID Wireless Power Transmission and Data Communication Applications

R. H. Chen, Y. C. Lee, and J. S. Sun
Graduate Institute of Computer and Communication Engineering
National Taipei University of Technology
Taipei, Taiwan

Abstract— This paper presents a low-cost rectifying antenna (rectenna) has been developed and measured at 900–950 MHz (Radio Frequency Identification Device, RFID band) for low-power applications involving wireless power transmission (WPT) and data communication. In order to validate the rectenna, we have been developed a loop antenna which was photo-etched from copper-clad FR-4 material ($\varepsilon_r = 4.4$) with the volume of $60 \times 80 \times 0.8\,\text{mm}^3$. The loop antenna used a meander line structure to reduce its size to 50% of the regular loop antenna and measured operating frequency of 925 MHz with bandwidth of 52 MHz at return loss −10 dB. The maximum antenna gain is 4.22 dBi and radiation efficiency is 97% at 925 MHz. Results show the satisfactory agreement for the loop antenna design to meet the RFID specifications.

Furthermore, to contribute a rectenna for RF power conversion, the back side of the loop antenna is the doubler rectifier circuit with input filter for efficiency optimization and rejects higher order harmonics produced by the rectifying diode. For the Schottky diode we used the commercial Agilent HSMS-285C surface mount zero bias schottky detector diode pair for small signal applications at frequencies below 1.5 GHz was used as the rectifying device, and there are two diodes are mounted into a single package to be the best in reduce the size and the efficiency.

In addition, the rectenna has a RF-DC conversion efficiency of 47% is achieved when 0 dBm RF power is received at 925 MHz. Measured results of rectenna proved that the rectenna is suitable for component of the WPT system.

Design of a Compact Dual-Band Loop-Slot Antenna

R.-H. Chen, **Y.-C. Lee**, **and J.-S. Sun**
Graduate Institute of Computer and Communication Engineering
National Taipei University of Technology
Taipei, Taiwan

Abstract— This article presents a new compact antenna with loop-slotted structure to achieve the dual-band operation. This loop-slotted structure on the printed antenna is presented, and is measured the impedance bandwidth, radiation patterns, and gain requirements of the 2.4- and 5-GHz wireless local area network (WLAN) applications. The investigated numerically and experimentally results demonstrate that a tunable dual-operating band and an enhancement of the antenna bandwidth are obtained owing to the proposed antenna with compact radiators. The geometry and configuration of the printed antenna with loop-slotted structure is designed and discussed. The compact design of proposed antenna has a loop-slotted structure and a rectangular-shaped plane on the coplanar ground plane. The inner fed conductor and the outer metal sheath of the coaxial line are connected to the feed point and the ground plane and both with a distance of 1.5 mm between two points. The proposed antenna is printed on the FR4 substrate with thickness of 0.8 mm, dielectric constant of 4.3, and loss tangent of 0.0245 and has a compact dimension of $32 \times 22.5\,\text{mm}^2$ in this study. The measured return loss of operation bandwidth portion has a 270 MHz within 2.39–2.66 GHz at the lower resonance mode. The upper resonance mode of 1350 MHz within 4.5–5.85 GHz is resulted. The maximum measured gain at all radiation planes is obtained a 4.98 dBi at the 2.5 GHz within the lower operating frequency band and from 5.16 dBi to 1.86 dBi within 5–6 GHz at the upper operating frequency band, respectively.

Power Feeding to RFID Tags Within Specific Distance and Transponder Control Signal

Kengo Ueyama, **Akitoshi Ito**, **Yukio Iida**, **and Noriaki Muranaka**
FSC, and Dept. of Electric and Electronic Eng., Faculty of Engineering Science
Kansai University, Japan

Abstract— We are proposing the method of supplying driving power of the RFID tag containing transponder control signal by the electromagnetic field besides the communication signal. From this viewpoint, we are also proposing power supplying method to RF tags within specific distance using two antennas. In the method, we use two properties: (1) The intensity of the electromagnetic field from two loop antennas sharply decreases depending on the distance, and (2) the supplied-signal phase difference sharply changes at a position $1/(2\pi)$ of the wavelength. In this paper, we demonstrate the power feeding method within specific distance experimentally. We used transmitting resonance-type antennas composed of capacitor of 1 pF and the five turns coil of 30 cm in diameter, and receiving antennas composed of variable capacitor from 10 pF to 120 pF and the card-type coil with five turns. The amplitude is 10 V at the transmitting side, and the resonance-frequency is about 17.6 MHz. Under this condition, we were able to drive an IC-encoder-chip of 2 V and 0.3 mA within the distance up to 70 cm. Next, we proposed the ball-type antenna to induce only magnetic fields mainly.

Coupling of Transmitting/Receiving Antennas and Super Regenerative Transponder (SRGT) for RFID Tags

Akitoshi Ito, **Kengo Ueyama**, **and Yukio Iida**
FSC, Department of Electric and Electronic Eng., Faculty of Engineering Science
Kansai University, Japan

Abstract— Recently, RFID technology to discriminate individuals with radio wave has fast been noticed and studied at full length in many fields. RFID has a great many possible applications. However, it is worried whether demands necessary hereafter can be satisfied or not because frequency bands allotted for RFID are not so broad. Thus we are considering utilization of faint radio wave. For, very broad frequency band can be used as well as its use requires no license.

Very many applications of RFID are possible. It seems impossible to prepare for future demands only with frequency bands that have been allotted for RFID. Accordingly, faint radio wave that requires no license is actively utilized though its definition will differ by country, too. As it can use a very broad frequency band, a large demand can be accommodated. In a common sense, it may be considered that reading probability from the tag must be near 100%. Sufficient role can be played even though reading probability is 70% or 50%. In the case of stray pet, for instance, it is considered that finding probability can get fairly higher than with past methods by installing sensors from place to place. Application range becomes very broad when including such ways of use.

Thus we are proposing utilization of faint radio wave and SRGT (super regenerative transponder) for demand expansion RFID system. In this paper, we study the circuit coupling the transmitting/receiving antennas with SRGT circuit. Receiver sensitivity and transmitting electromagnetic field strength are clarified.

Calculation of Electromagnetic Wave Attenuation Due to Rain for Various Percentages of Time

M. Zilinskas[1,2], **M. Tamosiunaite**[2,3],
S. Tamosiunas[2,3], **and M. Tamosiuniene**[4]

[1]Department of Radio Communication
Communications Regulatory Authority of the Republic of Lithuania
Algirdo 27, Vilnius LT-03219, Lithuania
[2]Faculty of Physics, Vilnius University, Sauletekio 9, Vilnius LT-10222, Lithuania
[3]Institute of Materials Science and Applied Research, Vilnius University
Sauletekio 9, Vilnius LT-10222, Lithuania
[4]Semiconductor Physics Institute, A. Gostauto 11, Vilnius LT-01108, Lithuania

Abstract— The electromagnetic waves attenuation due to its interaction with raindrops (rain attenuation) as a function of the rain rate has been analyzed at frequencies of 10 GHz and above. By using the rainfall amounts data, measured in Lithuanian weather stations, the values of rain rates for different percentages of time have been determined. The rain rate-values, obtained in Seacoast, were compared with ones in Continental Regions of Lithuania. In most cases, the integration time was ten minutes in measurements of rainfall amounts. The one-minute rain rate-values were determined according to the known model. Using measured rainfall data the relationship between rain rate and percentages of time was derived. This relationship is suitable for use under Lithuanian climate conditions.

It was obtained, that the average ratio between the R-values for 0.01% and 0.001% of time in Vilnius is equal 2.17. The suitability of the model, which was proposed in previous papers, was proven using the measured rainfall amounts data of longer period. It was concluded, that this model might be used for calculation of the $R_{0.01\%}$-value under Lithuanian climate conditions in cases, when only monthly rainfall amount data is available, and the rainfall data, measured with short integration time, is unavailable. Analysis of measured rainfall data shows that E-Zone rain rate-values proposed by ITU-R (International Telecommunication Union-Radio Communication Sector) coincide with one-hour rain rate values and are much lower than one obtained by using one-minute rainfall amounts data. It was concluded, that ITU-R rain rate-values must be re-calculated into one-minute rain rate-values before being used in calculation of rain attenuation under Lithuanian climate conditions. The specific rain attenuation was determined by using the rain rate-value obtained here.

A 2.4 GHz Low Phase Noise Voltage Controlled Oscillator

R. M. Weng and J. Y. Lin

Department of Electrical Engineering, National Dong Hwa University, Taiwan, R.O.C.

Abstract— Voltage-controlled oscillators (VCOs) are important parts of wireless communication systems, especially in frequency synthesizers and PLLs. VCO is widely used to generate the local oscillation (LO) carrier frequency for both up-conversion and down-conversion mixing of the input baseband and RF signals.

As a local oscillator in the transceiver, phase noise of VCO is one of the most important parameters for the quality and reliability. Phase noise in the oscillator can be determined by the VCO gain (K_{vco}). A large VCO gain will amplify the noise coupling to the control node and hence degrade the phase noise performance. It also makes VCO very susceptible to noise, because of AM to FM conversion. A VCO with a small K_{vco} is desirable because of its less susceptibility to noise. But when it suffers from process and temperature variations, small K_{vco} may cause VCO oscillation frequency drift corresponding to the desired frequency. There is trade-off between tuning range and phase noise in optimization of VCO performance. The tail current source is one of the major contributor to the phase noise of VCO. Besides, traditional biasing circuit needs an extra biasing voltage, which increase the power consumption and also introduces noise to the VCO.

In this paper, switched biasing transistors are used to force a trap and release its capture electrons, rendering the transistors to be memory-less. Since all the transistors are switched biasing, it is expected to have lower flicker noise.

The proposed extra coupling capacitor helps to decrease the K_{vco}, thus VCO with low phase noise can be achieved. The phase noise analysis of VCO are described in this paper. Simulation results and performance comparison show that the proposed VCO has superior phase noise performance.

The fully integrated VCO is fabricated in tsmc 0.18 µm 1P6M CMOS technology. With the memory reduction tail current source and the proposed coupling capacitor, the proposed VCO achieves the phase noise as low as −126.1 dBc/Hz at 1 MHz offset from 2.4 GHz carrier frequency. The output oscillation frequency can be tuned from 2.25 GHz to 2.58 GHz with 14% tuning range. A superior Figure-of-Merit (FOM) value at 2.4 GHz is around −188.8 dBc/Hz at 1 MHz offset. The proposed low phase noise VCO is suitable for $2.4 \sim 2.4835$ GHz ISM band of the Bluetooth standard with only 3.1 mW power consumption.

Novel Super Regenerative Transponder (SRGT) for RFID Tags and ASK signals

Yukio Iida
FSC, and Dept. of Electric and Electronic Eng., Faculty of Engineering Science
Kansai University, Japan

Abstract— Recently, RFID technology to discriminate individuals with radio wave has fast been noticed and studied at full length in many fields. RFID has a great many possible applications. However, it is worried whether demands necessary hereafter can be satisfied or not because frequency bands allotted for RFID are not so broad. Thus we are considering utilization of faint radio wave. For, very broad frequency band can be used as well as its use requires no license.

Very many applications of RFID are possible. It seems impossible to prepare for future demands only with frequency bands that have been allotted for RFID. Accordingly, faint radio wave that requires no license is actively utilized though its definition will differ by country, too. As it can use a very broad frequency band, a large demand can be accommodated. In a common sense, it may be considered that reading probability from the tag must be near 100%. Sufficient role can be played even though reading probability is 70% or 50%. In the case of stray pet, for instance, it is considered that finding probability can get fairly higher than with past methods by installing sensors from place to place. Application range becomes very broad when including such ways of use.

Thus we are proposing utilization of faint radio wave and SRGT (super regenerative transponder) for demand expansion RFID system. In this paper, we study the SRGT circuit that transmits and receives the digital signals.

A Low Cost 1 Watt Doherty Power Amplifier for WLAN and WiMAX Applications

Shilei Jin, Jianyi Zhou, Lei Zhang, and Wei Hong
State Key Lab. of Millimeter Waves, School of Information Science and Engineering
Southeast University, Nanjing 210096, China

Abstract— Because of the high peak-to-average power ratio (PAPR) signals in the WLAN and WiMAX transceivers, the linearity of the transmitter becomes one of the most key factors in the system design. In fact, as the power amplifier operates close to the saturation region where both high efficiency and high output power are achieved, the degradation in linearity becomes significant. Consequently PA must operate at a large amount of back-off from the peak output power, thus efficiency is rather poor. Many kinds of power amplification architectures are being considered to improve the power efficiency and linearity. However these architectures are complicated with high lost and high cost.

This paper presents the design and implementation of a low-cost 1-Watt Doherty Amplifier, working at 2.4 GHz, with high efficiency and simple circuit for WLAN and WiMAX applications. Two 1-Watt Heterostructure FETs with SOT-89 surface-mount package are adopted as the final stage of the carrier amplifier and the peak amplifier. The proposed Doherty amplifier has the characteristic of both high power added efficiency (PAE) and acceptable linearity. The research on the performance of the Doherty amplifier focuses on different bias voltage of peak amplifier. Through changing bias voltage the best operation point of the peak amplifier is selected to achieve the superior performance. Additionally by adjusting the off-set line the phase difference of carrier cell and peak cell is about 180 degree. So the intermodulation distortion is reduced by harmonic cancellation mechanism and therefore linearity and efficiency of the proposed Doherty amplifier are improved without any linearity enhancement techniques. The sweet point of the developed Doherty amplifier is about 3.5 dB back-off from the saturated power. According to the experimental results, the output P1 dB power is about 33.5 dBm. When the output power is 30 dBm, the tested PAE is about 31.5% and the IMD3 is about −34 dBc.

Planar Antennas for UMPC Integration

Cheng-Hung Lin[1], **Guan-Yu Chen**[2], **Jwo-Shiun Sun**[2], **Kwong-Kau Tiong**[1], **Yu-Hsiang Chen**[1], **Tsan-Hsuan Peng**[1], **and Y. D. Chen**[3]

[1]Department of Electrical Engineering, National Taiwan Ocean University, Taiwan
[2]Department of Electronic Engineering, National Taipei University of Technology, Taiwan
[3]Antenna and EMC Laboratory, HTC Corporation, Taiwan

Abstract— This UMPC will co-integration and co-design of the antennas (Fig. 1) for 2.5G/3G cellular, WLAN, BT, and GPS applications of 3G mobile handset, respectively. This 2.5G/3G antenna shows a wide operating bandwidth for low band and high band bandwidth, making it easy to cover the GSM, EDGE, CDMA, CDMA 2000, W-CDMA and UMTS band for wireless communication and dual mode operation of a mobile handset phone. Embedded Wi-Fi (2.4–2.5 GHz) and BT antenna in mobile handset for VoIP/IPTV and wireless connection. The resonance mode of a small PIFA antenna covers the GPS communication bandwidth of 1571.42–1579.42 MHz. The patch tuning expansion are introduced to confine the resonance mode region and to facilitate the frequency modes and impedance match expansion easily for antenna and wireless system integration design.

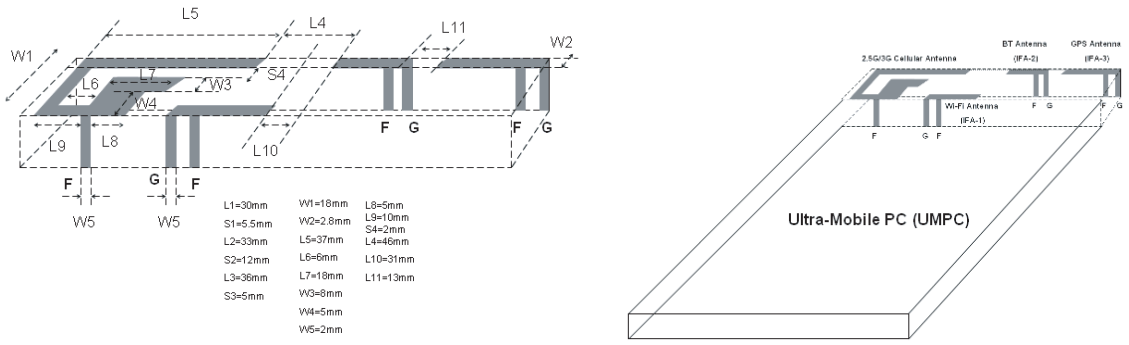

Figure 1: The proposed antennas structure for UMPC application and integration.

WLAN and Bluetooth Antenna Design

Kekun Chang[1], **Guan-Yu Chen**[1], **Jwo-Shiun Sun**[1], **and Y. D. Chen**[2]

[1]Department of Electronic Engineering, National Taipei University of Technology, Taiwan
[2]Antenna and EMC Laboratory, HTC Corporation, Taiwan

Abstract— A high performance monopole antenna fabricated using a folded planar line as radiator is presented. A prototype of the proposed monopole antenna with a compact area size of 20 mm × 8 mm is implemented, and the multi-band WLAN/Bluetooth antenna shows a wide operating bandwidth of about 200 MHz and 1000 MHz for low band and high band, bandwidth, making it easy to cover the IEEE 802.11a, IEEE 802.11b, IEEE 802.11g and IEEE 802.11n (MIMO) bands for wireless communication and future 4G wireless operation of a mobile VoIP/VoWLAN handset phone. An internal small antenna usually suffers from degradation in performance of narrow bandwidth and radiation efficiency. In this experiment, we design and fabricate a dual broadband interior type wire and shorting monopole with a high performance radiation pattern over a design operation band using dual path, as shown in Fig. 1. It has a measured return loss bandwidth (referenced −10 dB) about 200 MHz with center frequency at 2.45 GHz (2.35–2.55 GHz) and 600 MHz with center frequency at 5.7 GHz (5.4–6 GHz), as shown in Table 1.

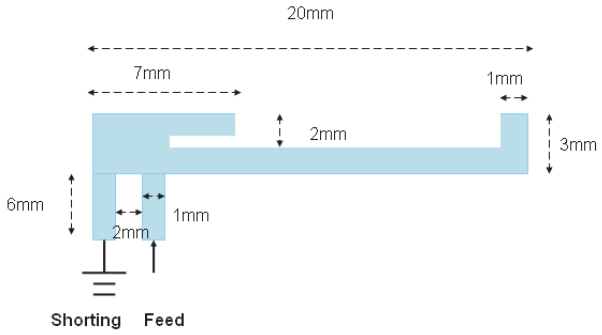

Figure 1: Dual-band shorting monopole antenna.

Table 1: Measured gain data.

Frequency (MHz)	2400	2450	2500	5400	5600	6000
Gain (dBi)	2.3	2.1	2.5	3.1	3.2	4.2

REFERENCES

1. Wong, K. L., *Planar Antennas for Wireless Communication*, John Wiley & Sons, Inc., 2003.
2. Balanis, C. A., *Antenna Theory*, John Wiley & Sons, Inc., 1997.
3. Kraus, J. D. and R. J. Marhefka, *Antennas for all Applications*, McGraw-Hill, 2002.

UMTS and DVB-H Antenna Co-integration

Kekun Chang[1], **Guan-Yu Chen**[1], **Jwo-Shiun Sun**[1], **and Y. D. Chen**[2]

[1]Department of Electronic Engineering, National Taipei University of Technology, Taiwan
[2]Antenna and EMC Laboratory, HTC Corporation, Taiwan

Abstract— In mobile TV technology, 3G UMTS and DVB-H antenna co-design for PDA phone in future. We have proposed a novel digital video broadcast for handheld (DVB-H) antenna for mobile handheld terminal using a meander monopole radiator and a simple matching circuit. The antenna impedance covers the DVB-H frequency band of 1400–1800 MHz. The proposed antenna was designed, fabricated, and measured. And the proposed 3G antenna covers the entire UMTS/WCDMA (1900–2200 MHz) band for VSWR < 2. The simulated antenna gain varies from 1 to 3 dBi over the operating frequency range. The obtained radiation patterns are very close to those of a conventional omni-directional antenna. Details of the proposed antenna design and the simulated and measured results are presented and discussed.

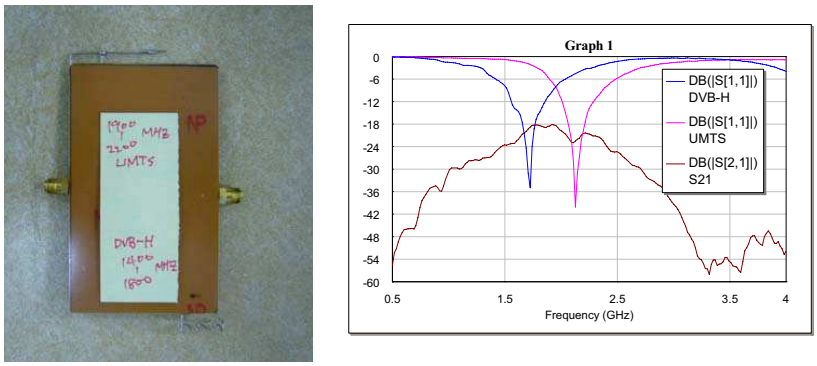

Figure 1: The proposed antenna and measured data.

REFERENCES

1. Balanis, C. A., *Antenna Theory*, John Wiley & Sons, Inc., 1997.
2. Kraus, J. D. and R. J. Marhefka, *Antennas for all Applications*, McGraw-Hill, 2002.

Design of Trapezoidal Ring Antenna Using Conductor-backed CPW Structure

S. W. Lee[1], **N. Kim**[1], **S. W. Park**[1], **S. K. Jeon**[1], **and S. Y. Rhee**[2]

[1]Chungbuk National University, South Korea
[2]Chonnam National University, South Korea

Abstract— In this paper, we design and fabricate the trapezoidal ring antenna using the conductor-backed CPW. The antenna has a broadband characteristic by the coupling effects through inserted H-shaped parasitic patch. The conductor-backed CPW shows more stable characteristics than the CPW structure when there is occurred the variation between the feed-line and the ground plane in the front side. The bandwidth of the designed antenna is 2.2 GHz∼4.6 GHz below −10 dB.

Design and Implementation of a Smart Antenna Using Butler Matrix for ISM-band

A. M. El-Tager and M. A. Eleiwa
Electronics Department, M. T. C., Cairo, Egypt

Abstract— Recently, switched beam smart antenna systems are investigated to improve the performance of wireless networks. The aim of this paper is to design and implement a smart antenna system using microstrip antenna array with beamforming network in the ISM-band at 2.45 GHz.

Four rectangular radiating patches on a low dielectric constant substrate ($\varepsilon_r = 2.2$) are designed in linear configuration to achieve required radiation properties. The antenna array is initially designed using PCAAD, then simulated and optimized using 3D EM modeling commercial software (HFSS).

Furthermore, a beamforming network using 4×4 Butler matrix technique is designed, analyzed, optimized and implemented using single layer microstrip substrate. The design methodology is verified by fabricating the main components in the network such as quadrature hybrid and crossover couplers. Measurements of both give excellent agreement with simulations. In addition, the 0.6 dB insertion loss and 38 dB isolation obtained from the crossover coupler are found to be better than that of published literature.

In order to verify the performance of the implemented Butler network, the linear antenna array of is attached to it in the same substrate and the whole smart antenna system is simulated. The resultant 2-D Polar Far Field patterns for uniform excitation are carried out and found to be matched with expected ones. This validates the performance of the implemented smart antenna network and shows that it is possible to implement a 4×4 Butler matrix with satisfactory antenna pattern.

A brief summery of the simulated and experimentally observed results is presented below:

1. The antenna array was observed to be operating at a center frequency of 2.46 GHz with an impedance bandwidth of 8%. These values are very close to the desired design frequency of 2.45 GHz and impedance bandwidth of 10%.
2. The array antenna gain of 13 dB was observed, whereas the designed antenna was required to have gain of 15 dB.
3. For the designed antenna array, the half power beam-width of 28° was observed.
4. Smart antenna efficiency and directivity are improved and found to be better than other smart antennas in literature. While obtaining smaller size than others; actually 21.3 mm × 18.6 mm.
5. The side lobe level was optimized to be −24 dB which is better than what is found in corresponding published literature.

The Current Status of Automotive Electromagnetic Compatibility Research

Yi Sun and Chaoqun Jiao
Department of Electrical Engineering, Beijing Jiaotong University, China

Abstract— With the growing development of automobile market and increasing electronic and electrical appliances in vehicle, automotive EMC (electromagnetic compatibility) study has become a new hot spot of research. Automotive EMC, which comes into being in recent years as the automobile technical term, is still unfamiliar to many people, but it relates to the particular electronic systems, the surrounding electric and electronic system of auto, up to the security and stability of the whole car system. In this paper, through collection and analysis of related literature, technical information and research reports, it detailed described the current automotive EMC research from these three aspects: the electromagnetic environment of the auto, international organizations and standards for automotive EMC, experiment testing technologies. Furthermore, it pointed out the long-term developing trend of automotive EMC research and analyzed its influence on the development of related study in China.

Introduction: With the rapid development of the auto industry and the electronic technology, more and more new technology in modern cars has been widely used, especially microelectronics technology, more effectively promoted the auto industry to the high value-added direction [2–4]. However, these new technologies also put forward higher requirements for the reliability of the entire vehicle system, that is, all electronic devices and electronic control systems must adapt to each other, automotive electronics applications will be related to a common problem — the automotive EMC [5–12].

In recent years, an increasing number of electronic products are widely used in automobiles, and gradually formed the automotive electronics. The car has also gradually transferred from the traditional mechanical control system into the electronic control system [7–11]. Automotive EMC, which come into being in recent years as the automobile technical term, is still unfamiliar to many people, so it is necessary to carry out a summary to introduce and expatiate on it.

Automotive Electromagnetic Compatibility Representation: Automotive EMC, is to ensure the car is running, the car's electrical and electronic equipments do not affect each other, which can compatibly work [1].

This paper collected and analyzed a large amount of related literature, technical information and research reports. For unceasing changes of driving environment of the car, the electromagnetic energy constitution in the work environment of the automotive electronics equipment would be very complex and changeable [6–9]. The article divides the vehicle electromagnetic environment into three: the inner electromagnetic interference, the body static interference, the outer electromagnetic interference. And they will be separately described in detail in the full paper. International organizations and standards for automotive EMC, experiment testing technologies, and the current automotive EMC research will also be specific introduced in this paper [3–8]. At Last, it pointed out the long-term developing trend of automotive EMC research and analyzes its influence on the development of related study in China. The detailed introduction will be expounded in the full paper.

Conclusion: The current EMC study can not provide engineering to effectively solve the problems of automotive EMC, yet to be further developed [1]. The new issues, which would emerge along with the development of automobile technology, also need to be discovered and solved. Furthermore, the present domestic automotive EMC research, including standard regulations, testing technology, design forecast and so on, have a wide gap comparing with other automotive developed countries [2]. It believes that with the related standard regulations constantly improving, the domestic automotive EMC will become a research hot spot, and the study will also carry to a new and higher level.

REFERENCES

1. Xu, L., "The development of automotive electromagnetic compatibility technology in China," *Safety and EMC*, Vol. 49, No. 1, 35–37, Jan. 2003.
2. Rybak, T. and M. Steffka, *Automotive Electromagnetic Compatibility*, 1st ed., Kluwer Academic Publishers, Dec. 2003.

3. Liu, Q.-S., L.-X. Ding, X.-L. Xu, B. Li, "Brief introduction on standard of automotive electromagnetic compatibility at home and abroad," *Communications Standardization*, Vol. 92, No. 2, 41–44, Mar. 2008.
4. Xu, L., *Automotive EMC Standards and Test*, 1st ed., Nation Technical Committee 79 on Radio Interference of Standardization Administration of China, Shanghai, 2007.
5. Yu, Z.-F. and M.-Q. Xu, "Automotive electromagnetic compatibility system approach," *Automobile Research and Development*, Vol. 77, No. 5, 54–57, Sep. 2002.
6. Chi, Q.-L., H. Liu, and Y.-Y. Zhao, "Technical analysis of automotive electromagnetic compatibility," *Journal of Heilongjiang Institute of Technology*, Vol. 20, No. 3, 38–40, Sep. 2006.
7. Dai, Z. and W. Zhou, "Electronic and magnetic disturbing source of automobile electronic system," *Journal of Wuhan Automotive Polytechnic University*, Vol. 21, No. 4, 4–7, Jul. 1999.
8. Guo, Z.-X., "EMC analysis in the application of automotive industry," *Electronic Test*, Vol. 174, No. 6, 35–38, Jun. 2008.
9. Rakouth, H., C. Cammin, L. Comstock, and J. Ruiz, "Automotive EMC: Key concepts for immunity testing," *IEEE International Symposium on Electromagnetic Compatibility*, 1–7, Jul. 2007.
10. Sakthivel, K. N., S. K. Das, and K. R. Kini, "Comparison of civilian EMC immunity standards with automative EMC immunity standards," *Proceedings of the International Conference on Electromagnetic Interference and Compatibility*, 63–69, Feb. 2002.
11. Liu, G.-P., C.-C. Chen, Y.-H. Tu, and J. L. Drewniak, "Anticipating full vehicle radiated EMI from module-level testing in automobiles," *IEEE International Symposium on Electromagnetic Compatibility*, Vol. 2, 982–986, Aug. 2002.
12. Zhao, Y., "Design of anti-jamming of digital in-car AV products," *Electronics Quality*, Vol. 98, No. 2, 58–60, Mar. 2006.

Transient High-energy Surge Protection Circuits for RF Transceivers

Liann-Be Chang, **Shen-Yio Liao**, **and Ming-Jer Jeng**
Department of Electronic Engineering, Chang Gung University, Taoyuan, Taiwan

Abstract— Electronic equipment is susceptible to the transient high-energy surge damage. How to protection these high-energy surges for electronic system is an important issue especially for the outdoor communication system. In this work, we proposed three different transmission band protection circuits to prevent surge damage to high frequency transceiver system. One is for the transmission frequency below 30 MHz, another is for the frequency below 100 MHz and the other is for the frequency range between 1 GHz and 2 GHz. The design ideas are based on the cascaded configurations (Two stages), which are paralleling the gas tube with solid-state protector (Metal oxide varistor and transient voltage suppressor). When high-energy surge enters to the protection circuit, the second stage of solid-state protector will conduct the initial surge to ground first and then build up the voltage at a voltage drop resistor, which is inserted between gas tube and solid-state protector. Next, the first stage gas tube conducts the main surge to ground when the voltage rises to a level to activate the first stage gas tube. It is noted that a voltage drop resistor has to be inserted to benefit the gas tube having enough time to be activated and to lead the main surge to ground. But, the resistor value will significantly affect circuit performance at high frequency. Impedance match is also a design issue for the front and back ends. Two types of transient high-energy surges were tested: one has the rise time of 1.2 50 µs and the other has the rise time of 1 ns. The maximum surge voltage is about 12 KV. It is found that our proposed circuits can effectively suppress the transient high-energy surges to a low value that is acceptable to a transceiver system.

Built-In-Self-Test (BIST) Circuitry for LVDS-type off-chip Transmission with Speed up to 640 Mb/s

Heng-Shou Hsu
Department of Electronic Engineering, Feng-Chia University
100 Wenhwa Road, Seatwen, Taichung 40724, Taiwan, R.O.C.

Abstract— This paper proposed the design and implementation of novel Built-In-Self Test Circuitry for LVDS-type off-chip transmission with speed up to 640 Mb/s. While the on-chip transmission rate can be easily optimized to the desired performance by careful circuit-level simulation, the inevitable off-chip transmission performance degradation due to Electromagnetic Interference (EMI) and signal crosstalk should be carefully justified to guarantee transmission signal integrity especially for high bit date rate applications. We proposed novel Built-In-Self-Test (BIST) circuitry embedded with the high speed output driver such as LVDS output buffer. The proposed novel circuitry posses much less smaller chip area compared with driver circuitry. The Built-In-Self-Test (BIST) circuitry can detect the off-chip transmitted signals through a hysteresis tunable detector and the output result of this detector then fed into a frequency divider to make the judgment for successful transmission. Therefore, the most important parts of signal transmission, signal amplitude and transmission frequency (data rate) have been completely examined. The proposed novel BIST circuitry for high data rate off-chip transmission posses the advantages of less chip area consumption, good system integration, can be used to monitor signal integrity when transmission rate up to 640 Mb/s, can be served as off-chip output driver performance judgment especially for chip mass-production. The circuits were implemented in a 3.3 v 0.35 μm CMOS process.

A Novel Electromagnetic Bandgap (EBG) Structure for Electromagnetic Compatibility (EMC) Application

Cheng-Chi Yu, **Meng-Hsiang Haung**, **Yao-Tien Chang**,
Luen-Kang Lin, **and Tsung-Han Weng**
Department of Communications Engineering, Feng-Chia University, Taichung, Taiwan

Abstract— The EMC issues become possible critical problems for high speed, large scale or complex systems consisting of a number of devices such as PCs, servers or automotive application, which cause significant time delay or extra developmental cost.

A novel electromagnetic bandgap (EBG) cell is proposed in this paper. It can be easily fabricated on standard PCB material and can be used where space is at a premium. This EBG unit cell consists of three elements: a square patch, slots and via. A 6×6 EBG array is built on a 0.8 mm thick FR4 substrate with relative permittivity of 4.4. The cells of EBG structures were placed between ground plane and transmission lines. They were designed and developed to provide two stop bands at 2.8 GHz $\sim$ 3.2 GHz and 4.3 GHz $\sim$ 4.8 GHz. By properly arranging the unit cell dimension and location, the mutual coupling between transmission lines in multi-layers structure can be reduced. Several cases of different layout skill have been studied in this paper. The results demonstrate that the mutual coupling between signal lines are effectively suppressed when the EBG structures are properly designed. They are suitable for EMC application.

Antenna Effect Analysis of Laptop Platform Noise on WLAN Performance

Han-Nien Lin, **Ching-Hsien Lin**, **Tai-Jung Cheng**, **and Min-Chih Liao**
Department of Communications Engineering, Feng-Chia University
100 Wen-Hua Rd., Taichung 40724, Taiwan, R.O.C.

Abstract— Due to increasingly high integration of multi-radios and high-speed digital system nowadays, serious platform noise is generated by ever higher speed digital clocking and signaling technologies. There are many sources of interference, such as EMI spectrum from CPU, LCD, and memory, which may be in the form of radiation or conduction emission and thus affect the quality of signal perceived at the transceiver. While encroaching into the wireless communication band, those noises could result in a significant degradation to the throughput performance of wireless communications. It is very important to analyze the proximity effect on antenna performance due to different locations and types of antenna. An antenna was used to measure the noise floor of RF systems and examine its performance for different locations on a laptop. The laptop tested and analyzed in this paper has the following modules: CPU (Intel(R) T9400:2.53 GHz) and built-in 802.11a/b/g WLAN module. The measurement result demonstrates the impact of LCD noise on throughput for 802.11g. We also found the sensitivity of the receiver decreases (throughput decreases) as the LCD interference was injected to the communication link between the AP and NIC card. Furthermore, we will also use the different type of antennas for 2.4G band to compare the communication performance, such as antenna efficiency, the radiation pattern, noise floor, for different locations. We will then show the increasing throughput of system by optimizing the design of antenna.

Application of EBG Structure to Suppress Digital Noise in the Integrated Module of 2.4 GHz CPW-fed Antenna and PCB

Han-Nien Lin, **Tai-Jung Cheng**, **Ching-Hsien Lin**, **and Jhih-Min Liao**
Department of Communications Engineering, Feng-Chia University
100 Wen-Hua Rd., Taichung 40724, Taiwan, R.O.C.

Abstract— The periodic EBG structure was intensively investigated and applied for noise isolation/suppression in PCBs recently. This paper will present a novel electromagnetic band-gap (EBG) structure on an integrated module with CPW-fed antenna and digital PCB. The proposed structure is to prevent the noise from digital area to degrade the RF signal quality at antenna input. When the 2.4 GHz band CPW-fed antenna and digital transmission line both share the same ground plane for economic purpose, the broadband digital noise may couple to antenna via the ground plane. Since the ground-bounce noise and power integrity problem occur due to simultaneous switching from the high-speed digital devices, we will utilize the EBG structure on the ground plane of integrated module of 2.4 GHz CPW-fed antenna with digital trace to reduce the noise coupling by suppressing harmonic noise. There are two different kind of EBG structures, one with defected ground structure (DGS) and the other with periodic sandwich layer between microstrip transmission line and ground plane. The advantage of DGS is that it doesn't need to waste additional single layer to implement the EBG structure, but it will suffer the significant signal integrity and EMI problem from splitting the ground plane. However, design of the sandwich layer EBG structure will bring great challenge to system engineers, because it may result in serious problems associated with signal integrity and S/N degradation. We will compare the level of digital noise coupled to antenna and show the noise suppression capability of integrated module for the cases with and without EBG structure.

Optimized ARC Filters Using Goal-lossy GIC

J. Sedláček, Z. Szabó, and R. Kadlec
Brno University of Technology, Czech Republic

Abstract— The ARC filters based on RLC ladder prototypes realized using non-cascade filter synthesis method exhibit some advantages- namely low sensitivities. On the other hand there are disadvantages which are coupled with ARC simulation of required ideal inductors of LC ladder prototypes what brings higher sensitivities to real parasitic properties of ARC simulation. Usage of new principle of goal-directed losssy RLC ladder prototypes enables to design ARC realizations with optimized parameters and minimized influence of real active elements. In paper here are new possibilities of ARC filter optimization in some practical examples presented.

REFERENCES

1. Hájek, K. and J. Sedláček, *Kmitočtové Filtry*, Vydavatelství BEN, Praha, 2002.
2. Hájek, K. and J. Sedláček, "Lossy LC ladder prototypes and their use for ARC filter optimization," *Wseas Transactions on Electronics*, Vol. 2, No. 3, 94–99, ISSN 1109-9445, July 2005.
3. Martinek, P. and T. Daša, "Evolutionary algoritmes by ARC filter synthesis," *ECCTD 05*, 155–159, Cork, 2005.
4. Hájek, K., V. Michal, J. Sedláček, and M. Steinbauer, "A simple method of goal-directed lossy synthesis and network optimization," *Advances in Electrical and Electronic Engineering*, 249–253, Žilina, ISSN 1336-1376, 2006.
5. Hájek, K., V. Michal, and J. Sedláček, "Modern operational amplifiers and their degeneracy effects on active filter performance," *IC-SPETO 2006*, 505–507, Gliwice-Ustroň, 2006.
6. Pavlovic, V. and M. Popovic, "An iterative method for lossy LC ladder filter synthesis", *Proc. 1987 ECCTD*, Vol. 1, 185–190, Paris, France, September 1987.
7. Martinek, P. and D. Přívratský, "Elliptic filters with lossy FDNRs," *Radioelektronika '97*, Bratislava, Slovak University of Technology, 58–61, 1997.
8. Hájek, K., J. Sedláček, and B. Sviezeny, "Improving of the active RC and SC filters by use of goal-directed lossy LC ladder prototypes," *Proc. ECCTD-03*, I-381–384, Krakow, September 2003.

Investigation into New Type Piezomagnetic Materials and Acoustical Transducers Exhibiting Piezoelectricity and Piezomagnetic Effect

Quanlu Li[1], **Yuan Li**[2], **and Zhaohui Huang**[2]

[1]Institute of Applied Acoustics, School of Physics and Information Technology
Shaanxi Normal University, Xi'an 710062, China
[2]Department of Prevention Medicine, Fourth Military Medical University
♯17, Changlexi Street, Xi'an 710033, China

Abstract— The design, preparation, etc of newly multipurpose ferrites (i.e., a magnetoelectric ceramic materials) $Ba_{6-x}R_{2x}$ $(Nb_{1-x}$ Fe_{2+x} $)O_3$, etc, which it exhibiting the piezoelectricity and the piezomagnetic effect (i.e., the ferrite is a multifunctional electroceramic) have been studied. The functional integrated devices including, with the magnetoelectric ceramic materials be made of a had piezoelectric vibration (electro-strctive type thickness extension vibration) and piezomagnetic vibration (magnetostriction type longitudinal extension vibration) both in the same vibrator (i.e., a functional integrated device of having two functions) which that is a composite acoustic transducer, and their applications have been investigated in acoustics etc, as may be noted.

Modal Analysis of an Antenna Feed System for a Multimode Monopulse Radar

A. M. El-Tager
Electronic Engineering Department, M. T. C., Kobry Elkoba, Cairo, Egypt

Abstract— Monopulse technique is commonly used in modern radars and communication systems for tracking targets or communicating partners because of its high angular accuracy. The aim of monopulse radar is to generate the signals required for E and H plane error channels (azimuth, and elevation).

A modal analysis for a multimode monopulse feed system is presented. Simulations for the complete system are performed. Measurements for different target positions in the 9–10 GHz frequency range are carried out to verify the modal analysis and the simulation results.

A dielectric loaded E-plane rectangular waveguide horn. The horn is dielectric loaded in order to allow the propagation of the desired higher order modes [TE_{01}, TE_{10}, TE_{20}, TM_{11}, and TE_{11}]. The horn is extended by a non standard waveguide allowing the propagation of the mentioned modes.

When the incident wave-front is on the antenna axis, the source is symmetrically excited, i.e., the distribution of the field on the horn aperture is even. Therefore, only TE_{10} mode is transmitted by the horn.

If the incident wave-front is offset in plane H of the horn, the diffraction pattern moves along X-axis of the horn aperture (Azimuth). The excitation becomes asymmetrical, such that higher order modes will propagate. The filtering action of the horn propagates only modes TE_{10} and TE_{20}.

Finally, if the incident wave-front is offset in plane E of the horn aperture, the diffraction pattern moves along the Y-axis of the horn aperture (Elevation). This asymmetric excitation produces modes TE_{10}, TM_{11}, and TE_{11}.

3D EM models are built using HFSS to obtain complete modal analysis. The analysis results verify the studied principle of operation.

To carry out the measurements the system is mounted and a transmitting horn antenna is used acting as a target. The transmitting horn is placed at different positions the output from each channel is measured with the other two ports matched. The channels output are measured at 5 positions (bore sight, $+20^\circ$ elevation, -20° elevation, $+20^\circ$ azimuth, and -20° azimuth).

Measurements showed excellent agreement with the analytical and simulation results.

Calculation of Electromagnetic Wave Logging Response by Using the Numerical Mode Matching Method

Yuan Zhao, **Yueqin Dun**, **and Jiansheng Yuan**
State Key Lab of Power Systems, Department of Electrical Engineering
Tsinghua University, Beijing 100084, China

Abstract— The Numerical Mode Matching (NMM) method as an efficient half-numerical and half-analytical algorithm has been successfully applied in the simulation of electromagnetic fields with multi-layer structure domains for both high and low frequency applications. The efficiency of the NMM method is based on the idea that a higher dimensional problem can be reduced to a series of lower dimensional problems. In this paper, the response of the Logging While Drilling (LWD) problem with multiple-layer structure soil is simulated by using the NMM method.

The simulated drill collar consists of one or two transmitting coils and two receivers. The transmitters operate at a frequency of 1 MHz. The two receivers can be used to cancel the direct coupling effect by taking the ratio of two receiver signals. This device can be applied to detect physical property parameters of the soil or medium surrounding the borehole, including the conductivity and the relative permittivity. According to the simulation results, the phase difference of signals received by the two receivers, but not the difference of the signal amplitude, is reflected by the parameters observably.

In the numerical simulation, a model of LWD problem including drill collar is adopted. The drill collar is considered as specific layers of the earth to simplify the simulation. The concerning algorithms for the complex number eigenvalue solution and the approaches for interface condition treatment will be introduced in the full paper. The software based on the NMM method has been developed, and verified by the finite element method software. The numerical experiments show that the NMM method is more efficient and accurate than other traditional numerical methods.

Analysis of Ridge Waveguide with Claddings of Metamaterials with Zero Index of Refraction

Wanzhao Cui[1], **Jia Chen**[2], **Tiancun Hu**[1], **Hongtai Zhang**[1], **and Enrang Zheng**[2]

[1]National Key Laboratory of Space Microwave Technology
Xi'an Institute of Space Radio Technology, Xi'an, Shannxi 710100, China
[2]Shannxi University of Science & Technology, Xi'an, Shannxi 710021, China

Abstract— In this paper, based on peculiar electromagnetic characteristics of metamaterials, peculiar properties of ridge waveguide with claddings of metamaterials with zero index of refraction are analyzed. These results provide some interested insights for potential applications.

A Simple Method to Measure the Unloaded Q of a Transmission-type Resonator

Tiancun Hu and Wanzhao Cui
National Key Laboratory of Space Microwave Technology
Xi'an Institute of Space Radio Technology, Xi'an 710100, China

Abstract— A simple method to quickly obtain the unloaded Q of a transmission resonator is presented. Input and output coupling coefficients can be directly obtained by measuring the transmission and reflection coefficient using a network analyzer.

Symmetric Unit Cell Models for Composite Right/Left-handed Transmission Lines (CRLH-TL) Metamaterials

Jia Chen[1], **Enrang Zheng**[1], **and Wanzhao Cui**[2]

[1]Shaanxi University of Science & Technology, Xi'an 710021, China
[2]National Key Laboratory of Space Microwave Technology
Xi'an Institute of Space Radio Technology, Xi'an 710100, China

Abstract— Based on the homogeneous composite right/left-handed transmissions lines (CRLH-TL) equivalent circuit model, an symmetric unit cell model for CRLH-TL metamaterials having left-handedness (LH), right-handedness (RH) at different frequencies presented. The CRLH TL unit model is a meta-structured TL composed of a series capacitance and a shunt inductance as well as a series inductance and a shunt capacitance. The series capacitance and the shunt inductance provide the LH nature at lower frequencies, whereas the series inductance and the shunt capacitance provide the RH nature at higher frequencies, an unique characteristic of CRLH-TL. We can obtain $|S_{21}| = 1$ at a desired center frequency and also make a desired phase shift over a unit cell possible. The unit cell model for CRLH-TL is analyzed using S-parameter formulations resulting in some useful closed-form expressions for design purposes. These results provide some useful references in facilitating the design of CRLH-TL.

Analysis and Simulation of Superresolution Image Restoration

Yi Zhang, **Quan Zhou**, **Minqi Li**, **and Wanzhao Cui**
National Key Laboratory of Space Microwave Technology
Xi'an Institute of Space Radio Technology, Xi'an 710100, China

Abstract— Superresolution image restoration reconstructs a frame of high-resolution (HR) image from low-resolution (LR) images. The resolution of the improved image is higher than any of the LR's. This kind of technique provides a novel method for obtaining HR image and reduces the cost, so it becomes one of the hotspots in the field of image processing, and has been widely used in the area of military affairs, weather, medicine and etc. Several aspects of superresolution restoration have been analyzed, and a frame of superresolution image has been reconstructed using a group of LR images in this paper.

THz Rectangular Microstrip Patch Antenna on Multilayered Substrate for Advance Wireless Communication Systems

Aditi Sharma[1], **Vivek K. Dwivedi**[2], **and G. Singh**[1]

[1]Department of Electronics and Communication Engineering
Jaypee University of Information Technology, Solan 173 215, India
[2]Department of Electronics and Communication Engineering
Jaypee Institute of Information Technology University, Noida 201724, India

Abstract— There are many advantages associated with increasing the operating frequency for majority of already well developed applications, including the potential for increased available bandwidth and improved resolution with directivity which can be obtained for a given antenna aperture. Gigabit data rate for future wireless communication systems will open the door to variety of applications demanding ultra-broad bandwidth. Among the applications that are already foreseen is the wireless extension of the next generation broadband access fiber-optic networks which will support data rates tens of gigabits, and are expected to replace xDSL and cable-modem access network [1–4]. Most of the present efforts towards higher data rates are aimed at enhancing the spectral efficiency of existing or currently developing microwave and millimeter wave wireless systems. However, the spectral bandwidth of such a system is limited, and they will not able to support data rates exceeding a few Gbps [4]. In the long run, there is no alternative but to turn towards higher carrier frequencies. Since it is commonly accepted that such high-data rates can not be achieved with IR systems, the THz range is a logical choice.

In this paper, we have simulated a rectangular microstrip patch antenna using multilayered substrate materials at THz frequencies for faster wireless communication systems with specified operational features. The 10 dB impedance bandwidth of the single-pin-shorted dual-band microstrip-line fed rectangular microstrip patch antenna on multilayered dielectric substrate is 33.67%. The radiation efficiency and gain of the antenna are 90.69% and 10.05 dB at 875 GHz, respectively. The operational features of antenna depend on the structural parameters and feed positions. The simulation of this antenna has been performed by using CST Microwave Studio, which is a commercially available electromagnetic simulator based on the finite difference time domain technique.

REFERENCES

1. Piesiewiez, R., T. K. Ostmann, N. Krumbholz, D. Mittleman, M. Koch, J. Aschoebel, and T. Kiirner, "Short-range ultra-broadband terahertz communications: Concepts and prospective," *IEEE Antenna and Prop. Magazine*, Vol. 49, No. 6, 24–39, Dec. 2007.
2. Zeadally, S. and L. Zhang, "Enabling gigabit network access to end users," *Proc. IEEE*, Vol. 92, No. 2, 340–353, Feb. 2004.
3. Driessen, P. F., "Gigabit/s indoor wireless systems with directional antennas," *IEEE Trans. Commun.*, Vol. 44, No. 8, 1034–1043, Aug. 1996.
4. Woolard, D. L., E. R. Brown, M. Pepper, and M. Kemp, "Terahertz frequency sensing and imaging: A time domain of reckoning future applications?," *Proc. IEEE*, Vol. 93, No. 10, 1722–1743, 2005.

Theoretically and Experimentally Investigation of Sparking of Metal Objects inside a Microwave Oven

Gholamreza Shayeganrad[1] **and Leila Mashhadi**[2]

[1]Islamic Azad University, Karaj Branch, Karaj, Iran
[2]Physics Department, Amirkabir University of Technology
P. O. Box: 15875-61390, Tehran, Iran

Abstract— Over the past years, some microwave oven experiments have been done by placing non-food objects such as metal objects, CDs, lightbulbs and etc. in the microwave oven cavity [1–4]. It is well understood, when a metal object is placed inside the oven cavity, sparking will result. Here, we have theoretically investigated the sparking of metal objects within the microwave oven, based on the electrostatic and alternating field. The resonant modes characteristics of both TE and TM electromagnetic fields in the oven cavity are determined. An approximate analysis for electric fields around the metal disks and sharp edges is carried out by solving Laplace equation in polar and elliptical coordinates. Some experiments are done for CD-ROMs and several types of metallic rings and wires. They have shown a good agreement with the theoretical predictions.

3D Joint Inversion of CSEM and MT Data with and without Anisotropy

C. Shen and R.-E. Plessix
Shell International E & P, The Netherlands

Abstract— Electromagnetic methods are commonly used to estimate the resistivity distribution of subsurface in geophysics. In hydrocarbon industry, marine control source electromagnetic (CSEM) methods generally send vertical electric currents into the Earth from an electric dipole source. Therefore, CSEM data are sensitive to thin resistive layers in subsurface. In presence of stack resistive layers or complex geology, for instance with large resistive bodies, the inversion results may be ambiguous and difficult to interpret. Magnetotelluric (MT) data, that relies on the natural electromagnetic field surrounding the Earth, allow us to image large-scale resistivity structures, especially at large depth thanks to the wide frequency range of the natural electromagnetic field. Because of the natural source distribution, MT data are almost insensitive to thin resistive layers. CSEM and MT data are complementary and it has been shown that a simultaneous inversion can reduce the ambiguities in the final inverted images. However, the presence of anisotropy may limit the benefits of a joint inversion. Indeed MT data are predominantly sensitive to the horizontal resistivity, while the inline CSEM data, that are sensitive to the presence of thin resistive layers, i.e., hydrocarbon layers, are mainly sensitive to the vertical resistivity. Broadside CSEM data are sensitive to both resistivities. In this presentation, we will further investigate the joint CSEM and MT inversion in the presence of anisotropy. We will discuss different formulations of the error functional for the joint inversion and possible regularization terms, based for instance on some a-priori assumption. We will illustrate the presentation with synthetic examples and a real example if we obtain permission.

A Congestion Control Algorithm Based on Onboard IP Switching

Yi Zhang, **Quan Zhou**, **Jun Li**, **Jie Li**, **and Wanzhao Cui**
National Key Laboratory of Space Microwave Technology
Xi'an Institute of Space Radio Technology, Xi'an 710100, China

Abstract— Onboard switching is a direction of satellite communication. Because of the limited satellite resources, the paper proposes an open-loop congestion control algorithm in onboard IP switches. We simply the RSVP in IP layer, in order to avoid the congestion in cache of onboard IP switches. The results of simulation show that the proposed algorithm can decrease the cell loss rate by sending path request message periodically.

A Broadband Two-stage MMIC Medium-power Amplifier

Yuanyuan Li and Long Jin
Research Institute of Electronic Science and Technology
University of Electronic Science and Technology of China, Chengdu, China

Abstract— A broadband two-stage MMIC medium-power amplifier operating from 6–20 GHz is developed for EW and communication applications using 0.15 μm low-noise PHEMT process. The amplifier use a single 3-volt DC power supply, each gain stage is self-biased for class-A operation for optimal power output with minimal distortion, the two-stage feedback power amplifier has 16.5 dB small signal gain with 2.0 typical noise figure and input and output VSWRs less than 1.7 over 6–20 GHz, the output power at 1 dB compression is 16.0 dBm at 20 GHz.

Session 2P1a
Plasmonics Nanophotonics: Experimental

Plasmonic Dipole Antennas, Simulation, Characterization and Applications

Weihua Zhang, **Holger Fischer**, **and Olivier J. F. Martin**
Nanophotonics and Metrology Laboratory, Swiss Federal Institute of Technology Lausanne
CH-1015, Lausanne, Switzerland

Abstract— Plasmonic dipole antenna is an optical analogue of conventional dipole antenna for radio wave. It not only 'focuses' the propagating light into its nanoscale gap, but also can enhance the emission of a quantum emitter. These properties make plamonic dipole antenna an interesting candidate for many applications, such as sensing, surface-enhanced spectroscopies, nonlinear optics, high performance near-field optical microscopy, etc. [1].

In order to understand the behaviours of plasmonic dipole antenna, we performed recently a systematic study. [2] Antenna structures with varying geometrical parameters were simulated using the Greens tensor method. We found that a plasmonic dipole antenna inherits features from both the traditional dipole antenna and plasmonic nanostructures: (1) its resonance wavelength linearly depends on its length; (2) its scattering cross-section is much larger than its geometrical size due to the excitation of localized plasmon resonances; (3) it generates huge field enhancement in its feeding gap; (4) the gap size has a strong influence on both the resonance wavelength and the field enhancement.

We verified those simulation results experimentally by fabricating the structures and measuring the scattering spectra of single antennas. Antenna structures with different geometrical parameters were made with a precision better than 10 nm. We characterized the spectral response of single nano-antennas using dark-field spectroscopy. The spectra show perfect lorenzian shape; their resonance wavelength red shifts linearly when the antenna length increases; red shift also occurs when the gap size decreases. All the experimental data quantitatively agrees with the simulation results.

As a resonance-tunable structure, plasmonic antenna dipole provides us with an ideal platform for surface-enhanced Raman spectroscopy (SERS). We investigated SERS effects on antennas with varying the length and gap size. On the antennas with a small gap size, temporal spectroscopic fluctuations were observed, indicating huge field enhancement in the feeding gap. A detailed comparison between the experimental result and the prediction by the classical SERS mechanism is performed on a large number of single antennas. The Raman spectra are consistent with the theoretical predictions, providing new evidence for the debated SERS theory.

REFERENCES

1. Mühlschlegel, P., H.-J. Eisler, O. J. F. Martin, B. Hecht, and D. W. Pohl, *Science*, Vol. 208, 1607, 2005.
2. Fischer, H. and O. J. F. Martin, *Opt. Express*, Vol. 16, 9144, 2008.

Analysis of Lightwave Propagation through Nano-wires and Plasmonic Waveguides for Nano-Photonic Circuit Application

El-Hang Lee[1, 2] **and S. H. Song**[3]

[1]OPERA National Research Center for VLSI Photonics Technology, INHA University
Incheon, 402-751, South Korea
[2]Graduate School of Information Technology and Telecommunication, INHA University
Incheon, 402-751, South Korea
[3]Department of Physics, College of Natural Sciences, Hanyang University
Seoul, 133-791, South Korea

Abstract— We present an overview of our work on the theoretical analysis of the propagation of electromagnetic waves, light waves, or plasmonic waves along the non-metallic dielectric nano-wires and plasmonic waveguides for applications in the design and fabrication of nano-scale photonic integrated circuits. First, we examine the lightwave propagation characteristics along the nano-wires and explain them in terms of plasmon waves propagating along the surfaces of the nano-wires. For the analysis of plasmonic wave propagation, we examine the characteristics of the slow light propagation and the fast light propagation. We then design and fabricate plasmonic waveguides to integrate them into either horizontally parallel directional couplers or vertically parallel directional couplers. Their characteristic performances are then compared. We first designed and fabricated vertical directional couplers consisting of metal stripe waveguides embedded in polymer. The fabricated vertical directional couplers were 9 mm long in total length with the arm separation of 200 μm at the input/output section. We also designed and fabricated a novel metal-waveguide structure for sustaining long-range surface-plasmon-polaritons (LR-SPP), which is basically composed of two asymmetric metal layers. We then examine the use of plasmonic waves for nano-photonic circuit applications. The plasmonic waveguide devices are integrated with other micro/nano-scale photonic devices, either on a board on on a chip, for VLSI photonic integrated circuit applications. We will present examples of devices and integrated circuits along with the scientific and engineering issues arising from the various mismatches between devices of diverse functional characteristics and properties.

Two-photon-induced Nano-scale Fabrication Technique of Three-dimensional Metallic Structures for Plasmonic Metamaterials

Takuo Tanaka
Metamaterials Laboratory, The Institute of Physical and Chemical Research, RIKEN
2-1, Hirosawa, Wako, Saitama 351-0198, Japan

Abstract— Plasmonic metamaterials are artificially designed materials. By engineering such materials, we can control the magnetic permeability even in the optical frequency region in which all materials in nature lose magnetic response. Recently, we have theoretically investigated the magnetic response of plasmonic metamaterials in the optical frequency region and we clarified that three-dimensional (3D) array of split-ring-resonators made of silver can give a strong magnetic response at the visible light frequency region. The magnetic response in the visible light frequency region enables us to expand the controllability of photons beyond what is achievable with natural substances. We found that the Brewster condition is satisfied even with *s*-polarized light at the interface between the materials that have different permeability. By using this phenomenon we proposed a novel non-polarizing Brewster device that transmits the light beyond the material boundary without any light reflection.In this paper, as a fabrication technique of plasmonic metamaterials, we report a technique that enables fabrication of three-dimensional (3D) metallic microstructures with a resolution of nano-scale by means of two-photon-induced metal-ion reduction. We demonstrate fabrications of continuous and electrically conductive silver or gold 3D structures self-standing on the substrates. Recently, by controlling the growth process of nano-metal-crystals with surfactant molecules, we successfully improved a spatial resolution up to 100 nm. In the presentation, the magnetic response of the plasmonic metamaterial fabricated by this technique is also presented.

High Density Optical Data Storage

Peter Török, **Carlos Macías Romero**, **Matthew Foreman**
Gung-Hsuan Ho, **Peter Munro**, **and Arthur Van de Nes**
Imperial College London, UK

Abstract— Optical data storage has played a significant role in the extremely fast development of consumer electronics during the last three decades. The direction of development has been the same ever since the fist CD disk was devised: for subsequent generations shorter wavelengths and higher focusing lens numerical apertures have been used. Unfortunately the natural limits of this development have been reached and further improvement does not seem to be possible using the same principles.

Recently holographic optical data storage has emerged as an extremely promising technique to pack around 1 TB/cm^3 information into an appropriate medium. Unfortunately this method has its significant drawbacks: holographic disks are at the moment cannot be mass replicated and they are not naturally compatible with current standards.

We have developed an alternative approach of storing data. The principle is that every pit ends up storing more than a single bit of information. This is achieved by introducing pits with various angles with respect to the spin direction. The angle of the pit stores the information. With this method it is in principle possible to store up to 1 TB per disk.

The talk will briefly overview current techniques of optical data storage and describe the principles of operation for the new solution. Experimental data will also be presented to demonstrate the full power of the method. Experimental data and system noise analysis shows that it is possible to obtain > 43 dB signal-to-noise ratios corresponding to a 14 fold increase in data storage capacity over any, currently existing solutions.

Fabrication of Functional Optical Devices Using Highly Ordered Anodic Porous Alumina

Hideki Masuda[1, 2], **Kazuyuki Nishio**[1, 2], **and Toshiaki Kondo**[2]

[1]Department of Applied Chemistry, Tokyo Metropolitan University
1-1 Minamiosawa, Hachioji, Tokyo 192-0397, Japan
[2]Kanagawa Academy of Science and Technology, 5-4-30 Nishihashimoto, Sagamihara
Kanagawa 229-1131, Japan

Abstract— The fabrication of functional optical devices based on the ordered structures from submicron to nanometer scales has attracted increasing attention due to its application in various fields due to its application in various fields, such as chemical or biological sensing. We describe here the results of the fabrication of highly ordered anodic porous alumina and its application to various kinds of functional optical devices. Anodic porous alumina, which is formed by anodization of Al in acidic solution, is typical self-ordered material [1]. The structure of anodic porous alumina consists of ordered triangular array of holes with high aspect ratios in alumina matrix. The ordered structures prepared from highly ordered anodic porous alumina showed unique optical properties originated from the localized surface plasmon, which was dependent on the size and shapes of the structures [2, 3]. In the report, several types of nanostructures composed of 2D and 3D ordered arrays of metal nanoparticles using highly ordered anodic porous alumina will be describe from the aspect of the preparation of functional plasmonic devices [3, 4].

REFERENCES

1. Masuda, H. and K. Fukuda, *Science*, Vol. 268, 1466, 1995.
2. Matsumoto, F., M. Ishikawa, K. Nishio, and H. Masuda, *Chem. Lett.*, Vol. 34, 432, 2005.
3. Kondo, T., F. Matsumoto, K. Nishio, and H. Masuda, *Chem. Lett.*, Vol. 37, 466, 2008.
4. Kondo, T., M. Tanji, K. Nishio, and H. Masuda, *Electrochem. Solid-State Lett.*, Vol. 9, C189, 2006.

Session 2P1b
Radio-Over-Fiber Communication System

Implementation of a Radio over Fiber System in a Geographically-distributed Optical Network

S. Arismar Cerqueira, Jr.[1], **D. C. Valente e Silva**[2], **M. A. Q. R. Fortes**[1], **L. F. da Silva**[2], **O. C. Branquinho**[2], **and M. L. F. Abbade**[2]

[1]Optics and Photonics Research Center, UNICAMP, Brazil
[2]Faculdade de Engenharia Elétrica, Pontifícia Universidade Católica de Campinas, Brazil

Abstract— The next generation of access networks is rushing the needs for the convergence of wired and wireless services to offer end users greater choice, convenience and variety in an efficient way [1]. This scenario will require the simultaneous delivery of voice, data and video services with mobility feature to serve the fixed and mobile users in a unified networking platform. In other words, new telecom systems require high-transmission bandwidths and reliable mobility. The Radio over Fiber (RoF) technology represent a key solution for satisfying these requirements, since it jointly takes advantage of the huge bandwidth offered by optical communications systems with the mobility and flexibility provided by wireless systems. RoF systems consist of heterogeneous networks formed by wireless and optical links. Unlike traditional optical communications networks, in which a baseband signal in transmitted into the optical fibers, in RoF systems one or multiple analogous carriers are transported into the fibers. The transmission is performed by directly or externally modulating lasers by the analogous radio frequency signal. On the receiver side, the transmitted signal is recovered by using a photodiode. Compared to traditional optical systems, RoF technology provides the advantage of eliminating the gateways, since there is no need for analogous-digital or digital-analogous conversions. This simplifies the system complexity and reduces the operational costs.

RoF technology has been investigated by many Research Groups in the last years. However, the great majority of works published in literature are based on simulations and/or experiments carried out in laboratories. This work presents an implementation of a Radio over Fiber system based on IEEE 802.15.4 standard, in a geographically-distributed optical network called KyaTera [2]. Lasers were directly modulated by a RF signal at 2.4 GHz with Quadrature Phase Shift Keying (QPSK) modulation. This signal was launched into hundreds of kilometers from KyaTera Network under real conditions of temperature, pressure, humidity and wind. The optical signal was received by a fast photodiode, converted to electrical signal and then retransmitted by an antenna with gain $G = 12$ dBi. Finally the wireless signal was obtained by a receiver antenna.

Simulations based on Split Step Fourier Method were carried out for predicting the system performance. The performance parameters evaluated in the experiments were the electrical Signal to Noise Radio (SNR) and Frame Error Rate (FER) of the transmitted RF signal. Experimental results show no performance degradation of the transmitted radio frequency signal.

REFERENCES

1. Jia, Z., J. Yu, G. Ellinas, and G.-K. Chang, "Key enabling technologies for optical wireless networks optical millimeter wave generation wavelength reuse and architecture," *Journal of Lightwave Technology*, Vol. 25, 3452–3471, 2007.
2. www.kyatera.fapesp.br.

60 GHz Radio over Fiber Transmission System Based on Integrative Cascade MZM

Cheng Hong, **Siyu Liu**, **Cheng Zhang**, **Zhangyuan Chen**, **and Weiwei Hu**
State Key Laboratory on Advanced Optical Communication Systems & Networks
Peking University, Beijing, China

Abstract— We experimentally demonstrated a Radio over fiber transmission system which works in 60 GHz band with 2.5 Gbps bit Rate over 22 km SMF, using an integrative cascade MZM modulator.

Introduction: Radio over fiber technology is considered to be a potential solution to the broadband access networks. Making use of convergence of mobility of wireless and good transmission channel property of optical fiber, Radio over fiber technology can easy transmit several Gigabit per second. Here we experimentally demonstrated the transmission system for 2.5 Gps on 60 GHz microwave over 22 km SMF. Cascade MZM modulation method is a simple way to generate two coherence optical modes to beat in photodetector for producing microwave signal.

Experimental Setup and Result:

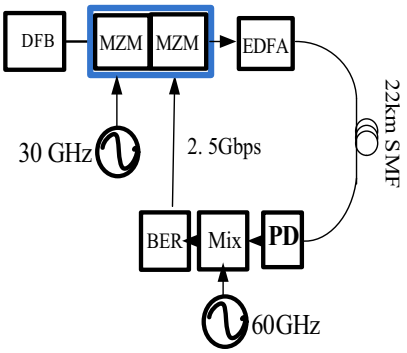

Figure 1: Experiment setup.

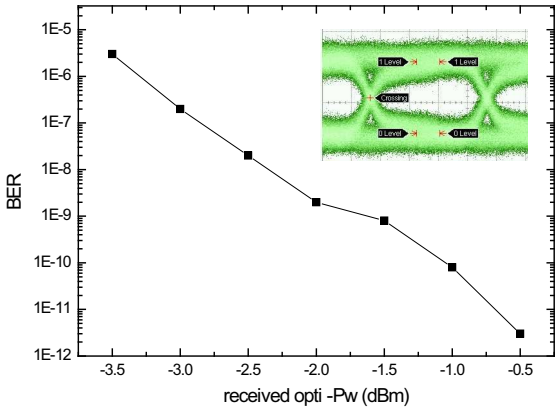

Figure 2: Received BER.

The experimental setup is show as Fig. 1. An integrative cascade MZM as modulator. One MZM is used as microwave carrier modulator bias at null point; the other is used as data modulator and set at linear bias point. The transmission bit error rate is verse received optical power is show as Fig. 2.

Conclusions: A primary demonstration of downlink Radio over system is realized by an integrative cascade MZM as modulator and coherent demodulation receiver.

ACKNOWLEDGMENT

This work is supported by The National High Technology Research and Development Program of China (863Program) under Grant 2006AA01Z261 and The National Natural Science Foundation of China (NSFC) under Grant 60736003.

REFERENCES

1. Koonen, T., "Fiber to the home/fiber to the premises: What, where, and when?," *Proc. IEEE*, Vol. 94, No. 5, 911–934, May 2006.

Single-mode Modulation Using Injection-locked Fabry-Perot Laser in Radio-over-Fiber System

Cheng Zhang, **Mingjin Li**, **Siyu Liu**, **Cheng Hong**, **Weiwei Hu**, **and Zhangyuan Chen**
State Key Laboratory on Advanced Optical Communication Systems & Networks
Peking University, Beijing, China

Abstract— Radio-over-Fiber (RoF) system has been considered a promising technology for future broadband wireless communication. Recently, many schemes have been proposed to realize a low-cost and high-performance RoF system. The commonly used method to generate millimeter wave (MMW) in these systems is optical heterodyning technique which use two correlated optical modes to beat a high-quality MMW. And usually the data is uploaded to the MMW by just modulating these two modes. However, standard modulation of two correlated modes will suffer from chromatic dispersion which results in a radio frequency (RF) fading and limits the transmission distance. Single-mode modulation is proposed to overcome this problem. But the former method using a Mach-Zehnder (MZ) interferometer filter is too complex to be practical. In this paper, we propose a new approach to realize single-mode modulation using injection-locked Fabry-Perot laser dioxide (FPLD).

In the experiment setup, the DFB laser's output is coupled into an intensity modulator which is driven by the reference frequency at 15 GHz from a signal generator. The modulator output is sent to an optical notch filter to select the first-order sidebands whose mode-spacing is 30 GHz. An EFDA and an attenuator are used to get the proper injection power and its output is connected with a 60 GHz mode-spacing FPLD through a three-port optical circulator (OC) for single-mode injection-locking. A polarization controller (PC) is used to control the input state of polarization to the FP laser diode. The intermediate frequency (IF) signal is uploaded by modulating the current of FPLD. Finally, the single locked mode and the other reflected mode are transmitted for 44.4 km and sent to a 70 GHz photo detector (PD) for 30 GHz MMW generation. The electrical signal sidebands on both sides of 30 GHz carrier are measured for different IF. Another experiment using standard dual-mode modulation has also been done to for comparing data.

Figure 1 compares the side power after 44.4 km SMF transmission for both single-mode modulation and dual-mode modulation. Different RF powers for single-mode modulation are also test in our experiment. Compared to dual-mode modulation, it can be found that the proposed single-mode modulation is immune to RF signal fading due to the chromatic dispersion.

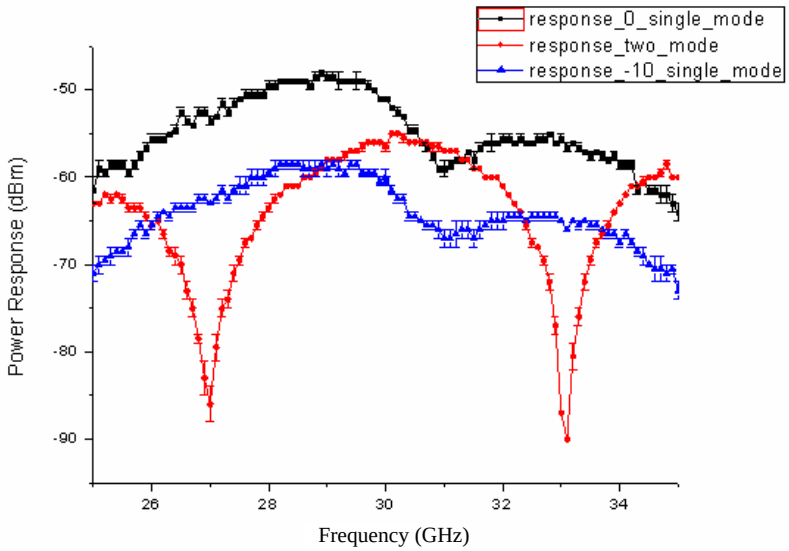

Figure 1: Received electrical power for different modulation frequency after 44.4 km SMF transmission.

ACKNOWLEDGMENT

This work is supported by The National Natural Science Foundation of China (NSFC) under Grant 60736003.

A Scheme of Photonic Notch Filter Using DGD Method for Radio-over-Fiber Communication Systems

Hanhong Gao, **Jinxuan Wu**, **Zhao Tu**, **Cheng Zhang**, **Dandan Wu**, **Weiwei Hu**, **and Zhangyuan Chen**
State Key Laboratory of Advanced Optical Communication Systems & Networks
Peking University, Beijing, China

Abstract— Microwave photonics has been a popular research field. The photonic filters can provide a large tunability and a high Q factor besides advantages such as low loss, light weight, immunity to electromagnetic interference and capability to overcome electronic bottleneck. Therefore, a number of photonic microwave filters have been reported in the literature. Several methods have been demonstrated using fiber delay lines, most of which use several fixed lengths of fiber to achieve stepped time delay. It is recently demonstrated that non-uniformly spaced taps can implement a photonic microwave filter with an arbitrary band-pass response, which would have the same spectral characteristics as a photonic microwave delay-line filter with true negative or complex coefficients. Another particular application of interest is the transversal microwave filter, which can be classified as two kinds: optically coherent and optically incoherent. Besides, a tunable ring resonator in polymeric wave-guides was exploited to implement an integrated photonic microwave band-pass filter operating at around 10 GHz.

We propose a reconfigurable and continuously tunable photonic notch filter implementing a technique using a differential group delay (DGD) element including a tunable laser source, a polarization beam splitter (PBS), an adjustable optical delay line, three polarization-preserving fibers (PPF) and one polarization-preserving fiber coupler. First, electro-optical modulator (EOM) modulates the laser output with RF signal. After passing PBS, the beam separates into two with orthogonal polarizations, which will travel separately along two PPF. In addition, one beam will experience delay through adjustable optical delay line. Therefore they will experience different time delay. They are combined using the polarization-preserving coupler and the electric signal is detected by photo detector (PD). Finally, a vector network analyzer is used to measure the characters of this microwave photonic filter.

The time delay is set to about 100 ps, and a filter with free spectral range (FSR) approximately 10 GHz is realized. The notch rejection ratio is larger than 20 dB. By varying the time delay, different FSR will be accomplished. What's more, the central frequency of laser source is adjusted deviating from the previous frequency from 0 to 10 GHz. In the meantime the filter varies from low-pass filter to band-pass filter and back to low-pass filter.

This filter configuration has several advantages comparing with previous schemes. Firstly, adjustable optical delay line can be used to adjust FSR of the filter, making it continuously tunable. This delay line can achieve a wide range of FSR. Secondly, it is reconfigurable through the adjustment of the central frequency of the laser source. The filter frequency response can be changing from band-pass filter to low-pass filter. Lastly, this configuration can be used in varieties of radio-over-fiber communication systems to achieve a better filter performance.

ACKNOWLEDGMENT

This work is supported by the National Undergraduate Innovative Test Program and the National Natural Science Foundation of China (NSFC) under Grant No. 60736003.

A Scheme of Microwave Photonic Filter Based on Hi-Bi Fiber

Dandan Wu, **Weiwei Hu**, **and Zhangyuan Chen**
State Key Laboratory of Advanced Optical Communication Systems & Networks
Peking University, Beijing, China

Abstract— Over the past several decades Microwave photonic filter (MPFs) has attracted a lot of interest due to the processing of radio-frequency (RF) signals in the optical domain, saving bulky OE and EO conversion parts, and with the advantages of wide bandwidth, immunity to electromagnetic interference, low loss, tunability and reconfigurability, therefore they are widely applied to phased-array beamforming, radar, mobile communications, and radio-over-fiber (ROF) systems. The MPFs can be operated in incoherent or coherent regime. Incoherent filters are more stable against environmental conditions. Therefore, until now many kinds of incoherent MPFs have been reported in literatures. The conventional incoherent MPFs have been proposed using different optical delay lines or electrically summing configurations, then the intensity of the modulated light outputs from different taps are added. However, the former limited the free spectrum range (FSR) of the MPFs, and the later lost the advantages of optical domain signal processing. Recently, polarization synthesizing method has been reported to realize incoherent operation, which is based on differential group delay (DGD) element with two fiber delay lines.

In this paper, we propose a novel structure of microwave photonic filter shown in Fig. 1. The radio frequency (RF) signal of a network analyzer drives an electrooptic modulator that modulates the output of a tunable laser source. The modulated optical signal transmits along a coupler and a three-port polarization beam splitter (PBS). One of the optical beams transmits clockwise along fast-axis of the Hi-Bi fiber, and the other transmits anti-clockwise along slow-axis of the Hi-Bi fiber. Because the Hi-Bi fiber has a large refractive index difference between its fast and slow axis, the time delay difference will be induced. The two orthogonal optical signals, which are differently delayed, are combined without interference and directed to the output of the coupler.

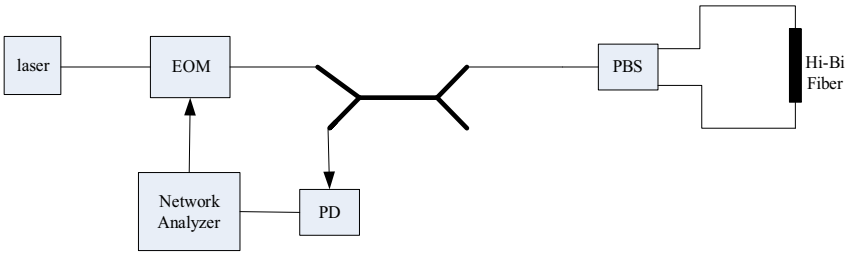

Figure 1: The experiment configuration of Microwave Photonic Notch Filter.

Theoretical calculation show that the MPF structure can provide approximately 10 GHz FSR corresponding to the 100 ps time delay. The notch rejection ratio is larger than 20 dB. This MPF has several advantages comparing with previous schemes. First, it's more stable and simpler due to using only one fiber delay line, which can implement a wide range of FSR. Second, through the employment of temperature controller or PZT to adjust the length of the Hi-Bi fiber, the MPF will be tunable and reconfigurable. The detailed experimental results will be discussed in the manuascript.

ACKNOWLEDGMENT

This work is supported by The National Natural Science Foundation of China (NSFC) under Grant 60736003.

The Trend of Designing Rotation Sensors Based on Highly Dispersive Resonating Structures

Zinan Wang, **Xiaomu Wu**, **Chao Peng**, **Rui Hui**,
Xuefeng Luo, **Zhengbin Li**, **and Anshi Xu**
State Key Laboratory on Advanced Optical Communication Systems & Networks
School of Electronics Engineering and Computer Science, Peking University, 100871, China

Abstract— Rotation sensors, which are also known as gyroscopes, are widely used for industrial and military purpose. The basic idea of it is to detect the phase shift induced by the Sagnac effect in a closed loop [1]. Over the past few decades, gyroscope designing based on different structures have been intensively studied [1–11], and highly dispersive structures are mostly considered [4–11].

It's recognized that dispersion cannot influence the magnitude of the Sagnac effect [2, 12]. But there are different manifestations in highly dispersive medium and resonator structure. For rotation sensors based on highly dispersive medium, as Doppler effect is proposed to be the intrinsic reason to enhance their sensitivity, they suit only situations when relative motion exists between the interferometer and the medium [10]. But it's different for sensors based on highly dispersive resonating structures, such as coupled-resonator slow-light waveguide structures [9] and various photonic crystal geometries. These structures may possess huge Q-factor and they are extremely susceptible to the phase perturbation in the light path. The Sagnac effect will induce additional phase shift in the light path when such a structure is rotating, and then influence its response. The total phase shift will be enlarged as a result. It shows that the highly dispersive resonating structure will improve the sensitivity in rotation sensing [10].

An example of highly dispersive resonating structures is the CRIT (coupled-resonator-induced transparency) structure, which has highly dispersive property with low absorption at its resonant frequency [13]. The gyroscope based on this CRIT structure is proved to be highly sensitive, and it has the potential to be made in a compact size [11]. The active CRIT structure, where the dispersion can be optically tailored, can further increase the performances of CRIT based gyroscopes [14].

Electrodynamics in rotating optical elements is quite useful in designing rotation sensors. This is widely used in modeling the Sagnac effect [8, 15–18]. One way of using it is the application in the Finite-Difference Time-Domain (FDTD) algorithm [18]. This FDTD method is a promising tool to accurately analyze, design and optimize rotation sensors.

REFERENCES

1. Post, E. J., "Sagnac effect," *Rev. Mod. Phys.*, Vol. 39, 475–493, 1967.
2. Arditty, H. J. and H. C. Lefevre, "Sagnac effect in fiber gyroscopes," *Opt. Lett.*, Vol. 6, 401–403, 1981.
3. Bergh, R. A., H. C. Lefevre, and H. J. Shaw, "An overview of fiber-optic gyroscopes," *J. Lightwave Technol.*, Vol. 2, 91–107, 1984.
4. Lefevre, H. C., *The Fiber-optic Gyroscope*, Artech House Publishers, 1993.
5. Leonhardt, U. and P. Piwnitski, "Ultrahigh sensitivity of slow-light gyroscope," *Phys. Rev. A*, Vol. 62, 055801, 2000.
6. Steinberg, B. Z., "Rotating photonic crystals: A medium for compact optical gyroscopes," *Phys. Rev. E*, Vol. 71, 056621, 2005.
7. Matsko, B., A. A. Savchenkov, V. S. Ilchenko, and L. Maleki, "Optical gyroscope with whispering gallery mode optical cavities," *Opt. Commun.*, Vol. 233, 107–112, 2004.
8. Steinberg, B. Z. and A. Boag, "Splitting of microcavity degenerate modes in rotating photonic crystals — the miniature optical gyroscopes," *J. Opt. Soc. Am. B*, Vol. 24, 142–151, 2006.
9. Scheuer, J. and A. Yariv, "Sagnac effect in coupled-resonator slow-light waveguide structures," *Phys. Rev. Lett.*, Vol. 96, 053901, 2006.
10. Peng, C., Z. Li, and A. Xu, "Rotation sensing based on a slow light resonating structure with high group dispersion," *Appl. Opt.*, Vol. 19, 4125–4131, 2007.
11. Peng, C., Z. Li, and A. Xu, "Optical gyroscope based on a coupled resonator with the all-optical analogous property of electromagnetically induced transparency," *Appl. Opt.*, Vol. 15, 3864–3875, 2007.

12. Leeb, W. R., G. Schiffner, and E. Scheiterer, "Optical fiber gyroscopes: Sagnac or Fizeau effect," *Appl. Opt.*, Vol. 18, 1293–1295, 1979.
13. Smith, D., H. Chang, K. A. Fuller, A. T. Rosenberger, and R. W. Boyd, "Coupled-resonator-induced transparency," *Phys. Rev. A*, Vol. 69, 063804, 2004.
14. Dumeige, Y., T. Nguyên, L. Ghişa, S. Trebaol, and P. Féron, "Measurement of the dispersion induced by a slow-light system based on coupled active-resonator-induced transparency," *Phys. Rev. A*, Vol. 78, 013818, 2008.
15. Shiozawa, T., "Phenomenological and electron-theoretical study of the electrodynamics of rotating systems," *Proc. IEEE*, Vol. 61, 1694–1702, 1973.
16. Anderson, J. L. and J. W. Ryon, "Electromagnetic radiation in accelerated systems," *Phys. Rev.*, Vol. 181, 1765–1775, 1969.
17. Van Bladel, J. *Relativity and Engineering*, Springer, Berlin, 1984.
18. Peng, C., R. Hui, X. Luo, Z. Li, and A. Xu, "Finite-difference time-domain algorithm for modeling Sagnac effect in rotating optical elements," *Appl. Opt.*, Vol. 8, 5277–5290, 2008.

Session 2P2
Metamaterial Technologies from Microwave to Optics

Metamaterial Technologies at Terahertz Frequencies

Fuli Zhang[1, 2], **Charles Croënne**[1], **Gregory Houzet**[1], **Davy P. Gaillot**[1], **Xavier Mélique**[1], **Eric Lheurette**[1], **and Didier Lippens**[1]

[1]Institut d'Electronique, de Microélectronique et de Nanotechnologie
(IEMN — UMR CNRS 8520), Université des Sciences et Technologies de Lille
Avenue Poincaré, BP 60069, 59655 Villeneuve d'Ascq, France
[2]Department of Applied Physics, Northwestern Polytechnical University, Xi'an 710072, China

Abstract— Terahertz metamaterials are now attracted much interest with the prospect to use their extraordinary electromagnetic properties for negative refraction, super and hyper-lensing along with cloaking. We address here the difficult problem of their fabrication with special attention on their frequency band width and on their losses (return and intrinsic losses). Two approaches will be more specially considered. The first one is based on Split ring Resonator — wire resonator arrays under a grazing incidence. In order to operate at Terahertz frequency with a relatively broad-band and low intrinsic loss, interconnected omega-type micro-arrays were fabricated and frequency assessed. Their magnetic dipole can be tune by means of a liquid crystal technology as recently demonstrated. On the basis of these studies, we then studied the possibilities afforded by sub-wavelengths metal arrays under front side illumination in a BCB technology. The second approach is based on the artificial magnetism which can be pointed out in high-κ ceramics such as Barium Strontium Titanate. The main advantage of such a route is related to the isotropy of their properties while the fabrication of an isotropic metamaterial from SRR-wire arrays is troublesome at Terahertz frequencies. The main targeted application is cloaking by implementing the gradients of the effective permeability values between zero and one. At last, the possibility to fabricate a double negative media through composite-size ceramics is also demonstrated.

Theoretical and Numerical Study of Surface Waves in a Grounded Slab Waveguide of Biaxially Anisotropic Metamaterial

Salma Mirhadi and Manoochehr Kamyab Hessari
Department of Electrical Engineering, K. N. Toosi University of Technology, Tehran, Iran

Abstract— In this paper, first we theoretically demonstrate grounded slab of biaxially anisotropic metamaterial can support surface waves. Specific conditions for the existence of surface waves at the interface of slab are investigated using graphical method and showed that these conditions are greatly dependent on tensor components of the constitutive parameters. Then, the finite-difference time-domain (FDTD) method based on piecewise linear recursive convolution algorithm (PLRC) in conjunction with convolutional perfectly matched layered (CPML) is employed to verify theoretical results. Furthermore, FDTD method provides a means for visualizing propagation of surface waves at the interface of slab.

Theory: The geometry under study is shown in Fig. 1. Region 1 is assumed to be a biaxially anisotropic slab place on a perfectly conducting ground plane. Region 2 is considered to be a semi-infinite isotropic RHM. An electric line source is located in region 2. The electric field is expressed in integral form in two regions. From boundary conditions on the perfectly conducting surface and the slab interface, we can obtain the equation of the guidance of surface waves as:

$$-\frac{\alpha_1}{\mu_{1z}}\coth(\alpha_1 d)=\frac{\alpha_2}{\mu_2} \tag{1}$$

where

$$\alpha_1 = \sqrt{\frac{\mu_{1z}}{\mu_{1x}}k_z^2-\omega^2\mu_{1z}\varepsilon_{1y}} \tag{2}$$

$$\alpha_2 = \sqrt{k_z^2-\omega^2\mu_2\varepsilon_2} \tag{3}$$

α_1 and α_2 are the attenuation constant in region 1 and 2 respectively. k_z is the longitudinal wavenumber which is found by using graphical solution of Eqs. (1), (2), and (3) simultaneously at certain frequency and with certain thickness of grounded slab. α_1, α_2, μ_2, and hyperbolic cotangent function in Eq. (1) always are positive and there are no real solution for Eq. (1) unless $\mu_{1z}<0$. We conclude that surface waves can be supported only by the anisotropic metamaterial. After determination the sign of the μ_{1z}, we will make our discussions based on four possible cases for the sign of the ε_{1y} and μ_{1x}.

Case I: $\varepsilon_{1y}>0$ and $\mu_{1x}>0$: Two conditions for supporting surface wave must be satisfied. 1) $\mu_2\varepsilon_2<\mu_{1x}\varepsilon_{1y}$, 2) k_z satisfies the inequality $\omega\sqrt{\mu_2\varepsilon_2}<k_z<\omega\sqrt{\mu_{1x}\varepsilon_{1y}}$.

Case II: $\varepsilon_{1y}<0$ and $\mu_{1x}>0$: Such a structure cannot support guided modes with imaginary transverse wavenumbers in this case.

Case III: $\varepsilon_{1y}>0$ and $\mu_{1x}<0$: When Eq. (1) has a solution for k_z that satisfies $\omega\sqrt{\mu_2\varepsilon_2}<k_z$, the surface waves can exist.

Case IV: $\varepsilon_{1y}<0$ and $\mu_{1x}<0$: The solutions of Eq. (1) must be satisfied $k_z>\max\left(\omega\sqrt{\varepsilon_{1y}\mu_{1x}},\,\omega\sqrt{\varepsilon_2\mu_2}\right)$ which ensures the existence of the surface wave.

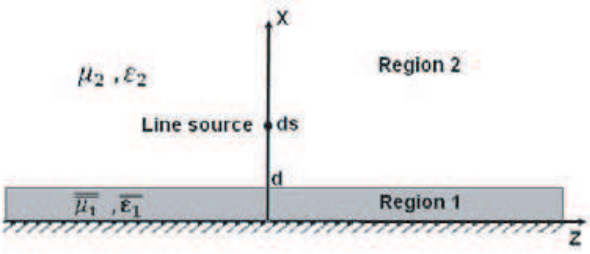

Figure 1: Geometry of an anisotropic grounded slab waveguide, electrical line source is located in region 2.

Examples and Numerical Results: Negative permittivity and permeability for FDTD simulation can be realized with the Lorentz dispersion relation

$$\varepsilon(\omega) = \varepsilon_o \left(1 - k_e^2 \frac{\omega^2}{\omega^2 - \omega_e^2 - j2\delta_e\omega}\right) \tag{4}$$

$$\mu(\omega) = \mu_o \left(1 - k_h^2 \frac{\omega^2}{\omega^2 - \omega_h^2 - j2\delta_h\omega}\right) \tag{5}$$

The parameters in Eq. (4) and Eq. (5) have been chosen such that the desired negative values of permittivity and permeability at $f_o = 10\,\text{GHz}$ are provided. Numerical simulations of four cases are shown in Figs. 2–5 which are in accordance with theoretical results.

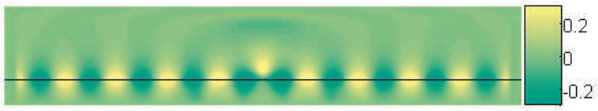

Figure 2: Electric filed distribution of surface waves at the interface of slab in case I. Slab boundaries are indicated by dark line in figure. $d = 1\,\text{cm}$, $\varepsilon_{1y} = 2\varepsilon_o$, $\mu_{1x} = 2\mu_o$, $\mu_{1z} = -\mu_o$, $\varepsilon_2 = \varepsilon_o$, $\mu_2 = \mu_o$.

Figure 3: Surface wave cannot be supported by anisotropic grounded slab in case II. Electric field has penetrated into the slab as guided modes. $d = 1\,\text{cm}$, $\varepsilon_{1y} = -0.5\varepsilon_o$, $\mu_{1x} = \mu_o$, $\mu_{1z} = -\mu_o$, $\varepsilon_2 = \varepsilon_o$, $\mu_2 = \mu_o$.

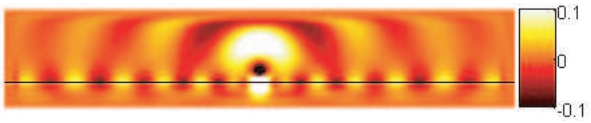

Figure 4: Electric filed distribution of surface waves at the interface of slab in case III as theory predicts. $d = 1\,\text{cm}$, $\varepsilon_{1y} = 2\varepsilon_o$, $\mu_{1x} = -2\mu_o$, $\mu_{1z} = -\mu_o$, $\varepsilon_2 = \varepsilon_o$, $\mu_2 = \mu_o$.

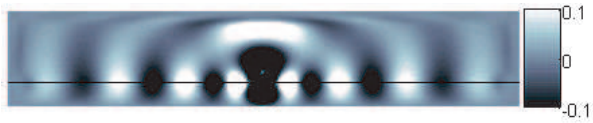

Figure 5: Electric field distribution of surface waves in case IV. $d = 1\,\text{cm}$, $\varepsilon_{1y} = -0.5\varepsilon_o$, $\mu_{1x} = -1.5\mu_o$, $\mu_{1z} = -\mu_o$, $\varepsilon_2 = \varepsilon_o$, $\mu_2 = \mu_o$.

All-dielectric Isotropic Metamaterial and Its Tunable Behavior

Qian Zhao[1, 2], Lei Kang[2], Bo Du[2], Hongjie Zhao[2], Bo Li[2], and Ji Zhou[2]

[1]State Key Lab of Tribology, Department of Precision Instruments and Mechanology
Tsinghua University, Beijing 100084, China
[2]State Key Lab of New Ceramics and Fine Processing
Department of Materials Science and Engineering
Tsinghua University, Beijing 100084, China

Abstract— Isotropic negative permeability resulted from Mie resonance is demonstrated experimentally and numerically in a three-dimensional (3D) dielectric composite consisting of an array of dielectric ceramic cubes. Measurements and simulations show that the dielectric composite exhibits a strong sub-wavelength magnetic resonance at the first Mie resonance and possesses isotropic negative permeability, resulting from the displacement current excited in the cubes. The dielectric particle was equivalent to a magnetic dipole at the magnetic resonance, which could be adjusted by the size and permittivity of the particles. And thus a tunable behavior is experimentally demonstrated in this dielectric composite by temperature changing. It shows that the first Mie resonance mode can be continuously and reversibly adjusted from 13.65 GHz to 19.28 GHz with the temperature changing from -15°C to 35°C. Accordingly negative permeability can be performed in the frequency range of about 6 GHz by adjusting the temperature. The results are promising for construction of novel isotropic 3D left-handed materials with simple structure, and design of adaptive metamaterials and 3D invisible cloak.

Ambient-permeability-controlling Based Magnetically Tunable Metamaterials

Lei Kang[1], **Qian Zhao**[2], **Hongjie Zhao**[1], **Rui Wang**[1], **Jingbo Sun**[1], **and Ji Zhou**[1]

[1]State Key Lab of New Ceramics and Fine Processing
Department of Materials Science and Engineering
Tsinghua University, Beijing 100084, China
[2]State Key Lab of Tribology
Department of Precision Instruments and Mechanology
Tsinghua University, Beijing 100084, China

Abstract— Different from those tuned by altering the capacitance of equivalent LC circuit, we present and experimentally demonstrate a novel approach to tunability of metamaterial. This tunability arises from the active inductance of equivalent LC circuit by controlling the ambient permeability. Yttrium iron garnet (YIG) that exhibits a variable permeability under different magnetic field at microwave frequency range, was cut into rod and introduced into the negative permeability metamaterial, left-handed metamaterial and electric resonant metamaterial, which are composed of elements of split ring resonator (SRR), SRR/wire, and eSRR, respectively. It shows that the resnonances of the metamaterials can be continuously and reversibly adjusted over a large range by external dc applied magnetic fields. These tunabilities would be useful for the construction of novel devices, e.g., broadband perfect lens.

Recent Developments in Free-standing Large-area S-string THz Metamaterials

H. O. Moser[1], **L. K. Jian**[1], **M. Bahou**[1], **S. P. Heussler**[1], **S. M. P. Kalaiselvi**[1], **S. M. Maniam**[1] **Shahrain bin Mahmood**[1], **S. Virasawmy**[1], **H. S. Chen**[2, 3], **X. X. Cheng**[3], **and B. I. Wu**[2]

[1]Singapore Synchrotron Light Source (SSLS), National University of Singapore (NUS)
5 Research Link, 117603, Singapore
[2]Research Laboratory of Electronics, Massachusetts Institute of Technology
Cambridge, Massachusetts 02139, USA
[3]The Electromagnetics Academy at Zhejiang University, Zhejiang University
Hangzhou 310058, China

Abstract— Due to their longitudinal extension, S-strings enable building large-area free-standing metamaterials that are neither embedded in matrices nor deposited on substrates. Free-standing metamaterials in which S-strings are held, at both ends, by a window-frame were experimentally demonstrated and characterized [1]. Two chips of such single-layer window-frames, separated by a spacer, are carefully aligned and assembled to form the resonance loops in a bi-layer chip. Their response is solely determined by geometrical parameters and metal properties. Gold samples built so far exhibit two left-handed pass-bands around 1.2 and 2.2 THz besides a right-handed electrical resonance around 2.8 THz depending on the incidence angle of the incoming wave. The left-handed pass-bands are assigned to the figure-eight loop formed by an S in one plane and its inverse in the other, as well as to the "cut-wire pair" formed by one S-leg in the top plane and the adjacent leg in the bottom plane. These resonances are best excited by tangential (90°) or normal incidence, respectively. The electrical resonance at 2.8 THz is right-handed and caused by a single layer alone. It is disregarded. Ongoing work aims at extending the architecture of window-frame-held S-strings to self-supporting grids without window-frames in which strings are interconnected by transverse rods, thus forming a locally rigid, globally flexible self-supporting grid. Simulations show that such structures also exhibit left-handed pass-bands and allow various periodicities of the interconnecting rods. Latest experimental results on such structures will be presented. Potential applications may arise in systems for THz communication or for the detection of explosives.

REFERENCES

1. Moser, H. O., J. A. Kong, L. K. Jian, H. S. Chen, G. Liu, M. Bahou, S. M. P. Kalaiselvi, S. M. Maniam, X. X. Cheng, B. I. Wu, P. D. Gu, A. Chen, S. P. Heussler, S. B. Mahmood, and L. Wen, "Free-standing THz electromagnetic metamaterials," *Opt. Express*, Vol. 16, 13773, 2008.

Resonance-induced Extraordinary Transparencies of Waveguides at Cutoff: A Tight Binding Study

Hao Xu, **Jiaming Hao**, **and Lei Zhou**
Surface Physics Laboratory (State Key Laboratory) and Physics Department
Fudan University, Shanghai 200433, China

Abstract— Inserting resonators of electric or magnetic types into a waveguide, we find extraordinary transmissions of EM waves at frequencies well below the waveguide's cutoff values for different polarizations [1]. In our previous work, such phenomena were explained by an effective medium theory [1]. Here, we employ a tight binding method (TBM) developed in [2] to further explore the underlying physics behind such unusual transparency. Adopting appropriate hopping parameters, we find that the TBM can provide clear pictures for many interesting phenomena discovered by brute-force numerical simulations and experiments previously [1], including the number and positions of the transmission peaks, the parities of wave functions, the band width and the group velocities of the transmission bands, and the defect modes, ect. [3].

REFERENCES

1. Xu, H., Z. Y. Wang, J. M. Hao, J. J. Dai, L. X. Ran, J. A. Kong, and L. Zhou, *Appl. Phys. Lett.*, Vol. 92, 041122, 2008.
2. Xu, Y., Y. Li, R. K. Lee, and A. Yariv, *Phys. Rev. E*, Vol. 62, 7389, 2000.
3. Xu, H., J. M. Hao, and L. Zhou, unpublished.

Effective-medium Properties of Meta-materials Studied by the Quasi-mode Method

Shulin Sun and Lei Zhou
Surface Physics Laboratory (State Key Laboratory), Physics Department
Fudan University, Shanghai 200433, China

Abstract— In the spirit of the generalized coherent potential approximation, we applied a "quasi-mode" method developed in [1] to study the effective media properties of electromagnetic (EM) meta-materials. Embedding the meta-material under study into a background medium with tunable permittivity and permeability, we calculate the Green's functions of EM waves traveling inside the medium by considering the scatterings caused by the meta-material. The density of states (DOS), the self-energy, and the mean free path of a mode can be calculated with the knowledge of the Green's function given. The effective permittivity and permeability of the meta-materials can then be determined by maximizing the DOS, which is a function of the permittivity and permeability of the background medium. Compared with the standard S-parameter retrieval method [2], the present approach overcomed the multiple solution problems that exist in previous methods. Moreover, the "mean free path" obtained in present method is helpful to judge qualitatively how good are the effective medium parameters that we obtained for the meta-materials. As the illustrations of our theory, we performed numerical calculations based on the finite element method to study the effective-medium properties of both split ring and metallic wire resonators.

REFERENCES

1. Sheng, P., *Introduction to Wave Scattering, Localization, and Mesoscopic Phenomena*, Academic Press, San Diego, 1995.
2. Smith, D. R., S. Schultz, P. Markos, and C. M. Soukoulis, *Phys. Rev. B*, Vol. 65, 195104, 2002.

Nanocluster Metamaterial

Qi Wu, **Jin-Hyoung Lee**, **and Won Park**
Department of Electrical & Computer Engineering, University of Colorado
UCB 425, Boulder, CO 80309-0425, USA

Abstract— We report a new metamaterial architecture based on metal nanoclusters. An array of metal nanowires exhibits a strong electric resonance due to the electric Mie resonance supported by the individual wires. When a finite-sized array is made, the nanocluster can support a strong magnetic resonance. The frequency of the magnetic resonance falls in the optical frequency region and is also tunable by controlling the array parameters such as nanowire size and filling fraction. If the nanoclusters are placed into an array, this nanocluster metamaterial exhibits optical frequency magnetism, where the effective permeability can reach negative values. By combining the nanocluster metamaterial structure with thin metal films or metal nanoshells, which provide negative permittivity, the combined metamaterial structure exhibits negative effective index. One of the most exciting features of nanocluster metamaterial is that it can be fabricated by a bottom-up self-assembly approach. We developed a new fabrication strategy in which metal nanoparticles are assembled to form nanoclusters by template-directed self-assembly method. The template is an array of nanoholes fabricated by the laser interference lithography. By properly treating the surfaces of the template and also of the nanoparticles, we successfully self-assembled nanoclusters. The nanocluster metamaterial exhibited strong absorption peaks due to the magnetic resonance. The peak position coincided very well with the theoretically predicted resonance frequency. The nanocluster metamaterial represents the first metamaterial architecture compatible to scalable manufacturing technology and holds a high promise to practical applications of metamaterial.

The Left-handed Property of the Composite with Metallic Wires Embedded in Mu-negative Medium

Yang Bai[1], **Fang Xu**[1], **Lijie Qiao**[1], **and Ji Zhou**[2]
[1]Corrosion and Protection Center
Key Laboratory of Environmental Fracture (Ministry of Education)
University of Science and Technology Beijing, Beijing 100083, China
[2]Department of Material Sciences and Engineering
Tsinghua University, Beijing 100084, China

Abstract— In recent years, left-handed material (LHM) is one of the most absorbing subjects in physics, which was proposed by Veselago in 1968. Because of its negative permeability and negative permittivity, LHM has abnormal electromagnetic behaviors, such as a left-handed set of $\overrightarrow{k}$, $\overrightarrow{E}$ and $\overrightarrow{H}$ for electromagnetic wave in it. Since the first LHM was made By Smith, various artificial structures, instead of natural materials, were supposed to construct LHMs, who gain the electromagnetic properties from structure rather than inheriting from the materials' nature. Then it becomes an interesting and challenging problem to realize LHMs using materials' intrinsic characters wholly or partially.

This paper reported the LH property of the composite with metallic wires and mu-negative (MNG) medium. The effect of material characters of isotropic or anisotropic media on LH properties was discussed.

First, the electromagnetic character of the composite structure with metallic wires in a homogeneous Lorentz medium was studied. The material characters of medium host affect the plasma of metallic wires remarkably. High permeability or permittivity will lower the plasma frequency of metallic wires, while near-zero permeability or permittivity can and zero ε or μ of medium can great raise the resonance frequency of wires' array. Both above influences narrow the range of negative permittivity of wire's array, which go against the realization of LHM. Negative-μ medium will destroy the wires' plasma resonance and prevent producing negative permittivity. High loss medium can also inhibit the metallic plasma resonance.

Second, the effect of the anisotropy of MNG medium was discussed under the condition of TEM wave. Because of the couple of medium with TEM wave and wires' array, μ_x, μ_y and μ_z of the medium play different roles to the LH properties. In this composite structure, metallic wires must be parallel to $\overrightarrow{E}$ of wave. The results indicates that negative μ_z (parallel to $\overrightarrow{H}$) is the necessary and sufficient condition for left-handed material. Negative μ_y (along $\overrightarrow{E}$) does not affect the metallic wires' plasma, while negative μ_x (along wave vector) destroys the wires' plasma and blocks the left-handed property.

Final, the electromagnetic character of the composite structure consisting of metallic wires and a gyromagnetic medium was studied. Based on above discussion, proper direction of magnetization is important for the realization of LH property. To reduce the influence of mu-negative host to wires' plasma to a great extent, it is a best choice to apply the bias magnetic field along the direction of wave vector.

This study can promote the development of LHM using materials' nature. It gives a clear direction to design LHM with isotropic, uniaxial and gyromagnetic media. Further research can greatly enrich the applications of LHMs owing to the multifunctionality of nature materials.

Two Types of Planar Chiral Metamaterials for Polarization Conversion

Benfeng Bai and Jari Turunen
Department of Physics and Mathematics, University of Joensuu
Joensuu, FI-80101, Finland

Abstract— Metamaterials are newly emergent artificial materials that cannot be found in nature and are designed to exhibit prescribed electromagnetic properties, among which the planar chiral metamaterials (PCMs) are the artificial planar micro- or nanostructures exhibiting extraordinary polarization effects much larger than those in natural materials. Since large optical activity can be achieved in a PCM with sub-wavelength thickness and can be optimized by proper structural design, the PCMs are very promising candidates to be developed as novel compact polarization-sensitive devices.

In this talk, we demonstrate two types of PCMs that we studied recently: the Type-I PCM made of isotropic achiral media but with chiral structural features, such as the gammadion-shaped TiO2 grating shown in Fig. 1(a), and the Type-II PCMs that are nanogratings containing magneto-optic materials, such as the perforated bismuth iron garnet (BIG) film shown in Fig. 1(c). Both of the two types of PCMs are found to be able to produce large (tens of degree) polarization rotation effect [see, for example, Fig. 1(b)], which leads to a gyratory power several orders of magnitude larger than that of natural chiral or magneto-optically active media. The large optical activity originates from circular birefringence/dichroism induced by the structural chirality or magneto-optic effect and is greatly enhanced by optical resonances (such as surface-plasmon resonance or guided-mode resonance) in the periodic sub-wavelength structures. The two types of PCMs are operated under normal illumination in the optical and near-infrared spectral ranges and can achieve multi-functional polarization manipulation (e.g., used as pure polarization rotator, phase retarder, or circularly-polarized beam splitter). Furthermore, since the polarization effect is reciprocal in the Type-I PCMs, whereas nonreciprocal (and tunable by switching on/off the external magnetic field) in the Type-II PCMs, they exhibit different functionality for application designs.

The talk reviews our recent theoretical and experimental work with regard to the two types of PCMs, covering fundamental theory, rigorous numerical simulation, design, nanofabrication process, and optical characterization. The physical mechanism of the large polarization effect enhanced by resonance is also explored and interpreted.

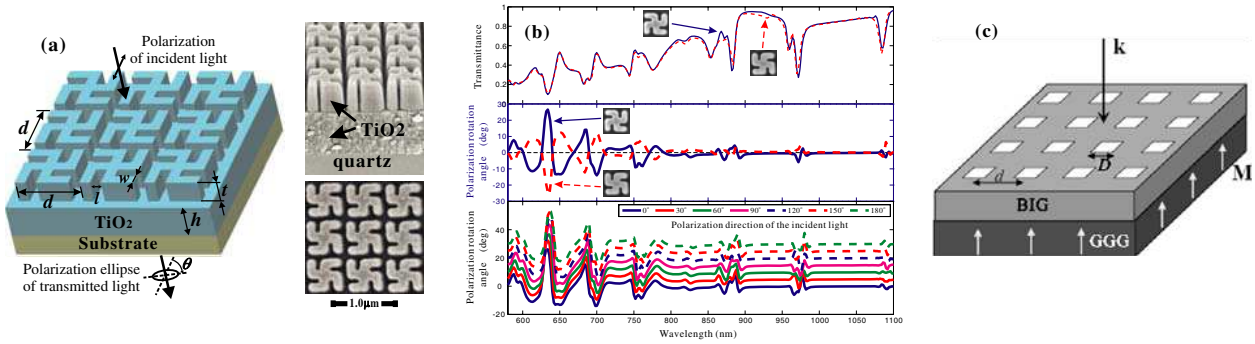

Figure 1: Geometry (a) and spectra (b) of the Type-I PCMs. (c) shows the structure of a Type-II PCM.

Anisotropy and Extreme Parameters: Waveguiding and DB Media

A. Sihvola and I. V. Lindell
Department of Radio Science and Engineering, Helsinki University of Technology
Box 3000, FIC02015 TKK, Espoo, Finland

Abstract— Media with extreme parameters have received increasing attention in the metamaterials community. Whereas in the "classical" metamaterial studies in the spirit of Veselago media [1, 2] where the emergent character arises from the simultaneously negative parameters for the electric permittivity and magnetic permeability, nowadays such media attract attention where one or both of the constitutive parameters are either very large or close to zero [3]. Examples of such media carry labels like ENZ (epsilon-near-zero) and EVL (epsilon-very-large) media.

Such media are isotropic. In this talk, the focus is on extreme materials with anisotropy. Especially, we focus on uniaxial anisotropy where the extreme quality is concentrated on the axial parameters of the permittivity and permeability. In other words, the in constitutive dyadics of the material

$$\bar{\bar{\epsilon}} = \mathbf{uu}\epsilon_z + \left(\bar{\bar{\mathrm{I}}} - \mathbf{uu}\right)\epsilon_t \tag{1}$$

$$\bar{\bar{\mu}} = \mathbf{uu}\mu_z + \left(\bar{\bar{\mathrm{I}}} - \mathbf{uu}\right)\mu_t \tag{2}$$

the axial components ϵ_z and μ_z are either very large or close to zero. (Here $\bar{\bar{\mathrm{I}}}$ denotes the unit dyadic and $\mathbf{u}$ is the unit vector along the optical axis.)

The case of both $\epsilon_z \to \infty$ and $\mu_z \to \infty$ corresponds to the so-called waveguiding medium which has been shown to lead to the possibility to mimic absolute boundary conditions [4]. The latter choice ($\epsilon_z = \mu_z \to 0$) leaves us with the so-called DB medium [5] which can be used as angular filter, a property that has been shown to be connected to ENZ materials in two-dimensional applications involving squeezing and channeling of electromagnetic waves [6]. Especially important is that the operation of the DB medium is independent of the polarization and excitation of the electromagnetic field it interacts with.

The talk will discuss the possible applications of these concepts and the realization of such materials.

REFERENCES

1. Veselago, V. G., "The electrodynamics of substances with simultaneously negative values of ϵ and μ," *Soviet Physics Uspekhi*, Vol. 10, 509–514, 1968.
2. Sihvola, A., "Metamaterials in electromagnetics," *Metamaterials*, Vol. 1, No. 1, 2–11, 2007.
3. Sihvola, A., S. Tretyakov, and A. de Baas, "Metamaterials with extreme material parameters," *Journal of Communications Technology and Electronics*, Vol. 52, No. 9, 986–990, 2007. (Also, "Metamaterialy s ektremal'nymi material'nymi parametrami (in Russian)", *Radiotekhnika i Elektronika*, Vol. 52, No. 9, 1066-1071, 2007.)
4. Lindell, I. V. and A. Sihvola, "Realization of impedance boundary," *IEEE Transactions on Antennas and Propagation*, Vol. 54, No. 12, 3669–3676, December 2006.
5. Lindell, I. V. and A. Sihvola, "Electromagnetic DB boundary," *Proceedings of the National URSI Meeting*, Espoo, Finland, October 28, 2008.
6. Alù, A. and N. Engheta, "Light squeezing through arbitrary shaped plasmonic channels and sharp bends," *Physical Review B*, Vol. 78, 035440, 2008.

Session 2P3
Synthetic Aperture Radar and Its Applications 2

A New Method for Imaging Avian Based on Frequency-stepped Chirp Signal

Feng Zhu[1], **Yong Wu**[2], **You-Qian Feng**[1], **You-Qing Bai**[1], **and Qun Zhang**[3, 4]

[1]Institute of Science, AFEU, Xi'an 710051, China
[2]Shaanxi Institute of Metrology Science, Xi'an 710048, China
[3]Institute of Telecommunication Engineering, AFEU, Xi'an 710077, China
[4]Key Laboratory of Wave Scattering and Remote Sensing Information (Ministry of Education)
Fudan University, Shanghai 200433, China

Abstract— It is quite significant for security and development of human's aviation that avian can be detected and monitored at real time. Radar with some special advantages is an important tool for observing birds' activities availably, which is all-weather and round-the-clock effective for working. Moreover, with the development of modern signal processing and high-speed computer technology, it becomes a novel and important approach for development of avian ecology and the prevention from avian influenza that avian can be imaged and identified accurately and successfully based on high-resolution radar imaging technology. Because of small size of birds, the ultra-large-wideband signal is necessary to be utilized for high range resolution. Frequency-stepped chirp signal is a kind of high-resolution range signal with some special advantages such as little instantaneous bandwidth and the virtue in synthesizing large bandwidth, and is considered as the major signal to imaging for birds.

The bird's moving status contains gliding status and flapping status. Because bird's moving velocity is generally very slow, on condition of few kilometers between targets and radar, bird must fly determinate distances which are required for imaging, in order to achieve necessary cross-range resolution during ISAR imaging. During this process, alternating changes between gliding status and flapping status would take place usually. Hence, the ISAR images with traditional RD algorithm could be contaminated, because of serious micro-Doppler effects generated by birds' flapping wings. Thus, a new method of imaging for birds is proposed in the paper, on the basis of identifying bird's moving status accurately. This method is simple and valid to operate, which avoids micro-Doppler extraction with lots of complicated computation burden. In the method, the different parts of bird's gliding spectrogram are connected without the flapping spectrogram and the minimum waveform entropy criterion is employed for phase compensation. Finally, a comparatively clear ISAR image can be achieved.

This paper is organized as follows: Section 2 describes the principle of ISAR imaging with frequency-stepped chirp signal; a new imaging method for avian proposed in the paper is introduced in Section 3; finally, some computer simulations are given in the last Section.

Dependency Analysis of Backscattering from Ocean Surface on Ocean Winds Using Airborne Dual-frequency Polarimetric Synthetic Aperture Radar

Akitsugu Nadai, **Toshihiko Umehara**,
Tatsuharu Kobayashi, **Takeshi Matsuoka**, **and Seiho Uratsuka**
National Institute of Information and Communications Technology, Japan

Abstract— The environment of the coastal ocean depends strongly to the ocean wind field, which has small-scale variation due to the topography. Therefore, the ocean surface wind field with high spatial resolution is important to analyze the coastal environment. To measure the ocean wind vector using single channel SAR, the external data is indispensable, because the winds have two components. The coarse spatial resolution of the external data leads a measurement error of ocean winds. In this paper, the dependency of backscattering from ocean surface on ocean winds is analyzed between the parallel polarizations using the results of multiple observations in same area in a short time by airborne dual-frequency polarimetric SAR with the L- and X-bands.

The dependency of NRCS of ocean surface on wind direction is analyzed with a geophysical model function. For the X-band HH polarization, the asymmetric dependency on wind direction, that is the difference of NRCS between the up- and down-wind conditions, is much larger than that of the X-band VV polarization, though the symmetric dependencies are almost same. This peculiarity of the asymmetric dependency of NRCS in the X-band suggests the possibility of measurement of ocean surface wind only using the X-band polarimetric SAR data. The polarimetric rate of X-band also changes with the wind direction. On the other hand, the dependency of the NRCS in the L-band parallel polarizations is almost same.

This study suggests the possibility of the ocean surface wind measurement with high spatial resolution using X-band polarimetric SAR.

Wind Direction Extraction from Coastal SAR Images Using Cross-spectral Method

Hiroyuki Saito and Yoshiharu Yamamoto
Hirosaki University, Japan

Abstract— A sensitive processing method for extracting the wind direction from SAR (synthetic aperture radar) images is presented. We transfer SAR images to the image spectra using two-dimensional FFT (fast Fourier transform) and take the integral of the image spectra between the wave numbers 400 m and 800 m, which is containing wind direction signatures in L-band SAR. From this and a reference signal (half or full wave rectified sinusoidal wave) we obtain the wind direction by using cross-spectral analysis. To examine the potential of our method, a set of simulated images with various SNR (signal to noise ratio) are used. It is shown that, even if the SNR is −30 dB, the agreement is to within ±3°. Therefore the processing technique we present allows us the precise estimation of wind direction. We also use 23 JERS-1/SAR scenes from the Tsugaru Strait located between Aomori and Hokkaido prefectures of Japan for the extraction of wind direction. The wind directions retrieved from these images have been compared with in situ wind data from the Kikonai, the Tappi and the Ooma lighthouse. Although the lighthouse estimates is lacking in directional resolution (16 direction, 22.5° interval), the SAR estimates obtained from spectra of 6.4-km-square images are shown to agree with the lighthouse estimates to within a mean absolute error of 21°. The estimates difference may be related to the directional resolution of in situ wind data, the SNR of JERS-1/SAR images, the effect of terrain around the lighthouse, and the ocean current.

Analyses of Synthetic Aperture Radar Images of Ocean Surface under Influence of Typhoons

C. S. Yang[1], **S. Taniguchi**[2], **S. I. Hwang**[2], **and K. Ouchi**[2]

[1]Ocean Satellite Research Group, Korea Ocean Research and Development Institute
Sa2-dong 1270, Sangnuk-gu, Ansan, Gyeonggi-do, 426-744, Korea
[2]Department of Computer Science, School of Electrical and Computer Engineering
National Defense Academy, 1-10-20 Hashirimizu, Yokosuka, Kanagawa 239-8686, Japan

Abstract— This paper describes the preliminary results on the analyses of synthetic aperture radar (SAR) images of ocean surface affected by typhoons. Despite several reports [1, 2], the SAR images of dynamic ocean waves under spatially and temporally varying severe atmospheric pressure such as typhoon and hurricane are not well studied due mainly to lack of data. In the present work, attempts are made to retrieve the parameters of ocean waves from ALOS-PALSAR images of the western coastal waters of Japan after the typhoon "SINLAKU" (number 200813) passed on the 19th of September, 2008. Several other SAR data of typhoon affected seas are sought, and the wave dynamics are investigated and discussed using the weighted cross-spectral analysis [3].

REFERENCES

1. Elachi, C., T. W. Thompson, and D. King, "Ocean wave patterns under hurricane Gloria: Observation with an airborne synthetic-aperture radar," *Science*, Vol. 198, 609–610, Nov. 1977.
2. French Institute for Exploration of the Sea, "Speckle wind from SAR imagettes," http://www.ifremer.fr/droos/anglais/programmes/sar/sar.htm.
3. Ouchi, K., S. Maedoi, and H. Mitsuyasu, "Determination of ocean wave propagation direction by split-look processing using JERS-1 SAR data," *IEEE Trans. Geosci. Remote Sens.*, Vol. 37, 849–855, 1999.

A Hybrid Approach Using MLCC and CFAR for the Improvement of Ship Detection by Synthetic Aperture Radar

Seong-In Hwang and Kazuo Ouchi
Department of Computer Science, School of Electrical and Computer Engineering
National Defense Academy, 1-10-20 Hashirimizu, Yokosuka, Kanagawa 239-8686, Japan

Abstract— In January 2006, the Advanced Land Observing Satellite (ALOS) was launched by JAXA (Japan Aerospace Exploration Agency), carrying a Phased Array L-band Synthetic Aperture Radar (PALSAR). Although PALSAR is aimed mainly at land, it can be a strong support to monitoring of maritime traffic, fishing control, surveillance of illegally operating boats, and those responsible for oil pollution.

In most of the previous experiments, "unknown" ships whose sizes were fairly large compared with SAR resolution cells were considered, but little was reported on the detection of "known" and "small" boats. In a same manner as for validation of image classification using ground-truth data, it is also essential to use "sea-truth" data in order to quantify the performance of ship detection algorithms and SAR parameters.

One of the goals of this study is to improve SNR (Signal to Noise Ratio) and to keep a low level constant false alarm rate combined with a high detection probability in the presence of clutter background. In our previous paper [1], we compared the performance of PALSAR and several ship detection algorithms, including MLCC (Multi-Look Cross-Correlation) [2], CFAR (Constant False Alarm Rate) [3], CCF (Cross Correlation Function) of co- and cross-polarization images, and 4-component decomposition analysis of polarimetric data [4], together with sea-truth data, maritime radar and AIS. As a result, it was found that some highly correlated noise around the targets still remained after applying MLCC, and therefore, the SNR of targets in the inter-look coherence image was not high enough to detect the targets with high accuracy in the MLCC method.

In order to improve SNR and high detection probability by MLCC, we propose, in the present paper, a hybrid approach of ship detection combining MLCC and CFAR. In this method, a probability density function (pdf) is first sought to describe the coherence image produced by MLCC, and using this pdf, CFAR is applied to the coherence image. Through the proposed approach, we are able to improve the SNR and keep a low level constant false alarm rate combined with a high detection probability in presence of clutter background.

REFERENCES

1. Hwang, S.-I. and K. Ouchi, "Detection of small fishing vessels by ALOS-PALSAR — Comparison of PALSAR modes and algorithms," *IEICE Tech. Rep.*, Vol. 108, No. 76, 35–40, 2008.
2. Ouchi, K., et al., "Ship detection based on coherence images derived from cross-correlation of multilook SAR images," *IEEE Trans. Geosci. Remote Sens. Lett.*, Vol. 1, 184–187, 2004.
3. Sekine, M. and Y. Mao, *Weibull Radar Clutter*, Peter Peregrinus, London, 1990.
4. Yamaguchi, Y., et al., "Four-component scattering model for polarimetric SAR image decomposition," *IEEE Trans. Geosci. Remote Sens.*, Vol. 43, No. 8, 1699–1706, Aug. 2005.

Estimation of Coniferous Tree Biomass by Second Intensity Moment from High-resolution Cross-polarization SAR Images

Kazuo Ouchi[1] **and Haipeng Wang**[2]

[1]Department of Computer Science, School of Electrical and Computer Engineering
National Defense Academy, 1-10-20 Hashirimizu, Yokosuka, Kanagawa 239-8686, Japan
[2]Key Laboratory of Wave Scattering and Remote Sensing
Department of Communication Science and Engineering
School of Information Science and Engineering
Fudan University, Shanghai 200433, China

Abstract— In our previous papers [1, 2], a regression model was developed to estimate coniferous tree biomass from hight-resolution airborne Pi-SAR (Polarimetric interferometric-Synthetic Aperture Radar) data. The model utilizes the strong correlation between the order parameter of the K-distribution in the cross-polarized amplitude images and "ground-truth" biomass measured in the Tomakomai national forests in Hokkaido, Japan. The comparison of model-based biomass and ground-truth biomass showed the model accuracy of 86% per forest stand.

In this paper, we present a new regression model using the same set of data as those used in the previous work [1, 2]. The new model is based on the relation between the second intensity moment of the cross-polarized Pi-SAR images and the ground-truth biomass. This moment model is robust in such a way that it does not require any probability density function which fits best to the observed image statistics, while keeping the ability of estimating biomass beyond the saturation limits of the conventional RCS (Radar Cross Section)-based models. In this presentation, we first give a brief description of the K-distribution model, followed by the regression analysis of the second intensity moment and ground-truth biomass. The accuracy of the moment model is then examined, and comparison is made between the moment model and K-distribution model. It was found that the accuracy of the moment model is 85% per stand, similar to the K-distribution model, and that the moment model underestimates the true biomass, while the K-distribution model overestimates the true biomass. This is because the second instensity moment is inversely proportional to the order parameter of the K-distribution. Finally, the moment model function is computed using all sets of ground-truth data, and as an example, a biomass map of the forests surrounding the test stands is produced using the model function.

REFERENCES

1. Wang, H. and K. Ouchi, "Accuracy of the K-distribution regression model for forest biomass estimation by high-resolution polarimetric SAR: Comparison of model estimation and field data," *IEEE Trans. Geosci. Remote Sens.*, Vol. 46, No. 4, 1058–1064, 2008.
2. Wang, H., K. Ouchi, M. Watanabe, M. Shimada, T. Tadono, A. Rosenqvist, S. A. Romshoo, M. Matsuoka, T. Moriyama, and S. Uratsuka, "In search of the statistical properties of high-resolution polarimetric SAR data for the measurements of forest biomass beyond the RCS saturation limits," *IEEE Trans. Geosci. Remote Sens. Lett.*, Vol. 3, No. 4, 495–499, 2006.

Investigation on Volume Scattering for Vegetation Parameter Estimation of Polarimetric SAR Interferometry

Y. S. Zhou[1, 2, 3], **W. Hong**[1, 2], **and F. Cao**[1, 2]

[1]National Key Laboratory of Microwave Imaging Technology, China
[2]Institute of Electronics, Chinese Academy of Sciences, China
[3]Graduate University of Chinese Academy of Sciences, China

Abstract— This paper investigates the volume scattering for the vegetation parameter estimation of Polarimetric Interferometric Synthetic Aperture Radar (Pol-InSAR) through three aspects. The first is to describe the volume scattering with models. The second is to investigate various factors that influence the volume scattering coherence. The third is to discuss the choice of radar parameters for a better estimation of vegetation parameters.

The Pol-InSAR technique is a combination of SAR interferometry and SAR polarimetry and has already shows its effectiveness and sensitivity to volumetric structures. It has been applied to parameter estimation of volume scatterers (e.g., forest height, extinction coefficient) based on the coherence diversity of the volume scattering with polarization. In order to improve the performance of estimation, it is necessary to investigate the volume scattering in detail within the scope of Pol-InSAR.

Firstly we present the models (e.g., Radon Volume over Ground (RVoG) and Oriented Volume over Ground (OVoG) model) for describing the volume scattering and analyze the interferometric properties of volume scattering as well as the polarimetric properties of volume scattering.

Secondly we investigate the effect of volume height, extinction coefficient, radar operational frequency, incident angle, and baseline length on the volume scattering coherence based on the RVoG and OVoG model respectively.

Then we describe a method to simulate Pol-InSAR data based on the RVoG model. With the simulated Pol-InSAR data, we investigate the effect of volume height, extinction coefficient, radar operation frequency, incident angle, baseline length on the estimation accuracy of vegetation parameters. Contrarily, for a given accuracy requirement of vegetation parameters, the allowable ranges of radar parameters for the acquisition of Pol-InSAR data is derived.

We conclude that the proper modeling of volume scattering and the suitable choice of radar parameters are important for a better estimation of vegetation parameters.

An Improvement of Vegetation Height Estimation Using Multi-baseline Polarimetric Interferometric SAR Data

Y. S. Zhou[1,2,3], **W. Hong**[1,2], **and F. Cao**[1,2]

[1]National Key Laboratory of Microwave Imaging Technology, China
[2]Institute of Electronics, Chinese Academy of Sciences, China
[3]Graduate University of Chinese Academy of Sciences, China

Abstract— This paper proposes a method for improving the estimation accuracy of vegetation height using multi-baseline Polarimetric Interferometric Synthetic Aperture Radar (Pol-InSAR) data.

Single-baseline Pol-InSAR technique has been applied to retrieve vegetation parameters based on the Random Volume over Ground (RVoG) model. There are two main error sources which may decrease the estimation accuracy. One is the non-volumetric decorrelation, such as thermal noise decorrelation, temporal decorrelation, quantization and coregistration decorrelation, etc. The other is the ideal assumption that volume-only coherence can be acquired in at least one polarization. This assumption may fail when vegetation is thick and dense, or penetration of electromagnetic wave is weak. These two problems have been solved by Cloude [IGARSS'00] and Zhou [IGARSS'08] respectively.

We now propose a method to solve both the abovementioned two problems at the same time (not respectively) based on the use of multi-baseline Pol-InSAR data. We first analyze the two main error sources and construct an inversion model based on the RVoG model to represent these error sources. This model consists of 8 unknowns, but conventionally, single-baseline Pol-InSAR data provides only six independent observables. Since multi-baseline data could provide more observables than the unknowns, it may be possible to solve the problem successfully. Then with the constructed model, we present the inversion procedure for estimating vegetation height using the multi-baseline Pol-InSAR data. The performance of this new method is validated using simulated Pol-InSAR data, and the ratio between each baseline length and their effect on the estimation accuracy are also discussed.

Analysis on SAR Optimization of Polarimetric Contrast Enhancement

Qiong Zhang[1, 2, 3], **Fang Cao**[1, 2], **and Wen Hong**[1, 2]

[1]National Key Lab. of Microwave Imaging Technology, China
[2]Institute of Electronics, Chinese Academy of Sciences, China
[3]Graduate University of Chinese Academy of Sciences, China

Abstract— The study on Optimization of Polarimetric Contrast Enhancement (OPCE) has been a key point for a long time. The methods solving the OPCE problem are usually comprised of analytical and numerical algorithms. Ioannidis et al. first developed a method using Lagrange Multipliers for OPCE, which was subsequently verified from programming by Cadzow and Swartz. Afterward, Yang et al. researched mainly on the numerical methods solving the problem, which was split into coherent case and incoherent case. For the coherent case, a method named Sequential Unconstrained Minimization Technique (SUMT), which focused on settling a minimized polarimetric scattering power function, was developed. SUMT made the traditionally analytical method altered from confirming single matched optimal vector for both of radar transmitting and receiving into respectively confirming the optimal transmitting and receiving vectors. However, although this method presented to be better than those using Co-Pol Nulls of the clutter, it needed too much iteration and may be not better enough than the form of a numerical model ascertaining polarimetric contrast. Then a numerical optimal method for the incoherent case was fully developed. This method was based on the contrast enhancement in the matched-polarized channel, could confirm different transmitting and receiving polarization states, fitted for the Kennaugh data matrices and could converge very fast. Generalized OPCE (GOPCE) algorithm was later developed and it introduced Similarity Parameters and Cloude Entropy, which showed more polarimetric information for analyzing targets scattering characteristics and better efficiency for roads discrimination from forest area.

This paper, in which the opinions could be effective indeed, studies the main methods for solving OPCE problems, presents better analysis and comprehension, and proposes some new ameliorations or advices for the algorithms.

On the Need of Developing Multi-Band Differential POLinSAR Theory and Algorithms for Remote Sensing and Monitoring of Natural Environments and Severe Environmental Stress Changes

Wolfgang-Martin Boerner[1] and Kun-Shan Chen[2]

[1]ECE/CSN Laboratory, University of Illinois at Chicago, USA
[2]Center for Space & Remote Sensing Research, National Central University, Taiwan

Abstract— Worldwide, medium- to short-term earthquake prediction is becoming ever more essential for safeguarding man due to an un-abating population increase, but hitherto there have been no verifiable methods of reliable earthquake prediction developed — except for a few isolated examples of earthquake prediction in China and in Greece. This dilemma is a result of previous and still current approaches to earthquake prediction which are squarely based on the measurement of crustal movements, observable only after a tectonic stress-change discharge (earthquake) has occurred. The prediction models were derived from past histories of measurements, mainly carried out during the past 30–40 years, although initiated soon after the San Francisco Earthquake of 1906. During the past decade it was proved and shown that it is not possible to derive reliable models for earthquake predictions from crustal movement measurements alone, and that an entirely new approach must be sought and rigorously pursued over years and decades to come.

In support of this conclusion, there have been reported throughout the history of man anecdotal historical up to scientifically verifiable earthquake precursor or "*seismo-genic*" signatures of various kind — biological, geological, geo-chemical and especially a rather large plethora of diverse electromagnetic ones on ground, in air and space, denoted as "*seismo-electromagnetic*" signatures. The existence of all of these signatures can no longer be denied even by the fiercest seismological expert opponents; and it is absolutely high noon that those signatures be more rigorously assessed in order to develop a strategy for designing and carrying out controlled "*seismo-genic*" and "*seismo-electromagnetic*" studies on how to set up world-wide a network of measurement sites for conducting a holistic set of measurements for providing an improved understanding on why and how such precursor signatures are generated, and how and where those may best be observed subject to the rather poor signal-to-noise ratio (SNR), requiring much improved digital instrumentation as time goes on due to the ever increasing man-made electromagnetic noise generation. Another viable novel method of detecting pre-seismic, co-seismic and post-seismic surface deformations is made available by the compatible rapidly advancing air- & space-borne Repeat-Pass Polarimetric Differential SAR Interferometry technology, now gaining increased applicability with the advent of the first fully polarimetric satellite SAR sensors such as the Japanese ALOS-PALSAR, the German Tandem TERRASAT-X 1 & 2 and the Canadian RADARSAT-2.

Similarly, the question on whether there do exist reliable prediction methods was answered long ago by the fauna living within the coastal littoral zone that are affected by tsunamis. Especially during the last devastating "*Boxing Day — 041226 Tsunami*" there were many verifiable episodes on how fish escaped the affected coastal region in time, elephants and other non-domesticated animals rushed for higher ground locations well in time before the tsunami crest approached. Indirectly, these observations provide proof that some electromagnetic or more likely infrasonic local warning signatures are received by these creatures relatively long before the approaching tsunami strikes. We presume that the signatures could be infra-sonic waves travelling at high speeds as under-water surface waves that could be detected by marine fauna as well as coastal animals and birds observing such precursors and acting instinctively without delay. Tsunamis have existed for eons and fauna of the affected coastal region has developed instinctive warning mechanisms — to be explored.

We require a more far-reaching ocean mapping technique which covers the affected wider region of for example the entire Indian Ocean — for now excluding satellite observations — from Sumatra around India to the African Coast from Somali down to the Cap. Next to implementation of GPS indirect telemetry due to ionospheric interaction of the transverse tsunami waves, such a device exists in principle, and it is based on the high-energy transmission and reception capabilities of the HF-OTHR (High Frequency — Over-The-Horizon-Radar) which makes use of the Ionosphere as a reflector. The HF-OTHR can detect minute disturbances in the atmosphere via troposphere to lower mesosphere but also minute changes of the relative ocean surface height at the order of several centimeters. Although major ionospheric disturbances may impact high resolution ocean surface imaging, it is however possible to detect instantaneously the initiation, the rapid

spreading of ocean-height and density changes generated by tsunamis and its impact on close to distant coastal shores indirectly again due to transverse tsunami ocean wave interaction with the ionosphere.

Session 2P4
Signal Processing for Communication Systems & Cognitive Radar 2

BGP Security Configuration in ISP Networks

Hexing Wang[1], **Cuirong Wang**[1], **and Ge Yu**[2]

[1]Northeastern University at Qinhuangdao, Qinhuangdao 066004, China
[2]School of Information Science and Engineering, Northeastern University
Shenyang 110004, China

Abstract— The Border Gateway Protocol (BGP) is the *de facto* inter-domain routing protocol used to exchange network reachability information between ISP networks in the global Internet. The border gateway router of ISP network runs BGP protocol and maintains a table of prefixes designating IP networks that can be reached. However, as the Internet routing infrastructure, BGP is vulnerable to both accidental misconfigurations and malicious attacks because it trusts unverified control plane information received from its peers.

This paper considers the security risks of BGP system and surveys works relating to BGP security. While a number of enhanced protocols for BGP (such as S-BGP, SO-BGP, PGBGP, etc.) have been proposed to solve BGP security problem, these generally relay on a public key infrastructure or a central authority like ICANN, or require substantial changes to the protocol, hence none of them has been widely deployed. We present a security configuration framework based on currently available technologies to improve the security of BGP routers. The security configuration framework provides a set of guidelines to protect the BGP routers from misconfigurations and malicious attacks. We describe the countermeasures and security mechanisms of BGP system when it encounters potential attacks, such as BGP peer spoofing, BGP session hijacking, malicious or unallocated route injection, etc. We also discuss how to use sinkhole tunnel technology together with the enhanced black hole routing technology triggered by BGP to reduce the attack damage when DOS/DDOS attacks occur. Our proposition is easily deployable in ISP networks without additional cost and can effectively improve the security of BGP system.

An Iterative QRD-M Detection Algorithm for MIMO Communication System

L. Liu, J. K. Wang, D. M. Yan, J. Gao, and Z. B. Xie
School of Information Science & Engineering, Northeastern University
Shenyang 110004, China

Abstract— Multiple input multiple output (MIMO) has been considered as a promising technique for its potential to significantly increase the spectral efficiency and system performance. Lots of detection algorithms have been proposed for MIMO systems in the literature. Among them, maximum likelihood detection (MLD) algorithm provides the best bit error rate (BER) performance. However, the complexity of MLD exponentially increases with the constellation size and the transmit antenna number. Therefore, it is impractical to use a full MLD without reducing its computational complexity, because it would be prohibitively large for implementation. Recently, several detection algorithms for MIMO systems achieving near-MLD performance have been proposed. The use of QR decomposition with an M-algorithm (QRD-M) and sphere decoding (SD) have been proposed to provide a tradeoff between the system performance and complexity in MIMO communications. However, with the exception of some special cases, their complexity still grows exponentially with increasing dimension of the transmitted signal. Moreover, the complexity of SD has big variations at different SNR values, which results in impractical to use in hardware implementation. To reduce these problems, a new detection scheme, named as iterative QRD-M (IQRD-M), is proposed in the paper. After performing QR decomposition of the channel matrix, the exhaustive search of the last layer is done, the accumulated metrics are calculated and sorted, which gives an order set of the last layer, then QRD-M algorithm are used to search the left layers with novel termination methods. The proposed algorithm provides the more near-ML performance and with low complexity.

Reconstruction of Multi-component Signals Based on Quasi Fourier Transform

Gang Bi and Yu Zeng
School of Information & Electrical Engineering
City College, Zhejiang University, Hangzhou 310015, China

Abstract— Parameter estimation and reconstruction of multi-component linear or nonlinear frequency modulated signals have a variety of applications, including sonar, radar and other communications. These signals have time-varying spectral properties and the Time-Frequency Representation (TFR) has been proved to be a powerful tool in analysis of such signals [1, 2].

In this paper, a novel time-frequency analysis technology named Quasi Fourier Transform is proposed for reconstruction of multi-component signals, and properties of this method are investigated. The QFT is as follows:

$$\begin{cases} S(\tilde{\omega}) = \int_{-\infty}^{+\infty} s(t)\alpha(t)e^{-j\tilde{\omega}\int_0^t \alpha(\tau)d\tau}dt \\ s(t) = \frac{1}{2\pi}\int_{-\infty}^{+\infty} S(\tilde{\omega})e^{j\tilde{\omega}\int_0^t \alpha(\tau)d\tau}d\tilde{\omega} \end{cases} \tag{1}$$

Some properties of the QFT are investigated as follows:

1. With $\alpha(t) = 1$, the QFT becomes the classical Fourier transform.
2. From the definition of the QFT, we can reach the conclusion:

$$\frac{1}{2\pi}\int_{-\infty}^{+\infty} \delta\left(\tilde{\omega} - \tilde{\omega}'_s\right) e^{j\tilde{\omega}\int_0^t \alpha(\tau)d\tau}d\tilde{\omega} = \frac{1}{2\pi}e^{j\tilde{\omega}'\int_0^t \alpha(\tau)d\tau} \qquad (\tilde{\omega}'_s \neq \tilde{\omega}_s = 1) \tag{2}$$

   Suppose that there are two component in the Time-Frequency Domain (TFD), as showed in Figure 1, where signal refers to $s_1(t)$ and noise to $s_2(t)$. By using QFT, these two signals can be separated by a reasonable curve $\alpha(t)$. The function $s_0(t) = \frac{1}{2\pi}\exp(j\int_0^t \alpha(\tau)d\tau)$ will be transformed to a Dirac function $\delta(\tilde{\omega} - \tilde{\omega}_s)$ in the $\tilde{\omega}$ frequency domain by F_α.
3. The QFT is a process of TFD mapping based on $\alpha(t)$. Let $\omega = \alpha(t)$ in Eq. (1). The Quasi STFT can be defined as follows:

$$S(t, \omega') = \frac{1}{\sqrt{2\pi}}\int s(\tau)h(\tau - t)e^{-j\alpha(t)\tau}d\tau \tag{3}$$

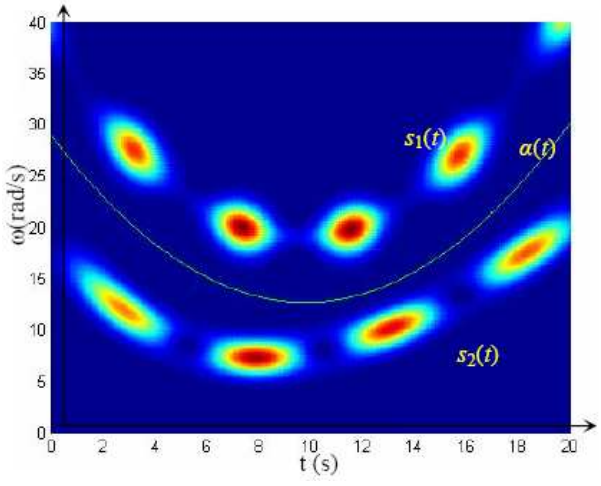

Figure 1: Spectrogram of signal $s(t)$.

Specifically, multi-component signals can be described as:

$$s(t) = \sum_{i=1}^{N} s_i(t) = \sum_{i=1}^{N} A_i(t) \exp(j\varphi_i(t)) \tag{4}$$

where $A_i(t)$ are amplitude modulated coefficients and $\omega_i(t) = \frac{d\varphi_i(t)}{dt}$ are the IF's.
Considering a multi-component signal $s(t)$ which contains two nonlinear FM components $s_1(t)$ and $s_2(t)$ as

$$\begin{aligned} s(t) &= s_1(t) + s_2(t) = 3^{2-\cos(1.5t)} \exp(j(0.07t^3 - 2t^2 + 38t)) \\ &\quad +20\sin(0.6t) \exp(j(-100\exp(-0.2t) + 0.017t^3)) \end{aligned} \tag{5}$$

Figure 1 shows the spectrogram of this multi-component signal, where the window functions is $h(t) = \sqrt{\frac{2}{\pi}} e^{-t^2}$. Figure 2 shows reconstruction results of the multi-component signal $s(t)$ in the time domain.

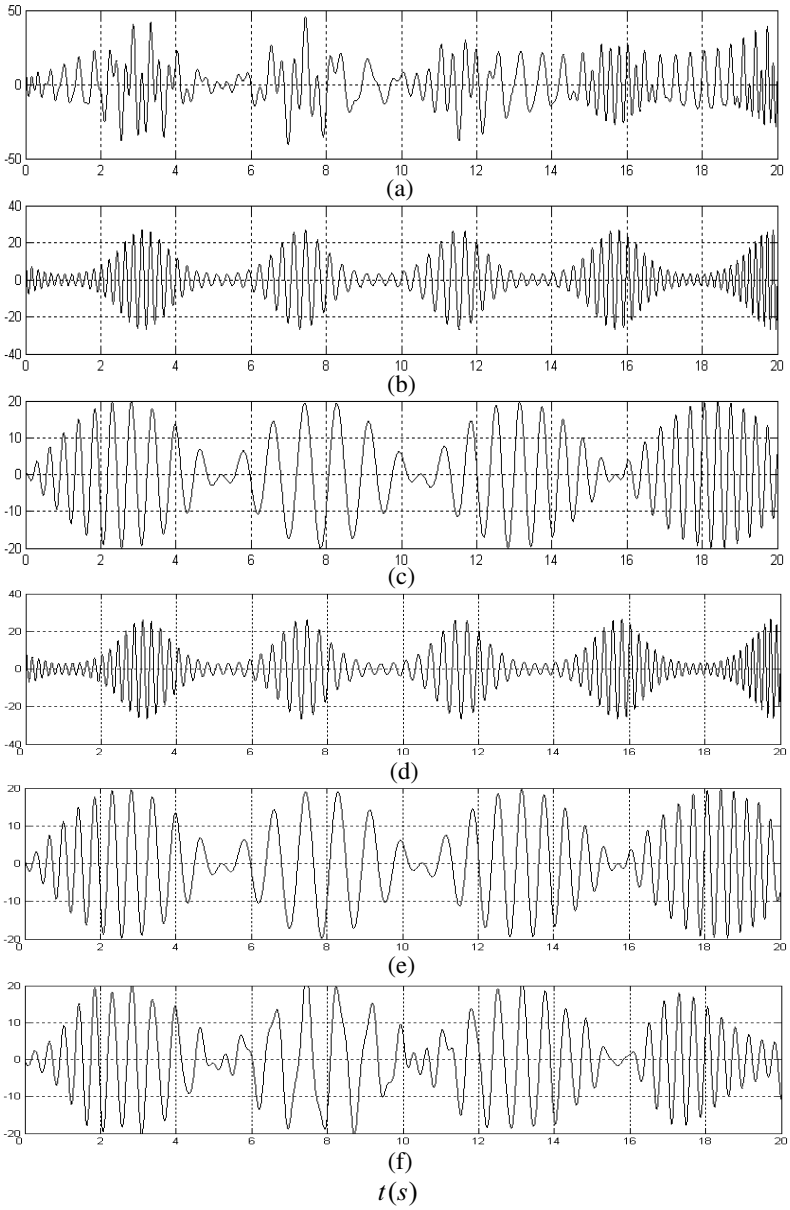

Figure 2: Comparison of the reconstructed signals and the original signals, (a) Multi-component signal, (b) Signal $s_1(t)$, (c) Signal $s_2(t)$, (d) Reconstructed signal $s_1'(t)$, (e) Reconstructed signal $s_2'(t)$, (f) Reconstructed signal $s_2'(t)$ using optimal filtering based on FRFT.

A QFT is proposed for the reconstruction of nonlinear frequency modulated and amplitude modulated multi-component signals. This method transforms signals which are aliased in the frequency domain, into the quasi frequency domain where the resulting spectra can be easily separated. The simulation results indicate that this method produces reliable reconstructed signals.

REFERENCES

1. Cohen, L., *Time-frequency Analysis: Theory and Applications*, 77–111, Prentice Hall, 1995.
2. Özdemir, A. K. and O. Arikan, "Fast computation of the ambiguity function and the Wigner distribution on arbitrary line segments," *IEEE Trans. Signal Processing*, Vol. 49, No. 2, 381–393, 2001.

Optimal Adaptive Waveform Selection for Target Tracking

B. Wang, J. K. Wang, X. Song, and F. L. Liu
Northeastern University, China

Abstract— Based on the new development of hardware of digital waveform modulator, performance of resolution, detection probability and tracking accuracy of radar system is substantively improved through adaptively adjusting parameters of transmitted waveform. Optimal waveform selection is an essential problem with the aim of selecting the optimal waveform and tracking targets with more accuracy. The problem of adaptive waveform selection can be viewed as stochastic dynamic programming. However, suitable scheduling algorithms are lacked, and optimality equations are themselves computationally intractable as a result that state variable space is very large.

To account for the aboved shortcoming, we can use forward dynamic programming algorithm approximating the expectation, which is one method of approximate dynamic programming (ADP). ADP offers a powerful set of strategies for problems that are hard because they are large. In this paper, based on stochastic dynamic programming model, we will show how to use this method to solve adaptive waveform scheduling problem. According to Bellman principle, Bellman's equation of waveform selection is gained. Then forward dynamic programming algorithm approximating the expectation is used to solve this equation effectively. The result is that we can minimize target tracking errors. And the problem of optimality equations themselves computationally intractable can be solved effectively.

The format of the reminder of this paper is as follows. In Section 1, the whole paper is briefly introduced. In Section 2, stochastic dynamic programming model of adaptive waveform selection is set up. In Section 3, forward dynamic programming algorithm approximating the expectation is used to solve adaptive waveform scheduling problem. In Section 4, how to chose parameters and reward function is introduced. In Section 5, the whole paper is summarized.

Adaptive Cooperative Coding in Fast Rayleigh Fading Channel

Li Li[1], **Tinghuai Wang**[2], **Yang Du**[1], **and Honglin Hu**[3]

[1]The Electromagnetics Academy at Zhejiang University
Zhejiang University, Hangzhou 310027, China
[2]School of Engineering, University of Warwick, Coventry CV4 7AL, UK
[3]Shanghai Research Centre for Wireless Communication (SHRCWC), Shanghai, China

Abstract— The relay technique is an effective way to enlarge the cell coverage and enhance the spectral efficiency in wireless network. A novel cooperative transmission protocol based on the channel coding, named the adaptive cooperative coding (ACC), has been proposed in our previous work. This ACC protocol is implemented by transmitting the rate-compatible punctured convolutional code (RCPC) sequence and its complementary punctured convolutional (CPC) sequence during the two-hop transmission. In this paper, we discuss and evaluate the ACC protocol performance in the fast and slow Rayleigh fading channel. The strict performance upper bound and its asymptotic expression are derived by the mathematical analysis. Through Monte Carlo simulation, the performance upper bound is proved to be tight with the simulation result, and the ACC protocol outperforms the traditional single hop (SH) transmission due to the considerable cooperative diversity, while maintaining the same transmit rate and power as that of the SH transmission.

MAC Scheduling Schemes and Cross Layer Optimization for IEEE 802.15.3

G. D. Yang[1], **L. Rong**[2], **R. F. Lin**[1], **and Y. Du**[1]

[1]The Electromagnetics Academy at Zhejiang University
Zhejiang University, Hangzhou 310058, China
[2]Shanghai Research Center for Wireless Communications, Shanghai 200050, China

Abstract— In this paper, the performances of varieties of HDR MAC scheduling schemes are examined. The scheduling schemes under investigation include 1) the shortest remaining processing time rule (SRPT); 2) the exponential rule (EXP); 3) the modified largest weighted delay first rule (M-LWDF); 4) the proportionally fair rule (PROP-FAIR); and 5) the maximum rate rule (MAX-RATE), most of which take advantage of wireless channel conditions to improve channel utilization. In addition, M-LWDF rule and EXP rule provide QoS guarantee to user traffic as well. The performances were studied under large number of simulation using ns-2, which take node mobility, channel fading and traffic characteristics into consideration in order to make the results more realistic. We also studied the performance gain of scheduling scheme combined with some cross layer mechanisms, including frame-decodability aware mechanism for MPEG traffic, adaptive MAC fragment size adjustment and Hybrid ARQ. The results show that with channel aware scheduling schemes, we provide a robust system, the performance of which has been greatly enhanced in particular with optimization mechanisms.

A Robust Beamforming Method Based on Space-time Averaging Techniques

Ruiyan Du and Jinkuan Wang
Engineering Optimization & Smart Antenna Institute
Northeastern University at Qinhuangdao, Qinhuangdao, China

Abstract— Robust beamforming is a ubiquitous task in array signal processing with applications, among others, in radar, sonar, acoustics, astronomy, seismology, wireless communications, and medical imaging, etc. Without loss of generality, we consider herein beamforming in array processing applications. Because of strict restrictions on the number of available snapshots, signal mismatches, or calibration errors, robust array beamforming has drawn considerable attention in the past years. In order to achieve high interference suppression and signal-of-interest (SOI) enhancement, an adaptive array must introduce deep nulls in the direction of arrival (DOA) of strong interferences, while keeping the desired signal distortionless. In subspace-based beamforming methods, it is clear that the performance of beamforming is directly determined by quality of correlation matrix. The conventional method of correlation matrix estimation is to average the output of sensor array. For a uniform linear array (ULA), the structure of correlation matrix of array output is Hermitian and Toeplitz. Based on this property, a robust beamforming method based space-time averaging techniques is presented in this paper. This proposed method can provide increased robustness against the mismatch problem as well as additional control over the sidelobe level. The simulation results show that the beamforming performance of the proposed method can be improved, especially on the condition that signal-to-noise ratio is low and the number of snapshot is not enough.

An Optimal ADP Algorithm for Waveform Selection in Cognitive Radar Systems

Fulai Liu and Jinkuan Wang
Engineering Optimization & Smart Antenna Institute
Northeastern University at Qinhuangdao, China

Abstract— One of the major issues in cognitive radar is obtaining an adaptive transmitting waveform based on environmental measurements. Modern phased array radars, with flexible waveform generation and beam steering capability, are able to adaptively modify their performance to suit a variety of environments. This power has not yet been fully exploited, in part because of the lack of suitable scheduling algorithms. In this paper, we consider the problem of adaptive waveform selection for tracking a single target in clutter using a cognitive radar with a fixed set of waveforms. The aim is to select the best sequence of waveforms to track the target with the highest possible accuracy. The problem of adaptive waveform selection is considered as the multistage stochastic problems, in this paper. For target tracking in cognitive radar system, an optimal approximate dynamic programming algorithm is proposed, taking account that the probability distribution of the underlying stochastic process is not known and the state space is too large to be explored entirely. This presented method combines Monte Carlo simulation in a pure exploitation scheme, in order to construct concave piecewise linear functions approximations. The function slopes are updated through stochastic approximation integrated with a projection operation. The result is a scheduling algorithm that minimises target tracking errors.

Reflection Cancellation from High Speed Transmission Line

Salahuddin Raju[1], **S. M. Salahuddin**[2], **and Ishfaqur Raza**[2]

[1]Department of Electrical and Electronic Engineering
American International University-Bangladesh, Bangladesh
[2]Department of Electrical and Electronic Engineering
East-West University, Bangladesh

Abstract— An IO driver architecture is presented here to compensate scattering in high speed transmission line circuits. In this methodology a system is calibrated initially to measure system response to a step or a lone pulse. The IO driver is then programmed to generate measured pulses at designated interval to compensate scattering responses due to impedance mismatch in the system transmission line. The compensation is done for every single bit or pulse transmitted from the driver end to eliminate sustained reflections and resonances. This methodology is demonstrated with high speed design tool. The architecture of the driver and calibration methodology is also outlined.

Special Approach for Estimation Ground Target Position in Passive Location

E. P. Voroshilina and V. I. Tislenko
Research Institute of Radiotechnical Systems, Tomsk, Russia

Abstract— Ground target tracking is difficult and actual problem. Because of the high target density and maneuverability, high clutter, low visibility due to terrain masking, etc., ground target tracking presents unique challenges not present in tracking other types of targets. But many tracking approaches have been developed for air targets and they may poorly when used to track ground targets.

This article includes results of the research work in estimation radar position in passive range-difference location. Radio source is not moving and perform circular scan. Signal from it is received in three points. But beside true measurements there are false measurements originated by clutter. Usually clutter measurements are modeled as independed identically distributed. But processing real experimental data shows that in cross-country it distribution may be multimodal. Therefore standard tracking algorithms are not efficient in this situation. Multimodal distribution is caused by re-reflected signal from underlying terrain. Some ground objects re-reflect signal and imitate true target.

We propose special approach to decide problem of position estimation in such high clutter environment and verify it on experimental data. Our algorithm consist of three part: 1 — track initiation, 2 — target state estimation (filtration), 3 — target identification (define class target — true or re-reflected object). Computer simulation shows that this algorithm works effectively. Estimation position error is about 50 meters on distance 2 Km long.

Session 2P5a
Bioeffects and Exposure Standards for RF Pulses

Exposure Standards for Radio Frequency Pulses

M. R. Murphy
Directed Energy Bioeffects Division, 711th Human Performance Wing
Air Force Research Laboratory, Brooks City-Base, Texas, USA

Abstract— Concomitant with the ever increasing use of Radio Frequency (RF) energy, there is also an increase in the opportunity, even certainty, for increased human exposure to RF emissions. Also, the nature of the exposures are entering new regimes, with possible exposure to RF pulses of nanosecond and picosecond duration and with extremely high-peak electric fields becoming more common Scientifically based human exposure standards are needed to both protect humans from the real hazards of exposure to RF pulses and to provide a relatively stable base for maximal safe exploitation of RF pulse-based technologies. Two widely used international RF exposure standards, one produced by the IEEE International Committee on Electromangetic Safety (ICES) (http://www.ices-emfsafety.org) "C95.1: IEEE Standard for Safety Levels with Respect to Human Exposure to RF Electromagnetic Fields 3 KHz to 300 GHz" (2005), and the other by the International Commission for Non-Ionizing Radiation Protection (ICNIRP) (http://www.icnirp.de) "Guidelines for Limiting Exposure to Time-Varying Electric, Magnetic, and Electromagnetic Fields (up to 300 GHz)" (1998), are similar in the total RF energy allowed within a specified averaging time, but differ greatly in their guidelines for limiting exposure to single RF pulses. IEEE ICES basic restrictions limit the Specific Absorption (SA) in any one pulse to 28.6 J/Kg and limit the peak *e*-field for any single pulse to 100 KV/m. ICNIRP basic restrictions limit the energy per pulse to 0.01 J/Kg (occupational exposure) or 0.002 J/Kg (public exposure) for any exposure that includes the head, but has no limit for peak *e*-field. The IEEE ICES limit on peak *e*-field is based on the possibility of air breakdown and subsequent spark discharge, whereas the ICNIRP limit on SA(J/Kg) is based on a concern to avoid the microwave hearing phenomenon. Thus, the basic restrictions for these two standards differ by as much as 14,300 times for the SA of a pulse and one controls peak *e*-field and the other does not. There is little scientific data to assure the public or industry that these limits are either safe or unnecessarily ultraconservative. With the increasing capability to emit shorter and higher pulses into the environment, additional mechanistic and safety research and predictive modeling are needed to develop a new generation of scientifically-based safety limits for pulsed RF exposure.

Low-level Pulsed Microwave Auditory Effect

C.-K. Chou
Corporate EME Research Laboratory, Motorola, Fort Lauderdale, Florida, USA

Abstract— Pulsed microwaves have been heard as sound by radar operators since radar was invented during World War II. In early 60's, a series of papers described the hearing phenomenon in a more controlled environment. In the 70's, we found that regardless of the peak power and pulse width the threshold was related to an energy density of 40 μJ/cm^2 per pulse, or a peak of specific absorption (SA) of 16 μJ/g per pulse [1]. At a low repetition rate, each individual pulse could be heard as a distinct click. Sound localization was impossible since the sound was heard inside the head. Subjects with high frequency hearing loss (above 5 KHz) cannot hear the RF sound. The RF sound may be perceived as clicks, buzzes, or hisses depending on the modulation characteristics of the microwaves. The threshold energy density per pulse for the auditory sensation is very low (2–40 μJ/cm^2). The maximal rise in temperature of the exposed tissue is on the order of 10^{-5} to 10^{-6}°C for exposure of an individual pulse at the threshold of energy density.

To better understand the microwave-induced auditory responses and to determine the thresholds of the effect, studies have been conducted using electrophysiological recordings and behavior paradigms in controlled experiments with laboratory animals. Data have been obtained from cochlear potentials recorded at the round window, from single-unit responses recorded at the eighth nerve, from evoked potentials recorded at various locations of the auditory pathway (eighth nerve to auditory cortex), and from surface potentials picked up by scalp electrodes. Behavioral studies include aversive behavior, discriminative control, and audiogenic seizures.

Microwave hearing is most easily explained by the mechanism of thermoelastic expansion [2], i.e., absorption of microwave energy produces non-uniform heating of the exposed head; a thermoelastic wave of pressure is then launched, presumably through bone conduction, to the cochlea where it is detected. After auditory-nerve excitation in the high-frequency portion of the cochlea, transmission of the microwave-induced neural response follows the same auditory pathways as do all of the acoustically induced responses through the brainstem and thalamus to the auditory cortex. Two reviews are available on this subject [3, 4].

From the above studies, it can be concluded:

1. Microwave hearing is a proven low-level pulsed RF effect in animals and humans.
2. Mechanism of the effect is understood.
3. The effect is thermally induced.
4. At threshold level, the temperature rise is about a millionth of a degree Celsius per pulse.
5. Hearing effect is not hazardous.
6. For setting safety standards, RF bioeffect studies must aim to establish dose-response relationship, and to understand its mechanism.

REFERENCES

1. Guy, A. W., C. K. Chou, J. C. Lin, and D. Christensen, "Microwave induced acoustic effects in mammalian auditory systems and physical materials," *Biologic Effects of Nonionizing Radiation, Annals NY Acad. Sci.*, Paul E. Tyler (Ed)., Vol. 247, 194–218, 1975.
2. Foster, K. R. and E. D. Finch, "Microwave hearing: Evidence for thermoacoustic auditory stimulation by pulsed microwaves," *Science*, Vol. 185, 256–258, 1974.
3. Chou, C. K., A. W. Guy, and R. Galambos, "Auditory perception of radio-frequency electromagnetic fields," *J. Acous. Soc. Am.*, Vol. 71, No. 6, 1321–1334, 1982.
4. Elder, J. E. and C. K. Chou, "Auditory response to pulsed radiofrequency energy," *Bioelectromagnetics*, Vol. 24, Supplement 6, S162–S173, 2003.

Studies on Effects of High Power Microwaves in Cell Cultures

M. Risling[1], **E. Malm**[1], **M. Angeria**[1], **and L. Malmgren**[2]

[1]Department of Neuroscience, Karolinska Institute, Stockholm, Sweden
[2]MaxLab, University of Lund, Sweden

Abstract— In previous studies we have reported a decrease in the content of the cytoskeletal protein tubulin in endothelial cells exposed to multiple pulses of high power microwaves (HPM). It may be assumed that a downregulation of tubulin could affect the complex structure of neuronal dendrites. In this study we have examined the effect of HPM in cultures of neurons from the hippocampus of rat embryos. The neurons were exposed to 1.6 GHz HPM pulses with a duration of 0.55 microseconds and a field strength of 21.7 KV/m. The spacing between the pulses was 3.3 ms and the cells were exposed for 10 seconds – 12 minutes. This relation between pulse duration and spacing is not assumed to produce heating in the tissue. The cultures were fixed and labeled with antibodies against tubulin and MAP2 (a microtubule associated protein) after 2, 6, 24 or 72 hours. The specimens were examined with a confocal microscope. The results showed extensive changes in dendrite structure in cultures exposed for more than 90000 pulses. This effect could be observed already 2 hours after exposure. Dendrite structure was gradually but not completely restored. In a subsequent study cultures of the rat C6 glia line were exposed to 90000 pulses of HPM with the same field parameters. After 24 hours the cultures were prepared for high-density oligonucleotide arrays and hybridized to each GeneChip® Rat Gene 1.0 ST Arrays (Affymetrix). Following normalization, the change in gene expression between the three control cultures and and three exposed cultures at each survival time was compared using an un-paired t-test. Low to moderate changes was observed in about 500 of the more than 27000 examined genes. This included changes in about 100 olfactory receptor genes. No significant changes in genes for cell death, cytoskeleton, inflammation or heat shock proteins were found. We conclude that the observed effects on tubulin probably are related to changes at the protein level and not a decrease in the expression of the mRNA for tubulin. In future studies, it will be important to reveal the threshold thermal effects in cells exposed to this type of fields.

Effects of Localised Pulsed Heating on Electrophysiological Responses in Brain Slices

J. E. H. Tattersall, N. C. D. Mifsud, I. R. Scott, and A. C. G. Green
Biomedical Sciences Department, Dstl Porton Down, Salisbury, Wiltshire SP4 0JQ, UK

Abstract— Exposure guidelines based on time-averaged heating effects of radiofrequency (RF) fields do not adequately address exposures to high peak power signals with low average power. Previous studies in our laboratory suggested that *in vitro* exposure to RF fields can affect both evoked and spontaneous electrical activity in rat hippocampal slices [3]; however, our more recent experiments have demonstrated that these effects may be explained by localised heating produced by interaction of the RF fields with the recording and stimulating electrodes [2]. We are now exploiting this electrode-mediated heating artefact to explore the effects of short pulses of localised heating on neurotransmission in the brain tissue. The results of this work will help to inform thermally-based standards for limiting exposures to pulsed RF fields.

Extracellular field potential responses were recorded in hippocampal slices prepared from adult rats and exposed to 380 MHz RF fields in a parallel plate transmission line [3]. An infrared camera (Cedip Infrared Systems Jade) was used to image the brain slice and the electrodes in order to measure the heating produced during RF exposure. This camera has a theoretical thermal resolution of 0.025°C and each pixel on the sensor corresponded to approximately 200 μm at the brain slice target. The acquisition rate was 50 frames.s^{-1}.

Initial experiments investigated the relationship between heating duration and the temperature rise required to abolish the evoked field potential recorded in CA1. For RF pulses at an input power of 100 W into the transmission line, the field potential was abolished at a pulse duration of 20 ms. For a lower input power of 10 W, a longer duration of exposure of 2 s was required to abolish the evoked field potential response. The pulse duration of 20 ms at 100 W produced a peak temperature increase to 58°C from the perfusion temperature of 33°C, a rise of 25°C. A plot of temperature increase against exposure duration showed an initial rate of temperature rise of 1438°C.s^{-1}. Assuming a specific heat capacity for brain tissue of 3850J.Kg^{-1}.°C^{-1} [1], this represents a specific absorption rate of RF energy of 5.54 MW.Kg^{-1}, which is far higher than could be achieved without exploiting the electrode heating artefact.

These results demonstrate that the RF-induced electrode artefact can be exploited to study the effects of millisecond periods of heating on neurotransmission in brain tissue, enabling the relationship between thermal threshold and heating duration to be determined. Future experiments will determine the threshold temperature rise for changes in the evoked field potential for a range of durations of RF exposure. The minimum heating duration that can be investigated is limited by the frame capture rate of the infrared camera.

This work was carried out as part of the Electronics Systems Research Programme for the Ministry of Defence.

REFERENCES

1. Mall, G. and W. Eisenmenger, "Estimation of time since death by heat-flow Finite-Element model. Part I: method, model, calibration and validation," *Legal Medicine*, Vol. 7, 1–14, 2005.
2. Mifsud, N. C. D., I. R. Scott, A. C. Green, and J. E. H. Tattersall, "Temperature effects in brain slices exposed to radiofrequency fields," *European Bioelectromagnetics Association*, abstracts S-3-6, 2007.
3. Tattersall, J. E. H., I. R. Scott, S. J. Wood, J. J. Nettell, M. K. Bevir, Z. Wang, N. P. Somasiri, and X. Chen, "Effects of low intensity radiofrequency electromagnetic fields on electrical activity in rat hippocampal slices," *Brain Res.*, Vol. 904, 43–53, 2001.

Biological Effects of High Power Microwaves

René de Seze[1], **I. Guimiot**[1], **M. Ammari**[1, 2], **C. Hernandez**[3, 4], **E. Bourrel**[3, 4], **C. Gamez**[1], **E. Maillot-Maréchal**[1], **J. F. Fontaine**[5], **and C. Fonta**[3, 4]

[1]INERIS, Parc technologique Alata, BP 2, 60550 Verneuil en Halatte, France
[2]Faculté des Sciences de Bizerte, laboratoire de physiologie intégrée, Jarzouna 7021 Tunisia
[3]CerCo, Université de Toulouse, UPS-31062 Toulouse, France
[4]CNRS, UMR5549, Faculté de médecine Rangueil-31062 Toulouse, France
[5]Unité d'Embryologie, Histologie et Anatomie Pathologique
Département des Sciences Biologiques et Pharmaceutiques
Ecole Nationale Vétérinaire d'Alfort-7
Avenue du Général de Gaulle-94704 Maisons Alfort Cedex, France

Abstract— High power microwaves can be used to inhibit electronic systems or to neutralise people. The aim of this study is to study the effects of high power microwaves on the central nervous system, and mainly on behaviour and the effects on astrocyte cell population indicating an inflammatory process.

Six-week rats were exposed to two different sources with pulse trains emitted at a repetition rate of 100 Hz.

	Source 1	Source 2
Beam diameter at output	13 cm	22 cm
Frequency	10 GHz	3.8 GHz
Total emitting power	350 MW	500 MW
Pulse duration	1 ns	2.5 ns
Train duration	10 s	Continuous
Emission duration	Every 5 min for 1 h	20 min
Peak surface power at output	20 GW/m^2	2 GW/m^2
Peak E-field	3 MV/m	1.7 MV/m
Peak SAR	95 MW/kg	31 MW/kg
Average SAR over total exposure	0.34 W/kg	4.7 W/kg

Performed behavioural tests were: avoidance, beam-walking, rotarod and T-maze. Besides that, the size and the number of astrocytes in the brain were assessed through quantification of GFAP filaments labelled by immunohistochemistry.

For each test, a group of 12 exposed animals was compared to a group of 12 sham-exposed animals, set at the same place and in the same ambient conditions as the exposed animals, but without emission by the source.

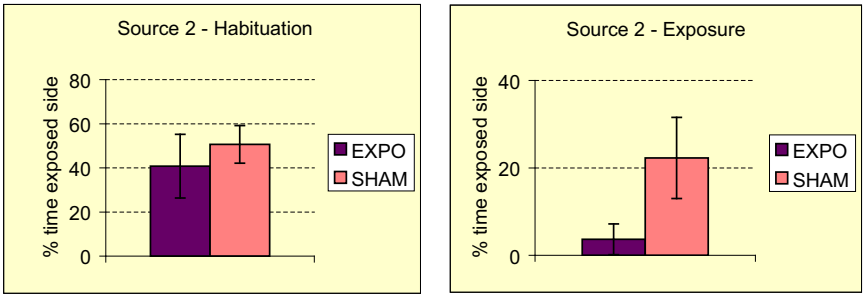

Figure 1: Time spent in non protected side-Source 2 (Mean±SEM).

For the avoidance test with source 2, the emission was closer to the antenna output, with two pulse trains of 8 minutes spaced by 10 minutes. The number of alternations between the two compartments was the parameter of interest. Exposure parameters were: peak SAR = 90 MW/kg; av SAR: 22 W/kg.

In the beam-walking, a 2 m-long, 2 cm-large rod was placed in front of the rat homecage. The rat was placed at different distances from the cage and the success to reach the cage was noted. In the rotarod, the ability of the rat to stay on the turning axis was recorded. In the T-maze, the rat learned to go in a first task to go in one single open arm (right or left). The consecutive task was to go in the second arm when both arms were open.

A chronic exposure was also performed on two groups of 24 animals, one was truly exposed, the second one was sham-exposed. This exposure lasted 20 minutes a day, 5 dys/wk for 8 weeks. Peak SAR: 3.3 MW/kg; av SAR: 0.8 W/kg. Residual X-rays: 20 mGy/day (total 0.8 Gy).

Results

Behavioural tests: Avoidance was significantly altered at a thermal SAR. Rotarod showed an increase performance in exposed animals.

Immunohistochemistry: With source 1, GFAP expression was not increased 2 days after exposure, but increased 7 days after exposure (+40%).

With source 2, GFAP expression was increased 2 days after exposure (+70%), probably reflecting the higher average SAR allowed by a continuous emission instead of spaced 10 s pulses.

During the first year after exposure, 8 from chronically exposed animals deceased following tumours, and only one sham-exposed animal died, without any tumours. Histopathological study is ongoing.

Table 1: Rotarod results.

	Training				Test	
	fail	succeed			fail	succeed
Sh	65	7		Sh	47	23
Ex	49	23		Ex	31	41
	p	$2.0\ 10^{-10}$			p	0.00001

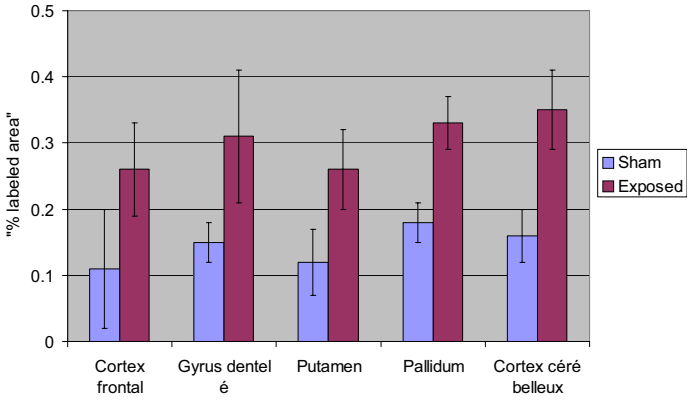

Figure 2: GFAP expression in different brain areas 2 days after exposure (Mean±SEM).

Although results suggest that rats are stimulated by the exposure in the rotarod, the increase of cancer incidence shows that this stimulation is not indicative in this case of a long-term beneficial effect after chronic exposure. It also shows that other behavioural tests are not helpful in detection of a chronic risk. Only effects on GFAP expression in rats could be a marker of a long-term risk, but this needs complementary studies to be confirmed.

If the observed important risk is not due to residual X-rays, this study suggests that a health risk could be produced by a chronic exposure at a SAR below the known level of health threshold of 0.08 W/kg, given that the peak SAR is of the order of 3.3 W/kg (E-field 1.5 MV/m). The threshold for such a risk must be further studied.

ACKNOWLEDGMENT

This study is funded by DGA, and by the MEEDDAT research program Pr189-Neurotox DRC07-AP05.

Effect of Electromagnetic Pulse on Embryo and Littles of Mice

Guozheng Guo
Department of Radiation Medicine, The Fourth Military Medical University
Xi'an 710032, China

Abstract—

Introduction: Effects of Electromagnetic Pulses (EMP) on the development of mammal embryo and litters haven't been clearly explored yet. To observe effects of EMP on pregnant mouse and embryo, and study the relation between the dose and effect of EMP.

Materials and Methods: Studies were carried out on BALB/c mice of about 2 months old. The treatment groups were exposed to EMP with different field intensity from 10 kV/m to 200 kV/m respectively. The teratological, sex ratio for embryo and the psychophysiological, learning ability were studied. The sex hormones for litters were tested. And also pregnant BALB/c mice were exposed to different dose of EMP in the period of organogenesis, the field intensity were 0, 50, 100, 200, 400 $kV \cdot m^{-1}$ respectively, then on day 18 of gestation, pregnant mice were sacrificed and the increase of the body weight, the ratio of the organ/body weight and the weight of placentas were measured. For the offspring, the weights of bodies, the length of bodies and tails were measured and the normal, abnormal and the ratio of the sex were checked. At last, according to the results, the EMP field intensity with the strongest inducing malformation effect was selected.

Results: The difference of the sex ratio between control and exposed group weren't significantly changed ($p > 0.05$). Whereas the absorbed and dead embryos, embryonic weight and placenta weight were significantly decreased ($p < 0.05$) compared with control group as well as the body length and tail length shorter than that of the control group ($p < 0.01$). Teratological assessment showed considerable differences ($p < 0.05$) between the exposed and the control group for litter appearance, visceral deformation, skeleton deformation including multirib and occipital bone. Examination of learning and memory capability tested on the 57th and 64th day after naturally born of the first filial generation whose mothers were undergone exposure to EMP were performed. Exposed group showed more error times and training times for either learning or memory test. Even though the exposed group could also reach the same criteria for learning and memory as the control, the conditioning times needed for the criteria were greatly reduced. No significant alternation ($p > 0.05$) was found between the females and males of the first filial generation. The sex hormones of the male litters were significantly decreased than that of control ($p < 0.05$).

In each EMP exposure group, the increase of the body weight and the ratio of the organ/body weight of pregnant mouse had no difference in all groups, but the weights of offspring and placentas, the lengths of offspring bodies and tails were all lower than those of control group ($p < 0.01$). The rates of dead, abnormal and hypoevolutism embryo in some exposure groups were higher than control groups' ($p < 0.01$), the number of malformation and the ratio of the female/male were increased in some EMP exposure groups, especially in 400 $kV \cdot m^{-1}$group.

Conclusion: In our condition, EMP can affect the development of mammal embryo and litters and have some damage effects on it. The damage effects were more and more serious with the EMP field intensity increasing.

ACKNOWLEDGMENT

This study was supported by National Natural Science Foundation of China (No. 60871068, No. 60601026 and 30700660).

Session 2P5b
Medical Electromagnetics, RF biological Effect, MRI 1

Ultra-high-sensitivity and Wash-free Assays on Bio-molecules Using Magnetic Nanoparticles and Superconducting Quantum Interference Devices

Herng-Er Horng[1], **Jen-Jie Chieh**[1], **Shieh-Yueh Yang**[2], **Chin-Yih Hong**[3], **Hong-Chang Yang**[4], **and Chau-Chung Wu**[5]

[1]Institute of Electro-optical Science and Technology
National Taiwan Normal University, Taipei 116, Taiwan
[2]MagQu Co., Ltd., Sijhih City, Taipei County 221, Taiwan
[3]Department of Mechanical Engineering
Nan-Kai Institute of Technology, Nantou County, Taiwan
[4]Department of Physics, National Taiwan University, Taipei 106, Taiwan
[5]Department of Primary Care and Internal Medicine, College of Medicine
National Taiwan University, Taipei 106, Taiwan

Abstract— Through bio-functionalizing magnetic nanoparticles with antibodies or single-strand nuclei acids, magnetic nanoparticles become able to associate with specific biomolecules, viruses, and nuclei acids. Due to the association, the ac magnetic susceptibility caused with the physical rotation of magnetic nanoparticles driven with ac magnetic fields is reduced. By measuring the reduction in the ac magnetic susceptibility of magnetic reagents, the to-be-detected biomolecules, viruses, and nuclei acids can be assayed. This assay technology is so-called magnetoreduction assay (MRA). To achieved an ultra-high sensitivity, a magnetosusceptometry consisted of high-T_c superconducting-quantum-interference-device (SQUID) magnetometer is utilized to detect the reduction in the ac magnetic susceptibility. The results show that the sensitivity can be down to 10^{-15} g. In addition, such technologies for assaying biomolecules reveal several advantages for clinical applications, e.g., wash free, single bio-conjugation, and high specificity.

Wavelet Analysis of Alterations of the Subcutaneous Microvasculature Signal Induced by Low Frequency-electromagnetic Fields Action in Vivo

L. Traikov[1,3], I. Antonov[3], A. Ushiyama[1], G. F. Lawlor[2], and C. Ohkubo[4]

[1]Department of Environmental Health, National Institute of Public Health, Saitama 351-0197, Japan
[2]Department of Public Health Administration & Policy, National Institute of Public Health
Saitama 351-0197, Japan
[3]Faculty of Medicine, Department of Medical Physics and Biophysics, Medical University-Sofia
Sofia-1431, Bulgaria
[4]Radiation and Environmental Health, World Health Organization
Avenue Appia 20, CH-1211 Geneva 27, Switzerland

Abstract— Microcirculatory changes in arterioles were examined in mice exposed to low frequency-electromagnetic fields (EMF), by direct, continuous intravital microscopy.

Conscious BALB/c mice ($n = 34$) assigned to 1 of 4 groups were exposed to EMF for 10 min: at 10, 16 or 50 Hz (28 mT), or no exposure (sham). Dorsal skin-fold chamber implanted mice were injected with FITC-Dextran-250, 2.5% in PBS, via caudal vein. Epi-illumination of arterioles (45–80 μm diameter) was monitored continuously over 33 min, that included: 3 min preliminary preparation and 10 min pre-, 10 min EMF-exposure, and 10 min post-exposure. In vivo alterations in vasomotion were measured using a high-speed digital-video recording and image enhancement system, employing an edge-gap detection algorithm (389 ms sampling time), to calculate arteriole diameters. Captured signal images were filtered and amplified to eliminated background fluorescence noise. Changes in frequency band magnitudes were determined by FFT (Fourier coefficients) and wavelet analysis.

Sham-exposed mice exhibited no significant changes in vessel diameters amplitude changes, during the 33 min evaluation. However, 16 Hz EMF significantly increased vasodilatation at post-exposure, period compared with pre- and exposure periods. No significant change with 10 Hz or 50 Hz exposure on vessels was seen throughout the monitoring, using Friedman's Chi-Square analysis. This on-line, automated and real-time methodology enables improved, advanced analysis of single frequency components among the compound signals monitored in vasomotion, toward better understanding signal transduction pathway interactions/factors related to the mechanisms of microvascular regulation and change.

The Role of Endogenous and Exogenous E-fields in Metaphase

A. H. J. Fleming
Biophotonics Research Institute, Melbourne, Australia

Abstract— Recently the mathematics of Self-Field Theory has been used to investigate the role of the photon as the binding energy inside the atom. Self-field theory provides deterministic eigensolutions to the Maxwell-Lorentz equations for the hydrogen atom. This is a mathematically distinct method to quantum mechanics and the more modern Lagrangian-based quantum field theories such as quantum electrodynamics. Fundamentally self-field theory obtains an expression for Planck's constant $\hbar = \frac{q^2}{4\pi\varepsilon_0\nu_e}$ as the energy per cycle of the principal eigenstate. Based on a composite photon, an analytic expression for photon mass is also obtained $m_\gamma c^2 = \frac{\hbar\omega_\gamma\nu_e}{4c}$, where ω_γ is an integer photon transition frequency within each cycle. This expression is compatible with the fine-structure constant $\alpha = \frac{\nu_e}{c} = \frac{4m_\gamma c^2}{\hbar\omega_\gamma}$, where $m_\gamma = 0.396 \times 10^{-55}$ Kg $(0.221 \times 10^{-19}$ eV). Within atoms and molecules photon substructure introduces a previously unknown quantum number by which bonds vary between strong and weak structures. A range of biological examples support this analytic bonding mechanism including the structures of DNA during the cell cycle. Most important metaphase is seen as a situation where the endogenous E-field can build up via cell-cell co-operation until the energy becomes sufficient to rupture the bond between the two daughter chromatids and metaphase continues into anaphase. The role of any exogenous field outside the body can be seen to related to the extracellular E-fields the resultant exogenous fields in the tissues in which the particular cells reside.

REFERENCES

1. "Self-field theory: Analytic spectroscopy of the ordinary photon," *EHE07*, Wraclow, Poland, Sep. 2007, http://www.iospress.nl/flyers_b/fl9781586038601.pdf.

Electromagnetic Pulses Radiation on Morphous and Gene Expression during Limb Development in Mice

Lihua Zeng, **Yongbin Chen**, **Jie Zhang**, **Xia Miao**,
Xiaowu Wang, **Yurong Li**, **Dongqing Ren**, **and Guozhen Guo**
Department of Radiation Medicine, Faculty of Preventive Medicine
Fourth Military Medical University, Xi'an 710032, China

Abstract—

Aim: To observe mice polydactylia induced by EMP and related genes expression (Gli3, Shh and Fgf4) during the developments of mice limbs.

Methods: Mature female mice were mated overnight with male mice (2 : 1). The morning on which a vaginal plug was found was designated as fetation-day-0. 1. The pregnant mice were randomly divided into control group and EMP radiation group. Mice in the EMP radiation group were exposed to EMP from fetation-day-7 to fetation-day-10. The fiedl intensity was 400 kv/m with 400 pulses. On the fetation-day-18, the embryos were taken out by cesarean section. The polydactylia were recorded. Morphological analysis of polydactylia was performed by using Alcian Blue-Alizarin red staining method. 2. The pregnant mice were randomly divided into negative control group, positive control group and EMP radiation group, Mice in the EMP from fetation-day-7 to fetation-day-10. The field intensity was 400 kV/m with 400 pulses. Mice in the positive control group were injected with 300 mg/kg of Brdu on the fetation-day-9 and fetation-day-10 days. On the fetation-day-11, the embryos were taken our by cesarean section. The expression of Gli3, Shh and Fgf4 were detected by Whole-mount in situ hybridization (WHISH).

Results: Morphological analysis indicated that the polydactylia rate of the EMP radiation group was significantly higher than that of the control group ($P < 0.05$). And it was also indicated that limb abnormality often occurred to the hindlimbs. In embryo limbs (fetation-day-11) of the EMP radiation group and the positive control group, the ectopic expression of Fgf4 was detected in AER, the overexpression and ectopic expression of Shh were detected in the ZPA; the decreased expression of Gli3 was detected in mesenchyme cells.

Conclusion: The occurrence of polydactylia in mice increased after EMP radiation and it may have some relationship with the abnormal expressions of the above-mentioned genes.

ACKNOWLEDGMENT

This study was supported by National Natural Science Foundation of China (No: 60601026), (No: 30700660) and Natural Science Foundation of Shaanxi (No: 2007$C_2$67) and National 863 project (No: 2008AA8030421B).

A Thermal Noise Analysis in the Biological Matter

Massimo Scalia[1], **Massimo Sperini**[2], **and Fabrizio Guidi**[3]

[1]Department of Mathematics, University of Rome "La Sapienza", Rome, Italy
[2]Technical Institute 'R. Rossellini', Rome, Italy
[3]Naval Technical Institute 'M. Colonna', Rome, Italy

Abstract— The discussion of the biological or health effects due to electromagnetic fields of low intensity in the whole region of non ionizing radiations (NIR) goes far beyond the mere scientific debate to invest health and environment problems, even in political decisions. Just in this context a relevant influence has been played along all these years by the statement of the Council of the APS (*American Physical Society*), written out in 1995, that excluded all biological and health effects from power lines, specially the promotion of cancers. Therefore, the directions of the APS statement disregard the risks associated to the exposure to the fields generated by power lines, in a substantial agreement with the WHO (*World Health Organization*) criteria on NIR emitted in 1984, assumed also by the ICNIRP (*International Commission on Non-Ionizing Radiation Protection*) successive guidelines. That statement has been reaffirmed by the Council of the APS in a more recent brief note (April 15, 2005).

The aim of the present communication is not to enter this debate, but, looking at the scientific bases of the APS position paper, to focus the one that has played a so relevant role up to day such to merit the name of "Adair's constraint". Really, Robert K. Adair proposed the concept of "thermal noise electric field" in some his papers (1990, 1991), and his "constraint" extends far beyond the possible cancer effects. It can be substantially summarized saying that weak electromagnetic fields ($E \leq 300\,\mathrm{V/m}$, $B \leq 50\,\mu\mathrm{T}$, $\nu = 50\,\mathrm{Hz}$) effects are impossible or, using his words: "To find them it is like looking for werewolves". R. Adair has kept on his arguments and his "constraint" in more recent papers (2000, 2003). We only mean to show that the consequences derived from the "thermal noise electric field" and the "Adair's constraint" are simply wrong relied.

Session 2P6
Elecromagnetic Field in Bio Magnetism Materials and Instrument and Dispersion in Cloaks and Metamaterials

3D GL Transform EM Modeling for Simulation of Cylindrical Cloaking

Jianhua Li, **Feng Xie**, **Lee Xie**, **and Lee Xie**
GL Geophysical Laboratory, USA

Abstract— The clocking material of cylindrical is different from the sphere clocking material, because they are based on different coordinate transformation. The Ez and Hz may be disturbed. In this paper, we develop a 3D Global and Local Transform (GLT) Electromagnetic (EM) field modeling for the simulation of cylindrical clocking. The circle annular cloaking material is anisotropic and dispersive in the circle annular zone. The conventional FEM and FD methods will meet difficulty in the full 3D simulation of the EM cloaking. We propose the electromagnetic field integral equation of the cylindrical annular cloaking anisotropic dispersive materials. Based on the EM integral equation, we develop GLT EM modeling for the simulation of the cylindrical annular EM cloaking which cloaked the central cylindrical space with any material, but there are low reflection disturbs into the out EM wave filed The 3D GLT EM cloaking simulation modeling is accurate and fast. The simulation results clearly and accurately show that the EM wave are propagating around the central sphere hole and can not going to inside of the hole. However, when the EM wave leaved the cloaking annular layer, the EM wave will suffer low reflection disturbs and mostly recovers to its original sample and direction. The central circle hole is complete cloaked and hiding from outside EM wave field. The 3D GLT EM cylindrical Cloaking Software (3DGLTEMCCC) is ready for many applications. We will show the movies of the 3D EM wave propagation around the cylindrical cloaking in EM Spring in PIERS 2009 in Beijing.

Analysis of Scattering from a Finite Linear Array of Dielectric Cylinders Using the Method of Auxiliary Sources

Naamen Hichem and Taoufik Aguili
Ecole Nationale d'ingénieurs de Tunis
Département Technologie de l'information et de Communications, Tunisia

Abstract— The numerical analysis, in the order to approximate scattered fields by larger bodies, is limited by the allowed computational cost and memory needs. The method of auxiliary sources is exploited to model the scattering properties from a finite linear array of dielectric cylinders taking into account the coupling between the different cylinders.

According to the MAS and for each dielectric cylinder, two bases of auxiliary sources must be considered; the first one distributed outside the physical contour and acts inside, the second is inside and acts outside.

The coupling modeled by the mutual satisfaction of the boundary conditions involving the continuity of the tangential field components just on the collocation points of every cylinder.

In the aforementioned global coupling model, we implement the fact that every cylinder is coupled only to the neighbouring cylinders (partial coupling), the linear system matrix in fully simplified entraining a significant decrease in the computational cost and memory requirements.

According to the global and partial coupling, numerical results (RCS, pattern field) reveal good agreement with references.

REFERENCES

1. Shubitidze, F., H. T. Anastassiu, and D. I. Kaklamani, "An improved accuracy version of the method of auxiliary sources for computational electromagnetics," *IEEE Transactions on Antennas and Propagation*, Vol. 52, No. 1, January 2004.
2. Anastassiu, H. T., et al., "Electromagnetic scattering analysis of coated conductors with edges using the method of auxiliary sources (MAS) in conjunction with the standard impedance boundary condition (SIBC)," *IEEE Transactions on Antennas and Propagation*, Vol. 50, No. 1, January 2002.
3. Kaklamani, D. I. and H. T. Anastassiu, "Aspects of the method of auxiliary sources (MAS) in computational electromagnetics," *IEEE Transactions on Antennas and Propagation*, Vol. 44, No. 3, June 2002.
4. Harrington, R. F., *Time Harmonic Electromagnetic Fields*, McGraw-Hill, New York, 1961.
5. Henin, B. H., A. Z. Elsherbeni, and M. Al Sharkawy, "Oblique incidence plane wave scattering from an array of dielectric cylinders," *Progress In Electromagnetic Research*, PIER 68, 261–279, 2007.
6. Elsherbeni, A. Z. and M. Hamid, "Scattering by parallel conducting circular cylinders," *IEEE Transactions on Antennas and Propagation*, Vol. 35, No. 3, March 1987.
7. Munk, B. A., *Finite Antenna Arrays and FSS*, IEEE Press, Wiley Interscience.

Light Localization in Quasiperiodic Dielectric Media

K. Wang
Laboratoire de Physique des Solides, CNRS/Universite Paris-Sud, Orsay 91405, France

Abstract— We study light wave behavior in octagonal and decagonal quasiperiodic dielectric media through the related approximate structures. We show the existence of a new light localization mechanism in these quasiperiodic dielectric media. As a matter of fact, due to local resonances between neighbor scatterers, light wave states inside the main photonic band gaps are localized on local structure patterns displaying the maximum symmetry of the quasiperiodic structure. In the present cases, the localized states, inside the two mains photonic band gaps, can be described as the s and p anti-bonding states formed from the first Mie resonant modes on respectively the D_8 and D_{10} local centers for the octagonal and decagonal structures. The formation of these localized states is favored by the high symmetry degree of the structure, without involving any disorder. We discuss the structural effects on the wave states by considering structure disorders as well as the different structure configurations at various scales. We show that, instead of reinforcing the localization effect, introduction of structure disorders leads to more extended wave states and strong increase in light propagation, with a group velocity increase that can reach almost one magnitude as compared to that for the perfect structure. This can be attributed to the fact that structure disorder breaks the local symmetry, and thus disfavors the formation of localized resonant states. Comparative studies on different classes of structures, characterized by different configurations at various structure scales, allow a better understanding of the relation between the localized states formation and the band gap opening in the quasiperiodic structures. In fact, the localization is determined by the local symmetry, while the band gap position depends on structure order at global scale. The opening of the gaps allows the existence of the localized states, and the symmetry degree of the local patterns determines the frequency level as well as the number of localized states inside the gaps. Finally, we investigate the coupling between the dielectric scatterers as a function of both the scatterer size and dielectric contrast, as well as the consequences on the localized wave states.

A Deformation-space Method for the Design of Spiral Longitudinal Biplanar Gradient Coils for Open MRI Systems

Minhua Zhu[1], **Ling Xia**[1], **Guofa Shou**[1]
Feng Liu[2], **and Stuart Crozier**[2]

[1]Department of Biomedical Engineering, Zhejiang University, Hangzhou 310027, China
[2]The School of Information Technology & Electrical Engineering, The University of Queensland St. Lucia, Brisbane, Queensland 4072, Australia

Abstract—

Introduction: In MRI, the gradient coils are usually composed of a series of discrete closed curves [1]. Here we design a spiral longitudinal biplanar gradient coil for use in an open MRI system by a deformation-space method [2]. The deformation-space method is a real-space (rather than reciprocal space) algorithm. Thus we can construct parametric equations to describe a longitudinal gradient coil based on Archimedes' spiral. These parameters are then used to define system rearrangements in the design procedure. An iterative optimization procedure is used to adjust the control parameters to minimize target/cost functions including gradient homogeneity. The spiral coils are composed of one or more sets of continuous curves.

Methods: Using Archimedes' spiral, $r = a\theta$ (see Fig. 1) as the candidate curve, we can construct a continuous curve/contour in the whole space. The system equation is:

$$r = R/\theta_{\max}^{p} \times \theta^{p} \tag{1}$$

where θ is an angle variable, p is the power of the variable, R is the magnitude of the coil, $\theta_{\max}^{p}$ is a normalization factor.

In the Cartesian coordinate system, the equation is:

$$\begin{aligned} x &= R/\theta_{\max}^{p} \times \theta^{p} \cos\theta \\ y &= R/\theta_{\max}^{p} \times \theta^{p} \sin\theta \end{aligned}$$

$\theta \in (0, +\infty)$, it means the spiral would be reversed if $\theta < 0$, where $[\frac{\theta}{2\pi}]$ can be used to represent the turn number.

With the normalization factor, the magnitude of the coil can be restricted to the size R, thus the wire gap between adjacent wires can be controlled. We set up two groups of (anti-clockwise) spirals, an outer group and an inner group. The spiral curve parameters are determined using a Multi-objective optimization routine in Matlab. During the optimization, the gradient field over the region of interest is calculated based on the Biot-Savart Law. As the coil contour is continuous, the field evaluation can be efficiently implemented using a 1D Gaussian integration method.

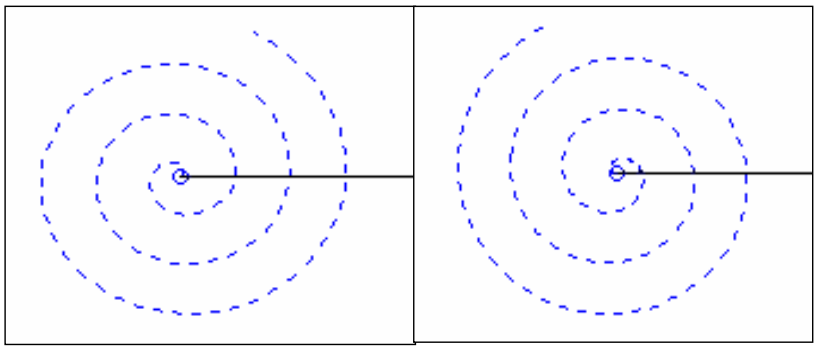

Figure 1: Archimedes' spiral. Left: $a > 0$ anti-clockwise; Right: $a < 0$ clockwise.

Results: Figure 2 shows the designed longitudinal gradient coil pattern and corresponding gradient field homogeneity inside the DSV. It can be seen that the method generates a well-connected coil structure with two continuous curves and a reasonably good gradient field. The

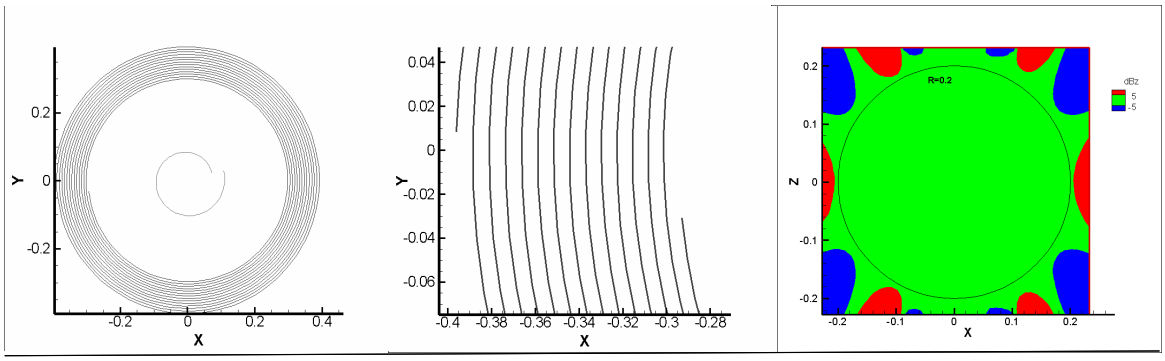

Figure 2: Spiral longitudinal gradient coil. Left: coil pattern in one plane; Middle: Local arrangement of two ends of outer group spiral; Right: the corresponding gradient homogeneity.

inner spiral has only about one turn and the outer spiral has 14 turns. The middle one in the Fig. 2 presents the details of a small part of the outer spiral where the start and the end of the spiral can be seen and the wire gap has been controlled to be not less than 7 mm.

Conclusion: In this work, we have demonstrated that the deformation-space algorithm can be conveniently and efficiently used for spiral gradient coil design. The spiral pattern can be readily manufactured. Both our previous studies for cylindrical systems [2] and the current work on planar systems illustrate the capability of the deformation-space methodology. However, here we only consider a simple regular shape condition for longitudinal gradient coils so the restriction condition is easy to define. In future work we will look at transverse gradient coils and irregular shaped coils.

REFERENCES

1. Turner, R., "Gradient coil design: A review of methods," *Magn. Reson. Imag.*, Vol. 11, 903–920, 1993.
2. Crozier, S., L. K. Forbes, and D. M. Doddrell, *J Magn. Reson.*, Vol. 107(A), 126–128, 1994.

Theory for the Detection of a Single Nuclear Spin in Magnetic Resonance Force Microscopy

Srinivasa Chemudupati and Vladimir Tsifrinovich
Polytechnic Institute of NYU, Brooklyn, NY 11201, USA

Abstract— We performed theoretical computations for the measurement of a nuclear spin state in a paramagnetic atom with Oscillating Cantilever-Driven Adiabatic Reversals (OSCAR) technique in Magnetic Resonance Force Microscopy (MRFM). We use a semi-classical approach, where, the electron-nuclear spin system, with hyperfine interaction, is treated quantum mechanically and the motion of the ferromagnetic particle is treated classically. Our calculations support the idea of the measurement of a nuclear spin state by detection of a single-electron spin.

Asymptotic Analysis of Modes of Composite Defects in Photonic Crystals

L. C. Botten[1], **K. B. Dossou**[1], **C. G. Poulton**[1], **A. A. Asatryan**[1], **S. Mahmoodian**[2], **R. C. McPhedran**[2], **and C. M. de Sterke**[2]

[1]CUDOS and Department of Mathematical Sciences
University of Technology, Sydney, Australia
[2]CUDOS and School of Physics, University of Sydney, Australia

Abstract— We demonstrate the existence of a class of defects in 2D photonic crystals, for which the eigenstates depend only on the defect geometry and not on details like photonic crystal parameters or defect size.

The study of photonic band-gap systems has evolved from an early focus on devising structures with total band gaps, through the creation of defects that are the foundation of useful devices, e.g., cavities, waveguides etc, and, most recently, to the application of unusual and interesting properties, including high dispersion and slow light (including band-edge properties of photonic crystals). In this paper, we consider the properties of the modes of compound defects in two-dimensional (2D) photonic crystals (PC), created by making small perturbations in an otherwise infinite, periodic photonic crystal. Such defect modes are well understood for electrons [1], and since the wave equation and the boundary conditions are similar for the 2D TM polarized electromagnetic case (i.e., with the electric field parallel to the cylinder axes), one might be confident that the behaviour exhibited by electrons should carry over to photons.

Our treatment [2, 3] combines analytic and numerical studies. In the near vicinity of the band edge, we assume the band surface is parabolic, and go on to deduce that the Green function of this 2D system is dominated by the contribution associated with the mode at the band edge — due a logarithmic dependence on the frequency difference between the defect mode ω and the band edge ω_L. This allows us to undertake a first-order perturbation treatment which, for the case of a simple (single) defect, leads to the following result, valid for both TM and TE polarization,

$$\frac{1}{\ln|\omega-\omega_L|} = -\frac{1}{S}\frac{\delta E_{WSC}}{E_{WSC}} = -\frac{1}{S}\frac{\displaystyle\int_{WSC}\delta\varepsilon(\boldsymbol{r}')\|E(\boldsymbol{k}_L,\boldsymbol{r}')\|^2 d^2\boldsymbol{r}'}{\displaystyle\int_{WSC}\varepsilon(\boldsymbol{r}')\|E(\boldsymbol{k}_L,\boldsymbol{r}')\|^2 d^2\boldsymbol{r}'},$$

$$\text{or} \quad |\omega-\omega_L| = A\exp\left(-\frac{S}{\delta E_{WSC}/E_{WSC}}\right), \tag{1}$$

in which the change in frequency $\delta\omega = \omega - \omega_L$ is related exponentially to the relative change in the electric energy $(\delta E_{WSC}/E_{WSC})$ (due to the defect) evaluated over the Wigner-Seitz cell, and where $S = 2/(\omega_L N_L)$ is the sensitivity parameter, involving the density of states N_L.

For compound defects, in which the same perturbation is applied in N multiple unit cells, the dispersion curve of the fundamental mode follows the form in Eq. (1), but in which the defects accumulate, with the energy change term δE_{WSC} scaled by the number of defects N. In addition, other defect modes arise, which are linked with the symmetry of the spatial arrangements of the defects. In the case when the defects are arranged in a regular polygon, it occurs that the matrix of coupling coefficients takes the form of a circulant matrix, the eigenvectors of which are independent of the particular values of the matrix elements. In the examples that we present, this means that the defect state depends only on the defect geometry and not, for example, on the separation of the defects.

The talk will present the theory and provide evidence of the asymptotic results through comprehensive simulations using the fictitious source superposition method [4] and the tight binding method.

REFERENCES

1. Economou, E. N., *Green's Functions in Quantum Physics*, 2nd ed., Springer-Verlag, Berlin, 1983.
2. Dossou, K. B., R. C. McPhedran, L. C. Botten, A. A. Asatryan, and C. M. de Sterke, "Gap edge asymptotics of defect modes in 2D photonic crystals," *Optics Express*, Vol. 15, 4753–62, 2007.

3. Dossou, K. B., L. C. Botten, R. C. McPhedran, C. G. Poulton, A. A. Asatryan, and C. M. de Sterke, "Shallow defect states in two-dimensional photonic crystals," *Phys. Rev. A*, Vol. 77, 063839, 2008.
4. Wilcox, S., L. C. Botten, R. C. McPhedran, C. G. Poulton, and C. M. de Sterke, *Phys. Rev. E*, Vol. 71, 056606, 2005.

Antireflection Coatings for 2D Photonic Crystals: A Rigorous Impedance Based Treatment

L. C. Botten[1], **F. Lawrence**[2], **K. B. Dossou**[1], **and C. M. de Sterke**[2]

[1]CUDOS and Department of Mathematical Sciences
University of Technology, Sydney, Australia
[2]CUDOS and School of Physics, University of Sydney, Australia

Abstract— We show how the concept of impedance can be defined rigorously in terms of PC Bloch modes and then exploit this to accurately and efficiently design multilayer anti-reflection coatings for photonic crystals.

The ability to define an impedance for photonic crystals (PC) would lead to significant improvements in key PC applications, particularly for superprisms, self-collimation, etc. which operate at frequencies outside of, but close to, a bandgap at which surface reflections can be very high. In such cases, the extension of the familiar concept of impedance to PC applications may facilitate the design of anti-reflection (AR) coatings and overcome the drawbacks associated with interface reflection.

The design of multi-layer anti-reflection coatings requires that the reflectance and relative position of the interfaces be tailored to minimize reflection at one or more wavelengths. In thin film optics, this is handled efficiently by encapsulating the optical properties of each layer in an *impedance*. Were this not the case, interface reflection coefficients would have to be recalculated *ab initio*, for each change in any layer. Accordingly, if AR coating design for PCs is to be practicable, it is vital to develop a rigorous definition of impedance for PC layers. To date, two approaches for defining PC impedances have emerged: (a) a generalization of field ratio E/H to account for spatial variation, and (b) inference from a Fresnel reflection coefficient. However, both are empirical and insufficiently rigorous to have confidence in their predictive ability. Here, we present a rigorous definition based on PC Bloch modes, and demonstrate its accuracy and applicability by designing two layer anti-reflection coatings — a computationally difficult otherwise.

We commence with plane wave representations of the electric (E) and magnetic (H) components of Bloch modes, computed by a transfer matrix method [1]. Since the transfer matrix is symplectic, orthogonality relationships of the form $\mathbf{E}^T\mathbf{H} = \mathbf{I}$ where $\mathbf{E}$ and $\mathbf{H}$ are matrices whose columns contain plane wave coefficients of the Bloch mode electric/magnetic fields, allow us to compute Fresnel reflection and transmission matrices between two semi-infinite PCs (PC1 and PC2) using least squares: $\mathbf{R}_{12} = \left(\mathbf{A}_{12}\mathbf{A}_{12}^T + \mathbf{I}\right)^{-1}\left(\mathbf{A}_{12}\mathbf{A}_{12}^T - \mathbf{I}\right)$, $\mathbf{T}_{12} = \mathbf{T}_{21}^T = 2\mathbf{A}_{12}^T\left(\mathbf{A}_{12}\mathbf{A}_{12}^T + \mathbf{I}\right)^{-1}$, $\mathbf{R}_{21} = \left(\mathbf{I} + \mathbf{A}_{12}^T\mathbf{A}_{12}\right)^{-1}\left(\mathbf{I} - \mathbf{A}_{12}^T\mathbf{A}_{12}\right)$, in which $\mathbf{A}_{12} = \mathbf{H}_1^T\mathbf{E}_2$ is a matrix of overlap integrals. Since $\mathbf{A}_{12}\mathbf{A}_{12}^T$ and $\mathbf{A}_{12}\mathbf{A}_{12}^T$ are relative impedances for crossing an interface in the 1→2 and 2→1 directions, it is impossible to define a unique impedance. Instead, there is the more fundamental $\mathbf{A}_{12}$, akin to the "square root" of the impedance. If, we introduce a reference medium (PC0), e.g., free space, and ensure that the mode bases in each region have a common dimension, we can deduce the useful approximation $\mathbf{A}_{12} \approx \mathbf{A}_{01}^{-1}\mathbf{A}_{02}$ (exact at full rank). We thus catalogue $\mathbf{A}_{0j}$ in each region, compute mixed coefficients $\mathbf{A}_{lj}$, and form the Fresnel coefficients.

We apply this technique [2] to design a V (two layer anti-reflection) coating for a square 2D PC in TM polarization. Fig. 1(a) shows the transmittance of an uncoated PC operating, while

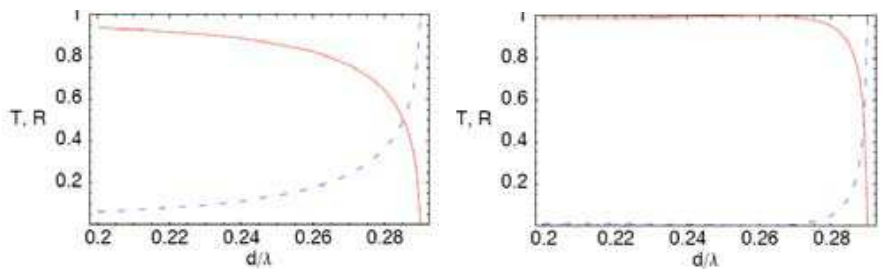

Figure 1: Transmittance (red) and reflectance (blue) curves for (a) the uncoated PC, (b) the 1.1 layer coating for the target frequency $d/\lambda = 0.26$.

Fig. 1(b) shows the transmission optimized for a normalized frequency $d/\lambda = 0.26$ using two single layer coatings. The approach clearly works well and the talk will outlines the method and presents a range of applications, including the slow light regime, in which both scalar and matrix impedances are required.

REFERENCES

1. Botten, L. C., T. P. White, A. A. Asatryan, T. N. Langtry, C. M. de Sterke, and R. C. McPhedran, "Bloch mode scattering matrix methods for modelling extended photonic crystal structures. Part I: Theory," *Phys. Rev. E*, Vol. 70, 056606, 1–13, 2004.
2. Lawrence, F. and L. C. Botten, "Antireflection coatings for 2D photonic crystals using a rigorous impedance definition," *Appl. Phys. Lett.*, in press, 2008.

Session 2P7
Electromagnetic Field Modeling and Inversion and Applications 2

A Method of Aperture Coupling Analysis and Computing Based on the BLT Equation

Jianshu Luo, **Wanjin Wang**, **and Xufeng Zhang**
College of Science, National University of Defense Technology
Changsha 410073, China,

Abstract— Carl E. Baum brought forward the BLT equation based on the multiconductor transmission line network model, which is a effective method to analyse and compute the coupling current/voltage generated at the inner key point of complex electronic system under high power microwave source excitation. Aperture of many geometry configurations can result in electromagnetic field leakage, so we brought forward a method of aperture coupling analysis based on the BLT equation. Different from other numerical methods, we computed the electromagnetic field penetrated in the shield cavity from excitation source by using the electromagnetic wave propagation mode and propagation character of rectangle waveguide or circle waveguide, then we obtained the large supermatrix equation of voltage or electric field intensity related with inner key point of complex electronic system based on the BLT equation, by solving this equation, we can compute the coupling voltage/current at the inner key point of complex electronic system. Last, we gave the coupling voltage/current numerical results of parallel two conductor line in a shield cavity with a rectangle trough under certain high power microwave source excitation.

GL TM Dielectric Parameter Inversion

Ganquan Xie, **Jianhua Li**, **Lee Xie**, **and Feng Xie**
GL Geophysical Laboratory, USA

Abstract— In this paper, we develop a 3D Global and Local Transform (GLT) Electromagnetic (EM) field modeling for the simulation of sphere clocking. The sphere annular cloaking material is anisotropic and dispersive. The conventional FEM and FD methods will meet difficulty in the full 3D simulation of the EM cloaking. We propose the electromagnetic field integral equation of the sphere annular cloaking anisotropic dispersive materials. Based on the EM integral equation, we develop GLT EM modeling for the simulation of the sphere annular EM cloaking which cloaked the central sphere space with any material. The 3D GLT EM cloaking simulation modeling is accurate and fast. The simulation results clearly and accurately show that the EM wave are propagating around the central sphere hole and can not going to inside of the hole. When the EM wave leaved the cloaking annular layer, the EM wave recovers to its original sample and direction without any distortion. The central sphere hole is complete cloaked and hiding from outside EM wave field and outside observer. The 3D GLT EM Sphere Cloaking Software (3DGLTEMSCS) is ready for many applications. We will show the movies of the 3D EM wave propagation around the sphere cloaking in EM Spring in PIERS 2009 in Beijing.

Electromagnetic Modeling of Plasma Etch Chamber for Semiconductor Microchip Fabrication

Zhigang Chen, **Shahid Rauf**, **Kartik Ramaswamy**, **and Ken Collins**
Applied Materials, Inc., Sunnyvale, California 94085, USA

Abstract— In the plasma etch chamber used to fabricate semiconductor microchips, maintaining the symmetry and uniformity of the electric field at the semiconductor wafer level is critical. Very high frequency (VHF) RF sources are attractive for such applications as they improve the efficiency of plasma generation. Electromagnetic effects become important at these frequencies, and etch reactor design requires careful investigation of the electromagnetic field spatial structure in the chamber. In this paper, we apply the finite-difference time-domain (FDTD) method to examine the various electromagnetic effects in the plasma etch chamber and investigate strategies for improved chamber design. These effects include the standing wave effects and asymmetric field distributions that can be caused by asymmetric RF power feed configurations. The FDTD method is formulated in both cylindrical and Cartesian coordinate systems to facilitate the modeling of rotationally symmetric chamber and asymmetric RF feed structures. To accurately and efficiently characterize the coaxial cable delivery of the RF power, the coaxial cable is excited with a TEM mode at discrete frequencies and truncated using the convolutional perfectly matched layer (CPML) absorbing boundary conditions. To decrease the transient time in a single frequency simulation, we choose a new time function based on the Hanning window function to replace the stepped monochromatic excitation. The electric field distribution generated by various RF feed configurations is studied at different VHF frequencies. Based on the FDTD simulations, we have been able to identify a variety of design approaches for ensuring electric field symmetry and uniformity. These design approaches are the foundation of new RF feed designs in our plasma etching chambers.

Analysis of Electric Field on Liquid Zoom Lens Based on Electrowetting

Shunan Shi
Department of Telecommunication, Xidian University, Shaanxi 710126, China

Abstract— Nowadays liquid Zoom lenses in imaging systems are becoming more and more important in both scientific research and industrial products. This paper reports the development and characterization of a novel design of a zoom lens system based on electrowetting. The lens system consists of a fixed cylinder electrode which contained liquid lenses made out of two immiscible liquids. The SnO_2 transparent conductive thin film cylinder electrode for liquid zoom lens was designed and implemented based on ultrasonic spray deposition method. This kind of transparency film can be easily prepared on the surface of glass at high temperature by spraying $SnCl_4$ solution. As for the liquid lenses, we have discussed a method that enables perturbation of the shape of a UV curable a droplet of silicone oil, this droplet of silicone oil confined in an aqueous solution (1% KCl) may works as a liquid lens. The changing applied electric field then controls the shape of the confined silicone oil and the focal length of the liquid lens varies depending upon an applied dc voltage of the cylinder electrode. As the applied electric field distribution affect liquid zoom lens' focus most, so this paper mainly shows the relationship between the external applied electric field of liquid zoom lens and its focus. The applied electric field distribution in both cylinder electrode and planar electrode will be simulated. After compare the different electric field that influence on the focal length of the liquid lens between cylinder liquid lens and planar liquid lens, the optimal distribution of applied electric field have been worked-out finally.

Nanosecond Pulsed Electric Field Treatment Proves Long-Term Effectiveness on Melanoma Metastasis Animal Model

Xinhua Chen[1, 2], **Richard Nuccitelli**[2], **R. James Swanson**[2], **Stephen J. Beebe**[2], **Karl H. Schoenbach**[2], **Shengyong Yin**[1], **Jinjun Li**[3], **and Shusen Zheng**[1]

[1]Department of General Surgery, The First Affiliated Hospital, College of Medicine
Zhejiang University, Hangzhou 310003, China
[2]Frank Reidy Research Center for Bioelectrics, Old Dominion University
830 Southampton Ave., Suite 5100, Norfolk, VA 23510, USA
[3]National Laboratory of Oncogenes and Related Genes
Cancer Institute of Shanghai Jiao Tong University
Shanghai 200032, China

Abstract—

Objectives: The recent use of nanosecond pulsed electric field treatment (nsPEF Tx) is recognized as a new tool for cancer treatment. Here we examine the long-term effectiveness *in vivo* of nsPEF, as a potential therapy in murine malignant melanomas over a 5-month period surviving study.

Methods: Female SKH-1 mice ($n = 36$) were injected with B16-F10 murine melanoma cells and then randomly assigned to 2 groups (17 in nsPEF treatment; 19 as controls). Mice were treated 1–4 times with nsPEF until the tumor shrank to invisible or no imaging manifestation. The control group was identical to treatment group except for nsPEF Tx. Both groups were imaged daily by photographing (1) external tumor surface and (2) transilluminated tumor. A mouse would be sacrificed if (1) the tumor ulcerated or exceeded the specified size limit 2 cm or (2) the tumor diminished to the point of no imaging visibility.

Result: All 17 mice in the treated group survived 3–5 months with the melanomas in complete remission while 14 of the 19 control mice died within 3 weeks due to fast tumor growth. Tumor volumes, survival times and tumor vessel numbers were statistically different ($P < 0.001$) between control and treatment groups. The nsPEF treated group had no metastasis. *In vivo* images and hematoxylin and eosin (H&E) staining revealed nsPEF initially disrupt and finally destroy tumor construction and blood supply. Immunohistochemistry (IHC) and tissue micro-array showed that CD31, a marker for micro vessel density, decreased significantly after nsPEF treatment and western blot analysis confirmed this reduced CD31 protein expression.

Conclusion: The high energy of nsPEF applied to solid tumors can destroy tumor construction and blood supply, but thermal damage to the skin tissue around the tumor. For 5-month long surviving observation no tumor recurrence on the primary site. Therefore nsPEF is a potential therapeutic candidate for solid tumors.

The Use of Ray-tracing and Genetic Algorithms to Optimize a Tapered Anechoic Chamber

S. M. J. Razavi and M. Khalaj-Amirhosseini
College of Electrical Engineering, Iran University of Science and Technology, Tehran, Iran

Abstract— The need for indoor testing of electromagnetic radiating devices, which began in the early 1950s, has led to a number of companies providing chambers and absorber products supporting a range of electromagnetic testing requirements.

Anechoic chambers are used for both emission and immunity testing. There are three major types of anechoic chamber including rectangular, tapered, and double horn. The illumination difference between the rectangular and tapered chambers is illustrated in Figure 1. This is accomplished by forcing the wall image close together at the source end of the chamber. The tapered chamber is an established design concept used for antenna testing below 1 GHz but the ferrite tiles used to line the inside of the chamber are extremely expensive.

This paper describes a method of reducing the number of tiles, whilst ensuring a reliable test environment. The method offered in this paper describes a new technique to reduce the need for full coverage of lining material and optimize the layout of absorbing material tiles to reach a good performance for the chamber and minimize the cost. The offered method has been simulated via computer programs and validated with CST MICROWAVE STUDIO.

In this paper, the ray-tracing method for waves propagation is used for evaluation the reflectivity level of an anechoic chamber, and genetic algorithms are used to optimize the layout of ferrite tile absorber in a partially lined enclosure to produce a best performance.

The results (for rectangular anechoic chamber) show that it is possible to cover just 80% of the surface of the enclosure with ferrite absorber and obtain good agreement by fully lined enclosure with an error of less than 3 percent over the whole test points.

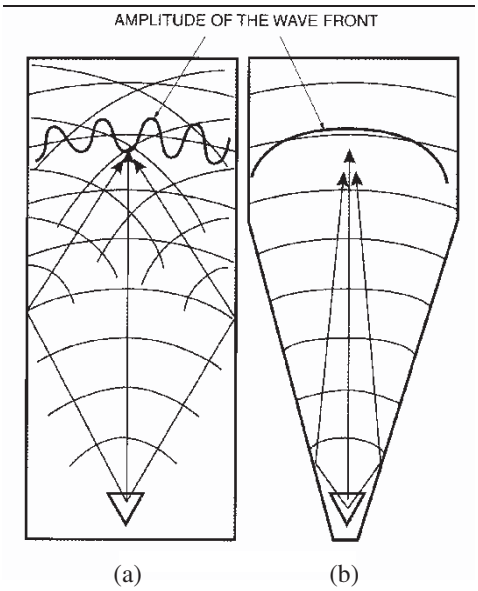

Figure 1: Test region illumination in (a) a rectangular chamber, (b) a tapered chambers.

An Improved Method of Determining Permittivity and Permeability by S Parameters

Hao Zhou, **Guizhen Lu**, **Yanfei Li**, **Song Wang**, **and Yue Wang**
Communication University of China, Beijing 100024, China

Abstract— In the paper, a new method is presented for determining the complex permittivity and permeability of the linear materials by S Parameters. The coaxial line fixture is used to facilitate the measurement of the material's scattering coefficients. With the scattering coefficients, the complex permittivity and permeability of the linear materials as a function of frequency can be determined by the method. The phase ambiguity of the imaginary part of propagator can be resolved by the real part of S_{21}. Compared with former methods, the period of propagator can be got from a series of reflection and transmission S Parameters in the frequency domain, the results of the improved method can be more accurate in the wideband.

Features and Mechanism of Satellite Infrared Anomaly before Ocean Earthquakes

Shanjun Liu[1,3], **Lixin Wu**[1,2], **Qunlong Chen**[3], **and Guoliang Li**[3]

[1]Institute for GIS/RS/GPS & Digital Mine Research, Northeastern University
Shenyang 110004, China
[2]Institute for GIS/RS/GPS & Subsidence Engineering Research,
China University of Mining and Technology, Beijing 100083, China
[3]College of Resources and Environment, Hebei Polytechnic University
Tangshan 063000, China

Abstract— The phenomenon of satellite thermal Infrared anomaly before earthquake has been reported since the late 1980s. The reported abnormal rise of surface temperatures reaches 2–4°C, occasionally higher. Usually, the anomaly appears one month to several days before the earthquake. Several mechanisms or hypothesis have been put forward to interpret the phenomenon: (i) the uplifted underground fluid leads to the emanation of warm gases; (ii) the uplifted well water and changed moisture contents in the soil leads to surface temperature rise; (iii) the diffuse CO_2 emanation causes a local greenhouse effect; (iv) the near-ground air ionization due to enhanced radon emission leads to the condensation of water vapor from the atmosphere and, hence, to the release of latent heat; (v) the thermo-elastic effect and friction heat due to tectonic stress; and (vi) the recombination of stress-activated positive hole in rock face leads to infrared emission.

There are more than five million earthquakes occur every years, and most of it occur in the ocean region. Taiwan and Japan region are located in the jointed position of Eurasia plate and Pacific Ocean plate. There are many earthquakes occurred every year due to the action of plate movements. The Jiji Ms 7.6 earthquake, which happened in Sep. 21, 1999, caused about 3000 people death and about 10000 people injured. After the terrible event, several violent earthquakes had happened in its adjacent area during the past years. For example, the Hengchun Ms 7.2 earthquake happened in Dec. 26, 2006 caused 2 people death and about 50 people injured. Besides, the Noto Peninsula Ms 6.9 earthquake happened in March 25, 2007 caused 1 people death and about 170 people injured. The laws and the omens of the ocean earthquake are of great importance.

In this paper, taking Dec. 26/2006 Hengchun Ms 7.2 earthquake and March 25/2007 Noto Peninsula Ms 6.9 earthquake as the cases of ocean earthquakes, the features of active satellite Infrared anomaly before the earthquakes are analyzed. The result shows that the satellite IR anomaly prior to earthquake is intimately linked with the geology tectonics of neighborhood of epicenter. To study the mechanisms of the infrared anomaly before the ocean earthquakes, a group of physical simulation experiments including the infrared radiation imaging detection on rock fracturing and sliding process, and a group of physical test and numerical simulation experiments on the heat transfer measurement of water, are carried out. Furthermore, the laws and the mechanisms of satellite infrared anomaly before the ocean earthquakes are discussed so as to reach valuable omens of ocean earthquake.

Sumudu Applications to Maxwell's Equations

Fethi Bin Muhammad Belgacem
Faculty of Information Technology, Arab Open University
P. O. Box 830, Al-Ardhia 92400, Kuwait

Abstract— A main attribute of the Sumudu transform lies in its units preserving property. Connected to Fourier, bilateral, two-sided, and ordinary Laplace transforms, the Sumudu is beginning to claim more fame through its unique advantages and pragmatic applications. Here, Maxwell's equations, pertaining to transient electromagnetic planar, (TEMP), waves propagation in lossy media, are shown to yield electric field solutions, through Sumudu transformation.

Inverse Scattering of Two-dimensional Dielectric Objects in Attenuating Media without Phase Information

Yanli Liu, **Lianlin Li**, **and Fang Li**
Institute of Electronics, Chinese Academy of Sciences, Beijing 100190, China

Abstract— An inverse scattering algorithm with intensity-only data to reconstruct both the permittivity and conductivity profiles of two-dimensional dielectric objects embedded in attenuating media is developed within the first Rytov approximation. The proposed method uses measurements of the intensity of the scattered field on a pair of lines shown in Fig. 1, which are beyond the object and perpendicular to the propagation vector s_0, in place of the usual phase measurements of the field.

The proposed algorithm consists of three steps. First, according to

$$\tilde{D}_{\Delta}(\kappa;\, l,\, \Delta) = \frac{i}{\gamma\Delta}\bar{\bar{F}}\left[\kappa\vec{s}_1 + (\gamma - k_c)\,\vec{s}_0\right] e^{i(\gamma-k_c)l}\left\{1 - e^{i[(\gamma-k_c)+(\gamma^*-k_c^*)]\Delta}\right\}$$

where $\tilde{D}_{\Delta}(\kappa;\, l,\, \Delta)$ is constructed from the spatial Fourier transformations Fourier transformations of both the total field intensity on two lines shown in Fig. 1, we can specify the 'pseudo' spatial Fourier transformation $\bar{\bar{F}}[\kappa\vec{s}_1 + (\gamma - k_c)\vec{s}_0]$ of the object function $f(\vec{r},\, \omega)$ over a set of spatial frequencies K that are constrained by the momentum transfer equation $K = k_c(\vec{s} - \vec{s}_0)$. $\vec{s}$ is a unit vector that can assume various directions depending the particular application, and $\vec{s}_0$ is the unit propagation vector of the incident plane wave. The reason for saying it as 'pseudo' spatial Fourier transformation is that the spatial frequencies K are complex valued in the condition of attenuating background where $k_c = k_0\sqrt{\varepsilon_b + i\eta_0\sigma_b/k_0}$ is the complex wave-number and by convention the real part of the wave-number is taken to be positive.

Second, by simultaneously rotating the incident wave field direction and measurement lines, a set of intensity measurements is acquired that can be used to reconstruct the object function.

Third, expand the object function with Fourier series, then

$$\bar{\bar{F}}[\kappa\vec{s}_1 + (\gamma - k_c)\vec{s}_0] = \sum_{m=-M}^{M}\sum_{n=-N}^{N} f_{m,\,n}\int_{-\infty}^{\infty}\int_{-\infty}^{\infty} e^{i(m\omega_1-\kappa)\xi'} e^{i[n\omega_2-(\gamma-k_c)]\eta'}\, d^2\vec{r}'$$

By virtue of regularization of the ill-posed matrix we can specify the object function from the 'pseudo' spatial Fourier transformation $\bar{\bar{F}}[\kappa\vec{s}_1 + (\gamma - k_c)\vec{s}_0]$. From the reconstruction steps given above we can see that this reconstruction algorithm needs only intensity information to rebuild the geometric and electric properties of an object embedded in an attenuating background.

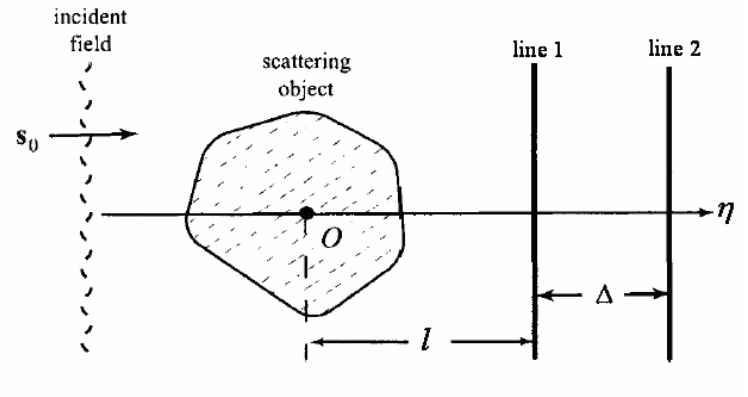

Figure 1: Measurement scheme for inverse scattering of the two-dimensional objects with only intensity measurements.

Session 2P8
Poster Session 3

Geometrical Effect of aperture on Shielding Effectiveness for Conductive Enclosures

A. Keshtkar[1], **A. Kalantarnia**[2], **and H. R. Karami**[3]

[1]University of Tabriz, Iran
[2]University of Applied and Science, Hamedan, Iran
[3]Amirkabir University of Technology, Tehran, Iran

Abstract— One of the environmental pollution is electromagnetic interference. Whereas use of electrical and electronics equipments is increased rapidly, consideration of EMI effects has been became important. Depending on strength and penetration, these interferences can derange electronics equipments in different levels. Shielding by high conductive materials is common and effective protection against EM. Whereas electronic systems have power cables or need ventilations, their protective shields have apertures or slots. By these apertures EM waves penetrate in shielding enclosures. Therefore evaluation of conductive enclosures with apertures is significance. In these cases, parameter that called SE (Shielding Effectiveness) is considered.

Definition of Problem: In this research we want to evaluate geometrical effect of aperture on SE.

The main goal: The main goal in this research is finding critical dimensions based on resonance frequency and new concept, "minus bandwidth" for SE, that is presented.

Solution Method: In this research, we use from RC (Reverberation Chamber) for making electromagnetic environment. Before SE computation we have considered different polarization of transmission antenna in field uniformity. On the basis of IEC 61000-4-21 standard, we present a new technique for increase of field uniformity. In other part, SE has been computed for different geometry of apertures by 3D-FEM. Furthermore in this research SE has been computed for enclosures with multiple apertures.

Dyadic Electromagnetic Green's Function for a Graphene Bilayer

Norman J. Morgenstern Horing[1] and S. Y. Liu[2]

[1]Department of Physics and Engineering Physics, Stevens Institute of Technology
Hoboken, New Jersey 07030, USA
[2]Department of Physics, Shanghai Jiaotong University
1954 Huashan Road, Shanghai 20030, China

Abstract— Graphene, a single-atom-thick two-dimensional planar layer of Carbon atoms in a hexagonal honey-combed lattice composed of two superposed triangular sub-lattices, has been receiving a great deal of attention, both experimental and theoretical, since the first report in 2004 of its unusual device-friendly material properties [1]. These properties include: high mobility at elevated temperature [2], reaching 200,000 cm^2/Vs (over two orders of magnitude higher than that of silicon-based materials, over twenty times that of GaAs, over twice that of InSb); high electron density, about $10^{13}\,cm^{-2}$ in a single subband; long carrier mean-free-path, $L \sim 400$ nm at room temperature, opening the possibility of Graphene-based ballistic devices; stability to high temperatures, ~ 3000 K; quantum Hall effect occurs at room temperature in Graphene; the planar form of Graphene generally allows for highly-developed top-down CMOS compatible process flows, a substantial advantage over Carbon nanotubes that are difficult to integrate into electronic devices and are difficult to produce in consistent sizes and electronic properties. All of these properties make Graphene an extremely promising material for future nanoelectronic devices. Such applications of Graphene are already in progress, including: Graphene *sensors* [3] that can detect minute concentrations (1 part per billion) of various active gasses; Graphene *spin valve* [4]; Graphene *electromechanical resonator* [5] can actuate an electromechanical resonator by an rf-gate-voltage superposed on a dc-voltage applied to the Graphene sheet, or by optical actuation using a laser focused on the sheet; Graphene *field effect transistor* [6] has already been produced; Graphene *quantum interference device* was built to manipulate electron wave interference effects.

The obvious promise of single and multiple Graphene sheets for new and improved electronic devices mandates a serious exploration of their electromagnetic properties. In this paper, we employ techniques that we recently used to develop an exact explicit analytical expression for the dyadic electromagnetic Green's function of a thin excitonic layer [7] (in a study of inhomogeneous radiative exciton polariton modes corresponding to the complex poles of the matrix Green's function). Here, we further extend this technique to determine the structure of the dyadic electromagnetic Green's functions for a bilayer, and apply it to examine Graphene bilayer electromagnetics.

REFERENCES

1. Novoselov, K. S., A. K. Geim, et al., *Science*, Vol. 306, 666, 2004; also see A. H. Castro Neto, et al., arXiv:0709.1163v1[cond-mat. other], Sep. 7, 2007.
2. Morozov, S. V., et al., *Phys. Rev. Lett.*, Vol. 100, 016602, 2008.
3. Schedin, F., K. S. Novoselov, et al., arXiv.cond-mat/0610809 (unpublished).
4. Hill, E. W., A. K. Geim, K. S. Novoselov, et al., *IEEE Trans. Magn.*, Vol. 42, 2694, 2006.
5. Bunch, J. S., et al., *Science*, Vol. 315, 490, 2007.
6. Georgia Tech Research News — http://gtresearchnews.gatech.edu/newsrelease/graphene.html; also, M. C. Lemme, *IEEE Electron Device Letters*, Vol. 28, 282, 2007.
7. Horing, N. J. M., et al., *J. Opt. Soc. Amer. B*, Vol. 24, 2428, 2007.

Open-ended MEMS Probes for Dielectric Spectroscopy of Biological Cells at Radio Frequencies

Hsin-Hung Li[1], **Jen-Yu Jao**[1], **Ming-Kun Chen**[1], **Ling-Sheng Jang**[1], **and Yi-Chu Hsu**[2]

[1]Department of Electrical Engineering and Center for Micro/Nano Science and Technology
National Cheng Kung University, Taiwan
[2]Department of Mechanical Engineering, Southern Taiwan University, Taiwan

Abstract— To increase the accuracy of impedance measurement for cell analysis, recent researches focus on various issues, such as frequency dependency, molecular dimensional normalization and interaction of electrode-electrolyte, in effort to obtain molecular behavior intrinsically not externally. Therefore, this study proposes a coplanar waveguide open-ended probe to perform the cell impedance measurement using MEMS (Micro-Electro-Mechanical Systems) technology at RF (Radio frequency) rather than lower frequency to eliminate the mentioned issues. The open-ended probe combines a microfluidic channel for cell capture and a CBCPW (Compound

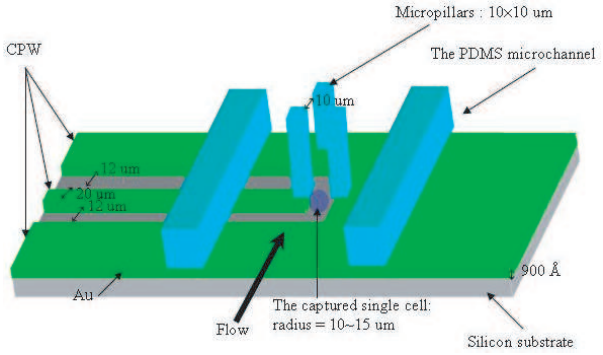

Figure 1: Schematic of coplanar waveguide on silicon.

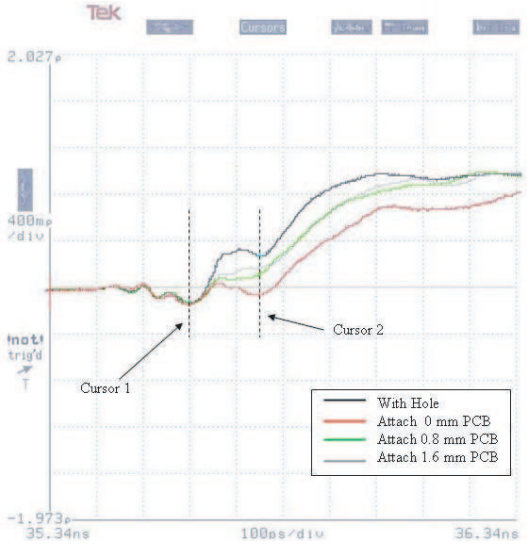

Figure 2: The characteristic impedance verified by TDR. Three different thickness of PCB are used to estimate the capacitance effect on the open ended probe, and a with hole case is used as a comparison.

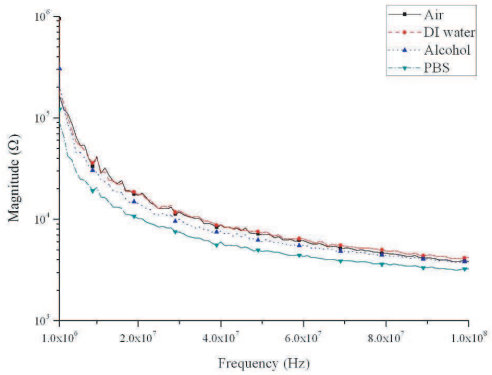

Figure 3: Measurement result of the impedance magnitude of various solution.

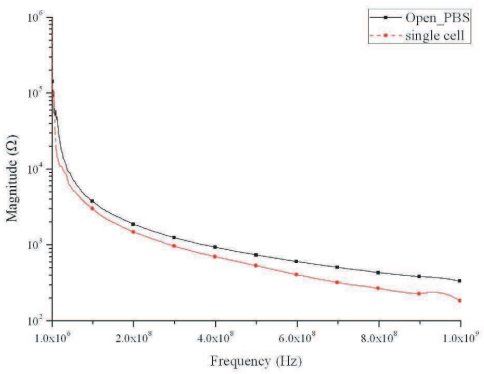

Figure 4: The impedance Magnitude of cells and PBS.

conductor backed coplanar waveguide for biological measurement (as shown in Figure 1)). The probe tip of exciting electrode is designed as 20 μm with respect to the cell radius ($15 \sim 20$ μm). The microfluidic cover is fabricated with PDMS (Polydimethylsiloxane) by silicon mold using lithography. The microfluidic channel and compound CBCPW are bonded after treated by 3-MPTMS (3-mercaptopropyltrimethoxysilane) and employed O_2 plasma. Leaning on the network analysis at radio frequency, quantitative analysis is investigated for the overall measurement device. Verified by TDR (Time-Domain Reflectometer) to tune the characteristic impedance to 50 Ω, conjunction interface of SMA-PCB, fabrication deviation, capacitance effect of substrate with/without engraving hole and various thickness of substrate are adjusted to improve signal-to-noise ratio on measurement and correct the calibration calculation of VNA (as shown in Figure 2). Contact area of solution is theoretically discussed to consider capacitance effect influence. Based on the measurement results, this device actually eliminates the shortcomings of measurement at low frequency for the double layer capacitances, and discriminates different concentration of electrolyte, various solution, and single cell (as shown in Figures 3 and 4).

Ferromagnetism in Substitutionally Mn Doped Ge Nanowires and Their Gate Potential Responsibility

Ungkil Kim[1], **Han-Kyu Seong**[1], **Myoung-Ha Kim**[1], **Il-Su Kim**[1], **Ryong Ha**[1], **Jae-Gwan Park**[2], **and Heon-Jin Choi**[1]

[1]Department of Materials Science and Engineering, Yonsei University
Seoul 120-749, Korea
[2]Nano-materials Research Center, Korea Institute of Science and Technology
Seoul 130-650, Korea

Abstract— Diluted magnetic semiconductors (DMSs), which transform spin-frustrated semiconductors to ferromagnets by magnetic doping, have garnered much interest due to their potential for introducing a spin degree of freedom into semiconductors, an important step toward developing spintronics. Room temperature ferromagnetism in DMSs has been predicted by system based on hole-mediation and reported in many transition metal doped semiconductor system. While ferromagnetism has been reported in many DMSs, there is still significant debate over the possible magnetic impurity phase separation and uncertainty of magnetic interactions. Furthermore, magnetic interactions are uncertain, because most of the transition elements form a trapping potential for holes in these semiconductors, making it difficult to realize hole mediated ferromagnetism. These problems related on the concept of simultaneously manipulating both the charge and spin in a single semiconductor medium pose obstacles to realizing their full potential for practical DMS-based spin devices. For solving these problems, we have investigated the ferromagnetism in Mn doped Ge nanowires because pure Ge nanowire system itself has a p-type characteristic. It is thus an ideal semiconductor to realize hole-mediated ferromagnetism when Mn is properly doped. It is also attractive because of a compatibility with current silicon complementary metal oxide semiconductor (CMOS) processes, and a nanowire system itself has a number of advantages over thin films with respect to studying ferromagnetism in DMSs. They specifically offer thermodynamically stable features and are typically single crystalline and defect-free. They can thus safely exclude the effect of defects and non-uniform distribution of dopants that are typically observed in DMSs prepared by non-equilibrium processing.

We successfully synthesized the single crystalline Mn:Ge nanaowires using a Au catalyst deposited silicon substrates in a germanium tetrachloride ($GeCl_4$) based chemical vapor transport system. For doping, $MnCl_2$ (purity 99.99%) powder is used as a doping source. The typical diameter and length of the Mn:Ge nanowires are from 60 nm to 80 nm and ten micrometers, respectively. The average concentration of Mn doped in these nanowires is c.a. 1.5%. Anomalous x-ray scattering measurement makes it clear that Mn atoms are substitutionally incorporated with the diamond network of host Ge sites. X-ray magnetic circular dichroism spectra at Mn $L_{2,3}$-edges showed that doped Mn has local spin moment with the $3d^5$ electronic configuration above room temperature, clearly meaning that the ferromagnetism originates from doped Mn^{2+} ions. Electrical characterization of a nanowire field effect transistor (FET) showed the real-time gate-dependent hysteresis that is due to formation of the acceptor level of Mn between the electron trap levels of Ge, resulting in Mn hole generation in the band gap. These findings suggest that the ferromagnetic coupling between Mn ions in Mn:Ge nanowires is driven by a carrier-induced mechanism that is mediated by the hole in the Mn band and carrier. Furthermore, we also vertically grew Mn:Ge nanowires and studied the magnetism. The outcomes indicate magnetic anisotropy that would be helpful to realize spin-based electronic.

Azimuth Ambiguity Removal for Multiple Channel SAR

Wei Jing[1], **Mengdao Xing**[1], **Cheng-Wei Qiu**[2], **Zheng Bao**[1], **and Tat-Soon Yeo**[2]

[1]Key Laboratory for Radar Signal Processing, Xidian University, Xi'an 710071, China
[2]Radar and Signal Processing Laboratory, Department of Electrical and Computer Engineering National University of Singapore, 4 Engineering Drive 3, Singapore 117576, Singapore

Abstract— Azimuth ambiguity occurs in synthetic aperture radar systems due to the well known constraint of minimum antenna area, especially at high resolution and wide swath. Thus the swath width can only be expanded at the cost of a coarse resolution or vice versa. In this paper, we use multiple channel system to solve the problem. In order to get image with wide swath and high azimuth resolution, low PRF is adopted. Then azimuth ambiguity is inevitable. The degree of freedom in space offered by multiple channel system make it possible to remove azimuth ambiguity. With the knowledge of space time processing, we present a modified space time domain method (STD) to determine the filter weight vectors. And use the filter weight vectors to process the signal in doppler domain to remove azimuth ambiguities. Our method is verified by simulation. And this approach was applied to the real data, which were collected by an experimental airborne multiple channel SAR system. During the processing of the real data, we found some factor which can influence our processing. Errors in both amplitude and phase are inevitable for real data due to nonideal analog circuits, such as the amplifier, radar mixer, and A/D converter. In addition, the space diversity leads to the difference in antenna patterns of each channel, which also contributes to the final error between channels. The STD processing degrades rapidly with increasing channel error. Finally, the errors between channels are investigated. The methodology to deal with these nonideal factors is discussed as well.

Analysis of Compact Polarimetry and Its Classification Capability

L. Chen[1, 2, 3], **F. Cao**[1, 2], **and W. Hong**[1, 2]

[1]National Key Laboratory of Microwave Imaging Technology, China
[2]Institute of Electronics, Chinese Academy of Sciences, China
[3]Graduate University of Chinese Academy of Sciences, China

Abstract— Compact polarimetry, an choice in the dual-pol SAR system designs, is based on basis measurement. The compact polarimetric SAR transmits a wave on circular or $\pi/4$ oriented linear polarization (the so-called CTLR mode and $\pi/4$ mode), while receives the backward wave on two orthogonal polarizations with phase coherence. Compared with the fully polarimetric SAR system, the compact polarimetric SAR halves its pulse repetition frequency, hence it reduces the average transmit power and increases the swath width, so it is considered to be compliant with low-cost/low-mass constraints of the space-borne polarimetric SAR systems.

In this paper, the varieties of compact polarimetric modes are illustrated at first, and then the relevant principles are analyzed. Although the compact polarimetric mode can be exploited to obtain some advantages of the quad-polarization mode, it cannot replace quad-polarization because it cannot obtain the complete scatter information. It should be analyzed to which extent the polarimetric information is preserved in compact polarimetric SAR data, by means of comparison with the fully polarimetric SAR data. Some analysis tools and indicators, such as scatter plots, Alpha-Entropy plots and root mean squared error are used.

Polarmetric information has been demonstrated to be useful to improve classification performance. Souyris [1] analyzed the potential of classification with compact polarimetric data ($\pi/4$ mode). This paper addresses the quantitative classification capability of compact polarimetric SAR. The classification accuracies of compact polarimetric SAR (CTLR and $\pi/4$ mode) versus fully polarimtric SAR, dual-polarization SAR, e.g., (HH+HV, etc.) are discussed, under the consideration that it can helps selecting polarization modes for various applications.

The experimental compact polarimetric SAR data are derived by transformation of fully polarimetric SAR data. For comparison, the dual-polarization analysis uses the same fully poarimetric datasets.

REFERENCES

1. Souyris, J. C., P. Imbo, R. Fjortoft, S. Mingot, and J. S. Lee, "Compact polarity based on symmetry properties of geophysical media: The $\pi/4$ mode," *IEEE Transaction on Geoscience and Remote Sensing*, Vol. 43, No. 3, 634–646, 2005.

C- and L-Band Radar Observations Acquired during the Corn Growth Cycle for Soil Moisture Retrieval Purposes

A. T. Joseph[1], **R. van der Velde**[2], **P. E. O'Neill**[1], **R. Lang**[3], **and T. Gish**[4]

[1]Hydrological Sciences Branch/614.3, Hydrospheric and Biospheric Sciences Laboratory
NASA/Goddard Space Flight Center, Greenbelt, MD 20771 USA
[2]International Institute for Geo-Information Science and Earth Observation (ITC)
Hengelosestraat 99, P. O. Box 6, 7500 AA Enschede, The Netherlands
[3]Department of Electrical and Computer Engineering, George Washington University
Washington, DC 20052, USA
[4]Hydrology & Remote Sensing Lab, USDA-ARS, Beltsville, MD 20705, USA

Abstract— At the USDA (United States Department of Agriculture)'s Optimizing Production Inputs for Economic and Environmental Enhancement (OPE^3) experimental site in Beltsville (Maryland, USA) a field campaign was conducted to analyze the impact of vegetation on microwave observations. This campaign took place during the corn growth cycle from May 10th to October 2nd, 2002. Ground conditions were observed through in-situ measurements. These measurements included soil moisture, vegetation biomass and surface roughness. Soil moisture of the top 5-cm was measured using a gravimetric sampling technique and portable impedance probes (Delta-T theta probe) at twenty-one sites located at the edge of a 67.1 m × 33.5 m rectangular area situated around the radar footprint. Vegetation biomass was quantified through the destructive measuring technique applied to a 1 m^2 area (approximately 12 plants). During this period the corn crops reached at peak biomass a vegetation water content of 5.1 kg/m^2 and soil moisture values ranging between 0.00 to 0.26 cm^{3}cm^{-3}. The range in biomass and soil moisture conditions observed during this field campaign forms a solid basis for a robust validation of the soil moisture retrieval algorithms.

One of the microwave instruments deployed for this campaign was a multi-frequency (C-band (4.75 GHz) and L-band (1.6 GHz)) and quad-polarized (HH, HV, VV, VH) radar. In the OPE^3 field campaign, radar observations were collected once a week (usually on Wednesdays weather permitting) at 8 am, 10 am, 12 noon and 2 pm. During each data run the radar acquired sixty independent measurements within an azimuth of 120 degrees from a boom height of 12.2 m and at three different incidence angles (15, 35, and 55 degrees). The sixty observations were averaged to provide one backscatter value for the study area and its accuracy is estimated to be 1.0 dB. By averaging of the measurements, row effects are assumed to be reduced.

In this investigation, an analysis is presented of the vegetation effects on C- and L-band radar observations and their sensitivity to soil moisture. It is shown that when the observations are corrected for the effects of vegetation soil moisture uncertainties can be obtained of 0.033–0.064 cm^{3}cm^{-3} for C- as well as L-band depending on the view angle and polarization.

SPECAN Azimuth Pre-processing for Bistatic Spotlight SAR Imaging

Lei Zhang[1], **Meng-Dao Xing**[1], **Cheng-Wei Qiu**[2], **Zheng Bao**[1], **and Wei Jing**[1]

[1]Key Lab for Radar Signal Processing, Xidian University, Xi'an 710071, China
[2]Radar and Signal Processing Lab, National University of Singapore
Singapore 117576, Singapore

Abstract— Modern synthetic aperture radar (SAR) is required to provide imagery with both high resolution and large processing scene. By illuminating the same scene during the data acquisition interval, the spotlight SAR is capable of obtaining high resolution imagery with a considerable scene. The receiving instantaneous Doppler bandwidth depends on the width of the scene in azimuth, which should be lower than the pulse repetition frequency (PRF). In the spotlight mode, the azimuth bandwidth is generally much higher than PRF and azimuth spectral aliasing occurs. Straightforward application of the precise imagery formation, such as the chirp scaling algorithm (CSA), is thus ill-suited. The spectral analysis (SPECAN) convolution is a mature technique widely used in the monostatic scan and spotlight SAR imaging. In SPECAN convolution, a quadratic phase azimuth deramping is used followed by a Fourier transform (FT) to focus the signal in azimuth. The azimuth deramping function is updated with range due to the azimuth focusing depth. One of its advantages is overcoming the azimuth spectral folding effect, as the quadratic phase of the returns is approximately compensated by the azimuth deramping operation. It is well suited for the situation of small range scene and low resolution imaging. In this paper, we expand this idea to support the generation of high resolution imagery over a large scene via bistatic spotlight synthetic aperture radar. An azimuth pre-processor based on SPECAN convolution is presented. The convolution overcomes the Doppler aliasing of the echoed signal, while the frequency domain analytic formula remains the same. Since the spatial characteristics of the returns are preserved, the pre-processor is compatible with conventional focusing approaches. The SPECAN convolution for our preprocessor includes three steps: 1) the product between returned signal (in the range wavenumber domain) and reference quadratic function approximately removes quadratic phase related to the center frequency; 2) taking a curve integration, which can be implemented by a Fourier transform (FT), and it approximately compresses the signal in azimuth, as the azimuth quadratic phase is approximately removed by the deramping; and 3) the residual quadratic phase is compensated, by which the spectrums in the two-dimensional frequency domain is aligned. The convolution is truly a time-frequency transform. By this convolution, the Doppler aliasing is resolved. Then the output data is transformed into the two-dimensional frequency domain, and after a quadratic phase term is removed, we have the preprocessed spectrum. The preprocessed spectrum is aligned and unfolded, its analytic formulation which is the same as conventional formulation of bistatic signal spectrum, can be derived by some current approaches, such as Loffeld's bistatic format (LBF), instantaneous Doppler frequency method, and series reversion. Then conventional bistatic SAR focusing approaches can be directly used to obtain wide-swath SAR image with high resolution. The proposed method is validated by simulated data.

Developing Polarimetric GPR System

Xuan Feng[1], **Li-Li Li**[1], **Li-Min Liu**[2], **and Cai Liu**[1]
[1]College of Geo-Exploration Science and Technology, Jilin University
No. 6 Xi Minzhu Street, Changchun 130026, China
[2]College of Instrumentation and Electrical Engineering
No. 6 Xi Minzhu Street, Changchun 130026, China

Abstract— Most ground penetrating radar (GPR) transmits and receives radio waves with a single polarization. That is, they measure the reflected power returned from the radar's horizontal pulses or vertical pulses. Polarimetric GPR measure the reflected power returned from both horizontal and vertical pulses. By comparing these reflected power returns in different ways (ratios, correlations, etc.), we are possibly to enhance signal and obtain more information on the size, shape, and physical property, etc.

We are developing a stepped-frequency (SF) polarimetric GPR system, which consists of two transmit antennas, two receive antennas, scanning platform, and vector network analyzer (VNA). VNA can generate ultra-wideband electromagnetic signal. Vivaldi antennas are employed in this system, because it is a kind of microstrip antenna, which possesses a wide bandwidth and a high cross-polarization ratio. Four antennas are oriented downwards to the ground and are organized into a tetrahedral square. The measurement method is to alternate between horizontal and vertical polarizations with each successive pulse. That is, first horizontal, then vertical, then horizontal, then vertical, etc. And, of course, after each transmitted pulse there is a short listening period during which the GPR receives both reflected horizontal and vertical polarization radio wave pulses.

We test the polarimetric performance of the GPR system using both copper plate reflector and copper trihedral corner reflector. When the reflector is the copper plate, strong co-polarimetric (VV polarimetric and HH polarimetric) signals are detected and very weak cross-polarimetric (HV polarimetric and VH polarimetric) signals are detected. When the reflector is the copper trihedral corner reflector, strong cross-polarimetric signals are detected.

Polarimetric GPR system may gain additional information about the subsurface characteristics by essentially controlling the polarization of the energy that is transmitted and received. But it should be noted that a polarimetric upgrade does not replace common GPR technology. Rather, it complements it.

Review of GPR Rebar Detection

Xian-Qi He, **Zi-Qiang Zhu**, **Qun-Yi Liu**, **and Guang-Yin Lu**
Info-physics and Geomatics School of Central South University, China

Abstract— Location of reinforcing bars is an important and popular application that has received particular attention with emphasis on the effects of bar size, spacing and depth upon ability to detect individual bars and the problems caused by masking of deeper features. In 1997, Concrete Society published the standard specification for the radar methodology, while in 2003 the Federation of Construction Material Industries of Japan proposed two drafts test standard.

Ground-penetrating-radar is an electromagnetic investigation method. Mostly it is used in reflection mode where a signal is emitted via an antenna into the structure under investigation. The arrival time and the ampleness of reflected signals caused by changes in material properties is recorded and analyzed.

For the reinforcement concrete, concrete could be regarded as isotropy medium in reinforced concrete structure, but the rebar would be regarded as abnormal objects. Radar wave would be shapely reflected at the interface between rebar and concrete because there exists strong abnormality between the two mediums. As a radar antenna is translated across the surface of the concrete a series of signals returning to the receiving antenna can then be presented as the raw results. Signal reflections from reinforcing bars displaying a hyperbolic image format.

Polarization, the direction and amplitude of the electromagnetic field as a function of time and space, can have a significant impact on the GPR response, and is therefore important to consider during data acquisition, processing and interpretation. Investigations have demonstrated the potential of using the polarization characteristics of GPR for defining the sizeshapeorientation and material properties of buried objects.

The scattering properties of rebar are strongly polarization dependent. The backscattered fields from rebar may be strongly depolarized depending on the orientation of the rebar relative to the antennas, and the radius of the rebar compared to the incident wavelength.

The detection of rebar diameter is also important. M. R. Shaw developed a neural network approach to automate estimation the diameter of reinforcing bars by analyzing the data taken with the transducer axis parallel and then orthogonal to the bar using a MLP neural network. It is estimated effectively, but not very accuracy and it is conditionally. Stolte and Nick investigate the relationship between cylinder radius and hyperbola eccentricity for the purpose of migration. S. Shihab also establish the following relation between R and the general hyperbola.

Different GPR signatures may be used for detecting internal corrosion of steel reinforcement within the concrete. Moisture and dissolved chlorides within the concrete attenuate the radar signals that are reflected from embedded rebar. They also decrease their average velocity of the reflected signal resulting in increased arrival times. Generally, lower relative reflection magnitudes and greater travel times are indicative of greater corrosion or deterioration of rebar. The amplitude of rebar reflection in sound section is strengthener the amplitude of the corrosion or deteriorated section.

Magnetic Properties Co, Ni, Fe Nano-wires Electro-deposited into AAO Nano-templates

Insoo Kim, **Bobomurod Hamrakulov**, **and Su Kwon Nam**
School of Advanced Materials and Systems Engineering
Kumoh National Institute of Technology, Gumi, Gyung Buk 730-701, Korea

Abstract— With the changing of fabrication method from micro-size to nano-size, porous alumina templates may play a key role in nano-technology evolution.

Anodic aluminum oxide (AAO) nano-templates have been widely used to prepare nano-wire arrays, because their cylindrical and uniform holes can be easily controlled by the changing of anodizing conditions in the subsequent procedure. There are many other potential applications for porous alumina templates, ranging from the simple fabrication of nano-structure arrays to the more complex processing of components for end-user products such as nano-integrated circuits, gas sensors, also potential applications in high density magnetic memory, giant magneto resistance (GMR) sensors, and magneto-electronic devices.

This study investigate the magnetic properties of several kinds of nano-wires such as Ni, Co and Fe which will be used as a main component in 3D nano-wire arrays for Magnetic Memory Devices or MRAM.

The AAO templates were prepared by a two step anodization process in a mixture phosphoric acid, sulfuric acid and oxalic acid. Ordered nano-wire arrays were prepared in this porous AAO templates using by the electro-deposition in Watt solution and additives. The ordered nano-wires were examined the microstructure, chemical composition and magnetic property by using Field Emission-Scanning Electron Microscope (FE-SEM), Energy Dispersive Spectrometer (EDS), X-ray diffractometer and Vibrating Sample Magnetometer (VSM) techniques, respectively.

Experimental results show that the magnetization reversal mode for multi-layer nano-wires depends on the magnetic layer thickness. The diameters of Ni, Co, and Fe nano-wires in the array were about 100 nm and the length is about 30 μm with the aspect ratio of about 300. Ni, Co and Fe nano-wires have high remanance (Br = 0.00140 emu) and have lower coercivity (Hc = 250 G).

Emissivity Estimation of Microwave Radiometer Calibration Load from Bistatic Measurements

Zhiping Li[1], **Ming Bai**[1], **Jungang Miao**[1], **and George Pan**[2]

[1]Electromagnetics Laboratory, Beijing University of Aeronautics and Astronautics, China
[2]Department of Electrical Engineering, Arizona State University, USA

Abstract— Microwave radiometers need to be calibrated by the loads with known emissivity and physical temperatures. In theory, the emissivity can be obtained by differential scattering coefficient measured in the full-space. Recently, there is increasing interest in utilizing reflectivity (either with or without global integration) to dynamically measure emissivity and improve the accuracy of the emissivity measurement. However, the full-space bistatic measurement system is often too expensive and inconvenient to be implemented in practice. Alternatively, the monostatic radar has been utilized to measure the back scattering from the calibration load, which could only provide a rough estimation on the emissivity. In order to realize the high accuracy of emissivity bistatic measurement as well as reducing its complexity, the bistatic scanning in the two principal planes with some approximation is introduced. The purpose of this study is to give an assessment on accuracy of the bistatic emissivity measurement system in obtaining the emissivity characterization of the calibration load.

In this paper, the measured emissivity of the calibration load is conducted, taking into account of some reasonable approximation. The calibration load, utilizing in the bistatic measurements, is constructed with a periodic metallic pyramid array coating absorbing material and is applied in the radiometer thermal/vacuum calibration. Several types of antennas, working on $10.65\,\mathrm{GHz} \sim 36.5\,\mathrm{GHz}$, are implemented as the sending and receiving antennas, inculding the spot-focusing lens antenna, conical antenna and choked antenna, etc. Moreover, based on the obtained emissivity in various measurements, an optimized bistatic measurement system with the optimized combination of the proper receiving antenna, orbit radius and sampling points can be implemented to provide more accurate emissivity measurement.

The Application of FDTD Method to UHF Electromagnetic Wave Analysis in Gas Insulated Switchgear

Xianglong Zhang and Yi Wang
School of Electrical Engineering, Beijing Jiaotong University, China

Abstract— Gas Insulated Switchgear (GIS) have the advantage of covering the smaller area, running more safely and reliably, less constant-maintenance, overhauling in a longer period and so on, so it develops very quickly and gets more and more application when it came out. Partial discharge(PD) phenomena is the most common characteristic before insulation breakdown in GIS. The UHF-method, as its name suggests working in the frequency range (300 MHz–3 GHz) has been widely used to obtain more exact PD signals. A lot of practical experience with the UHF-method has been reported in the past. But for the effective application in practice and the correct interpretation of the measurement results, it is necessary for us to research the characteristics of UHF electromagnetic waves. By UHF method of measuring GIS partial discharge, the big problem is to mark apparent discharge quantity. Moreover, it is hard to distinguish what the principal influence upon magnitude of UHF signals is. To solve them, wave-guide cavity configuration is utilized and FDTD method, which is a numerically exact technique to solve Maxwell's equations with given boundary conditions, is used to simulate transmission of PD (partial discharge) electromagnetic wave in wave-guide. The paper also introduce how to make a model structure setting and a subdivision setting with XFDTD. Therefore, factors influencing UHF signals are analyzed, which include position, dimension, PD current amplitude and pulse shape of PD source. From the experimental data, we can draw many useful and progressive conclusion. Such as, UHF singles have direct relation to the distance of PD source. Meanwhile, when the pulse width is constant, the square root of UHF single energy is direct ratio to the amplitude of the real pulse. According to UHF output signals, original PD pulse can be estimated, all of which will contribute to marking GIS partial discharge and studying mechanism of PD further.

Detection of Pseudo-singularities by Wavelet Technique for Extracting Leaky and Bulk Waves in Piezoelectric Material

D. Benatia[1], **T. Fortaki**[1], **and M. Benslama**[2]

[1]Département d'Electronique, Faculté des Sciences de l'Ingénieur
Université de Batna, Algeria
[2]Département d'Electronique, Faculté des Sciences de l'Ingénieur
Université de Constantine, Algeria

Abstract— In this paper, we propose a new numerical method for bulk and leaky detection of an acoustic microwave signal during the propagation of acoustic microwaves in a piezoelectric substrate (Niobate of Lithium $LiNbO_3$) excited by interdigital transducers. Moreover, we know that the Fourier transform presents a global spectral study of signal, this is not interesting if we want to study a signal locally and know its features in a more precise manner. By the use of wavelet transform, we can reduce this drawback. The originality of the wavelet transform consists of the local analysis of signal singularities (or signal pseudo-singularities) where abrupt events appear and hence access to hidden information by using the scale of this transform as up scaling parameters. These pseudo-singularities (correspond to abrupt variations) inform us of presence of bulk and leaky waves in piezoelectric materials.

For this, we based our analysis on the tensorial piezoelectric equations. These equations have been used thoroughly in the study of surface acoustic waves (SAW) or Rayleigh wave. In theses equations we have a very important parameter called acoustic velocity. Its importance is due to the fact that its variation begets the variation of the other parameters. On the other hand, it permits to provoke pseudo-singularities at the level of the wave. Some results are given, they lead to some interesting conclusions.

Furthermore, this transform proved its efficiency in many application, such as signal processing and the analysis of waves in microstrip structures. Hence, it can play an important role in the modelling of pseudo-singularities in acoustoelectronic.

Surface Latent Heat Flux (SLHF) Prior to Major Coastal and Terrestrial Earthquakes in China

Jinping Li[1,2], **Lixin Wu**[1,3], **Huanping Wu**[4], **Shanjun Liu**[3], **and Jieqing Yu**[1]

[1]Institute for GIS/RS/GPS & Subsidence Research, China University Mining & Technology
Beijing, China
[2]Department of Surveying and Engineering, Heilongjiang Institute of Technology
Harbin, China
[3]Institute for GIS/RS/GPS & Digital Mine Research, Northeastern University
Shenyang, China
[4]National Meteorological Centre, China Meteorological Administration
Beijing, China

Abstract— Satellite thermal infrared (TIR) imaging data have been proposed to map large linear structure and fault systems in the Earth's crust and to monitor geophysical phenomena associated with major earthquakes. TIR radiation anomaly can provide early warming information for impending earthquakes, and is considered to be a new precursor of shocking. The satellite TIR remote sensing, for the advantages of large observation area and short observation period, is becoming a promising technique for detecting earthquake and for monitoring tectonic activities. Surface Latent Heat Flux (SLHF), as an atmospheric parameter proportional to the evaporation from the Earth's surface, is dependent on meteorological parameters such as surface temperature, relative humidity, wind speed and underlaying surface.

Recently, analysis to SLHF from the epicentral areas of several coastal earthquakes in the world was found be possible to provide meaningful anomaly. The spatial-temporal anomalies of satellite SLHF, observed several months to several weeks before shocking, were suggested to be pre-seismic signals. The results of SLHF anomaly investigations in coastal regions had indicated that: 1) the SLHF anomaly is sensitive to earthquake above Ms5.0, 2) the SLHF anomaly usually appears from $2 \sim 19$ days before and disappears quickly after the shocking, 3) the anomalous behavior of SLHF is not found for terrestrial earthquakes in India.

In this paper, the SLHF behaviors of the epicentral areas of one coastal earthquake and three terrestrial earthquakes are analyzed. The spatial distribution of the SLHF behavior, from the NCEP-NCAR reanalysis data of the IRI/LDEO Climate Data Library (http://iridl.ldeo.columbia.edu/), prior to each event is studied in a 15° by 15° area with the pixel covering the epicenter. The data set is in resolution of global grid $1.8° \times 1.8°$, and the daily values of a months before and after shocking from 1991 to 2007 are taken for analysis. Since SLHF is affected by the winds, tides and monsoon, it is spatial-temporally changed. To analysis the SLHF anomaly prior to a shocking, the perennial spatial-temporal influences are considered as background trend, and the SLHF data of 16 years (exclude the year shocking) are used to calculate the mean values of SLHF for each pixel as perennial trend. To analyze the SLHF behavior of the epicenter and the adjacent regions of shocking, the procedures are as following:

1) The mean value and the standard deviation (the same month and the same day of 16 years) are calculated so as to get the background trend of each pixel.

2) The daily anomaly index of each pixel can be calculated as:

$$AI = \left(SLHF(r,t) - \overline{SLHF(r)}\right) / \sigma_{SLHF}$$

$SLHF(r,t)$ is the daily value of SLHF, $\overline{SLHF(r)}$ and σ_{SLHF} are the mean value and standard deviation of each pixel respectively;

3) If $AI > 1.5$, the pixel is considered to be an anomaly pixel;

4) The group of the anomaly pixels is considered to be a potential seismic active region.

The analysis shows that the maximum increase of SLHF was found to be $2 \sim 17$ days before shocking. It was suggested that SLHF together with other meteorological data such as surface temperature, water vapor, cloud liquid water and outgoing long wave radiation can be used for early warning of costal and territorial earthquakes in China.

Temperature Dependable Microwave Dielectric Model for Moist Soils

V. L. Mironov and S. V. Fomin
Kirensky Institute of Physics, SB RAS Krasnoyarsk, Russia

Abstract— Dielectric models of the soil and vegetation are an essential part in the algorithms used for data processing with regard to the problems of radar and radiothermal remote sensing. At present, the semiempirical dielectric model (SDM) proposed in [1] has become a routine instrument for predicting permittivities of moist soils in the microwave band. Wide spread occurrence of this model is partly caused by its direct linkage to conventional agro physical variables describing moist soils, which are the input parameters sufficient for dielectric predictions. At the same time, once the SDM was developed on the bases of limited dielectric measurements what really needs to be analyzed about this model is its accuracy when being applied to the soil types and used in the range of temperatures falling out of the domains encountered in [1]. In this context, the SDM was recently shown [2] to generate predictions for an assemblage of soils measured in [3] with three times as large error compared to that it does in the case of the prototypal soils. Meanwhile, the impact of temperature variations on the SDM accuracy has not been analyzed yet.

In this paper, such a task was formulated and accomplished using the soil dielectric data for a Silty Sand soil acquired in [3] at the temperatures of 10, 20, 30 and 40°C, over the frequency ranges from 45 MHz to 26.5 GHz, with a wide range of moistures. First, the predictions for dielectric constants and loss factors measured in [3] were calculated using the SDM, in which the temperature impact was taken in accordance with the formulas attained in [4] for the dielectric constant of soil water. The error calculated in terms of standard deviation of predictions, made with the SDM, was found to be as large as that at the temperature of 20°C, which was considered in [2]. Therefore, in this paper, the methodology of [2] was used to ensure dielectric predictions at all the temperatures, that is, 10, 20, 30 and 40°C, with much less error than the SDM does.

Moreover, for all the spectroscopic parameters used in the methodology of [2] there were obtained regression dependences on the temperature, relating to both the bound and free soil water types. Particularly, in the case of low frequency dielectric constant limit, the Clausiuss-Mossotii equation was taken as a theoretical regression equation describing temperature dependence, with the volumetric expansion coefficients and the starting dielectric constants becoming the only parameters accounting for temperature dependence. As to the relaxation time, for its theoretical regression equation, there was taken the Debye relaxation formula, with the activation energies and entropies of activation being determined through fitting procedure in order to ensure the relaxation time dependence on the temperature, for both soil water types. Finally, the temperature dependences for conductivities of both soil water types were well fitted with linear functions to provide for the starting conductivities and conductivity incrementations as regression parameters.

As a result, an assemblage of parameters consisting of volumetric expansion coefficients, starting low frequency dielectric constants, activation energies, entropies of activation, starting conductivities, and conductivity incrementations were derived with the use of dielectric data measured in [3]. These, in conjunction with dry soil complex dielectric constant and maximum bound water fraction, were found to be an all-sufficient set of parameters to make possible predictions of complex dielectric constants of moist soil as a function of frequency, volumetric moisture, and temperature. The error of these predictions in terms of standard deviation was found to be 3 times as small compared to the ones obtained with the SDM.

REFERENCES

1. Dobson, M. C., F. T. Ulaby, M. T. Hallikainen, and M. A. El-Rayes, "Microwave dielectric behavior of wet soil — Part II: Dielectric mixing models," *IEEE Trans. Geosci. Remote Sensing*, Vol. 23, No. 1, 35–46, 1985.
2. Mironov, V. L., L. G. Kosolapova, and S. V. Fomin, "Soil dielectric model accounting for contribution of bound water spectra through clay content," *PIERS Online*, Vol. 4, No. 1, 31–35, 2008.
3. Curtis, J. O., C. A. Weiss, Jr., and J. B. Everett, "Effect of soil composition on dielectric properties," Technical Report EL-95-34, December 1995.
4. Stogryn, A., "Equation for calculation the dielectric constant of saline water," *IEEE Trans. Microwave Theory Thech.*, Vol. 19, 733–736, 1971.

Investigation on Rolled Dipole Antenna Footprint for Ground Penetrating Radar (GPR)

Sugihartono[1], **Yuyu Wahyu**[2], **Adit Kurniawan**[1], **and A. A. Lestari**[3]
[1]School of Electrical Engineering and Informatics
Bandung Institute of Technology, Indonesia
[2]Research Center for Electronics and Telecommunications
Indonesian Institute of Science, Bandung, Indonesia
[3]International Research Centre for Telecom and Radar-Indonesian Branch (IRCTR-IB), Indonesia

Abstract— Ground Penetrating radar systems has been utilized for the detection and imaging of buried underground objects using electromgnetic waves, in 10 MHz to 1 GHz frequency range. In GPR terminology antenna footprint is defined as a collection of peak-to-peak amplitudes of the transmitted pulse in a horizontal plane. Antenna footprint indicates the shape and size of the area illuminated by the antenna on the ground surface or subsurface. Its importance lies in the fact that it determines the cross-range resolution of the GPR. If the size of the footprint is larger than the cross section of the target, it gives rise of clutter as the antenna illuminates not only the target but also the surrounding medium. Clutter can be maximally reduced if the size of the footprint is comparable with the cross section of the target. However, this is not always easily achieved as targets usually have different dimensions while the size of the antenna footprint remains fixed. In this work we investigate the GPR footprint of rolled dipole antenna operating at 600 MHz.

First phase of this research is the design of a rolled dipole antenna. The antenna is designed for a monocycle ground penetrating radar pulse which normally at 600 MHz operating frequency has relatively long dimension of 98 cm. 600 MHz frequency is suitable for GPR low resolution applications. A rolled dipole structure has been developed to obtain reasonable length of 25 cm. To obtain better pulse response in terms of ringing suppression, Wu-King resistive loading method has been applied. In each dipole arm, 65 resistors is used with 1 cm separation between resistor pair. The pulse response of this antenna is then simulated using FDTD method.

The second phase is the implementation of the rolled dipole antenna with single layer PCB using FR4 material. The third phase is the antenna parameter measurements; three antenna parameters has been measured, i.e., input impedance, monocycle pulse response and antenna GPR footprint. A special, indirect method of measurement setup has been developed to obtain the monocycle pulse response, while separate antenna measurement range is utilized to measure the antenna GPR footprint. In the pulse response measurement, S_{21} paremeter is measured with vector network analyzer; this frequency domain measurement result is then processed by a post processing software to obtain the time domain pulse response. The pulse response measurement shows significant improvement in the ringing reduction when Wu-King profile resistive loading is utilized in the dipole, leaving the main pulse representing a good GPR pulse.

In the antenna GPR footprint measurement a fixed transmitting antenna is buried in sand with 17 cm depth, while the rolled dipole antenna acts as receiving antenna, moving in the x-y directions with 3 cm clearance from the ground. The measured footprint is represented as contours of normalized peak-to-peak voltage (0 dB, -10 dB, -20 dB and -30 dB). The measured footprint dimension for 0 dB level is around 30×60 cm. It is concluded that the rolled antenna dipole is suitable for GPR application as the dimension of the antenna footprint is comparable with commonly found buried object dimensions. The next development using this type of antenna is antenna array realization to obtain adaptive GPR footprint.

Monioring of Satellite Thermal Pattern in the Azores Current Area

Shigehisa Nakamura

Kyoto University, Japan

Abstract— This is an introduction of the sea surface thermal pattern monitored by the satellites for the problems in the Azores Current area of the northeastern Atlantic. This thermal pattern is a typical sample case of the author's model for monitoring of satellite thermal pattern. The author has noted on this satellite monitoring in order to realize a ocean front evolution. Nevertheless, he could not have demonstrated any typical case of ocean thermal pattern for the sea surface temperature observed in-situ along a leg directly on the sea.

Professor Martins of the University of Azores introduced one of the typical case of the author's interest. The Professor Martins and her group has promoted oceanographic process in relation to fisheries problems to find the satellite thermal pattern noted above.

The author here gives you a note on the satellite thermal pattern found in the area of the Azores which supports the author's model for the ocean front evolution.

This note might give us a key to promote an application of the satellite monitoring for the ocean surface to promote the related research.

Radiometric Measurements of Maximum Bound Water Fraction in Soil

V. L. Mironov, **P. P. Bobrov**, **and A. S. Yascheko**
Kirensky Institute of Physics, SB, RAS, Krasnoyarsk, Russia

Abstract—

Introduction: So far, the radiometric remote sensing of moist soils has been focused on retrieving only volumetric soil moisture [1], with almost no studies having been developed to remotely sense hydrological properties of soils, such as the maximum bound water fraction (MBWF) retained by a given type of soil. This situation can be partly attributed to using the semiempirical dielectric model [2–4] in the majority of these studies, in which the MBWF was not explicitly introduced as a distinct parameter. At the same time, recently, the MBWF as a hydrological soil parameter was proposed to be used in the generalized refractive mixing dielectric model (GRMDM) for moist soils [5], which made possible, at least in principle, deriving this parameter from radiometric or radar remote sensing data. In this paper, a method of radiometric measurements of the MBWF is considered, using the GRMDM.

Measurement Methodology: First, on the basis of GRMDM parameters analyzed for a variety of soils in [6, 7], there were established regression relationships between the real, n_t, and imaginary, κ_t, parts of the complex refractive index regarding the soil with volumetric moisture equal to the MBWF, W_t, on the one hand, and the MBWF itself, on the other hand. These equations can be expressed in the following form: $n_t(f,T,W_t) = a(f,T)W_t + b(f,T)$ and $\kappa_t(f,T,W_t) = c(f,T)W_t + d(f,T)$, with the wave frequency, f, and physical temperature, T, being parameters.

Second, with the use of the GRMDM, the emissivity for moist soils was expressed through the real and imaginary parts of the complex refractive index at a given total volumetric moisture, W, as follows: $n(f,T,W_t,W_\Delta) = n_t(f,T,W_t) + [n_\Delta(f,T) - 1]W_\Delta$ and $\kappa(f,T,W_t,\ \Delta W) = \kappa_t(f,T)+\kappa_\Delta(f,T)W_\Delta$, where $n_\Delta(f,T)$ and $\kappa_\Delta(f,T)$ are respectively the real and imaginary parts of the complex refractive index of soil water, which is the exceeding of the total soil moisture, W, over the MBWF, $W_\Delta = W - W_t$. The emissivity of moist soil, χ, depends on the complex refractive index via the Fresnel reflection coefficient. As a result, it appears to be a known function of four arguments, $\chi = \chi(f,T,Wt,W_\Delta)$, provided the functions $n_\Delta(f,T)$ and $\kappa_\Delta(f,T)$ are determined from some other consideration.

Third, to derive the MBWF, it was proposed in this paper to measure the emissivity of thawed soil directly before freezing and after freezing, with the depth of frozen layer being equal to, or greater then, the depth of sensing and the temperature of soil being confined in a narrow range around the freezing point.

Finally, the values $n_t(f,T,W_t)$ and $\kappa_t(f,T,W_t)$ were supposed to undergo only small variations with the temperature, so that they were estimated at the temperature of 20°C with the use of data presented in [6]. While, in the case of thawed soil, the values of $sn_\Delta(f,T) = n_q(f,T)$ and $\kappa_\Delta(f,T) = \kappa_q(f,T)$ were calculated using the Debye formula for liquid water, according to [8], and, in the case of frozen soil, they were taken to be equal to the real and imaginary parts of the complex refractive index of ice: $n_\Delta(f,T) = n_c(f,T)$ and $\kappa_\Delta(f,T) = \kappa_c(f,T)$. In the final analysis, the system of two transcendental equation was obtained, $\chi_q = \chi_q(f,T,W_t,W_q)$ and $\chi_c = \chi_c(f,T,W_t,W_c)$, which is to be solved with regard to the MBWF, W_t, and liquid water fraction, $W_q = 0.917W_c$, using χ_q, and χ_c measured as input values.

Validation Of Results: To validate the proposed technique the emissivities at 6.0 GHz for two soil plots having different values of W_t were measured in the thawed and frozen conditions. Simultaneously, the MBWFs and bulk volumetric moistures for both soil types were determined as reference values with the use of other laboratory and field measurements. The difference between the reference values and the values measured with the proposed method was found not to exceed 10%.

REFERENCES

1. Wigneron, J.-P., Y. Kerr, P. Waldteufel, et al., "L-band microwave emission of the biosphere (L-MEB) model: Description and calibration against experimental data sets over crop fields," *Remote Sensing of Environment*, Vol. 107, 639–655, 2007. www.elsevier.com/locate/rse

2. Dobson, M. C., F. T. Ulaby, M. T. Hallikainen, and M. A. El-Rayes, "Microwave dielectric behavior of wet soil — Part II: Dielectric mixing models," *IEEE Trans. Geosci. Remote Sensing*, Vol. 23, No. 1, 35–46, 1985.
3. Peplinski, N. A., F. T. Ulaby, and M. C. Dobson, "Dielectric properties of soils in the 0.3–1.3 GHz range," *IEEE Trans. Geosci. Remote Sensing*, Vol. 33, No. 3, 803–807, 1995.
4. Peplinski, N. A., F. T. Ulaby, and M. C. Dobson, "Correction to 'Dielectric properties of soils in the 0.3–1.3 GHz range'," *IEEE Trans. Geosci. Remote Sensing*, Vol. 33, No. 6, 1340, 1995.
5. Mironov, V. L., M. C. Dobson, V. H. Kaupp, S. A. Komarov, and V. N. Kleshchenko, "Generalized refractive mixing dielectric model for moist soils," *IEEE Trans. Geosci. Remote Sensing*, Vol. 42, No. 4, 773–785, 2004.
6. Mironov, V. L., "Spectral dielectric properties of moist soils in the microwave band," *Proc. IGARSS'04*, Vol. 5, 3474–3477, Anchorage, USA, 2004.
7. Mironov, V. L., L. G. Kosolapova, and S. V. Fomin, "Soil dielectric model accounting for contribution of bound water spectra through clay content," *PIERS Online*, Vol. 4, No. 1, 31–35, 2008.
8. Ulaby, F. T., R. K. Moor, and A. K. Fung, *Microwave Remote Sensing, Active and Passive*, Vol. 3, Artech House, Dedham, MA, 1986.

New Method of Permanent Scatterers Selection for Changing City

Shibo Qu[1,2,3], **Yanping Wang**[1,2], **Wen Hong**[1,2], **and Fang Cao**[1,2]
[1]National Key Laboratory of Microwave Imaging Technology, China
[2]Institute of Electronics, Chinese Academy of Sciences, China
[3]The Graduate University of Chinese Academy of Sciences
No. 19, Bei Si Huan Xi Lu, Beijing 100190, China

Abstract— Permanent scatterers interferometry is a technique to exploit the temporal and spatial characteristics of interferometric signatures collected from point targets to accurately map surface deformation histories, terrain heights, and relative atmospheric path delays. It is a complicated technique composed several processing steps: PS selection, pixel triangulation, phase unwrapping.... Each step can affect the monitoring results to some extent. Among these steps, permanent scatterers selection is the first one. It will strongly affect the other following processing steps. So it is most important in PS technique.

Many methods has been developed for selecting permanent scatterers. These selection methods are based on pixel amplitude stability, pixel phase stability, and also spatial coherence. Coherence has been widely used as an indicator of interference quality. So the spatial coherence is used to obtain the maximum likelihood estimator of the coherence magnitude, and provides an estimation of the accuracy of the pixel's phase for each interferogram that is not dependent on the number of images available. The required estimation window decreases the spatial resolution, also can cause loss of isolated scatterers which could be selected with the amplitude or phase criteria. On the other hand, the selection based on amplitude presented by Ferretti estimates the phase standard deviation of every pixel from its temporal amplitude stability, which preserves the maximum spatial resolution of the images and allows detecting single isolated scatterers smaller than a resolution cell. These two methods are widely used by all researchers, and proved their effectiveness in most tests.

But these traditional PS selection methods have limitations, because they have not taken new building or house-breaking into consideration. The selection methods using amplitude stability and spatial coherence are not considered the temporal value variation, often mis-selecte new buildings as permanent scatterers. But in many areas, especially in many developing cities, many buildings are newly built, rebuilt, or disappeared for reprogramming the city. Cities change almost every year. There two pictures following are examples of the changing city.

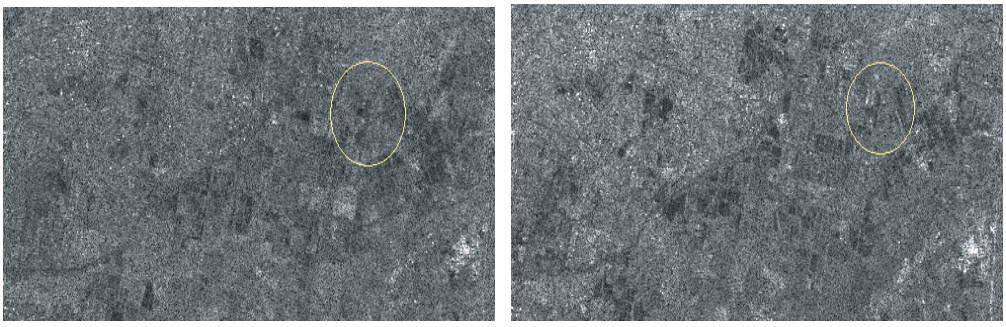

Figure 1: An example of an area from nothing to a new building.

Since China is a developing country, many cities there are changing in a high speed. Tianjin is one typical city of them. We applied permanent scatterers interferometric technique to the subsidence monitoring of Tianjin urban area. 17 ASAR images of this area, from April 25 in 2003 to June 3 in 2005, have been used. We get 16 interferograms in this experiment. Our PS selection method can choose out permanent scatterers with high reliability, solving the problem caused by changing city buildings.

Simulation System Development of Infrared Remote Sensing Images: HJ-1B Case

Gui-Jun Yang, **Qin-Huo Liu**, **Qiang Liu**, **and Xing-Fa Gu**
State Key Laboratory of Remote Sensing Science
Institute of Remote Sensing Application, Chinese Academy of Sciences
P. O. Box 9718, Beijing 100101, China

Abstract— Satellite image simulation is one of the key methods to check the expected performance of the satellites before they launched or when satellites can not provide images in other time. In order to provide a useful tool to analyze whether the payload of HJ-1B (a small satellite of the environment-monitoring constellation) is enough, we develop a simulation system for the infrared cameras, which consists of four bands including NIR band (0.75–1.10 μm), SWIR (1.55–1.75 μm), MIR (3.50–3.90 μm) and TIR (10.5–12.5 μm). The spatial resolution of NIR and SWIR band is 150 meter, while 300 meter for the MIR and TIR band. The sensor is an optical-mechanics multi-scanning system with maximum scanning degree of 29 degree.

The image simulation system consists of four main modules: 1) surface radiation transfer models including PROSPECT, SAILH, CUPID, GOMS model and etc; 2) Atmosphere transfer model MODTRAN is used to build simpler equations and setup Look Up Tables for different sun-viewer positions; 3) Sensor models including spectral response model, geometrical distortion model, MTF response model, noise model and A/D model; 4) Potential application models including the fire monitoring model and drought assessment model. We first use ASTER Products (one scene in Beijing, China, 2001.5.19) and ground measure data (2001, SHUNYI, Beijing) to get the ground true knowledge such as the land use map, vegetation cover and LAI and so on. We divided the land cover into 5 main classes: crop, forest, urban, rural residential area and water and inversed importance parameter for surface radiation transfer models according to their classes. Lacking of accurate BRDF models for urban, we have to adapt GOMS model to inverse urban and rural building density and height. For plant-soil system, we choose CUPID model (Norman, 1979) to simulate directional brightness temperature. For urban and rural area, we used statistics model to predict component temperature, e.g., the building temperature and road temperature, and used adapted GOMS model to simulate the angle effect of brightness temperature. Taking into accounts of the temporal importance, we maybe make use of new model based on physiology, physics and chemistry to inverse indispensable parameters in different time which are input above models, such as LAI, water content in soil and so on.

Among the four bands, the MIR range image simulation is the most difficult task because we have to consider the reflectivity and emissivity. We haven't found the published case to simulate the MIR band so far. We used Extended SAIL model and jerlhoff law for infrared range to simulate emissivity and BRDF for plant-soil system. For other classes, we didn't account for the directional effect in MIR band at present time. At present, we have finished the simulation system using Microsoft Visual C++ 6.0. The system was well designed because all modules are relatively independent, and easy to be extended. It can well describe the angle-dependant effect due to the swing of scanning system. For example, from the simulated image, we can find the "double eye" phenomenon at the edge. Also, the MTF blurring is significant. The potential application models are still under development. At the next step, we will make the simulation system general for different infrared sensors, different temporal images.

Time-domain Double Diffraction for UWB Signals

Peng Liu, **Jianying Wang**, **and Yunliang Long**
Department of Electronics & Communication Engineering
Sun Yat-Sen University, Guangzhou 510275, China

Abstract— Time-domain UWB multipath propagation channel model can characterize the most important electromagnetic wave propagation mechanisms, such as reflection, diffraction and transmission. Among these mechanisms, diffraction is the main reason causing the pulse distortion due to the consequences of the frequency dependency. Although a lot of papers have addressed the single time domain diffraction issues, in real environment the transmitted signals usually undergo multiple diffractions before it reaches the receiving antenna. So it is necessary to extend the single diffraction solution to multiple-diffraction. In this work the time-domain double diffraction case which can be extended to multiple-diffraction is investigated and a heuristic time-domain uniform theory of diffraction (TD-UTD) coefficient for a double wedge obstruction is presented. This coefficient is obtained by taking the inverse Laplace transform of an available and accurate corresponding frequency domain (FD) solution that incorporates higher-order diffraction coefficient. Furthermore, based on the fact that UTD is an asymptotic solution, it is valid only for early-time wavefronts and, consequently, to assume that the Fresnel reflection coefficients do not vary with frequency. This early-time approximations are employed to heuristically establish the double TD-UTD coefficients for the analysis of the diffraction by dispersive obstacle wedge. Finally, some numerical examples illustrating the utility of this TD-UTD are presented and to validate the proposed solution, comparisons are made between the TD solution and the numerical inverse fast Fourier transform (IFFT) of the FD solutions. The results show a very good agreement between the two solutions with the TD solution being more efficient in computation time and more straightforward for the analysis of pulse distortion.

Forward Scattering Indicatrix of Aircrafts In L and S Frequency Bands

V. A. Gromov and G. S. Sharygin
Tomsk State University of Control Systems and Radioelectronics
40 Lenin Ave., Tomsk 634050, Russia

Abstract— It is known that the radar cross section (RCS) of targets not transparent for radio waves depends both on the target aspect angle and on the two-position angles in horizontal and vertical planes (α and β). In case of bi-static barrier radar location, when α and β are about 180 degrees, RCS rapidly grows reaching $4 \cdot \pi \cdot (S/\lambda)^2$, where S is the target cross section and λ is the wave length. The value of this RCS does not depend on the target form and absorbing covering.

Unfortunately, publications do not provide data describing real targets RCS dependence on the angles α and β.

The authors simulated wave diffraction on eight aircrafts of Russia, USA, France and Great Britain basing on Huygens-Fresnel approximation. The target was described as an obstacle — the aircraft projection in the plane perpendicular to the illumination.

The simulation allowed to calculate the scattering indicatrixes (diffraction lobes of re-illumination) of targets in the horizontal and vertical planes and in 10 cm and 30 cm frequency bands for bi-static angles of (180 ± 55) degrees and different target aspect angle. Part of these data is given in the table. They illustrate the practical value of the simulation.

The aircraft type	F-22, USA		B-2, USA	
Target aspect angle	0	90	0	90
Wave length 10 cm				
RCS (dB/m^2) for $\alpha = \beta = 180°$	48	63	66	66
Indicatrix width at the level −3 dB (degr.):				
In horizontal plane	±2.5	±0.8	±0.5	±0.4
In vertical plane	±4	±2.5	±4	±1.5
Indicatrix width at the level −20 dB (degr.):				
In horizontal plane	±13	±6	±10	±3
In vertical plane	$> \pm 60$	±20	±27	±10
Wave length 30 cm				
RCS (dB/m^2) for $\alpha = \beta = 180°$	38	53	58	56
Indicatrix width at the level −3 dB (degr.):				
In horizontal plane	±8	±2.5	±1.5	±1.5
In vertical plane	±13	±7.5	±12	±4
Indicatrix width at the level −20 dB (degr.):				
In horizontal plane	±42	±18	±28	±7
In vertical plane	$> \pm 60$	$> \pm 60$	$> \pm 60$	±33

Coherent Terahertz Smith-Purcell Radiation from a Two-section Model

Zongjun Shi[1], **Ziqiang Yang**[1], **Feng Lan**[1], **Xi Gao**[1], **Zheng Liang**[1], **and D. Li**[2]

[1]Institute of High Energy Electronics, University of Electronic Science and Technology of China
Chengdu, Sichuan 610054, China
[2]Institute for Laser Technology, 2-6 yamada-oka, suita, Osaka 565-0871, Japan

Abstract— This paper presents a two-section model to produce beam bunching and obtain coherent Terahertz (THz) Smith-Purcell (SP) radiation. A schematic diagram of the two-section model is given in Fig. 1. Based on the mechanism of Cherenkov oscillator, a continuous beam is effectively bunched in the first section without external signal. In the second section, the coherent THz Smith-Purcell (SP) radiation is stimulated by the bunched beam interacting with open grating. From Fig. 2, we note the bunching is evident the particle-in-cell (PIC) simulations show that the strongest radiation is observed at 51° and the radiation frequency is 194 GHz at the simulation parameters, as illustrated in Fig. 3. In this scheme, the periodic bunches are generated by itself instead of the input signal, and the cost of the source will be reduced.

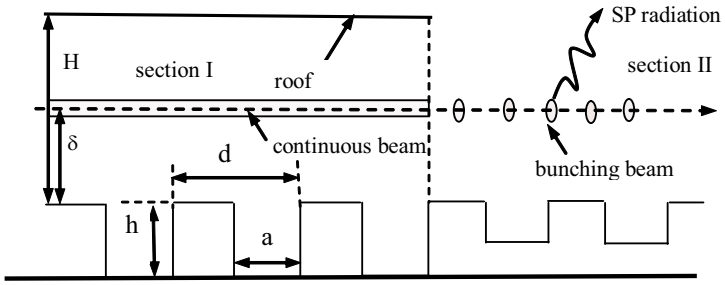

Figure 1: Schematic diagram of the physical model.

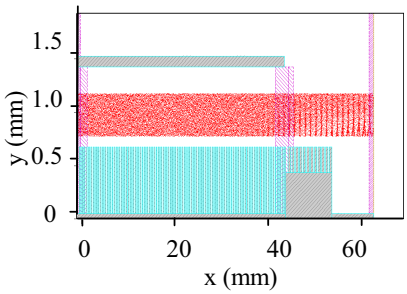

Figure 2: Density of electrons in the x-y plane at 3 ns, bunching is evident.

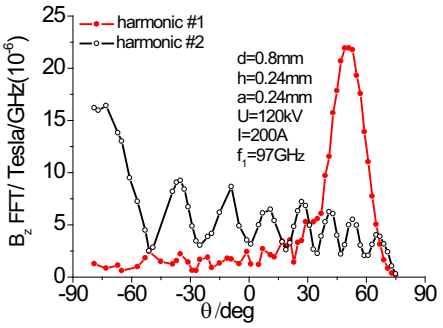

Figure 3: The peak of FFT amplitude of B_z as a function of angle.

Modeling the Electromagnetic Scattering from a Dielectrically Filled Groove Using the Method of Auxiliary Sources

Naamen Hichem and Taoufik Aguili
Département Technologie de l'information et de communications
Ecole nationale d'ingénieurs de Tunis, Tunisia

Abstract— Scattering of electromagnetic waves from a 2D groove filled with a lossy dielectric in an infinite conducting plane is modeled using the method of auxiliary sources. The scattering structure contain two mediums (perfectly electric conductor and the lossy dielectric) considered as strongly coupled.

According to the MAS, in order to approximate the electromagnetic fields in each domain, fictitious current sources verifying the Helmoltz equation in the considered domain are introduced and distributed around the physical boundary.

Three bases of AS must be taken into account, the satisfaction of the respective boundary conditions between the dielectric, the PEC and the upper free space model the strong coupling affecting the structure.

Therefore, the scattered field is the superposition of the scattered fields by the two mediums.

The implementation code was realized with Mathematica, and the numerical results (RCS, near field) agree very well with references.

The MAS in conjunction with the EM coupling model is able to analyze the scattering from finite gratings.

REFERENCES

1. Shubitidze, F., H. T. Anastassiu, and D. I. Kaklamani, "An improved accuracy version of the method of auxiliary sources for computational electromagnetics," *IEEE Transactions on Antennas and Propagation*, Vol. 52, No. 1, January 2004.
2. Anastassiu, H. T., et al., "Electromagnetic scattering analysis of coated conductors with edges using the method of auxiliary sources (MAS) in conjunction with the standard impedance boundary condition (SIBC)," *IEEE Transactions on Antennas and Propagation*, Vol. 50, No. 1, January 2002.
3. Kaklamani, D. I. and T. Hristos, "Aspects of the method of auxiliary sources (MAS) in computational electromagnetics," *IEEE Transactions on Antennas and Propagation*, Vol. 44, No. 3, June 2002.
4. Harrington, R. F., *Time Harmonic Electromagnetic Fields*, McGraw-Hill, New York, 1961.
5. Volakis, J. L., et al., *Finite Element Method for Electromagnetics, Antennas, Microwave Circuits and Scattering Applications*, 132.
6. Volakis, J. L., et al., *Finite Element Method for Electromagnetics, Antennas, Microwave Circuits and Scattering Applications*, 296.
7. Morgan, M. A., et al., "Mode expansion solution for scattering by a material filled rectangular groove," *Progress In Electromagnetics Research*, PIER 18, 1–17, 1998.

Analysis of Two-dimensional Scattering by a Finite Periodic Array of Conducting Cylinders Using the Method of Auxiliary Sources

Naamen Hichem and Taoufik Aguili
Département Technologie de l'information et de communications
Ecole nationale d'ingénieurs de Tunis, Tunisia

Abstract— According to the method of auxiliary sources and for conducting bodies, the scattered field is the summation of radiated fields by a set of auxiliary sources distributed on a fictitious inner contour near the physical one and satisfying the Helmoltz equation outside the considered domain. The satisfaction of boundary conditions leads to the unknown complex currents. The MAS applied to model coupling between a finite array of infinitely and parallel conducting cylinders, illuminated by a monochromatic plane wave. The coupling modeled by the mutual satisfaction of the boundary conditions just on the collocation points of every cylinder.

In the purpose to decrease the computational cost and to alleviate calculus, we suppose that every cylinder is coupled only to the eight neighbouring cylinders. The partial coupling implementation full simplifies the global matrix expression.

The comparison between the results obtained (RCS, field pattern) according to global and partial coupling for the same array reveals good agreement with references.

In this paper, we validate the MAS applicability for the global coupling and the approximation validity for the partial coupling for a finite array of conducting cylinders.

REFERENCES

1. Anastassiu, H. T., et al., "Electromagnetic scattering analysis of coated conductors with edges using the method of auxiliary sources (MAS) in conjunction with the standard impedance boundary condition (SIBC)," *IEEE Transactions on Antennas and Propagation*, Vol. 50, No. 1, January 2002.
2. Kaklamani, D. I. and T. Hristos, "Aspects of the method of auxiliary sources (MAS) in computational electromagnetics," *IEEE Transactions on Antennas and Propagation*, Vol. 44, No. 3, June 2002.
3. Shubitidze, F., H. T. Anastassiu, and D. I. Kaklamani, "An improved accuracy version of the method of auxiliary sources for computational electromagnetics," *IEEE Transactions on Antennas and Propagation*, Vol. 52, No. 1, January 2004.
4. Harrington, R. F., *Time Harmonic Electromagnetic Fields*, McGraw-Hill, New York, 1961.
5. Elsherbeni, A. Z. and M. Hamid, "Scattering by parallel conducting circular cylinders," *IEEE Transactions on Antennas and Propagation*, Vol. 35, No. 3, March 1987.
6. Henin, B. H., A. Z. Elsherbeni, and M. Al Sharkawy, "Oblique incidence plane wave scattering from an array of dielectric cylinders," *Progress In Electromagnetic Research*, PIER 68, 261–279, 2007.
7. Hichem, N. and T. Aguili, "Analysis of two-dimensional scattering by a periodic array of conducting cylinders using the method of auxiliary sources," *PIERS Online*, Vol. 4, No. 5, 2008.

Single Scattering Properties of Ice Particles in mm/sub-mm Waveband: Effects of Refractive Index and Shapes

Xinxin Xie and Jungang Miao
Electromagnetics Laboratory, School of Electronic Information and Engineering
Beijing University of Aeronautics and Astronautics, Beijing 100191, China

Abstract— Cirrus clouds play an important role in the radiation balance of the earth. Their distributions and microphysical parameters are vital to the global circulation models. Many kinds of ice crystals exist in cirrus clouds, including considerable amount of non-spherical shapes, like plate, pyramid, polyhedron, solid or hollow column, bullet and bullets aggregation, etc. The scattering and absorption characteristics of these ice particles are essential to perform radiative transfer in order to retrieve cirrus cloud parameters. Analytical and numerical methods, which are tested to be valid and accurate for regular shapes like spheroids etc., have been applied for calculating scattering properties of particles for remote sensing. For particles of irregular shapes, scattering properties can be solved by volume integral equation methods such as discrete dipole approximation (DDA), etc.

The scattering properties of an ice particle are determined by many factors, for example, the refractive index, the shape, the size parameter, the orientation and so on. In this paper, the effects of refractive index and shapes for single scattering properties are investigated. Mie theory is employed to simulate the effects of refractive index for ice spherical particles in mm/sub-mm waveband. The DDA method is also introduced to calculate the scattering properties of Koch fractals (first generation), bullets and their aggregation. Assuming that the ice particles are all randomly oriented, we have computed the average scattering results for several target orientations of each shape. Measurements are in process to validate the accuracy of computational results using DDA method. Based on the calculation and measurement results, we expect to have an insight into the scattering properties of ice particles.

Radio-frequency Characteristics of a Printed Rectangular Helix Slow-wave Structure

Chengfang Fu, **Yanyu Wei**, **Wenxiang Wang**, **and Yubin Gong**
National Key Laboratory of High Power Vacuum Electronics
University of Electronic Science and Technology of China, Chengdu 610054, China

Abstract— A new type of printed rectangular helix slow-wave structure (SWS) is investigated using the field-matching method and the electromagnetic integral equations at the boundaries. The radio-frequency characteristics including the dispersion equation and the coupling impedance for transverse anti-symmetric (odd) modes of this structure are analysed. The numerical results agree well with the results obtained by the EM simulation software HFSS. It is shown that the dispersion of the rectangular helix circuit is weakened, the phase velocity is reduced after filling the dielectric materials in the rectangular helix SWS. As a planar slow-wave structure, this structure has potential applications in compact TWTs.

Investigation of the Dielectric-loaded Folded Waveguide Traveling-wave Tube Amplifier

C. Q. Zhang, Y. B. Gong, H. R. Gong, Y. Y. Wei, and W. X. Wang
National Key Laboratory of High Power Vacuum Electronics of UESTC, Chengdu, China

Abstract— The cold-test characteristics of the dielectric-loaded folded waveguide traveling-wave tube (FWTWT) amplifier are investigated theoretically and the Pierce small-signal theory is employed to confirm the results. For the purpose of analysis, the discussions are separated into symmetric case and unsymmetrical case according to the loading form of the dielectrics. The calculation results indicate that both of them can significantly reduce the phase velocity and flatten the dispersion curve, especially the unsymmetrical form. However, loading dielectric in an unsymmetrical form will lead to a large decrease in the on-axis interaction impedance, thus it is recommended to use the symmetrical form. It is further found that when the thickness of the dielectric is small, i.e., $h_1/a \leq 0.1$, the interaction impedance is slightly affected for the variation on dielectric constant. The linear theory for the Q-band dielectric-loaded FWTWT amplifier shows that the bandwidth is increased from 15.08% to 27.03% and the operating voltage is decreased from 20.5 kv to 18.6 kv.

ACKNOWLEDGMENT

Project supported by the National Natural Science Foundation of China (Grant No. 60532010, 60401005).

Analysis of the Varying-period Folded Waveguide

Ao Xu, **Wen-Xiang Wang**, **Yan-Yu Wei**, **and Yu-Bin Gong**
National Key Laboratory of High Power Vacuum Electronics
School of Physical Electronics, University of Electronic Science and Technology of China
Chengdu 610054, China

Abstract— The dynamic velocity tapering is widely used to improve the efficiency of the beam-wave interaction in the slow wave structure of the TWTs. As an application of this technique, the varying-period folded waveguide has a series of the advantages such as the mode selection and the wide bandwidth. In this paper, the principle of taking a space harmonic to synchronize with the electron beam in the whole interaction process in a varying-period folded waveguide is present, the varying-period folded waveguide is analyzed by the simulation software, and the efficiency improvement is obtained.

ACKNOWLEDGMENT

Project supported by the National Natural Science Foundation of China (Grant No. 60532010, 60401005).

The Anisotropy of Dielectric Losses in Single Crystal of Al_2O_3 and SiO_2

Victor N. Egorov, **Vladimir L. Masalov**, **and Ivan B. Ozhogov**
East-Siberian branch of FSUE "VNIIFTRI", Russia

Abstract— The precision measurements of dielectric loss tangent were performed in single crystals Al_2O_3 and SiO_2 at X- and K-bands. The "whispering gallery" modes HE (quasi-E) and EH (quasi-H) with two polarizations in cylinder (disc) open dielectric resonator (DR) [1, 2] was used for longitudinal ($||$) and transverse ($\perp$) dielectric loss tangent (tgδ) measurements in uniaxial crystals. In measurements the disc specimen (open DR) with parallel orientation of optical and geometrical axises was mounted on copper post in central part of disc where the electromagnetic field of "whispering gallery" modes is negligible small. The heater and temperature sensor of DR were placed on this copper post. The excitation of HE_{n11} and EH_{n11} modes was performed by microstrip line at frequencies of X-band and by rectangular dielectric waveguide in K-band. The measured open DR was exiting as directional coupler in "running wave" regime. The azimuthal mode index n should be big sufficient for providing of negligible small radiation losses compared dielectric losses. In this condition the components tg$\delta_{||}$, tg$\delta_{\perp}$ are calculating as [3]

$$\mathrm{tg}\delta_{||} = \frac{Q_{0E}^{-1} \cdot K_{1E\perp}^{H} - Q_{0H}^{-1} \cdot K_{1E\perp}^{E}}{K_{1E||}^{E} \cdot K_{1E\perp}^{H} - K_{1E||}^{H} \cdot K_{1E\perp}^{E}} \qquad \mathrm{tg}\delta_{\perp} = \frac{Q_{0H}^{-1} \cdot K_{1E||}^{E} - Q_{0E}^{-1} \cdot K_{1E||}^{H}}{K_{1E||}^{E} \cdot K_{1E\perp}^{H} - K_{1E||}^{H} \cdot K_{1E\perp}^{E}}$$

where Q_{0E}, Q_{0H}-unloaded quality factor of HE_{n11} and EH_{n11} modes with negligible small radiation losses, $K_{1E||}^{E,H} = W_{1E||}^{E,H}/W_{\Sigma}^{E,H}$, $K_{1E\perp}^{E,H} = W_{1E\perp}^{E,H}/W_{\Sigma}^{E,H}$; $W_{1E||}^{E,H}$, $W_{1E\perp}^{E,H}$-electrical energy of field components $E_{||}$, $E_{\perp}$ in dielectric disc; $W_{\Sigma}^{E,H}$-complete energy of resonance. The upper indexes are corresponding to HE_{n11} (quasi-E) and EH_{n11} (quasi-H) modes. Difference between Q_{0E}, Q_{0H} for $K_{1E||}^{E}+K_{1E\perp}^{E} \approx K_{1E||}^{H}+K_{1E\perp}^{H}$ point to an anisotropy of tgδ due to the relationships $K_{1E||}^{E} \gg K_{1E\perp}^{E}$, $K_{1E||}^{H} \ll K_{1E\perp}^{H}$ in DR.

The measurements of quality factor Q_{0E}, Q_{0H} of sapphire and single crystal quartz "whispering gallery" DR show the significant difference between quasi-E and quasi-H modes. The experimental results of tg$\delta_{||}$, tg$\delta_{\perp}$ for SiO_2 at room temperature are given in table.

HE_{n11}					EH_{n11}				
n	f, GHz	$Q_{0E} \cdot 10^{-4}$	$K_{1E||}^{E}$	$K_{1E\perp}^{E}$	n	f, GHz	$Q_{0H} \cdot 10^{-4}$	$K_{1E||}^{H}$	$K_{1E\perp}^{H}$
18	33.63221	5.46	0.8752	0.0994	18	35.37845	3.45	0.0317	0.9302
$\mathrm{tg}\delta_{||} = 1.75 \cdot 10^{-5}$					$\mathrm{tg}\delta_{\perp} = 3.06 \cdot 10^{-5}$				

Experiments with isotropic DR show the same quality factor at close resonant frequencies for both polarization. Measurement results of tg$\delta_{||}$, tg$\delta_{\perp}$ for Al_2O_3 at X- and K-bands and SiO_2 at K-band in temperature range 293–363 K are given in paper.

REFERENCES

1. Vzyatyshev, V. F., V. S. Dobromyslov, V. L. Masalov, et al., *Tr. Mosk. Energ. Inst.*, No. 360, 51, 1978 (in Russsian).
2. Egorov, V. N. and I. N. Mal'tseva, "Asimuthal oscillation in anisotropical dielectric resonator," *Electron. Tekh., Ser.1: Electron. SVCh*, No. 2, 36, 1984 (in Russsian).
3. Egorov, V. N., "Resonance methods for microwave studies of dielectrics (review)," *Instruments and Experimental Techniques*, Vol. 50, No. 2, 143–175, 2007.

The Sensor for Local Dielectric Measurements on Non-flat Surfaces

Boris A. Vtorushin, **Victor N. Egorov**, **and Elena Yu. Tokareva**
East-Siberian branch of FSUE "VNIIFTRI", Russia

Abstract— The problem of homogeneity of dielectric properties in radio-transparent shields is need of sensor for local microwave dielectric measurements. Local measurements make it possible to solve a number of problems that sometimes do not require the measurement locality as such but that cannot be solved via conventional methods, e.g., a problem of measuring the dielectric parameters of ready articles of intricate shapes with curvilinear surfaces. In this case, the measurement locality must be such that, within the limits of the tested region, it would be possible to disregard the surface curvature at or introduce simple corrections on the basis of known radii of curvature at the measurement point. A frequent additional requirement is one-way access to an object and promptness of measurements.

The use of a hollow coaxial resonator with an open end allows a high measurement locality to be attained [1]. A theory of a sensor of dielectric parameters based on an open-end coaxial line is considered in [2]. An insignificant value of the relative changes in the resonance frequency imposes high requirements upon the thermal stability of the coaxial resonator's resonance frequency.

The highest measurement locality with high thermal stability can be achieved in quarter-wavelegth coaxial dielectric resonators (CDR) made from thermally stable high-Q ceramics. The nonmetallized end surface of such a CDR is sensitive to the dielectric parameters of the sample that is in contact with (or close to) this surface. In this case, the relative shift of resonance frequency may be (1-3)$\cdot 10^{-2}$.

The sensor for testing the homogeneity of the permittivity of radio-transparent shells at one-way access to the measured object has been developed on the basis of a CDR. This device is based on two generators in the form of transistor amplifier, the positive feedback loop of which includes a quarter-wavelength CDR specifying the oscillation frequency. One generator is the measurement channel and other is the reference channel. The sensitive surface of measurement CDR is open for access and reference CDR is shielded from external influence. The output signals of reference and measurement generators are fed to a mixer, at which an intermediate-frequency (IF) signal is obtained. If the measurement sample is absent, the oscillation frequency of the measurement generator is lower than the frequency of reference generator about IF $F_0 \approx 3\,\mathrm{MHz}$ in order to preclude their mutual synchronization and passage of the IF signal through zero during measurements. The area of sensitive CDR's end surface with their permittivity 20 is $4 \times 4.5\,\mathrm{mm}$. The device operating frequency is about 1.5 GHz. After the IF signal is amplified, its frequency F_ε is measured. The experimental dependence of measured value ε from relative frequency shift $x = (F_\varepsilon - F_0)/F_0$ was approximated as

$$\varepsilon = 1 + a_1 x + a_2 x^2 + a_3 x^3 + \ldots$$

The correction of measurement results for the curvature of studied sample surface has been obtained via expansion of the dependence $\varepsilon\,(R_1, R_2)$ into a series in terms of small parameters a/R_1, b/R_2, where $R_{1,2}$ are the radii of surface curvature in measured region along walls a and b of a rectangular CDR.

REFERENCES

1. Moschuring, H. and I. Wolff, *IEEE MTT-S Int. Microwave Symp. Dig.*, Vol. 7–12, 187, 1984.
2. Baker-Jervis, J. and M. D. Janezic, *Mat. Res. Soc. Simp. Proc.*, Vol. 347, 215, 1994.

Investigation on Wideband Filters Using Parallel Coupled Microstrip Resonators

Shinya Kohma[1], **Toshiaki Kitamura**[1], **Yasushi Horii**[2], **and Toshitaka Kojima**[1]

[1]Graduate School, Kansai University, 3-3-35, Yamate-cho, Suita-shi, Osaka 564-8086, Japan
[2]Graduate School, Kansai University, 2-1-1, Ryozenji-cho, Takatsuki-shi, Osaka 569-1095, Japan

Abstract— Since the Federal Communications Committee (FCC) authorized the unlicensed use of UWB frequency spectrum for short range and high speed wireless communication, wideband devices have been attracting much attentions. Recently, various kinds of wideband filters have been proposed. In these filters, attenuation poles play an important role in order to achieve sharp wide passband characteristics.

In this study, wideband filters using parallel coupled resonators are proposed. The resonators are composed of microstrip lines on which both ends are terminated. Using admittance parameters, we evaluate the scattering parameters of the proposed filters. We also investigate the characteristics through numerical simulations by means of the FD-TD method.

24 GHz Power Amplifier Design in 0.13 μm CMOS Technology

Se-Hwan Choi, **Jin-Sup Kim**, **Kyu-Bok Lee**, **and Kyu-Ho Park**
Korea Electronics Technology Institute, Republic of Korea

Abstract— Automotive collision warning systems have been developing in the license-free 24 GHz industrial, scientific and medical (ISM) band. Recently, FCC released the 22 GHz∼29 GHz ultra wideband (UWB) for vehicular radar applications. Many research about 24 GHz components and modules progresses steadily. Most papers use GaAs HEMT and SiGe BiCMOS. However, one of the problems of these processes is the high cost. Thus, low cost CMOS has become an alternative process in the millimeter-wave band. Specially, a CMOS power amplifier at 24 GHz is the most challenging part to be implemented because CMOS technology has the characteristics of low power gain and lossy on-chip passive elements inherently. In this paper, 24 GHz power amplifier in 0.13 μm CMOS technology is proposed. By using the three stage cascade structure, the power amplifier has a maximum output power of 6.8 dBm and the output P1 dB of 3.24 dBm. The supply voltage is 1.2 V and the current source is used for gate bias instead of voltage reference. The dissipated current is 90 mA totally. The proposed PA has the maximum power added efficiency (PAE) of 2.8% but this is owing to wire-bonding effect for connecting with package. The performance of PA will be improved by using on-chip proving test or flip chip bonding afterward.

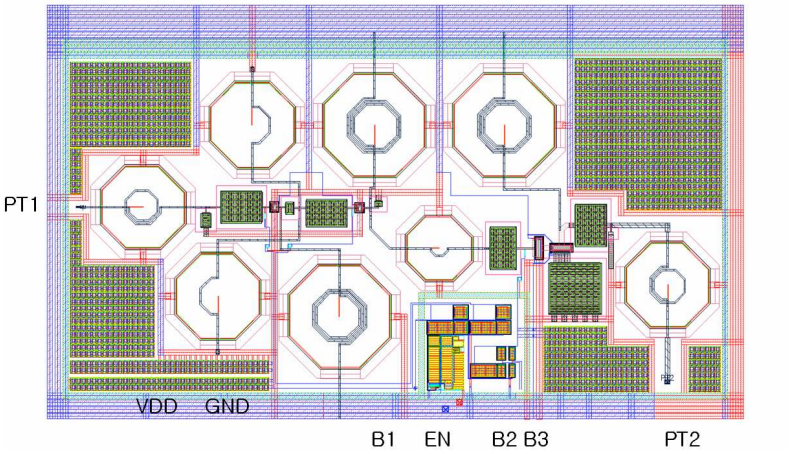

Figure 1: Layout of 24 GHz CMOS power amplifier.

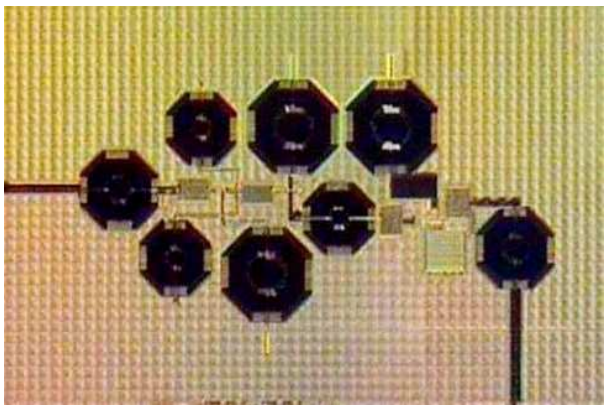

Figure 2: Die photograph of 24 GHz CMOS power amplifier.

Design of K-band CMOS VCO

Jin-Sup Kim, **Se-Hwan Choi**, **and Kyu-Ho Park**
Wireless Communication Research Center, Korea Electronics Technology Institute, R. O. Korea

Abstract— In this paper, a K-band voltage controlled oscillators (VCOs) is presented in a 0.13 µm CMOS technology. The simulated output power and the phase noise are −5 dBm and −110 dBc/Hz at 1 MHz offset from the carrier. The frequency tuning range is up to 550 MHz of the proposed VCO with FM modulation. The designed VCO consumes a dc power of 12 mW from a 1.2-V supply voltage.

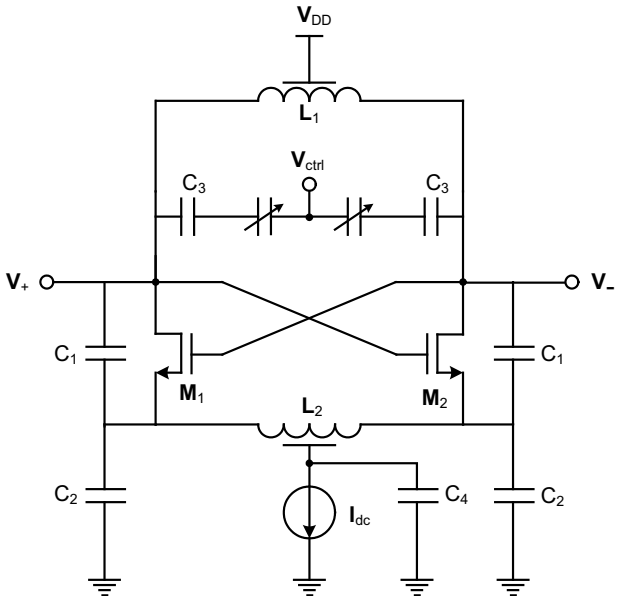

Figure 1: Schematic of K-band VCO.

REFERENCES

1. Wenger, J., "Automotive radar — status and perspectives," *Compound Semiconductor Integrated Circuits Symposium, 2005. CSIC'50. IEEE*, 21–24, 2005.
2. Boon, C. C., M. A. Do, K. S. Yeo, J. G. Ma, and X. L. Zhang, "RF CMOS low-phase-noise LC oscillator through memory reduction tail transistor," *IEEE Transaction on Circuits and Systems*, Vol. 51, No. 2, Feb. 2004.
3. Li, X., S. Shekhar, and D. J. Allstot, "Gm-boosted common-gate LNA and differential colpitts VCO/QVCO in 0.18-µm CMOS," *IEEE JSSC*, Vol. 40, No. 12, 2609–2619, Dec. 2005.

Analytical Calculation for DC Inductances of Octagonal and Circular RFIC Spiral Inductors

Chin-Chih Yeh[1], **Hao-Hui Chen**[2], **Jen-Tsai Kuo**[3], **Shyh-Jong Chung**[3], **and Ming-Huei Chen**[2]

[1]Department of Electronic Engineering, Huafan University, Taipei, Taiwan, R.O.C.
[2]Department of Electronic Engineering, National Kaohsiung First University of Science and Technology Kaohsiung, Taiwan, R.O.C.
[3]Department of Communication Engineering, National Chiao Tung University Hsinchu, Taiwan, R.O.C.

Abstract— With the rapid growth of the demand for low-power, low-cost, and high-integration wireless communication systems, development of on-chip passive devices for radio frequency integrated circuits (RFICs) has emerged as a critical issue recently. Among the passive circuits, on-chip spiral inductors are particularly essential and widely used in various RFICs such as mixers, amplifiers, and oscillators. To facilitate the analysis and design of RFICs, much research has been devoted to the investigation of RFIC spiral inductors. One attractive subject of these works is evaluating the DC (or low-frequency) inductance values from the layout parameters of spiral metal coil (line width, line spacing, inner or outer diameter, and number of turns). Several closed-form expressions such as Wheeler formula and Thomas formula have been established for the inductance calculation. These empirical expressions are practical but may be accurate to only limited inductor designs. On the other hand, [1] proposed an analytical formulation based the partial element equivalent circuit (PEEC) technique to carry out the inductance calculation. In this approach, the six-fold partial self and mutual inductance integrals resulted from the PEEC procedure are analytically evaluated by several concise formulas. The theoretically exact solutions can be therefore efficiently obtained. Nevertheless, as the formulas for calculating the six-fold integrals are limited to deal with the self inductance and the mutual one between two parallel metal strips, only the rectangular spirals were considered in [1]. In this work, the technique proposed in [1] is extended to investigate octagonal and circular spiral inductors (which are much more preferred than rectangular spirals in modern RFIC designs). In the calculation, the metal coil of an octagonal or circular spiral is first segmented into pieces of straight segment. By suitable segmentation, the octagonal and circular coil pattern can be approximated to be a combination of several straight metal sections, which are either parallel or perpendicular. The self inductances of each single section as well as the mutual ones among the parallel sections are then analytically evaluated by the integrating formulas presented in [1]. (Note that the mutual inductances between any two perpendicular sections are zero, thus there is no need to consider them in the calculation.) Finally, by summing up all of the calculated partial self and mutual inductances, one can then obtain the total inductance of the investigated inductor very efficiently. Various CMOS 0.18 µm and 0.13 µm octagonal and circular spiral inductors are tested to reveal the applicability of this efficient inductance calculation. The results and the detailed formulation will be presented and discussed in the symposium.

REFERENCES

1. Kuo, J.-T., K.-Y. Su, D.-Y. Liu, H.-H. Chen, and S.-J. Chung, "Analytical calculation for DC inductances of rectangular spiral inductors with finite metal thickness in the PEEC formulation," *IEEE Microw. Wireless Compon. Lett.*, Vol. 16, 69–71, Feb. 2006.

Behavior Study of Simultaneously Defected Microstrip and Ground Structure (DMGS) in Planar Circuits

M. Kazerooni, G. Rezai Rad, and A. Cheldavi
College of Electrical Engineering, Iran University of Science and Technology (IUST)
Narmak, Tehran, Iran

Abstract— In this paper several simultaneously defected microstrip and ground structures (DMGS) are proposed in order to study the behavior of these novel circuits by displacement of the defected patterns in circuit or ground planes. Investigation shows that the cascaded defects in one or two planes, makes to degrade the frequency response particularly in the high frequency, but by using the DMGS circuit enhances the stopband for wide range of frequency. Also the circuit parameters that related to the physical circuit configurations are extracted. The proposed DMGS circuit has larger effective inductance with respect to conventional DGS or DMS. These circuits have been analyzed and the performance of these circuits has been compared.

Design of 3.1 to 10.6 GHz Ultra-wideband Low Noise Amplifier with Current Reuse Techniques and Low Power Consumption

Pou-Tou Sun, **Shry-Sann Liao**, **Hung-Liang Lin**, **Chung-Fong Yang**, **and Yu-Hsuan Hsiao**
RF/MW Circuits Design Laboratory, Department of Communication Engineering
Feng-Chia University, 100, Wen-Hua Rd., Taichung 407, Taiwan, R.O.C.

Abstract— This paper presents a 3.1 to 10.6 GHz ultra-wideband (UWB) low noise amplifier (LNA) using a current-reused technique and wideband input matching network is proposed. The implemented LNA presents a maximum power gain of 12.8 dB, and a good input matching in the required band. An excellent noise figure (NF) of 2.97 to 6.04 dB was obtained in the frequency range of 3.1 to 10.6 GHz with a power dissipation of 10.13 mW under a 1.8-V DC power supply. The finished chip size is $1.26 \times 1.05\,\text{mm}^2$. The proposed UWB LNA is implemented by TSMC 0.18 µm CMOS technology.

A 3.1 to 10.6 GHz ultra-wideband (UWB) low noise amplifier (LNA) with a current-reused technique is fabricated in a TSMC 0.18 µm standard CMOS process. The LNA uses a current-reused technology to increase gain and save power consumption. The measurements are performed using on-wafer test. The LNA measurement at 3.1 to 10.6 GHz exhibits the minimum noise figure of 2.97 dB, maximum gain of 12.8 dB, input return loss is < -10 dB at 3.1 to 10.6 GHz and output return loss is < -9.3 dB at 3.1 to 10.6 GHz with a power consumption of 10.13 mW at V_{DD} is 1.8 V.

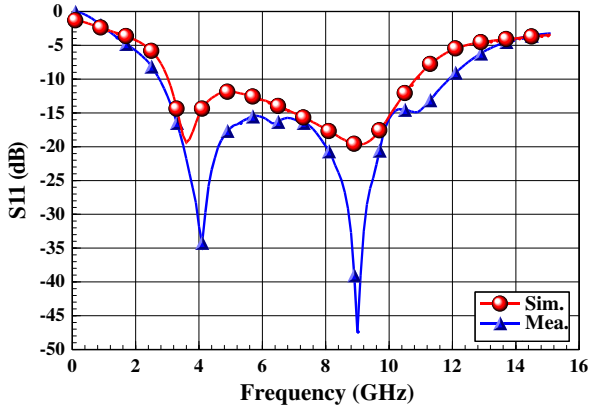

Figure 1: Simulation and measurement results of the input return loss.

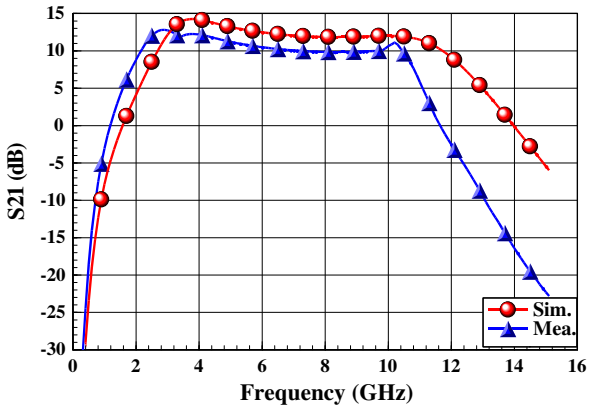

Figure 2: Simulation and measurement results of the gain.

REFERENCES

1. Bevilacqua, A. and A. M. Niknejad, "An ultra-wideband CMOS LNA for 3.1 to 10.6 GHz wireless receiver," *IEEE ISSCC Tech. Dig.*, 382–383, 2004.
2. Lin, Y.-J., S. H. Hsu, J.-D. Jin, and C. Y. Chan, "A 3.1–10.6 GHz ultra-wideband CMOS low noise amplifier with current-reused technique," *IEEE Microwave and Wireless Components Letters, Digest of Technical Papers*, Vol. 17, No. 3, March 2007.
3. Shaeffer, D. K. and T. H. Lee, "A 1.5-V, 1.5-GHz CMOS low noise amplifier," *IEEE Journal of Solid-state Circuits*, Vol. 32, No. 5, May 1997.
4. Lee, J. and J. D. Cressler, "Analysis and design of an ultra-wideband low-noise amplifier using resistive feedback in SiGe HBT technology," *IEEE Trans. Microw. Theory Tech.*, Vol. 54, No. 3, 1262–1268, March 2006.

The Design of Low Noise Amplifier with Gain-controlled and Low Power Consumption for WLAN Applications

Pou-Tou Sun, Shry-Sann Liao, Hung-Liang Lin, Chung-Fong Yang, and Tzu-Wei Yang

RF/MW Circuits Design Laboratory, Department of Communication Engineering
Feng-Chia University, 100, Wen-Hua Rd., Taichung 407, Taiwan, R.O.C.

Abstract— This paper presents a 5.2 GHz, 0.18 µm CMOS Low-Noise Amplifier (LNA) with gain controlled and low power consumption for an IEEE 802.11a WLAN application. The LNA fabricated with TSMC 0.18 µm 1P6M standard CMOS process, the current-reuse technique is used to increase the gain and reduce power consumption. The circuit performance is measured by using on-wafer test. The LNA exhibits a noise figure 2.94 dB at 5.2 GHz, the maximum power gain of 13.6 dB, the gain control range is 5 dB, and the power consumption of 4.2 mW at $V_{DD} = 1.8$ V. The finished chip size is 1.0 mm × 0.9 mm.

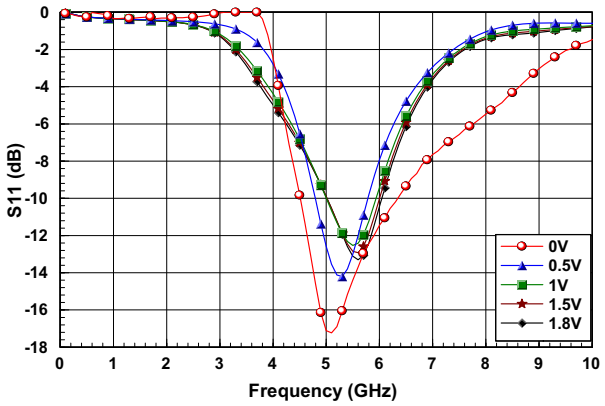

Figure 1: Measurement results of the S_{11} by control V_{crol} from 0 V to 1.8 V.

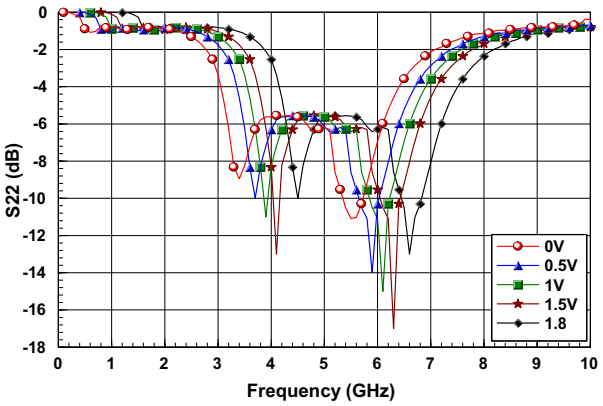

Figure 2: Measurement results of the S_{22} by control V_{crol} from 0 V to 1.8 V.

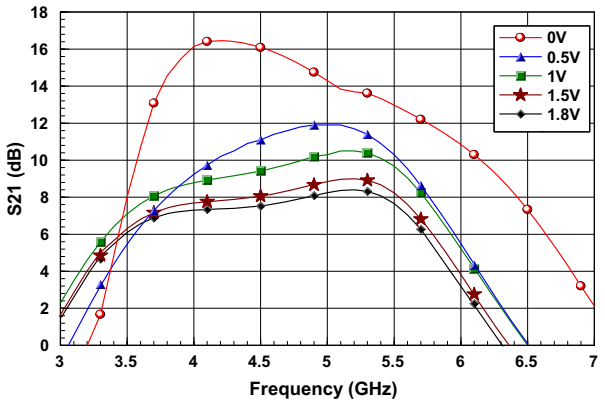

Figure 3: Measurement results of the gain S_{21} by control V_{crol} from 0 V to 1.8 V.

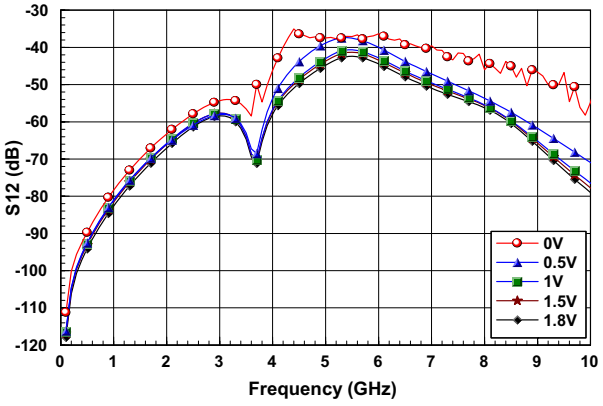

Figure 4: Measurement results of the S_{12} by control V_{crol} from 0 V to 1.8 V.

REFERENCES

1. Wang, X. and R. Weber, "Low voltage low power SiGe BiCMOS X-band LNA design and its comparison study with IEEE 802.11a LNA design," IEEE, 2005.
2. Wang, Y. S. and L.-H. Lu, "5.7 GHz low-power variable-gain LNA in 0.18/spl mu/m CMOS," Vol. 41, No. 2, 66–68, Jan. 20, 2005.

3. Liao, C.-H. and H.-R. Chuang, "A 5.7-GHz 0.18-/spl mu/m CMOS gain-controlled differential LNA with current reuse for WLAN receiver," Vol. 13, No. 12, 526–528, Dec. 2003.
4. Tsai, M.-D., R.-C. Liu, C.-S. Lin, and H. Wang, "A low-voltage fullyintegrated 4.5–6-GHz CMOS variable gain low noise amplifier," *European Microwave Conf.*, 13–16, 2003.
5. Raja, M., T. Boon, K. Kumar, and S. Wong, "A fully integrated variable gain 575-GHz LNA with on chip active balun for WLAN," *IEEE RFIC Symp.*, 439–442, 2003.

Design of a SiGe BiCMOS Power Amplifier for WiMAX Application

Cheng-Chi Yu, **Yao-Tien Chang**, **Meng-Hsiang Huang**, **Luen-Kang Lin**, **and Hsiao-Hua Yeh**
Department of Communications Engineering, Feng-Chia University
100, Wen-Hua Rd., Taichung 407, Taiwan, R.O.C.

Abstract— Worldwide interoperability for microwave access (WiMAX) wireless communication system has been gradually popular in recent years. WiMAX mainly provides a high data rate, long transmission distance, wide coverage, and good quality of service technology to improve the drawback in wireless fidelity (Wi-Fi).

Power amplifier is one of the most important components in WiMAX transmitter. A power amplifier operating at 3.5 GHz for WiMAX application is proposed in this paper. The TSMC 0.35-µm SiGe BiCMOS technology was used in this design. The choice of using SiGe BiCMOS technology for this design is based on its better breakdown robustness than CMOS and Si BJT (for same f_T), its technology availability and maturity, and its single-chip integration potential with multi-million gate digital CMOS. The proposed power amplifier was design with three stages open collector common-emitter amplifier. The results demonstrate that it can provide a reasonable efficiency, linearity and good output power.

Chiral Amino Alcohol Catalyzed Asymmetric Addition of Diethylzinc to Aldehyde

Ying-Chuan Wang[1] **and Hsien-Cheng Cheng**[2]

[1]Department of Nursing, Shu Zen College of Medicine and Management
Hwan-Chio Rd., Luju Kaohsiung 452, Taiwan, R.O.C.
[2]National Kaoshiung University of Applied Sciences
415 Chien Kung Road, Kaohsiung 807, Taiwan, R.O.C.

Abstract— In the study of chiral ligand, we used N atom and O atom as the main part of bidentate to be the chiral source. We have developed some bidentant chiral amino alcohol auxilaries. There are derived for the first time from Ketopinic Acid as chiral pool. Various bidentate chiral amino alcohol ligands were synthesized. Enantioselective addition of organometallic reagents to aldehydes affords optically active secondary alcohols. On the other hand, we also study substitution of chiral ligand, the does of chiral ligand, the reaction temperature, the reaction solvent, in order to get the best reaction condition and the best effect of enantioselectivity.

ACKNOWLEDGMENT

Acknowledgement from Ministry of Education Code No. SZN09602009.

Analysis of Performances of a Floquet Mode Preconditioner for Electromagnetic Scattering Computation by Rough Surfaces

S. Tournier[1], **J.-R. Poirier**[2], **and P. Borderies**[3]

[1]ONERA, 2 avenue Edouard Belin, 31055 Toulouse Cedex 5, France
[2]LAME-ENSEEIHT-INPT, 2 rue Charles Camichel, 31071 Toulouse cedex, France
[3]ONERA, 2 avenue Edouard Belin, 31055 Toulouse Cedex 5, France

Abstract— Scattering of electromagnetic waves by randomly rough surfaces is a subject of great interest in electromagnetism, including Radar and microwaves applications. Although analytical simulation techniques are now well-established for an efficient analysis of scattering by rough surfaces, it remains interesting to deal with them through the use of numerical approaches, with the goal of assessing the validity domain of the analytical ones or to substitute them in some cases.

Though various numerical approaches have been proposed in this context, this paper is about the use of the method of moments for solving the electromagnetic problem of scattering by rough surfaces. Then, major challenge of such approach is the numerical efficiency to cope with representative patches in terms of size and details.

Direct methods, such as LU decomposition, could be used to solve the resulting linear system. However, the computational complexity and the storage requirement of these methods grow hugely with the problem size. Iterative solvers based on the Krylov subspace method are the more suitable choice.

The convergence rate of a Krylov method is often in connection with the eigenvalues distribution. Rough surfaces need fine sampling and thereby the impedance matrix is in general poorly conditioned, so the convergence of the iterative solution may become very slow. Then, preconditioning matrices, which transform the initial linear system into an equivalent form with a eigenvalue distribution in a smaller cluster, are often introduced. The basic strategy to build an efficient preconditioner is to find a good approximation of the inverse of the impedance matrix with a computational cost as low as possible.

In this paper, a new physically preconditioner is proposed. It is developed for the fast computational analysis of 2D scattering from perfectly conducting rough surfaces in TM polarization.

The quasi planar nature of rough surfaces is exploited to construct the preconditioner. In the particular case of periodic flat plate, the spectral information (fitting Floquet's modes) of the impedance matrix is known, and this a-priori knowledge is introduced as approximate inverse matrix to build the Floquet Mode (FM) preconditioner.

Numerical examples are presented to exhibit the properties of this new preconditioner. We examine some theoretical aspects (eigenvalues clustering and condition number) and its convergence behaviour based on the number of preconditioned iterations for different Krylov methods. Large range of rms heights and correlation lengths for Gaussian and exponentially correlated rough surfaces is explored, and the efficiency of the FM preconditioner is determined as a function of the surface parameters. A variable but significant improvement is observed in most cases except when rms is high and oscillations fast.

Session 3A1a
Piezoelectric Devices and Systems

A Nut-type Ultrasonic Motor and Its Application on Focus System

Tieying Zhou[1], **Jun Zhang**[1], **Yu Chen**[1],
Cunyue Lu[1], **Deyong Fu**[1], **Yi Li**[2], **and Xiaoping Hu**[2]
[1]Department of Physics, Tsinghua University, Beijing 100084, China
[2]Boly Media Communications (Shen Zhen), Ltd., Shen Zhen 518031, China

Abstract— The ultrasonic motor (USM) is a prime candidate to meet the requirements of the cellular phone cameras due to its outstanding features of low speed, quick response and easy miniaturization etc. This article reports a polyhedron nut-type screw driving linear ultrasonic motor. It consists of an internal threaded metal nut as a stator and a matching external threaded screw as a rotor. The piezoelectric plates are bonded on the outer flat surface of the nut (Fig. 1). A circumferential traveling wave is stimulated on the stator when the harmonic electric signals are applied on the piezoelectric plates. The traveling wave drives the rotor to rotate and the threads transform the rotation into an axial linear motion. The lens could be fixed both on the rotor and on the stator to process auto focusing (AF) and zooming and the integration design of the focus module is achieved. The advantages of this structure are the absence of the retarder, the high accuracy of positioning due to direct drive and it is shockproof. The experiment results of this nut-type USM of M7 are obtained by applying the voltage of 20–40 Vp-p and the working frequency of 17 kHz for the second vibration mode. The power consumption is 0.25 W, the axial speed is 0.5–1 mm/s, the driving force is about 5 g and the response time is less than 10 ms. A mini size AF cellular phone module ($8.5 \times 8.5 \times 5.9\,\mathrm{mm}^3$) which driven by this motor has been made (Fig. 2). The image resolution of 3–5 Mp has been obtained in the module prototypes of the cellular phone.

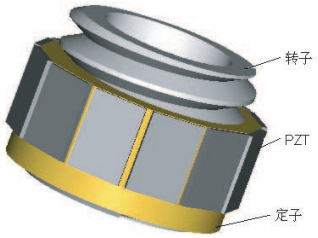

Figure 1: Nut-type USM.

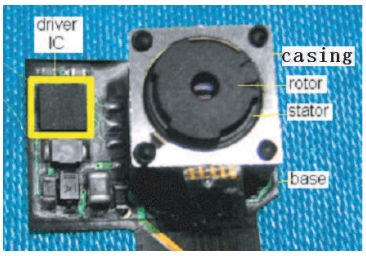

Figure 2: Integrated lens auto-focus system.

ACKNOWLEDGMENT

This work was supported by NSFC (50577035, 10676015) and 863 AA02Z472 of China.

R&D of a New Type Piezoelectric Transformer with a Composite Structure

Weige Zhou, **Jinlong Du**, **and Bin Wu**
China Electronics Corporation WeiHua Research Center, Beijing, China

Abstract— As we know, piezoelectric transformer (PT) has many advantages over the traditional transformers. In the past years, many new kind of PTs with very good performance were presented and analyzed. However, their applications were limited greatly due to the processing techniques limitations. Recently, with the rapid development of semiconductor processing techniques, it became much easier to realize the characteristics of PT, especially the reliability and conformity in the PT's mass production. Also, another key factor is that the years' endeavor of some PT's manufacturers. Their efforts make the mass production and actual applications possible.

In the paper, the technique developments of PT with different vibration modes were presented and analyzed. The situations of the PT's mass production in China were introduced with the examples of several manufacturers. The applications of PT were introduced and its typical driving and controlling circuits were presented.

In the final of the paper, the development tendency of PT's technology and techniques in mass production were analyzed. Its applications in new field were introduced.

Matrix Algorithms for Modeling Acoustic Waves in Piezoelectric Multilayered Media

Eng Leong Tan
School of EEE, Nanyang Technological University, Singapore

Abstract— This paper presents a review of matrix algorithms for modeling acoustic waves in piezoelectric multilayered media. One of the celebrated techniques for analysis of such media is based on the transfer matrix method, which facilitates the transition of fields across multilayers and leads to convenient determination of dispersion characteristics, generalized/dyadic Green's functions, and effective surface permittivity, etc. Despite its convenience, the transfer matrix method suffers from the numerical instability or exponential dichotomy problem, which often occurs when the frequency is high and/or the thickness is large. Many other algorithms that are capable of resolving the numerical instability of transfer matrix method are considered, including the conventional scattering and impedance matrices, as well as the more recent hybrid matrix. The formulation of basic matrices for these algorithm building blocks, and the development of recursive algorithms for the corresponding stack matrices, are systematically presented. Many variants of the algorithms are discussed, along with their respective usefulness and deficiency. Comparisons are made in their computational efficiency and numerical stability. For unconditional stability throughout large and small thicknesses, both scattering and hybrid matrix algorithms are applicable. For most efficiency, the algorithms that synergize both scattering and hybrid or impedance submatrices are superior, using surface matrix approach. Other aspects of algorithms such as formula conciseness, physical insight, versatility in incorporating boundary conditions, etc., are also noted. To bypass the intricacies of eigenvalue-eigenvector approach, the recursive asymptotic hybrid matrix method which requires only elementary matrix recursions along with thin-layer asymptotic approximation is described. The method enables simple and stable analysis of acoustic wave devices and transducers in piezoelectric multilayered media.

REFERENCES

1. Tan, E. L., "Matrix algorithms for modeling acoustic waves in piezoelectric multilayers," *IEEE Trans. Ultrason., Ferroelect. Freq. Contr.*, Vol. 54, No. 10, 2016–2023, 2007.
2. Tan, E. L., "Hybrid compliance-stiffness matrix method for stable analysis of elastic wave propagation in multilayered anisotropic media," *J. Acoust. Soc. Am.*, Vol. 119, No. 1, 45–53, 2006.
3. Tan, E. L., "Stiffness matrix method with improved efficiency for elastic wave propagation in layered anisotropic media," *J. Acoust. Soc. Amer.*, Vol. 118, No. 6, 3400–3403, 2005.
4. Tan, E. L., "A concise and efficient scattering matrix formalism for stable analysis of elastic wave propagation in multilayered anisotropic solids," *Ultrasonics*, Vol. 41, No. 3, 229–236, 2003.
5. Tan, E. L., "A robust formulation of SAW Green's functions for arbitrarily thick multilayers at high frequencies," *IEEE Trans. Ultrason., Ferroelect., Freq. Contr.*, Vol. 49, No. 7, 929–936, 2002.

Heavy Particle Collection by Ultrasonic Actuator

Junhui Hu, **Yanyan Liu**, **Tzehau Lam**, **and Huizhong Xu**
School of Electrical & Electronic Engineering, Nanyang Technological University
639798, Singapore

Abstract— This paper presents a new method to collect heavy particles by the ultrasonic actuator with two tapered metal strips. Heavy particles, such as medicine pills, can be trapped and transported in air by the actuator. We define the particle with a mass larger than 10 milligrams as heavy particle. A physical model is developed to explain the trapping mechanism. Effects of driving frequency, input voltage, particle size and weight, and structure of the actuator on the trapping capability are experimentally investigated.

Session 3A1b
Photonics Sensors

Optofluidic Cell Sorter by Integrating a Tapered Optical Fiber with Microfluidic Channel

Honglei Guo[1], **Gaozhi Xiao**[2], **Ping Zhao**[2], **and Jianping Yao**[1]

[1]Microwave Photonics Research Laboratory, School of Information Technology and Engineering
University of Ottawa, 800 King Edward Avenue, Ottawa, ON, K1N 6N5, Canada
[2]Institute for Microstructural Science, National Research Council
1200 Montreal Road, Bldg. M-50, Ottawa, ON, K1A 0R6, Canada

Abstract— The capability of handling small amount of cell particles is the prerequisite for the expanding of primary cells to large population as well as the dealing of precious cell particles. However, current available flow cytometers are only good at dealing with large amount cell particles. To address this issue, optofluidic cell sorters based on the principle of optical tweezers has been proposed and has shown some limited successes in the lab. Because the microscope is applied in this technique to provide both of the image and the gradient optical field, the whole system has the disadvantages of bulky size, high cost and difficulty of being integrated with the emerging lab-on-a-chip technology. Herein, we propose an optofluidic cell sorter design by integrating a tapered optical fiber with the microfluidic channel. In the proposed system, a tapered optical fiber is inserted into the microfluidic channel and is used to generate a strongly focused light beam to trap and manipulate the cell particle to the focused spot. By controlling the power of the light source and the position of the inserted tapered optical fiber, various cell particles could be pushed to different microfluidic buffers to realize sorting function. Compared with the conventional optofluidic cell sorters, it removes the table-top free-space optics, potentially reduces the cost, lowers down the power of the light source needed, increases the platform portability and is more flexible to operate.

Stacked Color Sensor with a Distributed Bragg Reflector

Noriyuki Kakimoto and Takahiro Numai
Department of Electrical and Electronic Engineering, Ritsumeikan University
1-1-1 Noji-Higashi, Kusatsu, Shiga 525-8577, Japan

Abstract— In conventional full-color imaging technologies using charge coupled devices (CCDs) and CMOS sensors, images are detected by separating colors into red, green, and blue (RGB) with lateral color filters. However, in the conventional full-color imaging technologies, each pixel detects only one color among RGB. Therefore, moiré fringes and color artifacts are produced, which degrades images. To suppress moiré fringes and color artifacts, stacked color sensors with vertical color filters inherent in silicon (Si) have been proposed. In the stacked color sensors, each pixel detects all colors, which leads to high quantum efficiency and high resolution in addition to less moiré fringes and less color artifacts.

To achieve ideal spectral photosensitivity, it is important to optimize both peak wavelengths and spectral widths of the spectral photosensitivity. However, the peak wavelengths and the spectral widths are simultaneously determined solely by thickness of absorption layers, because the vertical color filtering uses wavelength-dependent absorption coefficient in Si.

In this paper, the device parameters of the stacked color sensors incorporating the DBR, in which the peak wavelengths and the spectral widths of the photosensitivity can be designed independently, are optimized from the viewpoint of the measure of the goodness. The DBR is placed between the blue absorption layer and the green absorption layer, and only the blue light is reflected to the blue absorption layer. A dielectric layer, which is thicker than the coherent length of the incident lights, is inserted between the blue absorption layer and the DBR. Because the incident lights are partially coherent lights, the lights passing through the dielectric layer do not interfere with themselves. The simulated results reveal that values of the stacked color sensors incorporating the DBR were larger than those in previous work.

High Resolution Micro Spectrometers Based on Tunable Planar Lightwave Circuits

Gaozhi (George) Xiao[1], **Nezih Mrad**[2], **and Zhiyi Zhang**[1]

[1]Institute for Microstructural Science, National Research Council Canada, Canada
[2]Air Vehicles Research Section, Defence R & D Canada
Department of National Defence Canada, Canada

Abstract— High resolution micro spectrometers are sought after devices for optical fiber sensor interrogation, optical communication network monitoring, as well as bio-chemical analyzing and sensing applications, particularly in the case of field deployment. Currently, a typical micro spectrometer consists of two components, i.e., a light disperser (or a light demultiplexer), and a linear photo detector array. When a light signal coming into the micro spectrometer, the light is dispersed into its spectral components by the disperser and is directed to the detector array. Through suitable calibration, each detector can be assigned a certain wavelength range. However, due to the physical limitation of the number of the photo detectors that can be fabricated on a defined area, the spectrometer measurement resolution and range become two competing factors in the design. Depending on the spectrometer's operational and performance requirement, one parameter must be sacrificed at the expense of the other. For instance, if the measurement resolution is more critical, such as for the interrogation of optical fiber sensors, then the measurement range has to be compromised and vice versa. To address such design limitation, we propose to use tunable planar lightwave circuit (PLC) based demultiplexers to replace the light disperser. This approach would offer a spectrometer with good measurement resolution without sacrificing its measurement range.

Micro spectrometers based on two types of PLC demultiplexers, namely arrayed waveguide gratings (AWG) and echelle diffractive gratings (EDG), are reported here. Both types of devices are fabricated on semiconductor chips and have shown excellent reliability, as proved by their successful deployment in optical communication networks. By tuning the transmission wavelength of the demultiplexers, each AWG or EDG channel can be used to measure the spectra of certain wavelength range. Current technology can make an AWG or EDG with more than 100 channels. Therefore, an AWG or EDG based micro spectrometer can potentially measure the spectrum over hundreds nanometer. In the case of AWG, we have achieved a spectrum measure range of over 32 nm at a resolution of better than 1 pm; while in the case of EDG, spectrum measurement range of more than 25 nm at a resolution better than 1 pm is achieved. As the typical AWG and EDG size is about a few centimeter by a few centimeter or less, we would be able to stack several devices together and assemble a small size, lightweight, micro spectrometer to significantly increase the measurement range.

Modeling of the Potential Profile for the Annealed Polycrystalline PbSe Film

Gang Bi[1,2], **Fanghai Zhao**[1], **Jiangang Ma**[1], **Shaibal Mukherjee**[1], **Donghui Li**[1], **and Zhisheng Shi**[1]

[1]School of Electrical and Computer Engineering
University of Oklahoma, Norman, Oklahoma 73019, USA
[2]School of Information & Electrical Engineering
City College, Zhejiang University, Hangzhou 310015, China

Abstract— Narrow gap semiconductors such as lead salt materials are widely used to fabricate midinfrared optoelectronic devices [1, 2]. Thereinto, polycrystalline PbSe films grown on Si or SiO_2/Si substrates have attracted great interest mainly due to midinfrared imaging applications in the 3–5 and 8-12 μm atmospheric windows. Despite the continuous investigation of their properties, many aspects of the mechanism of photoconductivity in such films have not yet been completely resolved. Recently, we reported the photoluminescence intensity increased by more than two orders of magnitude at 4.5 μm after annealing the PbSe in an O_2 atmosphere at 350°C [3]. The results show that the optical and electrical property depends on the postgrowth processing significantly.

Modeling the mechanism of carrier transport for polycrystalline PbSe film such as their dependence on dopant concentration, type of dopant, and high-temperature processing becomes very important for the proper design of the devices. Most of the polycrystalline semiconductor devices are annealed structures with a complex potential relief, with which in such devices assigns its operational characteristics. Especially, potential profile is extremely important from the viewpoint of carrier transport phenomena. Therefore, the design of a potential relief of semiconductor devices is a topical question for engineering of new types and classes of devices.

The potential profiles between polycrystalline grains are greatly influenced by the grain-boundary (GB), doping concentration and temperature, grain-boundary interface states density. In this paper, a novel model for computing the potential profile in polycrystalline PbSe film is developed. The model is based on the mechanism of double heterojunction due to O_2 diffusing to grain, grain-boundary trapping, and thermionic emission as well as tunnel transportation through the inter-grain energy barriers at grain boundary. Figure 1 shows SEM image of the polycrystalline PbSe prepared in our lab to be used for the calculation of potential profile.

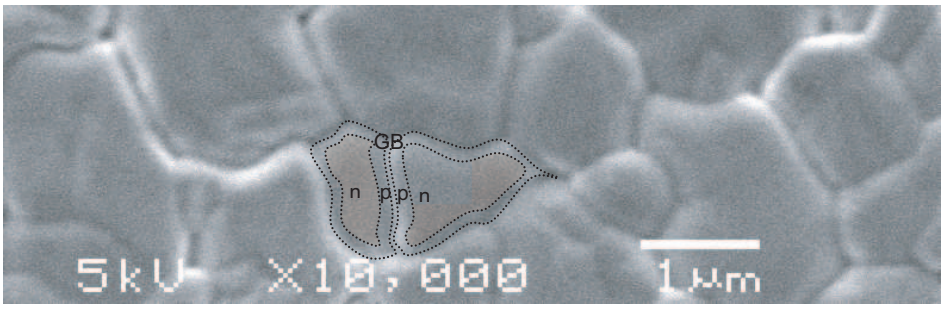

Figure 1: SEM image of a polycrystalline PbSe material at 10000× magnification. In high quality material, grains extend throughout the film thickness. The annealed condition is at 380°C for 20 hours. The double heterojunction due to the diffusion of O_2 at the grain boundary is formed, where n-type region in the semiconductor grain is packed by the p-type oxide at the grain boundary.

Figure 2 refers to the case of double abrupt junction, As a result of the diffusion of free carriers on both sides of the junction, where a space-charge depleted region is formed at the interface (Figure 2(a)). By solving the Passion equation for such structure, the electric field and potential distribution content with this charge distribution can be calculated (Figure 2(b)). The equilibrium energy-band diagram is also displayed (Figure 2(c)).

When a bias is applied to a polycrystalline PbSe film (Figure 3), we can also get the charge distribution, the electric field distribution, the potential profile (Figure 3(a)) and the energy

band diagram (Figure 3(b)). The dependence of potential profile on bias voltage is in detail discussed.

The dependence of potential profile on illumination intensity can also be calculated. As varying illumination intensity, the design of a potential relief of semiconductor device was discussed. These results provide an extremely important viewpoint of carrier transport phenomena for polycrystalline detector designs.

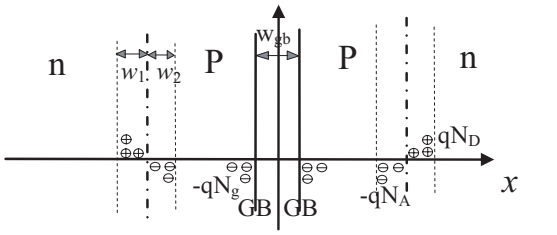

(a) Charge depleted region

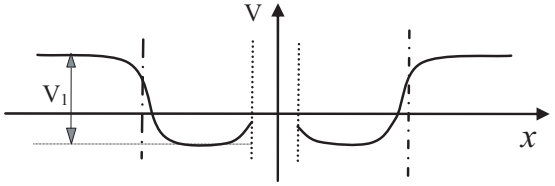

(b) Potential profile without bias voltage

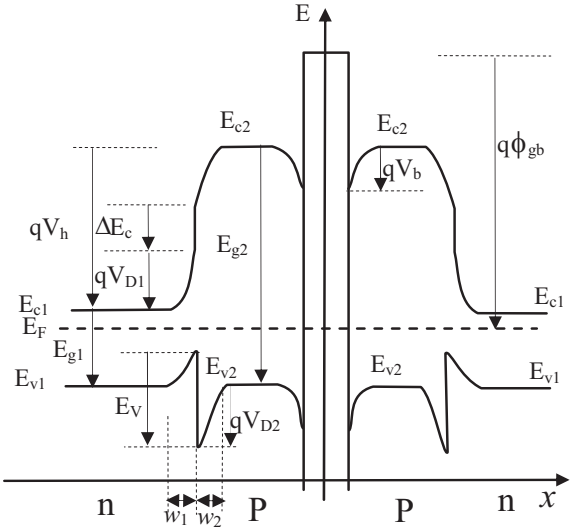

(c) Energy band diagram without bias voltage

Figure 2: Carrier thermal equilibrium at grain boundary without bias.

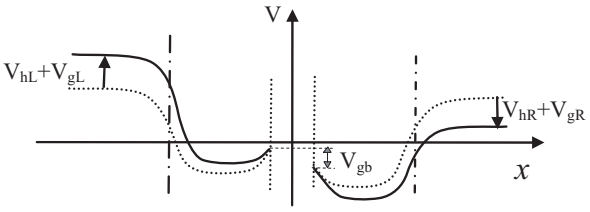

(a) Potential profile with a bias voltage V_0

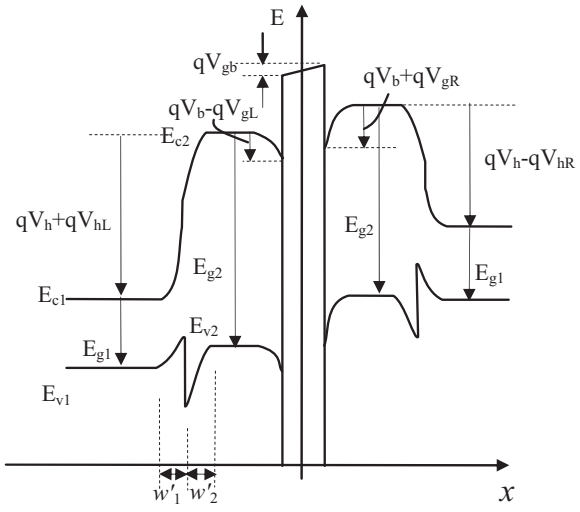

(b) Energy band diagram with a bias voltage V_0

Figure 3: A case of a bias voltage at grain boundary.

REFERENCES

1. Springholz, G., Z. Shi, and H. Zogg, *Thin Films: Heteroepitaxial: Systems*, edited by W. K. Liu and M. B. Santos, World Scientific, Singapore, 1999
2. Khokhlov, D., *Lead Chalcogenides Physics and Applications*, Taylor and Francis, New York, 2003.
3. Zhao, F., S. Mukherjee, J. Ma, et al., "Influence of oxygen passivation on optical properties of PbSe thin films," *Applied Physics Letters*, Vol. 92, 211110, 2008.

Interrogation of Tilted Fiber Bragg Grating Sensors by Mechanical Scanning an Arrayed Waveguide Grating

Honglei Guo[1], **Gaozhi (George) Xiao**[2], **Nezih Mrad**[3], **and Jianping Yao**[1]

[1]Microwave Photonics Research Laboratory, School of Information Technology and Engineering
University of Ottawa, Ottawa, ON, K1N 6N5, Canada
[2]Institute of Microstructural Science, National Research Council
M-50, Ottawa, ON, K1A 0R6, Canada
[3]Air Vehicles Research Section, Defence R & D Canada, Department of National Defence
National Defence Headquarters, Ottawa, ON, K1A 0K2, Canada

Abstract— Owning to its capability to sensing temperature and strain simultaneously, tilted fiber Bragg grating (TFBG) based sensors have shown great potentials in the development of smart structures. However, current available TFBG interrogation techniques for spectrally decoding the measurands are mainly based on conventional optical spectrum analyzer (OSA), which is bulky, expensive, and not suitable for in-field application. In this paper, we describe a novel wavelength interrogation method for TFBG sensing application, which is based on a mechanically-tuned arrayed waveguide grating (AWG). More specifically, the input light to the input coupler of the AWG is scanning along the facet of the input coupler by mounting the input optical fiber on a piezo motor. It has been found that by horizontally changing the position of the input light, the center wavelength of the AWG output channel will shift accordingly. In order to simplify the control, an open-loop piezo motor is applied in this design. But it causes position uncertainty due to the piezo hysteresis and the scanning speed non-uniformity. To address such practical limitation, we applied a sampled chirped FBG (SCFBG) to provide the reference of the mapping relationship between the multi-wavelength of the SCFBG and the number of DAQ sampling points, with which both the Bragg resonance and the first cladding mode (or ghost mode) resonance can be successfully interrogated. The proposed interrogator has the potential of being packaged into a chip-size, high performance, low cost and field deployable device.

Interrogation of Optical Fiber Sensors Using a Mechanically Scannable Arrayed Waveguide Gratings Demultiplexer

Gaozhi (George) Xiao[1], **Nezih Mrad**[2], **Zhiyi Zhang**[1]
Honglei Guo[3], **and Jianping Yao**[3]

[1]Institute for Microstructural Science, National Research Council Canada, Canada
[2]Air Vehicles Research Section, Defence R & D Canada
Department of National Defence Canada, Canada
[3]School of Information Technology and Engineering, University of Ottawa, Canada

Abstract— Optical fiber sensors have demonstrated many superior characteristics, such as excellent accuracy, light weight, small size, multiplexability, and immunity to electromagnetic interference. Some demonstration projects have shown that the fiber Bragg grating sensors being successfully embedded in aircraft structures and civil engineering works to monitor their performances. Some other experiments have shown that long period grating sensors, tilted fiber Bragg grating sensors, and Fabry-Perot fiber sensors can be used for bio and chemical sensing. Nevertheless, the field interrogation of those optical fiber sensors still remains to be a challenging task for many applications. The current available sensor interrogators are generally lab oriented, bulky, heavy and very expensive. To tackle this issue, in the last few years, we have been focusing our efforts on the development of a low cost, miniaturized sensor interrogator. In this presentation, we will report our progress in the development of a miniaturized fiber optical sensor interrogation system based on a mechanically scannable arrayed waveguide gratings (AWG) demultiplexer.

An AWG demultiplexer is a planar lightwave circuit type device and generally fabricated on silicon wafer. Its reliability has been proved by its successful deployment in the optical communication networks. The device usually measures few centimeters by few centimeters. We have noticed that by scanning the lateral position of the input light beam along the input coupler facet of the AWG demultiplexer, the transmission wavelength of the AWG can be linearly tuned. By using a special designed mechanically scannable AWG demultiplexer and a sampled chirped fiber Bragg grating (SCFBG) with multiple peaks as the reference, we have measured the central wavelength of LPG and FBG sensors. An interrogation resolution better than 1 pm and an interrogation range of 50 nm with a scanning speed up to 500 Hz have been demonstrated.

Fiber Optic Distributed Strain and Temperature Sensors

Lufan Zou and Omur Sezerman
OZ Optics, Ltd., 219 Westbrook Road, Ottawa, ON, K0A 1L0, Canada

Abstract— Although distributed Brillouin strain and temperature sensing has undergone significant evolution over the last decade, higher spatial resolution and longer sensing range challenge Brillouin-scattering-based distributed strain and temperature sensors (DSTS) that provide an excellent opportunity for structural health monitoring of civil structures by allowing measurements to be taken along the entire length of the fiber, rather than at discrete points, by using fiber itself as the sensing medium. One class of Brillouin scattering-based DSTS is based on the coherent pump depletion (CPD) technique, whereby two counter-propagating laser beams, a pulsed Stokes beam and a continuous wave (cw) pump beam, exchange energy through an induced acoustic field. The interaction magnifies the pulsed Stokes beam at the expense of depleting the pump beam coherently, which is then detected as a loss signal. The maximum depletion of the pump beam at a point along the fiber happens when the frequency of the acoustic wave ν_B at that point matches the beat frequency of two laser beams, i.e., $\nu_p - \nu_s = \nu_B$, where ν_p and ν_s are the frequencies of pump and Stokes beams, respectively. The frequency of the acoustic wave, hereafter called Brillouin frequency shift, is related to the fiber properties and laser wavelength. The sensing capability of Brillouin scattering arises from the dependence of the Brillouin frequency shift, ν_B, on the local acoustic velocity and refractive index in glass, which has a linear temperature and strain dependence. This type of sensing has tremendous potential for structural health monitoring since the spatial resolution can be adjusted for different applications simply by altering the pulse duration, even after the fiber is installed.

We conduct OZ' new product Foresight^{TM} DSTS based on CPD technique with 10 cm spatial resolution and up to 100 km round-trip sensing range and its application on micro-meter crack detection on ceramic tile, pipeline corrosion, pipeline erosion, pipeline buckling, power line monitoring, highway and bridge monitoring, and so on.

Session 3A2a
Metamaterial Applications: from Antennas to Cloaking

Quantifying Localization Characteristics of Plasmonic Waves

A. Sihvola
Department of Radio Science and Engineering, Helsinki University of Technology
Box 3000, FI-02015 TKK, Espoo, Finland

Abstract— Metamaterials [1] studies, especially when the frequency range of interest lies in the microwave region, deal often with artificial materials for which both the electric permittivity and magnetic permeability are negative. Such materials can be exploited for many interesting applications. However, also so-called single-negative media (in other words, media in which for example only permittivity reaches negative values) are known to be extremely exploitable, especially towards the optical and infrared frequencies. Plasmonics is the science of studying such phenomena [2]. In plasmonics, the effect of metal-insulator boundary geometry on the coupling of electromagnetic field to free-electron oscillations is in the center of study. In this talk, I will concentrate on various characterics of the plasmonic waves on surfaces and quantify their localization. I will approach the problem from the classical wave propagation point of view [3], the history of which can be traced back to Jonathan Zenneck and his seminal studies from the early 20th century [4].

REFERENCES

1. Sihvola, A., "Metamaterials in electromagnetics," *Metamaterials*, Vol. 1, No. 1, 2–11, 2007.
2. Maier, S., *Plasmonics: Fundamentals and Applications*, Springer, 2007.
3. Wait, J. R., "The ancient and modern history of EM ground-wave propagation," *IEEE Antennas and Propagation Magazine*, Vol. 40, No. 5, 7–24, October 1998.
4. Zenneck, J., "Über die Fortpflanzung ebener elektromagnetischen Wellen längs einer ebenen Leiterfläche und ihre Beziehung zur drahtlosen Telegraphie," *Annalen der Physik*, Vol. 23, 846–866, 1907.

Negative Permeability Derived from Resonance in Ceramic Dielectrics

Ji Zhou, **Qian Zhao**, **Hongjie Zhao**, **and Lei Kang**
Department Materials Science & Engineering
Tsinghua University, Beijing 100084, China

Abstract— Generation of negative permeability is a key issue for realization of left handed metamaterials (LHM). Most of LHM are based on artificial subwavelength metallic structures which exhibit magnetic resonances at a certain frequency to obtain abnormal permeability. However, there are some challenges for this class of metamaterials with the increase of the frequency, including difficult in the fabrication of 3D structure, size effects, anisotropic, and high dielectric loss. Nonmetallic dielectric materials supply another choice for metamaterials, as there are many electric or magnetic resonance mechanisms in dielectric materials, which may induce a negative permittivity or permeability. In this talk, two kinds of magnetic resonances, which derived from Mie resonance in dielectric particles and from ferromagnetic resonance in ferrites, are studied theoretically and experimentally. Negative permeability in X band are observed in both system. It is shown that the magnetic resonance in dielectrics supply a new way for generation of negative permeability other than metallic resonance structure.

Design of a Three-dimensional Metamaterial Exhibiting Isotropic Properties in the Near Infrared Range

Andrei V. Andryieuski, Radu Malureanu, and Andrei V. Lavrinenko
Technical University of Denmark, Kgs. Lyngby, DK-2800, Denmark

Abstract— Within the last years, the exciting new applications of metal-dielectric composites, called metamaterials, have showed up. These applications include, but are not limited to topics like near-field imaging on nanometer length scales, cloaking, nano-antennas, etc. Among the others there is an interest in assistance of coupling between waveguides [1]. The nanoscale core sizes of new photonic devices currently being tested for transporting and controlling light as interconnects (photonic crystal waveguides, photonic wires, plasmonic wires) raised up a serious problem of coupling between devices with large difference in cross-sections, e.g., between optical waveguides or fibers having characteristic core sizes of several microns and photonic wires with sizes of 100–300 nm. The important requirement for the metamaterial coupler is isotropy of its electric and magnetic properties exhibited in the real three dimensional space. Most of the metamaterials designs proposed so far show theoretically polarization independence at normal incidence in the best case.

We considered several designs of unit cells aiming that they can be constitutive blocks for the isotropic metamaterials at the telecom range. All of them have metallic parts arranged inside a unit cube, thus preserving the highest possible group symmetry. The restoration of effective parameters is made with the standard routine utilizing reflection/transmission data [2]. It reveals that the most potentially promising design is a "cube-in-cage" structure: cage made from metallic stripes containing a cube with non-connected plates. The cage is responsible for the Drude-like behavior of the effective dielectric permittivity like the 3D wire medium, while the plates act like 3D split-ring resonator and exhibit a pronounced magnetic resonance pushing the magnetic permeability to negative values. Both effects in cooperation lead effectively to a negative refractive index.

The optimal "cube-in-cage" design (technical parameters will be specified at the session) shows the negative refractive index for frequency range from 185 to 200 THz (wavelengths from 1.5 μm to 1.62 μm). The minimal value of $\mathrm{Re}(n) = -2.4$ (at 192.5 THz). The maximal figure-of-merit (FOM) is 2.4 (at 195 THz) and corresponds to $\mathrm{Re}(n) = -1.4$. The proposed unit cell has relatively high transmission of 16% in the region around the maximal FOM.

We report on the various numerical tests made to validate the isotropic response of the metamaterial with the "cube-in-cage" unit cell: bands dispersion analysis or reflection/transmission spectra obtained for oblique incidence on a slab made of such metamaterial. Obtained results are compared, and pros and cons for different approaches are discussed.

REFERENCES

1. Degiron, A., D. R. Smith, J. J. Mock, B. J. Justice, and J. Gollub, "Negative index and indefinite media waveguide couplers," *Appl. Phys. A*, Vol. 87, 321–328, 2007.
2. Smith, D. R., S. Schultz, P. Markos, and C. M. Soukoulis, "Determination of effective permittivity and permeability of metamaterials from reflection and transmission coefficients," *Phys. Rev. B*, Vol. 65, 195104, 2002.

Design of High-gain Antenna by Discrete Optical Transformation

Wei Xiang Jiang and Tie Jun Cui
State Key Laboratory of Millimeter Waves
Institute of Target Characteristics and Identification
Department of Radio Engineering
Southeast University, Nanjing 210096, China

Abstract— In real applications, the optical transformation media with complicated, strongly anisotropic and continuous electromagnetic parameters are difficult to realize. In this paper, we present a discrete and finite embedded optical transformation, from which a layered high-gain lens antenna and a multi-beam lens antenna are designed. Each layer of the lens antennas is composed of homogeneous and uniaxially anisotropic metamaterials, which are simple and realizable. Excited by a 2D line source which is normal to the plane of wave propagation, when the layered metamaterial lens is placed in the air, the incident cylindrical waves are partially converted into plane waves. When the layered lens is embedded in a horn antenna, the distributions of the electromagnetic fields at the aperture are almost uniform. Hence the lens antenna provides a high-directivity radiation beam. Simulation results show that the gain of the lens antenna is 6 dB higher than the horn antenna without the lens. We also use the discrete optical transformation to design a multi-beam high-gain antenna.

Planar Resonant Metamaterial Absorbers for All Polarizations at Microwave Band

Bo Zhu, Zhengbin Wang, Ziying Yu, Qi Zhang, and Yijun Feng
Department of Electronic Science and Engineering, Nanjing University, Nanjing 210093, China

Abstract— Metamaterials have the great potential of tailoring the electromagnetic (EM) parameters including the permittivity, permeability or the impedance in a manner not easily achieved with naturally occurring materials. Such advantage has recently been successfully applied to create resonant metamaterial absorbers and has been experimentally demonstrated at microwave and terahertz frequencies [1, 2]. The idea is to simultaneously minimize the wave transmission and reflection through the design of material impedance to match with the surrounding medium. However, the proposed design of the resonant metamaterial absorbers only works for one particular polarized EM wave.

In this presentation, we report the successful design of three different planar metamaterial structures that absorb electromagnetic wave of all polarizations by employing electric and magnetic resonance at Giga-hertz. Polarization insensitivity associated with these structures has been demonstrated through full-wave EM simulation which is carried out for calculating the absorption of two orthogonally polarized incident waves through the planar structure. Based on these designs we have fabricated the planar absorbers using normal print circuit board technique and experimentally verified the polarization insensitive absorbing feature (as shown in Fig. 1). The nearly perfect microwave absorbing has been successfully interpreted as the impedance matching at the resonant frequency through calculating the impedance based on the parameter retrieval from the measured data. We hope the designs could find more applications at higher frequencies (e.g., in terahertz) by shrinking the sizes of the structures.

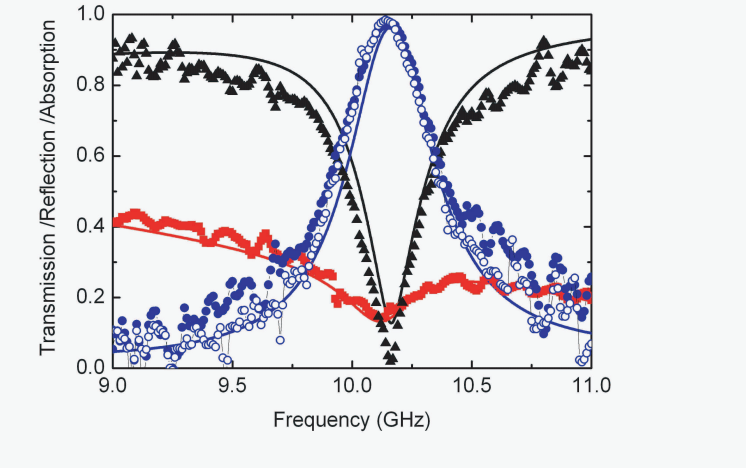

Figure 1: Measured EM transmission (square), reflection (triangle) and absorption (for two different polarizations, denoted as hollow circle, solid circle) for one of our designs. Solid lines correspond to the simulation results.

ACKNOWLEDGMENT

Supported by the National Basic Research Program of China (2004CB719800), and National Nature Science Foundation (No. 60671002).

REFERENCES

1. Landy, N. I., S. Sajuyigbe, J. J. Mock, D. R. Smith, and W. J. Padilla, *Phys. Rev. Lett.*, Vol. 100, 207402, 2008.
2. Tao, H., N. I. Landy, C. M. Bingham, X. Zhan, R. D. Averitt, and W. J. Padilla, *Opt. Express*, Vol. 16, 7181, 2008.

Leaky Coplanar Waveguide Antenna with Tunable Beamwidth and Radiation Angle Using Composite Right/Left-handed Materials

Abdelaziz Hamdi[1], **Ammar B. Kouki**[2], **and Abdelaziz Samet**[3]

[1]Ecole National d'Ingénieurs de Sousse, Technopole de Sousse, Sahloul, Tunisia
[2]École de Technologie Supérieure
1100, rue Notre-Dame O. Montréal (Qc) H3C 1K3, Canada
[3]Ecole Polytechnique de Tunisie, B. P. 743, La Marsa, Tunis 2070, Tunisia

Abstract— A new field of physics has appeared with the emergence of materials known as "Left handed materials" (LHM) or "metamaterials". These materials show very particular characteristics. Their index of refraction has a negative value, which results in the reversal of Snell's law. Whereas, in traditional material the Poynting vector S always forms a right-handed triplet with E and H ($S = E \wedge H$). In the left handed media, the Poynting vector S and the wave vector K are in opposite directions. Thus, the wave moves in the direction opposite to the direction of the energy flow: phase speed and group speed are anti-parallel. Therefore, a left-handed media is artificial and does not exist in nature. Indeed, when these materials are inserted into a guided wave device, one obtains the backward-wave effect. The goal of this work is to study more in details this physical phenomenon. To undertake this study, this paper presents also the design of a 10 GHz beam-scanning CPW-Antenna fabricated on metamaterial support.

Directive Emissions of Antennas on Metamaterial Ground Planes: Role of Anomalous Reflection Phases

Kun Ding[1], **Tao Jiang**[2], **Jiaming Hao**[1], **Lixin Ran**[2], **and Lei Zhou**[1]

[1]Surface Physics Laboratory (State Key Laboratory), Physics Department
Fudan University, Shanghai 200433, China
[2]The Electromagnetic Academy, Zhejiang University, Hangzhou 310027, China

Abstract— Efficiency and radiation pattern are two important characteristics of antenna radiations [1]. Recently, there has been much interest to employ metamaterials to control the radiation behaviors of antennas [2–5]. For example, directive emission can be achieved by simply putting a point source inside a metamaterial with zero refractive index [2], or inside a subwavelength cavity formed by specifically designed metamaterials [3]. In this work, we study the radiation properties of antennas put on ground planes formed by metamaterials, aiming to find the conditions under which the antenna emissions could be highly directive. We first applied a dyadic Green's function approach to analytically study the radiation properties of antennas put perpendicular or parallel to the ground plane, and found that the metamaterial ground plane should possess certain reflection phase properties in order to support directive emissions. We then employed finite-difference-time-domain (FDTD) simulations to successfully design realistic metamaterials structures as appropriate ground planes to support directive emissions for both orientations of antennas. Microwave experiments, in good agreements with FDTD simulations, were performed to verify the theoretical predictions [6].

REFERENCES

1. Jin, A. K., *Electromagnetic Wave Theory*, EMW, Cambridge, MA, 2000.
2. Enoch, S., et al., *Phys. Rev. Lett.*, Vol. 89, 213902, 2002.
3. Zhou, L., et al., *Appl. Phys. Lett.*, Vol. 86, 101101, 2005.
4. Li, H., et al., *Appl. Phys. Lett.*, Vol. 86, 121108, 2005.
5. Wu, B.-I., et al., *Microwave and Optical Technology Letters*, Vol. 48, 680, 2006.
6. Ding, K., et al., unpublished.

Session 3A2b
Mathematical and Numerical Tools for Metamaterials 1

Transformation Optics for Cloaking and Hyperlensing with Metamaterials

Charles Croënne[1], **Davy Gaillot**[1], **Fuli Zhang**[1, 2], **Wounjhang Park**[3], **and Didier Lippens**[1]

[1]Institut d'Electronique, de Microélectronique et de Nanotechnologie (IEMN — UMR CNRS 8520)
Université des Sciences et Technologies de Lille
Avenue Poincaré, BP 60069, 59655 Villeneuve d'Ascq, France
[2]Department of Applied Physics, Northwestern Polytechnical University
Xi'an 710072, China
[3] Department of Electrical & Computer Engineering, University of Colorado
UCB 425, Boulder, CO 80309-0425, USA

Abstract— We report here on the possibilities afforded by the numerical treatment of space transformations aimed at better controlling the light from microwave to optics. We illustrate these possibilities with two examples. The first one concerns cloaking applications which consist to coat a scatterer with a metamaterial. By proper designing the effective parameters of the cloak, a perfect matching at the interface between the embedding medium and the cloak can be achieved. Also, the light is deviated with a parietal flow along the cloak and a reconstruction of traveling waves behind the cloak. The difficulty to realize a perfect cloak, by monitoring both the permittivity and permeability gradients, is first pointed on the basis of the current metamaterial technologies. Secondly, we focus our attention about the frequency dependence of the Radar Cross Section (RCS) which is ultra narrow in essence. It is shown that the RCS depends on the dispersion but also on the scale of the cloaked scatterer. The second application concerns hyperlensing based on highly anisotropic metamaterial media. The condition of hyperlensing, namely the fact that the propagation of light shows a channeling effect is established. We then address the problem of magnification which permits one to increase the separation between two point sources with a sub-wavelength spacing. The originality of the work is the proposal of a flat configuration when the demonstrations, found in the literature, used round-shaped multi-layered microstructures. We conclude with the prospect to develop the reverse problem namely hyperfocusing.

Determination of the Effective Constitutive Parameters of Bianisotropic Metamaterials from Reflection and Transmission Coefficients

Zhaofeng Li and Ekmel Ozbay
Nanotechnology Research Center
Department of Physics, and Department of Electrical and Electronics Engineering
Bilkent University, Bilkent, Ankara 06800, Turkey

Abstract— We propose a method to retrieve the effective constitutive parameters of a slab of bianisotropic metamaterial composed of split ring resonators from the S parameters. Unlike the previous method [4], we only use the S parameters in one direction, which makes our method much simple. Analytical inversion equations are derived and firstly verified for a homogeneous bianisotropic media. Then, we use this method to extract the effective constitutive parameters of the bianisotropic metamaterials. The retrieved results corroborate well the conclusions in previous published papers.

REFERENCES

1. Smith, D. R., S. Schultz, P. Markos, and C. M. Soukoulis, *Phys. Rev. B*, Vol. 65, 195104, 2002.
2. Katsarakis, N., T. Koschny, M. Kafesaki, E. N. Economou, and C. M. Soukoulis, *App. Phys. Lett.*, Vol. 84, 2943, 2004.
3. Marques, R., F. Medina, and R. Rafii-El-Idrissi, *Phys. Rev. B*, Vol. 65, 144440, 2002.
4. Chen, X., B.-I. Wu, J. A. Kong, and T. M. Grzegorczyk, *Phys. Rev. B*, Vol. 71, 46610, 2005.

Homogenization of Finite Metallic Fibers and 3D-effective Permittivity Tensor

Guy Bouchitte and Cristophe Bourel
Universite de Toulon, France

Abstract— We consider a finite domain of $\mathbb{R}^3$ (scatter) filled periodically with high conductivity metallic fibers. Our aim is to describe mathematically the asymptotic of the harmonic diffraction problem (electromagnetic waves with a prescribed $\exp(-i\omega t)$ dependence) as the period η tends to zero. In the limit process, the conductivity in the fibers increases to infinity.

In this talk we will present two results, both obtained for a vanishing volume fraction of fibers (the section of fibers is infinitesimal with respect to the period): in the first situation fibers are e_3-parallel connected with length L. We find that the vertical component E_3 of the limit electric field induces a volumic current j density (solution of a 1D-propagation equation in which E_3 acts as a source term). The resulting diffraction problem involves (E, H) and j. Unfortunately the effective permittivity law is non local (convolution kernel with interaction distance of order L). This important feature is hidden when we assume a polarized electric field and $L = +\infty$: in this case the effective law can be interpreted through a scalar effective permittivity $\varepsilon^{\text{eff}}(\omega)$ which depend explicitely of the wave number. It becomes negative below *a cut-off frequency*. Notice however that fully 3D-negative tensors cannot be reached by this procedure (even if fibers are disposed in three orthogonal directions).

In our second variant we show that effective 3D-isotropic negative permittivity tensors can be reached: the trick consists in using the previous (non local) homogenized model at a very small scale by reiterating periodically our previous fibered structure (at macroscopic scale fibers are then very small and disconnected). We obtain a local effective law characterized by an effective permittivity tensor $\varepsilon^{\text{eff}}(\omega)$ whose eigenvalues depend on frequency and are ruled by a local spectral problem. The tensor $\varepsilon^{\text{eff}}(\omega)$ turns out to be negative wihin some range of frequencies (*band gaps*).

Case I: The inclusions are vertical parallel metallic fibers of radius $r \ll \eta$ (vanishing filling ratio) but scaled so that the average 2D-capacity of the cross sections remain positive. The permittivity ε has a large imaginary part. We find that the vertical component E_3 of the limit electric field induces a volumic current j density (solution of a 1D-propagation equation in which E_3 acts as a source term). The resulting diffraction problem involves (E, H) and j. It is non local in (E, H). However, in the case of a polarized electric field, we recover an homogenized medium characterized by an effective permittivity $\varepsilon^{\text{eff}}(\omega)$. This $\varepsilon^{\text{eff}}(\omega)$ depends explicitely of the wave number. It becomes negative below *a cut-off frequency*.

Case II: The filing ratio of inclusions is positive ($r \sim \eta$) but now the permittivity ε is scaled like $\frac{1}{\eta^2}$. Starting with e_3-invariant geometry we find an homogenized medium with a magnetic activity. It is described by an effective permeability $\mu_{\text{eff}}(\omega)$ depending explicitely on a elementary cell spectral problem. An important consequence is that, for certain ranges of frequencies, $\mu_{\text{eff}}(\omega)$ becomes negative (band-gap structure).

REFERENCES

1. Bouchitte, G. and D. Felbacq, "Homogenization near resonances and artificial magnetism from dielectrics," *C. R. Math. Acad. Sci. Paris*, Vol. 339, No. 5, 377–382, 2004.
2. Bouchitte, G. and D. Felbacq, "Left handed media and homogenization of photonic crystals," *Optics Letters*, Vol. 30, 10, 2005.
3. Bouchitte, G. and D. Felbacq, "Homogenization of wire mesh photonic crystals embdedded in a medium with a negative permeability," *Phys. Rev. Lett.*, Vol. 94, 183902, 2005.
4. Bouchitte, G. and D. Felbacq, "Low frequency scattering by a wire mesh photonic crystal: Homogenized limit in the capacitary case," submitted to *SIAM J. Applied Maths.*
5. Bouchitte, G. and D. Felbacq, "Homogenization of a set of parallel fibers," *Waves in Random Media*, Vol. 7, No. 2, 1–12, 1997.
6. Bellieud, M. and G. Bouchitte, "Homogenization of elliptic problems in a fiber reinforced structure. Nonlocal effects," *Ann. Scuola Norm. Sup. Pisa Cl. Sci.*, Vol. XXVI, No. 4, 407–436, 1998.
7. Bouchitte, G. and M. Bellieud, "Homogenization of a soft elastic material reinforced by fibers," *Asymptotic Analysis*, Vol. 32, No. 2, 153–183, 2002.

Homogenization of 3D-dielectric Photonic Crystals and Artificial Magnetism

G. Bouchitté[1], **C. Bourel**[1], **and Didier Felbacq**[2]

[1]Departement of Mathematics, Université de Toulon, BP 20132, 83957 La Garde Cedex, France
[2]GES UMR 5650, Place Bataillon, 34095 Montpellier Cedex 05, France

Abstract— In [1–4], a theory for artificial magnetism in two-dimensional photonic crystals has been developed for large wavelength (homogenization). The main idea was that a periodic crystal with high permittivity inclusions shows up micro-resonance effects from which an effective permeability law with anomalous dirpersion could be evidenced in a explicit way. The main drawback was however that in this model we assumed magnetic parallel polarization so that merely infinite photonic crystals (invariants in one direction) could be considered.

In this work we propose a full 3D generalization of previous results: the diffraction of a finite 3D- dielectric crystal is considered at a fixed wavelength and a limit analysis as the period tends to zero is performed. We evidence a new microscopic vector spectral problem which turns out to rule the macroscopic behavior of the crystal. We obtain then an extension to the 3D-case of the results in [1, 3] by proving rigorously that permeability tensor laws can be reached where the effective tensor exhibits negative eigenvalues in appropriate range of frequencies. This suggests that periodic bulk dielectric inclusions could be an efficient alternative to the very popular metallic split-ring structure proposed by Pendry [5].

REFERENCES

1. Bouchitté, G. and D. Felbacq, "Homogenization near resonances and artificial magnetism from dielectrics," *C. R. Math. Acad. Sci. Paris*, Vol. 339, No. 5, 377–382, 2004.
2. Felbacq, D. and G. Bouchitté, "Left handed media and homogenization of photonic crystals," *Optics Letters*, Vol. 30, 10, 2005.
3. Felbacq, D. and G. Bouchitté, "Homogenization of wire mesh photonic crystals embdedded in a medium with a negative permeability," *Phys. Rev. Lett.*, Vol. 94, 183902, 2005.
4. Felbacq, D. and G. Bouchitté, "Negative refraction in periodic and random photonic crystals," *New J. Phys.*, Vol. 7, 159, 10.1088, 2005.
5. OBrien, S. and J. B. Pendry, "Magnetic activity at infrared frequencies in structured metallic photonic crystals," *J. Phys. Condens. Mat.*, Vol. 14, 6383–6394, 2002.

Session 3A3
Microwave Remote Sensing of Soil Moisture

The Soil Moisture Active and Passive (SMAP) Mission

Dara Entekhabi[1], **Eni Njoku**[2], **Peggy O'Neill**[3]
Michael Spencer[2], **Kent Kellogg**[2], **and Jared Entin**[4]

[1]Massachusetts Institute of Technology, Cambridge, MA 02139, USA
[2]Jet Propulsion Laboratory, California Institute of Technology, Pasadena, CA 91109, USA
[3]Goddard Space Flight Center, Greenbelt, MD 20771, USA
[4]NASA Headquarters, Washington, DC 20546, USA

Abstract— The U.S. National Research Council Committee on Earth Science and Applications from Space issued the first decadal survey for Earth observations. This 2007 report recommended 17 missions grouped into several tiers based on factors such as science priority, risk and readiness. The Soil Moisture Active and Passive (SMAP) mission is one of four in the first tier of missions recommended by the report. In 2008, SMAP was selected by NASA to be a directedmission and is scheduled for launch in 2013. SMAP builds on concept development and risk-reduction studies carried out for the earlier Hydros mission concept. The SMAP mission measurement approach is based on simultaneous active (radar) and passive (radiometer) measurements in the 1.2–1.4 GHz range (L-band). The radar and radiometer share a feed and a 6-meter light-weight mesh deployable reflector. The observatory will launch into a sun-synchronous low-earth orbit. Conical scan measurements will be made across a wide swath (1000 km) resulting in a 2 to 3 days global data refresh rate. The radar resolution is enhanced through synthetic aperture processing and varies from 1–3 km over the outer 70% of the swath to about 30 km near the center of the swath. The radiometer resolution is 40 km across the entire swath. The SMAP mission soil moisture products will be based on combined radar and radiometer measurements (hydrometeorology product at 10 km, hydroclimatology product at 40 km resolution). The synergy of active and passive measurements enables global soil moisture mapping with unprecedented resolution and sensitivity.

Estimation of Soil Moisture with the Two Repeat-pass Radar Measurements

Jiancheng Shi
ICESS, University of California, Santa Barbara, CA 93016, USA

Abstract— Soil moisture is a key parameter in numerous environmental studies, including hydrology, meteorology, and agriculture. It plays an important role in the interactions between the land surface and the atmosphere, as well as the partitioning of precipitation into runoff and ground water storage. The spatial and temporal dynamics of soil moisture are important parameters for various processes in the soilvegetation-atmosphere-interface. The Soil Moisture Active and Passive Mission (SMAP) with both Active/Passive L-band instruments has been approved by NASA for monitoring global soil moisture and freeze/thraw. The SMAP instrument combines radar and radiometer subsystems. The radar operates with VV, HH, and HV polarizations and the radiometer operates with V, H and U (third Stokes parameter) polarizations at 1.41 GHz.

In attempt to use the active microwave remote sensors for estimation of soil moisture, we are mainly facing two common problems: effects of surface roughness and vegetation cover. Natural variability and the complexity of the vegetation canopy and surface roughness significantly affect the sensitivity of backscattering to soil moisture. Backscattering signals from vegetated areas is a function of water content and its spatial distribution as determined by vegetation structure and underlying surface conditions including surface roughness parameters and dielectric properties. Due to the limited observations from either active measurements alone, an ill condition, the number of measurements and equations are less than the number of unknowns, is expected. It results in the uncertainties in estimation of soil moisture.

In this study, we develop an active technique to estimate surface soil moisture with the focus on the short vegetated surfaces. We first simulated a database for both active and passive signals under SMAP's sensor configurations using the radiative transfer model with a wide range of conditions for surface soil moisture, roughness and vegetation properties that we considered as the random orientated disks and cylinders. Using this database, we developed a technique to estimate soil moisture with two repeat pass radar measurements. We will demonstrate this technique with the model simulated data and its validation with the experimental data from the ground and airborne PALS image data from the soil moisture SGP'99 and SMEX'02 experiments.

A Combined Use of ASAR and PALSAR Data for Soil Moisture Retrieval

Francesco Mattia, **Giuseppe Satalino**, **and Anna Balenzano**
Consiglio Nazionale delle Ricerche (CNR)
Istituto di Studi sui Sistemi Intelligenti per l'Automazione (ISSIA)
Via Amendola 122/D, Bari, Italy

Abstract— This paper investigates the use of multi-temporal L & C band SAR data for crop mapping and for the retrieval of the underlying soil moisture content. Its final aim is to contribute at defining and assessing retrieval strategies for monitoring agricultural crops using current and future satellite SAR data. Past studies have shown that a condition for successful retrieval algorithms consists of a thorough understanding and an appropriate modeling of the relationships between SAR measurements and soil and vegetation parameters. Besides, it is necessary to have updated information about land cover, at least in terms of main crop classes (e.g., small stems/broad leaves crops), in order to apply the appropriate retrieval approach. In view of this consideration, the development of retrieval and classification methods are strictly connected. In this respect, the use of multi-frequency and multi-polarimetric SAR data can be beneficial due to their different sensitivity to vegetation and soil components. For instance, for crop canopies characterized by a predominant vertical structure (e.g., cereal crops), it has been observed that the interaction between the vegetation layer and the SAR signal at L-band can be disregarded, at least at HH polarization. Conversely, at C-band there is a significant and differential attenuation of H and V polarizations. Therefore, the C-band HH/VV backscatter ratio can be employed to map cereal fields, whereas the L-band HH backscatter is well suited to retrieval the underlying soil moisture content.

In this context, the objective of this paper is to assess a combined use of ASAR AP and PALSAR data, acquired over the Capitanata plain (Southern Italy), for wheat mapping and soil moisture retrieval. The analyzed data consist of a temporal series of ground and ASAR and PALSAR data acquired from 2006 to 2008. Results indicate that the proposed approach permits to achieve classification and soil moisture retrieval accuracies of approximately 80% and 5%, respectively.

Retrieval Algorithm Development Based on SMEX02 Field Campaign Data for the Soil Moisture Active and Passive (SMAP) Mission

Steven K. Chan and Eni G. Njoku
Jet Propulsion Laboratory, California Institute of Technology, Pasadena, CA 91109, USA

Abstract— The Soil Moisture Active-Passive (SMAP) mission is a NASA directed mission aiming at providing global observations of soil moisture and land surface freeze/thaw state with unprecedented accuracy, resolution, and spatial coverage. The resulting hydrosphere state measurements will help advancing understanding of processes that link the water, energy and carbon cycles, as well as enhancing existing weather and climate forecast skills.

As a software tool to accurately assess the soil moisture measurement capability of SMAP, the SMAP Algorithm Development Testbed is currently under active development at NASA Jet Propulsion Laboratory. Among its diverse simulation capabilities, the Testbed allows objective evaluation of the relative merits of different microwave land surface models, retrieval algorithms, and ancillary data for satisfying SMAP's soil moisture and freeze/thaw science objectives.

In this work, we illustrate how a calibration/validation (CalVal) dataset acquired for an existing satellite can be utilized within the Testbed simulation framework to help develop better microwave land surface models and retrieval algorithms at L-band frequencies (1.4 GHz). Specifically, by using a subset of the Soil Moisture Experiment 2002 (SMEX02) dataset, we present how soil moisture variability in both space and time affects the observed brightness temperature and radar backscatter observed over a SMAP footprint scale. An inversion model is suggested and its performance evaluated against various independent ancillary datasets acquired in the same campaign. Sensitivity of retrieval accuracy to such factors as modeling errors, calibration errors, and ancillary data uncertainties is also investigated.

Development of an AMSR-E Soil Moisture Retrieval Algorithm through Field Experiments and Data Assimilation

Hui Lu, **Toshio Koike**, **Hideyuki Fujii**, **Tetsu Ohta**, **and Katsunori Tamagawa**
River and Environment Engineering Lab., The Department of Civil Engineering
The University of Tokyo, Hongo 7-3-1, Bunkyo-Ku, Tokyo 113-8656, Japan

Abstract— AMSR-E is highly expected to provide a state-of-the-art soil moisture observation in regional and continental scales. In this paper, three components which are the basis of our AMSR-E soil moisture algorithm are presented, and the performance of our algorithm is evaluated at a CEOP reference site.

The first task is the development of a new physically-based Radiative Transfer Model (RTM), in which the volume scattering effects of soil layer is simulated by Dense Media Radiative Transfer Theory (DMRT) and the surface roughness effects is simulated by Advance Integral Equation Method (AIEM).

The second attempt is to improve the understanding of vegetation effects. It is study through a long term experiment which monitors the growth cycle of winter wheat. Based on the analysis of winter wheat experiment results, the Polarization Index (PI) of 6.9 GHz and the Index of Soil Wetness (ISW) calculated from 18 GHz and 6.9 GHz horizontal polarization were recommended to compose the look up table.

The third progress is the development of a new parameterization method, optimizing model parameters by Land Surface Data Assimilation System developed at The University of Tokyo (LDAS-UT). The capability of LDAS-UT was validated successfully with winter wheat experiment data.

Finally, the new RTM and parameterization method was validated on AMSR-E match up data set. The results demonstrate that the simulated brightness temperature is in good agreements with the one observed by AMSR-E.

Exploring Uncertainty in the ERS-SCAT Soil Moisture Data with Monte Carlo Simulations

V. Naeimi and W. Wagner
Institute of Photogrammetry and Remote Sensing, Vienna University of Technology, Austria

Abstract— Recent technological advances in remote sensing of soil moisture have demonstrated the potential of microwave remote sensing techniques for the monitoring of soil moisture dynamics. In addition to improved instrumentation, equally important are the retrieval methods for soil moisture measurements. Dealing with and understanding uncertainty in the retrieval models is valuable for optimal soil moisture estimation and also for scientific applications such as data assimilation, which are very sensitive to observation and model errors.

In this study, we focus on problems existing in soil moisture estimation from ERS scatterometer (SCAT) data and provide an overview of the current state of uncertainty modeling and analysis of the retrieval model. The method initiates with a description of the variability and uncertainty of each input parameter representing by frequency distribution. A Monte Carlo simulation-based approach is used to propagate the uncertainty of input parameters within the system. Repeating the simulation several times allows an estimate to be made of the error implicit in the output parameters characterizing the uncertainty of the soil moisture product.

Satellite-based Atmosphere-land Coupled Data Assimi-Lation System

Toshio Koike[1], **David N. Kuria**[2], **and Mohamed Rasmy**[1]

[1]Department of Civil Engineering, The University of Tokyo
Hongo, Bunkyo-ku, Tokyo 113-8656, Japan
[2]Jomo Kenyatta University of Agriculture and Technology
Nairobi, P. O. Box 62000-00200, Kenya

Abstract— While GCMs are best at simulating evolving and future changes in climate systems, they are unable to produce mesoscale and local atmospheric phenomena. Thus downscaling methods are necessary to bridge the gap between global scales and smaller modeling scales. In this paper we use a high spatial resolution mesoscale model and nest it within a GCM. This nesting is realized using initial and boundary conditions from the GCM output. This approach alone is not adequate for reproducing local phenomena and extreme events because nesting does not include accurate land surface initial and boundary conditions, and thus the approach misses important physical processes such as convection and local circulation.

To physically address the mechanisms of atmosphere-land interactions based on land surface conditions, a land data assimilation system (LDAS) is used to augment the stand-alone regional atmospheric model. While this system addresses land surface heterogeneities, it does not address atmospheric components in a direct way. This system assimilates lower frequency microwave brightness temperatures to improve estimation of land surface conditions.

It has been argued that the structure of the atmosphere is strongly dependent on cloud microphysics because microphysical processes are responsible for the release of latent heat, formation of precipitation and precipitation evolution outside of clouds. A satellite-based cloud microphysics data assimilation system (CMDAS) was developed for assimilating brightness temperature at high microwave frequency to improve estimation of cloud properties over ocean and sea surfaces. CMDAS assimilates the satellite microwave radiometer dataset of the advanced microwave scanning radiometer for the Earth observing system (AMSR-E) and retrieves integrated water vapor and integrated cloud liquid water content.

A satellite-based atmosphere-land coupled data assimilation system (SALDAS) combines LDAS and CMDAS by refining and coupling them with a physically based land-atmosphere coupled radiative transfer model that can represent microwave radiative transfer in soil by considering surface roughness effects, volume scattering and emission in the soil volume, and atmospheric emission and scattering. Both data assimilation schemes use the advanced regional prediction system (ARPS), developed at the Center for Analysis and Prediction of Storms at the University of Oklahoma and the system is coupled with simple biosphere model 2 (SiB2). To account for precipitation estimation, SALDAS includes modifications allowing direct estimation of snow and rain rates as additional assimilation variables.

SALDAS was applied to the National Centers for Environmental Prediction (NCEP) global forecast system (GFS) reanalysis data and AMSR-E data, for downscaling to a mesoscale area of the Tibetan Plateau. The result of the SALDAS validation for assimilated integrated cloud liquid water and rain in the Tibetan Plateau shows better consistency with the satellite infrared observation.

TRMM Microwave Imager Soil Moisture Mapping and Flooding during CLASIC

T. J. Jackson, **R. Bindlish**, **Y. Wang**, **and M. Cosh**
USDA ARS Hydrology and Remote Sensing Lab, USA

Abstract— Passive microwave remote sensing has the potential to contribute to flood risk and impact assessment through the direct relationship between emissivity and soil moisture/standing water. Lower frequencies have greater potential because the impacts of atmospheric and vegetation attenuation are minimized. Although the current satellite sensor spatial resolution is quite coarse for some applications such as flash flooding, they can allow us to study large scale flooding events that extend over longer durations (greater than 2–3 days). Global products from sensors such as the Advanced Microwave Scanning Radiometer-AMSR are available approximately every other day. This may not be a useful interval for either warnings or post flood assessments. The TRMM Microwave Imager (TMI), especially near its maximum latitude bands of coverage ($+/-38^{\circ}$), provides high frequency temporal coverage during an approximate 6 hour time window every day. Although the time window changes systematically from day to day, this unique capability allows us to examine the temporal dynamics of soil moisture and standing water associated with flooding. The concepts described were evaluated using data collected as part of the Cloud Land Surface Interaction Campaign (CLASIC) conducted in Oklahoma during the summer of 2007. CLASIC was intended to examine the mechanisms that exist between land surface variables such as soil moisture and temperature and the atmosphere. Extensive ground and aircraft observations of these variables were made during June-July over a large region of the Oklahoma Southern Great Plains. Extreme conditions were encountered during the CLASIC field experiment. The summer precipitation over the Southern Great Plains was significantly greater than the average and resulted in new historic records in many areas. This rainfall resulted in widespread and repeated flooding throughout Oklahoma and Texas. In this study, TMI observations available during the CLASIC will be used to evaluate soil moisture and potential flood information.

Comparison of Soil Scattering Models Using Data vs. Image from EMSL Experiment

Q. Yin[1, 2], **W. Hong**[1, 2], **F. Cao**[1, 2], **W. X. Tan**[1, 2, 3], **and Y. Lin**[1, 2, 3]

[1]National Key Laboratory of Microwave Imaging Technology, China
[2]Institute of Electronics, Chinese Academy of Sciences, China
[3]Graduate University of Chinese Academy of Sciences, China

Abstract— In this paper, we study the performances of soil scattering models employing both the original scatterometer data from European Microwave Signature Laboratory (EMSL) and the images obtained from data by means of Circular SAR wavenumber algorithm. Data and imagery can reflect scattering properties from different perspectives. In fact, most physical models are proposed in terms of scatterometer data, and on the contrary, empirical ones are developed based on the analysis of SAR images. The experimental results show that the physical model Integral Equation Method (IEM) is more accurate than the empirical model Oh in retrieving parameters from data while Oh has higher efficiency than IEM in estimating parameters from images.

Soil roughness and moisture conditions are primary determinants of hydrology modeling, irrigation scheduling, pest management, and yield estimation. Scattering modeling is the effective way to relate soil parameters to those microwave sensor parameters, and they are generally divided into physical and empirical models. We take IEM and Oh model as representatives in this study.

We firstly apply Circular SAR wavenumber algorithm to obtain fully polarimetric single look complex images of L, Ls, and S band, with bandwidth of 500 MHz. Data were calibrated using the standard monostatic full polarimetric procedure, and basically the reciprocity theorem is met. Secondly the inversion technique is performed respectively according to the theory of IEM and Oh model using both the obtained images and the original data. Finally, we compare the ground truth measurement to the experimental results under different combination of source files and models, as shown in Fig. 1.

Soil scattering models developed upon different theory are compared in the inversion experimentation using data and imagery. In addition, we could probably find out some relationship between these models through further investigation.

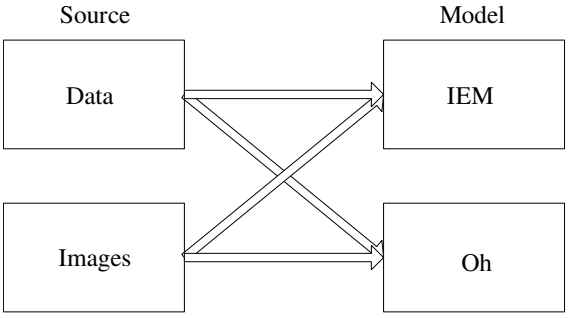

Figure 1: Combination of source and model.

Session 3A4
Electromagnetic Application in the Advanced Manufacturing Technology

Research on the Robotic Polishing Combined with Electromagnetic Field of Rapid Metal Tool

Guangchao Han[1], **Haiou Zhang**[2], **and Qichang Su**[2]

[1]School of Electronic Information & Mechanics, China University of Geosiences
Wuhan 430074, China
[2]School of Mechanical Science & Engineering
Huazhong University of Science and Technology
Hubei, Wuhan 430074, China

Abstract— In the rapid metal tooling, high efficient polishing process can improve the mould quality and shorten the lead time of the rapid tool, but the polishing process is frequently carried out manually. The application of industrial robot for the polishing process can minimize the production times and improve the working environment on a certain extent. In order to increase the robotic polishing efficiency continuously, the robotic polishing process combined with electromagnetic field is developed to fit for the application of commercial industrial robot, which is hard to be controlled online for its close control construction. Free abrasive and soft polishing tool are also applied in the robotic polishing process to cooperate with the electromagnetic field. A minitype electromagnet is trial-manufactured and connected to the robotic end-effector, which can act on the polished surface with the robotic moving. The electromagnet is canulate that the polishing tool and the electrical spindle can be fixed in the hollow. A partition & flexible mapping method based on CAM is developed to generate the uniform robotic polishing path, which can compensate the elastic deformation and the abrasion of the soft polishing tool. Experiments are executed to test the influence between the electromagnetic field and the polishing efficiency. The result shows that the polished material can increase over 50% when the metal surface is combined acted with the electromagnetic field about 160 Gs and the polishing tool.

Modeling of Thermal-metallurgical Behavior during Hybrid Plasma-laser Deposition Manufacturing

Fanrong Kong[1, 2], **Haiou Zhang**[1], **and Guilan Wang**[3]

[1]College of Mechanical Science and Engineering
Huazhong University of Science and Technology, Wuhan 430074, China
[2]Research Center for Advanced Manufacturing, Southern Methodist University
3101 Dyer Street, Dallas, Texas 75205, USA
[3]College of Material Science and Engineering
Huazhong University of Science and Technology, Wuhan 430074, China

Abstract— A three-dimensional nonlinear finite element method combining with Monte Carlo model was developed to investigate the temperature field and grain growth in the heat affected zone (HAZ) during the plasma-laser hybrid deposition manufacturing (PLDM) thin wall metal parts. The numerical study shows that the temperature gradient directly decides the grain growth speed in the HAZ of deposited wall. However, the effect of thermal impact due to continuous scanning of laser and plasma arc on the microstructure in the substrate material is negligible. This thermal-microstructure model could be further applied to study the variable high energy forming processes.

A Flexible Synchronous Powder Feeder for Electromagnetism Compress Digital Manufacturing of FGM Metal Component

Haiping Zou, **Haiou Zhang**, **and Guilan Wang**
Huazhong University of Science and Technology, Wuhan 430074, China

Abstract— Archiving functionally gradient materials (FGM) fabrication via digital manufacturing methods has attracted considerable attention in recent years. However, the application of multi-varieties powders flexible control mixing and feeding is still in its infancy. In this paper, a set of 3-units flexible synchronous powder feeder for electromagnetism compress FGM metal component digital manufacturing system was developed. The powder feeder unit was based on the timing belt driving and Pneumatic conveying principle. The feeding control hardware circuit was based on ADUC812 with appended TLC5620 D/A converter. The AD564 was used to transform 3-way analogy output voltage signals frequency pulse signal to actuate step motors. The Superior computer control program was based on lab windows/CVI program developing environment with good man-machine conversation interface. Tests were made with Ni-based alloy powders, Fe-based alloy powders and ceramic powders in the particle average diameter of 15–350 Microns. Results showed that powders mixtures obtained from the device are continuous and stable. The precision of delivering powders mixture can be within 2% error scope comparing to the desired mixture quality and the flexible proportion of mixture can be easy changed in the computer control program by synchronously controlling the powder feeder rotation speed. Further experiments were carried out to fabricate the gradient material PEN (positive electrode/electrolyte/negative electrode) of Solid Oxide Fuel Cell (SOFC) using the flexible control 3-units synchronous powder feeder as conveying mechanism to feed fine multi-varieties powders mixtures. Scanning Electron Microscopy (SEM) observation indicates that the variation of PEN composition is continuous gradient transition as expected.

Research on Relationship between arc Length and arc Voltage in the Plasma Deposition Manufacture Process

Haiou Zhang[1], **Chao Wang**[1], **Guilan Wang**[2], **and Hui Ai**[2]

[1]School of Mechanical Engineering
Huazhong University of Science and Technology, Wuhan 430074, China
[2]School of Materials Science and Engineering
Huazhong University of Science and Technology, Wuhan 430074, China

Abstract— The method of direct rapid metal prototyping and tooling can sharply shorten the lead-time and reduce the cost of product development, therefore it become the key technology in the RP&M. In this field, PDM (Plasma Deposition Manufacture) technology, based on low-cost and high efficiency plasma power resource caused attention.

This paper analysis the present status of direct rapid metal prototyping by PDM technology, and discusses the hardware and software scheme for a 5 axis movement system about PDM equipment. Experiments demonstrate that it is a friendly open system with satisfied operation and maintainability. In other hand, as it is difficult to measure the deposition height directly in the PDM process, a method for measuring deposition height by monitoring arc voltage is proposed because of the arc voltage is linear with arc length.

Research of Electromagnetic Effects on the Compound Arc Beam in the Hybrid Plasma-laser Manufacturing Process

Ying-Ping Qian[1], **Hai-Ou Zhang**[2], **Gui-Lan Wang**[3], **and Guangchao Han**[4]

[1]School of Mechanical Engineering, Hubei University of Technology, 430068, China
[2]School of Mechanical Engineering, Huazhong University of Science and Technology, 430074, China
[3]School of Material, Huazhong University of Science and Technology, Wuhan 430074, China
[4]China University of Geosiences, China

Abstract— The hybrid plasma-laser deposition manufacturing (PLDM) is a new technology for direct metal parts manufacturing. The shape and characteristics of compound arc beam has important influences on the molten-pool and, build-accuracy, as well as the performance of part and the internal quality. As plasma is a kind of gas ionized sufficiently, strong current pass the compound arc beam along the axial direction, which generate poloidal magnetic field. The magnetic field can contract the plasma arc beam and change the shape and features of compound arc beam. The study of electromagnetic influences on compound arc beam is essential to control the part quality. In this paper, the mechanism of electromagnetic influenced on the compound arc column is analyzed theoreticly, and the influence rule of electromagnetic on the compound arc beam is studied experimentally. The experimental results show that the compound arc column can absorb electromagnetic waves, and electromagnetic waves can compress the compound arc column. The compound arc column can maintain the same patterns only when the magnetic compressure and the expansive power outward are balance.

Multi-axis Path Planning for Electromagnetic-compressed Plasma Deposition Manufacturing Based on STL Format

Haiou Zhang[1], **Jiang Jiang**[2], **Guilan Wang**[2], **Xinhong Xiong**[2], **and Guangchao Han**[3]

[1]State Key Laboratory of Digital Manufacturing Equipment and Technology
Wuhan 430074, China
[2]State Key Laboratory of Plastic Forming Simulation and Die & Mould Technology
Wuhan 430074, China
[3]China University of Geosiences, China

Abstract— Super alloy was widely used in a variety of industry field such as aeronautics and astronautics, and plasma arc deposition has provided an effective way in fabricating refractory and intractable parts e.g., super alloy parts directly from their digital models. However, there is much difficulty in fabricating metal parts with large obliquity because of the flowing of molten pool caused by gravity field. In this paper, an innovated method named electromagnetic-compressed plasma deposition manufacturing is presented which employs the electromagnetic field to decrease the effectiveness of the flowing of molten pool. The influence of tool path to the performance of nickel-based alloy parts is emphasized. The result shows that the crystal grain was greatly refined with the help of electromagnetic and the complicated parts with big overhang structure and large obliquity could be fabricated under proper tool path and electromagnetic. Some parts with complex shape were trial manufactured which proves that electromagnetic-assisted plasma deposition manufacturing is a promising technology in direct rapid manufacturing of metal parts.

Integrated Robotic Plasma Spraying System for Advanced Materials Processing

Weisheng Xia[1,2], **Haiou Zhang**[2], **Gui-Lan Wang**[1],
Yunzhen Yang[1], **Guangchao Han**[3], **and Haiping Zou**[1]
[1]State Key Laboratory of Materials Processing and Die & Mould Technology
Huazhong University of Science and Technology, Wuhan 430074, China
[2]State Key Laboratory of Digital Manufacturing and Equipment Technology
Huazhong University of Science and Technology, Wuhan 430074, China
[3]China University of Geosiences, China

Abstract— During plasma spraying, to control the time dependent D.C. plasma jet behavior requires the comprehensive understanding of its electric, magnetic, thermal, thermodynamic phenomena. In this paper, influence of particles injection with different forms of suspension, solid state on the fluctuation of plasma jet is analyzed, and a control approach is presented to eliminate the effect. Moreover, an integrated robotic plasma spray (RPS) system for advanced materials processing, i.e., rapid metal tooling and solid oxide fuel cell (SOFC), is developed, which combines a PC-based controller with a six-axis robot. Communication between PC and Motoman UP-20 robot was established on the help of Ethernet, and robot control software was developed for the host control and the exchanging of working jobs by PC. Siemens S7-300 PLC was connected to the system through MPI (Multi-Point Interface). Finally, the robotic plasma spray forming system was established accompanied with forming process monitoring, intelligent adaptive adjustment of robot spraying trajectories, real-time control of robot and other functions. The intelligent adaptive adjustment of robot spraying trajectories and self-dispatch of manufacturing strategies were carried out by the resultant system according to the feedback of the temperature and thickness of sprayed coatings and other information during plasma praying. The flexibility of the forming system was promoted by integrating plasma spray forming with robot motion control. Excellent control performance is observed and the system can be effective to meet the requirements of different materials processing techniques.

Numerical Simulation of Electromagnetic Flux Leakage in Application of Internal Defects Prediction of Metal Parts

H. O. Zhang[2], **Y. Z. Yang**[1], **G. L. Wang**[1], **and Haiping Zou**[3]

[1]State Key Laboratory of Material Processing and Die & Mould Tech.
Huazhong University of Sci. & Tech., Wuhan 430074, China
[2]State Key Laboratory of Digital Manufacturing Equipment and Tech.
Huazhong University of Sci. & Tech., Wuhan 430074, China

Abstract— Metal products were widely used at a variety of industry, so it is essential to predict the security and the usability without the destructive testing for the desired production efficiency under the different their working conditions. Recently, the plasma deposition dieless manufacturing process (PDM) is an innovative and promising application of plasma heat source with extensive industrial potential for refractory and intractable material part or prototype, rebuilding of worn components and especially the direct rapid fabrication of functionally graded materials (FGMs). However, Residual stress and distortion induced by the highly localized transient heat and strongly nonlinear temperature distributions would likely promote undesired and unpredictable warps and cracks in this process. Thus, to distinguish the internal defect from the significant discontinuities during the nondestructive testing of the metal parts, in this paper, the finite-element method (FEM) was applied to predict the electromagnetic distribution. According to the difference the magnetic flux leakage analysis, distinction threshold was built by the ratio of the peak-to-peak amplitudes of the raw inspecting signal anomaly. Computational results show that it is potential to decrease the testing period and improve the security of metal parts, in particular, the micro-raw and hole in the metal parts can be predicted, thus the possibly-intended breakage would be improved.

Session 3A5a
Non-Thermal Mechanisms of Interaction between Electromagnetic Fields and Living Matter

Electrodynamic of Zwitterions in Aquaeus Solutions under the Action of Weak Magnetic Fields

E. Del Giudice[1, 2], **L. Giuliani**[1, 3], **Natalia Bobkova**[1, 4], **and M. N. Zhadin**[1, 4]

[1]International Commission for ElectroMagnetic Safety (ICEMS), Venice, Italy
[2]International Institute of Biophysics, Neuss, Germany
[3]National Institute for Ocuupational Health and Safety (ISPESL), Rome, Italy
[4]Institute of Cell Biophysics, Pushchino, Moscow Region, Russia

Abstract— The Zhadin effect [1] seems to be involved in fundamental mechanisms of interaction between EMF and living matter. In the previous papers [2–5] the effect is examined in the frame of QEM [6]. In [2] it is offered a model for the current arising in the a electrolytic cell where an aquaeous solution of glutamic acid (GLU) is exposed to an DC-AC combined magnetic field based on the poperties of water as a biphase liquid, whose a fraction (about 2/5 at room temperature) is coherent and the other fraction is bulk. The mechanism of the escape of the GLU ions was described and the current arising is deduced like the consequence of the motion of ions towards the electrodes, at a voltage of $-0.08\,\mathrm{V}$. In [3] is proposed that the current is due only to the motion of anions. In [4] the crucial role of GLU like a zwitterion which has a spectrum line close to a line of the spectrum of water is assumed in order to explain the formation of mixed GLU-water domain before the escape of ions from the coherent dominions. In [5] is proposed a slightly different experiment, where electrodes are no more employed and the GLU-solution in water is put in a flask, within a condenser at a voltage of $-0.08\,\mathrm{V}$, close to an induction coil, in which a current arising is detected when the previous combined DC-AC field is applied. The replication of the Zhadin effect in such new different configuration of the experiment allows to exclude that the Zhadin effect is due only to the passivation of the removed electrodes.

Because the phenomenon involved in the experiment is a multistep phenomenon, in the present paper the authors' aim is to connect the above described explanations of each step in a unique consequential theory.

Based on the perspective of the coherence the water is considered again as a biphase liquid patially coherent and partially bulk.

First is examined the approach of GLU to coherent dominions of water. Solution is kept at PH 2.5, at which the behaviour of GLU is that one of a zwitterion. The coherent dominion, a rotating ellipsoid, which can be considered, in the order of the time on the scale of a second, a sphere with a radius of 40 nm, offer a boundary depth of 4 nm. Each CD contains, at room temperature, about 5,500,000 water molecules. The coherent status $|S>$ of a CD is the coherent superposition of the fundamental state 1σ and the excitated state $5\delta >$. The LCAO provides the following coefficients:

$$< S|1\sigma >= 0.87 \qquad < S|5\delta >$$

then the CD is able to provide about 650,000 electrons to transform a GLU molecule in an ion, when the molecule enters the CD of water forming a mixed CD, according to the description in [4]. To promote the birth of the mixed CD we consider two forces are present on the water CD boundary: the dispersive force:

$$F_d = 1/(\omega^2_{\mathrm{GLU}} - \omega^2_{\mathrm{water}})\,\mathrm{grad}A^2$$

and the ponderomotive force:

$$F_p = -q^2/m\,\mathrm{grad}A^2 = qV_p$$

where $V_p = 0.1\,\mathrm{V}$.

The dispersive force is attractive because $\omega^2_{\mathrm{GLU}} - \omega^2_{\mathrm{water}} < 0$.

Then the zwitterion is forced towards the CD. Since the closeness of the spectrum lines of GLU and water — in an excited status — the GLU joins the CD because the slight difference of the lines is lower than kT, i.e., the environment provides the small quantity of energy which needs to match the two frequencies of GLU and of CD water [6]. When GLU is within shares the CD plasma of electrons of water meolecules of the CD and when it assumes an electron becomes a negative ion GLU.

The negative ion is repelled and stratched by the ponderomotive force that is repulsive and goes in the boundary where the following set on of the DC-AC combiened fields works like in [2].

The upper dynamic, in the frame of quantum physics, allows to consider ion motion in cells due to the combined action of weak autogenous magnetic fields, with the proper cyclotronic frequency, and the environmental static magnetic field of the earth, despite the classical statements that other authors previously accepted [7–9].

REFERENCES

1. Zhadin, M. N., V. V. Novikov, F. S. Barnes, and N. F. Pergola, "Combined action of static and alternating magnetic fields on ionic current in aqueous glutamic acid solution," *Bioelectromagnetics*, Vol. 19, 41–45, 1998.
2. Del Giudice, E., M. Fleischmann, G. Preparata, and G. Talpo, "On the 'unreasonable' effects of E.L.F. magnetic fields upon a system of ions," *Bioelectromagnetics*, Vol. 23, 522–530, 2002.
3. Comisso, N., E. Del Giudice, A. De Ninno, M. Fleischmann, L. Giuliani, G. Mengoli, F. Merlo, and G. Talpo, "Dynamics of the ion cyclotron resonance effect on amino acids adsorbed at the interfaces," *Bioelectromagnetics*, Vol. 27, 16–25, 2006.
4. Zhadin, M. and L. Giuliani, "Some problems in modern bioelectromagnetics," *Electromagn. Biol. Med.*, Vol. 25, 227–243, 2006.
5. Giuliani, L., S. Grimaldi, A. Lisi, E. D'Emilia, N. Bobkova, and M. Zhadin, "Action of combined magnetic fields on aqueous solution of glutamic acid: the further development of investigations," *BioMagnetic Research and Technology*, Vol. 6, 1, 2008.
6. Preparata, G., *QED Coherence in Matter.*, World Scientific, New York, 1995.
7. Adair, R. K., "Biophysical limits on athermal effects of RF and microwave radiation," *Bioelectromagnetics*, Vol. 24, 39–48, 2003.
8. Binhi, V. N., "A few remarks on 'combined action of DC and AC magnetic fields on ion motion in a macromolecule'," *Bioelectromagnetics*, Vol. 28, No. 5, 409–12.
9. Zhadin, M. N., F. Barnes, and L. Giuliani, "Response to a few remarks on combined action of DC and AC magnetic fields on ion motion in macromolecules by Binhi," *Bioelectromagnetics*, Vol. 28, No. 6, 412–413, 2007.

Influence of Calcium Cyclotronic Resonance on the Developmental Rates of *Xenopus Laevis* Tadpoles

M. Severini[1], **C. Giliberti**[3], **G. Tarantino**[2], **M. Loy**[2], **M. Bonori**[2], **A. Congiu Castellano**[2], **A. Bedini**[3], **R. Palomba**[3], **and L. Giuliani**[3]
[1]Department of Ecology and Economical Sustainable Development
Tuscia University, Viterbo, Italy
[2]Physics Department, University La Sapienza, Rome, Italy
[3]Institute for Prevention and Work Safety (ISPESL), Rome, Italy

Abstract— Recent studies (Zhadin 2008) suggest that Zhadin effect could have a role in changing the development rate of cells and animals. In particular, *in vivo* and *in vitro* experiments show that exposures to a weak ELF magnetic field close to Larmor frequency of Ca^{++}, increase the differentiation and maturation of cells and the development of the animals. Based on the preliminary results of several experiment on *X. laevis* tadpoles exposed to a weak low frequency magnetic field that is close to Ca^{++} cyclotronic resonance conditions. (In these experiments the tadpoles were exposed to a static field (B_0) fixed at 65 μT, in order to tune the Calcium cyclotron frequency resonance to the frequency (50 Hz) of the sinusoidal field applied (B_{ac}), whose mean value was 70.0 ± 5.0 μT), authors underline that, compared to unexposed conditions, the exposition to a weak low frequency magnetic field close to Ca^{++} cyclotronic resonance, doesn't affect development rates of exposed tadpoles. We suggest that, because of a compensation mechanism between the inhibitory effect of the melatonin, which induces a metamorphic effect, and the probable rise effects on the development due to frequency Ca^{++} cyclotron resonance, there isn't a statistically significant delay in the development rate of the exposed cohorts. For the amphibians, melatonin has an important role in their development rate because it acts as an antagonist of the thyroid hormone, essential for the development of the tadpoles. But for the amphibians, the role of Ca^{++} in the synthesis of melatonin has to be more investigated.

Another recent research shows also that under exposure conditions quite different from those of Ca^{++} cyclotronic resonance, ELF magnetic fields retard developmental rates of *Xenopus laevis* tadpoles. Comparing these results with the previous ones, it can be deduced that probably B0 plays an important role in the activation of some processes connected with the development rate of this specie. In order to find an interpretation of the interaction mechanisms occurring between field and biological matter at microscopic level according with the Zhadin effect, an estimation of the energies associated to the most important ions involved in the intra/extra cellular activities (K^+, Ca^{++}, Mg^{++}, Li^+) under different exposure conditions, has been performed.

The Weak Combined Magnetic Fields Induce the Reduction in Brain Amyloid-β Level in Two Animal Models of Alzheimer's Disease

Natalia V. Bobkova, **Vadim V. Novikov**, **Natalia I. Medvinskaya**, **Irina Y. Aleksandrova**, **Sergei Antonov**, **and Eugenii E. Fesenko**
Institute of Cell Biophysics of Russian Academy of Sciences, Pushchino 142290, Russia

Abstract— Amyloid-β (Aβ) peptides are widely believed to have a causative role in the pathogenesis of Alzheimer's disease. Earlier we revealed that a weak combined magnetic field (MF), produced by superimposing a constant component, 42 μT, and an alternating MF of 0.08 μT combined frequencies in the range 3.58–4.88 Hz, substantially accelerated the hydrolytic decomposition of Aβ into peptide fragments *in vitro*, which have a less pronounced neurotoxic effect and less capable of forming aggregates (Fesenko et al., 2003). Here we studied the subchronic effect of the same combined weak MFs on spatial memory and brain Aβ in olfactory bulbectomized and transgenic Tg (APPswe, PSEN1) mice, which are animal models of sporadic and heritable Alzheimer's disease accordingly (Aleksandrova et al., 2004). It was found that such fields induced the decrease of Aβ level in bulbectomized mice and reduction in number of Aβ plaques in the cortex and hippocampus of transgenic animals. However, the memory improvement was revealed in transgenic mice only, but not in the bulbectomized animals. One of the reason for this paradoxical observation is due to that the MF exposure started too late in bulbectomized animals, when there is already significant neuronal death in the structures that subserve memory (Nesterova et al., 1997; Bobkova et al., 2001; 2004). It is shown that in transgenic mice neurons are less subjected to degeneration. So for the greatest chance of success, MFs could be used for prevention of Aβ accumulation during the preclinical stages of Alzheimer's and other diseases involving amyloid protein deposition in other tissues. In work the comparison was made the effects of MFs and influence of immunization by fragments of acetylcholine receptors on memory and Aβ accumulation in two animal models of Alzheimer's disease.

ACKNOWLEDGMENT

Work was supported by Grant of RFBR No. 06-04-48710.

Link between Quantum Electro Dynamics and Biology: The Developing Concept of Informative Medicine

Alberto Foletti[1], **Emilio Del Giudice**[2], **Livio Giuliani**[3], **and Settimio Grimaldi**[4]
[1]Medico Chirurgo, Specialista in Chirurgia Generale, Milan, Italy
[2]International Commission for ElectroMagnetic Safety (ICEMS), Venice, Italy
[3]ISPESL, Italian National Institute for Health and Safety at Work, Venice, Italy
[4]Istituto di Neurobiologia e Medicina Molecolare, C.N.R., Rome, Italy

Abstract— According to Quantum Electro-Dynamical Theory by G. Preparata, liquid water can be viewed as an equilibrium between of two components: coherent and incoherent ones.

The coherent component is contained within spherical so called "coherence domains" (CDs) where all molecules synchronously oscillate with the same phase.

CDs are surrounded by the incoherent component where molecules oscillate with casual phases regarding each other.

The existence of coherent domain in water has been demonstrated in a set of experiments on pure water exposed to high voltage, under this condition the electric field concentrates inside the water, arranging the water molecules to form high ordered structure.

Recently we studied the influence of combined static and alternating parallel magnetic fields on the current through the aqueous solution of glutamic acid; outlining the relevance of low frequency electro-magnetic field in interacting with biological target.

In addition, our results demonstrate that when combined static and alternating parallel magnetic fields matching the ion cyclotron energy resonance of a particular charged molecule into biological tissue an intrinsic weak magnetic field is generated by ion currents in the cell.

These results should increase the reliability and the clinical feasibility of the use of electromagnetic field, tuned at ion cyclotron resonance of charged molecules, as a biophysical approach to interfere with biological mechanisms.

We demonstrate that exposure of human epithelial cell and in particular human adult stem cells (cardiac and mesenchimal) to ion cyclotron energy resonance tuned to calcium ion at 7 Hz act as a differentiation factor.

These experimental data can opening up the possibility to use particular extremely low electro magnetic field protocols as a tool in informative medicine.

Epidemiological Evidence Suggests Preference of the US Versus the EU Standards for Partial Body Exposure to Microwaves

L. Giuliani[1, 2] **and Francesco Boella**[3]

[1]International Commission for ElectroMagnetic Safety (ICEMS), Venice, Italy
[2]National Institute for Occupational Health and Safety (ISPESL), Rome, Italy
[3]National Institute of Occupational Prevention and Safety, Venice, Italy

Abstract— In December 1997, the US FCC released the regulation concerning human exposure to radiofrequency and microwave radiation from wireless and electronic devices on partial exposure of the body. The ceiling value for this kind of exposure has been fixed at 1.6 W/kg (SAR) averaged over 1 g of tissue. In July 1998, the EU Council of Health Ministries released a Recommendation (1999/512/CE), fixing the ceiling value at 2.0 W/kg (SAR) averaged over 10 g of tissue.

Who is writing voted no, as Italian representative in the Group of Experts of the EU Council, and suggested to adopt the same standard good in USA. The supporters of the new EU standard underlined that it was taking into account the continuity of the exposed tissue with peculiar reference to glands in the head. Obviously it was an abstract statement. The difficulty to model the SAR distribution in the body has vanished all that good aims in practical dosimetry.

The authors, as representatives in the Group of Experts of the EU Council, disagree with the EU recommendation and prefer adopting the US standard. Supporters of the EU standard insisted that their standard was based on exposure dosimetry in the head. However, since it is difficult to obtain detailed SAR distribution in the body, their basis is not valid.

Results from epidemiological studies, including some from the INTERPHONE Program since 2004, suggest a relationship between non-malignant brain tumours and long term exposures to mobile phone radiation. These results suggest a preference of the US over the EU standard or, better, with a standard based on the precautionary principle. The International Commission for Electromagnetic Safety (ICEMS) released in 2006 and 2008 two resolutions recommending prudent use of wireless communication devices, sources of radiofrequency radiation. Two non-thermal mechanisms of biointeraction of electromagnetic fields on living tissue, one in the ELF band, the so called Zhadin effect, and the other one in the microwave-UHF band, employed in the so called bioscanner — a simple medical device for early detection of prostate tumour — were demonstrated at the end of 1990s. New standards should be derived taking into account non-thermal mechanisms. The first author of this abstract suggested the frame of restrictions and consequences for partial exposure to EMF in Italy in 1998 and in a meeting in China in 2003, that some countries have subsequently adopted. Thus, a reduction of the limit for partial body exposure to radiofrequency radiation should be considered.

Biophisical Implications of Coherence in Water Involved in Fuchs' Water Bridges

E. D'Emilia[1], **L. Giuliani**[1], **S. Grimaldi**[2], **and A. Lisi**[2]
[1]Institute for Prevention and Labour Safety, Monteporzio Catone, Italy
[2]National Research Council (INMM), Rome, Italy

Abstract— When water in two beakers is exposed to a high voltage (15–25 kV at least), a floating water bridge forms between the beakers. This "unbelievable" bridge defying the gravity law has been produced in a famous experiment by Austrian scientists of Gratz University on 2007 [1]. The bridge, has a diameter of 1–3 mm and it does not collapse when the beakers are pulled apart at a distance — depending on the applied voltage — from 1.5 to 2.5 cm. Water density decrease to 0.93 and its temperature increases from 20°C to 65°C within a period of about 45 minutes, at the end of which the bridge collapses.

As the austrian researchers revealed the phenomenon is not yet fully undesrstood. Authors are replicating the experiment and are developing an interpretation of the result concerning the collapse time of the bridge. In the frame of QED [2] we suggest when the high electric field is applied the coherent dominions of water increase their angular momentum dissipating heat as in the Joule effect that causes the increase of the temperature. As temperature increases the volume of coherent dominions decreases until bulk water becomes dominant and water assumes all usual physical characters, but temperature, falling down.

REFERENCES

1. Fuchs, E. C., J. Woisetschläger, K. Gatterer, E. Maier, R. Pecnik, G. Holler, and H. Eisenkölbl, "The floating water bridge," *J. Phys. D: Appl. Phys.*, Vol. 40, 6112–6114, 2007.
2. Preparata, G., *QED Coherence in Matter*, World Scientific Publishing Co. Pte. Ltd., 1995.

Radio-over-fiber and Micro Cells: Can Be This a Way to Contrast the Increase of Human Exposure to Microwave Electromagnetic Fields?

Ing. Francesco Boella and Livio Giuliani
National Institute of Occupational Prevention and Safety, Venice, Italy

Abstract— The development of new networks, due to the introduction of new technologies and standards, will cause, in the near future, an increase of the electromagnetic exposure levels. We propose, for minimize the impact, a solution made by radio micro cells in conjunction with RoF technology, designed to substitute the conventional network and plants, with three goals:

1. To guarantee the coverage by a minimum signal level;
2. To adopt micro cells to lowering the uplink connections power to avoid user's high exposures;
3. To guarantee the indoor wireless coverage by bringing the signal over fibres to only pico cells.

On the request of the City of Venice we developed a study to compare the environmental pollution due to conventional grouped BTSs, operating in GSM, DCS and UMTS technologies, and the pollution due to a micro cell-based network interconnected using RoF technology, able to produce the same coverage in the same area.

The results suggest that the choice made in our Countries on '90 years has to be reconsidered.

Electromagnetic Mapping of Urban Areas: The Example of Monselice (Italy)

C. Giliberti[1], **F. Boella**[2], **A. Bedini**[1], **R. Palomba**[1], **and L. Giuliani**[2]

[1]Institute for Prevention and Work Safety (ISPESL), Rome, Italy
[2]Institute for Prevention and Work Safety (ISPESL), Venice, Italy

Abstract— In this work, the theoretical evaluation of the electromagnetic field (*emf*) produced by radio base stations (*rbs*) in the city of Monselice, sited in the northern part of Italy is presented.

An area of 16 Km^2, characterized by 11 *rbs* sites has been selected. A census of the *rbs* sites has been carried out, collecting: the location of the sites, the technical data of their antennas, the shape of the ground, the position of all the buildings (Gauss-Boaga coordinates) in the area and their heights.

Two different evaluations of the *emf* in this area are presented. The first one, representing the buildings by their barycentre placed at the height of each building, calculates in these points the electric field levels using the classical far field equation, assuming the *rbs* working at the maximum power declared.

Another theoretical evaluation of the *emf* has been carried out by the application of a calculation code working with the *ray tracing* method. It provides an output where a 3D map of the electric field produced by the *rbs* on the surfaces of the buildings in an area around a electromagnetic sites is shown, assuming the *rbs* working at the maximum power.

Session 3A5b
Progress in fs Laser Interaction with Matter 1

Polymer Photonics and Polymer MEMS: Fabrication by Femtosecond Lasers

Qi-Dai Chen, **Hong Xia**, **and Hong-Bo Sun**
State Key Laboratory on Integrated Optoelectronics
College of Electronic Science and Engineering
Jilin University, 2699 Qianjin Street, Changchun 130023, China

Abstract— Femtosecond (fs) laser rapid prototyping has been recently considered as a promising technology for fabrication of micro-optical and mechanical devices with complicated geometry [1–10]. The fundamental principle of the technology is, pinpoint scanning photopolymerizable resins according to a preprogrammed pattern with focal spot of a fs laser beam. The exposed or scanned trace, with linewidth as small as tens of nanometers, is solidified due to chain reactions of photopolymerization, while the unexposed portion is rinsed with solvent after scanning. The CAD designs are thus converted into matter structures, i.e., desired devices. Compared with other microfabrication approaches like lithography, the outstanding merits of the fs laser rapid prototyping lie in: (a) the capability in three-dimensional (3D) structural fabrication; (b) simplicity of technology, in another word, the increase of the device structural complexity doesn't lead to any significant increase of the difficulty in fabrication; and (c) ease of introduction of various functional components.

The fs laser rapid prototyping may find important uses in lab-on-chip field from two aspects: (a) realization of structures or devices that are otherwise not possible; and (b) use as a structural and functional simulation tool for batch production of complicated lab-on-chips. A systematical exploration of the method for lab-on-chip fabrication has not yet started. Here we show some devices that may be essential for a lab-on-chip system, including micro lens array [Fig. 1], micro oscillator [Fig. 2] and micro channels. The future development of the technology towards lab-on-chip application will also be discussed.

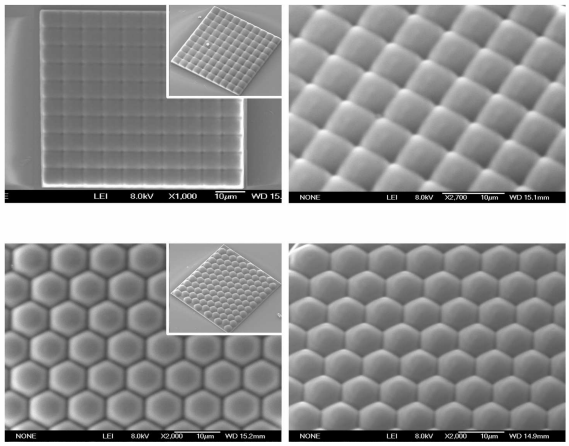

Figure 1: Aspheric micro lens arrays of 100% filling ratio with square (top) and hexagonal (bottom) lenslets arrangement.

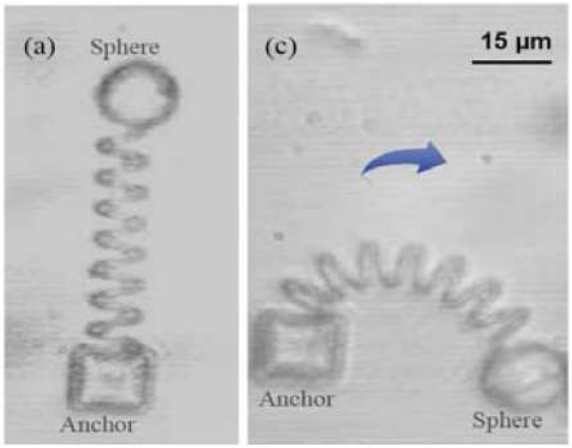

Figure 2: A micro-oscillator operated with a simple magnet. The same principle will be applicable to micro-pumps or micro-valves.

REFERENCES

1. Chen, Q.-D., X.-F. Lin, L.-G. Niu, D. Wu, W.-Q. Wang, and H. B. Sun, *Opt. Lett.*, Vol. 33, 2008.
2. Takada, K., K. Kaneko, Y. D. Li, S. Kawata, Q. D. Chen, and H. B. Sun, *Appl. Phys. Lett.*, Vol. 92, 041902, 2008.
3. Kaneko, K., K. Yamamoto, S. Kawata, H. Xia, J. F. Song, and H.-B. Sun, *Opt. Lett.*, Vol. 33, 1999, 2008.
4. Chen, Q. D., D. Wu, L. G. Niu, J. Wang, X. F. Lin, H. Xia, and H. B. Sun, *Appl. Phys. Lett.*, Vol. 91, 171105, 2007.

5. Nakanishi, S., S. Shoji, S. Kawata, and H.-B. Sun, *Appl. Phys. Lett.*, Vol. 91, 063112, 2007.
6. Sun, H.-B., A. Nakamura, K. Kaneko, S. Shoji, and S. Kawata, *Opt. Lett.*, Vol. 30, 881, 2005.
7. Sun, H.-B., T. Suwa, K. Takada, R. P. Zaccaria, M. S. Kim, K. S. Lee, and S. Kawata, *Appl. Phys. Lett.*, Vol. 85, 3708, 2004.
8. Sun, H. B., A. Nakamura, S. Shoji, X. M. Duan, and S. Kawata, *Adv. Mater.*, Vol. 15, 2011, 2003.
9. Sun, H.-B., K. Takada, M. S. Kim, K. S. Lee, and S. Kawata, *Appl. Phys. Lett.*, Vol. 83, 1104, 2003.
10. Sun, H. B., M. Maeda, K. Takada, J. W. M. Chon, M. Gu, and S. Kawata, *Appl. Phys. Lett.*, Vol. 83, 819, 2003.

Laser Micro-nanofabrication of High-quality Aspheric Microlenses and Microlens Array

Dong Wu, **Qi-Dai Chen**, **Li-Gang Niu**, **and Hong-Bo Sun**
State Key Laboratory on Integrated Optoelectronics
College of Electronic Science and Engineering
Jilin University, 2699 Qianjin Street, Changchun 130023, China

Abstract— Microlens arrays with diameters about several micrometers are key components for various micro-optical applications, particularly in optical interconnection, liquid crystal display, organic light emitting diodes and confocal microscopy. However, high fill factor and lens profile, two critical parameters determining lens functions, remains technological challenges for the common fabrication technology. Here, we report high-quality 100% fill factor aspheric microlens arrays with sub-20 nm precisions enabled by femtosecond laser direct writing [1, 2].

Shown in Fig. 1 are three kinds of 100% fill factor aspherical hexagonal microlens arrays with different NAs, 0.28, 0.40 and 0.52, deduced from the lens parameters of $\rho = 5\,\mu$m and the heights $h = 1.2\,\mu$m [Fig. 1(a)], $1.8\,\mu$m [Fig. 1(b)] and $2.4\,\mu$m [Fig. 1(c)], respectively. The lens surface is smooth and the average surface roughness, according to AFM measurement, is about 1.4 nm.

As we know, the resolution becomes higher as the numerical aperture increases. This property is obviously seen from the photos as shown in the middle images of Figs. 1(a), 1(b) and 1(c). We can evidently find that the image "F" becomes clearer as the numerical aperture increases, as shown in the right photos of Figs. 1(a), 1(b) and 1(c). This demonstrates that microlens arrays with high numerical aperture can be produced by femtosecond laser fabrication technology. This work is an important step towards creating and integrating complex micro-optical devices and systems and the high-quality microlens array will find wider applications in photonics, electronics and biotechnology.

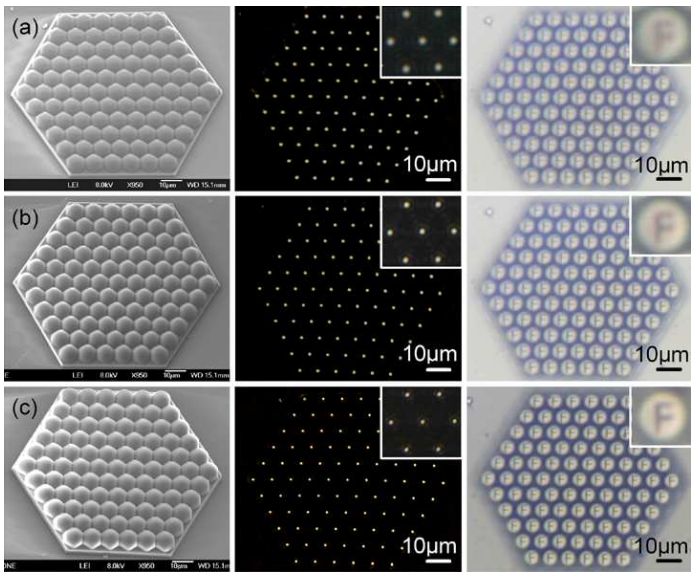

Figure 1.

REFERENCES

1. Sun, H. B., S. Matsuo, and H. Misawa, *Appl. Phys. Lett.*, Vol. 74, 786, 1999.
2. Wu, D., L. G. Niu, and H. B. Sun, *Opt. Lett.*, in press, 2009.

Design and Laser Fabrication of Polymeric Binary Micro-optical Components

Xiao-Feng Lin, **Qi-Dai Chen**, **Li-Gang Niu**,
Dong Wu, **Wen-Quan Wang**, **and Hong-Bo Sun**
State Key Laboratory on Integrated Optoelectronics
College of Electronic Science and Engineering, College of Physics
Jilin University, 2699 Qianjin Street, Changchun 130023, China

Abstract— Binary optical components has become more and more popular in optical systems due to the characteristics of high diffraction efficiency, high flexibility of design and relative ease of fabrication. Compared to the most prevailing etching technique, femtosecond laser induced polymeric micro-nanofabrication [1] has the unique merits of high accuracy and high tolerance to the structural complexity. By this means, we realized various binary optical components such as Dammann grating.

Shown in Fig. 1 are the scanning electron microscopic (SEM) images of the Dammann gratings fabricated by this new technology [2]. The thickness of phase retardation parts was designed to be 533 nm for splitting a 632.8 nm laser, thus the difference of the phase shifts that light travels through phase retardation parts and through hollow parts should reach π to ensure the theoretical maximum of diffraction efficiency. The whole process of fabrication takes no more than 30 minutes. In addition to short fabrication period, our Dammann gratings also show good performances [2]. Figs. 2(a)–(e) show the arrays of 2×2, 3×3, 4×4, 5×5, 6×6 spots generated by the corresponding structures in Figs. 1(b)–(f). Fig. 2(f) offers a direct view of the uniformity of spots in the fan-out. Each peak indicates the irradiance intensity of the corresponding spot in the dashed lines X and Y, and it can be told the peaks are of almost the same height that suggests a good uniformity.

This work shows not only the merits of femtosecond laser induced polymerization, but also the ease and promising prospect of polymeric binary micro-optical components enabled by this technology.

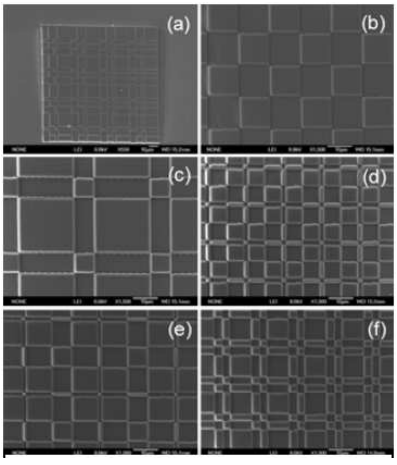

Figure 1: Dammann gratings fabricated by two-photon photopolymerization. (a) Top-view SEM image and locally magnified views of the Dammann gratings that generate (b) 2×2, (c) 3×3, (d) 4×4, (e) 5×5, and (f) 6×6 spot sources, respectively [Ref. 2].

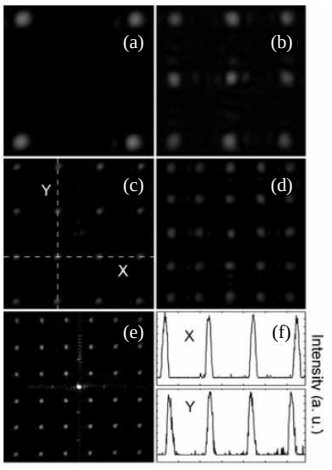

Figure 2: Diffraction patterns of Dammann gratings that generate (a) 2×2, (b) 3×3, (c) 4×4, (d) 5×5, and (e) 6×6 spot sources, respectively. (f) Intensity distribution of spots along dashed lines X and Y [shown in (c)] [Ref. 2].

REFERENCES

1. Sun, H. B., S. Matsuo, and H. Misawa, *Appl. Phys. Lett.*, Vol. 74, 786, 1999.
2. Chen, Q. D., X. F. Lin, L. G. Niu, D. Wu, W. Q. Wang, and H. B. Sun, *Opt. Lett.*, Vol. 33, 2559, 2008.

Session 3A6
Novel Mathematical Methods in Electromagnetics

Charge Moment Tensor and the Rotation Equation of a Charged Rigid Body in a Uniform Magnetic Field

Guo-Quan Zhou, **Cao Guan**, **and Si-Lei Zhang**
Department of Physics, Wuhan University, Wuhan 430072, China

Abstract— Based on a new concept, i.e., charge moment tensor, and Euler's equation in classical mechanics, the dynamic and kinetic equations of the fixed-point rotation for a charged rigid body under a uniform external magnetic field have been derived, its completeness and equivalence to its Lagrange dynamic equations are discussed.

Natural Introduction of Charge Moment Tensor and the Lagrangian of a Rotational Charged Rigid Body

Guo-Quan Zhou, **Si-Lei Zhang**, **and Cao Guan**
Department of Physics, Wuhan University, Wuhan 430072, China

Abstract— A natural method of Introducing a new concept, i.e., charge moment tensor, has been found. Its application in the Lagrange dynamic Equations of a rotational charged rigid body under a uniform magnetic field has been derived for the case of fixed-point rotation, and the corresponding invariants have also been recognized. Meanwhile some simple conclusions about a special symmetric case have been given.

Simplified Variational Principles for Barotropic Magnetohydrodynamics

A. Yahalom
Ariel University Center of Samaria, Ariel 40700, Israel

Abstract— Variational principles for magnetohydrodynamics were introduced by previous authors both in Lagrangian and Eulerian form. In a previous work [1] we introduced a simpler Eulerian variational principles from which all the relevant equations of magnetohydrodynamics can be derived. The variational principle were given in terms of six independent functions for non-stationary flows and three independent functions for stationary flows. This is less then the seven variables which appear in the standard equations of magnetohydrodynamics which are the magnetic field $\vec{B}$ the velocity field $\vec{v}$ and the density ρ. In this work we will attempt to improve on our previous results thus reducing the number of functions needed even further.

REFERENCES

1. Yahalom, A. and D. Lynden-Bell, "Simplified variational principles for barotropic magnetohydrodynamics," [Los-Alamos Archives — physics/0603128], *Journal of Fluid Mechanics*, Vol. 607, 235–265, 2008.

An in-depth Investigation of the Coupled Transverse-mode Integral Equation

Hung-Wen Chang and Shih-Min Lu
Institute of Electro-optical Engineering and Department of Photonics
National Sun Yat-Sen University, Kaohsiung 80424, Taiwan

Abstract— Many optical passive devices in nowadays optical communication systems are made of dielectric waveguides such as the smoothly bending waveguide, the power dividers, directional couplers, micro-ring cavities, waveguide crossing and arrayed waveguide gratings. Rigorous analysis of these waveguide devices is very difficult due to the shear size of the problem measured in the operating wavelength. Approximation methods such as the beam propagation method (BPM), time-domain finite-difference (FD-TD) and frequency-domain finite-difference (FD-FD) methods are used to analyze and optimize the design. However each of these methods has its limitation. Years ago, an integral-equation formulation as a full-wave analysis of 2-D dielectric waveguide devices was proposed. It holds a great potential to increase the accuracy and speed of numerical calculation. Only recently we are able to implement such a algorithm for a general 2-D complex structure under a stair-case approximation. Numerical examples such as multi-mode interferometer, waveguide crossing and quasi-adiabatic tapered waveguides are successfully studied with good convergent results.

Semi-analytical Approach for a Specific Microstructured Fiber

Kiyotoshi Yasumoto
Department of Computer Science and Communication Engineering
Kyushu University, Fukuoka 819-0395, Japan

Abstract— Photonic crystal fibers, with a core of a higher average index than the microstractured claddings, are now finding applications in diverse areas such as fiber-optic communications, fiber lasers, nonlinear photonic devices, highly sensitive sensors, and so on. The modal properties of photonic crystal fibers have been extensively investigated using the finite element method, the multipole method, the finite difference frequency domain method, and the finite difference time domain method. These numerical techniques can be versatilely applied to various microstructured configurations but are computationally intensive.

In this paper, we shall present a rigorous semi-analytical approach for a specific microstructured fiber as shown in Fig. 1. It consists of N-layered cylindrical arrays of circular rods located in a homogeneous background medium. The M number of circular rods are symmetrically distributed on each of the N-concentric circular rings with radii $d_\nu (\nu = 1, 2, 3, \ldots, N)$. The radii of the rings must satisfy the condition $d_{\nu+1} - d_\nu > r_{\nu+1} + r_\nu$ so that the circular rods on consecutive rings do not interpenetrate, where r_ν is the radius of the rods located on the ν-th ring. The circular rods should be identical along one ring but those on different rings need not be necessarily identical in material properties and dimensions. Fig. 1 shows a typical example with $M = 6$. In the proposed method, the reflection and transmission matrices for each layer of cylindrical arrays are first calculated for the incidence of cylindrical harmonics from the outer region and the inner region as shown in Fig. 1(b). These matrices are expressed in terms of the T-matrix of a circular rod in isolation and the translation matrices of cylindrical waves between the local coordinates $(\rho_j^\nu, \varphi_j^\nu)(j = 1, 2, 3, \ldots, M)$ attached to each circular rod and the global coordinate x-O-y. These reflection and transmission matrices are concatenated from the outermost layer to the innermost layer using a recursion formula. Then we can obtain the characteristic equations to determine the propagation constants and field distributions for the eigenmodes supported by the microstructured system.

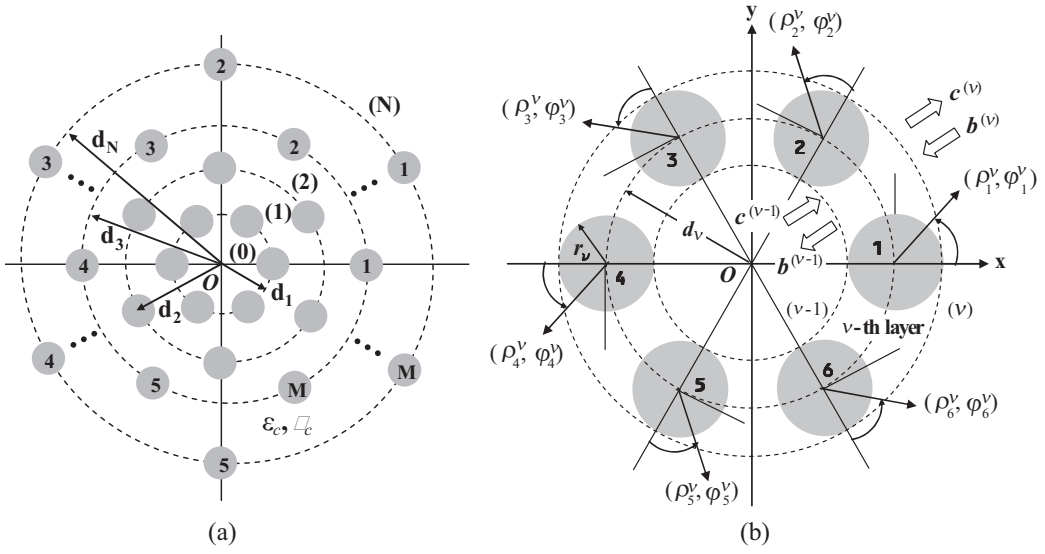

Figure 1: Cross sectional view of N-layered cylindrical arrays with M circular rods symmetrically distributed on each of N concentric circular rings with radii $d_\nu (\nu = 1, 2, 3, \ldots, N)$: (a) a general view of N-layered structure and (b) a typical view of the global coordinate system x-O-y, local coordinate systems $(\rho_j^\nu, \varphi_j^\nu)(j = 1, 2, 3, \ldots, M)$, and schematic of the scattering process in the cylindrical array on the ν-th layer when $M = 6$.

RCS Analysis of a Terminated, Semi-infinite Parallel-plate Waveguide with Four-layer Material Loading: Rigorous Wiener-Hopf Approach

E. H. Shang and K. Kobayashi
Chuo University, Japan

Abstract— The analysis of the scattering from open-ended metallic waveguide cavities has received much attention recently in connection with the prediction and reduction of the radar cross section (RCS) of a target. A number of two- and three-dimensional (2-D and 3-D) cavity diffraction problems have been analyzed thus far by means of high-frequency ray techniques and numerical methods, but it appears that the solutions obtained by these approaches are not uniformly valid for arbitrary cavity dimensions. In the previous papers [1–3], we have considered, as an example of canonical 2-D cavities, a terminated, semi-infinite parallel-plate waveguide with four-layer material loading, and analyzed the plane wave diffraction rigorously for both E and H polarizations by means of the Wiener-Hopf technique. It has been shown that our final solutions are uniformly valid for arbitrary cavity dimensions. In this paper, we shall summarize the research in our recent papers [1–3], and compare the results between two different polarizations.

The geometry of the waveguide is shown in Fig. 1, where ϕ^i is the incident field of E or H polarization. The waveguide plates at $x = \pm b$ and the planar termination at $z = -d_1$ are perfectly conducting and of zero thickness, and the four material layers I, II, III, and IV are loaded on the terminated plate. Introducing the Fourier transform of the scattered field and applying boundary conditions in the Fourier transform domain, the problem is formulated in terms of the simultaneous Wiener-Hopf equations satisfied by unknown spectral functions. The Wiener-Hopf equations are solved via the factorization and decomposition procedure leading to the exact solution, which requires numerical inversion of appropriate matrix equations. Taking the inverse Fourier transform of the solution in the complex domain and using the saddle point method, the scattered field inside and outside the waveguide is explicitly evaluated. Representative numerical examples on the monostatic RCS are shown for various physical parameters and the far field backscattering characteristics of the waveguide are discussed in detail. Our final results can be used as reference solutions for validating more general approximate methods.

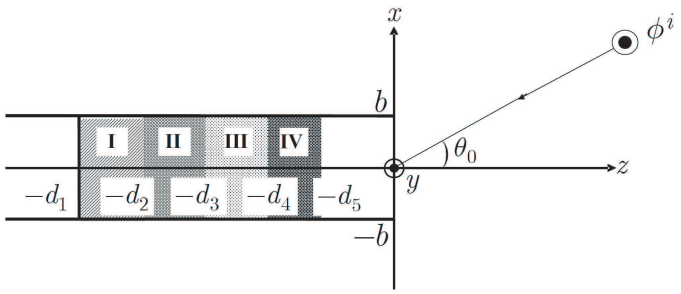

Figure 1: Geometry of the problem.

REFERENCES

1. Shang, E. H. and K. Kobayashi, "Diffraction by a terminated, semi-infinite parallel-plate waveguide with four-layer material loading," *IEEJ Technical Report*, No. EMT-07-38, May 2007.
2. Shang, E. H. and K. Kobayashi, "Diffraction by a terminated, semi-infinite parallel-plate waveguide with four-layer material loading," *Proc. 2007 URSI International Symposium on Electromagnetic Theory (EMTS 2007)*, No. O11-32-2, July 2007.
3. Shang, E. H. and K. Kobayashi, "Diffraction by a terminated, semi-infinite parallel-plate waveguide with four-layer material loading: The case of H polarization," *Proc. XXIX General Assembly of the International Union of Radio Science*, No. B01.10, August 2008.

Wiener-Hopf Analysis of the Diffraction by a Semi-infinite Parallel-plate Waveguide with Sinusoidal Corrugation

J. P. Zheng and K. Kobayashi
Chuo University, Japan

Abstract— The analysis of wave scattering by gratings and waveguides with periodic structures is important in electromagnetic theory and optics. Various analytical and numerical methods have been developed so far and the diffraction phenomena have been investigated for many kinds of periodic structures. However, there are only a few treatments of the diffraction by periodic structures using rigorous function-theoretic methods. In the previous papers [1, 2], we have considered a semi-infinite parallel-plate waveguide with sinusoidal corrugation, and analyzed the E-polarized plane wave diffraction by using the Wiener-Hopf technique combined with the perturbation method. The same diffraction problem has been analyzed in the past for the H polarization by Chakrabarti and Dowerah [3] following a method similar to that developed in [1, 2]. However, the analysis presented in [3] is incorrect from a mathematical point of view.

This paper is in continuation with our previous papers [1, 2]. We shall analyze in this paper the plane wave diffraction by a semi-infinite parallel-plate waveguide with sinusoidal corrugation for both E and H polarizations, and obtain analytical solutions in a complete form based on the Wiener-Hopf technique combined with the perturbation method. The geometry of the problem is shown in Fig. 1, where ϕ^i is the incident field of E or H polarization. The surface of the waveguide plates is assumed to be infinitely thin, perfectly conducting, and uniform in the y-direction, being defined by $x = \pm b + h \sin mz\,(z < 0)$, where m and h are positive constants. Assuming that the corrugation amplitude $2h$ is small compared with the wavelength, the original problem can be approximately replaced by the problem of diffraction by a semi-infinite parallel-plate waveguide with impedance-type boundary conditions. Taking the Fourier transform of the Helmholtz equation and applying approximate boundary conditions in the transform domain, the problem is formulated in terms of the simultaneous Wiener-Hopf equations. The Wiener-Hopf equations are then solved via the factorization and decomposition procedure together with the perturbation scheme leading to the efficient zero- and first-order solutions. Numerical examples of the scattered far field are presented, and the scattering characteristics of the waveguide are discussed in detail.

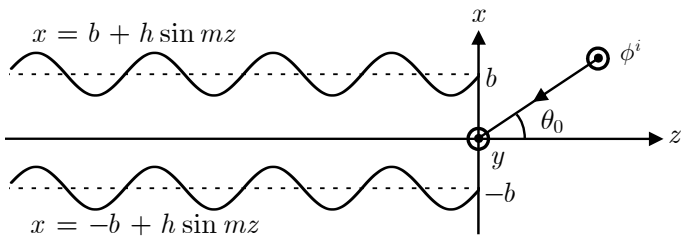

Figure 1: Geometry of the problem.

REFERENCES

1. Zheng, J. P. and K. Kobayashi, "Wiener-Hopf analysis of the plane wave diffraction by two parallel, corrugated half-planes," *Proc. 2007 URSI International Symposium on Electromagnetic Theory (EMTS 2007)*, O11-32-6, July 2007.
2. Zheng, J. P. and K. Kobayashi, "Plane wave diffraction by two parallel, corrugated half-planes: evaluation of the scattered field," *Progress In Electromagnetics Research Symposium Abstracts*, 698, Hangzhou, China, March 24–28, 2008.
3. Chakrabarti, A. and S. Dowerah, "Traveling waves in a parallel plate waveguide with periodic wall perturbations," *Can. J. Phys.*, Vol. 62, 271–284, 1984.

An Analytical Solution for the Logarithmic Singularity Associated with MoM Applied to Dielectrics and MFIE and Its Optimal Evaluation with Polynomial Quadratures

Thierry Gilles[1], **Marc Piette**[1], **and Christophe Craeye**[2]

[1]Ecole Royale Militaire, Laboratoire d' Electromagnétisme Appliqué (LEMA)
Avenue de la Renaissance 30, Bruxelles 1000, Belgium
[2]Université catholique de Louvain, Laboratoire TELE
Place du Levant 2, Louvain-la-Neuve 1348, Belgium

Abstract— A complete analytical solution is presented for the double integral with $1/R^3$ singularity occurring in electromagnetic problems involving dielectric materials or metallic objects treated with the magnetic field integral equation (MFIE). This analytical solution is then used to assess the accuracy obtained with high efficiency polynomial quadratures in the evaluation of the outer integral containing a logarithmic singularity. Many articles have been written on this logarithmic singularity and many complex schemes have been presented to deal with it. It is shown in this article that a simple integration method provides enough overall accuracy in the evaluation of this nasty integral. Moreover, an optimal choice for the number of integration points is proposed for the inner and outer integrals.

The Helmholtz Equation with Impedance Boundary Conditions

Aihua W. Wood
Department of Mathematics and Statistics, Air Force Institute of Technology
WPAFB, OH 45433-7765, USA

Abstract— Time-harmonic analysis of cavity-backed apertures with penetrable material filling the cavity interior has been examined by numerous researchers in the engineering community. It is a common assumption that the cavity opening coincides with the aperture on an infinite ground plane, and hence simplifying the modeling of the exterior (to the cavity) domain. This limits the application of these methods since many cavity openings are not planar. Here we present a well-posed math- ematical formulation for the analysis of the scattering characteristics of over-filled cavities in the frequency domain. Specifically we analyze the electromagnetic scattering phenomena induced by over-filled cavities that are embedded in an impedance plane. This is obviously more physically realistic, and at the same time more mathematically challenging. In particular, the more complex impedance (or mixed) boundary condition, as opposed the simple PEC (or Dirichlet) boundary condition, gives rise to a more complex boundary operator that is required to couple the infinite exterior domain and the finite interior domain. Furthermore, the radiation conditions will be dif- ferent due to the appearance of surface waves. Specifically, we first decompose the entire solution domain to two sub-domains via an artificial semicircle enclosing the cavity: the infinite upper half plane over the impedance plane exterior to the semicircle, and the cavity plus the interior region. The problem is solved exactly in the infinite sub-domain using a modal representation, while the other is solved using finite elements. The two regions are coupled over the semicircle via the intro- duction of a boundary operator exploiting the field continuity over material interfaces. In this way, cavity-backed antennas with dielectric lenses above the ground plane can be rigorously analyzed.

Session 3A7
Electromagnetic Near Field Effects in Problems of Wave Radiation from and Scattering by Ordered and Disordered Media

Coupled Surface States in Thin, Frequency Dependent Layers

M. Bergmair and Kurt Hingerl
CD-Labor für oberflächenoptische Methoden
Institut für Halbleiter-und Festkörperphysik
Johannes Kepler Universtät Linz, Linz 4040, Austria

Abstract— A negative dielectric function of e.g., a metal allows to excite surface plasmons (SP) along the interface of the metal and a positive dielectric material. The dispersion is derived by using continuity of the fields and reads $k_y = \omega\sqrt{\frac{\varepsilon_b\varepsilon(\omega)}{\varepsilon_b+\varepsilon(\omega)}}$ [1]. Here, k_y is the wave vector component which is parallel to the interface, ε_b the positive dielectric material (we use air with $\varepsilon_b = 1$ and $\varepsilon(\omega)$ the frequency dependent dielectric function of the metal (as a first approximation we use the Drude model including damping). The resulting dispersion is below the light line and therefore one has to use e.g., a grating or a prism to excite SPs.

The above solution for SPs at one interface is obtained by the given analytic equation. The next step is to study the coupling of SPs on parallel interfaces. Therefore we derive the two resulting modes (symmetric and antisymmetric mode) at a thin metallic sheet [2]. The dispersion is obtained from an implicit equation [3] and reads $\varepsilon(\omega)k_b/(\varepsilon_b k_m) = \tan(k_m d/2)^{\pm 1}$ where $k_i = \sqrt{k_y^2 - \varepsilon_i\omega^2}$ and d the thickness of the metallic sheet. It is suggested in literature [4] to solve this equation numerically by the Nelder-Mead minimization algorithm [5]. This algorithm works for minimization in arbitrary dimensions (we have a two dimensional minimization: $\Re(k_y)$ and $\Im(k_y)$).

For a single thin film one solution is hardly damped, the dispersion is very close to the light line below the asymptotic frequency and this asymptotic frequency shifts towards the plasma frequency of the metal as the thickness is decreased. The second solution is strongly damped and lies well below the light line.

In our contribution we investigate the coupling of surface plasmons over adjacent layers and therefore follow the derivation given in [2]. For each thin film one obtains two more solutions which are degenerate for large distances between the layers (or thick films). We study the coupling by means of the Nelder-Mead algorithm, investigate the influence of the geometry (distance between the metallic layers and their thickness) and give the dispersion of surface plasmons in a photonic crystal.

ACKNOWLEDGMENT

The authors would like to thank two EC grants (N2T2 and NanoCharM).

REFERENCES

1. Raether, H., *Surface Plasmons on Smooth and Rough Surfaces and on Grantings*, Springer, Berlin, 1988.
2. Economou, E. N., "Surface plasmons in thin films," *Phys. Rev.*, Vol. 182, 539–554, June 1969.
3. Zayats, A., I. Smolyaninov, and A. Maradudin, "Nano-optics of surface plasmon polaritons," *Physics Reports*, Vol. 408, 131–314, 2005.
4. Dionne, J., L. Sweatlock, H. Atwater, and A. Polman, "Planar metal plasmon waveguides: Frequency-dependent dispersion, propagation, localization, and loss beyond the free electron model," *Physical Review B*, Vol. 72, 075405, 2005.
5. Nelder, J. and R. Mead, "A simplex method for function minimization," *The Computer Journal*, Vol. 7, 308, 1964.

Non-radiating Field Wave Scattering from Discontinuities in Planar Surface

Feng Chen, **Huiling Zhao**, **and Wei Wan**
Northwestern Polytechnical University, Xi'an, Shaanxi 710072, China

Abstract— Any sources can be divided into radiation and non-radiation sources. The former provide propagating wave which is known to contribute to the far-field monostatic or bistatic scattering, while the latter provide non-radiating field which is confined in a certain region and can not be detected outside the region. However, non-radiating fields may contribute to propagating fields by local perturbations such as geometric or electromagnetic properties discontinuities. In this paper, one kind of non-radiating field wave — evanescent wave scattering by a slot in conducting planar surface was studied. The evanescent field was generate by a half wavelength dipole antenna, corresponding to the r^{-2} and r^{-3} part of the near field. The slot was located in the near field zone of the antenna. A modified Frequency Difference Time Domain (FDTD) method was utilized to calculate the far-field antenna pattern of this structure. Re-radiation boundary condition was introduce in the process in order to improve the calculation efficiency. The transformed propagating field from evanescent field was obtained by comparing the far field antenna pattern with slot and without slot. Affection of relative location and orientation between antenna and slot, working frequency, slot width and depth on the transformed propagating part were discussed. The conclusions can be advantageously used in overall arrangements of antennas on aircrafts, electromagnetic compatibility and microwave imaging.

REFERENCES

1. De Fornel, F., *Evanescent Waves: From Newtonian Optics to Atomic Optics*, Springer-Verlag Berlin and Heidelberg GmbH & Co. K, Jan. 2001.
2. Courjon, D., *Near-field Microscopy and Near-field Optics*, Imperial College Press, Mar. 2003.
3. Schultz, J. W., E. J. Hopkins, and E. J. Kuster, "Near-field probe measurements of microwave scattering from discontinuities in planar surface," *IEEE Trans. on Antennas and Propagation*, Vol. 51, No. 9, 2361–2368, Sept. 2003.
4. Diaz, R. E., "A simple stackable re-radiating boundary condition (rRBC) for FDTD," *IEEE Antennas Propagation Magazine*, Vol. 46, No. 1, 124–130, Feb. 2004.

High Harmonics Generation in Underdense Plasma from Relativistic Thomson Scattering

Fatemeh Abbasi
Vali-Asr University of Rafsanjan, Iran

Abstract— A high intensity laser incident ($10^{20}\,\mathrm{W/cm^2}$) on a vacuum-plasma interface, insert an Intensive electromagnetic force on electrons and charged particles. In this limit, the effect of light's magnetic field on electron motion should become comparable to that of its electric field, and the electron mass should increase because of the relativistic correction. Consequently, electrons in such high fields are predicted to quiver nonlinearly, moving in figure-eight patterns, rather than in straight lines, and thus to radiate photons at harmonics of the frequency of the incident laser light.

Harmonics can be produced coherently by strong plasma waves or incoherently by nonlinear Thomson scattering process. Theory for coherent emission in the direction of propagation of the laser beam indicates that-because of the mismatch between the phase velocities of the laser pulse the conversion efficiency should be low unless a means for phase matching or quasi phase matching, is implemented. In this paper, we study high harmonics generation by a normal incident, relativistically intense laser pulse on vacuum-**underdense** plasma. The equations of the "charge conservation" and the "momentum conservation" and Maxwell equations are written for the electromagnetic fields. Then the high order harmonics equations are derived, six coupled equations. We solved equations in phase matching and non phase matching conditions. We plot variation of density, velocity, electric field and magnetic field (in two direction, propagation of laser incident and normal to it) of high harmonics as a function of time and space. Comparison between results of two conditions (phase matching and non phase matching) lead to incoherent radiation and relativistic Thomson scattering.

Relativistic High Harmonics Generation in Underdense Plasma Produced by a Super Intense Femtosecond Laser Pulse

F. Abbasi[1] and K. Salimi[2]

[1]Vali-Asr University of Rafsanjan, Iran
[2]Sharif University of Technology of Tehran, Iran

Abstract— A high intensity laser incident on a vacuum-plasma interface, insert an Intensive electromagnetic force on electrons and charged particles. Relativistic charged particle movements lead to the high order harmonics generation of the incident wave. Efficiency of high harmonics increases with the intensity laser incident. So that the non-relativistic velocities of the particles vary to the relativistic velocities of particles. Efficiency of high harmonics increases with the intensity laser incident. The equations of the "charge conservation" and the "momentum conservation" and Maxwell equations are written for the electromagnetic fields. Then the high order harmonics equations are derived, six coupled equations. We plot variation of density, velocity, electric field and magnetic field (in two direction, propagation of laser incident and normal to it) of high harmonics as a function of time and space. One of considerable results in this paper is harmonics generation in direction of propagation of laser r incident and normal to it. considering $\vec{V} \cdot \nabla \vec{V}$ term in velocity equation (it means plasma is considered as a fluid) get this result. In previous works that has done in this field the researcher have reported-odd harmonics generated in direction of propagation of laser incident and even harmonics generated in normal direction of propagation of laser incident but in experimental results we can observe all harmonics in direction of propagation. The set of equations that are presented in other papers had been solved for SHG and THG while we have been presenting a set of equations and numerical analytic program do for any harmonics.

High Harmonic Generation in Magnetic Underdense Plasma

K. Salimi[1] and F. Abbasi[2]

[1]Sharif University of Technology of Tehran, Iran
[2]Vali-Asr University of Rafsanjan, Iran

Abstract— A high intensity laser normal incident ($10^{20}\,\mathrm{W/cm^2}$) on a vacuum-plasma interface produces high harmonics in reflected components. Efficiency of high harmonics increases with the intensity laser incident. So that the non-relativistic velocities of the particles vary to the relativistic velocities of particles. Consequently, electrons in such high fields are predicted to quiver nonlinearly, moving in figure eight patterns, rather than in straight lines, and thus to radiate photons at harmonics of the frequency of the incident laser light.

In this paper we study high harmonics generation by a normal incident, relativistically intense laser pulse on vacuum-**magnetic** plasma. The equations of the "charge conservation" and the "momentum conservation" and Maxwell equations are written for the electromagnetic fields. Then the high order harmonics equations are derived, six coupled equations. We plot variation of efficiency of high harmonics as a function of time and space. To meet the challenge of high power, short wavelength coherent radiation generation, it is quite to investigate the conditions under which harmonics generation efficiency can be maximized. We insert a magnetic field on plasma to increase the harmonics generation efficiency. Comparison between efficiency of high harmonics in underdense plasma and in magnetic underdense plasma shows, magnetic field can increases efficiency, considerably. one of the work we do in this paper is considering γ, relativistic factor, as a function of time and space such as other variables, velocity, density, electric and magnetic field (in other paper γ has been considered constant or as a function of laser intensity).

Manipulation of Thermal Emission via Tungsten Gratings

Jones T. K. Wan
Department of Physics, The Chinese University of Hong Kong, Shatin, Hong Kong, China

Abstract— Ordinary structured metallic surfaces exhibit various plasmonic excitations, in which the photon density of states is strongly modified. As a result, thermal emission of photons can be suppressed or enhanced accordingly. In this work, the author considers a model system consisting of tungsten gratings, and investigates the effects of the groove depth on the emission properties. By systematically increasing the groove depth, the emission at particular frequencies could be tuned to achieve that of the blackbody radiation limit, whereas the emission in other frequency ranges does not have noticeable changes.

Session 3A8
Poster Session 4

Applications of Silicon-based Photonic Crystal

Huihui Zhang, **Huajun Shen**, **Jingtao Zhou**, **and Xinyu Liu**
Institute of Microelectronics of Chinese Academy of Sciences, China

Abstract— Silicon photonic crystals provide an exciting new tool for the manipulation of photons in semiconductor industry. In this article, photonic crystal theory and applications of silicon-based photonic crystal are presented. Photonic bandgap is calculated and analysed, which are meaningful to the research of silicon-based photonic crystal devices.

Theoretical and Experimental Study of Complex Optofluidic Phenomena

J. A. M. Rojas, J. Alpuente, P. López-Espí, and R. Sanchez
Advanced Electromagnetism Research Group, Department of Signal Theory and Communications
Universidad de Alcala Escuela Politenica Superior, Campus Universitario Ctra. de Madrid a Barcelona km 33.600, 28871 Alcalade Henares, Madrid, Spain

Abstract— The study of electromagnetic processes in fluids has a long and rich tradition. Electrohydrodynamic, electroosmotic, dielectrophoretic and magnetophoretic phenomena are some of the most researched effects of the interaction of electromagnetic fields with fluids. The applications of these electromagnetic effects are extremely important in the chemical and pharmaceutical industries as well as invaluable tools in many laboratory procedures.

Optofluidics is an emerging research field with increasing theoretical and applied importance. Optofluidics study the interaction of dynamical electromagnetic fields with fluids. The theoretical understanding of these phenomena is very challenging because a complete description implies the coupling of the Maxwell equations, the Navier-Stokes equations, the equations of heat transfer in fluids and quantum effects related with the absorption of radiation by molecular species in fluids. In this sense, the understanding of electromagnetic interactions in fluids are of great importance for modelling other complex systems, like the biological ones. One example is the analysis of heat production and transfer in biological tissues due to the absorption of microwave radiation in the body. Such modelling is critical in many electromagnetic compatibility and medical physics issues.

Another extremely interesting theoretical challenge is the simulation of the interaction of electromagnetic radiation with complex structures in fluids. Certain phenomena like arrays of bubbles and turbulence can contribute to the formation of scattering structures with quasiperiodic variations of the refractive index inside the fluid. These fluid patterns can serve as photonic bandgap devices. The presence of photonic gaps inside a fluid permits the enhancement of light-matter interaction, increasing so the signal to noise ratio in the absorption spectrum. A clear understanding of the behavior of electromagnetic propagation in such structures would permit the fabrication of much more accurate and faster lab-on-a-chip instruments with innumerable applications.

The use of microfluidic channels as electromagnetic waveguides is also an exciting field of research. Fluids can be used as a flexible medium for propagation of light. The possible integration of tunable laser sources, adjustable gains and variable refractive indices make optofluidics a very promising technology in fields as diverse as sensors, robotics and telecommunications.

From an experimental point of view, optofluidics opens new possibilities for the study of electromagnetic propagation in complex media. The large coupling among the electromagnetic, hydrodynamic, acoustic and thermal phenomena constitutes an almost ideal laboratory to simulate, as a kind of analog computer, other poorly understood systems. The modelling of very complex systems beyond the present computational capabilites can be afforded in many cases by careful observation of analogous optofluidic devices.

Our group is researching new analytical and numerical approaches to the problem of light propagation in optofluidic structures formed by a combination of bubbles, electromagnetic and acoustical fields, thermal gradients and electrolytes with applications to new sensors and photonic devices. In analytical approaches, much of this coupling is expressed through the dependence of the dielectric permittivity on the physical parameters of the fluid. New powerful theories of effective permittivity inside fluids are needed in order to simulate the desired effects. From a numerical point of view, while finite elements are traditionally used for simulating fluids, finite differences are increasingly used in computational electromagnetics. Numerical schemes based on equivalent discretized systems, such as transmission line matrix (TLM) theory, have been successfully applied to both kind of problems and constitute a promissing line of research.

Experimental work is being developed in parallel with special focus on the transition between macroscopic and microscopic regimes. An special effort is dedicated to the reduction of complexity and cost of optofluidics devices, trying to search alternatives to integrated silicon structures in the mesoscopic and microscopic scale. The ultimate goal is the design of microfluidic photonic devices with a minimum of solid optical components and with the ability to guide, filter and collect the light with minimal losses and optimal wavelength tunability.

Focusing Properties of Radially Polarized Beam with Radial Cosine Phase Wavefront

X. Gao[1, 2], **J. Wang**[1], **L. Sun**[1, 3], **and S. Zhuang**[2]

[1]Electronics and Information College, Hangzhou Dianzi University
Hangzhou 310018, China
[2]University of Shanghai for Science and Technology, Shanghai 200093, China
[3]Key Laboratory of RF Circuit & System (Hangzhou Dianzi University)
Ministry of Education, China

Abstract— The focusing properties of radially polarized beam with radial cosine wavefront phase are investigated. For radially polarized beam without any wavefront phase, focus pattern is ring for low numerical aperture, while only one intensity peak for high numerical aperture due to stronger longitudinal field component in focal region. When the radially polarized beam with radial cosine wavefront phase is focused, focal pattern differs with frequency parameter in cosine function. For high numerical aperture, focal shift occurs, and novel focal patterns also evolve considerably, for instance, from only one peak to two or multiple peaks. Focal shift value fluctuates for low frequency parameter, drops sharply, and then comes back slightly. Simultaneously, Peak intensity ratio of radially polarized component to longitudinal polarized component in focal region decreases slowly, and then increases very quickly.

Investigation of Slow Wave Structure with Metal PBG Structures

Xi Gao, **Ziqiang Yang**, **Limei Qi**, **Zongjun Shi**, **Feng Lan**, **and Zheng Liang**
Institute of High energy Electronics, University of Electronic Science and Technology of China
No. 4, Section 2, North Jianshe Road, Chengdu 610054, China

Abstract— The dispersion curves of TM modes of two-dimensional (2D) photonic band gap (PBG) structure formed by triangular arrays of metal posts are calculated using Finite-Difference Time-Domain (FDTD) method. Then the global frequency band gaps of TM modes of the PBG structures with different ratios r/a can be obtained from the calculated dispersion curves, as shown in Fig. 1. The obtained results are in agreement with that in [1]. Using the band gap diagrams in Fig. 1, we have designed a PBG cavity, which only supports TM_{01}-like mode in TM_{0n}-like mode [2]. Furthermore, electromagnetic field characteristic and coupling impedance of a slow wave structure consisting of metal PBG structures are investigated. The electronic field patterns of π-mode of the operation mode TM_{01}-like mode and calculated coupling impedance are respectively shown in Fig. 3 and Fig. 4.

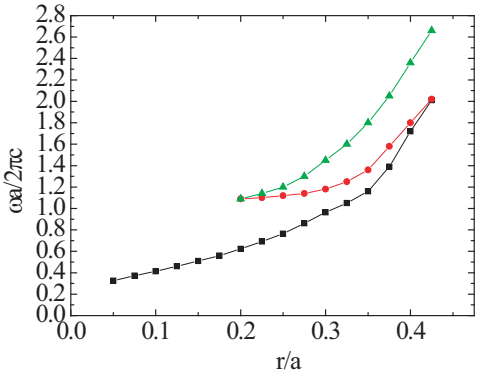

Figure 1: Global frequency band gap for TM mode as function of r/a for triangular lattice.

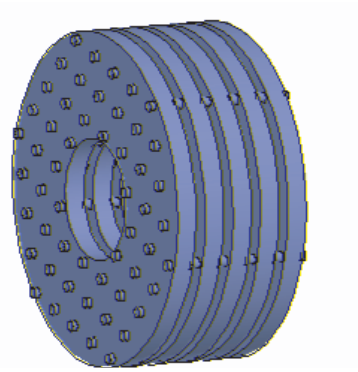

Figure 2: Physical model of high frequency system.

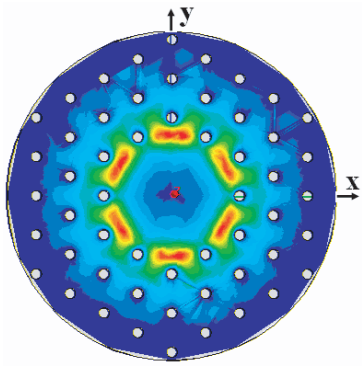

Figure 3: The electric field pattern of π-mode in a cross section of SWS.

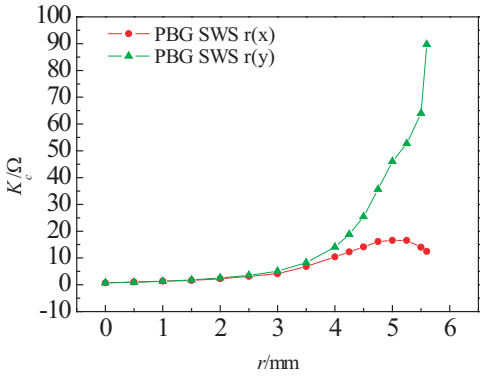

Figure 4: Coupling impedance at different position in SWS.

REFERENCES

1. Smirmova, E. I., C. Chen, M. A. Shapiro, J. R. Sirigiri, et al., *Journal of Applied Physics*, Vol. 91, 0021, 2002.
2. Gao, X., Z. Yang, et al., *Nuclear Instruments and Methods in Physics Research A*, Vol. 592, 292–296, 2008.

Transmission Characteristics of Electromagnetic Waves in Plasma Photonic Crystal by a Novel FDTD Method

Limei Qi, **Ziqiang Yang**, **Xi Gao**, **Feng Lan**, **and Zongjun Shi**
Institute of High Energy Electronic, University of Electronic Science and Technology of China
Chengdu, Sichuan 610054, China

Abstract— Plasma photonic crystal (PC) has been attracted much attention because of their new particular characteristics in which electromagnetic waves with frequency below plasma frequency can propagate. In this paper, we analyze the transmission characteristics of electromagnetic waves for two types of plasma PC-the one with plasma rods arranged in dielectric background periodically and an antiparallel one for the second type. A novel Finite-difference time-domain (FDTD) formulation for plasma is derived, the high accuracy and efficiency is confirmed by computing the reflection coefficients of electromagnetic waves through a collision plasma slab in one dimension.

ACKNOWLEDGMENT

This work is supported by National Nature Science Foundation of P. R. China (60571020 and 60178011).

3D FDTD Method Analysis of Light-beam Scattering from a RAD-MSR Disk Models

Di Yang, Akira Yokoyama, and Toshitaka Kojima
Graduate School of Electronics, Kansai University
3-3-35 Yamate-cho, Suita-shi, Osaka 564-8680, Japan

Abstract— We have developed numerical simulation techniques for the light-beam scattering and the detected signal characteristics from various types of optical disks such as digital versatile disks (DVD) and magneto optical (MO) disks so far and demonstrated that the finite difference time domain (FDTD) method can be a powerful tool for the numerical simulation of light-beam diffraction from conventional MO disk structures [1].

In order to break the optical resolution limit, various technologies are proposed for the higher density version of MO disks. In those technologies, the magnetically super resolution (MSR) is one of excellent readout methods [2]. The rear aperture detection (RAD) is proposed to increase the capacity by ten times or more [3]. The center aperture detection (CAD) is also proposed for advanced storage magneto-optical (ASMO) disks. Moreover, narrower focused beam can be realized by using blue laser light, so that the track pitch can be much more reduced. Therefore, narrower track pitches give rise to the increase of the crosstalk between adjacent tracks.

In the present paper, we try to apply the three-dimensional finite-difference time-domain (FDTD) method to the analysis of the light-beam scattering and the characteristic of detected signal from rear aperture detection-magnetic super resolution (RAD-MSR) disk model and to examine how the disk structure parameters affect the readout-signal characteristics including the influences of the groove depth on the crosstalk characteristics.

REFERENCES

1. Kobayashi, I., T. Kojima, S.-I. Fukai, and Y. He, "Numerical analysis of light-beam diffraction from magneto-optical disk medium by FDTD method," *IEICE Trans. Electron*, Vol. E84-C, No. 9, 1189–1195, Sep. 2001.
2. Kaneko, M., "Prospects of magneto-optical disks using magnetically induces super-resolution," *The Magnetics Society of Japan*, Vol. 23, No. 10, 1999–2004, July 1999.
3. Shinoda, M., A. Nakaoki, M. Kanno, and M. Kaneko, "High-density magneto-optical disk using land/groove recording and magnetically induced super-resolution by rear aperture detection," *The Magnetics Society of Japan*, Vol. 21, No. 4-2, 329–332, Oct. 1997.

Application of Laser Plasma Source with a Gas-puff Target in Calibration of Extreme Ultraviolet Detectors

J. Mikolajczyk and R. Rakowski
Institute of Optoelectronics, Military University of Technology
2 Kaliskiego Str., 00-908 Warsaw, Poland

Abstract— The paper presents a laser plasma source with gas puff target as metrology tools for EUV technology. The measurement of energy radiation is important issue in the technology. The experimental research show that the metrology parameters of the control instruments can be changed during exploitation. The changes could be caused with time degradation, chemical reactions with gases, debris's produced during experiments with some EUV sources or high radiation intensity. That is why the determination of the instrument responsivity in the EUV wavelength range is the main issue of any calibration procedure. The construction of the laser-plasma source with gas-puff target at the Institute of Optoelectronics MUT gives opportunity to design a calibration setup. In the paper, investigations results of the laser plasma source are described. The energy efficiency, spectrum and angle distribution of radiation emitted by the source were measured. The results made it possible to design a calibration procedure with a special metrology chamber. In the chamber, the optical beam splitter was mounted. The splitter consists of two special mirrors which reflect radiation into the chamber flanges. Using the chamber, the source radiation was measured simultaneously by a tested detector and model one. Developed system is characterized by very low outlay and good metrology features. In comparison with currently used systems, the presented setup is future alternative for small factories and laboratories producing for example EUV detectors.

Electromagnetic Modes in Hybrid Periodic-non-periodic Dielectric Porous Silicon Multilayers

José Escorcia-García[1] and Miguel E. Mora-Ramos[2]

[1]Centro de Investigación en Ingeniería y Ciencias Aplicadas
Universidad Autónoma del Estado de Morelos
Ave. Universidad 1001, Cuernavaca 62209, México
[2]Facultad de Ciencias, Universidad Autónoma del Estado de Morelos
Ave. Universidad 1001, Cuernavaca 62209, México

Abstract— Quasiregular structures were originally predicted to have peculiar electronic, vibrational and optical properties. In the case of electrons and phonons, the forecast was of critical states and highly fragmented fractal energy spectra. It still remains as an open question whether this kind of systems can outperform the periodic structures, or to exhibit novel features in comparison. In the case of optical capabilities, these structures can achieve better performance regarding second and third harmonic generation as well as the localization of light. At the same time, hybrid-order devices, based in the combination of periodic and quasiregular blocks have been proposed as well. It was established that hybrid systems are able to show complementary optical properties [1]. In addition, from the point of view of the vibration pattern of linear atomic chains, hybrid periodic-Fibonacci structures were found to possess selective confinement of the vibrations in the different parts of the structure for defined frequency ranges [2].

Porous silicon multilayers are easy to fabricate thanks to the rather simple electrochemical process used in their obtaining. They show great prospective for application in optical devices such as periodically layered dielectrics acting as Bragg mirrors, as well as different kinds of light filters. In general, such systems behave as one-dimensional photonic crystals with optical gaps in the visible and near infrared regions of the light spectrum.

In this work, we study the main features of the spectra of electromagnetic modes propagating in porous Si layered systems. We consider the case of the combination of periodic (Bragg-like) and quasiregular layered components, taking into account both periodic-quasiregular-periodic and quasiregular-periodic-quasiregular geometries. Among the aperiodic sequences used to simulate the quasiregular regions are the Fibonacci Thue-Morse and Period Doubling. Normal incidence transfer matrix formalism is used to calculate the eigenmodes as well as the electric field amplitudes corresponding to each of them. The possible existence of a localized behavior of some modes in the structures is particularly discussed for each studied system.

REFERENCES

1. Maciá, E., *Phys. Rev. B*, Vol. 63, 205421, 2001.
2. Montalbán, A., V. R. Velasco, J. Tutor, and F. J. Fernández-Velicia, *Phys. Rev. B*, Vol. 70, 132301, 2004.

Study on the Influence of the Incidence Direction on the Photonic Band Gap in Porous Si-based Dielectric Heterostructures

José Escorcia-García[1] and Miguel E. Mora-Ramos[2]

[1]Centro de Investigación en Ingeniería y Ciencias Aplicadas
Universidad Autónoma del Estado de Morelos
Ave. Universidad 1001, Cuernavaca 62209, México
[2]Facultad de Ciencias, Universidad Autónoma del Estado de Morelos
Ave. Universidad 1001, Cuernavaca 62209, México

Abstract— The capability of creating layered structures endowed with diverse properties has attracted great attention to study the optical properties of the photonic crystals (PC). These structures provide an effective means to control and manipulate the propagation of electromagnetic radiation in and out of the structure. In the case of one-dimensional case, a typical PC consists only of a periodically layered dielectric; for example, the Bragg mirror. This structure is able to reflect any electromagnetic within a wide range of the electromagnetic spectrum radiation, independently of the incident angle [1]. There are different proposals for enhancing the omnidirectional behavior of the PC, such as a combined system composed of a periodic and a quasiperiodic Fibonacci structure [2]. In this work we theoretically study the dependence of the photonic band gap (PBG) in porous Si multilayered systems with respect to the incidence angle for different structural distributions, regarding both the width of the layers and the refractive indices involved. We are considering both the cases of purely non-periodic heterostructures and the combination of periodic (Bragg-like) and quasiregular ones — the so-called hybrid systems. Among the different geometries taken into account there are the Gaussian, rugate, quasiregular Fibonacci, Thue-Morse and Period Doubling, as well as the case of random layer distribution. Oblique angle transfer matrix formalism is used to simulate the light propagation for different incidence directions. The possible omnidirectional behavior of the PBG is particularly discussed for each studied system and comparison is made between the distinct cases.

REFERENCES

1. Bruyant, A., G. Lérondel, P. J. Reece, and M. Gal, *Appl. Phys. Lett.*, Vol. 82, 3227–29, 2003.
2. Dong, J. W., P. Han, and H. Z. Wang, *Chin. Phys. Lett.*, Vol. 20, 1963–5, 2003.

Improved Property in Inverted Bottom-emission Organic Light-emitting Diodes Using 8-Hydroxyquinolinolatolithium Layer

J. F. Li[1, 2], **W. L. Chang**[2], **and F. J. Zhang**[1]

[1]School of Physical Science and Technology, Lanzhou University, Lanzhou 730000, China
[2]School of Mathematics, Physics & Software Engineering
Lanzhou Jiaotong University, Lanzhou 730070, China

Abstract— We demonstrate inverted bottom-emission organic light-emitting diodes (IBOLEDs) using 8-Hydroxyquinolinolatolithium (Liq) as an electron injection layer and an indium-tin-oxide coated glass substrate directly as cathode. The performances of devices with different thickness of Liq were investigated. Experiment results show that the efficiency of device with 1-nm-thick Liq is four times higher than that without Liq. The turn-on voltage of devices decreased from 20 to 9 V as the 1-nm-thick Liq was employed. Liq itself is an organic material which has a very similar electronic structure to Alq3. Therefore the energy level mismatch would be minimal and made the number of injected electrons and holes balance, and it significantly improves the device properties by inserting Liq electron injection layer between the emitting layer and cathode.

At the same time, we also demonstrate IBOLEDs using LiF as an electron injection layer and an indium-tin-oxide coated glass substrate directly as cathode. We found that the device using Liq as an electron injection layer is less sensitive to the Liq thickness than using LiF in efficiency. This property of Liq would be very important in the mass production. The difference may be attributed to the fact that Liq is an organic semiconductor and LiF an insulator, it can only be used when deposited as an ultra-thin layer. Our experimental results support the assumption that free lithium released from lithium quinolate is responsible for the improved device performance, and this release is more effective than that observed in devices with LiF. The results prove that Liq layer is also suitable for electron injection in IBOLEDs with an indium-tin-oxide coated glass substrate directly as cathode. This IBOLEDs can be integrated readily with the n-channel of the α-Si TFT backplane, which is proved to be useful in manufacturing. Active-matrix organic light emitting device with high-power efficiency and long device stability for future large-size OLEDs display applications.

Analysis of the Injection Layer of Liq in Inverted OLEDs Using Atomic Force Microscopy and X-ray Photoelectron Spectroscopy

J. F. Li[1,2], **W. L. Chang**[2], **and F. J. Zhang**[1]

[1]School of Physical Science and Technology
Lanzhou University, Lanzhou 730000, China
[2]School of Mathematics, Physics & Software Engineering
Lanzhou Jiaotong University, Lanzhou 730070, China

Abstract— A comprehensive understanding of the electronic states of the surface and interface is meaningful for organic light-emitting devices (OLEDs). 8-Hydroxyquinolinolatolithium (Liq)/indium-tin-oxide (ITO) thin film are analyzed using X-ray photoelectron spectroscopy (XPS). Atomic force microscopy (AFM) is also applied to investigate the morphology of Liq/ITO film. The above-mentioned ITO is directly employed as cathode and Liq as electron injecting layer in inverted OLEDs. AFM observation indicated that the surface is complanate, the Liq growth is uniform and defects cover basically the surface of ITO. Furthermore, the number of pinholes is small. And what is more, the analysis of the sample surface and interface further verifies this result by using XPS. XPS results show, the core-levels of Li1s, C1s, N1s, O1s, In3d5/2, and Sn3d5/2, spectra slightly shift towards lower binding energy with the increase of the sputtering time, which may be caused by the effect of oxygen, indium and tin in ITO diffusing into Liq layer. At the same time, Liq is found to have the ability of restraining the diffusion of chemical constituents from ITO to the electron transport layer, which is beneficial to the improvement of the performance and useful lifetime of the inverted OLEDs. Besides these, the single feature of the Li1s peak becomes two peaks, indicating there is the interaction of Li atoms with ITO. This reaction has caused a chemical change in Liq, which also might be an important reason that Liq layer can enhance the injection of electron. Our experimental results support the assumption that free lithium released from Liq. These results may explain that Liq is very effective to be used as an electron injection layer for inverted bottom-emission organic light-emitting diodes.

Low Cost 1×2 Acrylic-based Plastic Optical Fiber Coupler with Hollow Taper Waveguide

Abang Annuar Ehsan[1], **Sahbudin Shaari**[1], **and Mohd Kamil Abd. Rahman**[2]

[1]Institute of Microengineering and Nanoelectronics (IMEN), Universiti Kebangsaan Malaysia
43600 UKM, Bangi, Selangor, Malaysia
[2]Faculty of Applied Science, Universiti Teknologi MARA
40450 Shah Alam, Selangor, Malaysia

Abstract— A 1×2 Plastic optical fiber (POF) Y-coupler has been designed and fabricated using a simple acrylic (PMMA) mold insert. The device is composed of three segments: an input POF fiber, an intermediate hollow taper waveguide and output POF fibers. The acrylic mold insert has been fabricated using EGX-400 desktop engraver machine with a spindle speed of 15 K rpm and feed rate of 5 mm/sec. The engraved regions which is a form of U-groove allows 1 mm core step index PMMA POF fibers to be slotted into the mold insert. The short POF fibers at the input and output ends are slotted inside the mold insert before the interfaces of the taper waveguide. A top acrylic plate is then placed on top of the fabricated device and sealed. The final device has been tested for both splitter and combiner operations for an effective power of 1 mW. The device has an insertion loss of 10.48 dB. In the splitter operation, the device has a splitting ratio of 52 : 48. In the combiner operation, the combined power is −11.15 dB for input power of −11.90 dB and −12.05 dB.

Analysis of a New Measurement for Electromagnetic Field with Polarization Imformation of Fiber Grating

Yang Su, **Hui Peng**, **and Yuquan Li**
Institute of Communications Engineering
PLA University of Science and Technology, Nanjing, Jiang Su, China

Abstract— Fiber grating is sensitive to the stress, temperature and other entironmental factors. It has caused much attention and has been used widely. In this paper a new magnetic field measurement using polarization imformation of fiber grating is proposed. The polarization parameters include polarization dependent loss (PDL), different group delay (DGD) and so on.

When the magnetic field applied the refractive index difference of the two circularly polarized light in fiber grating will be changed because of the faraday effect. So the polarization imformation of fiber grating such as DGD or PDL will be changed.

Through the formula derivation in certain condition, the linear relationship between the peak value of DGD or PDL and magnetic field in measurement range is gained. Then through the simulations the effect of applied magnetic field, fiber length and index modulation coefficient on the peak value of DGD or PDL are shown and proved the theoretical analysis. On the other hand, the linearity will tend to saturation when magnetic field exceed the measurement range. So we can determine the mesurement range given the designing parameters.

In the experiments the DGD or PDL of FBG without and with magnetic field are performed. The peak value of DGD or PDL increase with the applied magnetic field linearly. The fit curve of experimental and simulated results is parallel approximately and the gap is because of the intrinsic DGD or PDL of fiber grating.

In DGD experiments using the optical vector analyzer with precision of 10^{-5} ps we get the sensitivity of 0.001 Gs. In PDL experiments the sensitivity of this sensor is 6.3×10^{-6} dB/Gs when the PDL resolution of OVA is 10^{-5} dB and the minimum value of magnetic field that can be measure is 2 Gs. The simulations and experiments validate this method.

Optoelectronic Sensor for NO_x Detection

J. Wojtas[1], **Z. Bielecki**[1], **J. Mikolajczyk**[1], **M. Nowakowski**[1], **T. Stacewicz**[2], **and A. Czyzewski**[3]

[1]Institute of Optoelectronics, Military University of Technology
2 Kaliskiego Str., 00-908 Warsaw, Poland
[2]Institute of Experimental Physics, Warsaw University
69 Hoza Str., 00-681 Warsaw, Poland
[3]Institute of Applied Optics, 18 Kamionkowska Str., 03-805 Warsaw, Poland

Abstract— The paper presents opportunities of application Cavity Enhanced Absorption Spectroscopy (CEAS) technique in nitrogen oxides (NO_x) detection. CEAS technique is a modification of Cavity Ring Down Spectroscopy (CRDS) technique. It is based on off-axis arrangement of an optical cavity. In this system, an absorbing gas concentration is determined by a decay time measurement of a light pulse trapped in a optical cavity. Measurements are not sensitive to laser power fluctuation and photodetector sensitivity fluctuation. In this configuration, setup includes the resonance optical cavity, build with spherical and high reflectance mirrors. As light sources pulsed lasers are used. NO_x detection is carried out in the visible and infrared range. The signal is registered with a developed low noise photoreceiver.

The features of a designed sensor show that it is possible to build a portable trace gases sensor, the sensitivity of which could be comparable with that of chemical detectors. Such a kind of system has several advantages; relatively low price, small size and weight, and possibility of detection of other gases.

Continuum Electronic Bound States in Rectangular Quantum Wells and Barriers

E. A. Carrillo-Delgado, **I. Rodríguez-Vargas**, **and S. J. Vlaev**
Unidad Académica de Física, Universidad Autónoma de Zacatecas
Calzada Solidaridad Esquina Con Paseo La Bufa S/N, Zacatecas, Zacatecas 98060, México

Abstract— We present numerical calculations that support the existence of electronic states confined in the continuum part of the spectrum in single rectangular quantum wells and barriers. We study the conditions necessary for the creation of these states. We find strong energetic and spatial localization of quasi-bound states at high energies in the conduction band. The results can be used in the design of optoelectronic devices that operate on the basis of continuum bound states.

Characteristic of Pentacene Thin Films

Chunlan Tao, **Xuhui Zhang**, **Maojun Dong**, **and Fujia Zhang**
School of Physical Science and Technology, Lanzhou University, Lanzhou 730000, China

Abstract— A comprehensive understanding of the organic semiconductor material pentacene is meaningful for organic filed-effect transistors (OFET). Thin films of pentacene are the most mobility molecular films known to date. They were fabricated by two ways on SiO_2 layer by dry oxidation, which were solution process and thermal evaporation.

The authors used O-dichlorobenzene to dissolve pentacene at 60°C and then raise the temperature, at 60°C, 100°C, 160°C fabricated the pentacene thin films respectively. Thermal evaporation was the other way to fabricate the penacene thin films under the vacuum of 10^{-5} Torr. Using the atomic force microscopicAFM images analyzed the surface morphologies and X-ray diffraction (XRD) patterns analyzed the crystal structure of the samples. The UV-visible spectroscopy analyzed the position of pentacene's absorption peaks.

From the images of thin films morphology, we learned that solution processed thin films of pentacene formed dendritic structure in large range, island structure could be observed in microscopy, which were extremely apparent at 100°C, so the optimum temperature of forming thin films was 100°C. The pentacene thin films of formed by thermal evaporation were very homogeneous, it better for fabricate organic filed effect transistors. From the solution processed pentacene thin films XRD peaks, according to Bragg Equation: $n\lambda = 2d\sin\theta$, it was obtained that the spacing of c-axis was 1.45 to 1.48 nm, which was close to bulk-phase and apart from thin film phase, but the thermal evaporated thin films were close to thin film phase.

ACKNOWLEDGMENT

Supported by the National Natural Science Foundation of China under Grant (No. 60676033).

Scanning Tunneling Microscope Studies of Co Growth on the Ru(0001) Surface

H. J. Zhang[1], **Y. F. Xu**[1], **X.-S. Wang**[2], **H. F. Wu**[1], **H. Y. Li**[1], **S. N. Bao**[1], **and P. He**[1]

[1]Department of Physics, Zhejiang University, Hangzhou 310027, China
[2]Department of Physics, National University of Singapore
Lower Kent Ridge Road, Singapore 119260, Singapore

Abstract— Co growth on the Ru(0001) surface from submonolayer to multilayer at room temperature and with different annealing temperature treatment were studied by using scanning tunneling microscope (STM). At room temperature, the Co forms a 2-D wetting layer at the first layer and followed with grow in the 3-D clusters mode from the second layer. In multilayer with different annealing temperature treatment case, 3-D Co clusters changed into 3-D islands and their height increased with the annealing temperature and then decreased at even higher annealing temperature. In about one monolayer case, the individual Co 2-D islands coalesced together to form Co wetting layers and the Co layer diffused away from the edges of the Ru steps with their shape changed from uniform to compact as the annealing temperature increased, no 3-D Co islands were observed.

Childhood Leukemia Risk Due to High Voltage Transmission Line in Tehran — Iran

Navid Khaledi and Nima Khaledi
Science and Research Campus, Young Researchers Club of Islamic Azad University
Tehran, Iran

Abstract— Up to the best of our knowledge, the first report on the relationship between childhood cancer and electromagnetic field emitted from power lines dates back to 1979. In our research, a group of 202 children suffering from leukemia has been studied (as case group). Map of Tehran was divided to 921600 square regions using AUTOCAD software. Using random number generator 4000 square regions were selected of which 86 were located 100 meters or less from the power line (as simulated control group), corresponding to 0.2 μT. Out of 202 children 7 were living in these selected area. Statistical analysis shows that Odds Ratio is equal to 1.63 (95% CI = 0.8 − 3.6) that shows a causal relationship between electromagnetic field and childhood leukemia.

Electromagnetic Pulse Alter Permeability of the Blood-brain Barrier in Rats

Guirong Ding, Xiaowu Wang, Kangchu Li, Yongchun Zhou, Lianbo Qiu, and GuoZheng Guo
Department of Radiation Medicine, School of Public Health
Fourth Military Medical University, Xi'an 710032, China

Abstract—

AIM: To study the effect of electromagnetic pulse (EMP) exposure on blood-brain barrier (BBB) permeability in rat brain.

Methods: 36 Male Sprague-Dawley rats were whole-body exposed or sham exposed to EMP at 200 KV/m for 400 pulses (1 Hz). At 1, 3, 6 h after EMP exposure, the rats were anaesthetized with sodium pentobarbital (ip, 40 mg/Kg), the heart was exposed and 100 ml 0.9% saline were perfused through the left ventricles, followed with lanthanum nitrate solution (for transmission electron microscopy observation) or 4% paraformaldehyde (for immunohistochemistry assay). The rats were sacrificed, their heads were removed and brains were excised. Disruption of BBB integrity in rat frontal cerebral cortex was detected by transmission electron microscopy and immunohistochemistry using lanthanum nitrate and endogenous albumin as vascular tracers respectively. The efficacy of the vascular tracer was confirmed with a positive control group exposed to adrenaline known to increase vascular permeability in the brain.

Results: In control rat brain, lanthanum nitrate tracer was limited to the capillary lumen, no lanthanum nitrate and albumin tracer extravasation was found. After EMP exposure, lanthanum nitrate ions reached the tight junction, basal lamina and the pericapillary tissue. Similarly, albumin immunopositive staining was also found in the pericapillary tissue. The changes of BBB permeability were transient, the leakage of BBB was found at 1 h, and reach the peak at 3 h, then began to recover at 6 h after EMP exposure.

Conclusions: These results suggest that exposure to EMP at 200 KV/m for 400 pulses (1 Hz) could increase the permeability of BBB in rat frontal cerebral cortex and this change is recoverable using lanthanum nitrate and endogenous albumin as vascular tracers.

The Research on the Harm of Biological Effect of Mobile Phone Radiation to Human Body

Yang Li and Guizhen Lu
Information Engineering School, Communication University of China
Beijing 100024, China

Abstract— This paper presents recent situations about the biological effect of mobile phone radiation, and enumerates some relative investigations and experiments. The former theoretic research has been reviewed, and then it indicates that classical theory may be not suitable to explain microcosmic phenomena and the methods should be ameliorated. The viewpoint that the interaction between the DNA molecule and adscititious electromagnetic wave can be analyzed with the quantum theory in the microcosmic domain namely in the nucleus has also been given. It is proposed that one reason of the electromagnetic biological effect is due to that the DNA molecule is affected by adscititious electromagnetic waves and then molecular energy level structure changes. The formula derivation of the quantum theory is listed and the explanation of its quantum theory effects is put forward. Finally, the paper points out that the results of action between microwave radiation and DNA molecule is probably belong to a kind of biological effect which is long-time and slow-effect.

Suppression of Static Magnetic Field in Diffusion Measurements of Heterogeneous Materials

Eva Gescheidtova[1] and Karel Bartusek[2]

[1]Faculty of Electrical Engineering and Communication, Brno University of Technology
Kolejni 2906/4, Brno 612 00, Czech Republic
[2]Institute of Scientific Instruments, Academy of Sciences of the Czech Republic v.v.i
Kralovopolska 147, Brno 612 00, Czech Republic

Abstract— The paper describes a magnetic resonance (MR) method for establishing the diffusion coefficients in heterogeneous materials. The pulsed field gradient stimulated-echo methods have a reduced coupling between the applied magnetic field gradient and a constant internal magnetic field gradient caused by different susceptibilities throughout the sample. When studying systems where it is necessary to keep the duration of the pulse sequence at a minimum or to study diffusion as a function of observation time, the spin-echo method should be chosen. The basic idea is to acquire the spin echo amplitude with pulsed field gradient of opposite signs and to subtract in a suitable way the NMR signals measured. The measuring method and the digital signal processing enable eliminating the effect of static magnetic field on the accuracy of measuring.

The experimental tests were made by measuring the diffusion coefficient of water both inside and outside of selected samples of porous materials of different properties. The change in the diffusion of water in porous materials was studied. The measuring method was experimentally tested on the MR tomograph 200 MHz/120 mm (4, 7 T) in the ISI ASCR in Brno. The 6-interval sequence (PFG-SE), shown in Figure 1, was used in the measurement. The error measured for the determination of spin echo magnitude for $G_{\mathrm{D}} = 0$ and $G_0 = 0$ is $\delta_{\mathrm{M}} = 1.8\%$.

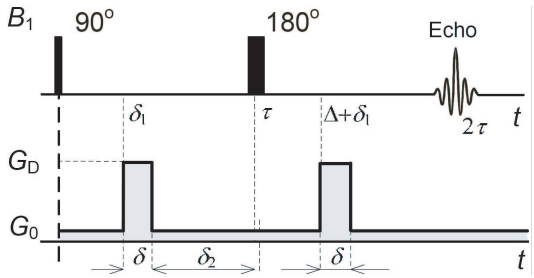

Figure 1: PFG-SE sequence.

In the paper, the measurement of the diffusion coefficients of water in heterogeneous systems is described. It is characterized by a special method of measuring, digital image processing, and calculation of the diffusion coefficients. An advantage of the three measurement arrangement is the elimination of both the cross terms $G_{\mathrm{D}}G_0$ and the term with G_0^2. The diffusion constant being measured depends on the time parameters of measurement, stability of the RF channel for nucleus excitation and MR signal reception, accuracy of the determination of spin echo magnitude, and on the magnitude of the diffusion gradient.

The technique will be made use of in the measurement of diffusion-weighted images of solids or gas found in porous materials, and in the development of new MR tomography measuring methods in the Institute of Scientific Instruments of the Academy of Sciences of the Czech Republic, v.v.i.

Compensating the Effect of Static Magnetic Field in MR Measurement of Diffusion

Karel Bartusek[1] and Eva Gescheidtova[2]

[1]Institute of Scientific Instruments, Academy of Sciences of the Czech Republic, v.v.i.
Kralovopolska 147, Brno 61200, Czech Republic
[2]Faculty of Electrical Engineering and Communication, Brno University of Technology
Kolejni 2906/4, Brno 61200, Czech Republic

Abstract— When studying the properties of live tissues and also inanimate materials, one of the currently most important methods can be seen in imaging techniques based on the magnetic resonance (MR) principle. These methods allow measuring the very slow motion (diffusion) $10^{-10} \div 10^{-12}\,\mathrm{m^2/s}$ of atomic nuclei and molecules in substances examined. The knowledge of the motion of atomic nuclei in porous materials brings new diagnostic potentials. The very first method for diffusion measurement, the Pulsed Field Gradient Spin Echo (PFGSE), was described as early as 1965. It can only be used to measure diffusion in substances with sufficiently long relaxation times T_1 and T_2. The nuclei of substances encountered in porous materials have short relaxation times (units of milliseconds).

Our proposed method employs the PFGSE measuring sequence, in which three or four diffusion gradients of different polarities are generated. Simple calculations can be used to compensate for the inhomogeneities of static magnetic field, which are due to the magnetic susceptibility of the substance being measured. Shaped impulses in the measuring sequence extend the diffusion measurement time, which is always limited by relaxation time T_1 of the substance under measurement. To be able to measure diffusion in substances with short relaxation times T_1, we must reduce the measuring time to a minimum while maintaining sufficient precision of the measurement.

The proposed method was verified experimentally by measuring diffusion in deionized water at temperatures of $20 \pm 0.2°\mathrm{C}$. The measurements were carried out on an MR tomography 200 MHz/120 mm (4.7 T) in the Institute of Scientific Instruments, Academy of Sciences of the Czech Republic in Brno. The relaxation times of the water measured were $T_1 = 2700\,\mathrm{ms}$ and $T_2 = 380\,\mathrm{ms}$. The 6-interval PFGSE sequence was used in the measurement. The sequence parameters were set at $\delta = 5\,\mathrm{ms}$, $\Delta = 20\,\mathrm{ms}$. The diffusion gradients chosen were $G_D = \pm 72$ and $\pm 144\,\mathrm{mT/m}$. The static gradient was measured in the range $G_0 = 0 \div 144\,\mathrm{mT/m}$.

The method described in the paper has been proposed for measuring diffusion coefficients in heterogeneous systems. Its characteristic feature is a special measuring procedure and the calculation of coefficients. The advantage of conducting three of four measurements is the elimination of the influence of cross terms between the diffusion and the static gradients, and the elimination of the influence of the static gradient itself. The diffusion constants are dependent on the time parameters of the measuring sequence, the stability of the RF channel of tomograph for the excitation of nuclei, the accuracy of determining the spin echo magnitude, and on the level of the diffusion gradient. The method will be used when measuring diffusion-weighted images of solids and gases that are present in porous materials.

REFERENCES

1. Stejskal, E. O. and J. E. Tanner, "Spin diffusion measurements: Spin echoes in the presence of a time-dependent field gradient," *J. Chem. Phys.*, No. 42, 288, 1965.
2. Tanner, J. E., "Use of the stimulatsd echo in NMR diffusion studies," *J. Chem. Phys.*, Vol. 52, 2523–2526, 1970.
3. Bartusek, K. and E. Gescheidtova, "MRI method of diffusion measurement in heterogeneous materials," *Measurement Science and Technology*, Vol. 19, 1–8, 2008.

Wavelet Filtering and Level Set Segmentation of NMR Images for Monitoring the Development of Growing Cultures

J. Mikulka[1], **E. Gescheidtova**[1], **and K. Bartusek**[2]

[1]Department of Theoretical and Experimental Electrical Engineering
Brno University of Technology
Kolejni 4, Brno 61200, Czech Republic
[2]Institute of Scientific Instruments, Academy of Sciences of the Czech Republic
Kralovopolska 147, Brno 61264, Czech Republic

Abstract— NMR images serve the purpose of following the development and quantitative measurement of tissues. Segmentation can be applied to images and subsequent evaluation of the parameters of individual regions such as circuit, area or volume in case images from several slices are available. The paper describes the pre-processing and subsequent segmentation of NMR images of growing tissue cultures. Images obtained by the NMR technique give three separately growing cultures. The aim of the work was to follow the speed of their development depending up environment. Images obtained by means of the NMR device used are of very low resolution and contrast and there are no sharp edges between regions. Processing such images may prove to be quite difficult. A suitable algorithm was found, which consists of the pre-processing of the image by wavelet filtering and subsequent multiphase level set segmentation. The wavelet filtering method smoothes a noise in image and increases the low contrast. The proposed level set method segments the image based on the intensity of the regions sought, and is suitable for working with NMR images in which there are no sharp edges. The method also has some filtering capability. The length of contour or the area of segmented region can be minimized. The level set method is described by partial differential equations that were transformed into corresponding difference equations solved numerically. Processing the observed images and measuring the sequence of NMR data give a graph of the growth development of the tissue cultures examined in comparison with manual measurement of their content.

REFERENCES

1. Aubert, G. and P. Kornprobst, *Mathematical Problems in Image Processing*, Springer, ISBN 0-387-32200-0, New York, 2006.
2. Vese, L. and F. Chan, "A multiphase level set framework for image segmentation using the Mumford and Shah model," www.math.ucla.edu/ lvese/PAPERS/IJCV2002.pdf.
3. Chan, F. and J. Shen, "Image processing and analysis: Variational, PDE, wavelet and stochastic methods," *SIAM 2005*, ISBN 0-89871-589-X, Philadelphia, 2005.
4. Osher, S. and R. Fedkiw, *Level Set Methods and Dynamic Implicit Surfaces*, Springer, ISBN 0-387-95482-1, New York, 2003.

Perimeter Measurement of Spruce Needles Profile Using MRI

J. Mikulka[1], **E. Gescheidtova**[1], **and K. Bartušek**[2]

[1]Dept. of Theoretical and Experimental Electrical Engineering, Brno University of Technology
Kolejni 4, Brno 612 00, Czech Republic
[2]Institute of Scientific Instruments, Academy of Sciences of the Czech Republic
Kralovopolska 147, Brno 612 64, Czech Republic

Abstract— The paper describes using of MRI methods to perimeter of spruce needles profile assesment. The aim of this work is creation of multi-instrumental equipment for research on heavy metal (cadmium and lead) influence on development of spruce needles cellulate germ (somatic embryos). During the research were observed differences in germ grow with different concentration of cadmium. With a certain concentration of cadmium the perimeter of needle increases more than with other. It is due to more intensive water usage from cultivation medium and then attenuation of heavy metal concentration inside the needle. As one of the observational method mentioned phenomenon was chosen analysis of NMR image susceptible estimation of needle growth by the perimeter of needle profile. Slices of spruce needles were observed on MR tomograph UPT AV CR with induction of magnetic field 4.7 T. Concurrently a method in AF MZLU was applied by cutting the needles on hand microtome, the images of slices were observed by digital camera with 1600×1200 pixels resolution and by using binocular magnifying glass. The aim of the article is comparison of experimental results observed by both mentioned methods.

REFERENCES

1. Aubert, G. and P. Kornprobst, *Mathematical Problems in Image Processing*, New York, Springer, ISBN 0-387-32200-0, 2006.
2. Vese, L. and F. Chan, "A multiphase level set framework for image segmentation using the mumford and shah model," www.math.ucla.edu/ lvese/PAPERS/IJCV2002.pdf.
3. Chan, F. and J. Shen, "Image processing and analysis: variational, PDE, wavelet and stochastic methods," *SIAM*, Philadelphia, ISBN 0-89871-589-X, 2005.

Characterization of Acetylcholine Hydrolysis under Continuous and Pulsed Microwaves Radiation Using Broadband Dielectric Measurement

C. Gilbert[1], **C. Pareige**[1], **A. Fourrier-Lamer**[1], **F. Maurel**[2], **and O. Meyer**[1]

[1]LGEP Supelec, CNRS UMR-8507, Univ. UPMC Paris 06, Univ. Paris Sud
11 rue Joliot Curie, F91192 Gif-sur-Yvette cedex, France
[2]ITODYS, CNRS, CNRS 7086, University of Paris 7, Bâtiment Lavoisier 15
rue Jean de Baïf, F75205 Paris cedex 13, France

Abstract— In this paper, we will describe the statement of our current advance in continuous and pulsed wave analysis on AchE activation. Acetylcholinesterase (AchE) is a major enzyme that catalyzes the hydrolysis of the neurotransmitter Acetylcholine into Choline and Acetic Acid [1, 2], a reaction necessary to allow a cholinergic neuron to return to its resting state after activation. In a more general way, it controls nervous and neuromuscular impulses in mammalians species. We will try to determine how continuous waves (CW) or Pulsed Waves (PW) interact with this polarized entity. Dielectric relaxation determination in real time, will give us information about the synthesis output, and power density measurement, the energy activation threshold.

Instrumentation & Application: The instrumental bench takes again the one of Belhadj [3] and Meyer [4] for CW and will be modified to take into account Pulsed Waves, previous literature describe that PW produce more effect on the reaction [5]. This instrumentation allows dielectric characterization in broadband frequency (1 MHz–1.8 GHz under microwave heating, 100 Hz–18 GHz in ambient temperature) during the microwaves treatment [4]. The sample to be characterized is placed into two types of cylindrical cell at the end of coaxial waveguide [3], one using multimodal and non homogeneous propagation and the other one propagates only fundamental mode but in a homogeneous way. CW generator characteristics are 2.45 GHz frequency and up to 50 W of Power. The last is applied during few seconds before measuring the admittance of the characterized material. The resolution of direct problem is analytical, and inverse problem resolution gives dielectric complex permittivity, which leads to conductivity.

PW generator characteristics are 2 ns rise time, 100 ns fall time, maximum repeatability of 10 KHz and maximum voltage of 7 KV. The very quick peak of energy is supposed to polarize the enzyme, which could lead to inactivation or on the contrary to fasten the hydrolysis via the so called 'Athermal Effect'. That's what the study is about.

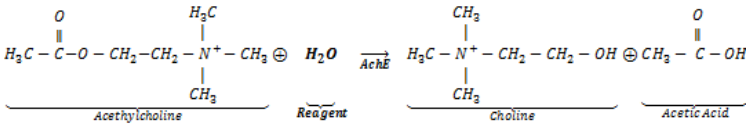

Equation 1: Hydrolysis reaction.

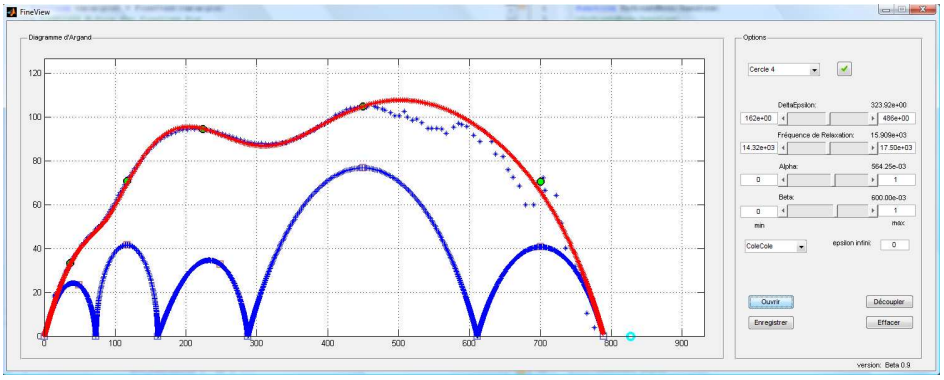

Figure 1: Example in determination of dielectrics parameters on $Li_{0.2}V_2O_5$.

Development: A new user-friendly fitting tool has been developed in order to perform the findings of relaxation time and static conductivity among the various coupled entities present in the reaction. It shows Argand representation with Cole-Cole, Cole-Davidson and Havriliak-Negami semi-empirical modeling. CW results are already available and soon in PW.

The fully automated bench allows knowing the immediate broadband admittance (100 Hz–18 GHz) after heating period, which leads to get immediate effect on the reaction. Conclusion will be carried out according to the state of the reaction. According to molecular static conductivity, it will easy to know the present entities in the reaction and consequently the hydrolysis evolution. This study is supported by *Direction Générale de l'Armemen*t (DGA), REI n°05.34.054.

REFERENCES

1. Dvir, H., M. Harel, S. Bon, W. Q. Liu, M. Vidal, C. Garbay, J. L. Sussman, J. Massoulié, and I. Silman, "Structural insight into tetramerization of the synaptic form of Acetylcholinesterase: Interaction of polyproline II helix with four WWW motifs," *EMBO J.*, Vol. 23, 4394–4405, 2004.
2. Massoulié, J., "The origin of the molecular diversity and functional anchoring of cholinesterase," *Neurosignal*, Vol. 11, 130–143, 2002.
3. Belhadj-Tahar, N. and A. Fourrier-Lamer, "Broadband analysis of a coaxial discontinuity used for dielectric measurements," *IEEE Trans. on Micr. Th. and Tech.*, Vol. 34, No. 3, 346–350, March 1986.
4. Chevalier, S., O. Meyer, A. Fourrier-Lamer, A. Petit, A. Loupy, and F. Maurel, "New instrumentation for the comprehension of chemical reactions under microwave and classical heating with the aid of a wide frequency band dielectric spectroscopy," *Eur. Phys. J. AP*, Vol. 15, 223–229, 2001.
5. Michaelson, S. M., E. C. Elson, and L. E. Anderson, *Biological and Medical Aspect of Electromagnetic Fields*, Vol. 3, 60–96.

Effect of Seed Pretreatment by Magnetic Fields on Seed Germination and Ontogeny Growth of Agricultural Plants

Ahmad Majd[1] **and Azita Shabrangi**[2]

[1]Islamic Azad University, North Branch, Tehran, Iran
[2]Physics Society, Plasma Physics Research Centre, Science and Research Campus
Islamic Azad University, Tehran, Iran

Abstract— Lentil belongs to Fabaceae family which has been cultivated since 8000 years ago. Nowadays different varieties of lentil are considered to be optimized because of its nutrient importance and some medicinal properties. An experimental study of the influence of external magnetic field on the germination, ontogeny growth and anatomical structure were carried out. In this research, seeds of Lentil (*Lens culinaris L.*) were magnetically pretreated by different magnetic field intensities from 0.06 to 0.36 tesla (T) for different periods of time 5, 10, 20 minutes. Some seeds were plunged into the water during exposure to magnetic fields. Then seeds were placed in germinator and seed germination rate and seedling excretion rate were measured.

Mean germination time showed a reduction for most of magnetic treatments therefore their rate of germination was increased. The range of greatest increase of germination were obtained from 0.18 T to 0.24 T. 15 days seedlings grown from pretreated seeds, which were plunged into the water during exposure to magnetic fields with 0/06 tesla intensity in 10, 20 minutes treatments, showed less and disorder growth in comparison to control. This decreased growth in 20 minutes treatment was more than 10 minutes treatment. On the other hand, 15 days seedlings grown from pretreated seeds in the same condition, but without water, showed more growth and leaf size increased too. Anatomical examination were carried out on 15 days seedlings, which were grown up from pretreated seeds in green house condition with natural light cycle 14-h light/10-h darkness and $25 \pm 3^{\circ}$C daily night temperture. The results of experiments suggested that stele and xylem vessels develop and grow more than control and parenchyma cells are larger than control. The greatest difference was observed in leaf section. Air chambers and parenchyma cells were larger than control. These results suggested that some intensities of magnetic field improve significantly seed germination and growth of plants.

Effect of Magnetic Fields on Growth and Antioxidant Systems in Agricultural Plants

Azita Shabrangi[1] and Ahmad Majd[2]

[1]Physics Society, Plasma Physics Research Centre, Science and Research Campus
Islamic Azad University, Tehran, Iran
[2]Islamic Azad University, North Branch, Tehran, Iran

Abstract— Magnetic fields are considered as an environmental factor that has significant effects on function and growth of plants. In this research, seeds of Lentil (*Lens culinaris L.*, which contains significantly Fe^{2+} as a ferromagnetic element) were magnetically pretreated by different magnetic field intensities from 0.06 to 0.36 tesla (T) by using Zeeman system for different periods of time 5, 10 and 20 minutes. Seedlings growth data were measured in green house condition with natural light cycle 14-h light/10-h darkness and $25 \pm 3^{\circ}$C daily and night temperature. Activity changes assay of Ascorbate peroxidase (APX) and Superoxide Dismutase (SOD) were carried out by spectrophotometer in 15 days seedlings.

The greatest root growth in 3 days seedlings was observed in seedlings which were grown up from pretreated seeds by 0/3 tesla magnetic field intensity in 20 minutes pretreatment. The greatest shoot growth was also seen in 0/24 tesla magnetic field intensity in 20 minutes pretreatment. The results of experiments suggested that in 15 days seedlings, the greatest growth and biomass was observed in 0.18 T. Root had more growth than shoot under effect of magnetic fields. Leaf size and stem thickness were increased too. These seedlings were more resistant to drought stress. Activity enzymes assay suggested that APX activity increased in both root and shoot by increasing magnetic field intensities and SOD activity also increased in root of pretreated plants. All the results suggested that pretreated plants by magnetic fields are more resistant against harmful environmental factors. `Moreover` growth data of seedlings changed in comparison with control and in some intensity of magnetic fields increased.

The Weak Combined Magnetic Fields Reduce the Brain β-Amyloid in an Animal Model of Sporadic Alzheimer's Disease

N. V. Bobkova, **V. V. Novikov**, **N. I. Medvinskaya**,
I. Yu. Aleksandrova, **and E. E. Fesenko**
Institute of Cell Biophysics, Russian Academy of Sciences, Pushchino 142290, Russia

Abstract— Subchronic effect of weak combined magnetic fields (MFs) on spatial memory and level of brain β-amyloid (βA) was studied in mice with ablation of the olfactory bulbs and control sham-operated (SO) animals. The bulbectomized (BE) mice show the main signs of Alzheimer's type degeneration such as memory impairment, the increase of the βA level in the brain, pathology in the acetylcholinergic system, and the loss of neurons in the brain structures responsible for memory (Bobkova et al., 2001; Aleksandrova et al., 2004, Bobkova et al., 2005; Nesterova et al., 2008). The combined MFs consisted of the constant component 42 μT and of the variable component 0.08 μT. The variable field was the sum of two signals of frequencies of 4.38 and 4.88 Hz. Exposure to the MFs (4 hours for 10 days) induced the reduction of the βA level in the brain of the BE mice, but did not protected their memory from impairment. However, the same MFs improved the spatial memory in SO mice. The beneficial effect of the MFs in the SO animals was prolonged and was revealed for a month after exposure to the MFs. The results suggest that the MFs can be used to prevent the Alzheimer's disease in a group of risk as well as in other diseases involving amyloid protein deposition in different tissues.

Weak Combined Magnetic Field Accelerates Hydrolysis of βAmyloid-Protein *in vitro*

E. E. Fesenko, **V. V. Novikov**, **and N. V. Bobkova**
Institute of Cell Biophysics, Russian Academy of Sciences
Pushchino, Moscow Region 142290, Russia

Abstract— Previously, we determined that weak combined magnetic fields substantially accelerate the spontaneous hydrolysis of some proteins and peptides into fragments in solutions. Here we have shown that a weak combined variable magnetic field of 0.05 μT with frequencies 3.58–4.88 Hz and constant magnetic field of 42 μT accelerate the hydrolytic decomposition of β-amyloid in solution. The region of the molecule that is most sensitive to the weak magnetic field was determined. This region is located between residues Asp7 and Ser8. In this region the hydrolysis of β-amyloid under the action of the magnetic field takes place. It is known that β-amyloid is the key neurotoxic protein in the brain of patients with the Alzheimer's disease, accompanied by loss of memory and death. At present one of the main elements of the current strategy of AD treatment involves the active modification of the structural-functional characteristics of protein and peptide molecules participating in the pathological process. Therefore our results can form the basis for new approaches to treatment the diseases related to the accumulation of pathological proteins in different pathologies, including the Alzheimer's disease.

Electromagnetic Wave Absorption in K Band and V Band with Carbon Microcoils

Kuan-Ting Lin[1], **Jian-Yu Hsieh**[1], **Tao Wang**[1], **Cheng-Hung Li**[2], **Neng-Kai Chang**[2], **Shey-Shi Lu**[1], **Shuo-Hung Chang**[2], **and Ying-Jay Yang**[1]

[1]Graduate Institute of Electronics Engineering, National Taiwan University, Taiwan, R.O.C.
[2]Department of Mechanica Engineering, National Taiwan University, Taiwan, R.O.C.

Abstract— With the dramatic development of wireless communication technology in recent years, the safety of radiated electro-magnetic (EM) wave becomes a more and more controversial issue. Regardless of the debate that whether radio signals are harmful to human bodies, relevant works on the prevention from EM wave exposure have been kept on going.

In this paper, an EM wave absorption materials consisting of carbon microcoils is realized in K band and V band of EM wave frequency. The powders of carbon microcoils of $10 \sim 100\,\mu m$ length doped in the polydimethyl siloxane (PDMS) are used as samples for measuring. The length, width, and thickness of carbon microcoils sample are 4 cm, 3 cm, and 3 mm, respectively. Besides, samples containing carbon fibers and carbon microcoils with different lengths were used as contrasts in the absorption experiment. In order to observe the EM wave absorption rate of carbon-microcoils, the measuring equipments include a signal generator (SG), narrower beamwidth rectangular horn antennas, and a spectrum analyzer (SA) are utilized. This experiment was performed in an anechoic chamber to minimize the effects of signal reflections and unwanted interferences.

The measured results of the carbon microcoils show that the absorptions are 15 dB (97%) at 26 GHz and 20 dB (99%) at the region from 64 to 70 GHz. In addition, the measured results of carbon microcoils with different lengths reveal that the EM wave absorption rate of long microcoils are better than short ones. The experimental results show that the carbon microcoils are superior in EM wave absorption and may be considered as a useful tool in future EMI/EMC applications.

Non-linear Heating of the Upper Thermosphere Due to Auroral Electric Field

S. S. De, **B. Bandyopadhyay**, **Suman Paul**, **M. De**, **and D. K. Haldar**
Centre of Advanced Study in Radiophysics & Electronics, University of Calcutta, India

Abstract— The electric field in the auroral zone and in the polar cap accelerates the movement of the upper thermosphere. The motion is associated with the movements of the constituent medium particles where electrons are highly affected by the driving force rather than heavy neutral and charged particles, and mainly responsible for the movement of thermosphere.

The thermospheric region above altitudes of about 160 Km is characterized by different non-linear phenomena due to variation of the velocity distribution of the thermospheric constituents, medium temperature, ionizing frequency, effective collision frequency and recombination co-efficient of electrons and ions.

The penetration, diffusion and precipitation of auroral electrons into the medium introduce heating which is further enhanced by the level of geomagnetic activities, multiple scattering and Coulomb interactions with atomic nucleus and orbital electrons of atmospheric constituents. Energy distribution also depends on the variation of the atmospheric density with altitude. Analyses and interpretation of precipitation patterns, latitudinal distribution of energy and dynamics of the incoming particles have been modeled by various earlier workers.

Auroral electric currents and charged particle precipitation produce Joule heating, gravity waves and travelling ionospheric disturbances which initiate temperature enhancement and temperature fluctuations. The presence of fluctuating electric field initiates Joule heating along with viscous heating. Magnetosphere-Ionosphere coupling mechanism also provides informations about Joule heating rate along with various other electrodynamic parameters. These heating make the largest contribution to the total energy budget in the medium. Both of these would give rise to detectable pressure fields beyond the boundaries at which the auroral currents remain confined.

In this presentation, magnetohydrodynamic formalism has been used to derive an analytical expression of the velocity of the upper thermosphere in the auroral region. The effects of ionization and recombination processes, density and temperature fluctuation of the thermospheric medium along with the influence of gravity and viscosity are taken into account in the analyses. The spatial distribution of the velocity and its altitude dependence within the auroral zone has been explored. The expressions of Joule heating and viscous heating are derived. Numerical analyses are carried out to estimate their magnitudes as well as the rate of their variations with time. For different characteristic times, the variations of velocity with altitude are studied. The results have been presented graphically.

The numerical results of the present analysis support the observations made by DE-2 satellite. The results may be considered to reflect the enhanced influence of geomagnetic activities.

Computer Simulation of Emission Spectra in Plasma Generated by an Alternating Electric Field

E. V. Koryukina
Tomsk State University, Lenin avenue 36, Tomsk 634050, Russia

Abstract— An electric field in a gas discharge is one of the most important discharge parameters. The presence of the electric field is a reason for the Stark effect. In plasma physics, the Stark effect is widely used for plasma diagnostics, in particular, for the determination of energy distribution functions, density and temperature of electrons, etc. It is obvious, the presence of the Stark effect leads to the change in the transition probabilities and spectral line intensities of atomic and ionic emission spectra observed in plasma under consideration.

Of special interest is the investigation of the emission spectra of rare gases widely used in plasma physics. In particular, the investigation of the rare-gas emission spectra in a circular polarized electric field is actual problem because such field is realized in a high-frequency discharge and under laser excitation. In the given work a theoretical method considered in [1] is used for obtaining the wave functions of atoms in the electric field. This method, free from limitations inherent in the perturbation theory, allows us to carry out the investigation of shifts and splitting of spectral lines of atoms and ions and also the transition probabilities between the Stark levels and atomic state lifetimes in the wide range of frequency and strength of the electric field.

The algorithm of using this method was realized in a special software package written in FORTRAN. Input data of this package are the unperturbed energy-level positions, the frequency and strength F of the electric field. Output data obtained at sequential passing of the code blocks are following: the wave functions of atom, spectral-line shifts and splitting, transition probabilities and Stark-level lifetimes in the electric field.

Based on the simulation results, the regularities inherent in the behaviour of spectral-line shifts and splitting of atoms in dependence on the frequency and strength of the electric field were revealed and investigated. As results have shown, an increase in the nucleus charge at an increase in the electric-field strength leads to the change of the spectral-line shift direction. The Stark-level interactions increasing with the growth of the electric-field strength lead to anomalies in the behaviour of spectral lines and an appearance of forbidden lines. Further, obtained results have shown that the interaction of the Stark levels leads to an anisotropy of transition probabilities. It was found that the transition probabilities and lifetimes have a polynomial dependence on the electric-field strength, and the bigger the electric-field frequency is, the bigger a degree of polynomial is.

Theoretical results obtained by the computer simulation allow us to explain the processes taking place in plasma. In particular, based on the calculated data one can determine the electric-field strength inside a discharge, clarify a mechanism of filling of the excited levels and causes of the change of spectral-line intensities. Further, simulated probabilities and lifetimes can be used as input data in other theoretical calculations, for example, at a solution of the population density balance equations. Moreover, the regularities revealed in the simulation process can be useful for a prediction of results necessary for a creation of new devices.

REFERENCES

1. Koryukina, E. V., *J. Phys. D: Appl. Phys.*, Vol. 38, 3296–33, 2005.

Abnormal Refraction of Microwave in Ferrite Based Composite Metamaterials

Hongjie Zhao[1, 2], **Lei Kang**[2], **Ji Zhou**[2], **Qian Zhao**[3], **Rui Wang**[2], **and Jingbo Sun**[2]

[1]Aerospace Research Institute of Special Materials and Processing Technology
Beijing 100074, China
[2]State Key Laboratory of New Ceramics and Fine Processing
Department of Materials Science and Engineering, Tsinghua University
Beijing 100084, China
[3]State Key Lab of Tribology, Department of Precision Instruments and Mechanology
Tsinghua University, Beijing 100084, China

Abstract— An abnormal refraction of microwave is observed experimentally in a composite metamaterial consisting of an array of ferrite rods combined with metallic wires. In a prism arranged with the parallel rods and wires we observe negative refraction (NR) whose frequency can be adjusted dynamically by an applied magnetic field, while we detect a positive refraction (PR) at those frequencies slight lower than that of the NR. The PR is resulted from large self-inductance of the wire, which is induced by the extremely increased permeability of adjacent rod to the wire in the vicinity of ferromagnetic resonance. By crossing the rods and wires, the self-inductance is decreased and only NR is observed correspondingly. The tunability of NR would be helpful for the design of novel subwavelength devices such as broadband perfect lens.

Light Harvest Induced in Cloaking Shells

Pu Zhang[1, 2] **and Yi Jin**[1]

[1]Centre for Optical and Electromagnetic Research, Zhejiang University
Hangzhou 310058, China
[2]Joint Research Centre of Photonics, The Royal Institute of Technology, Sweden

Abstract— In the last two years, transformation optics [1] has been actively exploited and applied to design the unusual electromagnetic (EM) cloak (cloaking shell) [2], which has the power to redirect EM waves around a hidden volume and transmit them as if nothing exists. The theoretical prediction was then successfully confirmed by analytical analysis [3] and numerical simulation [4]. A proof-of-principle experiment [5] based on a simplified model was also conducted to demonstrate the cloaking effect. Besides EM cloaking, other novel phenomena, like field concentration [6], subwavelength imaging [7] and arbitrary wavefront manipulation [8], are observed in devices designed by transformation optics.

Here, light collecting and guding functions of 2D cloaking shells are utilized to induce light harvest. Perfectly matched outer boundary of a cloak can collect incident light without reflection, light is then redirected by the shell (around the inner boundary) toward the two ends. Consider an elliptic cloak with a large aspect ratio and uniform thickness. In a wide range, incident light perpendicular to the major axis can be totally collected and redirected to the two ends. Note that the considerable amount of light concentrated at the two ends with finite thickness can be havested for solar energy use. Analytical and numerical methods are used to elucidate the aforementioned phenomena.

REFERENCES

1. Leonhardt, U. and T. G. Philbin, *Transformation Optics and the Geometry of Light*, arXiv: 0805.4778v2, 2008.
2. Pendry, J. B., D. Schurig, and D. R. Smith, "Controlling electromagnetic fields," *Science*, Vol. 312, 1780, 2006.
3. Chen, H., B. I. Wu, B. Zhang, and J. A. Kong, "Electromagnetic interactions between a fast electron beam and metamaterial cloaks," *Phys. Rev. Lett.*, Vol. 99, 063903, 2007.
4. Cummer, S. A., B. I. Popa, D. Schurig, D. R. Smith, and J. B. Pendry, "Full-wave simulations of electromagnetic cloaking structures," *Phys. Rev. E*, Vol. 74, 036621, 2006.
5. Schurig, D., J. J. Mock, B. J. Justice, S. A. Cummer, J. B. Pendry, A. F. Starr, and D. R. Smith, "Metamaterial electromagnetic cloak at microwave frequencies," *Science*, Vol. 314, 977, 2006.
6. Rahm, M., D. Schurig, D. A. Roberts, S. A. Cummer, D. R. Smith, and J. B. Pendry, "Design of electromagnetic cloaks and concentrators using form-invariant coordinate transformations of Maxwell's equations," *Photon. Nanostruct. Fundam. Appl.*, Vol. 6, 87, 2008.
7. Tsang, M. and D. Psaltis, "Magnifying perfect lens and superlens design by coordinate transformation," *Phys. Rev. B*, Vol. 77, 304, 2008.
8. Lin, L., W. Wang, J. Cui, C. Du, and X. Luo, "Design of electromagnetic refractor and phase transformer using coordinate transformation theory," *Opt. Express*, Vol. 16, 6815, 2008.

Terahertz Science and Technology and Applications

B. Zhu[1], **Y. Chen**[2], **K. Deng**[2], **W. Hu**[2], **and Z. S. Yao**[3]

[1]Center of Information and Networks, Chengdu University, China
[2]Institute of Astronautics and Aeronautics
University of Electronic Science and Technology of China, China
[3]National Key Laboratory of Space Microwave Technology, China

Abstract— In the past two decades, with the rapid development of the small-scale semiconductor technology, ultra-fast laser technology, as well as ultra-fast photonics technology, terahertz (THz for short) science and technology has shown great potential application. THz radiation, as a new kind of coherent light source, shows great scientific value and a wide range of applications in the field of basic researches such as physical chemistry, information and biology, etc., as well as in the field of technology researches, such as the materials, national security and medical technology, etc. The article summarizes the applications of THz technology in the field of basic research and civilian technology comprehensively, and focusing on its applications in security communication, anti-stealth radar, chemical and biological agent detection and the fields of national defense and military.

Cherenkov Radiation Formed by a Charge Moving Parallel to the Boundary between Normal and Double-negative Media

Zhaoyun Duan[1], **Bae-Ian Wu**[2], **and Min Chen**[3]

[1]Vacuum Electronics National Lab, School of Physical Electronics
University of Electronic Science and Technology of China, Chengdu 610054, China
[2]Research Laboratory of Electronics, Massachusetts Institute of Technology
Cambridge, MA 02139, USA
[3]Department of Physics, Massachusetts Institute of Technology
Cambridge, MA 02139, USA

Abstract— Cherenkov radiation by a charged particle that moves parallel to the interface of normal and double-negative media has been theoretically investigated. The simplest case of this kind is the one in which the charge moves in vacuum parallel to and over a semi-infinite anisotropic double-negative metamaterials. This case, as an example, is discussed in great detail. The Cherenkov group cone, the spectral density and the total radiated energy are presented. This particular problem is also of interest for various radiophysical purposes, primarily problems involving the generation of microwaves or (sub)-millimeter waves.

ACKNOWLEDGMENT

This work was supported by the Office of Naval Research under Contract N00014-06-1-0001, the Department of the Air Force under Air Force Contract F19628-00-C-0002, National Natural Science Foundation of China (Grant Nos. 60601007, 60532010 and 60531020), Youth Science and Technology Foundation of UESTC (Grant No. JX05018) and Chinese Scholarship Council.

Influence of Shielding in Asymmetric Planar Structures for MMICs Applications

A. Khodja[1], **C. Boularak**[1], **R. Touhami**[1], **H. Baudrand**[2], **and M. C. E. Yagoub**[3]

[1]Instrumentation Laboratory, Faculty of Electronics and Informatics
U.S.T.H.B University, Algiers, Algeria
[2]ENSEEIHT, 2 rue Charles Camichel 31071, Toulouse Cedex 7, France
[3]SITE, University of Ottawa, 800 King Edward, Ottawa, Ontario, K1N 6N5, Canada

Abstract— This article describes the shielding effect of electromagnetic fields appearing in unilateral asymmetric transmission lines (see Figure 1) which can support two different modes of propagation usually defined by "C" and "π" modes [1]. For this purpose, an integral method used in hybrid mode, especially transverse resonance method (TRM) is used in conjunction with an adequate choice of trial functions. The mathematical process of this method makes use of operators formalism in electromagnetism which consists to emphasize systematic character in this method [2], this allows to analyze efficiently the dispersion effect of those asymmetric structures.

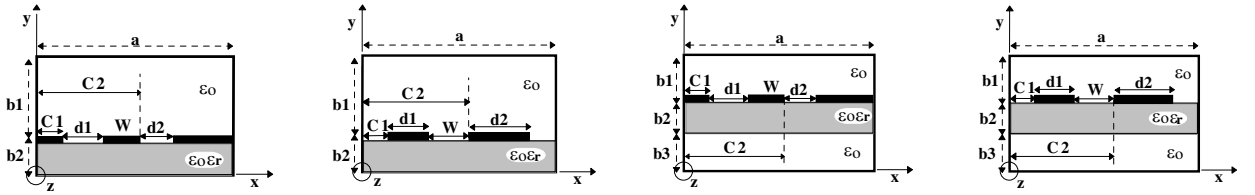

Figure 1: Cross sectional view of shielded unilateral asymmetric transmission lines.

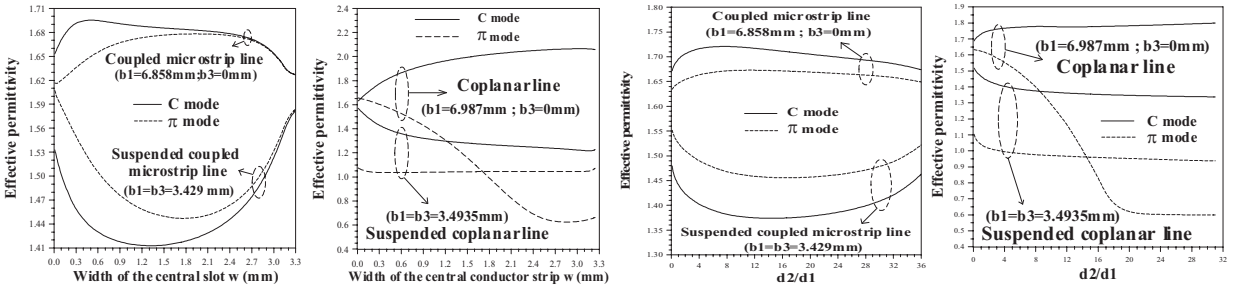

(d1= d2=0.08mm, b2=0.254 mm, C1=0.1mm, ε_r=2.22, F=10GHz)

(d1= d2=0.1mm, b2=0.125mm, C1=0.1mm, ε_r=2.2, F=33GHz)

(b2=0.254 mm, d1=0.08mm, C1=0.1mm, w=0.45mm ε_r=2.22, F= 10GHz)

(b2=0.125mm, d1=0.1mm, C1=0.1mm, w=0.2mm, ε_r=2.2, F=33GHz)

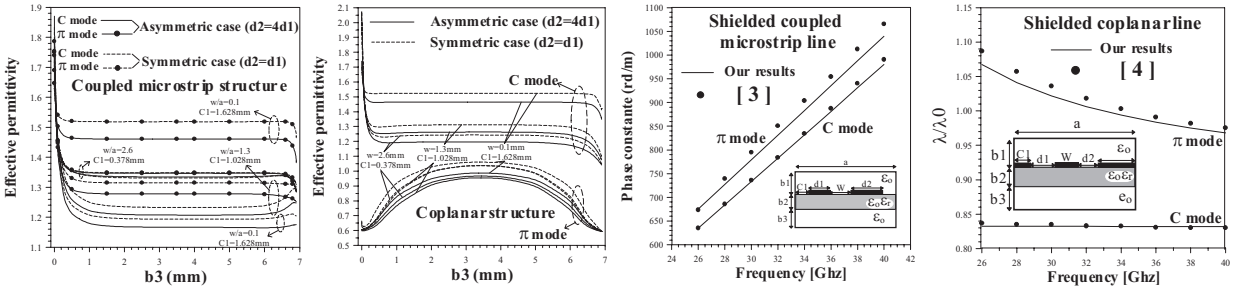

(b2=0.125mm, d1=0.1mm, ε_r=2.2, F=10GHz)

(b2=0.125 mm, d1=0.1mm, ε_r=2.2, F=33GHz)

(a=3.556mm, b2=0.254mm, b1=b3= 3.429mm, d1=d2=0.08mm, ε_r=2.22, w=0.45mm, C1=0.473mm)

(a=3.556mm, b1=3.556mm, b2=0.127mm, b3=3.429mm, d1=0.1mm, d2=0.3mm, ε_r=2.22, w=0.2mm, C1=1.578mm)

Figure 2: Influence of horizontal and vertical metallic sides of shielding on effective permittivity.

The TRM method is based on the evaluation of the impedance operator $\hat{Z}$ (or admittance operator $\hat{Y}$) to which the Galerkin's technique is applied. So, the full-wave behavior of shielding is analyzed with respect to the dispersion parameters. Cosine trial functions with edge singularities were used. The obtained results have been validated with a good precision compared with those available in the literature [1, 2].

REFERENCES

1. Khodja, A., M. L. Tounsi, M. C. E. Yagoub, R. Touhami, K. Idinarene, and S. Gaoua, "Optimal choice of trial functions in the modeling of unilateral asymmetric microwave structure by integral method," *4th Mediterranean Microwave Symposium (MMS'2004)*, Marseille, France, June 1–3, 2004.
2. Khodja, A., "Optimisation des fonctions d'Essai dans la modélisation de la ligne à ailettes unilatérale par la méthode de résonance transverse," Master Thesis, USTHB, Algiers, Algeria, April 2000.
3. Achkar, J., O. Picon, V. F. Hanna, and J. Citerne, "Analysis of symmetric and asymmetric coupled suspended striplines and some associated discontinuities," *20th EMC*, Budapest, Hungary, 1990.
4. Biswas, A. and V. K. Tripathi, "Analysis and design of asymmetric and multiple coupled finline couplers and filters," *MTTS*, Vol. 1, 403–406, 1990.

Electronic States in Mixed Cantor-like Potentials

D. S. Díaz-Guerrero, F. Montoya, and L. M. Gaggero-Sager
Facultad de Ciencias, Universidad Autónoma del Estado de Morelos
Ave. Universidad 1001, Cuernavaca, Morelos, México

Abstract— The transmittance is studied, using the transfer matrix method, for various multi-barrier systems. The calculations are made in the framework of effective mass theory. The transmittance is calculated for one system increasing the number of layers (generations). The systems are built by mixing a Cantor-like potential with a superlattice. Both cases, barriers and wells, for the Cantor-like potential, are considered to compare the variations beteween the known superlatice and the proposed mixed system. The resulting potential is as follows, first a superlattice, next a Cantor and finally another superlattice. Another interesting feature is to study the effect of the width and number of layers for the superlattices. The fractal dimension of the transmittance and the potential is calculated, using an image processing technique, to determine if some correlation exists between the fractality of the potential and the fractality of the transmittance.

REFERENCES

1. Gaggero-Sager, L. M., E. R. Pujals, and O. Sotolongo-Costa, "Self-similarity in a Cantor-like semiconductor quantum well," *Phys. Stat. Sol. (b)*, Vol. 220, 167–169, 2000.
2. Griffiths, D. J. and C. A. Steinke, "Waves in locally periodic media," *Am. J. Phys.*, Vol. 69, No. 2, 137–154, 2001.
3. Pérez-Álvarez, R. and F. García-Moliner, "The spectrum of quasiregular heterostructures," *Some Contemporary Problems of Condensed Matter Physics*, invited chapter, 1–37, ed. by S. Vlaev and M. Gaggero-Sager, Nova Science Publishers, 2000.

Eigenvalues and Eigenfunctions in a Cantor-like Potential

L. M. Gaggero-Sager[1], **E. Pujals**[2], **and D. S. Díaz-Guerrero**[1]

[1]Facultad de Ciencias, Universidad Autónoma del Estado de Morelos
Ave. Universidad 1001, Cuernavaca, Morelos, México
[2]Instituto de Matemática Pura e Aplicada — IMPA
Dona Castorina 110, Rio de Janeiro, Brasil

Abstract— We study the so called Cantor-like potential, probably one of the closest potential we can imagine as selfsimilar. The numerical calculation was carried out for the effective mass equation miming a GaAs-AlGaAs heterostructure made by following a Cantor algorithm. We show that the first eigenfunctions exhibit in a great extend a selfsimilar aspect. Another main result is that a fractal dimension is found for the spectrum. This can be seen as a demonstration that this kind of potentials have this peculiarity. It is reasonable to think that other similar potential show this property.

REFERENCES

1. Pérez-Álvarez, R. and F. García-Moliner, "The spectrum of quasiregular heterostructures," *Some Contemporary Problems of Condensed Matter Physics*, invited chapter, 1–37, ed. by S. Vlaev and M. Gaggero-Sager, Nova Science Publishers, 2000.
2. Maciá, E. and F. Domínguez, *Phonons and Excitons in Low Dimensional Aperiodic Systems*, Editorial Complutense, Madrid, 2000.
3. Mandelbrot, B. B., *The Fractal Geometry of Nature*, W. H. Freeman and Company, New York, 1983.
4. Bovier, A. and J. M. Ghez, "Spectral properties of one-dimensional Schrödinger operators with potentials generated by substitutions," *Commun. Math. Phys.*, Vol. 158, No. 1, 45–66, 1993.
5. Bovier, A. and J. M. Ghez, "Remarks on the spectral properties of tight-binding and Kronig-Penney models with substitution sequences," *J. Phys. A: Math. Gen.*, Vol. 28, No. 8, 2313–2324, 1995.
6. Gaggero-Sager, L. M., E. R. Pujals, and O. Sotolongo-Costa, "Self-similarity in a Cantor-like semiconductor quantum well," *Phys. Stat. Sol. (b)*, Vol. 220, 167–169, 2000.
7. Pérez-Álvarez, R. and F. García-Moliner, *Transfer Matrix, Green Function and Related Techniques: Tools for the Study of Multilayer Heterostructures*, ed. Universitat Jaume I, Castellón de la Plana, Spain, 2004.
8. Bastard, G., *Wave Mechanics Applied to Semiconductor Heterostructures*, Éditions de Physique, Paris, 1989.
9. Halsey, T. C., M. H. Jensen, L. P. Kadanoff, I. Procaccia, and B. I. Shraiman, "Fractal measures and their singularities: The characterization of strange sets," *Phys. Rev.*, Vol. A33, No. 2, 1141–1151, 1986.
10. Jitomirskaya, S. Y. and Y. Last, "Dimensional Hausdorff properties of singular continuous spectra," *Phys. Rev. Lett.*, Vol. 76, No. 11, 1765–1769, 1996.
11. Griffiths, D. J. and C. A. Steinke, "Waves in locally periodic media," *Am. J. Phys.*, Vol. 69, No. 2, 137–154, 2001.
12. Simon, B., "Almost periodic Schrödinger operators: A review," *Adv. Appl. Math.*, Vol. 3, 463–490, 1982.
13. Simon, B., "Schrödinger operators in the twenty-first century," *Mathematical Physics*, 283–288, eds. A. Fokas, A. Grigoryan, T. Kibble, and B. Zegarlinski, Imperial College, London, 2000; Also *J. Math. Phys.*, Vol. 41, 3523–3555, 2000.

Relative Mobility and Relative Conductivity in ALD-FET (Atomic Layer Doped-field Effect Transistor) in GaAs

O. Oubram, L. M. Gaggero Sager, and D. S. Díaz-Guerrero
Facultad de Ciencias, Universidad Autónoma del Estado de Morelos
Av. Universidad 1001, Col. Chamilpa, CP 62209, Cuernavaca, Morelos, Mexico

Abstract— We calculate the relative mobility and relative conductivity between source and drain as function of gate voltage for Atomic Layer Doped-Field Effect Transistor (ALD-FET) in a GaAs matrix. The mobility is described via a relative quantity that was presented in [1]. That expression does not have empirical form, neither empirical parameter. Also a phenomenological expression of the conductivity is presented, which is derived from the mobility expression. The calculation this relative quantities was performed with a model for the ALD-FET that was shown in [2]. In the end, we report for the first time an analytical mobility of electronic relative ALD-FET. With these tools, it looks that different behaviour of transport properties for ALD-FET.

REFERENCES

1. Rodriguez-Vargas, I., L. M. Gaggero-Sager, and V. R. Velasco, "Thomas-Fermi-Dirac theory of the hole gas of a double p-type delta-doped GaAs quantum wells," *Surf. Sci.*, Vol. 537, No. 1, 75–83, 2003.
2. Mora-Ramos, M. E. and L. M. Gaggero-Sager, "A simple model for atomic layer doped field effect transistor (ALD-FET) electronic states," *Rev. Mex. Fis.*, Vol. 44, No. 3, 165–167, 1998.

Design of a Novel Wideband Planar Inverted-F Antenna for Mobile Applications

Xingyu Zhang and Antti Salo
Adaptive Terminal Team, Nokia Research Center, Beijing 100176, China

Abstract— Nowadays, wireless communication technologies have being developed rapidly, which results in the co-existence of multi-systems, such as GSM (Global System for Mobile Communication), DCS (Digital Communication System), PCS (Personal Communication System), WCDMA (Wideband Code Division Multiple Access), UMTS (Universal Mobile Telecommunication System), WiBro (Wireless Broadband Access Service), Bluetooth, DMB (Digital Multimedia Broadcasting) and so on. Planar inverted-F antenna (PIFA) with the characteristics of small size, light weight, low profile, easy fabrication and easy integration is widely adopted in mobile terminals. However, one drawback of conventional PIFA is its narrow bandwidth. Design of wideband PIFA applicable in multi-systems has been a hot topic. In this paper, a compact internal wideband PIFA with single-layer and single-patch is proposed. Two symmetrical rectangular slots just below the radiating element are cut off on the ground plane. In the feeding part, the inner conductor of the $50\,\Omega$ SMA coaxial cable is connected to the radiating patch by a trapezoidal plate as a impedance transformer. Besides, the antenna is shorted to the ground plane by a shorting plate. It is shown that the bandwidth of the presented antenna defined by $S_{11} < -10$ ranges from 1.67 to 4.05 GHz, which is much larger than those of the existing antennas with similar structures and makes the designed antenna cover the frequency bands of DCS1800, PCS1900, WCDMA, UMTS, WiBro, Bluetooth and DMB simultaneously. Furthermore, the radiation patterns, gain and total efficiency of the reported PIFA in free space are analyzed. The prototype was fabricated and measured. Good agreement between the measurement and simulation results can be achieved.

Interaction between Two Photorefractive Bright Solitons in Different Dimensions

A. Keshavarz
Department of Physics, Faculty of Science, Shiraz University of Technology
P. O. Box 71555-313, Shiraz, Iran

Abstract— Optical solitons are self-trapped and localized wave packets existed by an exact balance between the diffraction or dispersion that tends to expand the wave pockets and the non linear effect. Nowadays many model equations of nonlinear phenomena are known to express soliton generation, and many methods of solution are introduced to solve them mathematically. Among optical solitons, photorefractive spatial solitons are more attractive than other types due to the fact that they are interesting for application in optics and photonics, also solving governed equations in mathematics. In this paper we introduced a suitable numerical method according to the Crark-Nicholson scheme to solve coupled nonlinear equations in one and two dimensions and simulated the interaction between two solitons in different dimensions. Results exhibited very interesting phenomena and show how we can control light by light.

REFERENCES

1. Kuroda, K., *Progress in Photorefractive Nonlinear Optics*, Taylor and Francis, 2002.
2. Crosignani, B., P. DiPorto, A. Degasperis, M. Segev, and S. Trillo, *J. Opt. Soc. Am.*, Vol. B14, 3078, 1997.
3. Yeh, P., *Introduction to Photorefractive Nonlinear Optics*, John Wiley, New York, 1995.
4. Zakery, A. and A. Keshavarz, *J. Phys. D: Appl. Phys.*, Vol. 37, 3409, 2004.

Second Harmonic Generation from Periodic Arrays of Metallic Sub-wavelength Slits

M. Centini[1], **A. Benedetti**[1], **M. Scalora**[2], **C. Sibilia**[1], **and M. Bertolotti**[1]

[1]Dipartimento di Energetica, Università di Roma, La Sapienza
Via A. Scarpa 16, Roma 00161, Italy
[2]Charles M. Bowden Research Center, AMSRD-AMR-WS-ST, RDECOM
Redstone Arsenal, Alabama 35898-5000, USA

Abstract— We numerically investigate second harmonic generation from metallic sub-wavelength apertures. Enhanced transmission from sub-wavelength apertures has been extensively studied and observed in the linear regime. The phenomenon in based on plasmon excitation and fulfilment of resonant conditions inside the aperture as a function of the screen depth. It is well known that metals do not have intrinsic quadratic nonlinear term. However, several theoretical and experimental works report on the possibility to generate a second harmonic signal impinging on a metallic screen. This is a direct consequence of the presence of a magnetic dipole due to the Lorentz force ($\sim J \times H$) and of an electric quadrupole-like contribution due to the Coulomb force ($\sim E[\nabla \cdot E]$). In a recent publication second harmonic generation from narrow slits on metallic substrates in the enhanced transmission regime was investigated by considering the nonlinear contributions arising from the magnetic contribution to the Lorentz force only. Here we compare and contrast the Coulomb and magnetic contributions, and find that in the plasmonic regime the Coulomb term can improve conversion efficiencies between one and two orders of magnitudes compared to the magnetic contribution alone. We consider P-polarized plane waves and femto-second pulses tuned to $\lambda = 800\,\text{nm}$ impinging on apertures carved on a thick Ag or Au substrates. The nonlinear polarization terms acting as a source for the second harmonic field may be calculated according to Equation (1):

$$\vec{\nabla} \wedge \vec{\nabla} \wedge \vec{E}_2(\vec{r}) - k_0^2 \varepsilon(2\omega, \vec{r}) \vec{E}_2(\vec{r}) = -\frac{k_0^2}{\varepsilon_0} \left(P_{NL}^{Coulomb}(\vec{r}) + P_{NL}^{Magnetic}(\vec{r}) \right) \tag{1}$$

We calculated the generated second harmonic field by integrating Equation (1) using a Green function approach in undepleted pump approximation. We finally plot the second harmonic field generated by considering both nonlinear polarization terms and magnetic terms only (Figure 1(a)-(b)). BY taking advantage of periodicity, the method we have developed allow us to calculate the generated second harmonic fields for an array of metallic scatterers and they are suitable to investigate nonlinear properties of metallo-dielectric nanostructures.

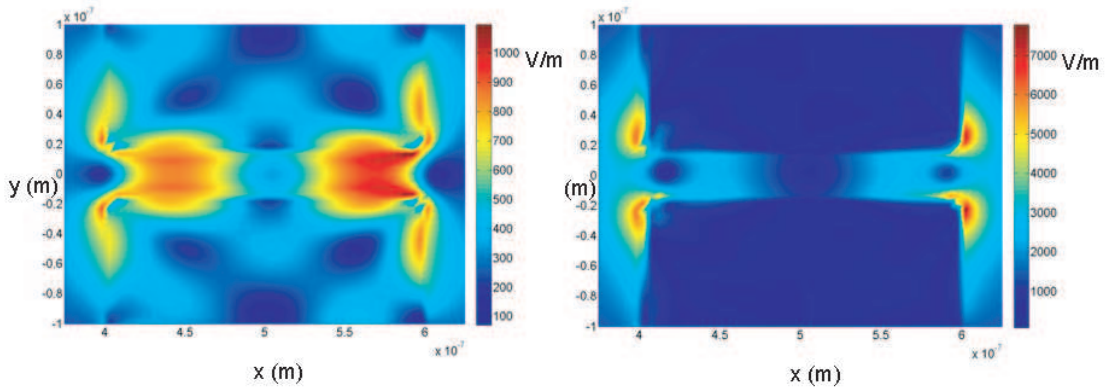

Figure 1: (a) Modulus of the second harmonic electric field generated by the magnetic term contribution. (b) Modulus of the second harmonic electric field generated by both terms.

Structural and Magnetic Properties of Mn Implanted GaN

Abdul Majid[1, 2], **Akbar Ali**[1], **Rehana Sharif**[3], **J. J. Zhu**[2], **and X. F. Han**[3]

[1]Advance Materials Physics Lab, Physics Department
Quaid-i-Azam University, Islamabad, Pakistan
[2]State Key Laboratory on Integrated Optoelectronics
Institute of Semiconductor, Chinese Academy of Sciences, Beijing 100083, China
[3]State Key Laboratory of Magnetism
Institute of Physics, Chinese Academy of Sciences, Beijing 100083, China

Abstract— (Ga, Mn)N with Mn concentration of 0.04–5 at. % has been achieved by Mn ion implantation into MOCVD grown GaN. Structural and magnetic properties of the material were studied by X-ray diffraction and vibrating sample magnetometer respectively. Ferromagnetic properties of the samples at room temperature have been observed. The saturation magnetization reached to its maximum value with Mn concentration of 2 at. %.

Session 3P1
Mathematical and Numerical Tools for Metamaterials 2

Virtual Antenna Method as Applied to the Study of the Scattering by 2-dimensional Non-linear Metamaterials

Frédéric Zolla, **Pierre Godard**, **and André Nicolet**
Institut Fresnel, Marseille, France

Abstract— We are interested in the electromagnetic scattering by a finite set of parallel non-linear rods (optical Kerr-effect, for instance) of any shape. Associated with perfectly matched layers, the Finite Element Method (FEM) is well suited for this kind of problems. Nevertheless, when using the FEM, the sources have to be put inside the meshed area; it is then clear that this method fails whenever the sources are far from the obstacles (for instance, when dealing with plane waves). In this paper, a new route for obtaining the scattered field by non-linear obstacles is proposed. The basic idea consists in simulating the real incident field by a virtual field emitted by an appropriate antenna, located in the meshed domain, and encompassing or lying above the obstacles. This general procedure is of course adapted to the diffraction by nonlinear metamaterials. Some results are given in order to illustrate the versatility of our method: transmission through a finite Kerr photonic crystal, Kerr gratings, etc.... We check the numerical results via a verification of the power balance.

We study the scattering by a non-linear finite photonic crystal (See, for example, [1]), made of rods that are invariant along one direction. For linear polarized light in the TM case the problem amounts to solving the equation:

$$\left(\Delta + k_0^2 \varepsilon_r(u)\right) u = \rho \tag{1}$$

with $u := u^d + u^i$ where u^d is the unknown scattered field satisfying an Outgoing Wave Condition (OWC) and u^i is a given incident field. The sources ρ of u^i can be currents, or it vanishes in case of incident plane waves. This study is tackled by numerical simulation and the FEM revealed to be appropriate, for its ability to treat inhomogeneous permittivities (hence this method seems more general than [2] or [3]).

The method we use for conveying the sources in the meshed area is to solve the equation for the total field (Equation (1)) and to bring the incident field u^i by a current j located on a simple curve $\partial\Omega$ (the interior of which is denoted by Ω) in the meshed area and enclosing the target. More precisely, we find j such that it radiates a field u^0 satisfying an OWC,

$$\left(\Delta + k_0^2\right) u^0 = \rho_v := \mathrm{j}\, \delta_{\partial\Omega}, \tag{2}$$

and such that u^0 has the following fundamental property: $u^0|_\Omega = u^i|_\Omega$.

The function ρ_v is called a *virtual antenna*. It is able to simulate almost any incident field in a bounded region. As a consequence, the problem of scattering amounts to looking for the scattered field by near sources which is solved by traditional tools of FEM [4].

In order to check the model coherence, we compare the dissipated power, computed by two different methods: on the one hand through the flux of the Poynting vector flowing through a surface encompassing the scattering object, and on the other hand by evaluating the Joule effect. The relative error, less than 8×10^{-5}, stimulate us to simulate more realistic experiments; in particular, we are interested in the study of the harmonic generation, without the usual approximations of the undepleted pump.

REFERENCES

1. Boyd, R. W., *Non Linear Optics*, 2nd edition, Academic Press, Amsterdam, 2003.
2. Centeno, E. and D. Felbacq, "Optical bistability in finite-size nonlinear bidimensional photonic crystals doped by a microcavity," *Physical Review B*, Vol. 62, No. 12, 7683, 2000.
3. Xie, P. and Z. Q. Zhang, "Multifrequency gap solitons in nonlinear photonic crystals," *Physical Review Letters*, Vol. 91, No. 21, 213904, 2003.
4. Deuflhard, P., *Newton Methods for Nonlinear Problems, Affine Invariance and Adaptive Algorithms, Series Computational Mathematics*, Vol. 35, Springer, 2004.

Computation of Layered Media Green's Functions in Metamaterials

Boping Wu, **Jeremy Q. Bagley**, **and Leung Tsang**
Department of Electrical Engineering, University of Washington-Seattle, USA

Abstract— In our recent research, we used the fast all modes method (FAM) combined with the numerical modified steepest-descent path method (NMSP) to solve the Green's functions for layered NIM media. The FAM method is able to calculate accurately hundreds of mode locations in the complex plane. The modes include surface wave modes (SWMs), leaky wave modes (LWMs), and improper modes. The NMSP method integrates along the steepest-descent path (SDP) using minimal CPU time by sampling only a few integration points after the extraction of the nearby singularity poles. The half-space extraction method has been used to benchmark the results of the FAM/NMSP method. Recently, J. B. Pendry has shown that a layer of material with relative permittivity and relative permeability both equal to -1 behaves as a perfect two-dimensional lens for an object closer than the thickness of the layer. Later, the experimental fabrications did by Shelby et al., have verified this claim. Although the techniques of construction of such materials still remain an experimental challenge, the theoretical analysis and research based on the homogenization approach is investigated assuming that an effective permittivity and permeability can be used. In the present paper, we extend the FAM/NMSP method to examine the results by calculating the electromagnetic fields on the semi-infinite metamaterials. The formulations and the fields of Ez, Ex and Hy will be presented. The Poynting vector is calculated to show the power distribution inside the metamaterials. We examine the limiting behavior of a passive medium as it approaches the perfect-focus condition when both relative permittivity and relative permeability are equal to -1. We also study the case of transient solution of Hertzian dipoles in layered lossy and dispersive metamaterials.

Coupling of Terahertz Surface Plasmon Polaritons in Corrugated Stacks of Dielectric and Semiconductor

Xin Wu, **De Li**, **Wei-Hua Sun**, **Feng Gao**, **Zhi-Jian Zhang**, **and Ru-Wen Peng**
National Laboratory of Solid State Microstructures and Department of Physics
Nanjing University, Nanjing 210093, China

Abstract— We present a theoretical approach that terahertz surface plasmon polaritons (THz-SPPs) are tuned by temperature in a stack of dielectric and semiconductor with periodic corrugations. Based on Rayleigh hypothesis, we show that when THz electromagnetic wave illuminates the waved stack, temperature-dependent THz-SPPs are excited. At resonant modes, reflection dips or Fano-type resonance shape are found. With increasing the temperature difference of the upper and lower semiconductor layers in the stack, transmissions increase and reflections decrease significantly. Our investigation indicates that such stacks may achieve potential applications in thermally controlled THz devices.

ACKNOWLEDGMENT

This work is supported by the grant from National Natural Science Foundation of China.

Omnidirectional Transmission in the Photonic Bandgap of Periodic Metamaterials Stacks

Wei-Hua Sun, **Ye Lu**, **Xin Wu**, **De Li**, **Zhi-Jian Zhang**, **Ru-Wen Peng**, **and Mu Wang**
National Laboratory of Solid State Microstructures, Department of Physics
Nanjing University, Nanjing 210093, China

Abstract— It is well known that in conventional photonic crystals, Bragg scattering gives rise to the photonic band gap. The defect mode will appear within the Bragg gap when the periodicity is broken such as by introducing a defect in the structure. Both the Bragg gap and the defect mode will shift dramatically when the incident angle of light varies. It becomes interesting to overcome the angular effects and obtain omnidirectional transmission properties by using the metamaterials. In this work, we present the propagation of electromagnetic wave through a type of metamaterial, where positive and negative index materials are alternatively stacked. It is found that electromagnetic waves can transmit perfectly and omnidirectionally through this system. The resonant tunneling in the photonic band gap is robust against incident angles and optical polarization. The numerical calculations are in good agreement with the analytical predictions. The findings are expected to achieve the potential applications in the optoelectronic devices.

ACKNOWLEDGMENT

This work is supported by the grant from National Natural Science Foundation of China.

A Density Matrix Approach to Wave Propagation in Nanostructures

D. Felbacq[1] and B. Guizal[2]

[1]Nanophotonics group UMR-CNRS 5650, University of Montpellier 2, France
[2]Institute FEMTO-ST, University of Besançon, France

Abstract— The recent interest in the imaging possibilities of photonic crystals (superlensing, superprism, optical mirages etc. ...) call for a detailed analysis of beam propagation inside a finite periodic structure. In particular, the in uence of evanescent waves is crucial [1]. We propose to use the full spectrum of the transfer operator to quantify the relative in uence of the different (i.e., propagative or evanescent) modes [2]. We do so we define projection ratios that lead to a density operator. This operator can then be used to define the analog of a quantum entropy. This quantity proves to be well-suited to the super-resolution effect.

ACKNOWLEDGMENT

This work is supported in part by the Eu-NoE project N 511616 PhOREMOST "NanoPhotonics to Realise Molecular Scale Technologies" and by the ANR project POEM PNANO 06-0030.

REFERENCES

1. Felbacq, D. and R. Smali, *Phys. Rev. Lett.*, Vol. 92, 193902, 2004.
2. Smaâli, R., D. Felbacq, and G. Granet, *Physica E*, Vol. 18, 443, 2003.

Rigorous Analysis of Metamaterials by Means of the Parametric Fourier Modal Method

Gérard Granet and Antoine Moreau
LASMEA, UMR6602, 24 Av. des Landais, Aubière 63177, France

Abstract— The electromagnetic properties of Metamaterials are due to the periodic arrangement of some elementary structure that may introduce electric dipole or magnetic moments. In order to be considered as an equivalent homogeneous media, the size of the unit cell, i.e. the wavelength should be large compared to the periodicity. In practice, it often happens that the wavelength is of the order of magnitude of the periodicity. Hence exact grating codes are natural numerical tools to investigate the properties of metamaterials.

Modal methods and mode matching techniques are well established methods to solve wave guide and scattering problems. One of their interesting features is that they easily allow to understand and to give some physical insight in the physical phenomena. Such methods lead to an eigenvalue problem that is transformed into a numerical matrix eigenvalue problem by the method of moments. At this stage, the boundary conditions that the field of the physical problem has to satisfy are included in the chosen expansion basis. For periodic structures the Fourier basis is a natural one. From the numerical point of view one obtains very simple code. However the main drawback of most Fourier based methods is that they are not able to describe efficiently electromagnetic fields with sharp variations as is the case in nano structures that include metals. As a consequence, convergence is achieved with rather huge matrices. For 2D problems it does not matter, but what about 3D structures? In that case, the situation is not that simple and it is our opinion that there is a need for fast, reliable, and easy to implement algorithms. For structures with single or double negative materials, the Parametric Fourier Modal is one such method.

The Fourier modal method has recently been improved with the idea of adaptive spatial resolution. By using a non-uniform sampling scheme that places more sampling points around the permittivity discontinuities, the total number of spatial harmonics required to achieve a given accuracy is significantly reduced. The idea of stretching thinner the space around the discontinuities is not entirely new in the larger context of rigorous numerical methods. What is new in our parametric approach as applied to gratings is that Maxwell's equations are written in the stretched coordinates under the covariant form. Thus the matrix operator takes into account the new information.

In our presentation, we shall show the effectiveness of the Parametric Fourier Modal Method as applied to the analysis of different structures known to produce artificial electric or magnetic response.

Dirichlet-to-Neumann Map Method for the Analyzing Photonic Crystal Slabs

Lijun Yuan and Ya Yan Lu
Department of Mathematics, City University of Hong Kong, Kowloon, Hong Kong, China

Abstract— For a photonic crystal slab, we construct a matrix approximation to the Dirichlet-to-Neumann (DtN) map of its unit cells and use it to calculate the transmission and reflection spectra for propagating modes of the slab incident upon a finite number of air-hole arrays.

Photonic crystal (PhC) slabs are dielectric slabs with a two-dimensional (2D) periodic structure, such as a triangular lattice of air holes. Based on defect structures in PhC slabs, many useful components and devices have been developed for applications in photonic integrated circuits. Numerical simulations are necessary to the design of PhC slab and related devices. The finite difference time domain (FDTD) is widely used, but it has a huge demand on computer resources. Standard frequency domain methods, such as the finite element method, give rise to large linear systems that are difficult to solve. More sophisticated frequency domain methods, such as the multipole method and the boundary integral equation method, are often more efficient.

In this paper, we consider a slab with a few air-hole arrays. Let the slab be parallel to the xy (i.e., horizontal) plane and perpendicular to the z (i.e., vertical) axis, we assume that the lattice of air holes is infinite and periodic in the x direction and finite in the y direction. The slab without holes supports a few propagating modes that decay exponentially when $|z|$ is increased. Our problem is to analyze the scattering of a propagating mode (with a plane wave dependence on x and y) by the finite number of hole arrays. For ideal 2D PhCs composed of parallel and infinitely long cylinders, the Dirichlet-to-Neumann (DtN) map method [1–3] is particularly efficient. The method relies on the DtN map of the unit cells, which maps the wave field to its normal derivative on the boundary of the cell, to avoid computing the wave field in the interiors of the unit cells completely. The DtN map is constructed by assuming that the general solution in the unit cell can be written as a sum of special solutions. For cells with a circular inclusion, the special solutions are simply the cylindrical waves. Unlike the multipole method and the boundary integral equation method, the DtN map method does not require lattice sums. For PhC slabs, the unit cell is now a cylinder parallel to the z axis. For a triangular lattice of air holes, the cross section of the unit cell is chosen to be a hexagon. The DtN map of the unit cell is an operator that maps two field components to their normal derivatives on the boundary (which is a surface) of the unit cell. Clearly, the DtN map for a unit cell of a PhC slab cannot be approximated by a small matrix. Nevertheless, it is still advantageous to calculate the DtN map, since it allows us to reduce further calculations to surfaces. For that purpose, we truncate the z variable by perfectly matched layers, calculate the vertical modes based on a fourth order finite difference scheme, and find special solutions around a single hole using mode expansion in z and Fourier-Bessel expansion in the xy plane. Since the vertical modes inside and outside the hole (i.e., in the slab) are different, it is necessary to match the solution at the hole boundary. Finally, we obtain a matrix approximation of the DtN map by assuming that the general solution around a single hole is a linear combination of the special solutions obtained above. Using the DtN maps of unit cells, we are able to calculate the transmission and reflection spectra for finite arrays of air holes using a generalized operator marching method.

ACKNOWLEDGMENT

This research was partially supported by a grant from the Research Grants Council of Hong Kong Special Administrative Region, China (Project No. CityU 102008).

REFERENCES

1. Huang, Y. and Y. Y. Lu, *J. Lightw. Technol.*, Vol. 24, 3448–3453, 2006.
2. Huang, Y. and Y. Y. Lu, *Journal of Computational Mathematics*, Vol. 25, 337–349, 2007.
3. Wu, Y. and Y. Y. Lu, *J. Opt. Soc. Am. B*, Vol. 25, 1466–1473, 2008.

Analyzing Diffraction Gratings by Neumann-to-Dirichlet Maps and Boundary Integral Equations

Yumao Wu and Ya Yan Lu

Joint Advanced Research Center of USTC and CityU, Suzhou, Jiangsu, China
Department of Mathematics, City University of Hong Kong, Kowloon, Hong Kong, China
Department of Mathematics, University of Science and Technology of China
Hefei, Anhui, China

Abstract— Diffraction gratings are important in many applications. Recently, a Dirichlet-to-Neumann (DtN) map method was developed for scattering of periodic arrays of cylinders. In this paper, we present a general DtN-map method for diffraction grating problems. Our method uses boundary integral equations without involving the quasi-periodic Green's function and lattice sums techniques. Our method also avoids the multi-layer approximation used in Fourier modal method. Numerical examples are used to illustrate the efficiency of our method.

For diffraction grating problems, many numerical methods have been developed, including the finite element method (FEM), the Fourier modal method (FMM), the boundary integral equation (BIE) method, etc. The FEM is very general, but it gives rise to large, sparse, complex and indefinite linear systems that are difficult to solve. The FMM is suitable if the grating is a layered structure, but it is not so efficient when a general grating structure with sloping interfaces must be approximated by a layered one. The BIE method is suitable if the grating structure involves a small number of interfaces and the refractive index is piecewise constant, but it is somewhat complicated to implement, since the integral operators are related to the quasi-periodic Green's function which requires lattice sums to evaluate.

We consider two-dimensional diffraction grating problems (with one periodic direction), where the refractive index n is piecewise constant. More specifically, $n = n(x, y)$ is periodic in x with period L and is constant for $y < 0$ and $y > D$, then the problem can be reduced to a rectangle G given by $0 < x < L$ and $0 < y < D$, with a quasi-periodic condition in the x direction and boundary conditions at $y = 0$ and $y = D$. We divide G into sub-domains (of constant refractive index) $\Omega_1, \Omega_2, \ldots, \Omega_m$, where Ω_j is bounded by two curves Γ_{j-1} and Γ_j, and two vertical lines at $x = 0$ and $x = L$. The Dirichlet-to-Neumann (DtN) map method solves the diffraction grating problem by manipulating two operators from Γ_0 to Γ_m [1–3]. On Γ_j, we define operators Q_j and Y_j by $Q_j u|_{\Gamma_j} = \partial_\nu u|_{\Gamma_j}$ and $Y_j\, u|_{\Gamma_j} = u|_{\Gamma_0}$, where u is any solution of Helmholtz equation satisfying the quasi-periodic condition and the boundary condition at $y = 0$, and ν is a unit normal vector of Γ_j. The key step is to march these two operators from Γ_{j-1} to Γ_j. This requires the NtD map Λ of the sub-domain Ω_j. In Ω_j, the refractive index n is a constant. Using the fundamental solution of the Helmholtz equation $G(\mathbf{x}, \mathbf{y}) = \frac{i}{4} H_0^{(1)}(k_0 n|\mathbf{x} - \mathbf{y}|)$, we define the integral operators $\mathcal{S}$ and $\mathcal{K}$ as

$$(\mathcal{S}\varphi)(\mathbf{x}) := 2\int_{\partial\Omega_j} G(\mathbf{x}, \mathbf{y})\varphi(\mathbf{y}) ds(\mathbf{y}), \quad (\mathcal{K}\varphi)(\mathbf{x}) := 2\int_{\partial\Omega_j} \frac{\partial G(\mathbf{x}, \mathbf{y})}{\partial \nu(\mathbf{y})}\varphi(\mathbf{y}) ds(\mathbf{y}), \quad \mathbf{x} \in \partial\Omega_j,$$

where φ is an arbitrary function defined on $\partial\Omega_j$. Then, on the boundary of Ω_j, we have $(1+\mathcal{K})u = \mathcal{S}\partial_\nu u$. Therefore, the NtD map of Ω_j is $\Lambda = (1 + \mathcal{K})^{-1}\mathcal{S}$. In practice, Λ is approximated by a matrix. We discretize the integral equation by a Nyström method using a graded mesh.

ACKNOWLEDGMENT

This research was partially supported by a grant from the Research Grants Council of Hong Kong Special Administrative Region, China (Project No. CityU 102008).

REFERENCES

1. Huang, Y. and Y. Y. Lu, *J. Lightw. Technol.*, Vol. 24, 3448–3453, 2006.
2. Huang, Y. and Y. Y. Lu, *Journal of Computational Mathematics*, Vol. 25, 337–349, 2007.
3. Wu, Y. and Y. Y. Lu, *J. Opt. Soc. Am. B*, Vol. 25, 1466–1473, 2008.

Longitudinal-elliptical-polarized EM Waves in off-diagonal Chiral Media

Weihua Wang[1], **S. T. Chui**[2], **Zhifang Lin**[1], **and Lei Zhou**[1]

[1]Surface Physics Laboratory (State Key Laboratory), Physics Department
Fudan University, Shanghai 200433, China
[2]Batrol Research Institute, Department of Physics and Astronomy
University of Delaware, Newark, DE, USA

Abstract— We study a chiral medium [1] with constitution relation $\vec{B} = \mu\vec{H} + \alpha\vec{E},\ \vec{D} = \varepsilon\vec{E} + \beta\vec{H}$ in which the magnetoelectric elements $\alpha,\ \beta$ are off-diagonal matrices [2]. The propagations of electromagnetic (EM) wave inside such a medium exhibit many fantastic properties. We find that, under certain conditions, the electric field of a particular EM wave mode becomes longitudinally elliptical-polarized in the propagating direction and the Poynting vector has a component that is perpendicular to the plane of incidence. We present a phase diagram to show the optimal parameters for the chiral medium to exhibit such unusual wave polarization behaviors, and illustrate such an extraordinary effect by designing a double-refraction experiment at the air/medium interface. We finally perform FDTD simulations on realistic structures to verify such unusual wave phenomena.

REFERENCES

1. Lindell, I. V., A. H. Sihvola, S. A. Tretyakov, and A. J. Viitanen, *Electromagnetic Waves in Chiral and Bi-Isotropic Media*.
2. Chui, S. T., W. Wang, Z. Lin, and L. Zhou, unpublished.

Electromagnetic Resonance, Negative Refraction, Transparency by Coated Spheres: Radial Anisotropy

Lei Gao
Department of Physics, Suzhou University, Suzhou 215006, China

Abstract— In this talk, we first study light scattering of individual coated spherical particles with the emphasis on the conditions of achieving resonant light scattering including magnetic resonance and negative refraction. It is found that the resonant scattering is controllable with fine adjustment of the core-shell ratio, varying from enhancement to suppression in the scattering. For a collection of such small coated inclusions, effective medium parameters are derived, and the resonances in both electric and magnetic responses result in the negative refraction of the system for a given core-shell ratio. Then, when the radial anisotropy in the core or (and) the shell is taken into account, we establish an account of electromagnetic scattering by coated spheres with radial dielectric and magnetic anisotropy. Within full-wave scattering theory, one may make the anisotropic coated particle nearly transparent or invisible by the suitable adjustment of the radius ratio. In the quasistatic case, we take one step forward to derive effective permittivity and permeability for the coated particle, and the near-zero scattering radius ratio can be well described within effective medium theory. To one's interest, the introduction of radial anisotropy is helpful to achieve better transparency quality such as much smaller scattering section and wider range of near-zero scattering ratio. Moreover, when the coated particle is anisotropic, the position of near-zero scattering radius ratio can be tunable.

REFERENCES

1. Gao, L., T. H. Fung, K. W. Yu, and C. W. Qiu, *Phys. Rev. E*, (revised) 2008.
2. Qiu, C. W. and L. Gao, *J. Opt. Soc. Am. B*, (revised) 2008.
3. Alu, A. and N. Engheta, *Phys. Rev. E*, Vol. 72, 016623, 2005.
4. Tribelsky, M. I. and B. S. Luk'yanchuk, *Phys. Rev. Lett.*, Vol. 97, 263902, 2006.
5. Wheeler, M. S., J. S. Aitchison, and M. Mojahedi, *Phys. Rev. B*, Vol. 73, 045105, 2006.

Application of General Transmission-line Equations on Left-handed Materials

Xiao Liu, **Chao Li**, **and Fang Li**
Institute of Electronics, Chinese Academy of Sciences, Beijing 100190, China

Abstract— General transmission-line equations (GTLEs) are first-order differential equations of the transmission line. They have given good performance for analyzing transmission line with discontinuities. Compared with traditional parameters of the transmission line, two additional terms α, β were introduced, which represent the local radiation effect. The broadband property of GTLEs on certain structures is especially useful. By using only one set of exacted parameters at one frequency or several frequencies, responses over a certain frequency band can be restored. In this paper, GTLEs are applied to analyze left-handed (LH) transmission lines. The analyzed model is a typical LH structure which consists of a gap capacitance or a interdigital capacitor in series and a microstrip shunt inductance. Four parameters L, C, α, β of the left-handed structure are extracted at assumed frequencies. By restoring the voltage and current distributions with these parameters, the dispersion characteristic over a frequency band can be obtained. The results based on GTLEs agree well with the results from full-wave simulations. It's shown that GTLEs offer an alternative method to analyze LH structures, and their broadband property could find application in evaluating the dispersion characteristics of LH materials, thus to improve the design technique for specific applications.

Magnetic Resonance Transmission and Its Suppression in Metallic Ring-plate Composite Metamaterials

Zheng-Gao Dong[1], **Hui Liu**[2], **Tao Li**[2], **and Shi-Ning Zhu**[2]

[1]Physics Department, Southeast University, Nanjing 211189, China
[2]National Laboratory of Solid State Microstructures
Nanjing University, Nanjing 210093, China

Abstract— Magnetic resonance is investigated in a metallic metamaterial comprising rings and plates. A transmission band, instead of a stop band, around the magnetic resonance frequency is found as long as the electric field of the incident wave is polarized parallel to the ring plane. This implies that the magnetic resonance transmission is omnidirectionally responded. We also observe a suppression phenomenon of the magnetic resonance transmission by tailoring the plate scales, which implies a magnitude modulation of magnetic resonance. The equivalent LC circuit model is applied to analyze the geometry dependence of the magnetic resonance frequency, which is consistent with the numerical results by parametric simulations on the structural variations. In addition, the comparable results between the ring-ring and ring-plate metamaterials are discussed.

Session 3P2a
Radar Polarimetry

Advancements in Active Multimodal Microwave (SAR) Remote Sensing

Wolfgang-Martin Boerner and Jorge J. Morisaki
ECE/CSN Laboratory, University of Illinois at Chicago, USA

Abstract— Whereas optical and passive microwave radiometric remote methods are well integrated into existing GIS templates, there still exists a great need for the practitioner to comprehend the enormously rich additional information that active microwave sensing and imaging can provide due to its day and night all-weather operational capabilities. Both single or compact and fully polarimetric multi-band scatterometer and synthetic aperture radar (SAR) remote sensing techniques proved that essential basic scattering information cannot be recovered with standard GIS information gathering methods alone.

Methods of Radar Polarimetry and Multimodal Polarimetric SAR Interferometry:

Considerable progress was made in advancing basic and applied methods of radar polarimetry and of polarimetric SAR interferometry during the past two decades. This advancement was based on the underlying research on fully polarimetric (scattering matrix) synthetic aperture radar (SAR) and on differential SAR interferometry and it mergers. The resulting concepts and SAR image processing algorithms were verified with the aid of airborne and shuttle platforms supporting single/multi-band POLSAR and also POLinSAR sensor systems; culminating in the very successful SIR-C/X-SAR shuttle missions of 1994. In the mean time space-borne SAR systems were developed progressing with the recent successful launches of the compact polarimetric ESA ENVISAT (C-band) and the fully polarimetric JAXA ALOS-PALSAR (L-band), the fully polarimetric DLR Terra-SAR-X (X-band) plus the fully polarimetric RADARSAT-2 (C-band) launched from early 2006 to the end of the 2007, respectively. Applications dealing with the global remote sensing of vegetative cover and geo-environmental stress-change monitoring will be presented and discussed including deteriorating aspects of SAR imagery due to meteorological propagation-path effects especially within the tropical and subtropical belts.

Forest LAI Estimation from Radarsat-2 Polarimetric SAR Data

Erxue Chen, **Zengyuan Li**, **Feilong Ling**, **Qisheng He**, **and Xin Tian**
Institute of Forest Resources Information Techniques, Chinese Academy of Forest, China

Abstract— Forest canopy Leaf Area Index (LAI) is normally estimated from optical data because of its good co-relationship with NDVI and other vegetation index. But in rainy or cloudy regions, it maybe very difficult to acquire right optical data for opertinal applications, so SAR data can be a good replacement if it can be used to estimate forest canopy LAI. One test site located in Qianlian mountain area was established for validating the capability of C-band Radarsat-2 quad-polarization data for estimating forest canopy LAI. Two scenes of Radarsat-2 polarimetric SAR data with different orbiting direction (one ascending and another descending) and different looking angles have been acquired. Field work has been carried out and LAI of some forest plots has been measured with both LAI-2000 and TRAC instrument. The relationships between ground measured LAI and various kinds of SAR polarimetric parameters will be analyzed, models to inverse LAI from C-band multi-angle polarimetric SAR data will be established, and model performance will be discussed.

Crop Type Identification in Jiangsu, China Using Fully Polarimetric Radarsat-2 Data

F. Ling, Z. Li, and E. Chen
Institute of Forest Resources Information Techniques, Chinese Academy of Forestry
Beijing 100091, China

Abstract— Synthetic Aperture Radar plays an important role in agriculture monitoring in cloudy south China due to its day-and-night and all-weather data acquisition capability. Radarsat-2 provides higher performance than its predecessor Radarsat-1 with its full polarimetric imaging capability thus providing a good chance for SAR polarimetry research and application. In this paper, we examined the crop identification capability of Radarsat-2 by applying the H/A/Alpha Decomposition followed by the unsupervised Wishart H/A/Alpha Classification to its fully polarimetric data. To enhance the coherence in the polarimetric decompositions, data had been multi-looked and de-speckled before decomposition. An agricultural site was chosen in Jiangsu province, China for its large scale plantations and smooth topography. Emphasis was put on two predominant crops: rice and mulberry trees. The planting patterns and crop calendars were analyzed to gain a solid understanding of the backscattering mechanisms and to identify crop types based on the unsupervised Wishart H/A/Alpha Classification. The classification map was validated by combining multispectral, high spatial resolution optical image and field work. The result shows that it is promising to identify different crop types given the right acquisition time of the SAR data according to the crop calendar and the planting patterns of the crops.

Study on Forest Biomass Extraction Based on ALOS PALSAR Data

Qisheng He[1, 2], **Erxue Chen**[1], **Zengyuan Li**[1], **and Chunxiang Cao**[2]

[1]Institute of Forest Resource Information Technique, The Chinese Academy of Forestry
Beijing 100091, China
[2]Institute of Remote Sensing Applications, Chinese Academy of Sciences
Beijing 100101, China

Abstract— In this paper, the feasibility of the forest biomass extraction in mountainous area was analyzed utilizing ALOS (the Advanced Land Observing Satellite) PALSAR (the Phased Array type L-band Synthetic Aperture Radar) data, based on a three dimensional radar backscatter model of forest canopies which takes full account of spatial position of trees in a forest stand. In mountainous area, topography changes the local radar incidence angle and vegetation spatial structure in the radar field of view. Changes in radar incidence angle caused by terrain slope can have several effects on radar image data including foreshortening and layover. So the slope correction is necessary to eliminate the impact of the topography in forest parameters extraction. In this paper, we utilized the field data in the Qilian Mountain area within Gansu province, western China and the three dimensional model to analyze the backscattering changes of coniferous forest in L band HH and HV polarizations in different slopes and aspects. Also the parameters sensitivity and the vegetation spatial location changes to radar signals were analyzed. Then the digital elevation model and the simulation results were used to correct the topography impact. Finally we used ALOS PALSAR data acquired in L band HH and HV polarization to extract forest biomass in study area and analyzed the feasibility. The results indicated that the L-band ALOS PALSAR data can be useful for estimating forest biomass in mountainous areas, but there are also some restricts.

Session 3P2b
Microwave Remote Sensing and Global Climate Change

Target Detection beneath Canopy Using PolSAR Images

C. F. Hu[1, 2], J. D. Xu[1], N. J. Li[2], and L. X. Zhang[2]

[1]Electronic Engineering Department, Northwestern Polytechnic University, China
[2]National Key Laboratory of UAV Specialty Technique
Northwestern Polytechnic University, China

Abstract— Polarization information is applied to detect target underneath forest by synthetic aperture imaging. At first, hard-in-loop PolSAR system is constructed in an anechoic chamber, then the resolution and sampling interval of system are analyzed. In order to obtain accurate polarization data, polarization scattering matrix measurement and calibration method are used. The data of echoes are processed by an improved back-projection algorithm. After comparing the difference of images, target beneath canopy is detected according to the best combination polarization information. In the experiment, a PNA transmits two signals by wide-band antennas, and another two antennas receive returned signals coming back to the PNA. The antennas maintain downward at an incident angle of 20 degrees with ground. The area of scene is 1 square meter, which consists of three fir trees and a scaled tank. The height of trees is about 1 meter, and the scaled tank is located beneath trees. The frequency is working at L-band, and the frequency sampling interval is 12.5 MHz. Scanner moves 3 meters along the center of scene, and the spatial sampling interval is 1.5 cm. The resolutions of cross-range and ground-range are 0.17 m and 0.15 m respectively. The results show that HH polarization image has a good effect for target detection beneath canopy at L-band.

An Inverse Model for Sea Ice Thickness Retrieval Using Active Microwave Remote Sensing

Y. J. Lee[1], **W. K. Lim**[1], **H. T. Ewe**[2], **and H. T. Chuah**[2]

[1]Multimedia University, Malaysia
[2]Tunku Abdul Rahman University, Malaysia

Abstract— Sea ice encompasses a large area within the polar region and greatly influences the earth's climate system. One particular sea ice parameter of interest in understanding the dynamics of the sea ice cover and the heat exchange between the ocean and the atmosphere is its thickness. Due to this, there has been an increase in interest towards research in the polar region. Yet the harsh environment proves a great challenge to scientists doing research in those regions. The use of microwave remote sensing to retrieve physical data of the polar region, in particular sea ice thickness serves as a practical solution to the problem. In this paper, an RT-DMPACT Inverse Model to retrieve sea ice thickness from active microwave remote sensing data is presented. The inverse model is a combination of the Radiative Transfer Theory with Dense Medium Phase and Amplitude Correction Theory (RT-DMPACT) forward model and the Levenberg-Marquardt Optimization algorithm. The RT-DMPACT forward model is an improved forward model and is applied to generate the radar backscatter data, where the DMPACT is included to account for the close spacing effect among the scatterers within the medium. The Levenberg-Marquardt Optimization algorithm is then applied to improve on the set of input parameters until the sea ice thickness can be estimated. Data from ground truth measurements carried out in Ross Island, Antarctica, such as sea ice surface roughness and temperature, together with radar backscatter data extracted from purchased satellite images, are used as inputs to estimate the sea ice thickness in an area. The estimated sea ice thickness is then compared with the ground truth measurement data to verify its accuracy. The results from the simulation show promise towards the use of the RT-DMPACT inverse model to retrieve sea ice thickness from actual conditions in the polar region.

Monitoring Crop Phenology with MERIS Data — A Case Study of Winter Wheat in North China Plain

Jihua Meng, **Bingfang Wu**, **Qiangzi Li**, **Xin Du**, **and Kun Jia**
Institute of Remote Sensing Applications, Chinese Academy of Sciences, China

Abstract— Crop phonology monitoring is an important part of growth monitoring. On the other hand, the analysis on crop phenology can improve the accuracy of crop classification and crop yield estimation. Crop phenology mainly has relation not only to weather variety, but also to the regional planting habit. Crop phonological stages and growth period vary in different areas and different years. With the development of remote sensing technique, the detection of crop phenology and it s mechanism using remote sensing data on regional or global scales have become popular topics in remote sensing applications. The MERIS data can provide time-serial terrestrial parameters at a several-day frequency, with which we can track the growing process of crops (take winter wheat for example) and study its variation in the growing season. The normalized different vegetation index (NDVI) derived from red band and near infrared band of MERIS sensor is a directly remote sensing indicator that reflects crop growth situation. However, due to reasons such as the influence of cloud and atmospheric conditions, the residual noise in the time-series NDVI derived from MERIS will induce erroneous result in crop phenology monitoring. Thus in this study, after the time-series NDVI was computed from MERIS data, a Savitzky-Golay filter was used to smooth out noise in NDVI time-series at pixel scale, and a time-series NDVI dataset at day frequency was produced (reconstructed). Then indicators such as the peak were extracted from the crop NDVI profile for each pixel. After that the relation between these indicators and different phonological stages for winter wheat was analyzed and a model to estimate certain phonological stage for winter wheat was developed from the analysis.The model was validated with the field observation data collected from Fengqiu, Henan province and Yucheng, Shandong province. The validation result shows that the error in monitoring result for Heading Date and Flowering date of winter wheat is less than 3 days.

Passive Microwave Remote Sensing for Sea Ice Thickness Retrieval Using Neural Network and Genetic Algorithm

H. J. Yap[1], **W. K. Lim**[1], **H. T. Ewe**[2], **and H. T. Chuah**[2]

[1]Multimedia University, Malaysia
[2]Tunku Abdul Rahman University, Malaysia

Abstract— Over the years, global warming has gained much attention from the global community. The fact that the sea ice plays an important role and has significant effects towards the global climate has prompted scientists to conduct various researches on the sea ice in the polar regions. One of the important parameters being studied is the sea ice thickness as it is a direct key indication towards the climate change. However, to conduct studies on the sea ice scientists are often facing with tough challenges due to the unfavorable harsh weather conditions and the remoteness of the polar regions. Thus, microwave remote sensing offers an attractive mean for the observation and monitoring of the changes of sea ice in the polar regions for the scientists. In this paper, we will be presenting 2 approaches using passive microwave remote sensing to retrieve sea ice thickness. The first approach involves the training and testing of the neural network (NN) by using data sets generated from the Radiative Transfer Theory with Dense Medium Phase and Amplitude Correction Theory (RT-DMPACT) forward scattering model. Once training is completed, the inversion for sea ice thickness could be done speedily. The second approach utilizes a genetic algorithm (GA) which would perform a search routine to identify possible solutions in sea ice thickness that would match the corresponding brightness temperatures profile of the sea ice. The results obtained from both approaches are presented and tested by using Special Scanning Microwave Imager (SSM/I) data with the aid of the sea ice measurements in the Arctic sea.

Interpolation Techniques to Improve RIO Boundary Detection

Avijit Hira, **Shaik Ashraf Hossain**, **and Md Ishfaqur Raza**
Department of Electrical and Electronic Engineering, East West University
43 Mohakhali C/A, Dhaka-1212, Bangladesh

Abstract— In non-invasive imaging techniques, the boundary of an object of unknown material characteristics embedded in a known region is detected without any physical penetration. The imaging is however, accomplished by analyzing the field propagation patterns around the object. A finite pulse generator located around the periphery of the known region is used as the source. Recorders are also placed at the periphery of the known region to record propagating field distribution. The recorded field consists of both the original pulse and the field scattered by the discontinuity of the object impedance. Using numerical modeling, recorded field is back propagated to reconstruct field around the object. An imaging operator is then used on the reconstructed field distribution to locate the boundary of the object. For numerical analysis, the region of interest is modeled using a spatial mesh. Due to physical constraints, the density of the recorders will be limited. Field propagating between the recorders will be lost. To improve the reconstruction of field distribution, a numerical mesh with cell size smaller then recorder intervals is designed. The source nodes that do not have recorded data are excited with signal estimated using interpolation techniques. Different numerical techniques such as cubic spline and linear interpolation methods are used to calculate the source data for source nodes without recorder data. Finer meshes are also modeled with several nodes between adjacent recorders. Imaging results for the different interpolation techniques are compared. It is also shown that the image definition improves with finer mesh.

A Microwave Scattering Model for the Remote Sensing of Oil Palm Plantations

Jun-Yi Koay[1], **Tuck-Yew Yan**[1], **Ka-Sing Lim**[2], **and Hong-Tat Ewe**[1]

[1]Universiti Tunku Abdul Rahman, Malaysia
[2]Multimedia University, Malaysia

Abstract— The soaring prices of palm oil in the world markets in the last few years have, up till recently, lead to a boom in the palm oil industry in South East Asian countries such as Malaysia and Indonesia [1]. With the rapid increase and expansion of oil palm plantations in these regions, there is a need for local authorities to monitor their growth, since these regions are also rich in biodiversity. Rainforests, as well as being critical to the survival of many species, serve as carbon sinks for the removal of CO_2 in the atmosphere; yet they are continually sacrificed to make way for oil palm plantations [2]. Remote sensing is expected to play a crucial role in the monitoring of these large expanses of plantations in the near future by providing relevant information to decision makers so that a balance can be struck between economic development and environmental concerns.

However, research in the remote sensing of oil palm is almost insignificant at present, with only a few brief studies conducted on the backscattering coefficient of oil palm canopies as obtained from satellite data [3]. A preliminary scattering model has been developed based on the radiative transfer approach with the phase matrix of the leaves obtained from the scattered field of elliptic disks [4]. In this study, a similar model will be developed, but needle-shaped scatterers will be used instead for the development of the phase matrices of the leaves. This scattering model will be used in the simulation of the backscattering coefficient of oil palm canopies based on ground truth parameters measured at plantations in Bangi, Selangor, Malaysia. The simulation results of the model developed in this study will be compared with that obtained using elliptic-disks [4] to determine if needle-shaped scatterers provide a better match with C-band scatterometer measurements. A detailed analysis of the backscattering coefficient at various angles of incidence, frequencies and polarizations will also be carried out to study the backscattering behavior of oil palm. These theoretical model simulations and analyses will provide a platform for future work in the development of monitoring applications in the remote sensing of oil palm.

REFERENCES

1. "Historical crude palm oil prices," Available: http://www.palmoil.com.
2. Watkins , K., *United Nations Human Development Report 2007/2008 — Fighting Climate Change: Human Solidarity in a Divided World*, Palgrave Macmillan, New York, 2007.
3. Rosenqvist, A. and H. Oguma, "Phenological characteristics of cultivated vegetation covers in JERS-1 and ERS-1 synthetic aperture radar data," *Proceedings of International Symposium on Vegetation Monitoring*, No. 8, 194–195, 1995.
4. Koay, J. Y., K. S. Lim, H. T. Ewe, H. T. Chuah, H. Jamil, and S. Bahari, "Preliminary study in the backscattering measurements and theoretical modeling of oil palm canopies," *Proceedings of the Asian Conference on Remote Sensing*, Kuala Lumpur, Malaysia, November 12–16, 2007.

EM Scattering from Multiple Cylinders

W. Z. Yan[1], **D. W. Liu**[1], **H. T. Ewe**[2], **and Y. Du**[1]

[1]The Electromagnetics Academy at Zhejiang University
Zhejiang University, Hangzhou 310058, China
[2]Tunku Abdul Rahman University, Petaling Jaya 46200, Malaysia

Abstract— During the past several decades, several theoretical models have been constructed to study the scattering mechanisms in the vegetation medium and are very useful for forest stand or short crops. Usually, these approaches treat the vegetation medium as a random collection of discrete scatterers with different sizes, shapes and orientations. For instance, the branches and trunks are usually modeled as finite dielectric cylinders, and in coniferous vegetation needles are used to model leaves. Determining the electromagnetic properties of those key constituents such as branches and trunks requires knowledge of the scattering properties of dielectric cylinders. Thus, finding an effective method to evaluate the total scattered electromagnetic field which results from the interaction of an incident wave with a group of cylinders distributed in a homogeneous medium is an interesting and important research topic.

In this paper, the problem of electromagnetic scattering from multiple cylinders is divided into two stages as follows: the first stage is to calculate the electromagnetic scattering from an isolated finite cylinder. We use a new iterative technique based on the T-matrix approach, where hypothetic surfaces are used to divide a long cylinder into a cluster of N identical sub-cylinder, for each the T matrix can be directly calculated. Since any two neighboring sub-cylinder are touching via the division interface, the conventional multi-scatterer equation method is not directly applicable. The coupling among sub-cylinder and boundary conditions at the interfaces are taken care of in our approach. As the second stage, a recursive solution that accounts for multiple electromagnetic scattering, which is associated with each particle of the system, is proposed. The first order solution can easily be obtained by calculating the response of isolated cylinders to arbitrary excitation. To get the higher order solution, the scattered field from one particle is considered as the illuminating wave for the other particle and vice verse. The procedure is repeated until all the coefficients converge. Vector translational addition theorems for the spherical basis functions are used not only to connect different sub-cylinder of an isolated cylinder, but also to take care of multiple scattering between the cylinders. Moreover, the formalism is universal because the scatterers may have different shapes and may be of different types as long as the T matrix of each particle can be accurately obtained.

Bearing the impact of errors in applying the translational addition theorems and T-matrix approach, the iterative procedure may become an ill-conditioned one, and therefore the linear system cannot be numerically solved by direct inversion techniques. To overcome this problem, we use a method similar to the successive over-relaxation method (SOR), which takes the form of a weighted average between the previous iterate and the computed new iterate successively for each component.

In order to validate this new formalism, we compare numerical results for bistatic scattering from two adjacent cylinders. We show that the results obtained with the recursive method are in good agreement with results by numerical technique.

Bistatic Vehicle under Foliage Modeling

L. Villard and P. Borderies
Département Electromagnétisme et Radar
Office National d'Études et de Recherches Aérospatiales, ONERA
Toulouse, France

Abstract— This paper aims at studying the electromagnetic behaviour of a target under vegetation and at assess the detection feasibility.

In a first step is presented the scattering model, on one hand according to the scene description, having in mind the military advantages of bistatic systems and on the other hand according to the electromagnetic aspect particularly focused on the target contribution. We will then get at the analysis of the results for several set of radar and scene parameters.

The scene is constituted with a forest area generated with a classical multi layer description except the fact that it contains the target. Indeed, each layer is characterized by its own canonical elements (flat ellipsoids or cylinder respectively for leaves or branches and trunks). They are then appropriately arranged following to statistics representative of in-situ measurement data in terms of size, orientation, humidity and concentration. The soil is also taken into account thanks to the ground truth by means of its root mean square height, its two dimensional exponential correlation function and water content. On the contrary, the target is deterministic , computed by FDTD and characteried in terms of diffracting points for which we know its type (giving the scattering matrix) and its position (cf. Figure 1). Furthermore, the shadowing effects of the target under foliage is taken into account by the introduction of an inner perfectly absorbing zone inside the forest patch. Finally, emitter and receiver may be located arbitrarily (cf. Figure 2).

To ensure the coherence and the fully polarimetric response of the model, the electromagnetic computation adds in phase the contribution of each element according to their own mean incident field thanks to the Foldy-Lax approximation associated to a ray tracing process and their own scattering matrix. (This process enables us to take into account shadowing effects). We distinguish different mechanisms: the volume, the soil contribution and their interaction (the double bounce with modified Fresnel coefficients) and also the target contribution and its coupling with its near environment, that is to say the closest scatterrers (among vegetation and soil).

In a second step simulations results are presented and analyzed. In particular, emphasis is put on the role of the shadowing effects associated with the presence of the target under foliage.

We will finally assess which configuration makes the detection easier, according to the bistatic radar geometry which will affect the proportion between the mechanisms or between the polarizations and with regards to the frequency which will have a great impact on extinction as the forest area type.

Session 3P3a
Antenna Applications and Measurement

Analysis of the Electromagnetic Properties of High Impedance Surfaces Using Genetic Synthesis

N. Lassouaoui, **H. Hafdallah Ouslimani**, **and A. Priou**
Applied Electromagnetism Group (GEA), Scientific and Technical Pole
University of Paris Ouest Nanterre La Defense
50, rue de SEVRES 92410, Ville d'AVRAY, France

Abstract— In this paper, we consider an artificial high-impedance surface (HIS) based on a thin 2D lattice of plates attached to ground planes by metal-plated via. The HIS was proposed [1] as a new simplest example of textured electromagnetic surface having thickness lower than the traditional quarter-wavelength deep. They can be analyzed as a resonant LC circuit where the reduction of thickness can be obtained by capacitive loading [2].

Most realizations of HIS are based on a planar frequency selective surface (FSS) at the interface of a metalbacked dielectric slab either including vertical via or not. However, it is not easy to define the characteristics of the HIS (period, distance between the elements, etc.) which:

- Check the behaviour of HIS in a desired frequency band,
- Ensure a resonant frequency stable; indeed, it varies according to the polarization and the incidence angles,
- Allow a good bandwidth.

The models of planar array of metal elements excited by electromagnetic plane waves can be roughly split into two categories [1, 5]: computational and analytical methods. Here in, we propose to use the analytical model developed by the authors [1, 2, 4, 5] combined with the genetic algorithms [3] to search the best characteristics of the HIS which ensure a stable resonant frequency and an optimal wide bandwidth. For that, a multi-objective function has been proposed and used to direct the genetic research forward the best configuration.

The HIS is analysed by computing the surface impedance, reflection phases and the propagating properties in TE and TM polarized waves. In this analytic model, the surface is described using parallel lumped circuit elements.

Figure 1(a) shows the Jerusalem cross patch array studied by genetic synthesis. The objective is to search the characteristics which ensure a resonance at 6 GHz for normal incidence. The optimized parameters are respectively: $\varepsilon = 1.027 - i^*0.1$ (relative permittivity); $T_L = 5.52\,\text{mm}$ (dielectric layer thickness); $D = 12.13\,\text{mm}$ (unit cell period); $g = 0.69\,\text{mm}$ (slit gap); $h = 0.25\,\text{mm}$ (wide) and $d = 4.12\,\text{mm}$ (internal length of the cross).

Figures 1(b)–(d) presents the surface impedance in (b), the phase of the reflection parameter in (c) and the dispersion diagram properties of the surface wave in (d). We obtain a resonance at the desired frequency of 6 GHz with a large bandwidth from $-\pi/4$ to $\pi/4$ of 22%.

During the conference, we will present more simulations results using the analytical model and HFSS software.

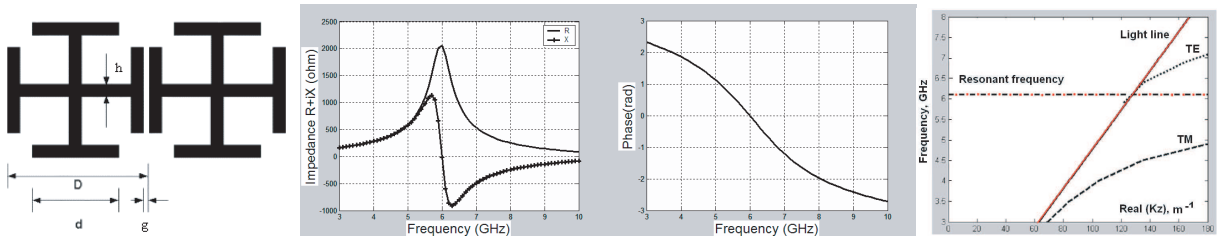

(a) (b) (c) (d)

Figure 1: (a) Jerusalem crosses patches, (b) Real and Imaginary Parts of Impedance, (c) Phase of reflection parameter for normal incidence, (d) The propagation properties of the surface waves along the HIS.

REFERENCES

1. Sievenpiper, D. F., "High-impedance electromagnetic surfaces," Doctorate Thesis, University of California, 1999.
2. Sievenpiper, D. F., "Review of theory fabrication and applications of HIS ground planes," *Metamaterials: Physics and Engineering, Explorations*, Edited by N. Engheta and R. Ziolkowski, Wiley Interscience, Chap. 11, 287–311, 2006.
3. Goldberg, D. E., *Genetic Algorithms in Search, Optimization and Machine Learning*, Addison-Wesley, 1989.
4. Simovski, C. R., P. D. Maagt, and I. V. Melchakova, "High-impedance surfaces having stable resonance with respect to polarization and incidence angle," *IEEE Transactions on Antennas and Propagation*, Vol. 53, No. 3, 908–914, March 2005.
5. Luukkonen, O., C. Simovski, G. Granet, G. Goussetis, D. Lioubtchenko, A. V. Räisänen, and S. A. Tretyakov, "Simple and accurate analytical model of planar grids and high-impedance surfaces comprising metal strips or patches," http://arxiv.org/, 1–20, May 2008.

Electromagnetic Modelling of High-impedance Surface for Antenna Applications

L. Y. Zhou[1], **H. Hafdallah Ouslimani**[1], **O. Maas**[2], **and A. Priou**[1]
[1]Applied Electromagnetic Group (GEA), University Paris-Ouest-La Defense
50 rue de Sèvres, Ville d'Avray 92410, France
[2]Thales Air Systems, Division Air Systems, Hameau de Roussigny, Limours 91470, France

Abstract— Recently, high-impedance surface (HIS) has been attracting a great deal of interests in improving planar antenna performances [1]. HIS can significantly reduce the surface waves and the parasitic radiation which enhance the antenna radiation efficiency. Furthermore, HIS has also demonstrated its advantage in antenna miniaturization, especially for antenna arrays [2, 3]. However, it is still very challenging in analyzing the complex coupling phenomena between the HIS and the radiating elements.

In this paper, a dipole antenna based on metamaterial is designed and experimentally characterized in the L-band. The simulation data are obtained by using HFSS software.

In the frequency band supposed to be the nominal one, the radiation patterns, particularly in the H plane of the antenna, are strongly modified versus frequency. The observed phenomena may be explained by the existence or the suppression of surface and/or leaky waves in this propagating plane.

In order to understand the coupling mechanism between the HIS and the dipole antenna, and also to characterize the propagating modes in the HIS it self, we developed additional experimental and modelling tools. Experimental techniques consist in using microstrip and coupling suspended lines above the total structure to measure. Modelling approach is based on the existence of leaky-wave radiation in the H plane. Next, this approach has been validated using circuit simulations. This mixed circuit and radiation analysis give access to the surface wave number confirmed by the experiments.

During the conference, some of experimental, modelling and circuit analysis results will be presented in details.

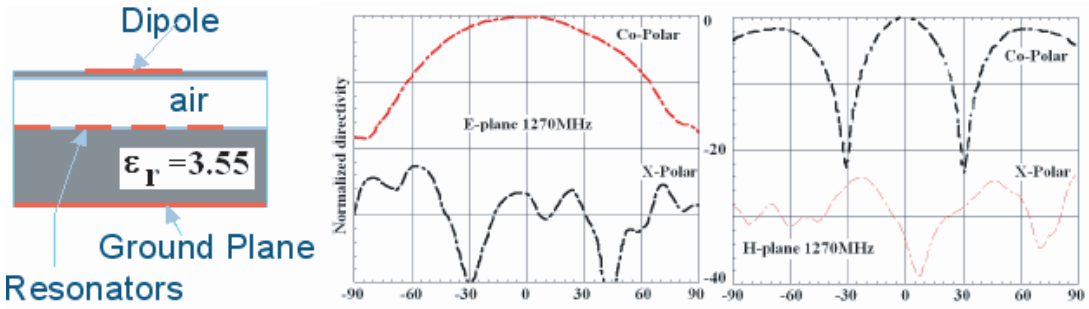

(a) Measured co- and cross-polarized radiation pattern E and H planes (Fields are normalized to the maximum value)

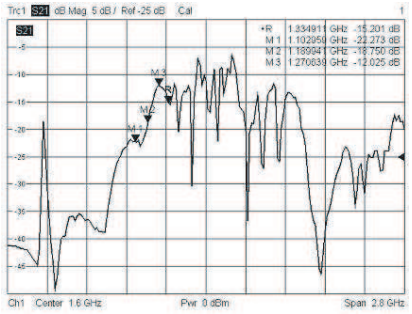

(b) Measured transversal propagation mode in the HIS array (through the H plane)

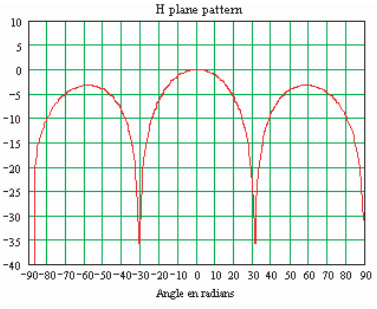

(c) Simulated co-polarized radiation pattern at 1.27 GHz in the H plane using the leaky wave and circuit approached

REFERENCES

1. Sievenpiper, D., "High-impedance electromagnetic surfaces," PhD Thesis, University of California, Los Angeles, 1999.
2. Akhoonszadeh-Asl, L., D. J. Kern, P. S. Hall, and D. H. Werner, "Wideband dipoles on electromagnetic bandgap ground planes," *IEEE Trans. on Antennas and Propagation*, Vol. 55, No. 9, 2426–2434, Sep. 2007.
3. Bell, J. M., M. F. Iskander, and J. J. Lee, "Ultra wideband hybrid EBG/ferrite ground plane for low-profile array antennas," *IEEE Trans. on Antennas and Propagation*, Vol. 55, Issue 1, 4–12, Jan. 2007.

Development of a Portable Field Meter for Measuring Specific Absorption Rate

Benjamin Loader[1], **Mike Manning**[2], **and Alex Miller**[3]

[1]National Physical Laboratory, UK
[2]IndexSAR Ltd, UK
[3]TUV Product Service Ltd, UK

Abstract— Antennas for wireless computer networks and mobile telephony are increasingly found in public areas such as airports, railway stations, and shopping centres. In such environments, it can be difficult to determine whether the antennas may represent a hazard to workers and members of the public, in particular whether touching the antennas could result in a specific absorption rate (SAR) of energy that exceeds exposure limits. This paper describes the development and testing of a portable meter for in-situ measurement of SAR from radio transmitters over the frequency range 800 MHz to 3 GHz. This covers the majority of second-generation and third-generation mobile phone base stations, and also the Industrial, Scientific and Medical (ISM) band at 2.45 GHz.

The portable SAR meter, shown in Fig. 1, consists of a three-axis electric field probe embedded within a dielectric phantom. The electric field probe is used to measure the fields at one point within the phantom resulting from proximity to a radio transmitter, from which mass-averaged SAR values are estimated. A tablet PC is used for data acquisition, and displays the SAR averaged over a 1 g or 10 g mass as the device is moved over the surface of the transmitter. The phantom is constructed as a machined Perspex shell filled with an emulsion into which the SAR probe is inserted. The emulsion is formulated to closely match the complex permittivity specified by SAR testing standards over the frequency range 800 MHz to 3 GHz. The flat face of the phantom is placed directly against the transmitter to be measured. The opposite face is contoured to reduce the effect of the energy reflected from the liquid-air interface on the electric field at the position of the probe sensors. The tapered section used is based on the Dolph-Chebyshev polynomial, since this minimizes the reflected energy.

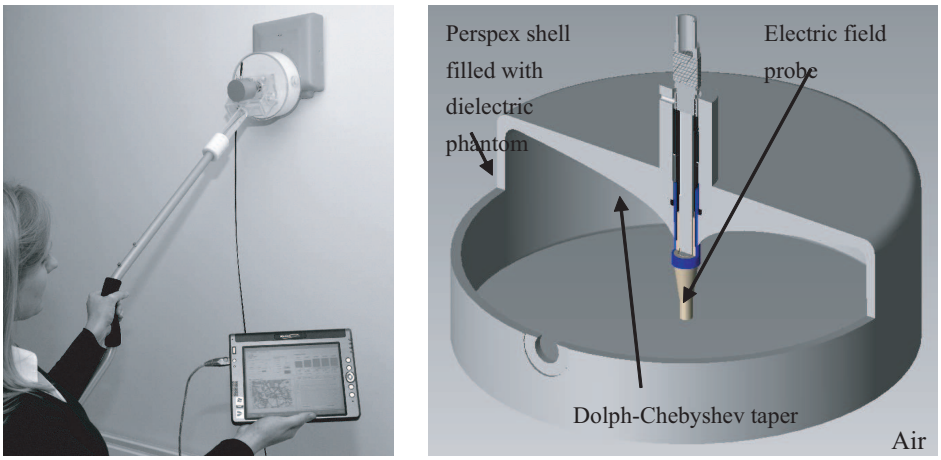

(a) (b)

Figure 1: (a) Prototype portable SAR meter being used to measure an indoor base station antenna, and (b) design of the phantom and electric field sensor.

To validate the performance of the meter, five indoor transmitters were measured with the portable SAR meter, and the results compared to those obtained using a full robotic scanning SAR measurement system. This allowed the measurement results to be verified against existing product testing standards. The maximum SAR levels averaged over 1 g are within ±45% of the full scanning SAR results, with the exception of one antenna type that showed poorer agreement. Note that the measurement uncertainty for SAR using a laboratory based system is typically ±30% at $k = 2$, so that this is good performance for a portable device.

Obtaining the Normal Field Component from Measurement

George G. Cheng, **Yong Zhu**, **and Jan Grzesik**
Allwave Corporation, California, USA

Abstract— We have evolved a novel technique to acquire the normal field components in planar, spherical, and cylindrical near-field measurements. It is commonly understood that measuring the normal field component is difficult to achieve due to the limitations of probe antennas suitable for capturing radial fields. For example, the z-, r- and ρ-components, respectively in planar, spherical, and cylindrical near-field measurements, in practice cannot always be measured easily and accurately. Specially designed normal-component probe antennas, e.g., optical probes, have been investigated and developed to some extent, but the accuracy and quality of the test data remain as key issues to date.

We propose a new way of obtaining the normal field component at any point from knowledge of two tangential field components over the entire measurement surface. For planar, spherical, and cylindrical near-field measurement methods, we introduce three algorithms which compute the z-, r- and ρ-component fields respectively from two tangential data streams over the measurement surface. The algorithms are direct, closed-form solutions which are numerically straightforward and efficient. The normal field component can thus be obtained numerically instead of our being required to actually measure it.

Verification of algorithms has been demonstrated by analytic examples, numerical simulations, and hardware measurements. Excellent agreement is evident in all cases tested to this point.

Session 3P3b
Antennas in RFID and Mobile Communications

Meander-line Antenna Design for UHF RFID Tag Using a Genetic Algorithm

D. Zhou, **R. A. Abd-Alhameed**, **C. H. See**, **M. S. Alkhambashi**,
Z. Zainal Abidin, **K. N. Ramli**, **M. M. Abusitta**, **and M. Usman**
Mobile and Satellite Communications Research Centre
University of Bradford, Bradford, West Yorkshire, BD7 1DP, UK

Abstract— In recent years Radio Frequency Identification (RFID) has become very popular in many commercial applications such as access control, animal tracking, security, and toll collection, because of its ability to track moving objects and its low-cost implementation [1, 2]. A typical RFID system is always made up of two components, including the tags (transponders) and readers (interrogators). A tag comprises an antenna and an application-specific integrated circuit (ASIC, or microchip) that is given a unique electronic product code. The antennas, as a key part of the system, enable the tag or reader to send and receive the signals. Readers are devices that read tags, and they equipped with antennas, a transceiver, and a processor (server with software system). The tag antenna design is quite challenging. This is because tag antenna is required directly connected to the tag IC, whose input impedance always presents capacitive reactance in nature. It means that the reactance part of tag antenna has to be designed and optimised to be complex conjugate impedance of tag IC in order to realize the maximum transmission using RF power induced from the antenna tag.

In this paper, an approach of using Genetic Algorithm (GA) in cooperation with an electromagnetic simulator was adopted to design and optimise the RFID tag antenna for UHF band. The benefit of applying GA is that it provides fast, accurate and reliable solutions for antenna structures. Genetic algorithm driver [3], written in Fortran, was adopted in this work in conjunction with the industry-standard NEC-2 Fortran source code [4], which was used to evaluate the randomly generated antenna samples. A meander-line antenna configuration, as shown in Fig. 1, was proposed in this study in order to achieve a tag design with compact size at UHF band. Moreover, a paralleled meander line arrangement was used to enhance the impedance bandwidth for the proposed design. A Higgs IC [5], designed to follow EPCglobal Class-1 Gen-2 specification, was selected for the tag IC, input impedance of which was found to be $(12.23–j135)\,\Omega$ at 900 MHz.

Table 1 presents the GA input parameters in which the possible range of parameters magnitudes were shown. There are seven parameters used to define the proposed tag antenna, including a matching circuit (i.e., parameters w_2 and h_2). For this optimisation, real-valued GA chromosomes were used. The optimisation of input impedance of the proposed tag antenna at 900 MHz is considered inside the GA cost function. The randomly generated antenna configurations were evaluated for maximum fitness using a cost function. The geometry configuration of the optimal antenna was found within the maximum generations and the best solutions are listed in Table 1. For validation, the performance of the proposed antenna was evaluated and validated with a commercial EM simulator and the comparative results of VSWR show fairly good agreement. The results are encouraging for practical implementation of this tag antenna.

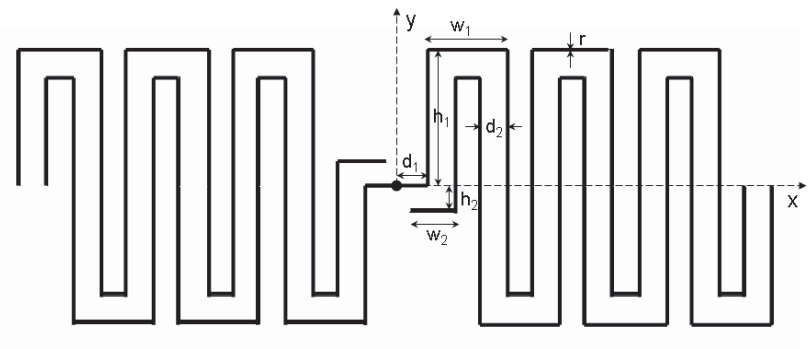

Figure 1: The new RFID antenna tag model.

Table 1: Summary of GA input parameters, antenna variables and best solutions.

GA parameters	GA-optimised RFID passive tag antenna	
	Parameters (m)	Optimal (m)
	Feeding wire length (d_1) (0.0025–0.0025)	0.0025
No. of population size = 4,	Spacing between wires (d_2) (0.001–0.003)	0.00222
No. of parameters = 7,	Outer wire width (w_1) (0.006–0.01)	0.00651
Probability of mutation = 0.02,	Matching wire width (w_2) (0.0015–0.0055)	0.00372
Maximum generation = 250,	Outer wire height (h_1) (0.005–0.015)	0.01110
No. of possibilities = 32768,	Matching wire height (h_2) (0.001–0.003)	0.00214
	Wire radius (r) (0.0002–0.0002)	0.0002

REFERENCES

1. Finkenzeller, K., *RFID Handbook*, 2nd edn., John Wiley & Sons, Ltd., Chichester, 2004.
2. Bhatt, H. and B. Glover, *RFID Essentials*, O'Reilly, January 2006.
3. Carroll, D. L., *FORTRAN Genetic Algorithm Driver*, Version 1.7, Download from: http://www.staff.uiuc.edu/ carroll/ga.html, 12/11/98.
4. Burke, G. L. and A. J. Poggio, *Numerical Electromagnetics Code (NEC)-Method of Moments*, Lawrence Livermore Laboratory, Livermore, CA, 1981.
5. http://www.alientechnology.com

A Miniature Chip Antenna Design for a Passive UHF RFID Tag to Be Built in a Portable Device

Yu-Shu Lin, **Hsien-Wen Liu**, **Kuo-Hsien Wu**, **and Chang-Fa Yang**
Department of Electrical Engineering
National Taiwan University of Science and Technology
Taipei, Taiwan

Abstract— In this paper, a miniature antenna for a passive UHF RFID tag is designed, which may be built in a portable device. Matching techniques for a Gen2 tag IC are employed to enhance the readable distance of the tag for long-range reading purposes, where quasi-lumped and lumped elements are used to match the chip antenna to the tag IC having complex input impedance. A commercial simulator, HFSS^{TM} is used to analyze the performance of the antenna. Also, measurements in an anechoic chamber of the RFID education and research center at National Taiwan University of Science and Technology are performed to evaluate the readable range of the chip tag, which is more than 5 m for a reader with an EIRP equal to 4 W. The chip antenna operating in the 900 MHz RFID band proposed here has dimensions of only $10 \times 9.5 \times 0.8\,\text{mm}^3$. Thus, this miniature tag may be flexibly built in a portable device to allow long-range reading.

A Metal Tag Antenna for Passive UHF RFID Applications

Hsien-Wen Liu, **Yu-Shu Lin**, **Kuo-Hsien Wu**, **and Chang-Fa Yang**
Department of Electrical Engineering
National Taiwan University of Science and Technology
Taipei, Taiwan

Abstract— In this paper, a passive tag antenna operating in RFID UHF band is presented, which may be mounted on a metallic object. This metal tag antenna design is composed of a slot radiator, a capacitive coupling structure and a coplanar waveguide (CPW) feed to provide a good power transfer to the tag IC. No additional matching network is required to achieve a conjugated matching between the tag IC and the proposed tag antenna. A commercial simulator, HFSS is used to analyze the proposed antenna performance. This tag antenna for the 900 MHz RFID band has dimensions of only $93(L) \times 20(W) \times 3.4(H)\,\mathrm{mm}^3$, and therefore can be flexibly attached on metallic surfaces, such as license plates for vehicle managements. Also, the antenna with low cost, easy fabrication and high efficiency are achieved by using a 0.4 mm FR4 PCB attached on a 3 mm PP substrate. For the metal tag mounted on the license plate, the maximum readable range measured in an anechoic chamber of the RFID education and research center at National Taiwan University of Science and Technology is more than 7 m for a reader with an EIRP equal to 4 W.

Dual-frequency Balanced Mobile Antenna for WLAN and Short Range Communication Systems

D. Zhou[1], **R. A. Abd-Alhameed**[1], **C. H. See**[1],
S. W. J. Chung[1], **A. G. Alhaddad**[1], **and P. S. Excell**[2]

[1]Mobile and Satellite Communications Research Centre
University of Bradford, Bradford, West Yorkshire, BD7 1DP, UK
[2]Glyndwr University, Wrexham, LL11 2AW, Wales, UK

Abstract— Over the recent years, the need to expand the bandwidth of antennas in mobile handheld devices follows from the ever-increasing data rates, and hence spectrum requirements, of mobile devices. The implementation of antenna designs causing minimised coupling with the human head/hand and hence minimised SAR would be attractive to many consumers, thus increasing the market acceptance of devices using such antennas. A good candidate is a balanced antenna [1]. An antenna with symmetrical structure that is fed with balanced currents to make it electrically symmetrical is said to be a balanced antenna. Dipoles and loops are the most commonly encountered balanced antennas [2]. In this type of antenna, balanced currents only flow on the antenna element, thus dramatically reducing the effect of current flow on the ground plane. As a result, balanced antennas should have good efficiency and more important to maintain their performance when in use adjacent to the human body.

This paper presents the design and analysis of a low profile dual-frequency (i.e., 2.4 GHz and 5.2 GHz bands) balanced-dipole antenna for WLAN and short range wireless communication. Basically, the proposed antenna is a planar dipole with folded structure, in which each monopole represented by a dual arm thin plates.The antenna is mounted on the top of a rectangular conductor plate (100×40 mm) as shown in Fig. 1 that can be represented as the mobile handset chassis or ground plane of a practical mobile phone. Initially, an antenna (referring as 'arm 1': see Fig. 1), operating at around 2.4 GHz, was designed and optimized using EM simulation package. In addition, a new technique was applied by inserting an additional thin-strip arm (referring as 'arm 2': see Fig. 1) that will generate the resonant frequency 5.2 GHz band.

The length of the folded two arms, together with other parameters of the proposed antenna, was optimized to ensure that the design entirely covered the required frequency bands. The proposed antenna has a compact size, with dimension of $38 \times 8 \times 8$ mm. In addition, current distribution on the mobile phone ground plane was analyzed using the EM simulator: it was observed that most of the current induced on the ground plane concentrated in the area beneath the antenna and minimum current distribution appeared on the rest of the ground plane, as expected. This proves the model advantage of using a balanced antenna in designs for mobile handsets. For results validation, the performance of the proposed antenna was evaluated and validated through a hardware realisation: the comparative results showed good agreement (see Fig. 2). The results are encouraging for practical investigation of this antenna in finding the performance of radiation and SAR of this new development.

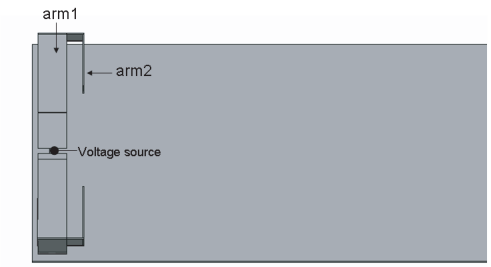

Figure 1: Antenna structure with ground plane.

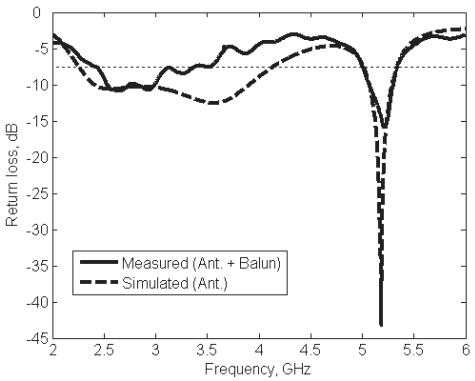

Figure 2: Simulated return loss.

ACKNOWLEDGMENT

The authors would like to gratefully acknowledge the support by the Engineering and Physical Sciences Research Council (EPSRC) under grant EP/E022936.

REFERENCES

1. Morishita, H., H. Furuuchi, and K. Fujimoto, "Performance of balance-fed antenna system for handsets in vicinity of a human head or hand," *IEE Proc.-Microw. Antennas Propag.*, Vol. 149, No, 2, 85–91, April 2002.
2. Abd-Alhameed, R. A., P. S. Excell, K. Khalil, R. Alias, and J. Mustafa, "SAR and radiation performance of balanced and unbalanced mobile antennas using a hybrid formulation," Invited paper, *IEE Proceedings-Science, Measurement and Technology sSpecial Issue on Computational Electromagnetics*, Vol. 151, No. 6, 440–444, November 2004.

Enhanced-bandwidth PIFA Antenna with a Slot on Ground Plane

Xingyu Zhang and Anping Zhao
Nokia Research Center, Beijing 100176, China

Abstract— Modern portable communication systems have experienced high market demand in recent years and it is very likely to continue in the years coming. With the rapid progress of wireless communication technologies and the extensive usage of multi-system application, wideband and multiband internal antennas have been a necessity for mobile terminals. Planar inverted-F antenna, which has the advantages of compact structure, low profile, light weight, easy fabrication, low manufacturing cost and easy integration with portable devices, is referred to as a preferable candidate for mobile applications. However, a disadvantage of conventional PIFA is its narrow bandwidth. In order to overcome this shortcoming, a new novel bandwidth enhancement solution for multiband handset antennas is proposed in this paper. In particular, a rectangular slot with an appropriate location and proper size is introduced into the system printed circuit board to improve the bandwidth of handset antennas in both the low (GSM850 and GSM900) and high (DCS1800 and PCS1900) bands. Influences of slot location and size on antenna bandwidth are studied and analyzed comprehensively. It is shown that, when the slot with a proper size is located at certain location, the bandwidths of the low and high bands can be significantly broadened. In particular, for the low band a double-resonant mode can be created by the slot. Based on this study, a PIFA antenna prototype (with 6 mm high) that can cover the frequency bands of GSM850, GSM900, DCS1800 and PCS1900 was fabricated and measured. Good agreement between the measurement and simulation results is achieved.

Design of Multi-band Antenna Using Different Radius Wires

Tsutomu Yokoyama[1], **T. Hoashi**[2], **K. Murata**[2],
S. Egashira[2], **K. Egashira**[3], **and T. Nakamiya**[4]

[1]Department of General Education, Sojo University, 4-22-1 Ikeda, Kumamoto 860-0082, Japan
[2]Department of Electronics, Computer and Network, Sojo University
4-22-1 Ikeda, Kumamoto 860-0082, Japan
[3]Saga Denshi Kogyo Co., Ltd., 2-7-13, Kaisei, Saga, Japan
[4]Department of Electronics and Intelligent Systems Engineering, Tokai University
9-1-1, Toroku, Kumamoto 862-8652, Japan

Abstract— The development of mobile communication standards that can operate different type of communication leads to have a great demand on designing compact mobile terminals such as Global System for Mobile Communication and Digital Communication System. The concept of multi band antenna is that each operating band resonates on the portion or the entire antenna geometry such that there is almost no extra size required to create multi band characteristics.

We have investigated the characteristics of the multi band antenna by measuring the current distribution of the antenna using a shield loop [1, 2]. When a shielded loop is near a test antenna, the electromotive force (EMF) on the loop is induced by the whole current on the antenna. Therefore, as the shielded loop is moved along the antenna, the current distribution can be inferred the relative value of EMF on the loop. The measurement of current distribution is important to estimate the radiation pattern of the linear antenna.

In this paper, we have designed the multi band antenna for mobile and digital communications using the different radius wires. This different radius antenna is composed of wires with a different radius. The current distribution and VSWR of the different radius antenna are measured using a shield loop. When the operation frequency was changed from 500 MHz to 2500 MHz, the value of VSWR became 1.3 at 800 MHz and 1.2 at 2.1 GHz, respectively.

In addition, we have developed the simulation model of different radius antenna. The simulation results of the current distribution and VSWR of the antenna are fairly good agreements with the experimental results. We have confirmed that the different radius antenna can be used for a multi band antenna.

REFERENCES

1. Yokoyama, T., K. Koga, and S. Egashira, "Estimation of radiation pattern by near field measurement of linear antenna," *International Conference on Microwave and Millimeter Wave Technology*, 357–360, 2002.
2. Nakamura, T., S. Yamaguchi, T. Yokoyama, and S. Egashira, "Ladder antenna," *3rd International Conference on Microwave and Millimeter Wave Technology*, 369–372, Bejjing, August 2002.

Balanced MIMO Antenna for Mobile Phones

Muhammad Usman, **Raed A. Abd-Alhameed**, **and D. Zhou**
Mobile Satellite Communications Research Centre, University of Bradford
Richmond Road, Bradford, West Yorkshire, BD7 1DP, UK

Abstract— MIMO for short, which stands for Multiple Input, Multiple Output) systems are theoretically able to provide increased throughput, and better error performance than traditional systems. The particular aspect that is used by MIMO systems is called *Multi*-Path propagation. This effect occurs when the radio signals sent from the transmitter bounce off intermediate objects before reaching the receiver. Some of these reflected signals may travel along entirely separate paths, and even reach the receiver at different times. Hence the name "multi-path" propagation. Currently, there are a number of MIMO applications, development platforms [1–6], and tools that are showing great promise in the quest for wireless systems with higher bandwidth and greater capabilities. The major advantage of MIMO technology is digital beam forming, which is now making its way out of research laboratories and into real-world applications with great speed.

The main aim of this present work was to design two elements antenna structure having a ground plane whose dimensions are compatible with a mobile phone at 5 GHz band for MIMO applications of the future wireless mobile communications. The antenna proposed here is made of two wideband balanced antenna elements and placed in parallel, as shown in Figs. 1 and 2. The proposed 2×2 MIMO balanced antenna system was designed optimized using commercial simulator HFSS (High Frequency Structure Simulator), which uses a 3D full-wave finite element Method (FEM). The antenna geometry and location on the ground plane can be found in Fig. 2. As can be seen, the antenna is fed at the centre with differential feeding which provide equal magnitude but 180 degree out of phase current for the two arms of the antenna. The input impedance of the antenna is 50 Ω.

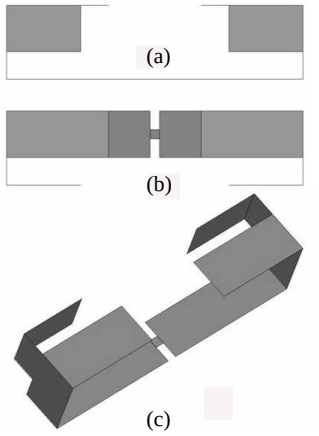

Figure 1: Antenna design; (a) Front view, (b) Top View, (c) 3D view.

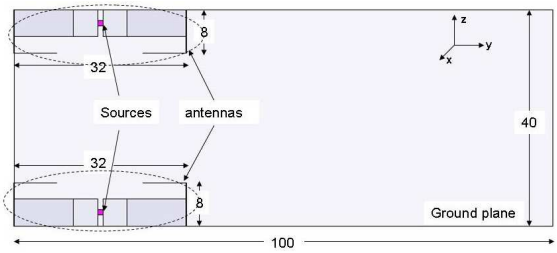

Figure 2: 2×2 Balanced MIMO antenna.

The optimal configuration of the elements was chosen to minimize the coupling between elements. The two balanced antenna elements were placed inside the limits of the ground plane and the distance between them is 24 mm (see Fig. 2). The simulated results of return loss and isolation performance of this 2×2 antenna system were examined. As observed in the upper band range, the return loss is lower than 8 dB and the isolation lower than −13 dB for both elements.

The radiation property of the proposed 2×2 MIMO balanced antennas was also investigated. Two pattern cuts were taken for four selected operating frequencies that cover the designated whole bandwidth in this study. The radiation patterns in the xz plane and yz plane for the antenna systems at 5.2 GHz and 5.8 GHz were measured.

The simulation results shows that the coupling between the antennas can be reduced with enhanced channel capacity. The balanced MIMO design discussed in this paper can be used for mobile handsets. The 2×2 balanced MIMO antenna systems with less volume can be incorporated efficiently into mobile phones. This design can also be used for PDAs and small handheld wireless devices.

REFERENCES

1. Foschini, G. J. and R. A. Valenzuela, "Initial estimation of communication efficiency of indoor wireless channel," *Wireless Networks*, Vol. 3, 141–154, 1997.
2. Winters, J. H., J. Salz, and R. D. Gitlin, "The impact of antenna diversity on the capacity of wireless communication systems," *IEEE Trans. Commun.*, Vol. 42, 1740–1751, Feb. 1994.
3. Andrews, M. R., P. P. Mitra, and R. deCarvalho, "Tripling the capacity of wireless communications using electromagnetic polarization," *Nature*, Vol. 409, No. 6818, 316–318, Jan. 2001.
4. Svantesson, T., "On capacity and correlation of multi-antenna systems employing mulTiple polarizations," *IEEE Int. Antennas Propagation Symp. Digest*, 202–205, San Antonio, TX, June 2002.
5. Stancil, D. D., A. Berson, J. P. Van't Hof, R. Negi, S. Sheth, and P. Patel, "Doubling wireless channel capacity using co-polarised, co-located electric and magnetic dipoles," *Electron. Lett.*, Vol. 38, No. 14, 746–747, July 2002.
6. Andersen, J. B. and B. N. Getu, "The MIMO cube — A compact MIMO antenna," *5th Int. Symp. Wireless Personal Multimedia Communications*, 112–114, Honolulu, HI, Oct. 2002.

Design of RFID Reader Antenna for Exclusively Reading One Single Tag

Chi-Fang Huang and I-Feng Huang
Graduate Institute of Communication Engineering, Tatung University
40, Chung-Shan N. Rd., Sec. 3, Taipei 104, Taiwan

Abstract— This paper presents a design of RFID reader antenna, which is equipped on a chip-attaching machine producing the RFID tags. Such an antenna is constrained to read exclusively one tag only for the purpose of functional check of the whole tag when it passes the reader antenna, namely, the other neighbour tags on the same rolling band are ignored that time. A wideband microstrip antenna is designed and a fixture with shielding material is set up for such a reading constraint.

Session 3P4
Fiber Optics, Optical Sensors, and All-optical Signal Processing

Reduction of Four Wave Mixing Noises in FDM Optical Fiber Transmission Systems with Quaternary Bit-phase Arranged Return-to-zero

Yoshitaka Ito, **Takuya Tamo**, **and Takahiro Numai**
Department of Electrical and Electronic Engineering, Ritsumeikan University
1-1-1 Noji-Higashi, Kusatsu, Shiga 525-8577, Japan

Abstract— Transmission characteristics in frequency-division-multiplexing (FDM) optical fiber transmission systems with low-dispersion optical fibers such as dispersion-shifted fibers (DSFs) are limited by four-wave mixing (FWM). In recent years, several FWM suppression techniques such as optical multiplexers and demultiplexers with the combination of delay lines, modified return-to-zero (RZ) signals, hybrid wavelength-/time-division multiplexing (WDM/TDM) technique, arrangement of polarization allocations of channels, separation between signal frequencies and the zero-dispersion frequency, combination of frequency/polarization allocations and separation of signal frequencies from the zero-dispersion frequency, the hybrid amplitude-/frequency-shift keying (ASK/FSK) modulation with prechirped pulses, and unequal channel spacing have been reported.

Characteristics of FWM are also closely related to frequency allocations and modulation formats. From the viewpoint of frequency allocations, unequally-spaced (US) allocations, repeated US (RUS) allocations, and modified RUSs such as equally-spaced RUS (ERUS) and unequally-spaced RUS (URUS) allocations have been demonstrated to overcome the problems in equally-spaced (ES) allocation. It was found that RUS, ERUS, and URUS have lower FWM light intensities with channel frequencies than ES and narrower total bandwidths than US. From the viewpoint of modulation formats, FWM noises have been analyzed for non-return-to-zero (NRZ), random RZ, differential phase-shift keying (DPSK), and bit-phase arranged RZ (BARZ) in ES, RUS, ERUS, and URUS, and it has been revealed that FWM noises are lowest in URUS with BARZ.

In this paper, to reduce FWM noises further, quaternary BARZ (Q-BARZ) is proposed as a modulation format, and FWM noises are analyzed. It is found that FWM noises with channel frequencies vanish in RUS, ERUS, and URUS with Q-BARZ. In our calculations, it is assumed that an oscillation wavelength for a light source is 1550 nm. A DSF is assumed to have the derivative dispersion coefficient $\mathrm{d}D_\mathrm{c}/\mathrm{d}\lambda$ of 0.07 ps/km/nm^2, the fiber length L of 80 km, and the decay rate α of 0.2 dB/km. The base unit and the channel spaces are common in all frequency allocations which are studied in this paper, and the frequency separations are the same as those in to make the pulse delay and pulse broadening as small as possible.

ACKNOWLEDGMENT

This research was partially supported by the Japan Society for Science, Grant-in-Aid for Scientific Research (C) 20560379, 2008.

An All Optical XOR Logic Gate for NRZ Based on TOAD

Yaping Wang, **Chongqing Wu**, **Xiaojun Shi**,
Shuangshou Yang, **and Yongjun Wang**
Key Lab of Education Ministry on Luminescence and Optical Information Technology
Institute of Optical Information, Beijing Jiaotong University, Beijing 100044, China

Abstract— The XOR logic gate has attracted particular attention because it is a basic and crucial element to perform a wide range of operations such as header recognition, comparison, pseudo-random bit generation and so on. Various configurations including the single SOA structure using cross gain modulation and interferential structures such as TOAD, UNI and MZI have been reported to realize XOR gate. Among them, TOAD is widely researched, due to slow optical nonlinearities presented in semiconductor and requiring less than 1 pJ switching energy. To the best of our knowledge, there is no report for all optical XOR gate for NRZ based on TOAD. This paper proposed a novel all optical XOR gate for NRZ based on TOAD by adjusting the position of SOA in the loop advisably and introducing assistant light and frame synchronizing signal as probe beam. The feasibility of this scheme is theoretically analyzed with the principle of TOAD. Based on this, all optical XOR gate operation at 40 Gb/s is successfully simulated with common SOA' parameter and the result shows that this program can get 13.29 dB extinction ratio of output by introducing advisable assistant light, while the input extinction ratio is 20 dB. For the experimentation, it is impossible to fix the power of assistant light and signals on the precise value. So the analysis of impact of nonlinear phase shift difference departure from π and 2π in actual system is necessary. The result shows that when a fluctuant rang of nonlinear phase shift difference is confined within 0.1 rad, the more than 13 dB extinction ratio of XOR operation still be obtained. Therefore the demander of debugging is degraded. The experiment give chance to demonstrate all of the possibilities of XOR gate at 10 Gb/s. The experimental result is consistent with that of theoretic analysis.

Ultra-low Power Frequency Conversion in Two-photon-absorption Free Micro Ring Resonator

M. Ferrera[1], **L. Razzari**[1,2], **D. Duchesne**[1], **R. Morandotti**[1], **Z. Yang**[3], **M. Liscidini**[3], **J. E. Sipe**[3], **S. Chu**[4], **B. E. Little**[4], **and D. J. Moss**[5]

[1]INRS-EMT, 1650 Boulevard Lionel Boulet, Varennes, Québec J3X 1S2, Canada
[2]Dipartimento di Elettronica, Università di Pavia, via Ferrata 1, 27100 Pavia, Italy
[3]Department of Physics and Institute for Optical Sciences, University of Toronto
60 St. George St., Toronto, Ontario M5S 1A7, Canada
[4]Infinera Corp., 9020 Junction Dr., Annapolis, Maryland 94089, USA
[5]CUDOS, School of Physics, University of Sydney, New South Wales 2006, Australia

Abstract— Up to date, the world of electronics has always been an inexhaustible source of solutions to satisfy the continuous request for larger bandwidth in communication systems. Unfortunately the bit rate limit of electronic devices (around 50 Gb/s) will soon be reached, and the world of science and technology is struggling for alternative solutions. Between them all-optical signal processing appears to be one of the most viable since it brings the promise to drastically increase the performances of transmission networks and, at the same time, to keep the associated costs low. However, in order to fulfill the goal of realizing all-optical agile communications systems and improve overall all-optical devices performances, it is mandatory to optimally perform fundamental network operations such as optical switching, data storage, ultrafast modulation, etc. In particular, wavelength conversion is required to realize wavelength division multiplexing systems capable of substantially increasing the bit rate by channeling the information on different frequency carriers [1]. Recently ultra-low CW pump power (5 mW) wavelength conversion based on Four Wave Mixing (FWM) has been reported in silicon micro-ring resonators [2]. Nevertheless, it is of paramount importance to study other material systems, since silicon is well known to suffer from two-photon absorption (TPA) that in turn induces free carrier losses and may affect the performance of silicon based devices [3]. In this work we demonstrate, by means of C-MOS compatible Hydex® glass [4] based micro ring resonators, efficient wavelength conversion by FWM using ultra-low continuous-wave pump power (< 5 mW, @1553.38 nm).

In our ring, the Q factor was 65,000 and the free spectral range was 575 GHz. By using the experimental value of the FWM efficiency we estimated the nonlinear refractive index (n_2) of Hydex waveguides to be as much as five times larger than that of standard Silica, and the nonlinear γ parameter to be around 250 times higher than that of typical single mode glass fibers [5]. Furthermore, the overall field enhancement factor of our device was shown to be $\cong 1.4 \cdot 10^7$, much larger than in semiconductor structures where losses tend to be in the order of several dB/cm.

Our results are comparable to the highest values reported to date in silicon ring resonators [2], and in addition they combine the advantages of ultra-low optical loss (0.06 dB/cm) with the absence of two-photon absorption (near $\lambda = 1.5$ μm. We believe that these achievements may bring us a step forward in the quest to create very efficient all optical communication networks.

REFERENCES

1. Fukuta, H., K. Yamada, T. Shoji, M. Takahashi, T. Tsuchizawa, T. Watanabe, J. Takahashi, and S. Itabashi, *Optics Express*, Vol. 13, 4629, 2005.
2. Turner, A. C., M. Lipson, M. A. Foster, and A. Gaeta, "CLEO," post-deadline paper, CPDA3, Baltimore, Md, 2007.
3. Yin, L. and G. P. Agrawal, *Optics Letters*, Vol. 32, 2031, 2007.
4. Little, B. E., "A VLSI photonics platform," *Proc. Optical Fiber Communications Conf.*, Vol. 2, 444, 2003.
5. Fu, L., M. Rochette, V. Ta'eed, I. C. M. Littler, D. J. Moss, and B. J. Eggleton, *Optics Express*, Vol. 13, 7637, 2005.

Highly Birefringent Hybrid Photonic Crystal Fiber

S. Arismar Cerqueira, Jr., **H. E. Hernandez-Figueroa**, **and H. L. Fragnito**
Optics and Photonics Research Center, UNICAMP, Brazil

Abstract— Highly birefringent fibers provide strong birefringence deliberately introduced during the fiber fabrication process. There are two ways to achieve the required birefringence: the shape of the refractive-index profile that defines the waveguide can be made noncircular (form or shape birefringence); or the material that forms the fiber can itself be made birefringent, typically by introduction of stresses as in bow-tie or PANDA fibers.

The Hybrid Photonic Crystal Fiber or Hybrid PCF [1, 2] is a novel type of microstructured fiber, in which for the first time, light was guided and manipulated simultaneously by two different propagation mechanisms: modified total internal reflection from an array of air holes and antiresonant reflection from a line of high-index inclusions. The Hybrid PCF is composed of air holes and Germanium-doped silica rods disposed around an undoped silica core. The air holes are arranged in a hexagonal pattern as in index-guiding PCFs, whereas the high-index rods replace a single row of air holes along one of the PCF axes. These unique properties make Hybrid PCF naturally high birefringent, since light is guided along its two orthogonal polarization states by two different propagation mechanisms.

We present an experimental investigation of the birefringent properties of a Highly Birefrigent Hybrid PCF. The experimental setup is based on the following pieces of equipment: a tunable external cavity laser, a fiber polarization controller (PC), some objective lenses, an optical spectrum analyzer (OSA) and a CCD camera. PC and OSA have been used to change the polarization at the fiber input and to measure the output power, respectively. Experimental results show that fiber birefringence is much more intense on the photonic bandgap edges, where power variation between the two orthogonal polarization states (ΔP) is about 21 dB. This physical phenomenon can be qualitatively observed by analyzing the near field images obtained by the CCD camera at the fiber output. This work also presents curves of ΔP as a function of wavelength and other near field images in different bandgap regions.

The very strong birefringence of Hybrid PCFs comes from the significant stress field produced by Ge inclusions; and since they are positioned along a line through the structure, they give rise to an asymmetric stress field within the core that induces a sizeable birefringence [3]. The asymmetric stress distribution will split the two polarization modes and cause a polarization dependent loss. Hybrid PCFs can be efficiently applied to the development of gyroscopes, fiber polarizers, and fiber lasers and amplifiers to ensure linearly polarized output.

REFERENCES

1. Arismar Cerqueira, Jr., S., F. Luan, C. M. B. Cordeiro, A. K. George, and J. C. Knight, "Hybrid photonic crystal fiber," *Opt. Express*, Vol. 14, 926–931, 2006.
2. Arismar Cerqueira, Jr., S., C. M. B. Cordeiro, F. Biancalana, P. J. Roberts, H. E. Hernandez-Figueroa, and C. H. Brito Cruz, "Nonlinear interaction between two different photonic bandgaps of a hybrid photonic crystal fiber," *Opt. Letters*, Vol. 15, September 2008.
3. Schreiber, T., et al., "Stress-induced single-polarization single-transverse mode photonic crystal fiber with low nonlinearity," *Opt. Express*, Vol. 13, 7621–7630, 2005.

Efficient Generation of Cascaded Four-wave Mixing in Very Short Optical Fibers

S. Arismar Cerqueira, Jr., **J. D. Marconi**, **H. E. Hernandez-Figueroa**, **and H. L. Fragnito**
Optics and Photonics Research Center, UNICAMP, Brazil

Abstract— Four-wave mixing (FWM) is a nonlinear phenomenon, based on optical Kerr effect, which is very attractive for developing nonlinear devices. FWM occurs when four different waves interact in such way that their energy and momentum are conserved. The momentum conservation is often referred to as phase matching and depends strongly on the chromatic dispersion of the nonlinear medium. As the waves propagate through the fiber, FWM processes may occur involving the new generated waves, creating in this manner photons at further new frequencies. This is referred to as cascaded or multiple FWM [1]. For the simultaneous propagation of multiple intense pulses, FWM can provide an efficient mechanism for broadband redistribution of the energy to new wavelengths. This frequency cascading is formed by signals with well-defined frequency and phase differences.

We have previously proposed a two pumps-based method for generating broadband four-wave mixing products [1]. By using this method large bandwidths of FWM products spaced by large spectral spacing, such as 2.5 and 6.5 nm, have been reported. This work presents an efficient technique for generating cascaded four-wave mixing spaced by only 0.8 nm or 100 GHz, which is the standard separation between Dense-Wavelength Division Multiplexing channels. It consists of using very short optical fibers, few meters, and three strong pumps launched near their zero-dispersion wavelengths. The advantages of using very short optical fibers result from three effects: reducing the relative phase difference $\Delta\Phi$ of non-polarization maintaining fibers; avoiding undesirable variation of the zero-dispersion wavelength and preserving the phase matching condition by keeping the product $\Delta\beta L$ small. On the other hand, the use of three pumps instead of two pumps, as in the previous publication, has been shown extremely interesting for improving the cascaded FWM efficiency. Simulations based on Split Step Fourier method demonstrate the number of FWM products with OSNR above 30 dB is enhanced by a factor of three by using three pumps not equally spaced, 100 GHz between the two initial pumps and 200 GHz for the two last pumps. This configuration ensures the products will continue spaced by 100 GHz with the advantage of obtaining an improved distribution of energy between the FWM products.

Experimental results, obtained by using highly nonlinear fibers with low dispersion slope, present 250 cascaded FWM products spanning over 200 nm at ITU-T grid specification. Cascaded four-wave mixing can be useful for the following potential applications: development of broadband multi-wavelength sources; generation of ultra-short pulses; frequency comb generation; broadband high-resolution spectroscopy; optical metrology and astronomy.

REFERENCES

1. Arismar Cerqueira, Jr., S., J. M. Chavez Boggio, A. A. Rieznik, H. E. Hernandez-Figueroa, H. L. Fragnito, and J. C. Knight, "Highly efficient generation of broadband cascaded four-wave mixing products," *Opt. Express*, Vol. 16, 2816–2828, February 2008.

High Performance, Low-loss Nonlinear Integrated Glass Waveguides

D. Duchesne[1], **M. Ferrera**[1], **L. Razzari**[1, 2], **R. Morandotti**[1], **M. Peccianti**[1], **B. Little**[3], **S. T. Chu**[3], **and D. J. Moss**[4]

[1]INRS-EMT, 1650 Boulevard Lionel Boulet, Varennes, Québec, J3X 1S2, Canada
[2]Dipartimento di Elettronica, Università di Pavia, via Ferrata 1, Pavia 27100, Italy
[3]Infinera Corp., 9020 Junction Dr, Annapolis, Maryland 94089, USA
[4]CUDOS, School of Physics, University of Sydney, New South Wales 2006, Australia

Abstract— Photonic research for telecommunications has become an important subject of investigation largely due to the high bandwidth and low energy costs of signal processing performed using photonics over electronics. In spite of the fact that optical fibers have been established as the standard for long-haul all-optical data transportation, several key operations and optical components are still at their infancy. In particular, frequency conversion, switching and routing are primary functions that can be accomplished using nonlinear optical media.

Recently, a considerable amount of research has been dedicated to semiconductors, such as AlGaAs and SOI [1], since they exhibit a very large nonlinear coefficient, allowing the possibility of achieving strong nonlinear processes with low power and short length scales. However, these materials also tend to show both linear and nonlinear absorption, thereby putting a threshold to their nonlinear response. Whereas highly nonlinear glasses, such as chalcogenides, have also been investigated, these suffer from nonlinear absorption and/or an immature fabrication technology. In an effort to achieve a compromise between the excellent linear properties of optical fibers (low propagation loss, ease of fabrication) and the nonlinear properties of semiconductors, a high index glass ($n = 1.7$) called Hydex© was developed by Little Optics in 2003 [2]. This material platform has since then been used for several applications, including the fabrication of high order filters using ring resonators [3]. Here we present high index contrast waveguides that have an extremely low propagation loss and absence of nonlinear absorption, matched to a significant nonlinear response.

Fully CMOS compatible waveguides were obtained by surrounding a $1.45\,\mu m \times 1.5\,\mu m$ Hydex© core with standard silica glass. The large index contrast between core and cladding results in a tightly confined mode of $2\,\mu m^2$, which in turn allows waveguide bends of less than $50\,\mu m$ with negligible losses. Several different length waveguides were fabricated on a $1\,cm \times 1\,cm$ chip, including a spiral waveguide of 45 cm in length. The chip is fully fiber coupled using pigtail mode converters, with coupling losses as low as 0.75 dB. From transmission measurements carried out in waveguides of different lengths, we estimated the propagation losses to be 0.06 dB/cm. The group velocity dispersion of the waveguides was obtained through a spectral interferometric technique, resulting in a low group velocity dispersion of $\sim 0.5\,ps^2/m$. The nonlinear properties of the waveguides were investigated using 110 W peak power, 900 fs pulses from a mode-locked fiber laser. Through self-phase modulation measurements, we determined the nonlinear parameter γ to be as high as $250\,W^{-1}/km$ (approximately 250 times larger than that of single mode fibers). Moreover, using $\sim$ 450 fs pulses we observe spectral broadening of more than 200 nm at the output of the 45 cm waveguide, whereas the total transmission from the device remained intensity-independent for input intensities up to $25\,GW/cm^2$ (this value is in fact the limit of our source). These promising results offer an exciting alternative for the fabrication of low-loss integrated nonlinear optical devices.

REFERENCES

1. Salem, R., M. A. Foster, A. C. Turner, D. F. Geraghty, M. Lipson, and A. L. Gaeta, "Signal regeneration using low-power four-wave mixing on silicon chip," *Nature Photonics*, Vol. 2, 35–38, 2007.
2. Little, B., "A VLSI photonics platform," *Optical Fiber Communication Conference*, 444, 2003.
3. Little, B. E., S. T. Chu, P. P. Absil, J. V. Hryniewicz, F. G. Johnson, F. Seiferth, D. Gill, V. Van, O. King, and M. Trakalo, "Very high-order microring resonator filters for WDM applications," *IEEE Photon. Technol. Lett.*, Vol. 16, 2263–2265, 2004.

Investigation of the Localization of the Electric Dipoles

Shuang Zhao and Chong-Qing Wu
Key Laboratory of Luminescence and Optical Information, Ministry of Education
Institute of Optical Information, Beijing Jiaotong University, Beijing 100044, China

Abstract— The research of dipole source localization has great significance and importance for both clinical and research applications, such as using EEG recordings from the scalp is widely used for the localization of sources of electrical activity in the brain. The regular expression of the electric field of dipoles isn't useful for obtaining the localization of the electric dipoles directly. This paper presents a closed formula that describes the electric field of dipoles at arbitrary position, it is a linear transformer called as transfer matrix. From this closed formula we obtain: the electric field is linear with the electric moment; for a certain observation point, the transfer matrix is a symmetric matrix, it is the function of the displacement vector from the observation point to the dipole; the electric field from several dipoles at the same position obeys superposition theorem. The expression of transfer matrix and its many useful characteristics are presented in this paper, which can be used for analyzing the electrical fields of dipoles. This paper presents the closed formula for determining the location and magnitude of single-dipole or multi-dipoles according to its electrical field distribution. A calculation results for a single dipole show that the dipole will be at the midpoint of a line segment if there are equivalent fields in its two ends. We also present the matrix method for the localization of multi-dipoles.

ACKNOWLEDGMENT

The authors thank the support of NSFC, No. 60577020.

Birefringence Vector Computation and Measurement for Fiber with Polarization Dependent Loss

Zhengyong Li, **Chongqing Wu**, **Qingtao Zhang**, **and Huiyuan Zhang**
Key Lab of Education Ministry on Luminescence and Optical Information Technology
Institute of Optical Information, Beijing Jiaotong University, Beijing 100044, China

Abstract— We introduce a high-speed measuring method to monitor the state of polarization (SOP) for optical pulse with ns-magnitude duration. The experimental configuration composes of a high-speed SOP generator, a 5-km single mode fiber (SMF), a 4×4 fiber coupler, some 1/4 retarders and fiber polarizers, while the SOP is finally obtained from a 4-channel optical detector. The SOP generator is based on a polarization-sensitive semiconductor optical amplifier, which provides the stable SOP with pulse duration of 10, 50, 100, 200, and 500 ns. After transmission in a 5-km SMF, the optical pulse with SOP $S = [S_0, S_1, S_2, S_3]^T$ is split equally to four parts by a 4×4 fiber coupler. Before entering the optical detector each of them passes through a 1/4 retarder and a polarizer whose polarization axis is at 0°, 45°, 135°, and 22.5° respectively. Given detected optical intensities I_1, I_2, I_3, and I_4 for those four parts, based on Mueller matrix method we get the SOP parameters as $S_0 = (I_2 + I_3)/2$, $S_1 = I_1 - (I_2 + I_3)/2$, $S_2 = 2I_4 - I_1 - \sqrt{2(I_2 - I_3)/2}$ and $S_3 = (I_2 - I_3)/2$. Experimental results show our scheme is accurate and convenient for high-speed SOP measurement, and the speed limitation is just determined by the bandwidth of optical detector. Since the employed detector has a −3-dB bandwidth of 100 MHz, the least pulse duration can reach 5 ns. By statistic analysis of the results for pulse widths of 10, 50, 100, 200, and 500 ns, we find the average error is ~ 0.085 rad on the Poincaré sphere, which is applicable to polarization-based fiber sensing such as the polarization optical time domain reflectometry (POTDR).

Spectrum Property of 6.5 W Multi-mode Output Laser Diode

Lanlan Liu, **Chongqing Wu**, **Guodong Lin**, **and Luyao Zhai**
Key Laboratory of Luminescence and Optical Information, Ministry of Education
Institute of Optical Information, School of Science, Beijing Jiaotong University
Beijing 100044, China

Abstract— There are three kinds of light sources used in fiber communications: Laser Diode (LD), Light-emitting Diode (LED) and non Laser Diode. Because non Laser Diodes are huge, such as, gas lasers, solid-state lasers and so on, they are not suitable to match the small volume fiber, and are only used in some special places at present. LED is non-coherent light source, and is suitable for the short distance, medium and small-capacity optical fiber communication systems. Laser Diode is a kind of semiconductor device whose working style is semiconductor diode stimulated luminescence, it sends out the laser, and plays an important role in the optical communication system. Since Laser Diode was developed, people have kept on improving its structure. From the initial luminescence only driven by impulse current in low temperature to the continuous luminescence in room temperature, LD has had the advantages of small bulk, simple structure, high efficiency, long life span and high electricity-photo conversion efficiency presently. Along with the appearance of the high-power Laser Diode, the laser using LD as the pump source has been an important research direction. However, because LD laser has a low coupling efficiency with the single-mode fiber, its application is limited. Along with the appearance of the high power multi-mode output semiconductor laser and the manufacturing technology's consummation of the double-clad fiber, high power fiber amplifier and fiber laser developed rapidly. We have developed an amplifier based on the Er-Yb co-doped double-clad fiber fiber, which used the multi-mode output LD with nominal peak wavelength 975 nm and nominal power 6.5 W as the pump, and have obtained the gain over 30 dB. Because the pump LD's spectrum property has obvious influence to the fiber amplifier and laser, we have conducted the experimental study to the spectrum property of the 6.5 W multi-mode output LD. The LD's maximal operating current is 8.5 A, and experiment shows the LD's lasing threshold current is 0.3 A. Along with the rise of LD's temperature and the increase of the infusing driving current, the LD's lasing peak wavelength has a drift to the long-wave direction. LD's emission spectrum in different infusing currents was obtained in the experiment and the experiment result shows that, in the process of the driving current increasing from 0.3 A to 5 A, LD laser's peak wavelength drifted from 964.2 nm to 972.5 nm.

An Optical Time-Division Multiplier for RZ Optical Clock by Means of Stabilized Delay Interferometers

Junichi Miyashita, **Yuki Adachi**, **and Hiroyuki Toda**
Department of Electronics, Graduate School of Engineering, Doshisha University
Kyotanabe, Kyoto 610-0321, Japan

Abstract— An optical time-division repetition frequency multiplier for return-to-zero (RZ) optical clock is proposed and demonstrated. The multiplier, which can be considered as a delayed interferometer (DI), was stabilized by the use of continuous wave (CW) tunable laser in order to stabilize the phase between adjacent output optical pulses. Here, the wavelength of the input pulse and the CW laser is denoted by λ_{P} and λ_{CW}. The DI is stabilized at a certain point (null point, for example) of the interference for the CW laser. If λ_{CW} is tuned, while the DI is stabilized and λ_{P} is fixed, the DI is stabilized at any point of λ_{P} interference curve. This means that the phase difference of adjacent optical pulses can be continuously controlled and stabilized by tuning λ_{CW}. Using this principle, phase stabilized optical clock 2x multiplication can be performed. By serially concatenating the 2x multiplier, we constructed an optical clock quadruple multiplier. In the experiment, 10 GHz mode-locked fiber laser with 1546.1-nm wavelength and 10-ps pulse width was used as an optical clock source. The time-delay of the first and the second DIs were set to be 25 ps and 50 ps, respectively. When TL turns on, the feedback loop is automatically locked and the DIs are stabilized. We have observed the temporal waveforms and optical spectra when RZ ($\lambda_{\mathrm{CW}} = 1551.4$ nm) and CS-RZ ($\lambda_{\mathrm{CW}} = 1551.2$ nm) optical clocks were generated, respectively. In the optical spectra, the undesired optical sidebands were suppressed to be more than 15 dB for both cases, while TL was turned on. From this result, we can conclude that the phase between adjacent optical pulses are successfully stabilized to 0 and π for RZ and CS-RZ cases. Therefore, 40 GHz RZ and CS-RZ optical clocks were successfully generated from 10 GHz optical clock.

Evolution of Beat Signal in a Nonlinear PCF Considering the Stability of the Light Source

L. M. Zhang, Z. Wang, K. L. Yu, and C. Q. Wu
Key Laboratory of Luminescence and Optical Information, Ministry of Education, China
Institute of Optical Information, School of Science, Beijing Jiaotong University, China

Abstract— The photonic crystal fibers (PCFs) have attracted a lot of attentions recently due to their intriguing properties, potential applications. In this paper, firstly we analyze the propagation properties of a kind of PCF with the "Compact supercell method", which was developed by our group. Considering self-phase modulation, fiber loss and dispersion, we establish the nonlinear Schrodinger equation to describe the transmission and evolution of the beat signal in the PCF. By using Split-Step Fourier Method to solve the equation, we analyze the transmission process of the beat signal propagating along the PCF, and get the emulational results of the signal spectrum, which is shown in Fig. 1. At present, the spectrum evolvement of the beat signal can be used to measure the nonlinear coefficient of the fiber. One method is to use the intensity of the zero- and first-order harmony to calculate the nonlinear coefficient. By theoretical simulations, for the first time, we analyze the effect of the stability of the output power and the frequency of lasers, in addition to a certain linewidth of the spectrum on the method of measuring nonlinear coefficient and make experimental validation. It shows that the stability of the laser output power has little effects on the measurements, but the stability of the wavelength and a particular linewidth have more effects, especially the effect of the linewidth is larger. Fig. 2 shows the spectrum of when those three factors all exist, with the power stability of 10%, the wavelength stability of 10%, and the linewidth of 0.02 nm. As to measure the fiber nonlinearity, two high stable lasers with rather narrow linewidth should be employed to get a more accurate experimental result. Fig. 3 shows the experimental spectrum of the beat signal propagating along the 200 meters long PCF. In our experiment, the linewidth of the laser is 0.02 nm, central wavelength difference between both signals is 0.12 nm. Besides, by studying the effect of the dispersion and the signal power to the evolution of the spectrum, we think the dispersion influences the spectra broadening speed, whereas the input power influences the peak value of the spectra range more.

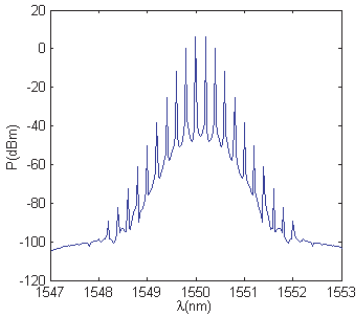

Figure 1: Simulated output spectrum.

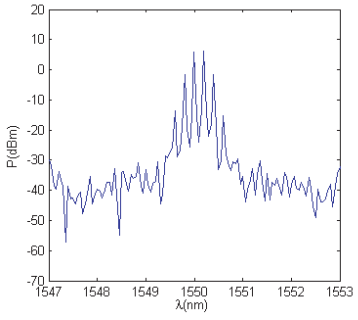

Figure 2: The spectrum considering the laser stability and linewidth.

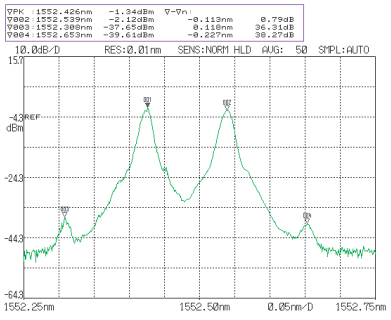

Figure 3: Experimental spectrum.

Investigation on Traffic Grooming of OPS Edge Node Base on FDLs

Kai-Qiang Gao, **Chong-Qing Wu**, **Xin-Zhi Sheng**, **and Kai Chen**
Key Laboratory of Luminescence and Optical Information, EMC
School of Science, Beijing Jiaotong University, China

Abstract— FDLs (Fiber Delay Lines) is usually used as time delay buffer in optical network and it can be used in a edge node for traffic grooming which functioned as packet header processing, time slot searching and implementing scheduling algorithm. According to its physical structure, a model was designed which described the node logical structure and scheduling algorithm based on FDLs to simulate and analysis on network efficiency in edge node. Self-similar traffic sources were imported to this model. Packets may arrive in an uncoordinated fashion. When contention occurs, fiber delay lines are needed to delay the contention packets to some future time slots for the desired output ports by some algorithm such as first fit or best fit. FDLs module simulates the packet time delay and sends packet to coupling module in precise simulation time. There are a few important factors on the network efficiency and the key parameters involved include: throughput capacity, packet lost rate, average delay time and buffer queue size. Because the main function of FDLs is traffic grooming in the model, the lost rate and average delay time play more important role than other parameters. With simulating based on a special scheduling algorithm, different network traffic load, FLDs' total number, FDLs' unit delay time and FDLs' availability lead to different lost rate, average delay time and network utilization. Modelling and Simulating give us key parameters with reference values which are important to design an optical network edge node. From the analysing result physical node can be established for special network demand.

The Diffusion Process of Dye in Polymer Film

Ying-Chuan Wang
Department of Nursing, Shu Zen College of Medicine and Management
Hwan-Chio Rd., Luju Kaohsiung 452, Taiwan, R.O.C.

Abstract— The diffusion of dye doped polymer film at various temperatures has been investigated by laser induced holographic grating relaxation technique (HGR). The decay of signal provides the information about the diffusion process of excited or unexcited dye in polymer host. The relaxation time constants can be derived from the time dependence of the diffraction signal by two exponential functions. By varying the grating spacing, we can obtain the diffusion coefficients from the plots of reciprocal of the relaxation versus the square of grating vector in this study.

Session 3P5
Progress in fs Laser Interaction with Matter 2

PW/cm^2 Femtosecond Laser-condensed Matter Interaction Resulting in X-ray Pulse Emission

Koji Hatanaka
Center for Ultrafast Intense Laser Science, Graduate School of Science
The University of Tokyo, Japan

Abstract— Interaction of tightly-focused femtosecond laser pulses at the power density more than PW/cm^2 with condensed matter such as metal solid or aqueous solution results commonly not only in ablation or plasma formation but also in hard X-ray pulse emission even in atmospheric pressure. However time course of interaction mechanisms in a short pulse width has been uncovered completely and such laser pulse shape (pulse width and chirp) and sample surface conditions (physical/chemical) for X-ray emission has not been fully optimized yet. Such knowledge is indispensable for further advance in X-ray pulse application as well as fundamental understanding and control of intense and short laser pulse interaction with condensed matter. In this presentation, effects on X-ray emission intensity/spectra of various parameters of laser pulses such as laser polarization and laser pulse width (chirp) and of samples such as surface structures and chemical components are reviewed.

Estimation of Local Force of Biological Cellular Adhesion by Femtosecond Laser Micro "Tsunami"

Y. Hosokawa[1], **A. Ito**[2], **K. Okano**[1, 3], **Y. Murakami**[2], **and H. Masuhara**[1, 4]

[1]Graduate School of Materials Science, Nara Institute of Science and Technology, Japan
[2]The Institute of Medical Science, The University of Tokyo, Japan
[3]Tohoku Fukushi University, Japan
[4]Department of Applied Chemistry, National Chiao Tung University, Taiwan

Abstract— When an intense femtosecond laser pulse is focused in a cell culture medium through an objective lens, a transient stress is generated and propagated from the laser focal point after shockwave and cavitation bubble generations. We have applied the transient stress, which we named femtosecond laser micro "Tsunami", to individual manipulation of cultured animal cells. For example, non-destructive isolation of a single cell from a substrate [1], transfer of a cell model object [2], and micro-patterning of animal cultured cell [3] have been demonstrated. In this work, the "Tsunami" was applied to estimate local adhesion force between cells. The force was evaluated by our original force measurement system utilizing an atomic force microscope (AFM). When a cell was detached from another cell by the force of the "Tsunami" due to the cavitation bubble generation and collapse, it was an order of μN. The adhesion condition for several kinds of cells was discussed in terms of the force dependence.

REFERENCES

1. Hosokawa, Y., J. Takabayashi, S. Miura, C. Shukunami, Y. Hiraki, and H. Masuhara, *Appl. Phys. A*, Vol. 79, 795, 2004.
2. Jiang, Y., Y. Matsumoto, Y. Hosokawa, H. Masuhara, and I. Oh, *Appl. Phys. Lett.*, Vol. 90, 061107, 2007.
3. Kaji, T., S. Ito, H. Miyasaka, Y. Hosokawa, H. Masuhara, C. Shukunami, and Y. Hiraki, *Appl. Phys. Lett.*, Vol. 91 23904, 2007.

Dynamics of Femtosecond Laser Processing inside Glasses — Dependence on Pulse Duration

Masaaki Sakakura[1], **Masahide Terazima**[2], **Yasuhiko Shimotsuma**[1], **Kiyotaka Miura**[3], **and Kazuyuki Hirao**[3]

[1]Innovative Collaboration Center, Kyoto University, Kyoto 615-8520, Japan
[2]Graduate School of Science, Kyoto University, Kyoto 606-8502, Japan
[3]Department of Material Chemistry, Graduate School of Engineering, Kyoto University
Kyoto 615-8510, Japan

Abstract— Femtosecond (fs) laser processing inside transparent materials has attracted interests in this decade [1]. Because small microstructures without any cracks can be created around the fs-laser focal region inside a glass, this technique is very useful for producing various kinds of three dimensional microoptics. Although there have been a lot of applications related to fs-laser processing, the dynamics of the induced structural change have not been elucidated and still been under investigation. We have investigated the dynamics of the structural change around the fs-laser focal region inside glasses, and observed the pressure wave generation after photoexcitation [2]. We have expected that the fs-laser induced pressure wave should be important factor for determining the structural change around the laser focal region inside a glass. In this paper, we will present the time-resolved observation of pressure wave generation in fs laser processing inside glass and show how the intensity of the pressure wave depends on the pulse duration.

We used a Transient lens (TrL) method for the time-resolved observation. The principle of a TrL method is described in our previous publication. In short, the refractive index distribution is created due to temperature increase in the laser focal volume inside glass after photoexcitation. The refractive index distribution works as a lens and affects the intensity profile of the probe beam, which passes through the photoexcited region. The probe beam intensity profile change is observed as the intensity of the central part of the probe beam (TrL signal). Because the refractive index distribution changes as the density distribution changes, the TrL signal also changes as the density distribution changes. Therefore, we can observe the material deformation process from the TrL signal. We used a 100 fs and 800 nm laser pulse for excitation and its second harmonic generation for a probe beam. The excitation pulse was focused inside a silica glass plate by a 20X objective lens.

We observed oscillating intensity change in a TrL signal (Fig. 1). Because the amplitude of the oscillation is determined by the intensity of the fs-laser induced pressure wave, we plotted the oscillation amplitude against laser pulse energy (Fig. 2). There is a sharp threshold of generation of a pressure wave, and the amplitude of the pressure wave increases as the pulse energy increases. Interestingly, while the threshold is lower when the pulse width is shorter, the slope is larger when the pulse width is longer. The larger slope in longer pulse width suggests that the photoionization by fs-laser irradiation is determined by not only multiphoton ionization but also light absorption by photoexcited electrons or photoinduced defects, because the longer pulse width gives photoexcited electrons and photoexcited defects longer time to interact with laser field.

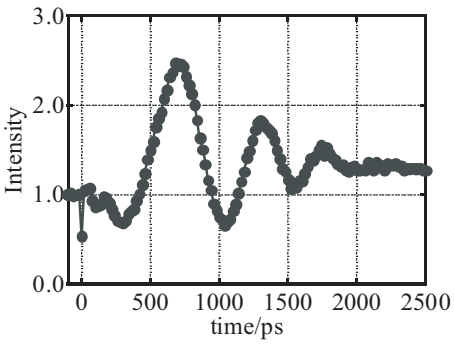

Figure 1: Typical TrL signal after the femtosecond laser irradiation inside a glass.

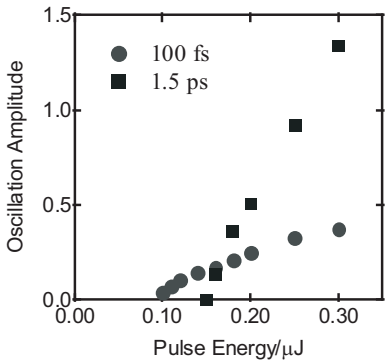

Figure 2: Oscillation amplitude plotted against pulse energy of a fs-laser.

REFERENCES

1. Davis, K. M., K. Miura, N. Sugimoto, and K. Hirao, *Opt. Lett.*, Vol. 21, 1729–1731, 1996.
2. Sakakura, M., M. Terazima, Y. Shimotsuma, K. Miura, and K. Hirao, *Opt. Express*, Vol. 15, 5674–5686, 2007.

Applications of the Laser 3D-structured Materials

S. Juodkazis and H. Misawa
Research Institute for Electronic Science, Hokkaido University
N21W10 CRIS Bldg., Sapporo 001-0021, Japan

Abstract— Femtosecond (fs) laser pulses allow to perform large-scale three-dimensional (3D) micro-/nano-structuring of materials with typical feature sizes of 0.1–1 μm. These characteristics make fs-laser microfabrication a highly suitable technique for the fabrication of 3D photonic crystals (PhCs) and their templates. Here, we discuss physical principles underlying the 3D laser structuring techniques: holographic [1] and *direct laser writing* [2]. We discuss application of these techniques for the fabrication of 3D PhCs, and demonstrate some recent results achieved in this field as well as discuss mechanisms of light-matter interaction taking place during 3D material processing.

The PhCs are expected to play an important role in photonics and optoelectronics due to their capabilities to control the emission and propagation of light via the photonic band gap (PBG) effects. These capabilities can be best exploited in the 3D PhC. However, the direct large scale 3D microfabrication of PhCs from semiconductor materials is expensive and does not yet provide required resolution; hence, more efficient fabrication strategies are highly required. Some of these strategies are based on microfabrication of PhC templates using more feasible techniques and materials. The templates can be subsequently infiltrated by other materials having higher refractive index, e.g., silicon [3]. Also, the photo-polymerized templates can be coated by metals using electroless deposition [4], which forms an uniform layer of 50–200 nm nm of metal (Ni, Ag, Au, etc.) over the frame of the structure. Such metal coated photonic structures perform as edge filters with a controllable spectral position of the edge, typically, in IR spectral region. The structures are "seen" by light as metallic since only the skin-depth of tens-of-nanometers is necessary to determine their optical response, while the spectral position of the edge filter is determined by the geometry of the polymeric template [4]. These structures can be used for spintronic (coated by Ni, Fe, Co) and plasmonic (Ag, Au, Cu) applications. We demonstrate that mechanical properties, e.g., the bulk modulus, of the photo-polymerized structures can be flexibly tuned to the required range by controlling the volume fraction and cross-linking of the polymers [5].

Creation of high pressure and temperature conditions inside the bulk materials by tightly focused laser pulses can be used to reach dynamic shock-compression pressures reaching and exceeding ∼1 TPa [6] (much higher than those attainable in a static *diamond anvil cell*). The application potential of the shock-processed materials is discussed as well as a possibility to create new high-density phases of nano-crystallites using this *"photonic" anvil cell*, where the 3D enclosure of the micro-explosion creates unique ultra-fast thermal quenching conditions favorable for a recovery of new materials when ultra-short laser pulses are implemented.

ACKNOWLEDGMENT

Support via a Grant-in-Aid from the Ministry of Education, Science, Sports, and Culture of Japan No. 19360322 is highly acknowledged.

REFERENCES

1. Kondo, T., S. Juodkazis, V. Mizeikis, S. Matsuo, and H. Misawa, *New J. Phys.*, Vol. 8, No. 10, 250–25, 2006.
2. Seet, K. K., V. Mizeikis, S. Matsuo, S. Juodkazis, and H. Misawa, *Adv. Mat.*, Vol. 17, No. 5, 541–545, 2005.
3. Seet, K. K., V. Mizeikis, K. Kannari, S. Juodkazis, H. Misawa, N. Tetreault, and S. John, *J. Selec. Topics Quant. Electr. (IEEE)*, Vol. 14, No. 4, 1064–1073, 2008.
4. Mizeikis, V., S. Juodkazis, R. Tarozaitė, J. Juodkazytė, K. Juodkazis, and H. Misawa, *Opt. Express*, Vol. 15, 8454–8464, 2007.
5. Juodkazis, S., V. Mizeikis, K. K. Seet, H. Misawa, and U. G. K. Wegst, *Appl. Phys. Lett.*, Vol. 91, No. 24, 241904/1–3, 2007.
6. Juodkazis, S., K. Nishimura, S. Tanaka, H. Misawa, E. E. Gamaly, B. Luther-Davies, L. Hallo, P. Nicolai, and V. Tikhonchuk, *Phys. Rev. Lett.*, Vol. 96, No. 16, 166101/1–4, 2006.

New Phenomena in Ultrafast Laser Interaction with Matter

Peter G. Kazansky[1], **Weijia Yang**[1], **Martynas Beresna**[1], **Yasuhiko Shimotsuma**[2], **Masaaki Sakakura**[2], **Kazuyuki Hirao**[2], **Jiarong Qiu**[3, 4], **and Yuri P. Svirko**[5]

[1]Optoelectronics Research Centre, University of Southampton, SO17 1BJ, UK
[2]Department of Material Chemistry, Graduate School of Engineering, Kyoto University
Kyoto 615-8510, Japan
[3]Department of Materials Science, Zhejiang University, Hangzhou 310027, China
[4]State Key Laboratory of High Field Laser Physics
Shanghai Institute of Optics and Fine Mechanics, Chinese Academy of Sciences
Shanghai 201800, China
[5]Department of Physics and Mathematics, University of Joensuu, FI-80101, Finland

Abstract— Modification of transparent materials with ultrafast lasers has attracted considerable interest due to a wide range of applications including laser surgery, integrated optics, optical data storage, 3D micro- and nano-structuring [1]. Three different types of material modifications can be induced with ultrafast laser irradiation in the bulk of a transparent material, silica glass in particular: an isotropic refractive index change (type 1); a form birefringence associated with self-assembled nanogratings and negative refractive index change (type 2) [2, 3]; and a void (type 3). In fused silica the transition from type 1 to type 2 and finally to type 3 modification is observed with an increase of fluence. Recently, a remarkable phenomenon in ultrafast laser processing of transparent materials has been reported manifesting itself as a change in material modification by reversing the writing direction [4]. The phenomenon has been interpreted in terms of anisotropic plasma trapping and heating by a tilted front of the ultrashort laser pulse. Moreover a change in structural modification has been demonstrated in glass by controlling the direction of pulse front tilt, achieving a calligraphic style of laser writing which is similar in appearance to that inked with the bygone quill pen [5]. It has also been a common belief that in a homogeneous medium, the photosensitivity and corresponding light-induced material modifications do not change on the reversal of light propagation direction. More recently we have observed that in a non-centrosymmetric medium, modification of the material can be different when light propagates in opposite directions (KaYaSo effect) [6]. Non-reciprocity is produced by magnetic field (Faraday effect) and movement of the medium with respect to the direction of light propagation: parallel (Sagnac effect) or perpendicular (KaYaSo effect). We anticipate that the observed phenomena will open new opportunities in laser material processing, laser surgery, optical manipulation and data storage.

REFERENCES

1. Gattas, R. R. and E. Mazur, "Femtosecond laser micromachining in transparent materials," *Nature Photonics*, Vol. 2, 219–225, 2008.
2. Shimotsuma, Y., P. G. Kazansky, J. Qiu, and K. Hirao, "Self-organized nanogratings in glass irradiated by ultrashort light pulses," *Phys. Rev. Lett.*, Vol. 91, 247705, 2003.
3. Bhardwaj, V., E. Simova, P. Rajeev, C. Hnatovsky, R. Taylor, D. Rayner, and P. Corkum, "Optically produced arrays of planar nanostructures inside fused silica," *Phys. Rev. Lett.*, Vol. 96, 057404-1, 2006.
4. Kazansky, P. G., W. Yang, E. Bricchi, J. Bovatsek, A. Arai, Y. Shimotsuma, K. Miura, and K. Hirao, "'Quill' writing with ultrashort light pulses in transparent materials," *Appl. Phys. Lett.*, Vol. 90, 151120, 2007.
5. Yang, W., P. G. Kazansky, Y. Shimotsuma, M. Sakakura, K. Miura, and K. Hirao, "Ultrashort-pulse laser calligraphy," *Appl. Phys. Lett.*, Vol. 93, 171109, 2008.
6. Yang, W., P. G. Kazansky, and Yu. P. Svirko, "Non-reciprocal ultrafast laser writing," *Nature Photonics*, Vol. 2, 99–105, 2008.

Nanoaquarium Fabricated by Femtosecond Laser for Dynamic Observation of Microorganisms

Koji Sugioka, **Yasutaka Hanada**, **and Katsumi Midorikawa**
RIKEN Advanced Science Institute, Wako, Saitama 351-0198, Japan

Abstract— Much attention is currently being paid to use microchips in chemical & biomedical research and development such as DNA analysis, medical inspection, new drug development, synthesis of new materials, environmental monitoring, etc. due to their performance of high-speed, high-sensitivity and high-efficiency as well as low sample and reagent consumption, and low waste production. Femtosecond (fs) laser is a very attractive and powerful tool for fabrication of such microchips since it can directly form three-dimensional (3D) microstructures inside transparent materials due to multiphoton absorption. In this paper, we demonstrate fabrication of 3D microfluidic structures embedded in glass chips by fs laser direct writing followed by thermal treatment and successive wet chemical etching in HF acid solution. The fabricated microchips are applied for observation of living bio-cells and microorganisms. The use of microchips possessing different microfluidic structures and different functions enables biologists to perform dynamic analysis of various kinds of bio-cells and microorganisms very efficiently. We referred to these microchips as ***nanoaquarium***. Observation and analysis on 3D movement of *Euglenas*, information transmission process in *Pleurosia Leavis*, high-speed motion of *Cryptomonas*, and *Phormidium* assemblage to seeding root are demonstrated using the ***nanoaquarium***.

Integration of Multifunctional Microdevices with Femtosecond Laser Pulses

Ya Cheng[1], **Jian Xu**[1], **Yang Liao**[1], **Fei He**[1], **Zenghui Zhou**[1], **Haiyi Sun**[1], **Zhizhan Xu**[1], **K. Sugioka**[2], **and K. Midorikawa**[2]

[1]State Key Laboratory of High Field Laser Physics
Shanghai Institute of Optics and Fine Mechanics
P. O. Box 800-211, Shanghai 201800, China
[2]Laser Technology Laboratory, The Institute of Physical and Chemical Research
RIKEN, Hirosawa 2-1, Wako, Saitama 351-0198, Japan

Abstract— Integrating three-dimensional (3D) functional microcomponents to form microdevices on/in single substrates is a challenge to current planar microfabrication technology. In the past decade, femtosecond (fs) laser microfabrication has received significant attention because of its powerful 3D integrating and manufacturing capabilities [1, 2]. A series of multifunctional microcomponents and microdevices, including microoptics, microfluidics, micromechanics, microelectronics, microplasmonics, and so on, can be fabricated and integrated in microchips with true 3D configurations using a unified fs laser microprocessing technique. For this reason, this technology is particularly suitable for fabricating lab-on-a-chip (LOC) devices, which have already created a revolution in the fields of chemical, biological, and medical research.

In this talk, we will review our recent progress in 3D fs laser fabrication of the multifunctional micro-components in chips as well as their integration. In particular, we first show the fabrication of a microfluidic optical waveguide on a glass chip by fs laser direct writing [3] which allows for switching between single mode and multi-mode waveguiding. We then present the selective metallization on dielectric surfaces based on fs laser modification combined with electroless plating [4]. Lastly, we demonstrate the integration of electronics and photonics in electro-optic (EO) crystal with fs laser pulses. A Mach-Zehnder Interferometer (MZI) EO modulator in crystal is fabricated by this technique, which is composed of optical waveguides inscribed by fs laser and embedded microelectrodes subsequently fabricated using fs laser ablation and selective electroless plating [5]. The microelectrodes embedded in crystal give rise to homogeneous electric field across the waveguides and result in effective electro-optic overlap. For these reasons, our current technique based on fs laser microfabrication shows a promising potential for 3D integration of multi-functions, such as microoptics, microfluidics, and microelectronics in a single substrate in the future.

REFERENCES

1. Sugioka, K., Y. Cheng, and K. Midorikawa, *Appl. Phys. A*, Vol. 81, 1, 2005.
2. Cheng, Y., K. Sugioka, K. Midorikawa, and Z. Xu, *SPIE Newsroom*, 2006. http://spie.org/x8513.xml.
3. Sun, H., et al., *Opt. Lett.*, Vol. 32, 1536, 2007.
4. Xu, J., et al., *Opt. Express*, Vol. 15, 12743, 2007.
5. Liao, Y., et al., *Opt. Lett.*, Vol. 33, 2281, 2008.

Complex Nanopatterns on 6H-SiC, ZnO Crystals Induced by the Interference of Multi-beam Femtosecond Laser

T. Q. Jia[1], **X. Jia**[1], **P. X. Xiong**[1], **Z. R. Sun**[1], **J. R. Qiu**[2], **and Z. Z. Xu**[2]

[1]State Key Laboratory of Precision Spectroscopy, Department of Physics
East China Normal University, Shanghai 200062, China
[2]State Key Laboratory of High Field Laser Physics
Shanghai Institute of Optics and Fine Mechanics, Shanghai 800211, China

Abstract— Holographic lithography has become an important technology to fabricate two- and three- dimensional micro- and nanostructures by adjusting the number of laser beams and their arrangement [1]. Short periodic nanostructures have been observed on some semiconductors, dielectrics and metals irradiated by femtosecond laser pulses [2], where the laser polarization plays an important role. The linearly polarized laser pulses induced nanoripples with the orientation perpendicular to its polarization, while the circularly polarized ones induced nanoparticles. The period of the nanostructures was much less than the laser wavelength (about $\lambda/3 \sim \lambda/5$).

Combining the fabrication of the short periodic nanostructures induced by femtosecond laser with HL technology, we have achieved 2D complex nanostructures by two-beam interference [3]. In this paper, we reported three types of complex nanostructures on 6H-SiC, ZnO crystals induced by the interferences of three femtosecond laser beams by arranging three types of laser polarization combinations. The nanostructures are composed of two parts: two-dimensional long periodic spots determined by the interferential intensity pattern, and self-organized short periodic nanoripples and nanoparticles determined by the interferential polarization pattern. Theoretical calculation indicates that the different polarization combinations will lead to distinct complex interferential polarization pattern and intensity pattern, and it accords well to the experimental results.

REFERENCES

1. Kondo, T., S. Juodkazis, V. Mizeikis, and H. Misawa, *Opt. Express*, Vol. 14, 7943, 2006.
2. Shimotsuma, Y., P. G. Kazansky, J. R. Qiu, and K. Hirao, *Phys. Rev. Lett.*, Vol. 91, 247405, 2003.
3. Jia, T. Q., M. Baba, M. Suzuki, R. A. Ganeev, H. Kuroda, J. R. Qiu, X. S. Wang, R. X. Li, and Z. Z. Xu, *Opt. Express*, Vol. 16, 1874, 2008.

Three-dimensional Surfaces of Inorganic Materials Fabricated by Femtosecond Laser Lithography

H. Nishiyama[1], **M. Mizoshiri**[1], **J. Nishii**[2], **and Y. Hirata**[1]

[1]Division of Materials and Manufacturing Science, Graduate School of Engineering
Osaka University, Japan
[2]National Institute of Advanced Industrial Science and Technology, Japan

Abstract— Three-dimensional (3D) surfaces of inorganic optical materials were created by femtosecond laser lithography assisted micromachining (FLAM), a combined process of nonlinear lithography and plasma etching. Hybrid diffractive-refractive optical elements are promising candidates for various photonic applications such as integrated sensors and high-density storages. In particular, silica-based elements are attractive because of their high transparency, physical and chemical stabilities. For obtaining these hybrid elements, microfabrication onto nonplanar substrates such as convex lenses is required. However, the current semiconductor process, which is well established for the production of complex fine structures, can not be extended to such fabrication because of the difficulty in obtaining uniform resist coating on nonplanar substrates. In this paper, we propose FLAM for microfabrication on nonplanar substrates, and demonstrate the formation of silica diffractive-refractive hybrid microlenses.

We used a femtosecond fiber laser system. This system delivers laser pulses at $\lambda = 780\,\mathrm{nm}$ with a pulse duration of 68 fs and repetition rate of 50 MHz. The patterns transfer was carried out by electron cyclotron resonance plasma with CHF_3 gas.

MicroFresnel lens patterns were directly written inside resists on convex lenses by femtosecond laser-induced nonlinear optical absorption. The patterns were transferred to the underlying lenses by plasma after development and baking processes. We could obtain constant pattern widths even for nonuniform resists because nonlinear absorption occurs only near the focal volume. The surfaces of hybrid lenses were smooth and there were no thermal damage and cracks. When He-Ne laser light of 632.8 nm wavelength was coupled to the hybrid lens, the shift of focal length by 200 μm was confirmed by CCD camera observation. This amount of shift well agreed with theoretical values. The FLAM is an effective way for the microfabrication of highly functional DOEs.

Three-dimensional Microstructuring inside Transparent Solid Substrates Assisted by Femtosecond Laser Pulses

Shigeki Matsuo, **Satoshi Kiyama**, **Kensuke Tokumi**,
Takuro Tomita, **and Shuichi Hashimoto**
Department of Ecosystem Engineering, The University of Tokushima
2-1 Minamijosanjimacho, Tokushima 770-8506, Japan

Abstract— Recent progress in femtosecond (fs) laser technology enabled us material processing of micro/submicrometer scale using tightly focused fs pulses. One of the application fields is three-dimensional (3D) removal processing inside transparent solid. The procedure of this processing consists of two steps. The first step is irradiation of focused fs pulses, which results in a modification of host material in the vicinity of the focus. By moving the sample, modified spots are fabricated along the pre-designed pattern. The second step is wet etching. If the modified region is more soluble than the un-modified host material, the modified region is selectively etched out and empty space is fabricated from the surface to the inside of the sample. Because we can fabricate a modified spot at an arbitral position, this removal processing inherently has a 3D capability in fabricating microchannels and microcavities.

We have developed this processing technique for silica and borosilicate glasses, and an inert material of sapphire. Here we report fabrication of microchannels inside glasses with a length of 10 μm to 10 mm scale, and microcavities inside sapphire by consecutive two-step process. In addition, we report fabrication of "ship-in-a-bottle" movable structure and its non-contact manipulation by optical tweezers. We have modified and etched out a cuboid region in a substrate, but a part of the cuboid was un-modified and remained after etching. As a result, a microcavity was fabricated with a movable object inside. Then, the optical tweezers (or laser trapping) technique was applied after filling the empty space with water. The movable object was trapped, and simultaneously rotated owing to its chiral shape.

Multi-photon Induced Polymerization for Three-dimensional Metal/polymer Fine Structures

Nobuyuki Takeyasu, **Takuo Tanaka**, **and Satoshi Kawata**
RIKEN, Japan

Abstract— Multi-photon induced polymerization is a promising fabrication method for three-dimensional (3D) nano/micro structures. In this method, a high-power femtosecond laser pulse is tightly focused in a photo-polymerizable resin. Multi-photon absorption is induced only at the focal spot and a solidified polymer spot is created. The size of the polymer spot is smaller than the diffraction limit of the irradiated laser due to the nonlinear effect. By scanning the focal spot in the photo-polymerizable resin three dimensionally, we can fabricate arbitrary 3D nano/micro structures. We have performed the multi-photon fabrication by multi-focusing spots prepared with micro-lens array for mass-production. In order to extend the application fields, we fabricated electrically conductive 3D fine structures by coating the 3D fine polymer structures with metal through electrochemical deposition. To advance this work, we have developed a controlled metal deposition technique capable of fabricating metal/polymer hybrid fine structures. The polymer template decides the size of the 3D metal/polymer structures, so then, enhancement of the fabrication resolution of polymer structure is expected. We numerically analyzed the multi-photon induced polymerization, and estimated the achievable minimum size of polymer voxels and polymerization threshold in this method.

Femtosecond Laser Modifications in Polymer Materials

Wataru Watanabe
Photonics Research Institute
National Institute of Advanced Industrial Science and Technology
1-8-31, Midorigaoka, Ikeda, Osaka 563-8577, Japan

Abstract— When femtosecond laser pulses are focused inside the bulk of polymer materials, different types of modifications are produced. In this talk, the morphology and properties of induced modifications are investigated depending on the focusing conditions, the materials, scanning speeds as well as the laser parameters.

Experiments were performed using a regeneratively amplified Ti:sapphire laser system at a repetition rate of 1 kHz and a wavelength of 800 nm. In order to induce structural modifications, 100-fs femtosecond laser pulses were focused into bulk polymers by microscope objectives with different numerical apertures. The mechanisms of the observed phenomena and applications of the modifications are reviewed and discussed.

Session 3P6
Scattering by Canonical Objects

Looking into Transient Scattering

Giorgio Franceschetti[1], **James Tatoian**[1], **and George Gibbs**[2]

[1]EurekaAerospace, Inc., Pasadena, CA, USA
[2]MARCORSYSCOM, Quantico, VA, USA

Abstract— Recent advances in remote sensing via Impulse SAR (ImpSAR) make use of carrierless impulse transmitted signals: applications have already been explored in the Homeland Security scenario. Appropriate processing of received data requires an improved knowledge of scattering in time-domain.

It is obvious that available solutions in frequency domain provide the corresponding solution in time domain by inverse Fourier transform. However, this approach is not satisfactory for at least two reasons: first of all, the frequency domain solution may be very complicated; secondly, its inverse Fourier transform may be usually done only numerically. We conclude that it would be beneficial to ignore the frequency-domain solution and implement instead an electromagnetic numerical solver. A question that deserves attention is the following one: which is the role, in this era of fast, efficient, precise and reliable computers, of the analytical solution?

We believe that the so called *analytical solution* is useful only if it is totally transparent, thus providing physical insight, suggesting a model of the underlining electromagnetic behavior. In this spirit we address the canonical problem of backscattering by a metal sphere of arbitrary radius a, when the incident plane wave is a Dirac-pulse. Thus, we address the problem of evaluation, leading to a simple readable form, of the scattering impulse response of the metal sphere.

We start from the well known Mie-series solution, and then proceed to the Laplace domain, $i\omega = p$, where we examine the features of the series terms. It turns out that each term can be cast as the product of two factors: one, containing all the propagation factors, can be analytically transformed in time domain, and verifies causality; the other one is essentially a rational function of p, and can be transformed in time domain in terms of the residues at its poles. After further manipulation, the impulse response solution is cast in the following form

$$f(t) = -f^r(t) \otimes f^p(t) - f^p(t)$$

where $f^p(t)$ is the time counterpart of the first factor, $f^r(t)$ that of the second factor, and $\otimes$ is the convolution operator. At this stage all these function are represented by a series. Additional elaboration shows that the last factor in the equation essentially reduces to a Dirac-function, thus being identified with the early-time response; the first factor is related to the sphere resonances, is represented by a very fast convergent series, and is identified with the late-time response. This analytical solution verifies above mentioned requirement of simplicity and transparent reading.

Theory, numerical results and confirmations will be presented at the Conference.

PO-based Analysis of Double-bounce Scattering

Andrey V. Osipov
Microwaves and Radar Institute, German Aerospace Center (DLR)
Muenchner Str. 20, 82234 Wessling, Germany

Abstract— Multiple reflections between different parts of a non-convex scattering surface or between a scatterer and its environment may significantly contribute to the radar cross section (RCS) of the scattering configuration. The incident wave gets reflected at different parts of the scattering surface and, when some of these parts are flat and oriented as in a corner reflector such that the conditions for a chain of specular reflections are satisfied, the scattering diagram shows a pronounced peak at the corresponding scattering direction. The effect is particularly strong at high frequencies when the wavelength is shorter than the typical size of the reflecting sub-areas.

Shooting and bouncing of rays (SBR) is an established method to simulate the multiple reflections between interacting parts of a scatterer. The approach is based on the laws of geometrical optics (GO) which, as is known, assumes sharp shadow boundaries and fails to describe the transformation of the plane wave reflected at a flat scattering surface into a spherical wave as the distance from the scattering surface increases. Thus, the use of SBR may lead to significant errors in the RCS values if the scattering geometry includes distant features (i.e., lying in the far zone of each other) that interact via the multiple-bounce mechanism.

To model correctly the far-zone interactions, physical optics (PO) solutions are necessary, and in the paper a PO-based solution is used for modeling the double-bounce reflection. Furthermore, a simple test geometry consisting of two rectangular metallic plates, each several wavelengths in size, is proposed which can serve as a canonical geometry for modeling the double-bounce mechanism. This geometry is employed to compare accuracy of GO and PO solutions. The parameters of the scattering configuration are the distance between the plates, their mutual location (lit or not lit by the GO reflection), the frequency, and the incident and scattering directions. These parameters are varied and the GO solution is shown to become inadequate when the plates are in the far field of each other.

Plane-wave Scattering by an Elliptic Cone

L. Klinkenbusch
Christian-Albrechts-Universität zu Kiel, Germany

Abstract— The scattering of a plane electromagnetic wave by a perfectly-conducting semi-infinite elliptic cone is treated in sphero-conal (conical) coordinates, where this geometry is one of the coordinate surfaces. By choosing the ellipticity parameters that elliptic cone includes a large variety of interesting degenerations, such as the circular cone, the wedge, and the plane angular sector. The practical interest in these structures is because they possess tips and corners. The fields belonging to these geometric singularities could be used to complete various asymptotic methods in Electromagnetics.

As in spherical coordinates, any electromagnetic field in sphero-conal coordinates within a homogeneous domain can be expanded in form of a vector spherical-multipole expansion. The vector expansion functions are deduced from solutions of the scalar homogeneous Helmholtz equation in sphero-conal coordinates. These solutions are given as products of spherical Bessel functions, non-periodic Lamé functions and periodic Lamé functions, where the latter two are solutions of a two-parametric eigenvalue problem with two coupled Lamé differential equations. Moreover, a modal form of the dyadic Green's function can be derived in sphero-conal coordinates, for the domain outside the PEC elliptic cone (satisfying appropriate boundary conditions) as well as for the free space.

For the solution of the scattering problem, first the exact surface current on the PEC cone is found from the dyadic Green's function of the elliptic cone. An incident plane wave is obtained by locating a Hertzian dipole in the far field and by multiplying the resulting modal expansion by a suitable correction factor. The scattered field is caused by this surface current and can be found by means of the equivalence theorem and applying the bilinear form of the dyadic Green's function of the free space in sphero-conal coordinates. The resulting double-sum series is valid in the far field only.

All of the obtained coupling integrals are solved completely analytically. The attempt to obtain a convergent partial-sum sequence by a simple summing-up procedure fails because we are describing a far-field distribution with plane and/or cylindrical wave portions by means of a *spherical*-multipole expansion. It has been shown that a linear summation technique is sufficient to obtain useful approximate results. Alternatively, we may subtract from the exact multipole amplitudes those one describing the Physical-Optics far field, and, hence we are able to dramatically improve the convergence properties for certain cases.

Integral Equations for 3-D Scattering: Finite Strip on a Substrate

Egon Marx
National Institute of Standards and Technology
Gaithersburg, MD 20899-8212, USA

Abstract— The simulation of the image of a finite strip on an infinite substrate is based on the solution of three-dimensional Maxwell equations reduced to singular integral equations. This applies to a line on a wafer as used by the semiconductor industry. The scattering problem is a special case of the scattering by a finite body located in the interface of two semi-infinite regions (Fig. 1).

The electromagnetic field is decomposed into the sum of incident, reflected, and refracted fields, determined by the substrate in the absence of the scatterer, and scattered fields. The latter are expressed in terms of unknown tangential vector fields, χ_{ij} and υ_{ij}, defined on the interfaces between the homogeneous media. One integral equation is

$$\left[\vec{L}_{21}^{\,\mathrm{t3}}\vec{M}_{11}^{\,\mathrm{t1}}+\vec{M}_{21}^{\,\mathrm{t3}}\left(\frac{1}{2}+\vec{L}_{11}^{\,\mathrm{t1}}\right)\right]\{\vec{\chi}_{11}\}+\left[\vec{L}_{21}^{\,\mathrm{t3}}\vec{M}_{12}^{\,\mathrm{t1}}+\vec{M}_{21}^{\,\mathrm{t3}}\vec{L}_{12}^{\,\mathrm{t1}}\right]\{\vec{\chi}_{12}\}+\left(\frac{1}{2}-\vec{L}_{23}^{\,\mathrm{t3}}\right)\{\vec{\upsilon}_{23}\}-\vec{M}_{23}^{\,\mathrm{t3}}\{\vec{\chi}_{23}\}$$
$$= -\vec{L}_{21}^{\,\mathrm{t3}}\left\{\hat{n}_1\times\Delta\vec{E}^{\,\mathrm{h}}\right\}-\vec{M}^{\,\mathrm{t3}}\left\{\hat{n}_1\times\Delta\vec{H}^{\,\mathrm{h}}\right\},$$

where vectors such as $\hat{n}_1$ are unit normals to a surface S_1 and the functionals have the form

$$\vec{L}^{\,\mathrm{t}}\left\{\vec{\xi}\right\}(\vec{x})=\hat{n}\times P\oint_S dS'\frac{(1-ikR)\vec{\xi}(\vec{x}')\times\vec{R}}{4\pi R^3}\exp(ikR).$$

Once integral equations are solved, the electromagnetic fields are obtained by integration. For the two-dimensional configuration the unknown functions diverge at the edges, which we expect to be the case in the three-dimensional problem as well. At the vertices P_i (Fig. 2) the divergences would be worse. It is possible to obtain hypersingular equations or one can stay away from the corners. The image at a selected focus height is computed from the electromagnetic fields by Fourier methods.

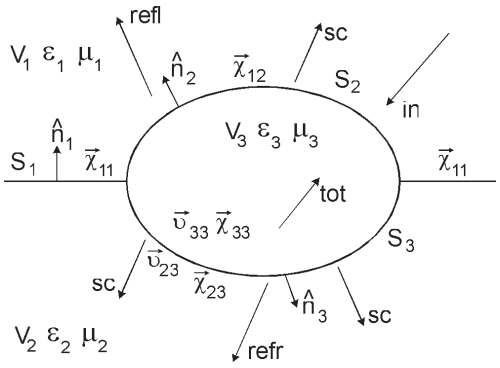

Figure 1: Finite scatterer in a plane interface.

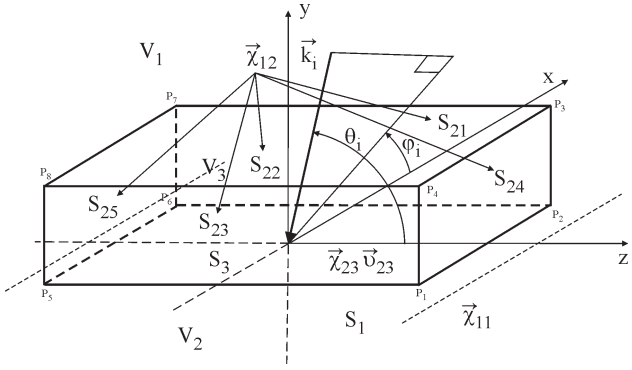

Figure 2: Finite strip on an infinite substrate.

Computational Parameters in Simulation of Microscope Images

Egon Marx and James Potzick
National Institute of Standards and Technology, Gaithersburg, MD 20899-8212, USA

Abstract— Lines on a wafer or photomask used by the semiconductor industry can be represented by two-dimensional dielectric or conducting strips on a substrate, a simple scattering configuration. Simulation is required in the determination of the width of a feature from its image, especially when this feature is smaller than the wavelength of the light used in the microscope. Simulated optical images of such a strip and similar cylinders are obtained from fields computed above the substrate and the strips. This has been done both for the reflection and the transmission modes. The latter involves a light source under a transparent layer of finite thickness. This paper presents the effects of computational parameters such as the number of patches on the interfaces and the number of plane waves representing the light illuminating the target.

The scattered fields are determined from unknown boundary functions satisfying singular integral equations [1] that are solved by the point-matching method. Sinusoids require at least six or ten points per wavelength in numerical integrations. The unknown boundary functions diverge where the regions have sharp corners, as has been extensively studied for dielectric and conducting wedges [2]. The corners have to be avoided but points may be chosen to accumulate near them. Ideally, if one knew the behavior of the unknown functions near edges one could incorporate this information in the computations. A different approach using hypersingular integral equations [2] results in unknown functions that are constant near the edges, but integrals are more difficult to compute due to the large spatial variation of the kernel.

Computational parameters include numbers of points on the interface, equispaced or accumulated at corners, number of points for a Fourier transform, height above the substrate where the scattered fields are computed, distance out on the theoretically infinite interface between the substrate and the medium of incidence, and number and distribution of patches covering the illumination aperture. Here a standard image is computed using large parameters as permitted by the available computing resources. This image is compared to images using smaller parameters by determining a quality of fit based on the squares of distances between the curves, either for the same abscissa or perpendicular to the curves. If the latter method is chosen, the plotting parameters should be dimensionless. Alternatively, one can express the discrepancy in the images in terms of the apparent line width or space width [3] difference. Visual comparison of graphs can indicate rough differences but is inadequate for high precision determination of feature size. When simulated images are compared to measured ones, the differences due to imperfections of the instrument and simplifications of the feature characteristics are much larger than those between simulations [4]. Results differ for different materials, sizes of features, wavelength, focus height, numerical apertures, and so on. A reduction in the computational parameters can lead to savings in computer run time, required memory, or both.

REFERENCES

1. Marx, E., "Images of strips on and trenches in substrates," *Appl. Opt.*, Vol. 46, 5571–5587, 2007.
2. Marx, E., "Scattering of an arbitrary plane wave by a dielectric wedge: Integral equations and fields near the edge," *Radio Sci.*, Vol. 42, RS6S09, doi:10.1029/2006RS003568, 2007.
3. Marx, E. and J. Potzick, "Simulation of optical microscope images for photomask feature size measurements," *2005 Digest of the IEEE Antennas and Propagation Society International Symposium*, 2116–2119, 2005.
4. Silver, R., R. Attota, M. Stocker, J. Jun, E. Marx, R. Larrabee, B. Russo, and M. Davidson, "Comparison of measured optical image profiles of silicon lines with two different theoretical models," *Metrology, Inspection, and Process Control for Microlithography XVI, Proceedings of the SPIE*, Vol. 4689, 409–429, 2002.

Diffraction of a Creeping Wave on an Elongated Object by an Edge

F. Molinet
MOTHESIM, L'Hay-les-Roses 94240, France

Abstract— It has been shown in previous publications that the amplitude of the magnetic creeping wave propagating on a strongly elongated perfectly conducting body is enhanced. One expects therefore a stronger diffraction process when these waves strike a sharp edge.

In this paper we present new formulas for the diffracted field for all configurations encountered in practical applications involving a combination of surface and edge diffraction on a strongly elongated object. The technique used for establishing explicit expressions for the corresponding hybrid diffraction coefficients is an extension of Michaeli's procedure developed for the classical creeping wave asymptotics. In a first step, the Heun functions appearing in the Fock integrals giving the creeping wave field at a point M with height n in the boundary layer of the penumbra region, are expanded in Taylor series in the parameter $\nu = \frac{kn}{m}$ (k = wave number, m = Fock parameter) which is supposed to be small. Then by using Heun's equation, it is shown that the first terms are also the series expansions of sine and cosine functions and represent therefore quasi-plane waves. Hence, as in the classical asymptotics, the Fock field can be written in the form of a spectral representation of inhomogeneous incident and reflected plane waves. But the reflection coefficient R of these waves depend now on the elongation parameter $\kappa = \frac{k\rho}{m}$ where ρ is the radius of curvature of the wave front. It is shown that R is identical to the reflection coefficient of an impedance surface with equivalent impedance $Z = -\frac{i}{2m_\kappa}$. By applying the spectral theory of diffraction we obtain therefore expressions for the hybrid diffraction coefficients which involve the diffraction coefficient of a plane wave by an impedance wedge. However in most practical situations only normal incidence on the wedge is of importance since enhanced creeping waves on a strongly elongated object arise in paraxial propagation and strike usually a truncation which is orthogonal to its axis. We limit therefore our analysis to normal incidence.

A list of new hybrid diffraction coefficients for strongly elongated objects involving Heun's functions and Malyuzhinets diffraction coefficients will be presented comprising the diffraction of a creeping wave into a space wave and vice versa and the diffraction of a creeping wave into another creeping wave with observation of the field on the surface or at large distance from it.

Reflection of a Plane Electromagnetic Wave in a Right-angled Interior Wedge with Anisotropic Faces

A. V. Osipov[1] and T. B. A. Senior[2]

[1]Microwaves and Radar Institute, German Aerospace Center (DLR), Wessling, Germany
[2]Department of Electrical Engineering and Computer Science
The University of Michigan, Ann Arbor, USA

Abstract— We consider the reflection of a plane electromagnetic wave incident obliquely in a right-angled corner region with anisotropic faces (in this paper, we mean by "corner" an intersection of two planes). This geometry is a useful model for a variety of applications. In radar applications, for example, the corner is a basic model of a dihedral corner reflector which is used for calibration of radars. Similar, dihedral-like, geometries are encountered in RCS simulations if a target has flat facets at 90 degrees to each other or if a target is placed over a ground plane. The corner geometry is also relevant to rectangular waveguides with corrugated walls and to the propagation of radio waves inside buildings, and the examples from wireless propagation are junctions of walls in a room, or a corner between a building wall and the ground in a street environment.

To describe material properties of the corner faces, we use impedance boundary conditions in their most general tensor form. The impedance boundary condition [1] is a convenient tool for simulating the material properties of a surface. For most materials the surface impedance is a scalar, but there are materials whose properties are anisotropic for which a tensor impedance is required. The simplest cases are those for which the tensors are diagonal but recent work with metamaterials has made possible the creation of very general materials for which the tensor may be non-diagonal. These are the focus of the present study.

We show that in general the solution consists of plane waves reflected off the two faces of the wedge and a diffracted field associated with the edge of the wedge, but if the surface impedances satisfy certain restrictions the diffracted field disappears. The exact solution is then the sum of four plane waves, one of which is the incident field. We derive the restrictions on the impedances for which this is so, and present a number of images showing the simulated behavior of the field in the corner region with various impedance tensors.

REFERENCES

1. Senior and Volakis, *Approximate Boundary Conditions in Electromagnetics*, IEE, 1995.

E-polarized Diffraction Coefficients of a Composite Wedge Composed of a Perfect Conductor and a Lossy Dielectric

S. Y. Kim
Korea Institute of Science and Technology, P. O. Box 131, Cheongryang, Seoul, Korea

Abstract— Ordinary ray-tracing provides the geometrical optics (GO) field. Keller suggested a generalization of the Fermat's principle on diffracted rays produced by an incident ray which hits edges, corners, or vertics of boundary surfaces. But the geometrical theory of diffraction (GTD) could not be implemented by employing only the ray-tracing data because the initial value of diffracted rays should be determined from the exact diffraction coefficients of some canonical structures, e.g., perfectly conducting half-plane, wedge, and cone. Hence the applicability of the GTD scheme has restricted due to the lack of rigorous diffraction coefficients of such canonical structures as penetrable wedges and cones. Recently an approximate but analytical solution to the diffraction by a composite wedge consisting of a perfect conductor and lossless dielectric was constructed using the hidden rays of diffraction (HRD) method. The hidden rays obey the usual principle of geometrical optics (GO) but do not exist in the physical region. These rays can be traced only in the complementary region, in which original media inside and outside of the wedge are exchanged each other.

The HRD method is applied to E-polarized diffraction by a composite wedge composed of a perfect conductor and a lossy dielectric. Ordinary rays are easily traced by employing the usual principle of GO in the physical region. Multiple reflections inside the lossy dielectric can be accounted accurately by determining the modified propagation constants for non-uniform plane wave transmission through conducting media. After the ordinary ray-tracing is terminated in the physical region, the hidden rays can be traced only by extending the usual principle of GO in its complementary region. Multiple reflections in the complementary dielectric region continue before the last hidden ray penetrates into the next periodic physical dielectric region. The amplitudes of hidden rays are obtained routinely by multiplication of the Fresnel's reflection coefficients. Then the HRD diffraction coefficients may be expressed by finite series of cotangent functions, which correspond to not only the ordinary rays in the physical region but also hidden rays in the complementary region. It should be noted that the angular period of the cotangent functions is adjusted to satisfy the edge condition at wedge tip. In a typical example, the diffraction coefficients and field patterns are plotted here. The accuracy of the HRD diffraction coefficients in the physical region may be accounted by checking how closely the diffraction coefficients satisfy the null-field condition in the complementary region.

Plane Wave Scattering by a Dielectric Wedge

Jung-Woong Ra
Department of Electrical Engineering and Computer Science
Korea Advanced Institute of Science and Technology
373-1, Kusong-dong, Yusong-gu, Taejon 305-701, Korea

Abstract— An analytic solution for electro-static fields in the presence of dielectric wedge is known [1]. An analytic solution for the dynamic electromagnetic fields scattered by the dielectric wedge is unknown to date because it is non-separable problem.

Physical optics (PO) approximation is obtained in analytic forms [2] for a plane wave incidence. By multiplying a factor $(1 - e^{-\alpha\rho})$ to make the geometric optical (GO) fields along the wedge interfaces zero at the wedge edge ($\rho = 0$) for an arbitrary large parameter, α, one may obtain a similar PO approximation. The correction surface currents satisfying the static edge condition near the edge and matching the phase variation of GO fields along two wedge interfaces may be synthesized and its expansion coefficients may be obtained as a function of angular spectrum from two extinction integrals in the mathematically complementary regions of the free space and the dielectric wedge, respectively. Expansion coefficients satisfying the extinction theorem in the complementary regions for each GO plane waves are analytically continued into those of the Sommerfeld's wave integrals for the diffracted fields of the correction sources in the physical regions, air and dielectric regions of the wedge. The PO solutions plus the diffracted field integrals give full analytic expressions for the fields scattered by a dielectric wedge of arbitrary wedge angles, permittivites and permeabilities. Sommerfeld's integrals may be evaluated asymptotically for large $k\rho$, where k and ρ are the wave number and the distance of the field point from the wedge tip, respectively.

REFERENCES

1. Van Bladel, J., "Field singularities at metal-dielectric wedge," *IEEE Trans. on Antennas and Propagation*, Vol. 33, 450–455, 1985.
2. Kim, S. Y., J. W. Ra, and S. Y. Shin, "Diffraction by an arbitrary-angled dielectric wedge I, physical optics approximation," *IEEE Trans. on Antennas and Propagation*, Vol. 39, No. 9, 1272–1281, 1991.

Diffraction by an Infinite Singly-negative Material Wedge

M. A. Salem[1] and A. H. Kamel[2]

[1]New Jersey Institute of Technology, Newark, NJ 07102, USA
[2]Advanced Industrial, Technological and Engineering Center
P. O. Box 433, Heliopolis Center, Cairo 11757, Egypt

Abstract— Electromagnetic fields, excited by an electric phased line source in the presence of an infinite singly-negative (negative electric constant) wedge, are determined by application of the Kontorovich-Lebedev transform. The Maxwell's equations together with the conditions of continuity of the tangential field components at the wedge interfaces are formulated as a vector boundary-value problem. By representing the field components as Kontorovich-Lebedev integrals, the problem is reduced to a system of singular integral equations for the unknown spectral functions.

The system of singular integral equations is derived by analytically continuing that of the ordinary material wedge [1]. Numerical solutions to those equations are constructed permitting fields evaluation for arbitrary negative values of the wedge electric constant and for arbitrary positioned source and observer. Numerical results showing the influence of a wedge presence on the directivity of the phased line source are presented and verified through finite-difference frequency-domain simulations. Obtained results are also compared to the results reported in [2] and contrasted to the results of the ordinary material wedge in [1].

REFERENCES

1. Salem, M. A. and A. H. Kamel, "Electromagnetic fields in the presence of an infinite dielectric wedge: The phased line-source excitation case," *Q. J. Mechanics Appl. Math.*, doi: 10.1093/qjmam/hbm029, 2008.
2. Feigenbaum, E. and M. Orenstein, "Nano plasmon polariton modes of a wedge cross section metal waveguide," *Opt. Express*, Vol. 14, 8779–8784, 2006.

Session 4A1a
Nano Scale Electromagnetics

A Physical De-embedding Method for Silicon-based Device Applications

Hsiao-Tsung Yen[1], **Tzu-Jin Yeh**[1], **and Sally Liu**[1, 2]

[1]Taiwan Semiconductor Manufacturing Company Ltd.
9, Creation Road, Hsinchu Science Park, Hsinchu, Taiwan, R.O.C.
[2]RFMP Department of Taiwan Semiconductor Manufacturing Company, Taiwan, R.O.C.

Abstract— In the recent years, de-embedding method of "open-short", "open-thru", and TRL with dummy DUTs are mostly used for on-wafer devices. This paper shows a new method, called L2L, with two metal lines or transmission lines. One is two times the length of the other one. Based on the measurement data of two lines, we can get signal PAD parasitics and scalable length model to de-embed the GSG PAD and feed metal lines with certain width. Furthermore, the tape-out DUT numbers for our test-key are extremely minimized. The applications for inductors by 65 nm Low-K Si-based process and 0.18 µm FSG Si-based process, and for 0.13 µm transmission lines are also shown for benchmark in this paper.

Thermal Conductivity of Nanofluid with Magnetic Nanoparticles

T.-H. Tsai[1], **L.-S. Kuo**[1], **P.-H. Chen**[1], **and C.-T. Yang**[2]

[1]Department of Mechanical Engineering, National Taiwan University, Taiwan
[2]Department of Mechanical and Computer-aided Engineering, St. John's University, Taiwan

Abstract— The effect of viscous base fluid on the thermal conductivity of nanofluid is investigated in this study. By mixing proper proportion of diesel oil to polydimethylsiloxane (PDMS), the specific viscous base fluids are obtained. As the ratio of PDMS increases the viscosity of base fluid grows exponentially. Fe_3O_4 is used as nanoparticles dispersed in different viscous base fluids. Oleic acid is used as surfactant. It was observed that when the low viscous (4.44cP) base fluid is applied, the thermal conductivity ratio (K_{nano}/K_{bf}) of nanofluid is higher than that predicted by Maxwell equation. And $K_{nano}/K_{Maxwell}$ is 1.02 at 2.24% volume fraction of Fe_3O_4 nanoparticles. When the high viscous (140.4 and 648.5cP) base fluids are applied, the thermal conductivity ratios (K_{nano}/K_{bf}) of nanofluid are almost the same as that predicted by Maxwell equation. And $K_{nano}/K_{Maxwell}$ are 1 at 2.24 volume fraction of Fe_3O_4 nanoparticles. To sum up above results, the thermal conductivity of low viscous nanofluid is obviously higher than that predicted by Maxwell equation. As the viscosity of base fluid increases the measured thermal conductivity becomes closer to the predicted value of Maxwell equation and finally they become the same when the viscosity is above 140.4cP. This result can be explained that the Brownian motion in the low viscous base fluid is strong and increases the thermal conductivity of nanofluid. When the viscosity of base fluid increases, the Brownian motion is weakened and finally has no influence to the thermal conductivity of nanofluid.

Breakups of a Magnetic Drop Passing through a Micro-orifice

Ching-Yao Chen[1], **C.-H. Chen**[2], **and W.-F. Lee**[3]

[1]Department of Mechanical Engineering, National Chiao Tung University, Taiwan, R.O.C.
[2]Department of Automation Engineering, Nan-Kai Institute of Technology, Taiwan, R.O.C.
[3]Department of Mechanical Engineering
National Yunlin University of Science and Technology, Taiwan, R.O.C.

Abstract— We present an experimental study on the breakup instability of a ferrofluid drop, which could be potentially applied to generation of multiple micro-scale droplets in a non-invasive way. The experiments have shown the process of a ferrofluid drop passing through a micro passage under an applied magnetic field. Interesting fluids breakups are observed. To quantitatively describe the patterns of breakups and efficiency of ferrofluid transport through the orifice, characteristic measurements of the breaking droplets, such as their stretching lengths, sizes, numbers and process time periods, are documented systematically and analyzed against two important dimensionless control parameters, e.g., the magnetic Bond number $\mathrm{Bo_m}$; and the Ohnesorge number Oh, that represent the ratio of magnetic force to the surface force and the viscous effect to the surface force, respectively. The patterns of drop breakups can be characterized by the volume fractions and stretching lengths of breaking droplets. It is found that both the volume fractions V and stretching lengths of breaking droplets ΔL_d are mainly determined by the Ohnesorge number, regardless of the magnitudes of the magnetic Bond number. Smaller breaking droplets with greater stretching result from a higher value of the Ohnesorge number. However, the transport efficiency of ferrofluids through the orifice, which can be represented by the number of total breaking droplets N and the process time of the individual breakup cycle $\mathrm{t_p}$, is found to significantly depend on both the magnetic Bond number and the Ohnesorge number. A larger value of magnetic Bond number or Ohnesorge number leads to more breaking droplets and a shorter process time of breakup. Simpler correlations can be obtained by proper combinations of the two dimensionless parameters. A nearly linear proportionality is obtained between the number of break droplets N and the dimensionless combination of $\mathrm{Oh}^{3.7*}\ \mathrm{Bo}_m$, while the process time $\mathrm{t_p}$ appears a monotonically inversed dependence if plotted as a function of a dimensionless combination of $\mathrm{Oh}^{2.9*}\ \mathrm{Bo}_m$. The results indicate, while the breaking patterns are more dominated by the Ohnesorge number in the present situations, the transport volumes and speeds strongly depend on both the magnetic Bond number and the Ohnesorge number, which are consistent with the qualitative observations.

Short Pulsed Laser Processing in Liquid Media: From Single Silicon Nanocrystal to 3D Photonic Structures

Vladimir Švrček
Novel Si Material Team, Research Center for Photovoltaics
National Institute of Advanced Industrial Science and Technology (AIST)
Central 2, Umezono 1-1-1, Tsukuba 305-8568, Japan

Abstract— Among the semiconductrors the silicon plays the most important role in daily applications However, with indirect band gap and weak interaction with photons is not suitable for optoelectronic devices. Significant room temperature photoluminescence (PL) can be observed when the grain size is decreased (< 5 nm) and quantum confinement can take place. Compared to nanocrystals embedded in solid matrix, colloidal suspensions of silicon nanocrystals (Si-ncs) in solutions have multiple advantages for both fundamental investigation and nanotechnology applications. For instance, the surface electronic states of dispersed nanocrystals are easier modifying the overall properties could be better controlled more effective way [1].

Short pulsed laser fragmentation and ablation in solution is suitable and alternative method for fabrication of nanocrystals with room temperature PL [2, 3]. The confinement of pulsed laser-generated plasma and shock waves in liquids allow the formation of luminescent Si-ncs. Peculiar chemistry, accessible for instance in water and hardly achievable in any other nanotechnology way, allows tuning their properties by an efficient and an environmentally compatible way [2]. Figure 1 shows a photo of nanocrystals fabricated by ns laser fragmentation in water. Strong visible PL of the colloid can be observed under an excitation at 325 nm wavelength. An easy variation of the liquid media enables to fabricate for example polymer (Si-ncs)-based samples [4]. Embedded luminescence Si-ncs in polymer allow to prepare either self-organized structure on different surfaces or fabricate 1D, 2D and 3D photonic structures.

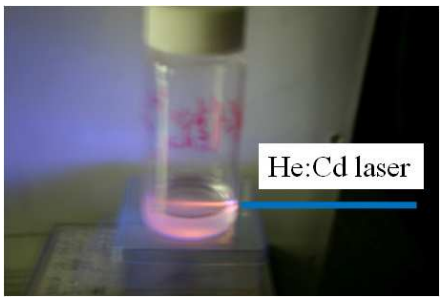

Figure 1: Photo of Si-ncs prepared by ns laser fragmentation of silicon micrograins in water and dispersed in water. The colloid is excited with the He:Cd cw laser at 325 nm wavelength.

We will present results of fundamental studies of made to synthesize blue and red room temperature luminescence-stable colloidal Si-ncs by short laser processing in liquid media. We show that the laser processing in different liquids allows stabilization of Si-ncs in carbon nanotube cavities and formation of 1D nanostructures [5]. The processing in polymers, in addition, leads to the Si-ncs surface passivation and direct fs laser writing enables formation of new types of 3D photonic luminescent structures. Lastly, the challenges and also future approaches will be overviewed.

REFERENCES

1. Švrcek, V., et al., *J. Appl. Phys.*, Vol. 95, 3158, 2004.
2. Švrcek, V., et al., *Appl. Phys. Lett.*, Vol. 89, 213113, 2006.
3. Švrcek, V., et al., *Chem. Phys. Lett.*, Vol. 429, 483, 2006.
4. Švrcek, V., et al., *J. Appl. Phys.*, Vol. 103, 023101, 2008.
5. Švrcek, V., appears in *J. Phys. Chem. C*, 2008.

On the Use Complex Susceptibility Measurements in Investigating the Field Dependence of Resonance and After-effect Function of Nano-particle Colloids

P. C. Fannin
Department of Electronic and Electrical Engineering, Trinity College, Dublin 2, Ireland

Abstract— From measurements of the field and frequency dependent magnetic complex susceptibility, $\chi(\omega, H) = \chi'(\omega, H) - i\chi''(\omega, H)$, ferromagnetic resonance, (as indicated by the change in the χ' component from $a + ve$ to $a - ve$ value) [1], may be identified and accurate data on the anisotropy constant, K, anisotropy field, H_A, gyromagnetic constant γ, and the damping parameter, α, determined. Also from polarized studies, one can identify the existence of any hysteresis.

The after-effect function, $b(t)$, or magnetization decay function, represents the decay of magnetization after the sudden removal of an external polarizing magnetic field, H [2] and $\chi(\omega)$ and $b(t)$ are related by the expression,

$$b(t) = 2\mathrm{Re}\left\{F^{-1}\left[\frac{\chi''(\omega)}{\omega}\right]\right\} \tag{1}$$

where in Eq. (1) F^{-1} denotes the inverse Fourier transform.

Since $\chi''(\omega)$ and $b(t)$, are an inverse Fourier transform pair, $b(t)$ is readily obtained and from this data. Fig. 1 shows a typical family of normalized after-effect functions for six different values of polarizing field; $H = 1$ to 6. It is apparent that $b(t)$ changes from an exponential decay to an oscillatory one. One also notices that the area under the $b(t)$ curves also changes with H. From this data a value of the precessional decay time, τ_0, may be determined.

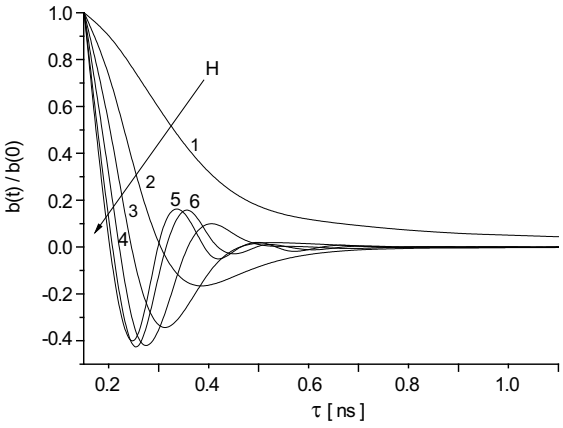

Figure 1: Plot of $b(t)/b(0)$ against t s.

In this paper, examples of results obtained for a number of magnetic fluid samples are presented and discussed; these measurements are obtained by means of the transmission line technique, over the frequency range 100 MHz to 6 GHz.

REFERENCES

1. Fannin, P. C., T. Relihan, and S. W. Charles, *J. Phys. D: Appl. Physics*, Vol. 28, 2003–2006, 1995.
2. Scaife, B. K. P., *Principles of Dielectrics*, Clarendon press, Oxford, 1998.

New Transport Regime of Electromagnetic Wave in Two-dimensional Photonic Crystal

Xiangdong Zhang
Department of Physics, Beijing Normal University, Beijing 100875, China

Abstract— A new transport regime of electromagnetic wave in two-dimensional photonic crystal near the Dirac point has been demonstrated by exact numerical simulation. In this regime, the conductance of photon is inversely proportional to the thickness of sample, which can be described by Dirac equation very well [1–3]. Based on it, We can not only construct "one-way waveguides" that allow electromagnetic energy to flow in one direction only, some unusual beating effects, which can be regarded as optical analogue to Zitterbewegung of relativistic electron, can also be observed near the Dirac point in a two-dimensional photonic crystal [4]. The superiority of such a phenomenon for photons is that it can be found in different scaling structures with wide frequency regions. It can be observed by measuring the time dependence of the transmission coefficient through photonic crystal slabs. Thus, it is particularly suited for experimentally observing this effect. We have observed such a phenomenon by exact numerical simulations, confirming a long-standing theoretical prediction [4].

REFERENCES

1. Haldane, F. D. M. and S. Raghu, *Phys. Rev. Lett.*, Vol. 100, 013904, 2008.
2. Sepkhanov, R. A., Y. B. Bazaliy, and C. W. J. Beenakker, *Phys. Rev. A*, Vol. 75, 063813, 2007.
3. Zhang, X. D., *Phys. Lett. A*, Vol. 372, 3512, 2008.
4. Zhang, X. D., *Phys. Rev. Lett.*, Vol. 100, 113903, 2008.

CFD Simulation of Gravitational Sedimentation and Clustering Effects on Heat Transfer of a Nano-ferrofluid

A. Jafari[1], **S. M. Mousavi**[2, 3], **T. Tynjala**[1], **and P. Sarkomaa**[1]

[1]Laboratory of Engineering Thermodynamics, Lappeenranta University of Technology
Lappeenranta, Finland
[2]Biotechnology Group, Chemical Engineering Department, Tarbiat Modares University
Tehran, Iran
[3]Department of Chemical Engineering, Lappeenranta University of Technology
Lappeenranta, Finland

Abstract— Nanofluids are produced by adding only a small amount of nanoparticles or nanotubes (up to 10%) into the base fluid [2]. The presence of these small particles has been shown to increase the heat transfer of the base fluid. As Keblinski et al., [4] explored there are different factors influencing the heat transport capability of nanofluids such as: brownian motion of nanoparticles; molecular-level layering of the liquid at the nanoparticle surface; nature of heat transport in nanoparticles; and the effects of nanoparticles clustering.

Ferrofluids are one type of nanofluids which are suspension of magnetic nanoparticles in a carrier liquid such as water or kerosene [3]. In the presence of an external magnetic field, a ferrofluid becomes magnetized as the particles align with the magnetic field [1]. So they have a wide range of potential application in biomedicine and technology.

In this attempt transport phenomena and hydrodynamics behavior of a kerosene based ferrofluid in a cylindrical geometry has been investigated using computational fluid dynamics (CFD). Effects of sedimentation and magnetic praticles's diameter on thermal treatment of ferrofluids have been studied. In order to compare the effect of single phase approximation and mixture model on prediction of nanofluid' behavior, both methods were investigated.

In the presence of natural convection for smaller magnetic particles' diameter Rayleigh rolls can be observed. The results show that some vortices can be observed in such systems. These rotations increase heat transfer, and their effect on thermal convection in ferrofluids is important in certain chemical engineering and biochemical situations. In addition it was found that sedimentation may lead to spatiotemporally chaotic convection and reducing the particle size decreases the rate of sedimentation observed.

REFERENCES

1. Borglin, S. E., G. J. Moridis, and C. M. Oldenburg, "Experimental studies of the flow of ferrofluid in porous media," *Transport in Porous Media*, Vol. 41, No. 1, 61–80, 2000.
2. Choi, S. U. S., "Enhancing thermal conductivity of fluids with nanoparticles," Siginer, D. A. and H. P. Wang, (Eds.), *Developments and Applications of Non-newtonian Flows*, FED-Vol. 231/MD-Vol. 66, 99–105, The American Society of Mechanical Engineers, New York, 1995.
3. Jafari, A., T. Tynjälä, S. M. Mousavi, and P. Sarkomaa, "CFD simulation and evaluation of controllable parameters effect on thermomagnetic convection in ferrofluids using Taguchi technique," *Computers and Fluids*, Vol. 37, 1344–1353, 2008.
4. Keblinksi, P., S. R. Phillpot, S. U. S. Choi, and J. A. Eastman, "Mechanisms of heat flow in suspensions of nano-sized particles (nanofluids)," *International Journal of Heat and Mass Transfer*, Vol. 45, 855–863, 2002.

Session 4A1b
Optics and Photonics 1

Electronic Properties of Quantum Wells Structures with Gaussian Potential Profiles

S. Jelev-Vlaev, **A. Enciso-Muñoz**, **and D. A. Contreras-Solorio**
Unidad Académica de Física, Universidad Autónoma de Zacatecas
Calzada Solidaridad Esquina con Paseo La Bufa s/n, C. P. 98060, Zacatecas, ZAC., México

Abstract— The design of many semiconductor devices containing quantum wells structures is based on numerical calculations of their electronic properties. The electronic spectrum of these heterostructures depends on the potential profile in the growth direction. A lot of confinement potentials have been exploited in the applications. The Gaussian profile causes specific features in the electronic structure of quantum wells and superlattices which have been used in some opto-electronic devices. A systematic study of the electronic structure in single and multiple quantum wells and superlattices with Gaussian profiles is conducted in the framework of the semi-empirical tight-binding model. We consider AlGaAs materials where the Al concentration x depends on the growth direction coordinate z and the functional dependence $x(z)$ is of Gaussian type. Due to the linear dependence of the conduction and valence band borders position on the Al concentration x, the confinement potentials for electrons and holes obey Gaussian profiles too.

The evolution of the mini-bands in finite and infinite superlattices is studied and the specific features of the electronic properties are shown. Comparison with available experimental data and known theoretical results are presented. Some possible practical applications are discussed.

Total Density of States in Rectangular Quantum Wells

S. Jelev-Vlaev[1], **Romeo de Coss**[2],
A. Del Río de Santiago[1], **and J. C. Martínez-Orozco**[1]

[1]Unidad Académica de Física, Universidad Autónoma de Zacatecas
Calzada Solidaridad Esquina con Paseo La Bufa s/n, C. P. 98060, Zacatecas, ZAC, México
[2]Departamento de Física Aplicada, CINVESTAV-Mérida
Mérida 97310, Yucatán, México

Abstract— The applications of the quantum wells are based mainly on the optical transitions around the high symmetry points in the two-dimensional Brillouin zone. By this reason the electronic structure of the quantum wells has been studied extensively only in these points. But all macroscopical properties of any condensed matter system depend on the integrated (total) density of states. The experimental methods photoemission and inverse photoemission measure directly the total density of states of the occupied and non-occupied electronic states respectively in atoms, molecules, crystals and nanostructures. The is few experimental and theoretical information about the total density of states in quantum wells. In the present work we have conducted numerical calculations of this quantity in typical rectangular quantum wells. The method of the special points was applied summing in 10, 36, 136, 528 and 2080 points of the two-dimensional Brillouin zone. We have studied the specific properties of the electronic spectrum in these quasi-bidimensional systems within the framework of the semi-empirical tight-binding model and Green function formalism.

Decline of Quantum Redundancy in a Thermal Environment

Srinivasa Chemudupati and Vladimir Tsifrinovich
Polytechnic Institute of NYU, Brooklyn, NY 11201, USA

Abstract— We study redundancy of quantum information first introduced by W. Zurek. We propose the model of a "thermal Universe", which is described by the density matrix rather than the wave function. We show that the redundancy of quantum information in a thermal environment decreases with increasing the environment temperature. We have calculated the mutual information as a function of the number of qubits in the environment. Partial information plots demonstrate that the quantum redundancy vanishes at $k_B T > 10\hbar\omega$, where ω is the characteristic energy of the environmental qubits. This provides an insight how the transition of the quantum information to the classical world can be controlled by varying temperature of the environment.

Session 4A2a
Millimeter-wave on-chip Antennas, Filters, and Passive Components

Scattering Parameters Measuring Technology Research on Two-port Surface Mounted Device

Hui Huang[1, 3], **Ke Wang**[2], **Xin Meng Liu**[3], **and Xin Lv**[1]

[1]Beijing Institute of Technology, Beijing 100081, China
[2]China Electronic Standardization Institute, Beijing 100007, China
[3]National Institute of Metrology, Beijing 100013, China

Abstract— This paper derives a novel principle how to design the fixture and the standard kit from the physical structure of surface mounted device (SMD). The characteristic coefficients of the standard are described. A perfect de-embedding algorithm is implemented. Then an example of two port surface acoustic wave (SAW) filter scattering parameters (S-parameters) measurement is used to show how to design the fixture and the calibration kit by applying the de-embedding algorithm.

A Ka Band LTCC-based Small Encapsulated Transceiver Module

Ye Yuan, **Yubo Cui**, **Shengchang Zhang**, **and Kai Zhang**
The 10th Institute of Chinese Electronic Technology Corporation
P. O. Box 94-13, Chengdu 610036, China

Abstract— With the development of the millimeter-wave system technology, system on chip (SOC) and system on package (SOP) millimeter wave system become an important direction. Low-temperature co-fired ceramics (LTCC) technology has been widely used in the design because of its relatively high dielectric constant, the technics stability and the three-dimention (3D)system on package in the millimeter-wave transceiver design.

In this paper, we describes a small Ka-band transceiver using LTCC technology and its application in a small channel extension. All part of the millimeter-wave circuit are built on Ferro A6 tape in a standard multi-layer LTCC technology, and be hermetic encapsulated with tungsten copper and kovar. This transceiver includes the internal components of a receiving channel and a transimitting channel, which are switched by a MMIC switch chip, and share a fourth subharmonic image rejection mixer which achieve the downconvert frequency image rejection and upconvert sideband constrain at the same time. The circuit in this transceiver is high-density integrated, system integration package (SOP) of the millimeter-wave MMIC chips and other passive circuit. In this paper it is described in detail on the principle of transceiver, LTCC waveguide-microstrip transition, the fourth subharmonic image rejection mixer, RF bandpass filters, LO bandstop filter and other passive circuits and the hermetic packaging technology of the small transceiver module.

Transceiver has the entire volume of 32 mm × 45 mm × 6 mm. Working in the 400 MHz bandwidth in the receiver gain measured greater than 35 dB, noise figure of less than 5 dB, image frequency compression of greater than 30 dB, output power greater than 21 dBm. The result provides a good high-volume production consistency of circuit, low-cost, easy assembly, with a high value of the LTCC encapsulated transceiver module.

A 60-GHz CPW-fed Integrated CMOS Bandpass Filter and on-chip Yagi Antenna

Pei-Chun Kuo, **Kai-Hsiang Tsai**, **Cheng-Ying Hsu**, **and Huey-Ru Chuang**
Department of Electrical Engineering, National Cheng Kung University
Tainan, Taiwan, R.O.C.

Abstract— In order to pursue the RF system-on-chip (SoC) for the 60-GHz radio and the antenna integrated with the low-cost monolithically integrated CMOS RF front-end circuitry, this paper presents a 60-GHz CPW-fed integrated CMOS bandpass filter and on-chip Yagi antenna fabricated with a 0.13-μm CMOS process. A feeding network is designed in coplanar waveguide (CPW) technology. The 0.13-μm 8-metal-layer CMOS process allows the on-chip antenna to utilize a simple coplanar waveguide (CPW) to coplanar stripline (CPS) feed transition and the first metal-layer to implement a reflector strip. An FEM-based 3-D full-wave EM solver, HFSS, is used for design simulation. The simulated input VSWR of the integrated CMOS on-chip Yagi antenna with the bandpass filter is less than 2 from 59 to 66 GHz. The front-to-back ration of the CMOS Yagi antenna (with the filter) is about 13 dB. The simulated antenna radiation efficiency and maximum antenna power gain are about 3.5% and −11.7 dBi, respectively. The chip size of the fabricated CMOS Yagi-antenna-filter is $1.35 \times 1.34\,\mathrm{mm}^2$.

A 60-GHz CMOS Millimeter-wave Wilkinson Balun

Y.-S. Lin[1], **L.-K. Yeh**[1], **C.-Y. Hsu**[1], **H.-R. Chuang**[1], **and C.-Y. Chen**[2]
[1]Institute of Computer and Communication Engineering
Department of Electrical Engineering
National Cheng Kung University, Tainan, Taiwan, R.O.C.
[2]Department of Electronic Engineering
National University of Tainan, Tainan, Taiwan, R.O.C.

Abstract— This paper presents a design and measurement performance of 60-GHz millimeter wave balun fabricated using 0.18 µm standard CMOS process. The proposed millimeter-wave balun was modified from traditional Wilkinson power divider structure. It can provide a phase differential 180 degrees of the two output ports by using modified transmission line length. The balun has bandwidth of 7 GHz at the center frequency of 60 GHz. The measured performances of the Wilkinson balun agree well with the results as that expected by simulation. The 3-D full-wave electromagnetic solver is used for design simulations. Dummy metals and via parasitic effects are considered in the design. The measured responses show good performances on S_{21} and S_{31} are above −5.3 dB and −4.7 dB, respectively. In additional, the matching ports and isolation ports are less than −17 dB and −13 dB, respectively. The measured phase differential is ±5° and power differential is 1.1 dB. The die size of the chip is $1.14 \times 1.2\,\mathrm{mm}^2$. This is to pursue the RF-SoC and single-chip transceiver for a 60-GHz radio.

Mm-wave Antenna Array Architecture to Enhance Multi-Gigabit Network Performance

Helen K. Pan, **Minyoung Park**, **and Hossein Alavi**
Intel Corporation, Hillsboro, Oregon, USA

Abstract— As new demands for high quality multimedia, voice, and data services such as high definition video and high-speed wireless data transfer arise, wireless mobile devices need to deliver multi-Gigabit data transfer capabilities [1]. 60 GHz millimeter wave radio technology has a license exempt 7 GHz-wide spectral band worldwide to provide multi-Gigabit data rates. Recent advances in CMOS process technology has enabled millimeter RFIC on silicon. CMOS millimeter chipset delivers the highest level of integration and the lowest cost solution when compared with SiGe, BiCOMS, InP and other manufacture processes. However, the inherently low output power of CMOS RFIC requires a high efficiency and high gain antenna system to meet the overall link budget.

A well designed antenna array can provide high gain and adaptive beam steering capability to enable millimeter wave communications. Microstrip antenna is an efficient antenna element and a good candidate for 60 GHz because of the advantages such as small size, planar profile, easy manufacturing process, integration, and low cost [2]. This paper describes a new microstrip antenna design that achieves 12% bandwidth with 9.5 dBi peak gain. This microstrip antenna design also preserves the similar broad beam radiation pattern performance across a broad bandwidth. Based on this high gain microstrip antenna design, 16-element 4×4 square antenna array was developed and achieved about 18 dBi peak gain at broadside beam scanning with 0.56λ element spacing. Various antenna array architecture designs can be constructed on mm-wave ICs to deliver 60 GHz systems. While linear, rectangular, square, circular, and irregular shapes antenna arrays have been studied in the past [3], the impact of the actual antenna array architecture and antenna array performance on the mm-wave network performance have not been addressed. In this paper, we study various antenna array architectures to compare their gain, beam width, and SLL (side lobe level) by adaptively changing their beam scanning angles, and investigate their impacts on mm-wave wireless network performance. We consider multiple mm-wave communication links in an office cubicle environment. The SINR (signal to interference plus noise ratio) of each link is measured by taking interference from the neighboring links into account. This paper will demonstrate the mm-wave antenna array selection criteria for a dense wireless networking environment.

REFERENCES

1. Yong, S. K. and C.-C. Chong, "An overview of multi-Gigabit wireless through millimeter wave technology: Potentials and technical challenges," *EURASIP J. Wireless Communication and Networking*, Vol. 2007, 2007.
2. Bahl, I. J. and P. Bhartia, *Microstrip Antennas*, Artech House, Inc., Dedham, 1982.
3. Hansen, R. C., *Phased Array Antenna*, A Wiley-Interscience Publication, 1998.

Session 4A2b
EM Based Modeling and CAD Techniques

Signal Integrity Analysis for 3D High-speed Interconnects Using Foldy-Lax Multiple Scattering Equations

Boping Wu and Leung Tsang
Department of Electrical Engineering, University of Washington, Seattle, USA

Abstract— One of the critical issues in signal integrity above 5 GHz range is to model the vertical electrical paths for the up-to-date package and interconnect designs with 3D integration techniques. The via structures, which are different from horizontally-routed strip and microstrip lines, cause significant signal discontinuity and crosstalk due to several reasons, such as large cylinder size, vertical orientation and other fabrication limitations. In our research, we used a semi-analytical approach, based on Foldy-Lax scattering equations and modal expansions, to compute the full-wave solution of massively-coupled multiple vias randomly positioned in multi-layered dielectric substrate. This method goes beyond the quasi-static analysis, equivalent circuit models and the analytic decomposition methods. The magnetic field Greens functions were derived and expressed in terms of waveguide modes in the vertical direction and vector cylindrical wave expansions in the horizontal direction. The network parameters were obtained by solving scattering matrix using Foldy-Lax method. After extraction of equivalent circuits of via structures using solved admittance matrices, system-level SPICE simulations was implemented to check the complete channel performance. Excellent agreements were shown when compared with Ansoft HFSS simulations. The results were also validated by hardware measurements for the entire board. Recently, this approach is extended to solve vias with arbitrary shape of antipads and pads by calculating the magnetic frill current at the antipad aperture using finite difference method. In the present paper, we show extensions of the Foldy-Lax approaches to other common and challenging structures. For example, the structure of offset via stack is widely adopted for the micro-via design inside the multilayered IC package. The structure of paring vias with shared void is the typical plated through-hole via (PTH) structure for the differential signaling in the core layer. The simulation results will be presented and compared with benchmark solutions. Even with these new complications in the structures, the CPU of Foldy-Lax approach is still about one thousand times faster than Ansoft HFSS.

HFSS$^{\mathrm{TM}}$ Modelling Anomalies with THz Metal-Pipe Rectangular Waveguide Structures at Room Temperature

Yun Zhou and Stepan Lucyszyn
Imperial College London, UK

Abstract— Air-filled metal-pipe rectangular waveguides (MPRWGs) represent the single most important form of guided-wave structure for applications above *circa* 100 GHz. Simple lengths of uniform MPRWGs can be accurately modeling using analytical equations [1], derived from first principles. However, for arbitrary 3D structures, numerical methods for determining electromagnetic behavior is required. To this end, Ansoft's commercial software package *High Frequency Structure Simulator (HFSS^{TM})* is considered by many to represent the industry standard, even though it can suffer from modeling anomalies [2]. This software employs the finite-element-method (FEM) and has many features for material definition data entry.

Surprisingly, even with the latest version (HFSS^{TM} v.11), the Drude model is not incorporated into the software, to represent the relaxation effect of conduction electrons within a metal. Relaxation effects result in bulk conductivity of metals being complex numbers that are frequency dependent. As a consequence, at (sub-)millimeter wave and terahertz frequencies, it is well-known that transmission losses increase within guided-wave structures [3] and cavity resonators experience frequency de-tuning. The solution is to either manually define a complex number for conductivity at each solution frequency or import data files that contain such information. Unfortunately, it has been found that neither solution works, and so an unorthodox approach has to be taken to model (sub-)millimeter-wave and terahertz structures accurately.

With electromagnetic modeling software, it is easy to generate simulation results that may or may not reflect the true nature of the structure. Our work highlights significant problems that can be found when modeling even the simplest air-filled MPRWGs and cavity resonators, because of inappropriate modeling of bulk conductivity, when using the latest version of HFSS^{TM}. Here, four different material definition data entry approaches were compared for structures in the Ka, W, G and Y bands. These structures are all based on the following waveguide standards: WR-28 (26.5–40 GHz), WR-10 (75–110 GHz), WR-5 (140–220 GHz), WR-2 (325–500 GHz) and WR-1 (750–1100 GHz), respectively. Results from numerical simulations are compared with those from analytical modeling; showing that an unorthodox approach must be taken for material definition data entry for the correct results to be obtained using HFSS^{TM} v.11. It can, therefore, be concluded that previously published simulations of (sub-)millimeter wave and terahertz structures, using the latest and previous versions of HFSS^{TM} with default material definitions may well have significant errors. These findings may also apply to other well-know commercial electromagnetic simulation software.

REFERENCES

1. Lucyszyn, S., D. Budimir, Q. H. Wang, and I. D. Robertson, "Design of compact monolithic dielectric-filled metal-pipe rectangular waveguides for millimetre-wave applications," *IEE Proceedings — Microwaves, Antennas and Propagation*, Vol. 143, No. 5, 451–453, Oct. 1996
2. Choi, J. Y. and S. Lucyszyn, "HFSS modelling anomalies with electrically thin-walled metal-pipe rectangular waveguide simulations," *10th IEEE High Frequency Postgraduate Student Colloquium (10th HF-PgC) Digest*, 95–98, ISBN: 0-7803-9500-X, Leeds, Sep. 2005
3. Lucyszyn, S., "Investigation of anomalous room temperature conduction losses in normal metals at terahertz frequencies," *IEE Proceedings — Microwaves, Antennas and Propagation*, Vol. 151, No. 4, 321–329, Aug. 2004

High-speed I/O Buffer Modeling for Signal-integrity-based Design of VLSI Interconnects

Yi Cao and Qi-Jun Zhang
Department of Electronics, Carleton University, Ottawa, ON, K1S 5B6, Canada

Abstract— Digital I/O buffers play an important role for the signal integrity (SI) simulation and timing analysis of high-speed VLSI interconnect networks, which often require the consideration of electromagnetic (EM) effects. In this paper, we give an overview of the recent advances in efficient macromodeling of nonlinear digital I/O buffers, including equivalent-circuit-based and neural-network-based approaches. The detailed equivalent circuit models are accurate but computationally slow. On the other hand, the simplified equivalent circuit models are fast but only provide limited accuracy. The neural-network-based models are good alternatives to those equivalent-circuit-based models, maintaining a good overall performance in terms of accuracy and speed. We demonstrate the neural-network-based approaches through an example of modeling a commercial high-speed integrated circuit (IC) device and its application to the SI simulation of high-speed interconnect networks.

Session 4A3
Active and Passive Microwave Sensing: Modelling and Simulations

Near Field Imaging of Synthetic Aperture Radiometer

C. Zhang, J. Wu, H. Liu, and W. Y. Sun
Center for Space Science and Applied Research, Chinese Academy of Sciences
Beijing 100190, China

Abstract— Synthetic aperture interferometic radiometer (SAIR) is a promising technique for passive remote sensing which can achieve high resolution without the problems associated with deploying large scanning antenna of traditional real aperture radiometer. The mass and weight are both greatly reduced. Several airborne SAIR systems have been developed, and space borne application projects have also been proposed. All the present applications of SAIR systems are operated in far field of the entire antenna array. While with the development and maturity of integrate digital correlator technology, there has been growing interest in applying SAIR in short viewing range applications such as security detection of concealed weapons or other contrabands, all weather reconnaissance and surveillance, and even ground penetrating imaging for landmine detection or archeology.

In condition of far field measurement, the curvature of the incoming wave fronts is neglected and performing as plane wave. The cross correlation of the antenna pairs with deferent antenna pair spacing (baselines), called visibility function, exactly yield the sample points of the space frequency of incoming brightness, so the original brightness can be imaged by standard Fourier inversion algorithm. While in near field applications, the typical distance from targets to antenna array is limited in range of less than 100 m, compared with the maximum baseline it is not large enough to neglect the incident wave front curvature. The paraxial approximation based Fourier relationship between the cross correlation results and incident brightness will not stand any longer. Therefore we should explore other appropriate techniques. The near filed imaging technique will also be helpful for SAIR on-ground calibration and characterization inside range limited anechoic chamber or at open air experimental field before launching into space.

This paper is devoted to analyze the near filed imaging problems of SAIR and develop an accurate near field imaging technique. Firstly we analyzed the system impulse response of Fourier algorithm in near field condition, the distortion features are exactly same as those described in, but noted that the main lobe shift is not appeared in the figure, because it is essentially determined by the geometrical arrangement of antenna pairs and can be eliminated by choosing an appropriate "center point" of the whole array as the coordinate origin point. Since it is impossible to analytically inverse the near-field visibility due to overmuch unknown variants, we can adopt a discrete form of the visibility, i.e., discretizing the visibility integral equation to form a vector product, then a numerical inversion like Moore-penrose Generalized Inverse formula can be implement to get the optimal discrete brightness distribution. The distance matrix between targets and each antenna pairs is needed for performing numerical inversion, but the targets spatial distribution is difficult to get without special ranger instruments, so we anticipate replacing it by a supposed simple surface like plane to estimate the distance matrix approximately. In some essence this corresponds to focusing the imaging array on a plane where the scene targets are equivalently located. Numerical simulation results show that this method has a better performance than the corrected Fourier method. More complicated 3D scenes are also tested to illustrate the feasibility of this plane focus method.

Numerical Study of Emissivity from Finite-size Cylindrical-shape Objects

Luis M. Camacho, **Mingyu Lu**, **and Saibun Tjuatja**
Wave Scattering Research Center, Department of Electrical Engineering
The University of Texas at Arlington, UTA Box 19016, Arlington, TX 76019-0016, USA

Abstract— All substances at a finite absolute temperature radiate electromagnetic energy. The radiation emitted into space by this substance is often partially polarized [1]. Knowing the polarization of the emission has application in passive remote sensing [2]. In most of the modeling that has been done for passive remote sensing, it is emphasized the emission from an area extensive target without considering any effect of embedded finite-size target. In realistic scenarios for remote sensing, the presence of finite-size objects is frequent. Hence, in order to incorporate the effects of the finite-size object into existing layer emission models, both an equivalent phase matrix and equivalent source model for emission from the object have to be obtained. This study is focused on the emission behavior from cylindrical-shaped objects as a function of their dielectric properties and dimensions. In [3] and [4], analytical expressions are reported to find the emission from a body. A general expression is given for an object with arbitrary shape. However, to obtain practical results, assumptions were made to make the formulation mathematically tractable. In this study, a 3D-FDTD algorithm is developed and used to compute the emissivity from finite-size objects. The approach can be used for any arbitrary-shape object; however we have focused our study in cylindrical-shaped objects. Under thermal equilibrium, the emissivity of an object is the same as its absorptivity. The absorptivity is a function of both the scattering and the absorption cross sections of the object. These cross sections were computed using the FDTD approach [6]. For the frequency and permittivity analyzed, it was found that for low conductivity the emissivity shows more variation with respect to the observation angle, having a peak or valley value at a specific polar view angle, depending on the dimensions of the object. Also, as the conductivity is increased, the emissivity tends to be more uniform with respect to the observation angle. Emissivity values for cylindrical objects as function of observation angle, polarization, permittivity and dimensions are generated and presented in this paper.

REFERENCES

1. Sandus, O., "A review of emission polarization," *Applied Optics*, Vol. 4, No. 12, 1634–1642, December 1965.
2. Tsang, L., *Theory of Microwave Remote Sensing*, John Wiley and Sons, Inc., 1985.
3. Tsang, L., "Thermal emission of nonspherical particles," *Radio Science*, Vol. 19, No. 4, 966–974, 1984.
4. Bertilone, D. C., "Stokes parameters and partial polarization of far-field radiation emitted by hot bodies," *Journal of Opt. Soc. Am.*, Vol. 11, No. 8, 2298–2304, August 1994.
5. Yueh, S. H. and R. Kwok, "Electromagnetic fluctuations for anisotropic media and the generalized Kirchhoff's law," *Radio Science*, Vol. 28, 471–480, 1993.
6. Taflove, A. and S. Hagness, *Computational Electrodynamics: The Finite-difference Time-domain Method*, 3rd Ed., Artech House, 2005.

A 2D Finite Difference Frequency Domain (FDFD) Application for Through-wall Sensing

David Insana and Carey Rappaport
Northeastern University, Boston, MA 02115, USA

Abstract— To measure the scattered fields from weak internal scattering targets buried deep within a building of unknown internal configuration, an accurate clutter model of the external and internal structural is required. This, along with the ability to accurately measure wideband scattering data for various transmit and receive locations surrounding the perimeter of the external structure is key to numerically determining the locations and scattering strengths of each target for a given clutter model.

Given an external view of a building, structural rules of thumb can be used to generate an initial clutter model of the external walls based on estimated thickness and content (i.e., brick, concrete block with reinforced rebar, etc.). To minimize the dispersive and attenuative effects through the external walls caused by vertically oriented reinforced rebar, TE_z polarized point-source excitations were propagated using a 2D FDFD method [1], terminating the computational domain by an 8-Layer PML [2]. Internal wall intersections with the external structure are located by removing the effects due to clutter from the total scattered field by direct subtraction. These points of intersection are used to update the clutter model with an estimated internal wall configuration and the process is repeated to isolate the received target scattering. To locate objects of known length, excitation frequencies can be tuned to correspond to the length of these objects, such as door and window headers.

Obtaining numerical Green's functions for the transmit and receive paths of propagation, based on a mature clutter model, provides a means to image the internal scatterers using the MUSIC [3] algorithm, in order to locate each target within the clutter. Integrating the results for various transmitter and receiver locations over a range of discrete frequency steps showed improved performance in accurately locating each target. Results show performance limitations depending on target location relative to strong clutter effects at various frequencies.

REFERENCES

1. Rappaport, C., Q. Dong, E. Bishop, A. Morgenthaler, and M. Kilmer, "Finite difference frequency domain (FDFD) modeling of two dimensional TE wave propagation and scattering," *2004 URSI Conference*, 1134–1136, Pisa, Italy, May 16–18, 2004.
2. Marengo, E. A., C. M. Rappaport, and E. L. Miller, "Optimum PML ABC conductivity profile in FDFD," *IEEE Trans. on Magnetics*, Vol. 35, No. 3, 1506–1509, May 1999.
3. Lehman, S. K. and A. J. Devaney, "Transmission mode time-reversal super-resolution imaging," *Journal of the Acoustical Society of America*, Vol. 113, No. 5, 2742–2753, 2003.

Adaptive Clutter Suppression Technique for Through-wall Radar Sensing Using 2D FDFD

David Insana and Carey Rappaport
Northeastern University, Boston, MA 02115, USA

Abstract— It is essential to reduce clutter when attempting to sense internal building structure and contents with radar. Clutter characterization is used twice in the process of locating targets within a building: first to suppress the clutter, and second, to generate numerical Green's functions used in imaging. In the first case, *a priori* knowledge of the internal clutter configuration is not needed. Previous work [1] used direct subtraction to suppress clutter in the received scattered field. Since clutter is the dominant scatterer in through-wall sensing, conventional time reversal was shown to be more sensitive to the effects of clutter, and thus less effective overall. Also, in most cases, *a priori* knowledge of the clutter channel within the building is not available and an incorrect hypothesis about the clutter configuration can be costly in the clutter suppression process. In locations where the scattering due to clutter is strong, decoupling the dominant effects of clutter from weak scattering targets is difficult and requires a wideband analysis to improve image resolution.

This work proposes a process for enhanced target resolution in the presence of strong clutter which consists of combining an adaptive time reversal technique with the MUSIC [2] algorithm over a range of stepped frequencies. The process of removing clutter from the received scattered field using direct subtraction is replaced by the Time Reversal Adaptive Interference Canceller (TRAIC) algorithm [3], which first characterizes the clutter channel alone, then uses time reversal twice to a) minimize the effects of clutter at each frequency, then b) focuses on the targets within the structure, in both cases removing the effects of the clutter characterized by the first step. This process adaptively removes clutter at each frequency, regardless of the internal configuration of the building. In this case, we define clutter as just the external and internal walls.

The TRAIC technique was applied in conjunction with a wideband version of the MUSIC algorithm by combining the MUSIC spectrum for all frequencies to produce a high resolution wideband image of the targets. The resulting images were compared to previous images obtained using direct subtraction to show improvement in identifying true target locations for various target orientations throughout the building.

REFERENCES

1. Insana, D. M. and C. M. Rappaport, "A 2D finite difference frequency domain (FDFD) method application for through-wall sensing".
2. Lehman, S. K. and A. J. Devaney, "Transmission mode time-reversal super-resolution imaging," *Journal of the Acoustical Society of America*, Vol. 113, No. 5, 2742–2753, 2003.
3. Moura, J. M. F. and Y. Jin, "Time reversal imaging by adaptive interference canceling," *IEEE Transactions on Signal Processing*, Vol. 56, No. 1, 233–247, January 2008.

Radar Target Modeling Based on Energy Content of Scattering Centers

Suman K. Gunnala, Jeffrey B. Hall, and Saibun Tjuatja

Wave Scattering Research Center, Department of Electrical Engineering
The University of Texas at Arlington, UTA Box 19016, Arlington, TX 76019-0016, USA

Abstract— Radar target can be modeled as collection of scattering centers in the image domain. Appropriate scattering center model provides an abstraction of the target which helps in effective target detection and identification. When the target of interest resides in the complex environment, such as in an inhomogeneous medium or itself is a collection of objects, effects of multi-bounce between objects and background interactions results in radar image with low signal-to-clutter ratio and significant dispersion of target scattering centers. This needs the extraction of true scattering centers corresponding to target and suppression of higher order scattering centers corresponding to clutter and other phenomena. A model based on energy content is proposed in this paper. The model approach is based on extracting the true scattering centers which correspond to the first few order terms of target returns. These low order returns have a high energy content compared to higher order multibounce clutter and it is this physical phenomenon which is exploited in this model. Data from Inverse Synthetic Aperture Radar Imaging (ISAR) measurements were utilized to validate the proposed model. Initial results show that significant first order scattering centers corresponding to target can be extracted based on the energy content using sparsity constraint. More details of model implementation and results of different experimental data sets will be presented in the full paper.

Independent Source Scattering Model for Radar Imaging

Jeffrey B. Hall, **Suman K. Gunnala**, **and Saibun Tjuatja**
Wave Scattering Research Center, Department of Electrical Engineering
The University of Texas at Arlington, UTA Box 19016, Arlington, TX 76019-0016, USA

Abstract— A pervasive issue with radar detection techniques is that of interference due to interactions of a target of interest and other closely spaced scatterers. As a method to improve the performance of systems presented with this phenomenon, a physics based scattering center model is used to extract the independent scattering centers within the field of regard. Published studies showed that the statistical distribution of radar signal is dependent on the scattering order; it approaches Gaussian as the scattering order increases. In this study, a model based on gaussianity employing Independent Component Analysis (ICA) is applied to returns of a radar system to extract independent scattering centers. As an example, this model of target extraction based on scattering centers is implemented in inverse synthetic aperture radar (ISAR) imaging of closely-spaced targets. The conventional ISAR image of these targets showed significant clutter due to the strong multiple scattering. In ICA-ISAR processing, the least Gaussian components are extracted from the radar returns to generate the ISAR image. The resulting ISAR image shows significant clutter suppression with well defined scattering centers associated with each target. Results of this study show that the application of this modeling technique has allowed extraction of independent scattering centers which are needed in target detection and identification.

Physical Model of Microwave Remote Sensing of Snow Using the Bi-continuous Random Media Model

Xiaolan Xu and Leung Tsang
Department of Electrical Engineering, University of Washington
Box 352500, Seattle, WA 98195-2500, USA

Abstract— The modeling of wave propagation and scattering in random media with discrete permittivity have widely applications in microwaves remote sensing on snow. Discrete permittivities refer to cases when the permittivity changes with discrete values from one part to the other. Dry snow is such kind of media, which consists of mixtures of ice particles and air. The permittivities vary discretely assuming the values of 3.2 for ice and 1 for air. In the past, we have modeled the bistatic scattering by considering the dense media of spherical ice grains and clusters. Both of the analytic methods (QCA) and numerical method (NMM3D) using Foldy-Lax equations have been developed.

In this paper, we consider a new approach to solve the scattering problem of media with discrete permittivities. Instead of using particles, the mathematical formalism of bicontinuous medium is applied in this study to simulate the morphologies of random porous structures. The model is based on a continuous representation of interfaces between inhomogeneities within the medium. The random structure is then defined by setting a level on this Gaussian random process according to the required volume fractions of inhomogeneities. The three dimensional bi-continuous structures generated by such random processes can be characterized by exact correlation functions. The scattering of electromagnetic waves by the simulated random media is calculated by using analytical and numerical approaches.

The analytic Born approximation is based on the derived correlation functions. NMM3D is also applied. In the numerical simulations, convergence tests are performed with respect to discretization, realization size and number of realizations. Results between the numerical and analytic approaches are compared. The polarization and cross polarization phase matrices are illustrated.

A Method to Estimated Winter Wheat Yield with the MERIS Data

Xin Du[1,2], **Bingfang Wu**[1], **Qiangzi Li**[1], **Jihua Meng**[1], **and Kun Jia**[1,2]

[1]Institute of Remote Sensing Applications, Chinese Academy of Sciences, China
[2]Graduate University of Chinese Academy of Sciences, China

Abstract— The MERIS data will provide us time-serial parameters, with which we can get the information that describe the growth process of winter wheat, so inputted these information into a biomass model such as CASA with the real time meteorological data, and then we could get the biomass of winter wheat. For calculating the yield of winter wheat, the harvest index (HI) must be estimated. There were very rarely people to estimated HI of crop with the remote sensing data. Based on the own character of winter wheat, we found that the correlation between HI and the post-anthesis biomass is quite well, and r^2 is about 0.6. Therefore, with the post-anthesis biomass calculated from remote sensing data, we can estimate the HI of winter wheat for every pixel. There is also another important parameter to estimate, the phenology of winter wheat. The same as estimating the other two parameters biomass and HI, we estimate the phenology of winter wheat with remote sensing data, too. There was a MERIS image every there or five days, and then with HANSZ model we can get everyday NDVI/LAI, the whole growth process of winter wheat is simulated. Subsequently, for different pixel there are different anthesis. Finally, we can use the follow expression to calculate the yield of winter wheat, YIELD = BIOMASS $\times$ HI, and HI = f(BIOMASS$_{\mathrm{PA}}$), where BIOMASS$_{\mathrm{PA}}$ express the post-anthesis biomass of winter wheat. With this method to estimate the yield of winter wheat, the temporal and spacial information of MERIS data has been used adequately. And the precision of the yield of winter wheat estimated with this method is expected to 80%. Because of the advantage and objectivity of the remote sensing data, this method is very useful and adequate for estimating the yield of winter wheat in daily operation.

Session 4A4
Electromagnetic and Optical Wave Technologies for Communication and Sensing 1

VLF Sferics Propagating in the Earth-ionosphere Waveguide

A. B. Bhattacharya[1], **S. Joardar**[2], **R. Bhattacharya**[3], **S. Sarkar**[1], **and S. Das**[1,4]

[1]Department of Physics, University of Kalyani, Kalyani 741235, West Bengal, India
[2]Giant Meterwave Radio Telescope, Tata Institute of Fundamental Research
Khodad, Narayagaon, Pune 410504, Maharashtra, India
[3]Department of Environmental Science, University of Kalyani
Kalyani 741235, West Bengal, India
[4]Department of Physics, Serampore College
Serampore, Hooghly 712201, West Bengal, India

Abstract— The electromagnetic waves originating in lighting discharges at frequencies in the VLF band are reflected by the ground as well as by the conducting layer of the ionosphere and thus they are guided efficiently around the earth. As in this earth-ionosphere waveguide sferics propagate with low loss, they can be detected even at long distances from their source locations. Our observations in a tropical country India, over three decades, on VLF propagation reveal some interesting phenomena under realistic conditions. The variations of the overall intensity of radio atmospheric signal at the time of sunrise and sunset as well as by the so called cosmic ray layer formation after sunrise have been critically examined besides investigations on geomagnetic effects producing long period fading in sferics level. The effects of land and sea thunderstorms in the sferics level occurring over this area have also been taken into consideration. As the wave propagates over greater distances, the excitation and attenuation vary significantly with the parameters of the waveguide, such as reflection height, anisotropy etc. which change over time and also over the typically long VLF propagation path. In fact, owing to anisotropic boundary at the ionosphere, waves traveling westward are attenuated more in comparison to the waves traveling eastward. In addition, we have noted that for frequencies $\sim 10\,\mathrm{kHz}$, the QTM modes propagating west have relatively higher longitudinal magnetic field components in comparison to the QTM modes propagating east; suggesting that the west bound wave modes have a higher level of "quasiness" than east bound modes. More interesting results are exhibited due to non homogeneity of the earth-ionosphere waveguide over an entire propagation path. Discontinuities in the wave guide parameters due to variation in the reflection height of the ionosphere are responsible for converting energy from one wave guide mode to another waveguide mode which appears to be more dominant when the path of propagation crosses the day-night terminator. All these processes affect the sferics waveforms as they propagate through the earth-ionosphere waveguide and are considered specially for sferics analysis with reference to distant sources.

A Roadmap for Detecting Extraterrestrial Intelligent Life

A. B. Bhattacharya[1], **S. S. Banerjee**[1], **and R. Bhattacharya**[2]

[1]Department of Physics, University of Kalyani, Kalyani 741235, West Bengal, India
[2]Department of Environmental Science, University of Kalyani, Kalyani 741235, India

Abstract— Search for extraterrestrial intelligence is indeed a great challenge to astronomers since its method of communication, direction of propagation as well as spectral pattern are all unknown beforehand. Due to all these various limitations, the problem has become complex and thus the science has become a "hard science". As galactic societies would be transitory, an obvious solution is an interstellar communications network, or type of library mostly consisting of automated systems to store the cumulative knowledge of vanished civilizations and thereby to communicate the knowledge through the galaxy. This is called "interstellar internet", where the different automated systems act as network servers. Intercepting such signals is highly difficult and extremely complex. The paper reviews the modern techniques and instruments for cosmic search. Theories and hypothesis developed for investigating life in the universe including some exciting findings have been critically examined. Finally mythology and exotheology about the Universe have been pointed out focusing the future role of where is everyone.

On Low-cost GPS/INS Integration for Footprint Chasing in Bistatic SAR

Stefan Knedlik, Junchuan Zhou, Zhen Dai
Ezzaldeen Edwan, and Otmar Loffeld
Center for Sensor Systems (ZESS), University of Siegen, Siegen 57068, Germany

Abstract— To meet the requirements for footprint chasing in bistatic SAR (to obtain overlapped antenna footprints from transmitter and receiver) at low cost, multiple GNSS receivers/antennas and multiple low-cost sensors (gyroscopes, acceleration sensors) or sensor units (IMUs) and other sensors like barometers and magnetometers can be considered.

In this paper, data fusion approaches based on dynamic modeling and Kalman filtering, which allow optimal integration of redundant position and attitude information, are in the focus.

Advantages and disadvantages of loosely-, tightly-, and deeply-coupled GPS/INS integration architectures (a few possible realizations of integration architectures are shown in Fig. 1) will be indicated and analyzed with respect to attitude and position determination of a SAR antenna mounted on an airplane.

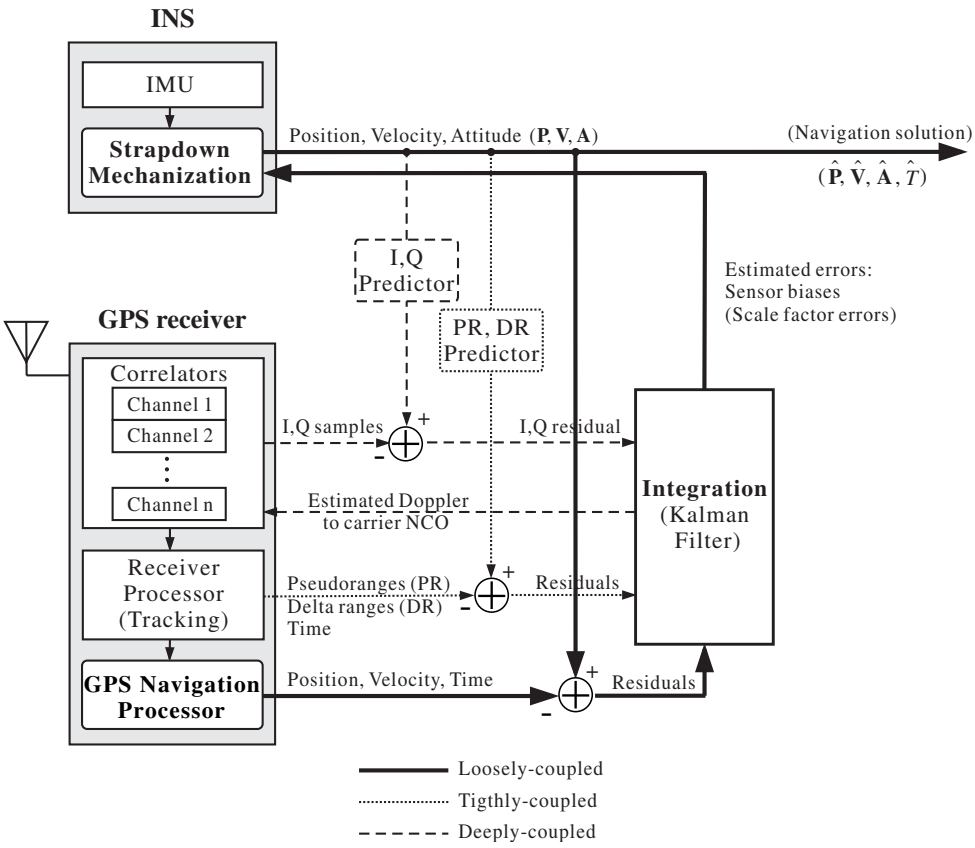

Figure 1: Example GPS/INS indirect feedback integration architectures.

Simulation results which are based on synthetic data (simulated trajectories and proper GNSS and IMU observables), and on experiments using GNSS measurements and an Open Source Software GPS receiver — or using a RF GPS Signal Simulator and a hardware-in-the-loop system-together with synthetic low-cost IMU data, are presented and discussed.

ACKNOWLEDGMENT

Part of the work reported herein has been funded by the German Science Foundation (DFG), grant number KN 876/1-1, which is gratefully acknowledged.

Analysis of Collided Signal Waveform on the Long Transmission Line of UART-CSMA/CD Control Network

Chuzo Ninagawa[1] and Yasumitsu Miyazaki[2]

[1]Mitsubishi Heavy Industries, Ltd., Japan
[2]Aichi University of Technology, Japan

Abstract— UART-CSMA/CD (Universal Asynchronous Receiver Transmitter Carrier Sense Multiple Access with Collision Detection) is a low-cost type of CSMA/CD media access control protocol of digital communication networks for building facility control as shown in Fig. 1. The UART-CSMA/CD protocol must detect signal collisions due to simultaneous transmission from other nodes. In the case of an extremely long transmission line, a collided signal waveform of digital bits may not be simple aggregation of original logical signals because of propagation delays and line terminal reflections. It is very important to predict collided signal waveforms on the transmission line under various conditions, such as the line length or termination reflectivity, before actual installation of a control network transmission line on site.

In this paper, waveforms of collided digital signal bits are analyzed by superposition of step responses of a distributed constant circuit for the transmission line. Instead of using a circuit simulator, we have chosen the analytical method using transient response calculations for fast evaluation. As a model of signal collision, we have calculated collision waveforms of two bit pulse trains with opposite logical levels. That is, while a node is sending a bit train of "Hi-Lo", the node simultaneously receives a train of "Lo-Hi" propagated from another node. Our analysis indicates narrow voltage spikes on the leading edges of bit pulses in the collided waveforms, and the transmission line length and the terminal reflection coefficients affect the width of the spikes. The widths and peaks of the spikes calculated by our analysis were matched with those of experiments as shown in Fig. 2.

In the severe cases of actual applications, the width of the voltage spike might reach significant portion of the bit pulse width. The spikes might cause collision detection failure, and there will be a possibility of causing deterioration of media access performance of the UART-CSMA/CD protocol. Therefore, our analysis is effective to estimate the allowable maximum line length and/or transmission bit rate in order to avoid collision detection failure keeping the communication throughput to the desired level.

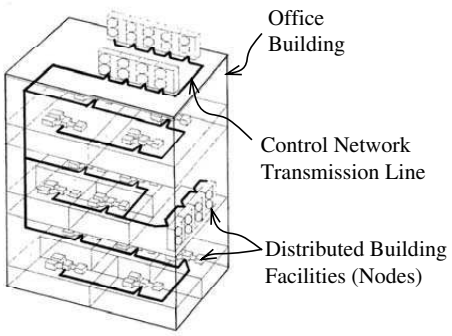

Figure 1: UART-CSMA/CD control network.

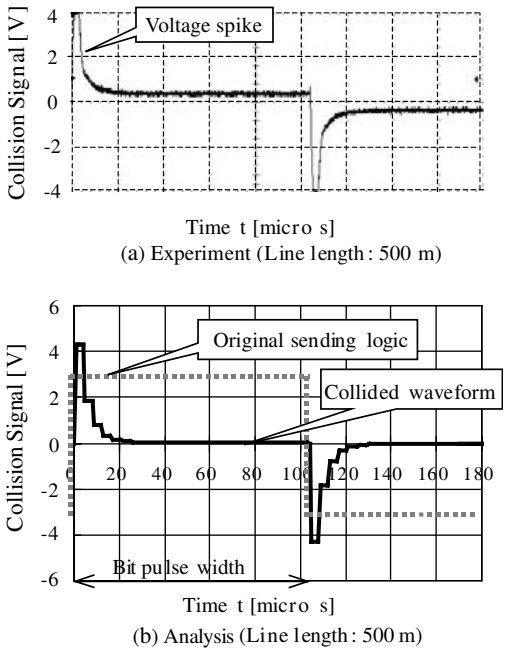

Figure 2: Analysis of collided signal waveforms.

Recognition of Wavelength-multiplexed Labels with Acoustooptic Waveguide Circuit for Hierarchical Photonic Routing

Nobuo Goto[1] **and Yasumitsu Miyazaki**[2]

[1]The University of Tokushima, Japan
[2]Aichi University of Technology, Japan

Abstract— Optical processing for packet routing can overcome bottleneck in large-capacity photonic networks. In label routing networks, various label processing methods have been proposed to use effectively the potential of optical signal processing. We have studied on collinear acoustooptic (AO) switches and applications to optical label recognition. Since parallel combination of collinear AO switches can handle WDM optical pulses, recognition for optical labels encoded in spectral and time domains can be realized. In this paper, we discuss recognition of layer-structure labels for hierarchical routing control.

A configuration of the optical label router is shown in Fig. 1. The extracted label of a packet is optically processed and the label information is used to reconfigure optical switches to forward the packet. We consider M-layer label, where M identifying bits are placed ahead of the routing coded labels. Each of the N_t-bit layered codes has different wavelengths. In the next section, we discuss recognition of the partial label.

An integrated-optic processor consisting of parallel AO switches and delay lines is shown in Fig. 2. The incident label is divided into $N_t + 1$ pulse trains. The layered labels to be matched in this device are represented by frequency-multiplexed SAWs. The label pulse trains are wavelength-selectively switched and the outputs are balanced detected with photodiodes (PDs). The electrical output signals are electrically multiplied. The M matched output pulses correspond to label matching of each layer label.

The recognition characteristics are discussed with computer simulation. It is shown that each layer label can be recognized with the proposed circuit.

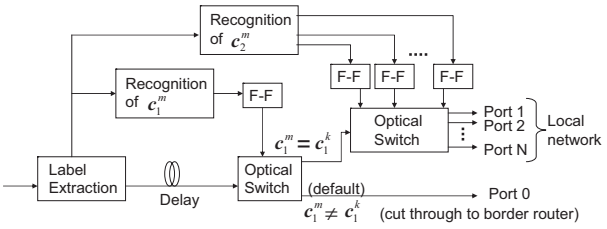

Figure 1: Optical label router with two-layer labels.

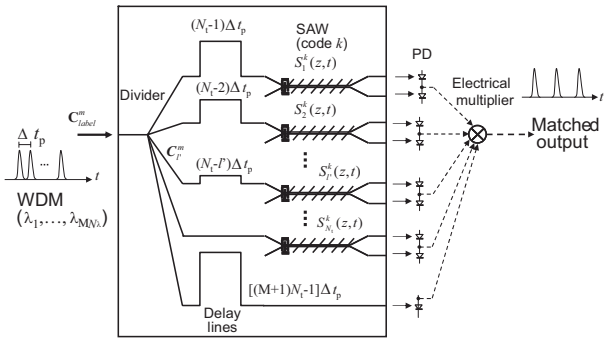

Figure 2: Configuration of collinear AO processor.

Development of Infrared Position Sensitive Detectors

Masafumi Kimata[1], **Takashi Kano**[1], **Masashi Asai**[1]
Akihiro Takahata[2], **Masayuki Morinune**[2], **Hideaki Kusuhara**[2]
Yoshiharu Shimada[2], **Fumio Yoshioka**[2], **Ikuo Yamamoto**[2], **and Masashi Yoshida**[2]

[1]College of Science and Technology, Ritsumeikan University, Japan
[2]Kodenshi Corporation, Japan

Abstract— Uncooled infrared focal plane arrays (IRFPAs) have made a rapid advance in these 10 or 15 years, and their performances have reached levels that are comparable to the second generation quantum IRFPAs. Although efforts are still made to enhance the performance, it seems that they will not impact on unexploited great commercial markets that are not covered by high-price large-format IRFPAs and low-price single-element infrared detectors. To fulfill requirements from the markets, we have developed an uncooled infrared array sensor that is classified into a new category.

The new device is called infrared position sensitive detector (IRPSD). IRPSD is a non-imaging two-dimensional uncooled infrared array sensor. It has two thermometers in each pixel. One thermometer is serially connected in a row and the other is serially connected in a column as shown in Fig. 1. The serial connection of these thermometers produces the sum of signals from all pixels in each row and column. Many infrared applications do not need complete image information, but use some specific characteristics extracted from images. Constructed as shown in Fig. 1, IRPSD can identify the position of a hot (or cold) object and can count the number of hot (or cold) objects in the field of view without digital image processing.

We have developed a thermoelectric IRPSD that has 36 (6×6) 500 μm-square pixels (Fig. 2). We have confirmed that the fabricated IRPSD has successfully performed the position detecting and hot object counting operations. The device exhibited a responsivity of 170 V/W. We have also developed a prototype infrared detection module with this IRPSD.

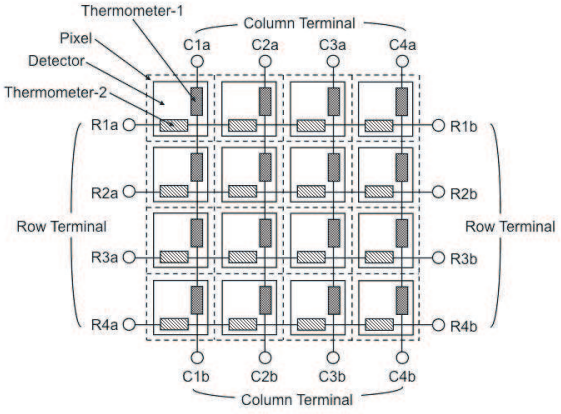

Figure 1: Construction of IRPSD.

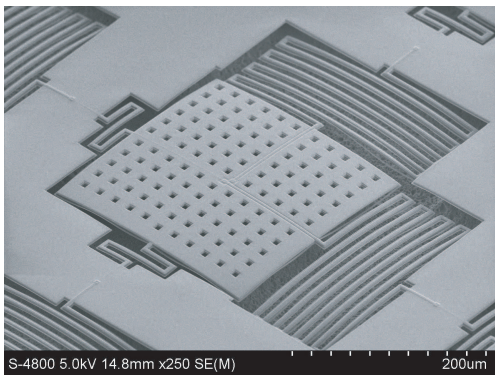

Figure 2: Pixel of thermoelectric IRPSD.

Input Impedances and Bandwidths of Meander Line Antennas with Planar Coupled Parasitic Meander Elements for Compact RFID Tags

K. Taki[1] and Y. Miyazaki[2]

[1]NID Research and Development Department, Brother Industries, Japan
[2]Department of Media Informatics, Aichi University of Technology, Japan

Abstract— Radio frequency identification (RFID) systems are widely used in various applications and small tag antennas are required for on-demand RFID label printing application. An RFID tag consists of an antenna and an IC chip and meander line antennas are an attractive choice in the UHF band, especially below 1 GHz. However, the input resistance of small meander line antennas is too low and it is difficult to achieve direct impedance match to an IC without adding any external matching networks. We have proposed meander line antennas with planar coupled parasitic meander elements in order to increase the antenna input resistance [1, 2].

In this paper, compact meander line antennas having planar coupled parasitic meander elements and short stubs are investigated in order to reduce antenna sizes and to increase bandwidths. As shown in Fig. 1, a parasitic element is placed close to a driven element in the same plane so that the narrower meander sections should be inserted into the meander sections of the driven element except for near the feed point where the parasitic element has straight section. By adding a short stub along the driven meander section having the feed point, proper impedance match is realized between this compact antenna and an IC chip whose input impedance has large capacitive reactance.

The length and width of the area occupied by the antenna were chosen to be $w_0 = 51.5\,\text{mm}$ and $D_0 = 17.5\,\text{mm}$, respectively. The line width of each element was set to be 0.5 mm. Each element is assumed to be lossless and the input impedance was calculated with the method of moment. When $w_1 = 3\,\text{mm}$, $w_2 = 1\,\text{mm}$, $w_3 = w_4 = 2\,\text{mm}$, $D_B = 8\,\text{mm}$ and $D_S = 7\,\text{mm}$ in Fig. 1, the input impedance of $28 + \text{j}86\Omega$ and the larege bandwidth of 45.9 MHz was obtained at 947 MHz. The current distributions along each meander element as well as the input impedances are also investigated for various D_B and D_S of short stubs.

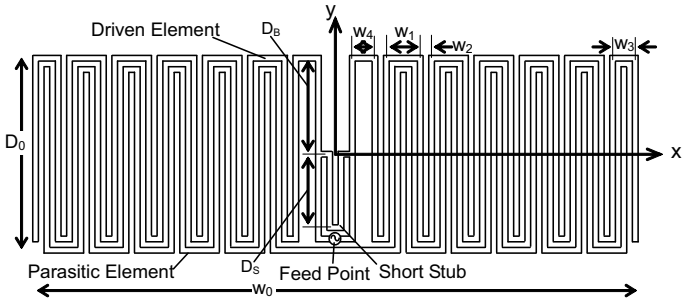

Figure 1: A meander line antenna with a parasitic meander element and a short stub.

REFERENCES

1. Taki, K. and Y. Miyazaki, *Proc. Progress In Electromagnetics Research Symposium*, 256, Tokyo, Japan, August 2006.
2. Taki, K. and Y. Miyazaki, *Proc. Progress In Electromagnetics Research Symposium*, 1700, Beijing, China, March 2007.

Design and Development of A FMCW Ground Based Imaging Radar System

Y. K. Chan, **C. Y. Ang**, **V. C. Koo**, **and C. S. Gan**
Multimedia University, Malaysia

Abstract— This paper describes the design and development of a low cost ground based Frequency Modulated Continuous Wave (FMCW) radar system in Multimedia Univeristy (MMU), Malaysia. In this project, a ground-based fully polarometric, C-band, high bandwidth linear FM-CW and real time imaging radar system is to be designed and constructed. The system should have the capability to measure the complex scattering matrices of distributed targets using FMCW system and the obtained fully polarimetric signals which can be used to provide more accurate identification and classification of the geophysical media.

The purposed system hardware consists of four major sections: an antenna, a radio frequency (RF) subsystem, an intermediate frequency (IF) electronic, and a data acquisition unit (DAU). The purposed antenna system consists of Microstrip based single polarised 2×2 planar antenna. The radiating element will be novel 2×2 planar array configurations which enable the array to scan horizontal and vertical signal. The RF section is constructed in-house from several RF components, which include voltage-controlled oscillator, stable local oscillator, high power amplifier, directional coupler, circulator, RF switches, band-pass filter, isolators, and mixers. In RF section, the received signal is mixed with a portion of the transmitted signal to produce low low frequency IF signals. The IF signals are pre-processed in IF section, before they are digitised in DAU. A mobile personnel computer with analog to digital converter card is used to store the measurement data and process the data on real time basics.

In paper, the high level design will be discussed and detail design parameters will be presented. It followed by radar electronics design, which outlined the detail in radar transmitter and receiver.

Design and Development of a Low Cost Chirp Generator for Airborne Synthetic Aperture Radar

Y. K. Chan and S. Y. Lim
Faculty of Engineering & Technology, Multimedia University
Jalan Ayer Keroh Lama, Bukit Beruang, Melaka 75450, Malaysia

Abstract— An airborne C-band Synthetic Aperture Radar (SAR) has been designed and developed over the past few years as a key geometric data source for environmental monitoring by the Centre for Applied Electromagnetic of Multimedia University (MMU), Malaysia. Several modifications and enhancement are underway on top of the successful construction of the current SAR prototype. The highlight of this continuation work is the hardware implementation of the airborne SAR, specifically on the modifications of the existing SAR sensor microwave transceiver, such as the design and development of one high-speed dual-channel chirp generator using a digital approach. The digital approach is selected over an equivalent analogue solution for its stability, repeatability and flexibility following breakthrough and advancement in the world of digital electronics.

This paper incorporates the simulation, development, and measurement of the output chirp signals of a newly constructed digital chirp generator, the name of which has been personalized from a common term "exciter" to the chirp generator. The primary function of the chirp generator is to generate a coded pulse waveform from a crystal oscillator that allows the input of reference signal from continuous tone STALO output. The pre-stored waveform approach taken to develop the chirp generator is proven at the end of the research to give maximum performance for short pulses.

Electromagnetic Scattering Theory of Car Body Imaging Using Scanning Millimeter Wave Radar

Yasumitsu Miyazaki
Department of Media Informatics, Aichi University of Technology
50-2 Manori, Nishihasama-cho, Gamagori 443-0047, Japan

Abstract— In the ITS, Advanced Information Transport Systems, technical and social subjects of automatic driving system and safety transport and traffic system are very important problems. Automatic driving and cruising systems using microwave and millimeter radars in the cars are sensor systems for measurements of distances among driving cars, detection of obstacles, and intelligent recognition of road environments [1–3]. Millimeter wave radar of short wavelengths and high frequency using short pulses of millimeter wave carriers yield precise distance measurement and image processing. ITS applications of millimeter wave radar are distance control system between driving automobiles, and auto-breaking system. Distance measurement using short pulse millimeter carriers are derived by time differences between transmitted pulse and received pulse, and image information are given by reflected waves by scanning millimeter beam waves, like optical vision information. Comparing with optical waves, millimeter waves have less attenuation characteristics due to rains, mist, fog, and snows, and can give millimeter size resolution. Shape image recognition systems of car bodies receiving scattered and reflected waves in scanning millimeter radars, are very useful for ITS. Temporal and spatial characteristics of electromagnetic scattering and reflection by driving car bodies are studied. Fundamental characteristics and application of scanning millimeter wave radars of synthetic aperture type and multi-wavelengths for image recognition of car body are shown.

Radiating millimeter beam packets from scanning millimeter radars and reflected beam packets of temporal Gaussian pulse form and spatial Gaussian beam form are expressed as Fourier components for time coordinates and as spectral functions expanded by Hermite-Gaussian functions for space coordinates [4]. Incident, reflected and scattered fields are studied using beam mode expansions derived by Hermite-Gaussian spectral functions. Boundary conditions of car bodies are applied to derive reflected and scattered field for spectral components. Car body imaging is analyzed by the Synthetic Aperture Radar Method. Correlation functions by transmitted and received fields yield image processing information for transverse image patterns at each driving time. Velocities of cars are given by frequency variations of received fields. Scanning millimeter wave radar in the front of car radiating short Gaussian pulse and forward Gaussian beam can construct spatial image at each time analyzing reflected and scattered waves by other cars and objects on the road. Based on this fundamental theory, safety driving systems may be constructed.

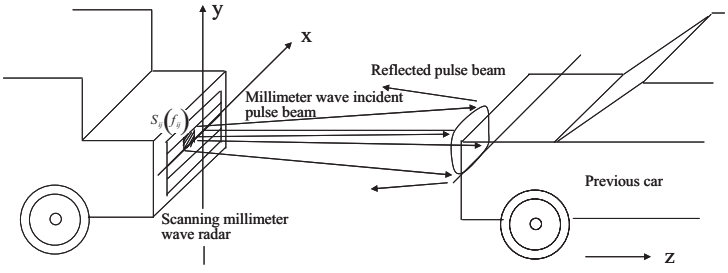

Figure 1: Scanning millimeter wave radar and car body imaging.

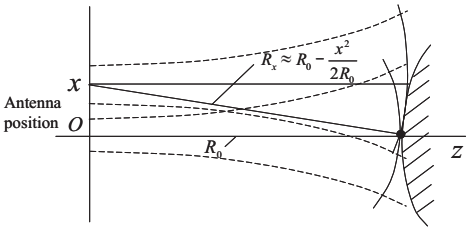

Figure 2: Antenna position and distances to cars.

REFERENCES

1. Tanaka, M. and Y. Miyazaki, *Trans. of IECE Japan*, Vol. 66-B, No. 8, 1005–1012, 1983.
2. Miyazaki, Y., *Proc. of OFSET 2000*, 361–364, 2000.
3. Takahashi, K. and Y. Miyazaki, *Trans. IEE Japan*, Vol. 120C-1, No. 1, 111–116, 2000.
4. Miyazaki, Y. and Y. Akao, *Trans. of IECE Japan*, Vol. 51-B, No. 1, 25–31, 1968.

FDTD Analysis of Electromagnetic Wave Propagation for Out-door Active RFID System

Yasumitsu Miyazaki[1], **Tadahiro Hashimoto**[2], **and Koichi Takahashi**[1]

[1]Department of Media Informatics, Aichi University of Technology
50-2 Manori, Nishihasama-cho, Gamagori 443-0047, Aichi, Japan
[2]Broadband Technology Department, Synclayer, Inc.
1-20 Himegaoka, Kani 509-0249, Gifu, Japan

Abstract— In recent years, RFID systems have received much attention in security, logistics and medical fields. However, most of these systems are used at in-door and the RF tags are passive tags that are controlled by reader. Security and protection systems in urban streets for school children can be constructed by RFID systems. We consider to use active RFID system of very weak UHF electromagnetic waves at out-door [1–3]. In this paper, we describe the characteristics of electromagnetic wave propagation by RF tags using FDTD method [4]. The reader of active RFID system receives periodic weak electromagnetic wave pulses of UHF carrier band from multiple tags and recognizes multiple tags. In order to correctly estimate the position when the reader of active RFID system receives transmitted signal from many tags, numerical simulation results of electric field intensity are studied. We considered to build human identification system for elementary schoolboys and schoolgirls by active RFID using UHF band. In transmitting and receiving points of the weak electromagnetic wave, receiving characteristics are influenced by the street environment of RF tags and readers. We consider the road models as this environment. RF tags are carried by the human on the road, and the readers are installed on the electric pole and connected to the cable network. Therefore, understanding of out-door propagation characteristics of RFID is necessary to develop high performance antenna of reader. In this paper, FDTD method is applied to show the propagation characteristics of RFID tags. The radiation field generated at tag locations on the road, which leads to weak intensity of electric fields at the position of reader are investigated.

As numerical examples, the analysis models for several types of roads are shown in Figure 1. These models are consisting of the straight road, the T-type road (a) and the cross road (b). The parameters of the straight road are length L and width W, and the parameters of the T-type and cross roads are horizontal length $L1$ and width $W1$ and vertical length $L2$ and width $W2$. In Figure 1, the points A, B and C indicate the positions of receiving reader antennas and the point Ts indicates the position of one tag. Transmitted wave is a modulated Gaussian pulse with carrier frequency of UHF band 300 MHz with pulse width of 30 nsec. Ni and Nj of $10^3 \times 10^3$ are number of divisions in x and y direction. The walls of the road are considered to be perfect conducting plane or concrete.

In this paper, propagation of electromagnetic wave transmitted from RF tag is analyzed and the intensity of electric field in several types of roads is shown numerically using FDTD method. These characteristics are very significant for optimum design of RFID systems. As a next step, we perform field experiments using actual tags and compact reader in out-door and compare numerical results of three dimensional simulations with the experimental results. These results yield basic foundation for the design of RFID system, and system design of resolving collision problems for multiple pulses.

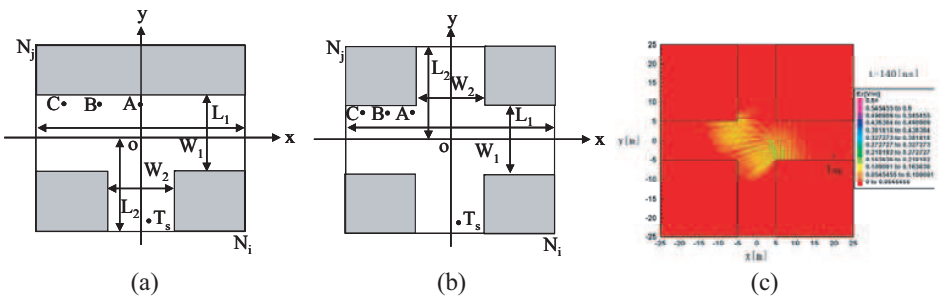

Figure 1: Analysis models and fields for FDTD method. (a) T-type road model, (b) Cross road model, (c) Field intensity, $t = 140$ (ns).

REFERENCES

1. Masuda, T. and Y. Miyazaki, *Trans. IEE Japan*, Vol. 118-C, No. 1, 112–117, 1998.
2. Taki, K. and Y. Miyazaki, *PIERS Proceedings*, 256, Tokyo, Japan, 2006.
3. Masuda, T., Y. Miyazaki, and Y. Kashiwagi, *PIERS Proceedings*, 1713–1715, Beijing, China, March 26–30, 2007.
4. Rodriguez, G., Y. Miyazaki, and N. Goto, *IEEE Trans. on Antennas and Propagation*, Vol. 54, No. 3, 785–796, 2006.

Session 4A5
Antenna Theory and Radiation, Microstrip and Printed Antennas 1

The Effect of Shorting Post on Axe-shaped Circular Antenna Miniaturization

Jingxian Liu[1], **Salman Naeem Khan**[2], **and Sailing He**[1,3]
[1]Centre for Optical and Electromagnetic Research
Zhejiang University, Zijingang Campus, Hangzhou 310058, China
[2]Department of Physics, COMSATS Institute of Information Technology
Defense Road, Off Raiwind Road, Lahore, Pakistan
[3]Division of Electromagnetic Engineering, School of Electrical Engineering
Royal Institute of Technology, S-100 44 Stockholm, Sweden

Abstract— An edge shorted circular axe-shaped patch antenna is studied for miniaturization. The effects of the location and number of shorting post on the resonance frequency, impedance match and radiation pattern are studied. By inserting a shorting post near the edge of circular axe-shaped patch, the antenna size (resonance at 1.36 GHz) reduced about is 72% compared to the antenna without shorting post (resonance at 2.58 GHz) and 91% compared to the conventional circular antenna (resonance at 4.6 GHz). Parametric analysis for the lowest resonant frequency is studied by moving the shorting post from the center to the edge of the patch. Parameters such as the distance between feeding point and shorting post, the number of shorting posts and the post radius are optimized for the best impedance match. Compared with placing the shorting post near the center, the edge shorted antenna has a 76% frequency reduction. The result shows that by putting a shorting post near the edge of the axe-shaped circular patch, the resonance is lower than adding a post near the center. Meanwhile, the feed should be excited near the shorting post for better impedance match.

The effect of increasing number of shorting post is also studied. If the number of shorting posts is changed from 1 to 3, the resonant frequency is 1.48 GHz, which is higher than that with only one shorting post. However, the design offers stable resonant frequency and broadside radiation pattern.

Microstrip Slot Antenna with a Finite Ground Plane for 3.1–10.6 GHz Ultra Wideband Communication

Huan-Cheng Lien[1], **Yung-Cheng Lee**[1], **Wen-Fei Lee**[2], **and Huei-Chiou Tsai**[2]

[1]Department of Security Management, WuFeng Institute of Technology, Taiwan
[2]Department of Electrical Engineering, WuFeng Institute of Technology, Taiwan

Abstract— This paper introduces an Ultra Wideband microstrip Slot Antenna (UWSA) conformed to craving for the band of IEEE802.15.3a UWB (3.1 GHz ∼ 10.6 GHz) communication. In this paper, the design for enhancing impedance bandwidth of wideband microstrip slotting antenna with a finite ground plane is proposed and studied. With this design, a matching impedance bandwidth (SWR ≤ 2) about of more than 146% was achieved; as a result, the bandwidth can be located at the wireless communications from 2.3 GHz to 12 GHz. The variations of gain are changing from 0.2 to 6.98 dBi. In addition, the design has been a planar profile and it can easily be integrated in small mobile units; besides, it also can be in the laptops or various remote-sensing devices etc..

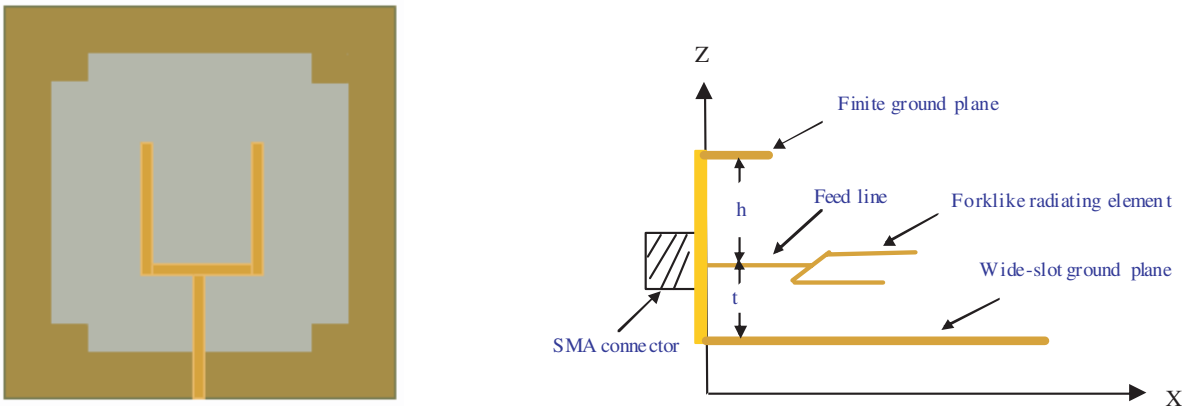

(a) Top view (b) Side view

Figure 1: The configuration of the wideband slot antenna with a finite ground plane.

Centerline Longitudinal Shunt Slot Excitation by Parabolic Shaped Single Ridge Waveguide

M. Moradian, **M. Khalaj-Amirhosseini**, **and M. Tayarani**
Department of Electrical Engineering, Iran University of Science and Technology
Narmak, Tehran 16846-13114, Iran

Abstract— Application of V-shaped ridge waveguide is presented for excitation of a centreline longitudinal shunt slot antenna. The proposed method is realized by adding V-shaped to the ridge of the single ridge waveguide. The V-shaped ridge is placed exactly under the longitudinal slot and the slot is place along centreline of the waveguide. It is shown that for a typical slot, the slot normalized conductance can be increased by increasing the V-shaped depth. The simulation results show that the proposed structure can be considered as a proper candidate for replacing the conventional longitudinal shunt slot.

Introduction: The slotted waveguide array is widely used in radars and communication duo to its simple feeding, easy manufacture, precise control of aperture distribution and low loss. Among all kind of slot antenna, longitudinal shunt slot antenna has been the most frequently used antenna for its pure linear polarization. However, despite its advantages, the conventional longitudinal slot antenna has several shortcomings. Its basic drawback is the appearance of second-order beams off the principal planes which are usually called butterfly lobes [1, 2]. These second-order beams decrease the antenna efficiency and increase the susceptibility of the radar to jamming. Therefore, it is desirable to eliminate these second-order beams.

The second-order beams are associated with the alternating offset of successive slots which is essential in order to avoid the grating lobe appearance. The alternating offset of the successive slots and consequently the second order beams can be eliminated by filling the waveguide with dielectric and selecting the spacing between the radiating elements equal to one guided wavelength instead of one half guide wavelength [2]. However this method adds extra loss and is difficult to realize.

Some methods have been proposed in the literature to suppress the second-order beams. Applying the corrugated narrow wall make it possible to form a collinear array of slots and eventually second order beam suppression [3]. The alternating offset of successive slots can be avoided by exiting the slot with an iris [4]. Placing finite length parallel plate on both side of the one half guide wavelength spacing radiating slots are also an effective way to produce tolerable uniform E-field and eventually suppression of the second-order beams [2, 5].

Application of V-shaped ridge waveguide fed slot arrays is presented. The proposed structure is realized by adding the V-shaped to the ridge of the single ridge waveguide. The V-shaped ridge is placed exactly under the slot. It can be shown that the radiation characteristic of the slot can be varied by changing both slot length and V-shaped depth. Applying the proposed method not only eliminate the required offset but also has the advantage of ridge waveguide in reducing the required waveguide width.

REFERENCES

1. Kurtz, L. A. and J. S. Yee, "Second-order beams of two dimensional slot arrays," *IRE Trans.*, Vol. AP-5, 356–36, 1957.
2. Forooraghi, K. and P.-S. Kildal, "Transverse radiation pattern of a slotted waveguide array radiating between finite height baffles in terms of a spectrum of two-dimensional solutions," *Proc. Inst. Elec. Eng., pt. H, Microwaves Antennas and Propagation*, Vol. 140, No. 1, 52–58, Feb. 1993.
3. Guenberg, H., "Second-order beams of slotted waveguide arrays," *Can. J. Phys.*, Vol. 31, 55–69, 1953.
4. Dudley, D. G., "An iris-excited slot radiator in the narrow wail of a rectangular waveguide," *IRE Trans.*, Vol. AP-9, 361–364, 1961.
5. Rengarajan, S. R., "Mutual coupling between waveguide-fed transverse broad wall slots radiating between baffles," *Electromagnetics*, Vol. 17, No. 5, 421–435, 1997.

A New Algorithm about Extrapolating Near Distance Field to Far-field of Large Size Antenna

N. J. Li[1, 2], **C. F. Hu**[1, 2], **J. D. Xu**[1], **and L. X. Zhang**[2]

[1]Electronic Engineering Department
Northwestern Polytechnic University, China
[2]UAV Specialty Technique Key Laboratory of Nation
Northwestern Polytechnic University, China

Abstract— In order to meet the approximate plane-wave irradiation condition, adequate large field or compact range system is needed for antenna pattern measurement, especially for large size antenna, an outside testing field site or a compact range system is very expensive. Near-field planar scanning system is another method, however it is time-consuming and only suited for directional antenna. In this paper, a new extrapolating technique by connecting near-distance field with far-field of large-size antenna is set up. If a large size antenna is short in vertical plane, its irradiating field in horizontal plane can be respected as cylinder wave distribution, an ideal aperture as a reference irradiating source is utilized, which width is the maximum size of the tested antenna. By the ideal aperture a phase-correction coefficient $g(x)$ connected spherical and plane wave can be deduced, which can be used to calculate the far-field of the tested antenna. In fact the convolution calculation between $g(x)$ and near-field can be replaced by Fast Fourier Transform, thus the calculating procedure could be completed simply and quickly. By theoretical simulation for a simple long antenna, the pattern extrapolated can be obtained correctly. Experimental results of complex antenna show that this new technique makes experiment agree to theory precisely, moreover, it permits the measurement distance reduced by 15 percent of the minimum distance of far-field. Also, there is no serious limitation of measurement for antenna in dimension of aperture and depth.

Planar Antenna Array Mutual Coupling Identification: A Direct Method Applied to Quasi-Yagi Elements

C. E. Capovilla[1], **A. Tavora A. S.**[1], **S. E. Barbin**[2,3], **and L. C. Kretly**[1]
[1]Department of Microwaves and Optics, School of Electrical and Computer Engineering
University of Campinas, Brazil
[2]Department of Telecommunications and Control Engineering, Polytechnic School
University of Sao Paulo, Brazil
[3]Center for Information Technology Renato Archer, Campinas, Brazil

Abstract— Mutual coupling between radiating elements is a critical issue for the design of antenna arrays. In this way, it is important to determine the influence of each type of coupling mechanism on the total mutual coupling. With this objective, surface waves and free space coupling were analyzed for an array of two identical quasi-Yagi antenna elements, aiming at proposing an optimization procedure for the structure. The quasi-Yagi antenna was chosen since it satisfies many requirements of modern communication systems such as small dimensions, reasonable wideband gain, and multi-band operation capability. Also its radiation pattern shows excellent stability over the entire operation band. Four array prototypes, including special details, were built and tested, with antenna elements placed in line and side by side. The prototypes were fabricated using FR-4 with $\varepsilon_r = 4.4$ and 1.6 mm thickness and operate at the ISM band 2.4–2.5 GHz. The design and optimization of the quasi-Yagi antenna elements is reported in [1]. The array was exhaustively simulated for several distances between the elements, aiming at reaching optimal performance. Small distances generate strong mutual coupling, degenerating the array overall performance, while great spaces favor the appearance of secondary lobes in the radiation pattern. In this work, a distance of $\lambda_0/2$ was adopted between the extremities of the adjacent drivers. The first prototype is a conventional array, without any modification in the structure. The second prototype, designed for analyzing the coupling of superficial waves excited by the feeding lines, has a cut in the ground plane between the elements, in order to suppress the waves [2]. The ideal opening length was experimentally found to be 15 mm. The third prototype was designed to investigate the mutual coupling due to superficial waves excited directly by the antennas and has an opening in the substrate. Finally, the last prototype was designed to test both effects together and has openings in the ground plane and in the substrate. The mutual coupling effects were observed using a ZVRE network analyzer from Rhode & Schwarz. The behavior of the first and the third prototypes is almost the same for the whole operation band, which means that the superficial waves excited directly by the antennas do not significantly influence the mutual coupling in the array. The second and fourth prototypes show the same behavior, presenting only small differences in comparison with the first and the third prototypes. One concludes that the mutual coupling in quasi-Yagi antenna arrays happens mainly through the free space i.e., superficial waves do not have significant influence on the coupling level. No changes in the elements structure are then necessary for the design of a quasi-Yagi antenna array; only correct positioning and appropriate feeding lines are required.

REFERENCES

1. Kretly, L. C. and C. E. Capovilla, "Analysis of radiation patterns and broad-band characteristics of a novel quasi-yagi antenna array for wireless communications," *IEEE International Symposium on Wireless Personal Multimedia Communications*, Vol. 03, 440–443, October 2003.
2. Song, H. J., M. E. Bialkowski, and P. Kabacik, "Parameter study of a broadband uniplanar quasi-yagi antenna," *13th International Conference on Microwaves, Radar and Wireless Communications*, Vol. 01, 166–169, 2000.

Study of High T_c Superconducting Microstrip Antenna

T. Fortaki[1], **M. Amir**[1], **S. Benkouda**[1], **and A. Benghalia**[2]

[1]Electronics Department, University of Batna, Algeria
[2]Electronics Department, University of Constantine, Algeria

Abstract— In the last years, a growing interest has been observed in the development and use of new materials in microwave and millimeter wave technologies. Some high T_c superconducting materials can be deposited in a thin film form on appropriate dielectrics, which makes them very suitable for microwave and millimeter-wave device applications. Advantages of using high T_c superconducting materials at high frequencies include [1]: 1) very small losses, which means reduction of attenuation and noise level; 2) very small dispersion up to frequencies of several tens of GHz; 3) smaller devises due to the lower losses, which leads to larger integration density; and 4) the propagation time can be greatly reduced because of the smaller size and the shorter interconnects. In the literature, the studies concerning the resonance characteristics of microstrip antennas using perfectly conducting patches are abundant. However, few works have been done for the case of microstrip antennas using superconducting patches. The determination of the resonant frequencies of superconducting antennas was initially carried out by means of the cavity model [2]. Later on, these resonant frequencies were obtained by using the rigorous full-wave analysis [3]. To validate the theoretical analysis, the authors in [3] have compared their numerical results with the experimental data of Richard et al. [2]. This comparison has not been done in a convenient way for two reasons: the variation of the permittivity of the lanthanum aluminate substrate with the variation of the temperature, as indicated by the experiment of Richard et al. [2], has not been take into account by Silva et al. [3] and the effect of varying the temperature on the resonant frequency is insignificant. In this paper, we present a theoretical and numerical analysis of the resonant frequencies of high T_c superconducting rectangular microstrip antennas which yields excellent agreement with the measured data of Richard et al. [2]. To include the effect of the superconductivity of the microstrip patch in the full-wave analysis, a surface complex impedance is considered. This impedance is determined by using London's equation and the model of Gorter and Casimir [4]. Numerical results for the effect of the temperature on the resonant frequency and half-power bandwidth of superconducting microstrip antennas are given. Finally, the influence of the thickness of the high T_c superconducting film on the resonant frequency is also presented.

REFERENCES

1. El-Ghazaly, S. M., R. B. Hammond, and T. Itoh, "Analysis of superconducting microwave structures: application to microstrip lines," *IEEE Trans. Microwave Theory Tech.*, Vol. 40, No. 3, 499–508, 1992.
2. Richard, M. A., K. B. Bhasin, and P. C. Claspy, "Superconducting microstrip antennas: an experimental comparison of two feeding methods," *IEEE Trans. Antennas Propagat.*, Vol. 41, No. 7, 967–974, 1993.
3. Silva, S. G., A. G. d'Assuncao, and J. R. S. Oliveira, "Analysis of high T_c superconducting microstrip antennas and arrays," *Proceedings of SBMO/IEEE MTT-S IMOC*, 243–246, 1999.
4. Gorter, C. J. and H. B. G. Casimir, "The thermodynamics of the superconducting state," *Physik. Z.*, Vol. 35, 963–966, 1934.

Directivity Enhancement of Microstrip Patch Antennas Using a Dieletric Superstrate

Yanfei Li[1], **Raj Mittra**[2], **Guizhen Lu**[1], **and Wenhua Yu**[1, 2]

[1]Information Engineering School, Communication University of China, Beijing 100024, China
[2]Electromagnetic Communication Laboratory, 319 EE East, The Pennsylvania State University University Park, PA16802, USA

Abstract— In this paper, we present a systematic design methodology for enhancing the directivity of microstrip patch antennas (MPAS), by using it as an exciter of a Fabry-Perot (FP) resonant cavity. The design procedure involves three steps: (i) determing the resonance frequency of the empty cavity, with the MPA removed, when operating in the receive mode; (ii) designing the patch antenna to operate at the same frequency in the presence of the superstrates; (iii) finally, we operate the composite system in the transmit mode to investigate its aperture distribution that provides us a clue for enhancing the directivity. We show that the directivity can be enhanced by more than 8 dB, over that of the MPA without the superstrate, by using either planar or curved superstrates as covers for the MPA.

Dual-band Dual-polarized Dielectric Resonator Antenna Array for SAR Applications

Xiao-Rong Tang, **Shun-Shi Zhong**, **Zhu Sun**, **and Jian-Jun Liu**
School of Communication and Information Engineering
Shanghai University, Shanghai 200072, China

Abstract— The modern synthetic aperture radar (SAR) systems require advanced antennas operating at multi-bands with multi-polarization shared a single aperture. In the last decade, a great deal of research has been devoted to enhance the performance of bandwidth, polarization purity, efficiency, and so on. Historically, Slotted waveguide arrays have used as SAR antennas, which is bulky, difficult for multi-bands, then some dual-band dual-polarized (DBDP) microstrip antenna arrays have been proposed.

The dielectric resonator antenna (DRA) has been widely discussed since it first reported in 1983. The DRA offers many attractive qualities, such as small size, low-cost, ease of excitation, no conductor loss, no dielectric loss and no surface wave excitation. Some papers have studied on the dual-polarized DRA in the past decade. In this paper, a novel design of dual-band dual-polarized DRA array for SAR application is presented. Microstrip dipoles and square DRA are used as the radiating elements at S- and X-band, respectively. For X-band, the hybrid feed technique is used to provide two orthogonal polarization. For S band, two separate single Microstrip dipoles are used to generate the horizontal and vertical polarization. The rectangular element of S band is narrow to decrease the mutual coupling with the adjacent X-band DRA. The balanced probe feed is used to achieved the symmetrical pattern and lower cross-polarization level. Since the array is scanning to 30° in azimuth and elevation both, the X-band element spacing is about $0.64\lambda_1$ at 9.6 GHz, and the S-band element spacing is triple the X-band one, about $0.61\lambda_2$ at 3 GHz. As a test model, interlaced S-band 1×1 elements and X-band 4×4 elements are used to form a share-aperture antenna array.

Results show that the antenna has isolation of 30 dB and cross-polarization level of −38 dB below the co-polarization for dual-band both. The peak gain reaches 6.5 dB in each port. Its return loss is less than −10 dB for the impedance bandwidth of 5.3% (2.92–3.08 GHz) for S-band and 9.4% (9.2–10 GHz) for X-band. The antenna has advantages such as small size, simple structure, low cost, perfect polarization purity and easy to expand into a large array. Thus it is promising candidate for the SAR application.

ACKNOWLEDGMENT

This work was supported by the National High-technology Research and Development (863) program of China, under Grant No. 2007AA12Z125, the Specialized Research Fund for the Doctoral program of High Education of China, under Grant No. 20050280016, and 2008 Shanghai University Graduate Innovation Fund.

Design and Properties of Compact Multimode Antennas for Diversity Applications

Heinz J. Chaloupka[1] **and Ludger Klinkenbusch**[2]
[1]Bergische Universität Wuppertal, Wuppertal, Germany
[2]Christian-Albrechts-Universität zu Kiel, Kiel, Germany

Abstract— For wireless digital communication links operating in a multi-path propagation scenario the use of multiple antennas at the receiver (RX) or/and transmitters (TX) is known to be an effective mean to increase the capacity efficiency (bits/sec/Hz). Examples of application range from signal-to-noise enhancement with RX antenna diversity (e.g., maximum ratio combining) to spatial multiplexing or space-time-coding enabled by multiple-input multiple-output (MIMO) systems.

This paper presents a novel concept for the realization of multiple antennas in case of a seriously limited platform size, e.g., in case of handheld mobile terminals like cellular phones and personal digital assistants (PDA).

The conventional approach is based on a group of M separate antennas, localized at different positions and/or with different polarization. Due to the limited space of the antenna platform relatively strong mutual coupling between co-polarized elements becomes unavoidable and leads to performance degradations with respect to matching efficiency and antenna correlation.

In order to gain a more appropriate solution for a compact M-port antenna one has to recall that there is no need to use decoupled antenna elements, but to decouple the antenna ports. Based on this fact one ends up with a general antenna structure which possesses multiple ports where any of these is in principle allowed to excite the entire antenna structure, provided that suitably defined equivalent current distributions corresponding to different ports are mutually orthogonal. It has been shown that the latter condition ensures isolated (decoupled) antenna ports. This type of multiple antenna system will be referred to as a multimode antenna.

The important feature of a multimode antenna, namely that each port uses the entire structure (including housing of the terminal) as radiating structure, is shown to allow (for a prescribed frequency bandwidth and a given number M of ports) for a higher degree of miniaturization than the conventional approach with quasi-decoupled separated antenna elements. This result is derived by applying general results [1] on the radiation quality factor of each term of a spherical-multipole field expansion to the multi-port antenna structures considered in this paper.

In order to allow an exploitation of the multimode antenna concept, systematic design procedures are needed. Two different approaches for finding multimode structures with isolated ports will be reported. The first approach is based on the eigenmode representation and was already used to design a compact three-port antenna [2]. The second design approach is based on a systematic introduction and adjustment of reactive loads. Examples for the application of both design concepts will be given.

REFERENCES

1. Yaghjian, A. D. and S. Best, "Impedance, bandwidth and Q of antennas," *IEEE Trans. Antennas Propagat.*, Vol. 53, 1298–1324, April 2005.
2. Eßer, D. and H. J. Chaloupka, "Design approach for a class of compact multiport antennas," *Proc. IEEE 2005 Int. Symp. on Microwave, Antenna, Propagat. and EMC Technol. for Wireless Commun. (MAPE 2005) Proceedings*, Vol. 2, 144–147, 2005.

Miniaturized Multimode Antenna Array for 2×2 MIMO Systems

Rashid A. Bhatti, **Nguyen Ngoc Anh**, **and Seong-Ook Park**
Information and Communications University (ICU), Daejeon, Korea

Abstract— Modern personal wireless communication devices are expected to support various high data rate communication services at multiple frequency bands. Multiple-input multiple-output (MIMO) communication techniques with multiple antennas at both the transmit and receive sides have shown potential to enhance the channel capacity and can be realized in small portable communication terminals. Such high performance MIMO-enabled communication devices require miniaturized multiband antenna arrays with low mutual coupling, low envelop cross-correlation, high mean effective gain (MEG), and high radiation efficiency for high capacity performance. In this paper, design of a dual-element multimode antenna array for MIMO-enabled handsets has been reported. The antenna array can operate at four frequency bands centered at 2.45 GHz, 3.5 GHz, 5.2 GHz, and 5.8 GHz with reasonable return loss and high isolation across each band. Each element in the array is designed within a volume of $11.50 \times 13.80 \times 4.0\,\text{mm}^3$ and is placed at the corner of a ground plane measuring $50 \times 100\,\text{mm}^2$. A conventional single-band planar inverted-F antenna (PIFA) is modified by introducing two slots in the structure realizing operation at three frequency bands. A quarter-wave resonator is integrated into the structure for the forth resonance. Additionally, a matching stub is used to optimize impedance matching in the high frequency bands. SMA connectors have been used to feed each element in the array from the bottom side of the ground plane. Due to the presence of ground plane underneath, the antenna is expected to exhibit low specific-absorption-rate (SAR) and will allow placement of electronic components below the antenna on back side of the ground plane without experiencing the undesired detuning effects. A prototype antenna array is fabricated and measured to validate the predicted results. The simulated and measured scattering parameters of the array are in good agreement. The MEG and envelop correlation analysis using 3-D radiation patterns have been included and discussed in the paper.

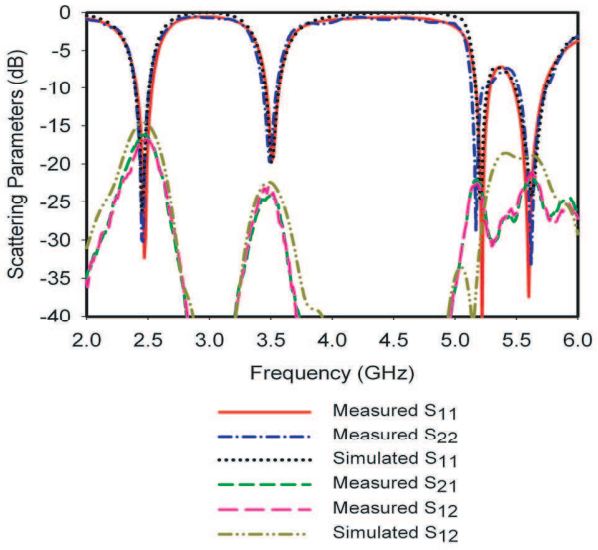

Figure 1: Comparison of the measured and simulated scattering parameters.

Session 4A6a
Scattering, and Inverse Scattering

On the Concept of Vector (Polarization) Electromagnetic Inverse Boundary Conditions for the Perfectly and Imperfectly Conducting Cases and Its Applications: Why Is Renewed Interest in EM-IBC Forthcoming?

Wolfgang-Martin Boerner[1] **and Harinder P. S. Ahluwalia**[2]

[1]ECE/CSN Laboratory, University of Illinois at Chicago, USA
[2]Info-Electronics Systems Inc., Canada

Abstract— The inverse problem of electromagnetic scattering pertains to the problem of recovering the size, shape, material surface and interior constituents of an unknown scatterer, given the incident and the scattered fields every where, together with the laws governing the interaction. In the direct problems of scattering and diffraction, the electric size, the shape and the material surface and interior constituents are known *a priori* together with the pre-specified incident field in terms of a computational coordinate system so that their unknown vector electric and vector magnetic fields can be derived from Maxwell's equations by incorporating the known parameters into the boundary conditions which are well established. In contrary, in the inverse problem such local boundary conditions must be sought which *in particular* do not depend on either the size, shape or the surface normal and material properties of the scattering body and its enclosing surface, but must allow to specify these parameters uniquely from the recovered near fields.

Here two separate cases are considered, a perfectly and an imperfectly conducting closed-shaped smooth body for which the total complex vector electric fields $\mathbf{E} = \mathbf{E}^{inc} + \mathbf{E}^{scat}$ and $\mathbf{H} = \mathbf{H}^{inc} + \mathbf{H}^{scat}$ are assumed to be given everywhere and expressed in terms of a computational coordinate system, where for a

1. Perfectly conducting closed-shaped, convex and smooth body, the following inverse boundary conditions hold

$$\mathbf{E}\cdot\mathbf{H} = 0 \quad \text{and} \quad \left|\mathbf{E}^{inc}\right| = \left|\mathbf{E}^{scat}\right| \qquad \text{necessary and sufficient} \tag{1}$$

$$\mathbf{E}\times\mathbf{E}^{*} = 0 \qquad \text{necessary and not locally sufficient} \tag{2}$$

2. Imperfectly conducting closed-shaped, convex and smooth body, for which the following inverse boundary conditions are derived from the Leontovich direct boundary condition

$$\mathbf{E}\times\hat{n} = \eta\hat{n}\times(\mathbf{H}\times\hat{n}) \tag{3}$$

where $\hat{n}$ denotes outward local surface normal, η defines the local normal Leontovich surface impedance

By inverting this Equation (3), two characteristic orthogonal vector quantities, $\mathbf{A}$ and $\mathbf{B}$, are obtained which are tangential to the local surface and independent of its local normal

$$\mathbf{A} = \mathbf{E}\times\mathbf{E}^{*} - \eta\eta^{*}\mathbf{H}\times\mathbf{H}^{*} \quad \text{and} \quad \mathbf{B} = \eta\mathbf{E}^{*}\times\mathbf{H} - \eta^{*}\mathbf{E}\times\mathbf{H}^{*} \tag{4}$$

Satisfying the following three necessary but not locally yet globally sufficient conditions

$$\mathbf{A}\cdot\mathbf{B} = 0 \qquad \text{orthogonality condition} \tag{5a}$$

$$\mathbf{A}^{2} = \mathbf{B}^{2} \qquad \text{normality condition} \tag{5b}$$

$$\hat{n}\cdot\mathbf{A} = 0 \quad \text{and} \quad \hat{n}\cdot\mathbf{B} = 0 \qquad \text{tangentiality condition} \tag{5c}$$

These two sets of boundary conditions are tested for the case of cylinders and spheres of different radii and for two slightly different frequencies for verifying that these conditions are indeed satisfied for (i) the perfectly conducting and (ii) the imperfectly conducting cases explaining why these conditions are exact, and why all of these conditions are necessary but some of the conditions are not locally but only globally sufficient.

Although attempts had been made soon after these vector inverse electromagnetic boundary conditions were first discovered forty years ago, verifying them with experimental data was not possible at that time due to the lack of measurement capabilities and accuracy. However, within the past decade this has changed and sufficiently accurate measurement data for near and far field measurements are now becoming available for testing them which is of considerable relevance to non-destructive material testing and also for advancing vector electromagnetic inverse scattering theory and techniques.

REFERENCES

1. Boerner, W.-M. and V. H. Weston, "A bistatic electromagnetic inverse scattering technique," *Canadian Journal of Physics*, Vol. 47, No. 11, 1177–1184, 1969.
2. Boerner, W.-M. and H. P. S. Ahluwalia, "On a continuous wave electromagnetic inverse boundary condition," *Canadian Journal of Physics*, Vol. 50, No. 23, 3023–3061, 1972.
3. Boerner, W.-M. and H. P. S. Ahluwalia, "Application of a set of electromagnetic inverse boundary conditions to the profile characteristics inversion of imperfectly conducting cylindrical shapes," *IEEE Transactions on Antennas and Propagation*, Vol. 21, No. 5, 663–672, 1973.
4. Boerner, W.-M. and H. P. S. Ahluwalia, "Profile characteristics inversion of spherical shapes," *IEEE Transactions on Antennas and Propagation*, Vol. 22, No. 5, 673–682, 1974.
5. Boerner, W.-M. and O. A. Aboul-Atta, "On the concept of electromagnetic inverse boundary conditions," *1975 Int. IEEE/AP-S Symposium Proc.*, 130–135, Urbana, IL, USA, June 2–5, 1975.
6. Boerner, W.-M. and O. A. Aboul-Atta, "Vectorial impedance identity for the natural dependence of harmonic fields in closed boundaries," *Canadian Journal of Physics*, Vol. 53, 1404–1407, 1975.

Exact Solutions for Microwave Holography — Part I: Planar Case

George G. Cheng, **Yong Zhu**, **and Jan Grzesik**
Allwave Corporation, California, USA

Abstract— We introduce exact solutions for microwave holography problems. All necessary information regarding an electromagnetic wave field can be determined exactly, everywhere, based on two tangential field components over a planar aperture. Fields in source regions can thus be obtained so as to generate holograms. Furthermore, one can also reconstruct any given wave propagation phenomenon likely to occur in practice, in real time over an entire region because these solutions provide full field information, i.e., all three components of both electric and magnetic fields.

Holography is treated as an inverse problem, and is tackled with exact solutions. A mapping algorithm is proposed which determines the field everywhere, in both interior and exterior regions, based on a single-plane near-field measurement sequence. In other words, these solutions not only "predict" the wave behavior in the future, but also "reveal" what has happened in the past. The field mapping algorithm is a direct, closedform solution which is numerically straightforward and efficient. Uniqueness and existence of the solutions will also be addressed and discussed.

Verification is carried out and demonstrated by analytic examples and numerical simulations, as well as by hardware measurements. Five test examples are given. Case 1, a circular aperture with uniform distribution, and Case 2, a dipole array antenna, represent analytic examples. Case 3 is a slot array antenna, its fields being generated by commercial simulation software. Cases 4 and 5 are based on hardware measurements. The first involves a slot array antenna, and the second a patch antenna. In both cases blockage is present in order to create diffraction and field interruption. Excellent agreement is evident in all five cases.

Exact Solutions for Microwave Holography — Part II: Cylindrical and Spherical Cases

George G. Cheng, **Yong Zhu**, **and Jan Grzesik**
Allwave Corporation, California, USA

Abstract— We introduce exact solutions for microwave holography problems. All necessary information regarding an electromagnetic wave field can be determined exactly, everywhere, based on two tangential field components acquired over a cylindrical or spherical surface. Fields in source regions can thus be obtained so as to generate holograms. Furthermore, one can also reconstruct any given wave propagation phenomenon likely to occur in practice, in real time over an entire region because these solutions provide full field information, i.e., all three components of both electric and magnetic fields.

Holography is treated as an inverse problem, and is tackled with exact solutions. Mapping algorithms are proposed which determine the field everywhere, in both interior and exterior regions, based on a near-field measurement across a single cylindrical or spherical surface. In other words, these solutions not only "predict" the wave behavior in the future, but also "reveal" what has happened in the past. The cylindrical/spherical field mapping algorithms are direct, closed-form solutions which is numerically straightforward and efficient. Uniqueness and existence of the solutions will also be addressed and discussed.

Verification is carried out and demonstrated by analytic examples and hardware measurements, five cases all told. Three of these are analytic and concern themselves with various arrangements of dipole antennas. The remaining two process near-field measurements from base-station and patch antennas, one each for the cylindrical and spherical geometries. Excellent agreement is evident in all instances.

The Calculation of Back Scattering Field of Unmanned Air Vehicle

N. Altın[1] and E. Yazgan[2]

[1]Turkish Aerospace Industries, Inc., Ankara, Turkey
[2]Electrical & Electronics Engineering Department, Hacettepe University, Turkey

Abstract— In this paper, GTD, GO and PO is employed in calculating the back scattering field of Unmanned Air Vehicle (UAV) in the 1 GHz. The calculated result is compared by FEKO analysis program result. When target's electric size is two times greater than its wavelength, higher order diffraction field is ignored. The first order diffracted field will be sufficient to calculate the target's RCS.

Estimation Error of Topographic Phase Based on RVoG Model Using POLinSAR Data

L. Bai[1, 2, 3], **W. Hong**[1, 2], **and F. Cao**[1, 2]

[1]National Key Laboratory of Microwave Imaging Technology, China
[2]Institute of Electronics, Chinese Academy of Sciences, China
[3]Graduate University of Chinese Academy of Sciences, China

Abstract— When the forest can be modeled as Random Volume over Ground, the complex coherences in all polarization states distribute along a straight line. Topographic phase, which is the interferometric phase of the topography, is one intersection of the straight line and the unit circle. Therefore, the topographic phase can be estimated from complex coherences of POLinSAR data.

However, the complex coherences in forest usually spread in a narrow ellipse or a narrow triangle region, not locate on a straight line. Consequently, the straight line and the estimation for the topographic phase would suffer from the shape of the coherence region. Besides, the SNR decorrelation and temporal decorrelation brings estimation error to topographic phase. This paper is to analyze the estimation errors caused by the coherence region and the SNR decorrelation so as to describe the estimation error in quantity. It is not based on the statistics of the interferometric phase, but based on the RVoG model and the inversion process.

To describe the estimation error using the RVoG model, we introduce a parameter called axis ratio. It is defined as the length ratio of the largest axis and the minimum axis of the coherence region. Since axis ratio indicates the matching degree of coherence region to the RVoG model, it is also a risk indicator for the estimation error. The axis ratio could be applied to the error analysis of topographic estimation in bare ground. Since the complex coherences in different polarization states provides the same interferometric phase theoretically, the coherences distributes along a straight line, too.

Besides the analysis of the coherence region, the SNR decorrelation γ_{SNR} influences the estimation of topographic phase. As shown in Figure 1, the decorrelation factor shifts the ideal brown line to the green line. Correspondingly, the estimation ϕ_3 shifts from the true topographic phase ϕ_0. We use the optimum coherence obtained by the coherence optimization to estimate the minimum scalar decorrelation so as to get the possible maximum estimation error in topographic phase.

To demonstrate the error analysis, experiments are applied on DLR E-SAR L-band fully polarized data acquired from Traunstein as shown in Figure 2. According to the topographic estimation

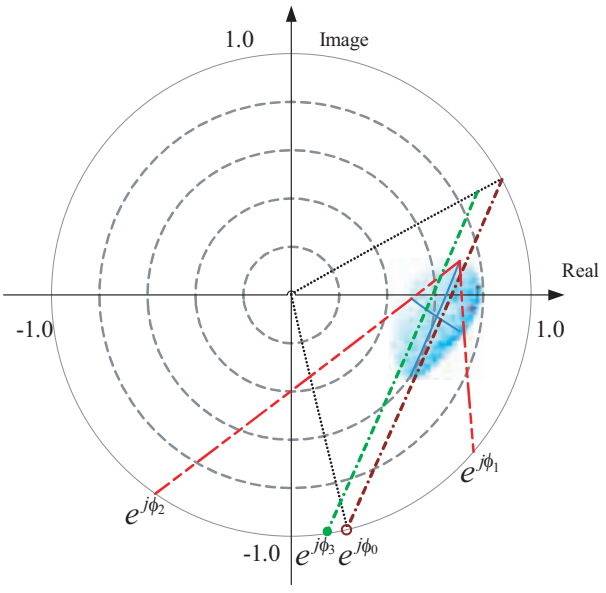

Figure 1: The schematic of error analysis.

Figure 2: Experiment data.

using different coherence samples, the estimation errors caused by the coherence region are shown. When the coherence region is very close to the straight line, the error caused by the decorrelation is calculated.

Antenna Measurement via Compressive Sensing

Wenji Zhang, **Lianlin Li**, **and Fang Li**
Institute of Electronics, Chinese Academy of Sciences, Beijing, China

Abstract— Recently, Compressive Sensing (CS) proposed by Donoho, Candes, Romberg and Tao et al. has become a revolutionary theory in signal processing and applied mathematics. It allows one to simultaneously sample and compress unknown signals which have a sparse representation in a known basis, such as DCT, wavelet, curvelet, Gabor, and so on. By using CS, one can exactly obtain the complete signal from highly incompletely sampled data. The CS measurements correspond to projections performed on the basis function coefficients. Interestingly, Candes and Tao et al has demonstrated that a randomly designed measurement matrix, such as i.i.d. Gaussian matrix, can be considered a universal and optimal encoding strategy.

In this paper, we constitute a rich multi-path background environment, much similar to the chaos time reversal cavitywhich is used to construct the CS projections via the background Green's function. The background environment is constructed with equally spaced thin wires which enables an accurate and fast estimation of the background Green's function. With the knowledge of the background Green's function, the antenna radiation pattern can be measured in a CS manner. This implies that the antenna radiation pattern in a wide range of observation angles can be recovered from a limited angle of measurement data.

Ionospheric Tomography Based on P-band Spaceborne SAR via Compressive Sensing

Lianlin Li, **Yin Xiang**, **Yanli Liu**, **and Fang Li**
Institute of Electronics, Chinese Academics of Sciences, Beijing, China

Abstract— In this presentation, the potential of the tomography of well localized ionospheric irregularities (LII) based on P-band spaceborne SAR via compressive sensing (CS) has been investigated.

A mandatory requirement of the proposed approach is that the echoes scattered by LII should be well separated from the SAR echoes scattered from the target(s) on the ground. According to this requirement, the lower pulse repetition frequency (PRF) of SAR should be mandated, which is not permitted by traditional P-band spaceborne SAR system; however, the new theory, named as compressive sensing (CS), developed recently by Donoho et al. has shown that the data required by traditional SAR can be retrieved from the data sampled by a PRF much smaller than the Nyquist sampling, i.e., the PRF required by traditional SAR system.

As for the procedure of the well LII tomography, a three-step strategy has been proposed: firstly, the data required by traditional SAR migration algorithm is retrieved by using CS; secondly, the SAR migration algorithm, such as Range-Doppler algorithm, is employed to determine the approximate size and position of LII; thirdly, the diffraction tomography algorithm is used to determine the value of electron density, exact size, position LII. During the third step, an ill-posed linear inverse problem should be solved. In order to alleviate the degree of ill posed and improve the imaging of LII, much independent data should be required. To do this, two approaches are proposed, i.e., the model of InSAR and increasing the bandwidth of SAR. The detailed procedure of proposed is following:

Step1. Data Retrieval from Data Sampled with Low PRF by Using CS Theory

The conventional approach to sampling signals, whether along range direction or along azimuth direction, follows the celebrated Shannon sampling theorem: the sampling rate must be at least twice the maximum frequency present in the signal (the so-called Nyquist rate). Following this criterion, the PRF of spaceborne SAR system is impressively designed. However, according to the CS theory developed recently by Donoho and Candes et al. has shown *that one can recover certain signals and images from far fewer samples or measurements than traditional methods use.* The crucial observation of CS is that one can design efficient sensing or sampling protocols that capture the useful information content embedded in a sparse signal and condense it into a small amount of data.

The review of CS theory is briefly summarized as following. Consider a complex $m \times 1$ vector u, that is compressible in the basis Ψ, with the columns of Ψ denoting orthonormal vectors that define the basis. One may therefore write $u = \Psi\theta$, where θ is nearly sparse $m \times 1$ vector in the sense that most of its coefficients may be set zero, with minimal effect on the representation of u. It is noted that in the traditional SAR system and SAR migration algorithm, the Fourier basis is specified; however, the Fourier basis is not optimal in application in the view of signal sparse representation. As a matter of fact, the wavelet or curvelet representations may be far better than Fourier representation. In CS rather than first measuring u and then performing transform coding, we can perform projection measurements of u. Specifically, let Σ represent an $n \times m$ matrix ($n < m$), and instead of measuring the m-dimensional signal u we measure the n-dimensional signal $v = \Sigma u = \Sigma\Psi\theta = \Phi\theta$. It has been demonstrated that where θ is sparse there are conditions under which Φ may be constructed which guarantee that for sufficiently large n (often for $n << m$) one may recover θ exactly using an l_1-regularized inversion.

Step 2. The Imaging of Well LII by Using Traditional SAR Migration Algorithm

As mentioned above, when the PRF of SAR system is lowed, there is no overlap of signal between received signals corresponding to two different transmitted signals, consequently, the echoes scattered from well LII can readily be separated by using the time window technique, at the same time the SAR imaging of targets on the ground can be safely realized after the complete data are retrieved. In this presentation, the Range-Doppler algorithm is employed to realize the imaging of well LII to determine the approximate position and size of ionospheric irregularities. Of course, any SAR imaging algorithm can be used, such as Chirp Scaling, ωK and SPECAN and so on.

As well known, by using the SAR imaging algorithm, one only obtain the imaging of LII projected on the plane consisted by the direction along the flight direction of SAR and the slant range

direction. It means that (1) the size and position of well LII along the x-direction can obtained with high precision; (2) In addition, due to the three dimensional ionospheric irregularities, the information along the z-and y-direction are confused; however, the approximate size of well LII can be easily estimated.

Step3. The Tomography of Well LII by Using Diffraction Tomography (DT) Algorithm

After the number, approximated size and position of well LII are estimated, the value of electron density, size and position of well LII can be obtained quantity by using diffraction tomography (DT) algorithm. During the course of discretion, because the imaging along the x-direction can be exactly obtained, only the region confined by z- and y-axis is discretized and is divided into $N \times N$ subgrids. It is stressed that due to ill posedness, some regularization technique should be employed; the truncated SVD technique is employed in this presentation. In order to alleviate the degree of ill-posedness, some independent information should be increased, to do this, the using of InSAR model and increasing the signal bandwidth are proposed in this paper.

Session 4A6b
Computational Techniques 1

Ferrite Image Lines Studies by Transverse Operator Method

H. Sakli[1], **H. Benzina**[2], **T. Aguili**[1], **and J. W. Tao**[3]

[1]SYS'COM Laboratory, Ecole Nationale d'Ingénieurs de Tunis, Le Belvédère, Tunis 1002, Tunisia
[2]Ecole Nationale d'Ingénieurs de Gabès, Rue Omar Ibn El Khattab, Gabès 6029, Tunisia
[3]Groupe de Recherche en Electromagnétisme (GRE), ENSEEIHT-INPT, Toulouse 31071, France

Abstract— In this paper, a rigorous study of the transverse operation method (TOM) formulation is presented by an inhomogeneous rectangular structure of ferrites with transverse anisotropy which will be followed by the application of the Galerkin Method.

Our study is essentially focused on the determination of the propagation constant in a ferrite image lines magnetised longitudinally by a static magnetic field.

The transverse operator which is another formulation of the Maxwell equations is here used to define the rectangular waveguide characteristics charged of ferrites. This method consists on eliminating the longitudinal components and resolving the propagation equation by developing the transverse fields in series of modes of a closed structure (empty metal guide).

The elimination of the longitudinal fields in the Maxwell equations lets appear an operator L named the transverse operator. The resolution of the propagation equation by the Galerkin method leads to an eigenvalues equations.

The transverse operator method has been applied to a generalized multidielectric waveguide structure. The theoretical results were obtained for the dielectric image lines and compared with others approaches and good agreement was obtained. The proposed method gives better numerical convergence than those approaches (The convergence stability of the propagation constant is obtained when reaching the value $N = 5$ modes) because of the appropriate choice of eigenfunctions. Other ferrite waveguides with arbitrary cross-sections can be studied using this procedure with no modifications.

By considering a longitudinal propagation in the direction Oz in the ferrite image lines and with the use of the TOM method, we obtain the following propagation equation:

$$\hat{L}' H'_t = k_z^2 H'_t$$

With:

$$\hat{L}' = k_0^2 \varepsilon_r \overline{\overline{\mu}}_{tt} - \eta_0 \partial_t \frac{1}{\varepsilon_r} \partial_t^+ \eta_0 \varepsilon_r - \eta_0 \overline{\overline{\mu}}_{tt} \eta_0 \partial_t \frac{1}{\mu_{zz}} \partial_t^+$$

The expression of ε_r in different mediums can be written as follows:

$$\varepsilon_r = 1 + (\varepsilon_{r2} - 1) \cdot U(X) \cdot U(Y)$$

where

$$\begin{aligned} U(X) &= U(x - x_1) - U(x - x_2) \\ U(Y) &= U(y) - U(y - y_1) \\ \delta(X) &= \partial_x U(X) \\ \delta(Y) &= \partial_y U(Y) \end{aligned}$$

U is the Heaviside function and δ is the Dirac impulsion.

The decomposition of the field $\overrightarrow{H}'_t$ on a complete basis (trigonometric functions) permits to obtain a system with eigenvalues which can be written as follows:

$$G \cdot H'_t = k_z^2 \cdot H'_t$$

G is a $(2N \times 2N)$ matrix with $N = m \cdot n$: number of modes; m and n are natural integers, verifying: $(m, n) \neq (0, 0)$.

The values and the eigenvectors of H' are respectively the propagation constants and the development coefficients of the guide field.

Transparent Boudary Condition for a Hybrid FD-FD Method

Hung-Wen Chang and Wei-Chi Cheng
Institute of Electro-optical Engineering and Department of Photonics
National Sun Yat-sen University, Kaohsiung 80424, Taiwan

Abstract— We combine a hybrid analytic mode expansion method with the finite-difference, frequency-domain (FD-FD) method to study passive optical waveguide devices. To reduce FD-FD computational domain, the input and output parts of the optical device are computed analytically. Only the internal complex domain is modeled by the FD-FD method. Along the interface of the two domains, a layer-mode based transparent boundary condition (LM-TBC) is employed to inject the incident wave field and simultaneous to allow the outgoing wave fields to leave the waveguide device. The reflection/transmission coefficient vectors of input and output waveguide are computed from the field points on the FD-FD boundaries. The accuracy and performance of this LM-TBC method is checked against a same FD-FD calculation employing two PML regions and with the exact Green's function solution. We show that for a line source in the free space and a layered dielectric structure, LM-ABC results are able to pass through wave fields with all incident angle including those nearly grazing and evanescent fields for both TE and TM polarizations.

The Dirichlet Problem for the Laplace Equation in a Cylindrical Domain

Diego Caratelli[1], **Bruna Germano**[2], **Matthew X. He**[3], **and Paolo E. Ricci**[4]

[1]International Research Centre for Telecommunications and Radar
Delft University of Technology, Mekelweg 4, Delft 2628 CD, the Netherlands
[2]Dipartimento di Metodi e Modelli Matematici per le Scienze Applicate
Università degli Studi di Roma "La Sapienza", Via A. Scarpa, 14, Roma 00161, Italia
[3]Nova Southeastern University, 3301 College Avenue, Ft Lauderdale, FL 33314-7796, USA
[4]Dipartimento di Matematica "Guido Castelnuovo"
Università degli Studi di Roma "La Sapienza", P. le A. Moro, 2, Roma 00185, Italia

Abstract— Many applications of Mathematical Physics and Engineering are connected with the Laplacian, however, the most part of BVP relevant to the Laplacian are solved in explicit form only for domains with a very special shape, namely intervals, cylinders or domains with particular (circular or spherical) symmetries [1].

In the two-dimensional case, the solution for more general domains is obtained by using the Riemann theorem on conformal mappings, and the relevant invariance of the Laplacian [2]. However, explicit conformal mappings are known only for particular domains. Of course, this method does not exist in the three-dimensional case, and the usual approach makes use of discretization.

We considered in [3, 4] an extension of the classical theory to the case of a starlike domain, i.e., a domain $\mathcal{D}$, which is normal with respect to a suitable polar co-ordinate system.

This theory was further extended in [5] to the case of a three-dimensional starlike domain in spherical co-ordinates.

In this article we show how to solve the Dirichlet problem for the Laplace equation in a cylindrical domain, whose section is a given two-dimensional starlike domain.

The solution is given by generalizing the classical procedure, i.e., by using the classical Fourier method, and splitting the problem in two cases (assigning zero values on the bases and non-zero values on the lateral surface and vice-versa).

The boundary of the bases we have considered in all our applications are defined by using the so called "superformula" due to J. Gielis.

Many numerical applications, we have performed by using the Computer Algebra system Mathematica©, confirm even in this more general case the theoretical results by Lennart Carlson, since we have found point-wise convergence in all regular points of the boundary, with possible oscillation usually occurring only in singular points.

REFERENCES

1. Andrews, L. C., *Special Functions of Mathematics for Engineers*, Oxford Univ. Press, Oxford, New York, 1998.
2. Krall, G., *Meccanica Tecnica Delle Vibrazioni*, Vol. 2, Veschi, Roma, 1970.
3. Natalini, P. and P. E. Ricci, "The Laplacian in stretched polar co-ordinates and applications," *Proceedings ISAAC Conference on "Complex Analysis, Partial Differential Equations and Mechanics of Continua"*, Dedicated to the Centenary of Ilia Vekua, (to appear).
4. Natalini, P., R. Patrizi, and P. E. Ricci, "The Dirichlet problem for the Laplace equation in a starlike domain of a Riemann surface," *Numer. Algorithms*, (to appear).
5. Caratelli, D. and P. E. Ricci, "The Dirichlet problem for the Laplace equation in a starlike domain," *Proc. Int. Conf. CSR 2008*, Las Vegas, July 14–17, 2008 (to appear).

Session 4A7
MIMO, DOA and Wave Propagation in Wireless Communication

Estimation of Direction of Arrival Using the Modulated Scattering Technique

Jung-Hwan Choi, **Byung-Yong Park**, **and Seong-Ook Park**
Information and Communications University, Daejeon, Korea

Abstract— In demanding of higher bit-rate wireless communications for various mobile services, multiple-input-multiple-output (MIMO) systems are being considered as the best solution for enhancing the capacity of the radio channel without investment of additional frequency resources. These systems use multiple antenna elements at the transmitter and receiver to improve the capacity over single-input-single-output (SISO) system when operated in multipath environments. Especially, in the non-line-of-sight (NLOS) regions, the channel correlation and the channel capacity are influenced by distribution of the incoming signal such as power azimuth spectrum (PAS), angle of arrival (AOA), and direction of arrival (DOA). So, estimating direction of arrival is essential in MIMO performance measurement. Prior to this issue, smart antenna and adaptive array antenna technologies have achieved improvement of efficiency by estimation of DOAs.

Beamforming and Bartlett DOA estimation methods which are one of the earliest methods have been used due to its simplicity although the resolution is limited by array's aperture size. Nowadays, the multi signal classification (MUSIC), the estimation of signal parameters via rotational invariance technique (ESPRIT) and the maximum likelihood (ML) have been used popularly in order to obtain high-resolution performance. And the DOA estimation method using electronically steerable parasitic array radiator (ESPAR) which has only one RF port has been studying because of inexpensive hardware structures. In this paper, the DOA estimation method using the modulated scattering techniques (MST) is proposed.

The MST has been popularly used for rapid near-field measurement without scarifying the acceptable level of accuracy. In order to characterize microwave fields at the probe's location with the amplitude and phase information, the MST uses non-linear devices loaded on the short dipole scatterer with modulating at the low frequency. The modulated scattering microwave fields can be discriminated from unmodulated parasitic signals that cause errors. Also, the MST can use several modulated scatterers placed at the pre-defined positions to increase the measurement speed. This configuration provides economical solution by using a low frequency switch instead of an expensive RF switch.

The DOA estimation system using the MST consists of one monopole antenna and optically modulated scatterers. And the detecting part of this system consists of a quadrature coupler, two mixers, and two single-phase lock-in amplifiers as a homodyne receiver. An optically modulated scatterer is a short dipole antenna that has the photodiode which is loaded at the center of the short dipole antenna and optically switched by a laser source through optical fiber. The monopole antenna for receiving the modulated RF signal is located at the center of the DOA detection system and connected to a RF port. It is surrounded by 12 optically modulated scatterers on a circle of radius 0.75 m, equally. A 7 kHz modulated laser optical signal feeds all photodiodes for switching operation sequentially by controlling the 12-channel high-speed relay.

A single sinusoidal signal was generated apart 15 m away from the DOA detection system. And then, the amplitude and phase of the modulated scattering signals were recorded driving the low frequency signal to each dipole scatterer sequentially. The output signal of the detection system is proportional to signal strength of operating sensor's location. The ratio of the strongest signal intensity and another sensor's one adjacent to the sensor which has the strongest intensity is proportional to the ratio of angles between the direction of incoming signal and sensors. The direction of the sensor which has the strongest intensity may be close that of the impinging signal because the intensity should be higher as the propagation distance is shorter. Therefore, we can estimate DOA precisely by this detection system with the inexpensive RF structure and without high computational complexity.

A Localization Scheme Using Bi-directional Metrics Joint Estimation

C. K. Seow, **S. Y. Tan**, **and S. W. Chen**
Nanyang Technological University, Singapore

Abstract— The proliferating growth of both the commercial and government applications of wireless localization has spurred the need for more accurate wireless location estimation schemes. Currently, wireless location estimation schemes use the Line of Sight (LOS) geometric relationship to establish the Euclidean distance between the reference and the mobile devices. The information that is used to determine this relationship, as well as the location of the mobile device, includes the Time of Arrival/Time Difference of Arrival (TOA/TDOA), the Angle of Arrival (AOA) or the Received Signal Strength (RSS) at the reference devices. A hybrid localization technique that uses a combination of the above metrics, such as combining TOA and AOA data, also exists.

Localization in a two-dimensional (2D) environment usually requires two and three reference devices, for AOA and TOA/TDOA localization schemes respectively. However, these conventional localization schemes may not be feasible when the channel environment consists of a multipath-rich medium with numerous scattering objects (scatterers). One or more reference devices may not be in the LOS range of the mobile device, thus rendering the geometrical relationship derived for LOS localization erroneous. Various Non Line of Sight (NLOS) mitigation techniques have emerged to overcome this problem. However, the NLOS mitigation techniques will not perform satisfactorily, as they require the number of LOS reference devices that are available to be greater than the number of NLOS reference devices deployed, which is not feasible.

In this paper, we propose a novel two step Least Squares (LS) localization scheme that is based on jointly estimating the AOA and TOA bi-directionally at both the reference and mobile devices. This can be done as both ends are equipped with antenna arrays for carrying out AOA estimation, such as those used in Multiple Input Multiple Output (MIMO) technology devices. The advantages of using bi-directional estimation for localization are twofold. Firstly, we can devise a NLOS path rejection mechanism to infer whether a path is LOS or NLOS. The underlying mechanism is the LOS angle relationship that exists between the reference and mobile devices. Secondly, bi-directional estimation allows an enhancement technique for readjusting and improving the accuracy of the AOA measurement values at both the reference and mobile devices to be designed. Through these readjustments, the accuracy of identifying the mobile device's location is improved.

By exploiting bi-directional measurement information, our proposed localization algorithm outperforms the conventional unidirectional localization schemes, especially under NLOS scenarios. In general, when coupled with the NLOS path detection and AOA adjustment techniques we have devised, our proposed localization scheme with one LOS reference device performs better than the conventional unidirectional schemes that use three reference devices. Cramer Rao Lower Bound (CRLB) and numerical simulation results in a typical real environment demonstrate that the proposed joint localization scheme which uses only one LOS reference device, provide much better location accuracy compared to the conventional unidirectional TOA and TOA/AOA localization schemes, which use disjoint metric estimation and three reference devices. The Average Location Error (ALE) simulation results indicate that our joint LS, which uses only one LOS reference device outperforms the conventional schemes for all cases of error variations with a much higher margin.

Propagation of Ultra Wideband Signals in Automotive Environment

Ching-Ping Wang and Wen-Jiao Liao
National Taiwan University of Science and Technology, Taiwan

Abstract— This work investigates the propagation of the ultra wideband signal in automotive environment, especially the car underhood. Measurements as well as simulations using high frequency numerical electromagnetic tool are performed to examine the interaction between broadband signals and obstacles in the propagation environment. The measurement setup contains two broadband antennas. A large metal plane and a box with conducting surfaces are put in the environment in various configurations. Transmission magnitudes and phases are recorded with a network analyzer by sweeping from 2 to 6 GHz. By applying the Fourier transform, the frequency spectrum is converted into time domain to examine the propagation characteristics of the environment. With adjustments in the propagation environment setup, the location of primary scatters can be identified.

A Simplified Statistical Modeling of Radioclimatological Parameters for LOS Links in South Africa

P. K. Odedina and T. J. Afullo
University of KwaZulu-Natal Durban, P. O. Box 4000, South Africa

Abstract— Different techniques has been proposed by various authors in different regions of the world to model the solution to radio wave propagation problems, but most of these techniques have not considered modeling the primary parameters on which other radioclimatological factors are based. This paper has therefore focused on working from the basics, by considering the initial parameters on which radioclimatological factors were based. These initial parameters namely; temperature, pressure and humidity were modeled with vertical height increase using one year radio propagation data and six years radio propagation data in Durban, KwaZulu Natal province of South Africa. A simplified statistical technique is employed in the analysis of this data.

The propagation of electromagnetic waves around the earth is influenced by the properties of the earth and the atmosphere. The earth is an inhomogeneous body whose electromagnetic properties vary considerably as we go from one point to another, its properties varying with temperature, pressure and humidity.

According to ITU-R Recommendation P. 530, the propagation loss on a terrestrial line-of-sight path relative to free space loss is the sum of different contributions which includes: attenuation due to atmospheric gases; diffraction fading due to obstruction or partial obstruction of the path; fading due to multipath and attenuation due to precipitation. Each of these contributions has its own characteristic as a function of frequency, path length and geographical location.

Some of the basic parameters in the field of radioclimatology includes but not limited to the weather parameters such as; temperature, pressure, humidity and water vapour pressure. Also included are the variables that account for the earth curvature such as effective earth radius factor (k-factor), surface roughness, multipath effect and geoclimatic factor. Parameters such as k-factor have been adequately studied, modeled and applied to line of sight link in Southern Africa. Temperature, pressure, humidity, water vapour, saturated vapour pressure and refractivity as it affects signal degradation and how they are related were discussed have been discussed elsewhere. This paper discussed a simplified statistical modeling of these basic parameters mentioned above and the steps involved were detailed in the paper.

Influence of Model Parameters on the Sub-aperture Propagation Method

J. Blas[1], **P. Fernández**[1], **R. M. Lorenzo**[1], **S. Mazuelas**[2], **A. Bahillo**[2], **D. Bullido**[2], **and E. J. Abril**[1]

[1]Department of Signal Theory and Computer Engineering, University of Valladolid, Spain
[2]Centre for the Development of Telecommunications of Castilla y León, Spain

Abstract— There are some cases where ray-tracing techniques do not provide a correct prediction of the E-Field envelope variations. The transition between outdoor and indoor propagation is one of them. The main problem is transmission through windows, which are structures whose size is approximately of the same order of magnitude as the typical mobile phone wavelength. Therefore they are incompatible with the geometrical optics assumption of electrically large objects. This fact together with inner walls effects, explain the complex field patterns found inside rooms which are directly illuminated from base stations. We propose to model window panes as apertures while inner walls can be replaced by equivalent sources applying the theory of electrical images. Each aperture is divided into several sub-apertures in order to relax far field conditions. The method provides an accurate statistical description of the spatial variability of the E-field envelope in a bidimensional region under test inside the room. The model is corroborated by a measurement campaign performed in a real room under controlled conditions. The maximum deviation found between the simulated and measured envelope Cumulative Distribution Function is less than 1%. Kolmogorov-Smirnov test guarantees the goodness of fit with P-values around 99%. This contribution describes the experimental setup employed to validate the model and explores the influence of different parameters of the sub-aperture model on the results. In particular we study the effects due to the three-dimensional position of the transmitter and variations in the sub-aperture shape and number. Theoretical justifications that support parameters are provided.

A Rigorous Model for Capacity Evaluations of Indoor MIMO Systems with Complex Radiators

Hao Gang Wang, **Li Wang**, **Huan Li**, **Hong Bing Song**, **and Kan Hong**
The Electromagnetics Academy at Zhejiang University, Zhejiang University, Hangzhou, China

Abstract— In the next generation of wireless communications, Multiple Input Multiple Output (MIMO) communication system will be a key technology to enhance the communication efficiency. A Multiple Input Multiple Output (MIMO) system sufficiently utilizes the abundant multi-paths resource to enhance the wireless communication channel capacity in multiples. In the last two decades, there exist a lot of research works in simulating the MIMO channels. However, the studied antennas are very simple, e.g., linear dipole arrays. To obtain higher gain and channel capacity, the shapes of the radiators should be complex. This suggests that higher efficient EM method is needed. In this paper, we fully develop a novel three-dimensional (3D) numerical model for rigorously simulating mutual coupling effects on the channel capacity of the Multiple Input Multiple Output (MIMO) systems. In this numerical model, the efficient integral equation method MutlilLevel Green's Function Interpolation Method (MLGFIM) is employed to fast calculate the input admittance matrix of the transmit antennas and the receive antennas, and the radiation patterns. To accurately model the EM wave propagation in the wireless environment, we 1) use the ray tracing method to obtain the multi-paths and 2) devise a new path loss model with a more generalized polarization transform scheme. Using this numerical model, we successfully analyze mutual coupling effects on the three dimensional correlation of a 2-by-2 monopole array and the indoor channel capacity of the 2-by-2, 4-by-4, 8-by-8, 20-by-20 planar array and the 20-by-20 icosahedron array. The numerical examples in this paper demonstrate that our numerical model is very efficient for simulate the MIMO system with very complex radiators.

ACKNOWLEDGMENT

This work is supported by the National Natural Science Foundation of China No. 60501017.

Regular Polyhedron Antenna Array Design and Simulation for MIMO Systems

L. Wang and H. G. Wang
The Electromagnetics Academy at Zhejiang University, Zhejiang University
Hangzhou, China

Abstract— Some MIMO applications require antennas to closely spaced, and it will cause the mutual coupling among antennas and high spatial correlation which will harmful for enhancing the system capacity. In order to solve this problem, many methods have been developed. The antenna array design is a feasible way to enhance the MIMO system performance. We developed the regular polyhedron antenna array, each monopole is fixed at the center of each surface of regular polyhedron. Regular polyhedron has excellent spatial symmetry, and it is vital in 3D environment. This kinds of regular polyhedron antenna array exhibit spatial correlation than the antenna array fixed on a plane. In numerical simulation, the efficient integral method MGLFIM is employed to fast calculate the input admittance and radiation pattern. In our simulation, the frequency is set to be 1.95 GHz, the radius and height of the monopole are set to be $\lambda/100$ and $\lambda/4$. All of the polyhedrons, i.e., dodecahedron, hexahedron, octahedron, tetrahedron and icosahedron are simulated. Using our numerical model for MIMO system developed in our recent research, we calculate the correlation coefficient matrix and the MIMO capacity of these polyhedron antenna arrays. The simulation shows that each regular polyhedron antenna array is possess of excellent efficiency in enhancing the MIMO system capacity. Using the same number of monopoles, the physical size of the regular polyhedron array can be smaller than that of the plane antenna array, while the system capacity of the former is larger than that of the latter.

ACKNOWLEDGMENT

This work is supported by the National Natural Science Foundation of China No. 60501017.

A Source Localization Scheme Based on Unitary ESPRIT and the City Electronic Map

Hong Bing Song, **Hao Gang Wang**, **Li Wang**, **and Da Qing Liu**
The Electromagnetics Academy at Zhejiang University, Zhejiang University
Hangzhou 310027, China

Abstract— In this paper, a novel source localization scheme is proposed based on the Unitary ESPRIT (UESPRIT) algorithm with back ray tracing technique and the city electronic maps. In this scheme, the UESPRIT is employed to estimate the angles and delays of the arrival rays radiated from the source. Based on the obtained information, we devise a back ray tracing techniques according to the Geometrical Theory of Reflections and the 2D city electronic map. The locating procedure is shown as follow: First UESPEIR is used to estimate the direction of arrival (DoA) and time delay of arrival (TDoA). With the estimated DoA and TDoA, the arrival angles and the lengths of the paths of signals can be obtained. Second, the Back Ray Tracing (BRT) emits signals from the receiver according to these angles. Then the transmitting waves will move forward, hit the building, and be reflected. They will not stop until lengths of the path reach the estimated ones. The stop position is the source location. For the case the signals hit around the corner of the building, the estimated position may far away from the actual position, when the estimated DoA and TDoA deviate a little from the real DoA and TDoA. In order to minimize the estimated error, a selection scheme is employed in this paper. After eliminating the wrong estimated position, the average of the estimated position will be made, which is the ultimately estimated source location. Error analyses have been made and show that the localization accuracy for a cell of about 80 m × 40 m can reach 1 m when the SNR is greater than 15 dB.

ACKNOWLEDGMENT

This work is supported by the National Natural Science Foundation of China No. 60501017.

Performance Analysis of OFDM Communication System over Correlated Nakagami-m Fading Channel

Vivek K. Dwivedi[1], **Pradeep Kumar**[2], **and G. Singh**[2]
[1]Department of Electronics and Communication Engineering
Jaypee Institute of Information Technology University, Noida 201307, India
[2]Department of Electronics and Communication Engineering
Jaypee University of Information Technology, Solan 173215, India

Abstract— Orthogonal frequency division multiplexing (OFDM) is broadly considered as an effective approach for the future high speed wireless multimedia communication systems [1, 2]. The basic principle of OFDM communication systems is to split the high data stream into number of lower rate data streams which are transmitted simultaneously over a number of sub-carriers. High spectral efficiency and multipath immunity are two major features of OFDM systems. However, diversity techniques can dramatically improve the performance over different fading channels. Thus the OFDM systems with diversity have very significant role in wireless communication [4]. So it is necessary to investigate the performance over different fading channels. Nakagami fading channel model [3] has received considerable attention due to its great flexibility and accuracy. In this paper, an effort has been made to analyze performance of OFDM communication system over correlated Nakagami fading channel using maximal ratio combining (MRC) diversity at the receiver. If the antennas are closely spaced at receiver then received signals are correlated which is the reason that correlated Nakagami fading channels are considered in this analysis. A novel mathematical formula of bit error rate (BER) for the MQAM OFDM communication systems using more than two MRC at receiver is analyzed. Since we are considering more two MRC combiners at the receiver, hence BER performance of presented system is improved.

REFERENCES

1. Moose, P. H., "A technique for orthogonal frequency division multiplexing frequency offset correction," *IEEE Trans. Comm.*, Vol. 42, 2908–2914, Oct. 1994.
2. Dwivedi, V. K. and G. Singh, "An efficient BER analysis of OFDM systems with ICI conjugate cancellation method," *PIERS Proceedings*, 166–171, Cambridge, USA, July 2–6, 2008.
3. Nakagami, M., "Them-distribution — A general formula of intensity distribution of rapid fading," *Statistical Methods in Radio Wave Propagation*, W. G. Hoffman, Ed., Oxford, U.K.: Pergamon, 1960.
4. Kang, Z., K. Yao, and F. Lorenzelli, "Nakagami-m fading modeling the frequency domain for OFDM system analysis," *IEEE Commun. Lett.*, Vol. 7, 484–486, Oct. 2003.

Session 4P1a
Medical Electromagnetics, RF Biological Effect, MRI 2

Numerical Investigation of Spectral Optical Coherence Tomography Based on Full-wave Solution of Maxwell's Equations

Ji Yi, **Wendy Yip**, **and Xu Li**
Department of Biomedical Engineering
Department of Electrical Engineering and Computer Science
Northwestern University, Evanston, IL 60208, USA

Abstract— Spectral optical coherence tomography (SOCT) is an optical imaging technique that has been under intensive investigation. It allows the simultaneous acquisition of potentially sub-micron-resolution images and backscattering/absorption spectra for characterizing subcellular properties of biological tissue. One of the challenges of interpreting SOCT images is the complex nature of tissue scattering, which includes both multiple-scattering effects as well as single scattering from particles with size larger than or comparable to the wavelength.

In this paper, we report numerical synthesis of SOCT images using a combination of rigorous solution of Maxwell Equations and diffraction theory to assist optical analysis of biological tissues and cells. In our numerical methodology, we first calculate scattered light from the sample at the pupil of the objective lens using the finite-different-time-domain (FDTD) method or Generalized Multiparticle Mie-solution (GMM) — both of which are full-vector numerical solutions of the Maxwell's equations. The second processing step involves numerically creating a reference signal and forming SOCT images based on diffraction theory. We validate this approach by comparing the numerically synthesized images with experimental results for dielectric microspheres. This comparison demonstrates that our algorithm provides an effect methodology for predicting SOCT images of arbitrary scattering structures.

Based on our numerical simulations conducted on aggregations of spherical particles, we investigate the impact of multiple scattering on SOCT images and spectra. Here, we generate realizations of particle ensembles with specified particle size and volume fraction in the simulations and calculate the corresponding SOCT images. The wavelength dependent scattering spectrum for a specific ensemble is then calculated by averaging spectra obtained at multiple positions in the SOCT image. This spectrum is compared to both single-particle scattering spectrum and incoherent multiple-scattering spectrum. Through these simulations, we demonstrate that through signal processing, SOCT provides the potential of extracting single-scattering properties even for high volume fraction of particle ensembles. These observations will guide us to improve the inverse algorithms for biological tissue characterization based on SOCT measurements.

Arrays of Waveguide Applicators for Microwave Thermotherapy

Jan Vrba
Department of EM Field, Czech Technical University in Prague
Prague, Czech Republic

Abstract— In this contribution we would like to describe our new results dealing with waveguide hyperthermia applicators, typically used for cancer treatment. We have designed and evaluated a water filled lens applicator (aperture of a the rectangular waveguide applicator is divided into 3 or 5 sectors with shifted excitation).

We would like to present theoretical model of this applicator, results of numerical modelling and experimetal evaluation as well. Focusing principle of the lens applicator enables to increase the depth of efficient heating in comparison with waveguide applicators.

The basic schematics of the discussed type applicator is shown in the following figure. The aperture of lens applicator is divided into 3 or 5 sectors with shifted excitation (i.e., different amplitude and phase). To achieve deep local treatment by aid of this applicator we can thus use a focusing principle.

In our contribution we will discuss our results with the design of this type applicator and also some first experiments will be presented.

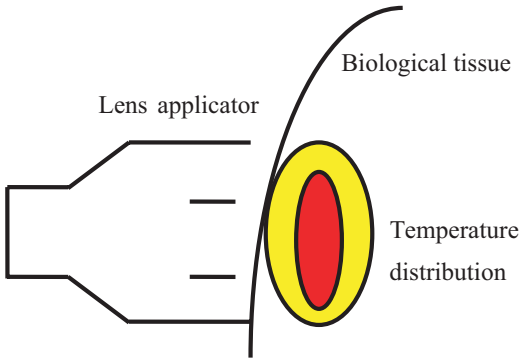

ACKNOWLEDGMENT

This research is supported by the Grant Agency of the Czech Republic and by the Ministery of Education, Youth and Sport of the Czech Republic.

Technical Equipment for Research of EM Field and Biological Systems Interactions

Jan Vrba[1], **Luca Vannucci**[2], **Paolo Togni**[1], **and Lukas Visek**[1]

[1]Dept. of EM Field, Czech Technical University in Prague, Prague, Czech Republic
[2]Institute of Microbiology, Czech Academy of Sciences, Prague, Czech Republic

Abstract— Research of interactions between EM Field and biological systems is of growing interests elsewhere. Also here in Czech Republic there are several groups working in this field, often in international co-operations. We will describe here mainly basic technical equipment developed for 5 different research projects in the discussed area of interactions of EM field and biological systems.

Microwave Medical Imaging and Diagnostics

Jan Vrba[1], **Ladislav Oppl**[1], **Jan Vrba, Jr.**[2], **and David Vrba**[1]

[1]Czech Technical University in Prague, Dept. of EM Field, Prague, Czech Republic
[2]RWTH Aachen University, Chair of Electromagnetic Theory
Kopernikusstraβe, Aachen 1652074, Germany

Abstract— Future trends in medical applications of microwave technique and technology can be seen in development of new diagnostic and imaging methods based on high frequency EM field. A significant importance for the future can be identified for the following methods: Microwave tomography, Microwave radiometry, Measurement of complex permittivity, Imaging in the Terahertz waves band and Microwave diagnostic radars.

Reversible Electroporation on a Microchip

H. S. Kim[1], **H. B. Kim**[2], **and J. H. Yi**[1]
[1]Department of Biomedical Engineering, Konkuk University, Republic of Korea
[2]Solco Biomedical Institute, Republic of Korea

Abstract—

Introduction: Electroporation technique uses application of extracellular electric field and involves rapid structural rearrangement and formation of pores on the lipid bilayer of the cell. The technique is becoming more important method for inserting biologically active molecules such as drug and gene into the cells. The technique uses a nonthermal process and relatively low external electric field pulses of short duration thereby maintaining the integrity of the outer cell membrane and preventing further irreversible damage.

Methods: In order to investigate electroporation, we fabricated a microchip applicator having six identical electroporation sites on a Pyrex substrate and each site has a electrode pair of 1mm inter-electrode distance. The experiment was performed using sequences of moniphasic pulses; pulse-width = 100 µs, pulse interval = 100 µs, pulse amplitudes = 375, 750, 1k, and 1.3 kV/cm, and number of pulses = 2 and 5. The pulses are applied across the cells between two electrodes on the microchip site so that we can investigate a relationship between efficacy of electroporation and the pulse parameters. We used PI and Calcein-AM to measure the efficacy of the electroporation. Cell viability was also measured after the electroporation experiment.

Results: The result of the experiment was analyzed using a confocal microscopy. The analysis have showed that the sample applied 1 kV/cm gated at a rate 15.9% and 88.9% than the control for 2 and 5 pulses respectively. The cell viability was over 91% for all the applied electrical conditions.

Conclusions: In vitro electroporation experiments were performed using a new microchip applicator and efficacy of the electroporation was evaluated. Our study shows that the new microchip applicator is a useful device to assess the efficacy of the electroporation with anti-cancer drug in vitro and the device can be used to assess electroporation-induced drug delivery for cancer treatment in vitro.

Session 4P1b
Microwave Devices and Circuits

Wideband Differential Phase Shifters Using Waveguides Filled by Inhomogeneous Dielectrics

Mohammad Khalaj-Amirhosseini
Iran University of Science and Technology, Iran

Abstract— A new structure is proposed for wideband differential phase shifter. This structure utilizes a waveguide filled by a longitudinally inhomogeneous dielectric along with a simple uniform waveguide. To optimally design the structure, the electric permittivity function of the inhomogeneous waveguide is expanded in a truncated Fourier series, firstly. Then, the optimum values of the coefficients of the series are obtained through an optimization approach to have low phase shift error and low reflection coefficient in the desired frequency bandwidth. The usefulness of the proposed structure is studied using a comprehensive example.

Introduction: Differential Phase Shifters (DPSs) have many applications in microwave circuits such as phase discriminators, beam forming networks, frequency translators, power dividers and phase array antennas. The main disadvantage of the conventional waveguide DPSs, which utilize dielectric cards or slabs in the waveguides, is their narrow band property. In this paper, we propose a new structure as a wideband DPS. The proposed structure as shown in Fig. 1 is a waveguide with dimensions a and b and of length d, whose cross section has been filled by a longitudinally inhomogeneous dielectric $\varepsilon_r(z)$ or several thin dielectric layers. The phase difference between two matched ends of the proposed DPS at frequency f is as follows

$$\varphi(f) = \text{Angle}\left(S_{21}(f)\right) \tag{1}$$

Also, the phase difference between two matched ends of a hollow waveguide of length d_0 at frequency f is as follows

$$\varphi_0(f) = \text{Angle}\left(\exp\left(-j2\pi f\sqrt{1-(f_c/f)^2}d_0/c\right)\right) \tag{2}$$

where c is the velocity of the light and $f_c = c/(2a)$ is the cutoff frequency of the hollow waveguide. We would like that the difference between these phase differences ($\Delta\varphi = \varphi - \varphi_0$), calling it the phase shift, be equal to the desired value $\Delta\varphi_d$ at all frequencies in the desired frequency bandwidth, i.e., from $f_{\min}$ to $f_{\max}$.

We designed a DPS in a frequency range from 8.0 to 12.0 GHz (X-Band), considering $a = 0.9$ inch, $b = 0.4$ inch (WR-90) and $\varepsilon_{r,\max} = 10$ for $\Delta\varphi = 90^\circ$ and $\rho_{\max} = -13$ dB. It is observed that the optimally designed structure yields a low phase error and also the absolute of the input reflection coefficient is less than -13 dB at the desired frequency band.

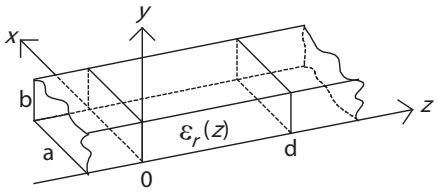

Figure 1: A waveguide filled by a longitudinally inhomogeneous dielectric designed as a Differential Phase Shifters (DPSs).

Analysis and Design of a Novel Reconfigurable Defected Ground Structure Resonator on CPW Technology

Heba B. El-Shaarawy[1, 2], **Fabio Coccetti**[1], **Robert Plana**[1, 2], **Mostafa El-Said**[3], **and Essam A. Hashish**[3]

[1]Laboratoire d'Analyse et d'Architectures des Systèmes
Centre National de la Recherche Scientifique (LAAS-CNRS), Toulouse, France
[2]University of Toulouse, Toulouse, France
[3]Electronics and Communications Department, Cairo University, Cairo, Egypt

Abstract— The increasing development of wireless applications introduces new requirements for transceiver architectures that feature excellent microwave performances and enhanced integration density that is achieved through miniaturization of modules as well as the introduction of multi standard functionalities.

A novel reconfigurable Defected Ground Structure (DGS) resonator fabricated on planar CPW technology is here presented. The cell is endowed with an original design which enables the arbitrary generation of multiple transmission zeros. The chosen design is indeed based on a slot transmission line defect created on the lateral ground planes of the CPW with the double advantage to allow a simple reconfiguration, by means of surface mounted (or fabricated) components, and a very compact solution, by exploiting the transversal dimension of the CPW-TL, as shown in Fig. 1(a). In this work, the reconfigurability is proven by means of short bridges mounted in specific locations of the slot patterns. The measured responses of the DGS cell with different states are presented Fig. 1(b).

Three basic configurations have been simulated and measured showing a very good agreement within each other. In the first state, the response shows three transmission zeros at 2.28, 7.44 and 9.85 GHz. In the second state, the upper bigger square is isolated from the rest of the structure, which gives a stopband filter response with a transmission zero at 5.7 GHz. In the third state, the upper square resonator is isolated as in the previous case, and the smaller resonator is divided into two unequal length resonators, each forming a $\lambda_g/4$ resonator that is terminated by a short circuit directly connected to the ground. Each resonator forms a transmission zero at the corresponding frequency (4.8 and 10.9 GHz).

Although that DGS has attracted the interest of many researchers, the work that has been published so far has explained the structure only by means of parallel RLC equivalent circuit to represent the transmission zeros in the response, providing no insight into the underlying electromagnetic wave propagation principle and hence providing no design rules. In this paper, in addition to the transmission line equivalent circuit using parallel RLC resonators, electromagnetic explanation of the structure, using the slot line waveguide design equations, is hereby presented providing simple and efficient design rules. These rules have been applied to the design of the

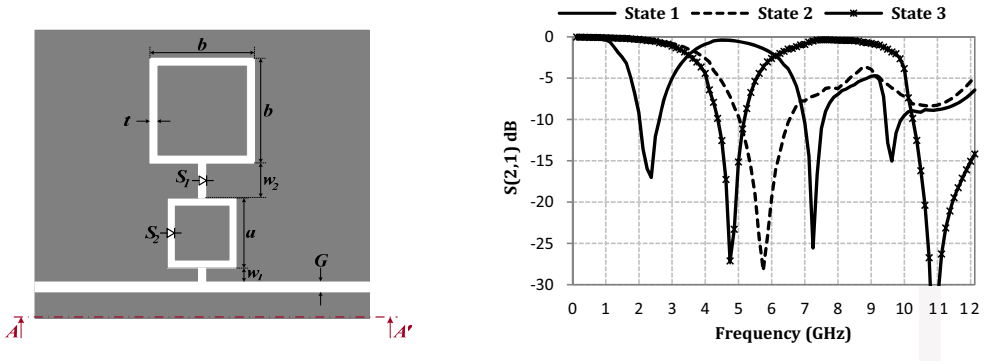

(a) (b)

Figure 1: (a) Proposed reconfigurable DGS resonator. (b) Measured responses of the DGS resonator at different states.

structures centered at different arbitrary frequencies and validated by simulated and measured responses, all in very good agreement with each other.

The DGS here presented represents a very promising building block for more complex structures (such as filters and phase shifters) where reconfigurability and size are at stake. Future implementation by means of integrate RF silicon and reconfigurability by means of RF MEMS switches/capacitors are expected in order to provide a further degree of improvement.

A Novel LTCC Wideband Filter with Good Out-band Performance

Kengyi Huang, **Chao Ping Hsieh**, **and Tsenchieh Chiu**
Department of Electrical Engineering, National Central University, Taiwan, R.O.C.

Abstract— Ultra-wideband (UWB) technology has been receiving great attention since the Federal Communication Committee (FCC) released the frequency band from 3.1 to 10.6 GHz for commercial communication applications in 2002. Many designs of wideband filters have been proposed in the past. For commercial and industrial applications, the frequency band from 3.1 to 10.6 GHz is divided into several band groups by ECMA subsequently in 2005. For instance, the band group #1 is from 3.1 to 4.8 GHz. In this paper, a compact wideband filter with good out-band selectivity will be proposed at the frequency from 3.1 to 4.8 GHz for the applications of the UWB band group #1. Based on a second-order combline filter, an extra capacitor is added to the combline structure to obtain the wideband impedance matching from 3.1 to 4.8 GHz. In modern wireless communications, out-band rejection and compactness of filters are both in great demand. In order to achieve better attenuation at lower and upper stop-bands, the proposed design is extended to third-order circuit structure. 30-dB attenuation at both 2.4 and 5.8 GHz is obtained in the proposed design. For compactness, the proposed design is fabricated by using low-temperature co-fired ceramic (LTCC) technology. The filter is simulated by using High Frequency Structure Simulator (HFSS). Simulated results are in good agreement with the measurement. The volume of the proposed wide-band filter is $2.5 \times 2.0 \times 0.8\,\mathrm{mm}^3$, which is suitable for commercial wireless applications.

Cascade Electromagnetic Pulse (EMP) Protection Using an AlGaN/GaN MSM 2-DEG Varactor

Liann-Be Chang, **Atanu Das**, **Ferng Yi Cherng**, **and Ming-Jer Jeng**
Chang Gung University, 333, Taiwan, R.O.C.

Abstract— A cascade electromagnetic pulse protection configuration comprised of AlGaN/GaN MSM 2-DEG varactor is proposed in this study. This proposed configuration can effectively protect sophisticated electronic configuration or equipment from faster introduced EMP or specially EMP with faster rise time. This work proposes a cascade EMP protection configuration integrated with an LEMP protection configuration and fast response element AlGaN/GaN MSM 2-DEG varactor with new architecture, which can be applied to a communication system and protect from common lightning damage as well as against various sudden EMP attacks. An electromagnetic pulse, which can damage the sophisticated electronic system, is classified into different categories including LEMP (Lightning induced electromagnetic pulse), NEMP (Nuclear electromagnetic pulse), HEMP (High altitude electromagnetic pulse) and PEMP (Portable electromagnetic pulse). The Lightning induced electromagnetic pulse has rise time 10–15 μs, whereas all other EMPs attacks mentioned above have faster rise times about 10 ns. Thus, a conventional LEMP protection configuration is unable to protect against the advanced EMP attack. Our proposed cascade EMP protection is capable of protecting electronic devices against EMP attacks with nano-second rise time. In this present work, a cascade EMP protection configuration, which integrates an LEMP protection configuration and a new type fast response protection, is comprised of a MSM 2-DEG varactor. The MSM 2-DEG varactor consists of two back-to-back connected Schottky diodes above a 2- DEG layered structure. Its electrical behavior is the key issue for the current EMP protection configuration. The capacitance of the unbiased MSM 2-DEG is determined by the electrode area and the distance to the 2-DEG channel, which acts as an equipotential plane. An applied bias voltage depletes the channel below the reverse-biased electrode. For large bias voltages, the depletion region penetrates deeply into device, and capacitance drops to a very low value within a small voltage region. The transition voltage from high to a low capacitance depends on the 2-DEG carrier density and is strongly related to threshold voltage of the corresponding device. For this case, the transition voltage is the threshold voltage of the reversed biased contact added by the voltage drop at the forward-biased contact.

The AlGaN/GaN heterostucture was grown by MOCVD on sapphire substrate for the fabricated MSM 2-DEG varactor diode. The room temperature Hall measurement yields a 2-DEG carrier concentration of $3.6 \times 10^{13}\,\mathrm{cm}^{-2}$ and a mobility of $600\,\mathrm{cm}^2$/V-sec. The device processing begins with mesa isolation performed by argon sputtering followed by Ni/Au metal pad deposition. The device passivation was performed by [P_2S_5 + (NH_4) S_2] solution for five minutes. The measured C_{max} and C_{min} ratio is found to be 24.4. The transition voltage is about 6 V for the device. This varactor is cascaded in series with the LEMP protection configuration. This fast response varactor has normally high capacitance (C_{max}) within a certain voltage range, and therefore offers low insertion loss in high frequency range. When an intense overvoltage EMP in front portion appears, the varactor has a low capacitance (C_{min}) and high impedance that impedes signal coupling, thus, protecting electronic elements from the damage of a surge pulse. Meanwhile, the LEMP configuration can sink the maximum portion of the overvoltage stress with slower response time. In this way the proposed cascaded Electromagnetic pulse protection configuration can properly accomplish its work.

In conclusion, a cascaded EMP protection configuration is proposed and investigated, integrated with LEMP protection configuration and a fast-response protection configuration, wherein a capacitive reactance varactor element is cascaded to the path of signal transmission. Due to the inherent electrical property of AlGaN/GaN MSM 2-DEG varactor diode, the proposed present protection configuration is capable protecting the front-end of a communication system against faster introduced EMP attacks.

The Design of Triple-Mode Low Noise Amplifier for SDR System

Yang Liu, **Sungju Choi**, **Sangho Lee**, **and Hyeongdong Kim**
Microwave Engineering Lab., Electrical & Computer Engineering Department
Hanyang University, Seoul, South Korea

Abstract— With the rapid development of communication technology, the research of convergence technology that can implement various communication services on a single terminal is desired. Software designed ratio (SDR) is the technology widely recognized as a means to realize these convergence technology which converts operation frequency band to suit the communication services decided by hardware according to the operation mode of SDR when the software decides the operation.

The low noise amplifier for CDMA 2000 1x, WCDMA and WiBro band applicable to SDR handset is designed by using TSMC RF 0.18 µm CMOS process in this work. The designed LNA achieves simultaneous power and noise matching, and narrow band voltage gains in three frequency bands of interest. The selection of operating frequency band is implemented by four switched-capacitor circuits, where every two of them located at the input and output matching network, each switch is realized by NMOS transistor, and it is shown as the followed Figure 1.

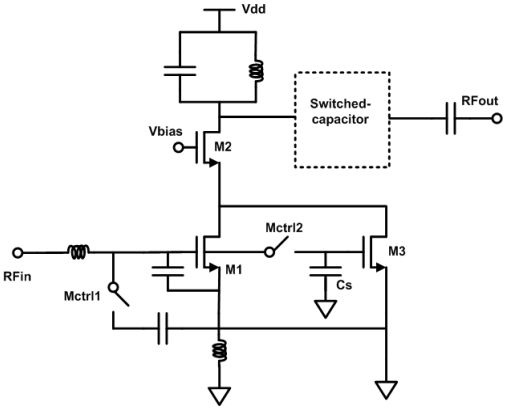

Figure 1: Schematic of the main amplifier.

In the proposed LNA, the CDMA 2000 1x band is selected when the transistor M_{ctrl1} and M_{ctrl2} is turned on at one time, and it can be changed to WCDMA band by turning off M_{ctrl1} and turning on M_{ctrl2} only, and when both the switches are turned off, the WiBro band can be selected. The capacitor, C_s, in parallel with M_{ctrl2}, connected from M1 to M3, it helps to reduce the noise figure greatly at each frequency band of interest while improving DC current consumption excellently. Three narrow band voltage gains are obtained by the control of switched-capacitor circuits at output matching network. The design of LNA is simulated by Cadence SpectreRF using TSMC RF 0.18 µm CMOS process. The simulation result shows 2.24 dB noise figure, −12.4 dB input reflection loss, 9.4 dB voltage gain at 1.85 GHz (CDMA 2000 1x), and 2.05 dB noise figure, −17.3 dB input reflection loss, 11.9 dB voltage gain at 2.14 GHz (WCDMA), and 2.23 dB noise figure, −19 dB input reflection loss, 12 dB voltage gain at 2.35 GHz (WiBro) respectively. With a 1.8 V supply voltage, the circuit consumes 5.8 mA DC current for the total process. The post-layout simulation of the circuit will be carried out and the results will be displayed in the final of this paper.

Unconditional Stability Criteria for Microwave Networks

Eng Leong Tan[1], **Xiaofeng Sun**[1], **and Kian Sen Ang**[2]
[1]School of EEE, Nanyang Technological University, Singapore
[2]DSO National Laboratories, 20 Science Park Drive, Singapore

Abstract— This paper presents a review of unconditional stability criteria for analysis and design of microwave networks. A linear two-port network is said to be unconditionally stable (in even mode) if for all passive load and source terminations, the moduli of the input and output reflection coefficients are smaller than one. There are many stability criteria stating the necessary and sufficient conditions for such unconditional stability. One classical set of these criteria is based on the combination of Rollett condition ($K > 1$) together with one auxiliary condition (e.g., $|\Delta| < 1$, etc.), which constitutes a family of dual-parameter stability criteria. Another family of stability criteria involves merely a single-parameter condition, which is often more convenient to analyze and utilize. Besides the popular geometrically-derived criterion ($\mu > 1$ or $\mu' > 1$), many other single-parameter criteria can be deduced that feature various specific advantages. One such criterion that is found to be most advantageous is the quasi-invariant single-parameter criterion ($K_t > 1$). With its simplistic form (like K), it can be shown that $K_t > 1$ if and only if a two-port network is unconditionally stable. The parameter K_t can be derived from the classical matrix invariants and the familiar stability criteria, leading to the straightforward proof of its unconditional stability condition. Moreover, it is invariant under arbitrary lossless termination and reactive matching at either port when unconditional stability exists. Such invariant property is retained so long as $|\Delta| < 1$, which occurs more frequently than $|\Delta| > 1$ for most microwave devices. The parameter can also be aptly related to the maximum available gain of an unconditionally stable device. Application of the quasi-invariant single-parameter criterion is extended for simplified graphical analysis of linear three-port stability. In particular, only one plot of a single-parameter condition needs to be constructed in each termination reflection plane. Such plot is useful to aptly depict the terminations at each port that result in unconditional stability between the remaining two ports. The three-port stability plots are exemplified to illustrate the convenience using the single-parameter condition. These stability plots find direct application in the stabilization of potentially unstable microwave networks.

A Low Cost and High Performance Design of X-band Short Range Doppler Radar Transceiver

Jingzhou Luo and Lixin Ran
Information Science and Engineering College, Zhejiang University, China

Abstract—

Introduction: Recently, more and more Doppler radar products are found in some commercial short-range use circumstances. The features of these Doppler radar products are with high sensitivity of target detection, low power radiation, low cost, easy circuits alignment, and small circuit size, etc. Based on this consideration, the authors made a computer-aided design for a continuous wave (CW) Doppler radar transceiver. The radar works at X band. It has an optimised system performance, and the transceiver PCB (FR4) size can reach $40 \times 40\,\mathrm{mm}^2$.

The design process is divided into three steps. Firstly, establish a system model by conventional radar equation. Secondly, design main module schematics including an oscillator, a mixer, and a TX/RX antenna. Finally, perform a system simulation using the optimised designed circuit parameters to verify the design goal.

Radar Transceiver Design Scheme

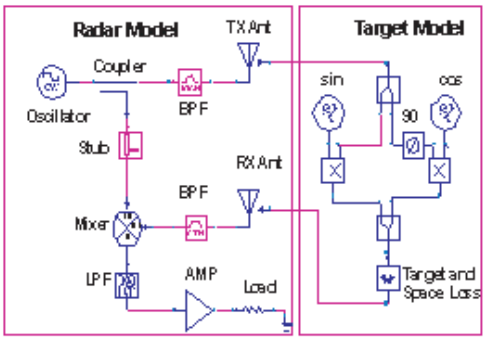

The diagram of designed radar transceiver is shown in the left part in above figure. It mainly consists of an oscillator, a mixer, and two antennas. The right part is a radar target model including frequency sources and phase-shifter relative to Doppler radar application, the attenuator representing the loss in free space and radar cross section (RCS). Our design goal is to determine correctly the target model parameters, optimize the performances of separate circuits, and make a systematic integration of the transceiver. This is done by systematical analysis of radar equation and in virtue of powerful design and simulation tool ADS.

Simulation and Experiment Results: Typical designed circuit specifications at frequency 10.07 GHz with available device model in ADS system are achieved: the oscillator output is 12 dBm, the mixer conversion gain is 13 dB, and the antenna gain is 8 dB. Integration simulations and experiments are also performed and it shows that this design scheme can meet our application requirement.

Session 4P2
Recent Advances in Metamaterials and Invisibility Cloaking 1

From the Perfect Lens to Anti-cloak, Superscatterer and Beyond

Huanyang Chen and C. T. Chan
Department of Physics, Hong Kong University of Science and Technology
Clear Water Bay, Kowlong, Hong Kong, China

Abstract— We find that the concept of the perfect lens, that is a folded geometry in the view of transformation optics, shows the way to design the anti-cloak, superscatterer and other devices. It is known that a negative refractive index medium "cancels" the space of a positive index medium that has the same impedance. An anti-cloak annihilates the functionality of the interior part of the invisibility cloak, and effectively shifts the enclosed region outwards to make contact with the outer part of the cloaking shell that is not "canceled". This leads to a finite cross section. The superscatterer annihilates some space outside and effectively maps the enclosed region outwards to make a large effective scattering region. This leads to the large scattering. The evanescent wave amplification by the double negative material is responsible for these spectacular effects.

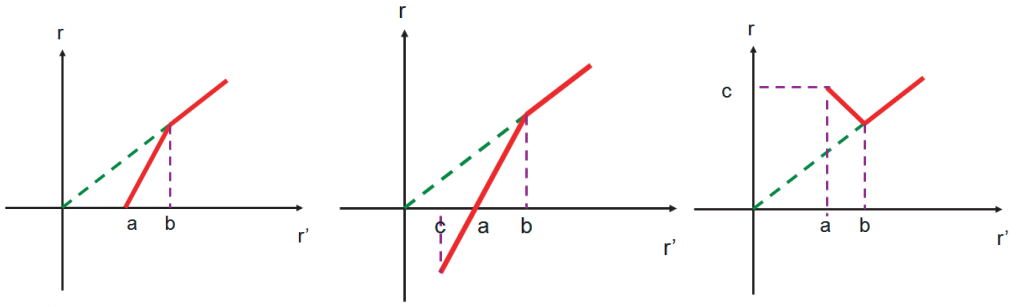

Figure 1: Left: The coordinate mapping for cloak. Middle: The coordinate mapping for anti-cloak. Right: The coordinate mapping for superscatterer.

REFERENCES

1. Chen, H. Y., et al., *Phys. Rev. B*, Vol. 76, 241104(R), 2007.
2. Chen, H. Y., et al., *Opt. Express*, Vol. 16, 14603, 2008.
3. Yang, T., et al., to appear in *Opt. Express*, 2008. http://arxiv.org/abs/0807.5038
4. Chen, H. Y., et al., to appear in *New J. Phys.*, 2008. http://arxiv.org/abs/0808.0536
5. Luo, X., et al., submitted, 2008. http://arxiv.org/abs/0809.1823
6. Ng, J., et al., submitted, 2008.
7. Lai, Y., et al., submitted, 2008.

Analytic Description of Non-ideal Electromagnetic Cloaks

Ilya V. Shadrivov
Nonlinear Physics Centre, Research School of Physical Sciences and Engineering
Australian National University, Canberra ACT 0200, Australia

Abstract— We use analytical solutions for the spatial transformation of the electromagnetic fields to obtain and analyze explicit expressions for the structure of the electromagnetic fields in non-ideal electromagnetic cloaks. We study the efficiency of non-ideal electromagnetic cloaks taking into account losses, impedance mismatch and truncation of the cloak.

The concept of the electromagnetic cloaking is based on the coordinate transformation of space and the corresponding transformation of Maxwell's equations, which provide the required expressions for the effective spatially varying dielectric permittivity and magnetic permeability of the cloak medium [1, 2]. The possibility of creating such cloaks has been confirmed experimentally [3], and it was further discussed and demonstrated in many numerical studies. Numerical simulations are usually performed either by using commercial finite-element equation solvers or by employing the decomposition of the electromagnetic fields into a set of the corresponding eigenmodes. Several studies have analyzed a possibility of creating simplified cloaks [4, 5], since the required media parameters for an ideal cloaking are extremely complex for their realization in experiment. One of the main limitations of the resonant medium used for creating electromagnetic cloaks is losses. In this work we calculate scattering of electromagnetic waves by a cloak with small losses, and show that such scattering effectively equivalent to electric and magnetic currents. These currents lead to the scattering radiation which can be easily evaluated either analytically or numerically.

Next, we estimate the effect of mismatched dielectric permittivity and magnetic permeability on the cloak performance. In this case we show that the non-ideal cloak scatters the waves as a cylinder of a particular radius (for the cylindrical cloak) with a scalar dielectric permittivity, thus giving a clear picture of the scattered field structure and strength.

The original results included in this presentation have been obtained in collaboration with Nina Zharova, Alexander Zharov and Yuri Kivshar.

REFERENCES

1. Pendry, J. B., D. Schurig, and D. R. Smith, "Controlling electromagnetic fields," *Science*, Vol. 312, 1780–1782, 2006.
2. Leonhardt, U., "Optical conformal mapping," *Science*, Vol. 312, 1777–1780, 2006.
3. Schurig, D., et al., "Metamaterial electromagnetic cloak at microwave frequencies," *Science*, Vol. 314, 977–980, 2006.
4. Cummer, S. A., et al, "Full-wave simulations of electromagnetic cloaking structures," *Phys. Rev. E*, Vol. 74, 036621, 2006.
5. Chen, H., et al., "Extending the bandwidth of electromagnetic cloaks," *Phys. Rev. B*, Vol. 76, 241104(R), 2007.

Electromagnetic Beam Modulation through Transformation Optics and Application to Invisibility Cloaking Structure

Yijun Feng, **Xiaofei Xu**, **Tian Jiang**, **and Zhengbin Wang**
Department of Electronic Science and Engineering, Nanjing University, Nanjing 210093, China

Abstract— Recently based on the form-invariant of Maxwell's equations under certain coordinate transformations, the transformation optics proposed in [1, 2] for controlling the electromagnetic (EM) fields has been proved to be an effective approach for manipulating the material properties to satisfy the desired ray traces of the EM waves. The successful application of the transformation optics to the invisibility cloaks has triggered more intensive explorations of this idea theoretically and experimentally, and many interesting theoretical results and practical approaches have been obtained. Besides the invisibility cloak, EM wave concentrators, rotators and other interesting devices have also been proposed with exotic EM behaviors by utilizing the transformation optics.

In this presentation, we will report on applying the finite-embedded coordinate transformation method [3] to design electromagnetic beam modulating devices both in the Cartesian coordinates and in the cylindrical coordinates. By designing the material constitutive tensors of the transformation optical structures through different kinds of coordinate transformations, either the beam width of an incident Gaussian plane wave could be modulated by a slab, or the wave propagating direction of an omni-directional source could be modulated through a cylindrical shell. We will present the design procedures and the full wave electromagnetic simulations that clearly confirm the performance of the proposed beam modulating devices.

Finally, we will discuss the application of the concept of the electromagnetic beam modulators to invisibility cloaking structures.

ACKNOWLEDGMENT

Supported by the National Basic Research Program of China (2004CB719800), the National Nature Science Foundation (No. 60671002).

REFERENCES

1. Leonhardt, U., *Science*, Vol. 312, 1777–80, 2006.
2. Pendry, J. B., D. Schurig, and D. R. Smith, *Science*, Vol. 312, 1780–82, 2006.
3. Rahm, M., S. A. Cummer, D. Schurig, J. B. Pendry, and D. R. Smith, *Phys. Rev. Lett.*, Vol. 100, 063903, 2008.

A New Strategy to Design Cylindrical Cloaks

Wei Xiang Jiang and Tie Jun Cui
State Key Laboratory of Millimeter Waves
Institute of Target Characteristics and Identification
Department of Radio Engineering
Southeast University, Nanjing 210096, China

Abstract— In the invisibility cloaks reported in most literatures, a big problem is that the material parameters have singularities on the inner boundary of the cloaks. Hence the changing range of some parameter components is from zero to infinity, which is difficult to achieve even using metamaterials. A new elliptical invisibility cloak is proposed using a coordinate transformation in the classical elliptical-cylindrical coordinate system, which crushes the cloaked object to a line segment instead of a point. The elliptical cloak is reduced to a nearly-circular cloak if the elliptical focus becomes very small. The advantage of the proposed invisibility cloak is that none of the parameters is singular and the changing range of all parameters is relatively small. An experimental realization of such a new cloak requires building blocks that have uniaxially anisotropic dielectric functions. With the advent of more and more new metamaterial structures, the approaches we proposed here can be much easier to realize.

Hiding Arbitrary Geometries with Dissimilar Cloaks

Kan Yao, **Chao Li**, **and Fang Li**
Institute of Electronics, Chinese Academy of Sciences, Beijing 100190, China

Abstract— Transformation optics, especially invisibility cloaks has received intense attention since a general recipe of designing complex electromagnetic material based on coordinate transformations was proposed. Researches from different viewpoints, like analytical or physical aspect, have been reported. Furthermore, experimental demonstrations have been carried out at microwave frequencies and optical frequencies with the help of metamaterial technology.

Besides the topics mentioned above, designing cloaks for arbitrary geometries is another interesting problem. Most early studies on invisibility cloaks were limited to circular cylindrical cases (2D) or spherical cases (3D) for the convenience of calculation. After that, square cloak, eccentric elliptic cloak, homocentric elliptic cloak, ellipsoidal cloak, etc. were proposed, which reduced the symmetry of the cloak devices and generalized the possible applications. However, all the objects to be cloaked are still regular in geometry. In this paper, we present a method to design arbitrarily shaped cloaks. The general expressions of constitutive tensors are derived by operating transformations in the polar coordinates.

In order to overcome the disadvantage of similar cloak, which is a cloak shell with geometrically similar inner and outer boundaries, when the object contains an elongated direction, a uniform-thick cloak for elliptic region was proposed. The design, although solved the problem in thickness, introduced discontinuities in the cloak shell, and might be not easy to calculate or fabricate, especially for complex geometries. In this paper, we also propose a nonlinear transformation to realize dissimilar cloaks. Combining this transformation and the above method, arbitrarily shaped cloak devices with limited thickness but without discontinuities can be obtained. Full-wave simulations are given to show the validity by using finite element method.

Concealing an Object from Electromagnetic Wave with Metamaterial

Yu Luo[1], **Jingjing Zhang**[1], **Hongsheng Chen**[1, 2], **Bae-Ian Wu**[1, 2], **Lixin Ran**[1], **and J. A. Kong**[1, 2]

[1]The Electromagnetics Academy at Zhejiang University
Zhejiang University, Hangzhou, China
[2]Research Laboratory of Electronics
Massachusetts Institute of Technology Cambridge, MA 02139, USA

Abstract— Isotropic metamaterial is adopted to design coatings which can conceal the size and position information of an object. It is also demonstrated that in small wave length case the incident light will always be deflected around some region inside this coating, making an object there appear invisible to the detector outside. The permittivity or permeability of this isotropic coating is not required to approach to zero, as long as the magnitude of the spatially varying refractive index is larger than one everywhere. Under this condition, concealment can be achieved with artificially structured metamaterials like phonic crystal or high dielectric resonator. Our approach suggests another way to conceal objects, which is probable to realize in physical practice.

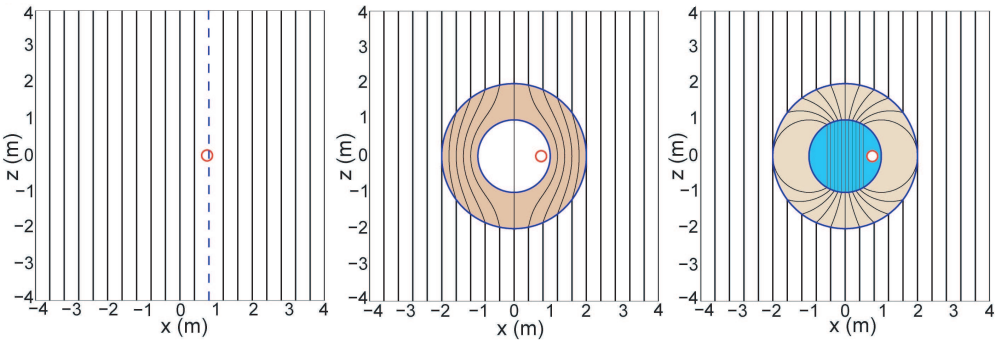

Photonic Crystal Based Subwavelength Imaging and Cloaking Optical Devices

O. Vanbesien[1], **N. Fabre**[1], **X. Mélique**[1],
L. Lalouat[2], **B. Cluzel**[2], **F. de Fornel**[2], **and D. Lippens**[1]

[1]Institut d'Electronique, de Microélectronique et de Nanotechnologie (IEMN — UMR CNRS 8520)
Université des Sciences et Technologies de Lille
Avenue Poincaré, BP 60069, 59655 Villeneuve d'Ascq Cedex, France
[2]Institut Carnot de Bourgogne (ICB — UMR CNRS 5209)
9, Avenue A. Savary, BP 47870, 21078 Dijon, France

Abstract— Potentialities of 2.5D dielectric photonic crystals for subwavelength imaging or invisibility cloaking operation at optical wavelengths are studied numerically and experimentally. First, a negative refraction based flat lens is designed, fabricated and characterized. Starting from the band structure of two dimensional photonic crystals (PCs) and from the resonance properties of finite dimension PC slabs, an optimization procedure in terms of refractive index and transmission to promote focusing is given. For the prototype, a two dimensional array of air holes defined by electron beam nanolithography and etched by ICP-RIE is defined on a multilayered stacked semiconductor InP/GaInAsP/InP heterostructure. Light is injected via a cut ridge waveguide acting as a subwavelength source ($\lambda/3$). Using scanning near-field optical microscopy, subwavelength imaging (0.8λ) for a deduced refractive index of -1 is obtained at 1.55 µm. Experimental results compare favorably to full three dimensional FDTD simulation of the complete device. Second, using a similar approach, original designs of structures aimed to operate as cloaking devices are proposed by combining photonic lattices operating under different regimes, exploiting both pass- and stop-band properties. An example combining spatially evanescence properties and negative refraction is more deeply analyzed. A cloaking effect for an incident Gaussian shaped plane wave is numerically demonstrated with the potential of hiding rather wide regions of space (much bigger than the operating wavelength) to the incident wave. Advantage in terms of bandwidth or limitations in terms of injection waveform of such a device are also studied and compared to other approaches based on permeability and/or permittivity engineering.

Broadband Acoustic Cloak with Multilayered Homogeneous Isotropic Materials

Y. Cheng, J. Y. Xu, and X. J. Liu
Key Lab of Modern Acoustics of MOE, Nanjing University, Nanjing 210093, China

Abstract— Invisibility cloaking has received much attention in the literature recently [1]. On the basis of coordinate transformation method and effective medium theory, we design an acoustic cloak using concentric multilayered structure with alternating homogeneous isotropic materials [2–5]. The cloak is analyzed by means of both rigorous scattering theory and finite element numerical simulations. The results demonstrate that efficient cloaking effect, i.e., low-reflection and power-flow bending, can be achieved for a wide frequency range in which the overall performance gradually degrades with increasing frequency. The mechanism of the cloaking is ascribed to a specific multiple scattering process determined by the microscopic material distribution and structural details of the cloak. We also demonstrate some interesting resonant phenomena when concealing penetrable materials. We observe that the cloak-induced reverse-phase monopole and dipole resonances can increase the total scattering cross-section (TSCS) around the resonant frequencies, while the in-phase monopole resonance decreases the TSCS. Further studies show that the zeroth and first order cylindrical wave components are the dominated elements in the cloak-induced resonance. All of these results may provide us with deeper insights into the cloaking phenomenon as well as a simple path to experimental realization of acoustic cloak.

REFERENCES

1. Schurig, D., J. J. Mock, B. J. Justice, S. A. Cummer, J. B. Pendry, A. F. Starr, and D. R. Smith, *Science*, Vol. 314, 977, 2006.
2. Cheng, Y., F. Yang, J. Y. Xu, and X. J. Liu, *Appl. Phys. Lett.*, Vol. 92, 151913, 2008.
3. Cheng, Y. and X. J. Liu, *Appl. Phys. Lett.*, Vol. 93, 071903, 2008.
4. Cheng, Y. and X. J. Liu, *Appl. Phys. A*, 2008, in press.
5. Cheng, Y. and X. J. Liu, *J. Appl. Phys.*, 2008, in press.

Limitations of High-order Transformation and Incident Angle on Simplified Invisibility Cloaks

Baile Zhang[1], **Hongsheng Chen**[1,2], **and Bae-Ian Wu**[1]
[1]Research Laboratory of Electronics
Massachusetts Institute of Technology, Cambridge, MA 02139, USA
[2]The Electromagnetics Academy at Zhejiang University
Zhejiang University, Hangzhou 310058, China

Abstract— In studies of the transformation based invisibility cloaks, simplified cylindrical cloaks for normally incident waves with only one polarization are often preferred in experimental demonstration, simulations and other practical designs. However, the scattering evaluation at only one incident angle is not sufficient to describe the performance of such simplified cloaks. Previously, scattering results for normal incidence were obtained only semi-analytically from commercial simulation tools. Therefore, a fully analytic method to evaluate the performance of simplified cylindrical cloaks at both normal and oblique incidences is needed in designing invisibility cloaks.

The main reasons for scattering from a simplified cloak are the mismatches at the outer and inner boundaries. There was study on the mismatch at the outer boundary that showed that impedance matching at the outer boundary applied by a high-order quadratic transformation is able to decrease the scattering efficiently, while there is little study on the mismatch at the inner boundary.

In this paper, the field solutions of the simplified cylindrical cloaks at both normal and oblique incidences are found. The reduced scattering from these simplified cloaks can be achieved only within a limited range of incident angles. The high-order transformation with impedance matched at the outer boundary may produce stronger scattering than the simplified linear one without impedance matched at the outer boundary due to inefficiency of guided waves close to the inner boundary.

Perfect Invisibility Using Isotropic Material with Negative Refractive Index

J. C. Nacher[1], **U. Leonhardt**[2], **and T. Ochiai**[3]

[1]Department of Complex Systems, Future University-Hakodate
116-2 Kamedanakano-cho Hakodate, Hokkaido, 041-8655, Japan
[2]School of Physics and Astronomy, University of St Andrews
North Haugh, St Andrews, KY16 9SS, Scotland
[3]Faculty of Engineering, Toyama Prefectural University
5180 Kurokawa Imizu-shi Toyama, 939-0398, Japan

Abstract— The aim of an invisibility device is to guide light around any object put inside, being able to hide objects from sight. Here, we propose a novel design of dielectric invisibility device based on an optically isotropic material with negative refractive index. Using an optical conformal mapping [1, 2], we show that this device creates perfect invisibility. In particular, it represents an example of possible cloaking devices where the time delay is zero. Furthermore, due to impedance matching of negatively refracting materials, the waves are completely transmitted when crossing different material index borders and consequently reflecting waves are zero [3]. Our device is composed of five artificial dielectric materials with different values of refractive indices n and different index profiles, which are combined with one another like building blocks. The cloaking device is then composed of two Riemann sheets. While the first Riemann sheet the material has refractive index $n = 1$, the second Riemann sheet is composed of four quadrants with negative alternated with positive refractive index profile n. While Pendry et al. [4, 5] suggested a complex and highly anisotropic media that leads to perfect invisibility, here we show that perfect invisibility in isotropic media is also possible. The condition is that these materials should be partially negatively-refracting. From the theoretical side, our approach has also shown that it is possible in isotropic media to get around the Nachman's theorem. In summary, our findings strongly indicate that perfect invisibility with isotropic materials is possible and open new possibilities on the way to perfect invisibility in the visible range of the spectrum.

REFERENCES

1. Leonhardt, U., *New. J. Phys.*, Vol. 8, 118, 2006.
2. Leonhardt, U., *Science*, Vol. 312, 1777, 2006.
3. Ochiai, T., U. Leonhardt, and J. C. Nacher, *J. Math. Phys.*, Vol. 49, 032903, 2008.
4. Pendry, J. B., D. Schurig, and D. R. Smith, *Science*, Vol. 312, 1780, 2006.
5. Schurig, D., et al., *Science*, Vol. 314, 977, 2006.

Session 4P3
Remote Sensing, GPR, SAR

Automatic Detection of Terain Surface Changes after Snowstorm from Multi-temporal Images of Fully Polarimetric ALOS PALSAR and Multi-channel AMSR-E

Ya-Qiu Jin, **Dafang Wang**, **Hao Chen**, **and Haipeng Wang**
Key Laboratory of Wave Scattering and Remote Sensing Information (MOE)
Fudan University, Shanghai 200433, China

Abstract— In January 2008, a big snowstorm and frost made a surprise attack on southern China. It is unusual to have such snowstorm and frost in warmly southern China over 50 years. However, the operational code for both passive and active microwave remote sensing failed to detect this snowstorm. It needs further study with applicability to monitoring snowstorm in both technology and operational analysis.

In active remote sensing, a method of two thresholds expectation maximum and Markov random field (2EM-MRF) is developed to automatic detection of terrain surface changes caused by snowstorm using multi-temporal fully polarimetric ALOS PALSAR images. The terain surface is first classified based on fully polarimetric scattering, and then three-kind changes, i.e., enhanced, reduced and no-changed, of polarimetric characteristic parameters, e.g., total power, VV-HH, VH, etc., are detected. Using the tool of Google Earth, the surface change situation can be demonstrated in multi-azimuth views as animated cartoon.

In passive remote sensing, the radiative transfer model is developed to analyze the scattering and polarization indexes from multi-temporal multi-channel AMSR-E data during snowstorm of southern China in 2008. A new algorithm and logic tree for snow and frost detection is presented, and well validated.

Pulse Electromagnetic Sounding of the Permafrost Layered Medium

V. L. Mironov and K. V. Muzalevskiy
Kirensky Institute of Physics, SB RAS Krasnoyarsk, Russia

Abstract—

Introduction: In view of the global climate change, the monitoring season variations of the permafrost area becomes a crucial factor for global climate prediction modeling. The adequacy of wave scattering model is crucial for the ground penetrating radars (GPR) to be used as an effective instrument for detecting and retrieving the subsurface structural discontinuities [1–3]. In this paper, propagation of a super wide-band electromagnetic pulse in a frequency dispersive medium representing the active layer permafrost area is theoretically modeled.

Methodologies Applied: On the basis of the spectroscopic soil dielectric model [4, 5], the GPR pulse complex amplitude was calculated using solution of a 3-D wave scattering problem. A point dipole was used to model a receiver/transmitter antenna. Transmitting antenna was excited with a pulse voltage form equal to the first time derivative of a Blackman–Harris window function having duration of one nanosecond. The complex permittivity profiles with depth were obtained using the spectral dielectric model [4, 5], and the temperature and moisture profiles in the permafrost active layer, which were measured at the North Slope, Alaska, near Toolik Lake, at N 68° 38', W 149° 35' [6]. The dielectric model employed takes into account contributions from the organic/mineral contents of soil, liquid soil water, bound soil water, arising due to interaction of soil water molecules with the surface of organic/mineral and ice particles, as well as from the ice particles in frozen soil themselves.

Analysis of Pusle Responce from a Permafrost Layered Medium: The numerical algorithm developed allowed to calculate the GPR pulse amplitude as a function of time delay, which finally resulted in a simulated GPR image representing a layered permafrost medium in the course of freezing and thawing processes. The impact of a frozen/thawed boundary on pulse propagation and the maximum depth of detecting that boundary were determined. In addition, pulse- spectral characteristics and attenuation of pulse energy in the course of propagation through thawed and frozen layers as well as the processes of pulse reflection from the thawed/frozen boundary were analyzed.

REFERENCES

1. Daniels, D., *Surface Penetrating Radar*, Inst. Elect. Eng., London, U.K., 1996.
2. Lambot, S., E. C. Slob, I. Van den Bosh, B. Stockroeckx, and M. Vanclooster, "Modeling of ground-penetrating radar for accurate characterization of subsurface electric properties," *IEEE Trans. Geosci. Remote Sensing*, Vol. 42, No. 11, 2555–2568, 2004.
3. Lu, T., W. Cai, and P. Zhang, "Discontinuous Galerkin time-domain method for GPR simulation in dispersive media," *IEEE Trans. Geosci. Remote Sensing*, Vol. 43, No. 1, 72–80, 2005.
4. Mironov, V. L., M. C. Dobson, V. H. Kaupp, S. A. Komarov, and V. N. Kleshchenko, "Generalized refractive mixing dielectric model for moist soils," *IEEE Trans. Geosci. Remote Sensing*, Vol. 42, No. 4, 773–785, 2004.
5. Mironov, V. L., R. D. Roo, and I. V. Savin, "Dielectric spectroscopic model for Tussock and Shrub tundra soils," *Proc. IGARSS'07*, Barcelona, Spain, July 22–27, 2007.
6. De Roo, R. D., A. W. England, H. Gu, H. Pham, and H. Elsaadi, "Groundbased radiobrightness observations of the active layer growth on the north slope near Toolik lake, Alaska," *Proc. IGARSS*, Vol. 4, 2708–2711, Denver, USA, 2006.

Experiments on Three-Dimensional Microwave Imaging of Human Body

W. Hong[1, 2], **W. X. Tan**[1, 2, 3], **Y. P. Wang**[1, 2], **Y. Lin**[1, 2, 3], **and Y. R. Wu**[1, 2]

[1]National Key Laboratory of Microwave Imaging Technology, China
[2]Institute of Electronics, Chinese Academy of Sciences, China
[3]Graduate University of Chinese Academy of Sciences, China

Abstract— Three-dimensional (3-D) microwave imaging has been developed as an important detecting and monitoring technique. In this paper, the 3-D imaging algorithm based on the cylindrical imaging geometry is investigated from the aspect of the point target's spectrum. Then the similarities and differences of the algorithms between the cylindrical imaging geometry and plane imaging geometry are analyzed. Finally, the experiments carried out in microwave anechoic chamber and the processing results are provided to illustrate the effect of the 3-D microwave imaging of the human body.

The property that microwave could penetrate the clothing barriers to reconstruct the three-dimensional (3-D) image of human body and the concealed objects beneath the clothing in the 3-D space domain has been demonstrated and developed by Huguenin (1991), Collins (1995) and Sheen (2001, 2005, 2006). The microwave radiation is harmless nonionizing to the human body with the very low transmit power. In addition, the high resolution 3-D imageries of the human body could be obtained with the 3-D microwave imaging technique. Therefore, 3-D microwave imaging technique of human body has been applied to various checkpoints, such as airports in Amsterdam, border crossings, commercial buildings and so on. Recently, due to the increasing threat of terrorism, the need for better security detecting and monitoring has further promoted the human body 3-D microwave imaging technique and applications.

Firstly, we analyze the representation of the spectrum of the point target in the 3-D wavenumber and deduce the 3-D imaging algorithm for processing cylindrical imaging geometry data from the aspect of Doppler frequency formation of the point target.

Secondly, we review the 3-D imaging algorithm based on the plane imaging geometry and present the similarities and differences of two algorithms through the simulations. Theoretically speaking, we can get the 3-D imagery of the human body from different angles (through three or more scanning planes), and then reconstruct the fully 3-D imagery of the human body.

Finally, the 3-D microwave imaging of human body experiments are conducted in anechoic chamber with the frequency ranging from 33 GHz to 38 GHz. As for the data collection in the experiment is very time-consuming, a little mannequin (about 1.2 meters high) is selected as the illuminated object. Two kinds of experiments for naked mannequin and clothed mannequin with concealed items using plane and cylindrical imaging geometry are performed, respectively.

In this paper, the 3-D imaging algorithm is studied and proven both theoretically and experimentally. With the 3-D microwave imaging technique, the high resolution 3-D microwave imageries of the human body could be obtained for personnel surveillance application.

Evaluation of Scattering in Collision Avoidance Radar Application

Wei-Han Lee and Wen-Jiao Liao
Department of Electrical Engineering, National Taiwan University of Science and Technology, Taiwan

Abstract— This work uses a high frequency electromagnetic numerical tool to evaluate the scattering characteristics of vehicles. The projected application is for use on the collision avoidance radar utilizing frequency modulated continuous wave. Experiment results show that a car is a relatively complicated scattering target, which can be regarded as a collection of several scattering sources. The distributions of scattered signals vary as the geo locations of the radio source and scattering targets change. Effects of critical parameters such as the longitudinal distance to the target, lateral offset of the target and the orientation of the target, are investigated. The findings can be used to develop detection and tracking algorithms for collision avoidance radars.

Monitoring of Satellite Thermal Patterns of Warm Core Ring in Subarctic Sea Surface

S. Nakamura
Kyoto University, Japan

Abstract— This notes a part of monitoring of satellite thermal patterns of warm core ring in subarctic sea surface. A modeling is introduced in a scope of hydrodynamics. In practice, satellite data should be combined to the data obtained by direct measurement of the related factors by the survey ships along the stretched legs.

Monitoring of Satellite Thermal Patterns of Ocean Front Evolution in Relation to Ocean Water Stratification

S. Nakamura

Kyoto University, Japan

Abstract— The author has studied satellite thermal patterns on the sea surface found when he had received the satellite signals directly by a simple system settled on the coast facing the ocean. Signals from a couple of the existing satellites with a polar orbital motion are obtained by a system for directly receiving satellite signal in a personal computer. In this work, the author introduces a note to a problem of satellite thermal pattern of ocean front evolution. His special interest in this work is what could be seen a vertical structure of the ocean to relate a result by monitoring of satellite thermal patterns of ocean front evolution.

With the author's understanding of the satellite thermal pattern on the sea surface under a scope of hydrodynamics, a hypothetical evolution of the ocean front between a warm ocean water mass and a cold ocean water mass is in the author's interest. In order to illustrate a typical thermal pattern in a vertical section of an ocean water stratification, several models are introduced.

The ocean scientists has been used to assume a two layered ocean for convenience of their mathematical modeling of ocean water motions. Any two layer model makes us it easy to analyze by a mathematical formulation and by a numerical computation. They use to assume several conditions for solving the model problem, though the solution is simply the solution of their model but the actual ocean.

Then, the author introduces three typical patterns for his interested vertical section of the ocean as follow.

The first pattern is a simple two layer model for a surface layer and deep layer. The surface layer might be formed by an inflow of river waters from the land, or, a layer which is taken as a layer above the thermocline. This layer is strongly affected by an atmospheric effect and by the solar radiation effect. In fact, the thermocline is found between the surface layer and the deep layer.

The second pattern is a case of a horizontal water intrusion into a slit formed between the two layer considered above in the fist case. The densimetric condition should be satisfied some condition of the salinity and the water temperature. Balance of buoyancy is interesting factor in this case.

The third case is the upper layer is formed after intrusion of the deep water layer. In this case also buoyant balance is interesting factor.

With a hydrodynamic understanding about what noted above, we could have a chance to have more advanced satellite monitoring system for the thermal pattern on the sea surface as a part of the global ocean.

Integrated Cryogen-free 2.5-THz Heterodyne Receiver for Spectroscopy and Security Applications

H. Richter[1], **A. D. Semenov**[1], **S. G. Pavlov**[1], **H.-W. Hübers**[1], **L. Mahler**[2], **R. Green**[2], **A. Tredicucci**[2], **H. E. Beere**[3], **D. A. Ritchie**[3], **K. Il'in**[4], **and M. Siegel**[4]

[1]German Aerospace Center (DLR), Institute of Planetary Research
Rutherfordstr. 2, Berlin 12489, Germany
[2]NEST CNR-INFM and Scuola Normale Superiore
Piazza dei Cavalieri 7, Pisa 56126, Italy
[3]Cavendish Laboratory, University of Cambridge
Madingley Road, Cambridge CB3 0HE, United Kingdom
[4]Institute of Micro- and Nano-Electronic Systems, University of Karlsruhe
Karlsruhe 76187, Germany

Abstract— Terahertz spectral range has recently attracted substantial interest due to expected prospects of introducing heterodyne terahertz technology into high-altitude astronomy for molecular spectroscopy or into public security for stand-off detection of hidden threats. In a heterodyne receiver the signal radiation and the radiation from a local oscillator are both applied to a nonlinear device (mixer), which converts frequency of the signal from the THz range down to a few GHz. The most sensitive for sub-terahertz frequencies are superconductor-insulator-superconductor mixers, while above approximately 1.5 THz superconducting hot electron bolometric mixers have better sensitivity. For spectroscopy the local oscillator has to be a narrow band, continuous wave, coherent radiation source. Typically, below 2 THz multiplied microwave sources are used as local oscillators. At higher frequencies, where the output power of multiplied microwave sources is too low, THz quantum cascade lasers are promising alternative. Initial experiments showed the potential of this approach and demonstrated its feasibility for Doppler limited high resolution molecular spectroscopy. Here we present a liquid-cryogen free 2.5 THz heterodyne receiver with the quantum cascade laser as local oscillator and the superconducting hot-electron mixer. The receiver is integrated in a pulse tube cooler and has a noise temperature of 2000 K in the 3 GHz intermediate frequency band. High degree of Gaussity of the receiver directional pattern provides easy coupling to external optics. Integrated receiver is an important step towards heterodyne instruments for space based or aircraft based missions as well as user-friendly turn-key systems for applications in public security.

Air Quality Monitoring with a Ground-based FTIR Solar Absorption Spectroscopy during the Beijing Olympic Games

Q. H. Liu, **J. Cheng**, **and Y. M. Du**
State Key Laboratory of Remote Sensing Science
Institute of Remote Sensing Applications, Chinese Academy of Sciences
Beijing 100101, China

Abstract— Atmospheric trace gases monitoring plays an important role in air quality evaluation. A ground-based FTIR solar absorption spectroscopy was employed to monitor the air quality during the Beijing Olympic games. The FTIR spectrometer with spectral resolution of 0.02 cm-1 had been developed by BVS (Beijing Vision Sky Co. Ltd) and the Canada ABB-Bomem. It was installed on the top of the IRSA building, nearby the Beijing Olympic Park. The solar rays are reflected into the FTIR spectrometer by the tracking mirror. Software of SFIT2, which was originally developed by C. Rinsland and B. Connor, has been selected as inversion code and the target gas profiles of CO, CH4, NO2, N2O, O3, HCL have been retrieved.

When we use the ground-based FTIR data to retrieve the trace gas profiles, the prior information is very important. This paper shows the dependence of a priori information on the trace gas profile inversion accuracy. The retrieved vertical column amount was validated with simultaneously observed DOAS system and consistent results were obtained. Based on the retrieved trace gases profile and vertical column amount, the variation trend and influence of anthropologic activities on several typical trace gases are analyzed in this paper. The results show that the air quality is excellent during the Beijing Olympic games.

Coupling the CUPID and TRGM Models to Study the Temporal Variations of Thermal Emission Directionality of Crop Canopies

H. G. Huang[1, 2, 3], **Q.-H. Liu**[1, 2], **and W. H. Qin**[1, 2, 4]

[1]State Key Laboratory of Remote Sensing Science
Institute of Remote Sensing Applications, Chinese Academy of Sciences
Beijing 100101, China
[2]Beijing Normal University, China
[3]Key Laboratory for Silviculture and Conservation of Ministry of Education
Beijing Forestry University, China
[4]NASA Goddard Space Flight Center, Greenbelt, Maryland, USA

Abstract— Many field experiments have observed the significant temporal variation of TIR (Thermal Infrared) emission directionality, so it is necessary to quantitatively explain this phenomenon to improve the application of the directional remotely sensed TIR observation. In this paper, the 3D Thermal Radiosity Graphics Model (TRGM) and a extended energy balance model CUPID are coupled to simulate the seasonal and daily variation of directional brightness temperature (DBT) of wheat canopies. The improvement of CUPID model mainly focused on simultaneously retrieving the shaded temperature and sunlit temperature of soil surface, which is very important for coupling with TRGM Vegetation structure, soil water content and micrometeorology data are the main input parameters that affect the component temperature distribution. Driven by the input data set *in situ*, the half-hourly DBT dataset of wheat canopy are simulated for 22 days. Several new variables are defined to analyze the DBT temporal variation, which include nadir DBT, "hot spot" DBT, azimuthally averaged DBT at zenith angle of 55°, standard deviation of DBT at zenith angle of 55°, etc. The validation results show that the simulated directional temperature differences have consistent trend with field measurements. Based on the sensitivity analysis, it is found that the soil water content and air temperature are the two most significant factors that affect the DBT distributions, while the wind speed and solar radiation affect DBT much more than air temperature.

Ray Tracing of CMP Antenna Array GPR System

Xuan Feng[1], **Motoyuki Sato**[2], **and Cai Liu**[1]

[1]College of Geo-Exploration Science and Technology, Jilin University
No. 6 Xi Minzhu Street, Changchun 130026, China
[2]Center for Northeast Asian Studies, Tohoku University
41 Kawauchi, Aob-ku, Sendai 980-8576, Japan

Abstract— Accidents caused by antipersonnel (AP) landmines remaining from past conflicts have received considerable public exposure in the last several years. Because ground-penetrating radar (GPR) is sensitive to changes in all three electromagnetic characteristics of a medium, electric permittivity, electric conductivity, and magnetic permeability, GPR is one of a number of technologies that has been extensively researched as a means of improving mine detection efficiency. There is much interest in vehicle mounted array GPR systems for landmine detection and work is being carried out on various national, because high speed array GPR systems can sweep a large area in a relatively short time to improve performance and efficiency.

We developed the vehicle mounted stepped-frequency (SF) CMP antenna array GPR system, which was installed in the mine hunter vehicle (MHV). The system has three vector network analyzers (VNA) and three pairs of Vivaldi antennas that configure a symmetrical CMP antenna array. Based on this configuration, multi-offset CMP data gather can be acquired at every measurement position.

Migration is an important signal processing method that can improve signal-clutter ratio and reconstruct subsurface image. Kirchhoff migration sums amplitudes along the migration trajectory that generally is hyperbolic. But when the ground surface varies acutely, we have to modify the migration trajectory by the technique of ray tracing. Firstly we build the 3D velocity model including the ground surface topography, which are extracted directly from GPR data, and the subsurface velocity, which are computed from the CMP GPR data. Secondly we separate the model into inhomogeneous two-layer grid. Then we compute the travel time between transmitter, receiver and each subsurface scattering point. At last, we search the propagation ray depending on the Fermat's principle.

The method is tested by an experiment data acquired by the SF CMP antenna array GPR system. The target is a metal ball that is buried under a sand mound. A nice result of ray tracing is shown in the case.

On Some Effects of India-Pakistan Border Earthquake on the Atmospherics Recorded at Tripura

S. S. De[1], **B. Bandyopadhyay**[1], **B. K. De**[2], **A. Bhowmick**[2], **Suman Paul**[1], **D. K. Haldar**[1], **and S. Barui**[1]

[1]Centre of Advanced Study in Radiophysics & Electronics, University of Calcutta, India
[2]Department of Physics, Tripura University, India

Abstract— There are different models on seismic waves and on the generation of electric field within the upper atmosphere due to seismo-ionospheric coupling phenomena during the occurrence of any strong earthquake. The emission and propagation of electromagnetic waves from large earthquakes in the ULF-ELF-VLF bands have been reported. Both precursory and post-seismic variations in ELF-VLF amplitudes and in ionospheric parameters are well-known from satellite-based observations surrounding the earthquake zones.

During the strong seismo-ionospheric coupling processes in the earthquake preparation zone, underground gas discharges carry submicron aerosols with them which enhance the intensity of electric field at the near ground due to the drop in air conductivity created by aerosols. Seismo-electromagnetic emissions have been observed at low frequency bands in the seismically active zones prior to the incidence of any large earthquake which are different from lightning induced and technogenic emissions. On the event of strong earthquakes, the near ground of the atmospheric layer becomes ionized and generates strong electric field which introduces particle acceleration thereby exciting local plasma instabilities.

Ion cluster mass and plasma concentration during the process of lithosphere-ionosphere coupling vary with the vastness of the earthquake. As a result, the seismo-electromagnetic emissions would be expected to cover almost the whole of ULF-ELF-VLF band. In the process, there will be increase of thermal plasma noise along with other types of emissions, e.g., Cerenkov and Bremstrallung.

In this work, the results of some significant observations by VLF receivers recorded over Agartala (Lat. 23° N, Long. 91°24' E) at 6 KHz and 9 KHz during the India-Pakistan border earthquake occurred on October 8, 2005 at Muzaffarabad (Lat. 34.53° N, Long. 73.58° E), Kashmir (under Pakistan) will be presented. The effects of the vast earthquake (M=7.7) are exhibited through the occurrence of discrete spikes. Numbers of spikes were observed first on September 28, 2005 and continued upto October 13, 2005. The number of spikes and their intensities as well as durations were found to be changed irregularly and reached the maximum value on the day of occurrence. The signatures ceased gradually and almost ended after October 13, 2005. These commencements may be considered to be precursory and post-seismic effects of this vast earthquake. The records were taken at Agartala which is about 2179 Km away from the place of occurrence. The effects at 6 KHz have been found to be more prominent than at 9 KHz records. Observations were taken at Agartala continuously at frequencies 1, 3, 5, 6, 9 and 12 KHz. No such effects had been observed except at 6 KHz and 9 KHz. The data were analyzed and the outcome of the results will be presented.

The earthquake at India-Pakistan border at Muzaffarabad occurred along with 156 after-shocks on the same day and almost at the same place having M: 4 to 5.9. Different quakes due to after-shocks are of various magnitudes and their hypocenters are located at different depths. As a result, the electromagnetic signals which are thought to be generated during the period get attenuated differently for different sources. The uneven distribution of intensity of spikes in Figures 10–12 may be due to anomaly in the after-shock effects which were present during the period.

ACKNOWLEDGMENT

This work is funded by Indian Space Research Organization (ISRO) through S K Mitra Centre for Research in Space Environment, University of Calcutta, Kolkata, India.

Studies on Solar Flare Effects on Propagation of Sferics and Transmitted Signal

S. S. De[1], **B. K. De**[2], **M. Pal**[2], **B. Bandyopadhyay**[1], **Suman Paul**[1], **D. K. Haldar**[1], **and S. Barui**[1]

[1]Centre of Advanced Study in Radiophysics & Electronics, University of Calcutta, India
[2]Department of Physics, Tripura University, India

Abstract— Solar flares cause significant perturbations in the received VLF signals propagating in the Earth-ionosphere wave-guide. Flares release energy in the form of electromagnetic radiation (from radio waves at the long wavelength end, through optical emission of X-rays and gamma rays at the short wavelength end), energetic particles (electrons and protons) and mass. All flares are high emissions in the wavelength range 1–8 Å. These wave-lengths ionize the D-region, which results in radio absorption.

The intense radiations from solar flares when travel towards the earth, there will be enhancement of D-region ionization. For this, the characteristic features of Integrated Field Intensity of Sferics (IFIS) are greatly affected. The Fourier spectrum of IFIS extends from extra low frequency to high frequency. The contribution is mostly from VLF band.

Stratospheric electric fields get modified due to conductivity enhancements caused by the energetic particles during solar flares. Works were reported earlier about the statistical relationship between the occurrences of solar flares and the variations of lower atmospheric electricity parameters.

There is always a correlation among atmospheric electricity, aurora, sunspots, geomagnetic activity, and solar X-ray flares. Very often, the observed responses on Sferics are confusing and are difficult to understand in terms of solar terrestrial interactions.

The present work deals with the observations of solar flare effects on the Integrated Field Intensity of Sferics (IFIS) recorded at Agartala (Lat. 23° N) at frequencies 1, 3, 6, 9 and 12 KHz. Observations exhibited substantial enhancement in the IFIS during the occurrences of solar flares in July, 2004. The effects of solar flares on sub-ionospheric signals at 16.3 KHz recorded on November 23, 2004 from Kolkata (Lat. 22°34' N) are also presented. The occurrences of flares are justified by GOES satellite data both in long and short X-ray range.

The comparative study of our recorded Sferics spectra during solar flares with those of GOES satellite data suggests some sluggishness, which is the time lag observed in between the occurrence of solar flares and sudden enhancement of atmospherics (SEA). This observed sluggishness is due to relaxation effect in the ionospheric region.

During solar flares, the intensity of solar X-ray fluxes heading towards the earth's atmosphere increases the ionization and hence the reflection coefficient as well as reflection height are altered for a short period. This is observed as a sudden change in the amplitude of ARNFS in the ELF-VLF range.

ACKNOWLEDGMENT

This work is funded by Indian Space Research Organization (ISRO) through S K Mitra Centre for Research in Space Environment, University of Calcutta, Kolkata, India.

Session 4P4
Electromagnetic and Optical Wave Technologies for Communication and Sensing 2

FDTD Analysis of Spatial Filtering of Scattered Waves for Optical CT of Medical Diagnosis

Yasumitsu Miyazaki and Kouhei Kouno
Department of Media Informatics, Aichi University of Technology
50-2 Manori, Nishihazama-cho, Gamagori 443-0047, Japan

Abstract— Medical image diagnosis and computer aided diagnosis are modern important medical techniques developed with computer technology. Particularly, medical image diagnosis using optical waves of lasers is very important technical tools for physiological examination of human body. Optical CT is effective for body tissues such as eyes, hands, children heads, and womens breasts, where transmitted signals of propagating optical waves can be received after propagation. Image responses of optical transmitted projection include optical scattering characteristics that disturb transmission properties through biological structures depending on optical absorption effects due to biological characteristics consisting of atomic and molecular structure. In this paper, technical methods of spatial filtering for optical scattering superposed on transmitted and attenuated waves are discussed to improve image diagnosis. Statistical theory of optical waves is numerically described for optical propagation, attenuation and scattering in random inhomogeneous biological media. Scattered and attenuated fields are studied by numerical computer simulation methods of FDTD. Spatial filtering characteristics of grid structure are shown for exact image optical projection excluding scattering effects through physiological media by FDTD method. Spatial filtering characteristics for off-axial scattering optical waves are discussed in inhomogeneous waveguide-type grids. Scattered fields of large scattering angles have large attenuations in waveguide grids and are filtered. Transmitted and scattered fields of small scattering angles have small attenuations and can pass through waveguide grids.

Statistical characteristics of optical propagation in random media consisting of biological tissues are discussed by numerical difference equation method and FDTD method, using particle models in random media. Biological tissues are consisted of random particles with several complex dielectric constants. Scattering characteristics of incident optical Gaussian beam in random physiological media consisting of biological materials such as biological cells are discussed. Electromagnetic filtering properties by optical inhomogeneous waveguides with lossy clad for off-axial scattered fields are discussed using optical inhomogeneous waveguides consisting of lossy metal clad by FDTD method. Image recognition of biological objects surrounded by random biomedical media, using optical lossy waveguide grid filter are discussed. Based on this computer simulation of scattered fields and waveguide grids, the optimum design of CT system may be accomplished.

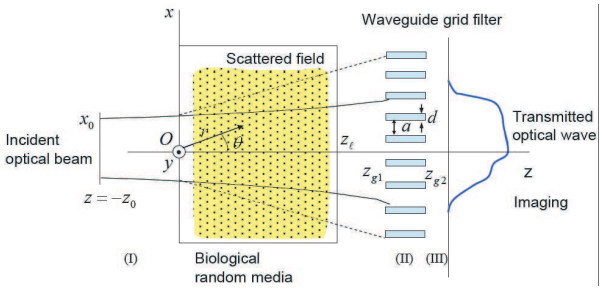

Figure 1: Optical scattering and optical grid filter.

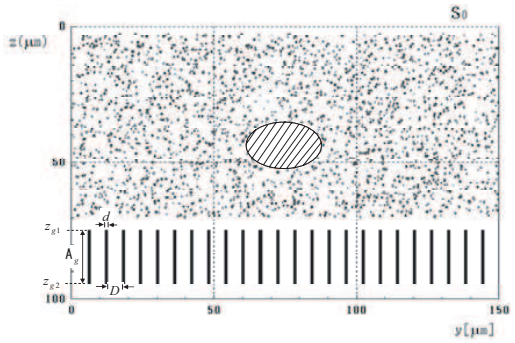

Figure 2: Random body tissue and waveguide grid filter.

REFERENCES

1. Miyazaki, Y., *Jour. of ME Eng.*, Vol. 23, No 7, 20–27, Japan, 1985.
2. Miyazaki, Y., *Jpn. Appl. Phys.*, Vol. 13, 1238–1248, 1974.
3. Miyazaki, Y., *Proc. of APMC 2007*, 527–530, Bangkok, 2007.

FDTD Analysis of Microwave Propagation and Scattering Characteristics over Forests for WiMAX Wireless Communications

Yasumitsu Miyazaki and Tatsutoshi Ikeda
Department of Media Informatics, Aichi University of Technology
50-2 Manori, Nishihasama-cho, Gamagori 443-0047, Japan

Abstract— WiMAX wireless communication has been rapidly developed for broadband mobile communication of image and TV transmission. Mobile WiMAX communication system uses microwave carrier of 2.5 GHz frequency band, and digital modulation system is mainly OFDM for transmission of signals. By using OFDM technique, WiMAX provide high speed and reliable communication against the multi pass interference due to the presence of obstacles in communication channels. To design excellent high performance wireless communication systems, accurate evaluations of communication signal propagation and scattering are indispensable. By using parallel FDTD, we studied fundamental characteristics of microwave propagation and scattering in urban area [1, 2]. In these analyses, building and street effects on high speed signal propagation have been investigated by computer simulation of FDTD method. However, wave propagation and scattering characteristics in presence of forest and trees are not so much studied [3, 4]. The effects of multiple scattering and attenuation of microwave by forest is severe factors of high speed wireless communications. Size of branches and leaves of trees are comparable with microwave wavelength and yield multiple strong interaction phenomena of broadband propagation.

In this paper, propagation and scattering characteristics of microwave over forests in WiMAX wireless communication is numerically analyzed using FDTD method. FDTD method can be applied for signal and interference analysis about several different complex models and inhomogeneous materials such as several forests in communication channels. By applying FDTD method, numerical simulations of signal propagation for various tree structures at different frequencies and digital signal bit rates are demonstrated. Incident wave is assumed to be a traveling wave from transmission antenna station at a far distance. The shape of forest assumed to be constructed by random surface and distribution of branches of trees are random inhomogeneous. The effects of multiple scattering and attenuation due to forests are evaluated using statistical functions, such as average, variance and correlation of conductivities and permittivities for trees. These results may yield important factors for design of high performance and more reliable WiMAX communication systems.

Parallel computation of FDTD using grid computer can be proceeded for these analyses of large area propagation. The electromagnetic fields in each divided subdomain $D_{u,v}(1 \leq v \leq My)$ are calculated by parallel processing. To proceed the parallel processing, data transfer between adjacent subdomains is carried out using MPI.

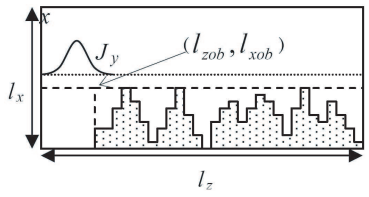

Figure 1: 2-dimensional model for FDTD method.

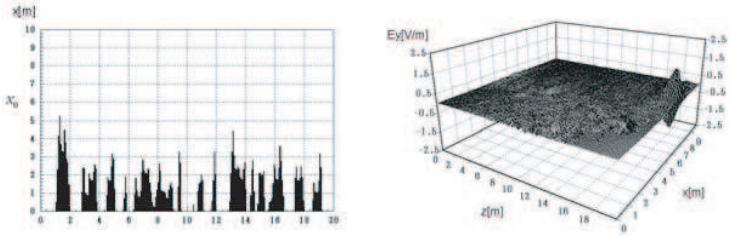

(a) (b) t =1500 Δt =30 (ns)

Figure 2: Forest model and field intensity.

REFERENCES

1. Selormey, P. and Y. Miyazaki, *Trans. IEE*, Vol. 119-C, No. 1, 97–104, Japan, 1999.
2. Rodriguez, G., Y. Miyazaki, and N. Goto, *IEEE Trans. Antennas & Propagat.* Vol. 54, No. 3, 785–796, 2006.
3. Masuda, T., Y. Miyazaki, and Y. Kashiwagi, *Proceeding of Progress in Electromagnetics Research Symposium*, 1713–1715, Beijing, China, 2007.
4. Miyazaki, Y., T. Takada, and H. Tomita, *IEICE Tech. Rept.*, MW2008-31, 1–6, 2008.

An Accelerated Frequency Domain Ray-tracing Simulator for Ultra-Wideband Communications

J. Diskin[1], **A. Alomainy**[2], **and C. Brennan**[1]

[1]Research Institute for Networks and Communications Engineering (RINCE)
School of Electronic Engineering, Dublin City University, Ireland
[2]Antennas & Electromagnetics Research Group
Queen Mary University London, United Kingdom

Abstract— Ultra-Wideband (UWB) is an emerging wireless technology that offers novel capabilities in wireless communication systems. Unprecedented data rates over short ranges are possible due to the large bandwidths of several gigahertz in UWB channels [1]. Ray tracing is an efficient deterministic modelling technique used to predict electromagnetic propagation over large scale environments. This asymptotic method offers accurate computationally practical modelling of wireless propagation in complex environments at high frequencies. Initially ray tracing was used to compute channels for narrow band wireless schemes, such as the IEEE 802.11 wireless LAN based systems. However with the advent of UWB based schemes ray tracing has been employed to compute wideband channels [2]. While some ray tracing simulators use time-domain computations [3], the channel simulations mentioned here are created using a frequency domain based simulator.

In this work results from a ray tracing simulated Ultra-Wideband channel are compared to measurements taken in a single room environment. An UWB channel was measured for 70 receiver points in a 3 by 2.1 meter grid using a Planar Inverted Cone Antenna (PICA) developed at Queen Mary University London [4]. Frequency and time domain received signals and channel statistical parameters are presented for both measured and simulated results.

The variations of material properties with frequency have been previously measured for common indoor building materials in [5]. In order to cope with these effects a frequency domain ray tracing simulator was used. A wideband channel is computed for 500 individual frequencies from 3 to 7 GHz, allowing for such frequency dependant variations to be fully accounted for.

The large bandwidth of UWB channels can pose a computational challenge for existing frequency domain ray tracing simulators. We propose an acceleration algorithm that reduces the number of frequency domain samples computed in order to simulate a wideband channel. This technique involves separating rapidly varying components due to propagation in air from a frequency domain channel associated with each individual ray, allowing the remaining components to be accurately approximated using a reduced set of frequency sample points.

REFERENCES

1. Yang, L. and G. B. Giannakis, "Ultra-wideband communications: An idea whose time has come," *IEEE Signal Processing Magazine*, Vol. 21, No. 6, 26–54, November 2004.
2. Attiya, A. M. and A. Safaai-Jazi, "Simulation of ultra-wideband indoor propagation," *Microwave and Optical Technology Letters*, Vol. 42, No. 2, 103–108, July 2004.
3. Yao, R., W. Zhu, and Z. Chen, "An Efficient time-domain ray model for UWB indoor multipath propagation channel," *2003 IEEE 58th Vehicular Technology Conference, VTC 2003-Fall*, Pt. 2, Vol. 2, 1293–1297, 2003.
4. Alomainy, A., Y. Hao, C. G. Parini, and P. S. Hall, "Comparison between two different antennas for UWB on-body propagation measurements," *IEEE Antennas and Wireless Propagation Letters*, Vol. 4, 2005.
5. Muqaibel, A., A. Safaai-Jazi, A. Bayram, A. M. Attiya, and S. M. Riad, "Ultrawideband through-the-wall propagation," *IEE Proceeding Microwave and Antennas Propagation*, Vol. 152, No. 6, December 2005.

Alteration of Quantum Fluctuations by Third-order Optical Nonlinearity in Semiconductors

H. Ju[1, 2] **and E.-C. Lee**[1, 2]

[1]Division of BioNano Technology, College of BioNano Technology, Kyungwon University Gyeonggi-do, 461-701, Korea
[2]Gachon BioNano Research Institute, Kyungwon University, Gyeonggi-do, 461-701, Korea

Abstract— Squeezing of quantum fluctuations of coherent light quadratures is theoretically investigated. Nonlinearity responsible for quantum squeezing is generated from third-order nonlinear optical susceptibility of semiconductor waveguide devices where ultrafast pulsed light is propagated. This nonlinearity leads to self-phase modulation via intensity-dependent refractive index (Kerr effects). Photon energy of propagating light can be chosen to excite nonlinear positive frequency chirping (positive Kerr effects) or nonlinear negative frequency chirping (negative Kerr effects), given a semiconductor band-gap energy. Our calculation which simulates quantum fluctuations with Gaussian-weighted random distribution of phase space phasors shows that Kerr effects produce, in a two-dimensional complex phase space, conversion of circular shape of quantum fluctuations into elliptical shape whose eccentricity becomes enhanced along propagation through a nonlinear waveguide.

It is revealed that the sign of the Kerr parameter, which is determined by propagating photon energy with respect to the semiconductor band-gap energy, governs the direction of nonlinear rotation of squeezed ellipse of quantum fluctuations along the propagation. This indicates that negative Kerr devices can be used to compensate for the positive-Kerr-effects-induced quantum squeezing as well as can be used as a compensator for frequency chirping caused by positive Kerr effects and group velocity dispersion in an optical fiber.

We also show that Kerr nonlinearity increases quantum fluctuations of optical phase but do not change those of optical intensity (photon-numbers) beyond our calculation error. To the contrary, two-photon absorption that stems from the third-order nonlinear optical susceptibility reduces quantum fluctuations of optical intensity below the standard quantum limit. However, our calculation shows that the rescaling of intensity-independent uncertainty area of propagating light occurs in a two-dimensional phase space by two-photon absorption whereas Kerr effects do not change the uncertainty area.

Experimental Study of Atmospheric Turbulence Effects on RoFSO Communication Systems

W. Ni[1], **Y. Miyamoto**[1], **K. Wakamori**[2], **K. Kazaura**[2], **M. Matsumoto**[2], **T. Higashino**[3], **K. Tsukamoto**[3], **and S. Komaki**[3]
[1]Hamamatsu Photonics K. K., 5000 Hirakuchi, Hamakita-ku Hamamatsu-shi, 434-8601, Japan
[2]GITS/GITI, Waseda University, 1011 Okuboyama, Nishitomida Honjo-shi, 367-0035, Japan
[3]Division of EEIE, Graduate School of Engineering, Osaka University 2-1 Yamada-oka, Suita-shi, 565-0871, Japan

Abstract— Many existing and emerging broadband wireless services benefit from the Radio on Fiber (RoF) technology offering high speed and large bandwidth over long distance at a low attenuation. Although RoF approach works well in many cases, in fiber not feasible area, free-space optics (FSO) communication techniques have received renewed interest as alternative for Radio-Frequency (RF) signal transmission-concept referred to as Radio on FSO (RoFSO)-because they can offer similar capacity while being cost effective and secure access without extensive installation of copper or fiber infrastructure. We are currently in the development stage of the advanced RoFSO system. On the other hand, atmospheric turbulence manifested as beam wander, intensity fluctuation and beam spreading has significant influence on the performance of conventional FSO as well as RoFSO systems. In order to measure, characterize and quantify the influence of atmospheric turbulence in our system deployment environment, we described in this paper a setup Radio Frequency-FSO (RF-FSO) link to test the basic characteristics of RF signal transmission under various atmospheric and weather conditions e.g., clear weather, clouds, rain, fog and snow. We have attempted to quantify the strength of atmospheric turbulence by calculating the refractive-index structure parameter C_n^2 from scintillation index indicating intensity fluctuation caused by atmospheric turbulence. Correlation analysis on carrier-to-noise ratio (CNR) and C_n^2 was also made and presented. In addition, a comparative measurement to characterize intensity scintillation and Angle-of-Arrival (AoA) variance has also been presented in this paper. The experimentally derived data and results will be available for antenna design, link margin prediction and evaluation of performance criterion of future RoFSO systems in different deployment environments.

Soft-lithography-based Inter-chip Optical Interconnects

Wei Ni[1], **Rubing Shao**[1], **Jing Wu**[2], **and X. Wu**[1]

[1]State Key Laboratory of Modern Optical Instrumentation, Department of Optical Engineering
Zhejiang University, Hangzhou 310027, China
[2]University of California at San Diego, La Jolla, CA 92093, USA

Abstract— The increasing performance of microprocessors leads to higher bandwidth requirements for the data flow to and from the processor. Today, all signaling on a PCB is performed electrically, using copper lines that are integrated in the board. However, issues such as propagation loss and inter-channel crosstalk limit the scalability of electrical interconnects to ever higher bandwidth densities. Optical interconnects feature a higher bandwidth × length product, are more power-efficient and enable a higher bandwidth density than electrical interconnects do. This paper describes a kind of two-dimensional monolayer optical interconnects providing interconnections between chips on conventional PCB. We have designed a soft-lithography-based, versatile coupling structure with a 45° total internal reflector (TIR), a beam duct, and a polymer waveguide in order to vertically couple light beams between transmitter (or receiver) and the waveguide layer. This proposed integrated architecture of a polymeric optical interconnection has been demonstrated to be advantageous in the aspects of misalignment tolerance, ease and low cost of fabrication, as well as relative simplicity in deployment. We also investigated the characteristics of in-plane connections including cross-over and branching nodes in the optical interconnects with experimental and theoretical analysis. The theoretical crosstalk, as calculated by a function of crossing angle, was determined for a set of interconnect pairs with varying cross-sections, and was compared with experimental measurements. Furthermore, a suitable branching angle was found for branching node and the effects of short-distance mode scrambling in highly multimode polymer waveguides were studied in detail in this paper too.

Experimental Study of the Multipath Propagation Effect on the Accuracy of GPSCo-ordinates Measurements in Case of Urban Conditions

P. V. Polyukhovich and B. P. Dudko
Tomsk State University of Control Systems and Radioelectronics
40 Lenin Ave., Tomsk 634050, Russia

Abstract— There are two main sources of co-ordinate estimation errors while using the GPS under urban conditions. They are the limited number of signals seen and the multipath radiowaves propagation due to reflections from buildings.

The error due to the limited number of signals seen can be minimized by the differential method of co-ordinate estimation.

The error due to the multipath radiowaves propagation can be minimized either by the trajectory correct calculation or by averaging the results of several measurements got by using number of satellites. Experience shows that the error becomes small if there are used 10 satellites or more, which happens rather rare.

The report presents the results of experimental study of GPS co-ordinate measurements by the differential method under urban conditions. The equipment was put near the buildings. Even the differential method gives the error of several meters, if the influence of the multipath propagation is high. The error can be minimized by the correct calculation of the signal trajectory from the satellites to the equipment. The authors suggest using the locality laser scanning in order to define more accurately the conditions of wave propagation. There has been estimated the possibility of the error compensation.

FDTD Simulation for Statistical Properties of Microwave Scattering and Attenuation Due to Randomly Distributed Rainfalls

Yasumitsu Miyazaki[1], **Koichi Takahashi**[1], **and Nobuo Goto**[2]

[1]Department of Media Informatics, Aichi University of Technology
50-2 Manori, Nishihasama-cho, Gamagori 443-0047, Japan
[2]Institute of Technology and Science, The University of Tokushima
2-1 Minamijosanjima-cho, Tokushima 770-8506, Japan

Abstract— Rain measurement system using propagation characteristics of microwave and millimeter wave is very effective for safety system of ITS and disaster prevention system to disasters caused by strong rainfalls. Measurement technique of electromagnetic scattering and attenuation characteristics by rain is one of useful evaluation methods of rainfall rate [1], as shown in Fig. 1. A parabolic antenna with diameter $2a = 0.5\,\mathrm{m}$ is used to transmit and receive microwave of 10–20 GHz. Gaussian beam with beam spot $r_0 = 0.15\,\mathrm{m} \cong 5\lambda \sim 10\lambda$ is transmitted. We evaluated rain attenuation of Gaussian beam with 20 GHz carrier frequency in random media of rainfall

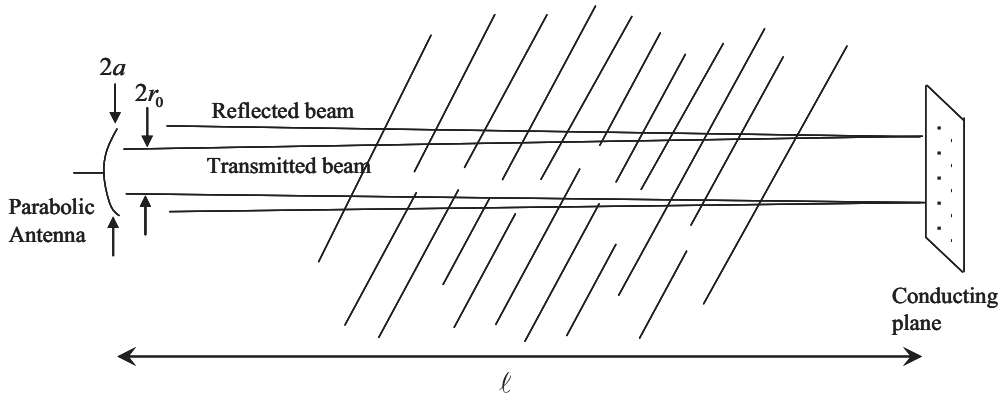

Figure 1: Measurement system of rain attenuation.

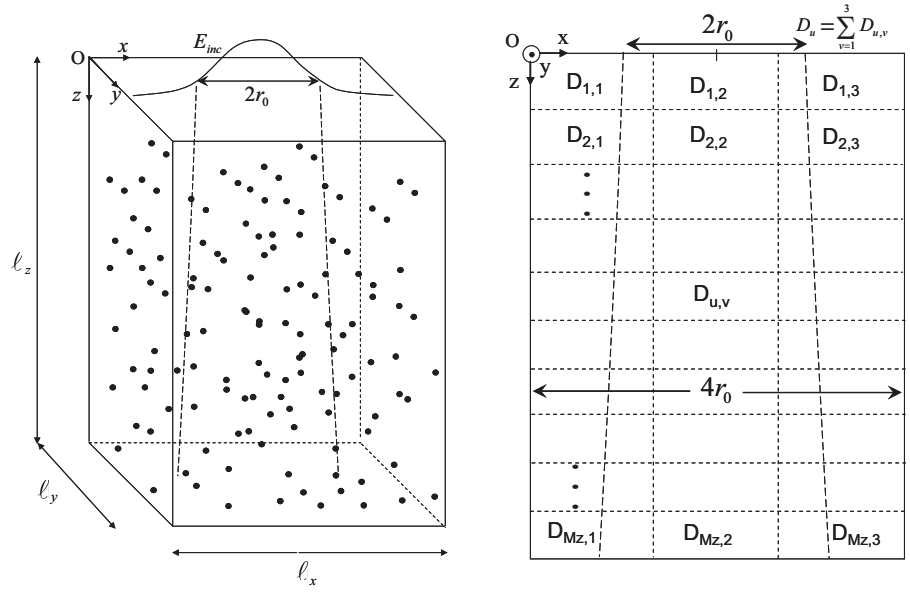

Figure 2: Analysis model for rain attenuation and division of calculation region.

rate $10 \sim 40$ mm/h using three-dimensional FDTD method [2]. To obtain accurate relationship between rainfall rate and rain attenuation, analysis of long distance propagation for the incident wave with relatively small beam spot is considered. For the analysis of large area, parallel and successive computing based on the division of large calculation region using grid computer is studied [3, 4]. Calculation model for rain attenuation and division of the calculation region are shown in Fig. 2. Firstly, we show precise comparison of scattering fields of a few raindrops by numerical FDTD method in small area with theoretical results derived by Rayleigh scattering theory, to confirm the accuracy of numerical simulation model. In small area calculations, scattering properties of cubic and non-cubic raindrop models are also evaluated. An example of comparison of numerical FDTD calculations and theoretical analysis for scattering field by single raindrop is shown in Fig. 3. Secondly, the field in the large area which contains more than hundred raindrops is calculated using parallel and successive FDTD method. Scattering of Gaussian beam mainly depends on the ratio of the correlation length of random media to the wavelength [5]. Forward scattering intensity obtained by FDTD method is compared with statistical theory of electromagnetic scattering in random media. The comparison of numerical calculations of specific attenuation with the experimental results is also considered. Based on these computer simulations, the optimum measurement and control systems of raindrops using microwave techniques for ITS and protection against calamities may be accomplished.

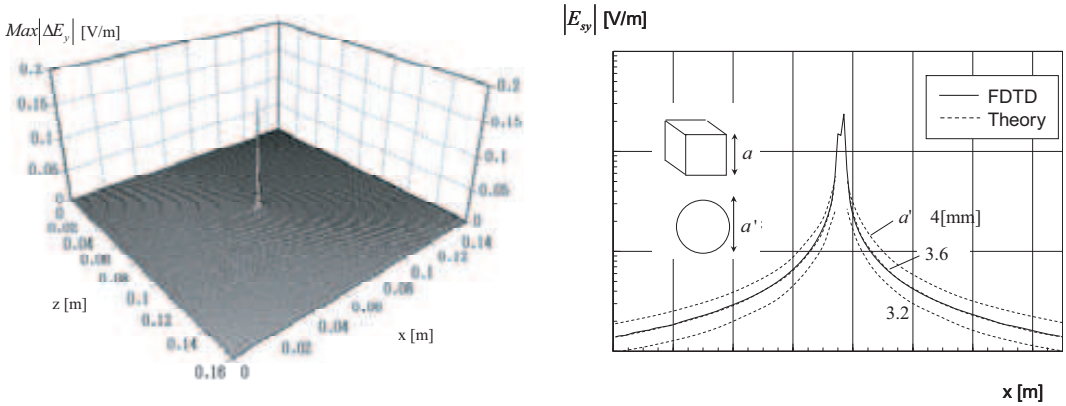

(a) Amplitude of scattered electric field at y= $\ell/2 = 0.075$ m

(b) Cubic raindrop ($a = 2$ mm)

Figure 3: Comparison of numerical calculation and theoretical analysis of scattered field by single cubic raindrop with side length a and sphere with diameter a' ($y = z = 0.075$ m).

REFERENCES

1. Oguchi, T., *IEEE Proc.*, Vol. 71, 1029–1078, 1983.
2. Miyazaki, Y., K. Takahashi, and N. Goto, *PIERS Proceedings*, 967–972, March 24–28, Hangzhou, China, 2008.
3. Rodriguez, G., Y. Miyazaki, and N. Goto, *IEEE Trans. Antennas & Propagat.*, Vol. 54, No. 3, 785–796, 2006.
4. Takahashi, K., Y. Miyazaki, and N. Goto, *IEEJ Trans. EIS*, Vol. 127, No. 12, 1973–1981, 2007.
5. Miyazaki, Y., *Jpn. Jour. Appl. Phys.*, Vol. 13, No. 8, 1238–1248, 1974.

Ubiquitous Network for Building and Home Control System with Refrigerant Pipe Communication and Sensor Network Technologies

Toshiyasu Higuma, **Noriyuki Kushiro**, **and Masanori Nakata**
Living Environment System Laboratory, Mitsubishi Electric Corp., Japan

Abstract— There is a growing interest to introduce a ubiquitous network for controlling and monitoring appliances and sensors dispersed in a building both for realizing comfortable living environment and reducing energy consumption. Wireless sensor network system, like IEEE802.15.4 is a promising solution for the system. It realizes the ubiquitous network in a space. However, some obstacles, such as wall and floor, attenuate the wireless signal and prevent the communication between rooms or floors. It is necessary to introduce a new solution, which relays the wireless signal into another room.

A hybrid network, which consists of a low power ad-hoc wireless network (IEEE802.15.4) and a refrigerant pipe line communication network with high frequency band dispersed-tone method, has been developed (Fig. 1).

Power Line Communication (PLC) is a widely known solution for extending communication without special wiring. In a small building, PLC would be the best way to extend the wireless network. In a large building system, the PLC solution is not useful, because of complexity topologies of the power line. In the example of an air-conditioning system in a building, outdoor units installed on the roof-top and indoor units equipped on the ceiling of each room, are connected via a central switch board of power distribution system. Generally, the length of the power line between the outdoor unit and the indoor unit is too long to communicate with PLC. Pipe lines for refrigerant of the air-conditioner are more simple and short in length. It would be the better solution to utilize the pipe line instead of power line as a communication medium.

The pipe line communication is similar to PLC. A pair of the refrigerant pipes of air-conditioners is utilized as communication media instead of the power line for PLC. The refrigerant pipes cannot transmit signals in normal ways because they are shortened in electrical. A couple of impedance upper changes the pipes into communication media by raising their impedance (Fig. 2).

We have constructed both simulation model of the pipe line communication and appliance control systems by utilizing the proposed hybrid network system and have installed them in an actual building and home to evaluate their reliability and capability. High reliability and capability of the network system have been confirmed by both simulation and field test.

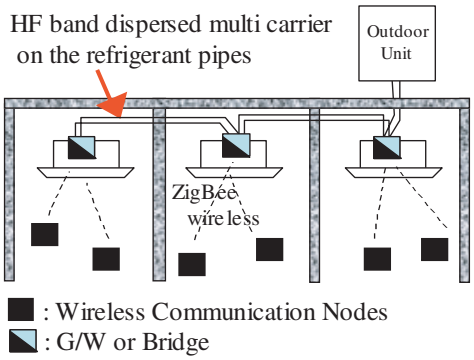

Figure 1: Diagram of a hybrid network system.

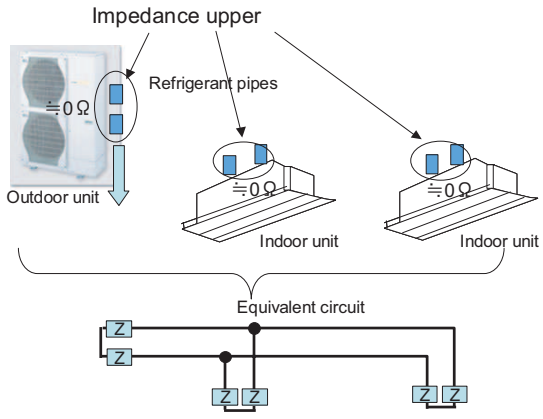

Figure 2: The pipe line communication network.

Session 4P5
Antenna Theory and Radiation, Microstrip and Printed Antennas 2

Pattern Reconfigurable Antenna Array for MIMO-enabled Handheld Wireless Communication Devices

Rashid A. Bhatti, **Nguyen Viet Anh**, **and Seong-Ook Park**
Information and Communications University (ICU), Daejeon, Korea

Abstract— Users demand wireless communication devices supporting high data transmission rates for high speed internet and multimedia applications. Multiple-input-multi-output (MIMO) communication techniques are promising to meet these emerging demands for high data-rate wireless communications. A lot of research work has been published on MIMO system implementations for both the fixed and mobile terminals. Experimental and theoretical published research reveal that the achievable MIMO system capacity can be improved in the rich scattering environment with reconfigurable antenna patterns at the mobile terminal side. Power angular spectrum is always changing in both the indoor and outdoor propagation scenarios as the mobile is moved from one location to another. Alignment of radiation pattern with the PAS improved signal-to-noise-ratio (SNR) thus improving the system capacity. However, implementation of multiple antennas each having reconfigurable pattern is a challenging task for antenna designers. In this paper, we have proposed a pattern reconfigurable antenna with four switching options covering 360 degrees angular domain at 3.5 GHz. The antenna consists of two elements located at the corners of a ground plane measuring 70 mm × 100 mm. Each antenna consists of a driven element and four parasitic elements that can be switched to direct the pattern in the desired direction. Driven and the parasitic elements are printed on a 0.508 mm thick substrate with dielectric constant of 2.2. Each antenna has been implemented in an area of 13 mm × 13 mm and is located at a height of 4.0 mm over the ground plane near the corners for better isolation or mutual coupling performances. Switching network has been implemented on the main ground plane using RF PIN diodes. The proposed implementation has the advantage that there is no DC block capacitor in the RF path as the switches has been implemented in the electromagnetically coupled parasitic elements. SMA connectors are used to feed the driven elements in the array from the bottom side of the ground plane. Measured input return losses are better than −10 dB with bandwidth greater than 200 MHz at the center frequency of 3.5 GHz. Mutual coupling between the elements is also within acceptable limits. Comparison of the measured and simulated scattering parameters of the proposed array is given in the paper. Co-polar and cross-polar 3-D radiation patterns for different switching options have been shown and discussed in the paper.

Research and Application on Scattering Matrixes of the Radar Target under Different Polarization Bases

Jian-Xun Liu, **Qiang Xu**, **Hou-Jun Sun**, **and Xin Lv**
School of Information Science and Technology, Beijing Institute of Technology
Beijing 100081, China

Abstract— The deduction and application of transition matrix of radar target polarization scattering matrix under different linear polarization bases were presented in this paper. The relation between different scatter matrixes of the same target under different linear polarization bases was studied.

This paper includes three parts:

In the first part, according to the representations of polarization vectors, the relation of scatter matrixes between the h/v and other linear polarization bases was given and transition matrix between two linear polarization bases was deduced. The transition matrix can be used to change the scattering matrix from a linear polarization base to another one. This method can be thought as theoretical foundation of simplifying the measurement and application of radar target polarization characteristics.

The second part is mainly concerned with validating the transition matrix. It was proved to be correct by exemplifying the relation of scatter matrixes of two polarization bases, h/v and (45°, 135°), and applied to virtual polarization synthesis successfully. The data indicated that the polarization scattering matrix given by the experimental results agrees well with the theoretical deduction under (45°, 135°) polarization base.

Moreover, the curve of co-polar scattering parameter to the inclining angle is presented. The inclining angle of a radar target can be given by measuring its polarization scatter matrix and comparing to the matrix under the known polarization base. This method can be used to identify the inclining angle of a plane when it is landing in the dark.

Electrically Small Top-loaded Monopoles Utilizing Space Filling Curves: Concept, Design and Experiment

Christopher Thajudeen and Ahmad Hoorfar
Department of Electrical and Computer Engineering, Villanova University
Villanova, PA 19085, USA

Abstract— In recent years, many researchers have investigated the mathematical concept of space-filling curves for antenna design miniaturization. An interesting property of space-filling curves, such as Peano and Hilbert curves, is that as one considers the higher orders in iterative filling of a 2-D region, a long "line" can be compacted into a small "surface" area. As a result a planar resonant radiator, based on a space-filling curve, can have a very small footprint. One draw back of such an antenna is its very small input resistance and bandwidth.

Recently, however, we have shown that the use of a space-filling curve as a planar top-load for a short vertical monopole provides a good impedance match with a stable monopole-like radiation pattern over a relatively wide bandwidth [1]. In this paper, we present an extension of this concept to further enhance the bandwidth and achieve reconfigurable designs by top loading the monopole with stacked layers of Hilbert or Peano curve elements. This novel class of top-loaded monopoles (TLMs) can achieve wide-band and reconfigurable radiation characteristics while remaining within an electrically small form factor.

Numerical as well as experimental results will be presented to demonstrate that the use of stacked Peano curves as top-loads can achieve an electrically small monopole with an impedance bandwidth of better then 30%. We will also show that the Hilbert-curve TLMs are able to achieve both wide-band and reconfigurable radiation chracteristics through the addition of electronic switches on the grounding posts of the curves. For both Peano and Hilbert TLMs, the effect of a finite ground plane, on the radiation patterns, is investigated using a method of moment simulation tool and verified using measurements. In addition, the radiation performance of these novel TLMs are numerically investigated for use in small Unmanned Areal Vehicles (UAVs); some of the results of this study will also be shown in the presentation.

REFERENCES

1. McVay, J. and A. Hoorfar, "Miniaturization of top- loaded monopole antennas using peano-curves," *IEEE Radio and Wireless Symposium*, Long Beach, CA, January 2007.

Beauty of Symmetry — Thinking from the Design of Logging-While-Drilling Propagation Resistivity Tools

Sheng Fang and Dan Georgi
Baker Hughes Inc., USA

Abstract— With the advancement of new technology, the design precision of an antenna could be very high. However, the precision can not be guaranteed in some special situations such as in a drilling environment that the temperature and pressure are very high. High temperature could cause electronic drift and change the moment of an antenna. Moreover, the tool string (metal mandrel) could bend and twist due to the torque of drilling process, which makes it more difficult to interpret the measured response. The solution to solve aforementioned difficulties is to use the beauty of symmetry from multiple antennas to compensate these effects, which is much simpler than trying to achieve the high precision for each single antenna.

In our standard Logging-Wile-Drilling (LWD) propagation resistivity tools, two transmitter and two receiver antennas are symmetrically mounted on a metal mandrel and used to resemble two three antenna measurement systems. The three antenna measurement system consists of a transmitter and two receivers. The differential signals from the two receivers are measured in terms of amplitude and phase. Then, the measurements from the dual systems are averaged to yield the final records. The combined measurements will 1) compensate the temperature drift; 2) reduce the precision requirement on magnetic moment of the antenna; 3) tolerate a certain degree of bending; and 4) reduce the near borehole environmental effects. In the paper, we discuss all these issues and verify the conclusions from modeling responses and field measurements. The pros and cons for the differential three antenna system are analyzed and compared with a three antenna bucking system. In addition, the fundamental differences and challenges between a hardware approach and a software implementation for the three antenna system will be addressed.

Air Gap Tuning Effect on the Resonant Frequency and Half-power Bandwidth of Superconducting Microstrip Patch

T. Fortaki[1], **S. Benkouda**[1], **M. Amir**[1], **and A. Benghalia**[2]

[1]Electronics Department, University of Batna, Algeria
[2]Electronics Department, University of Constantine, Algeria

Abstract— Rectangular microstrip patches can find an application in microwave integrated circuits as planar resonators for oscillators and filters. Also, rectangular microstrip patches can be used as resonant antennas fed by means of either coaxial probes, or microstrip lines. Since the bandwidth of microstrip patch resonators and antennas around their operating resonant frequencies is known to be very narrow, it is important to develop accurate algorithms for the computation of those resonant frequencies. The resonant frequency value of the rectangular microstrip patch depends on the structural parameters, and it is evident that if the resonant frequency is to be changed, a new antenna is needed. In order to achieve tunable resonant frequency characteristics, an adjustable air gap layer can be inserted between the ground plane and the substrate, resulting in a two-layer structure.

Apart from tunable microstrip patches, in the last few years, there has been a growing interest in the use of superconducting materials in microwave integrated circuits, which is due to their main characteristics, such as: small losses, very small dispersion, and reduction in the time of propagation of the signals in the circuits.

In this paper, a rigorous Full-wave analysis of an air gap tuned high T_c superconducting microstrip antenna is presented. To the best of our knowledge, this structure has not been analyzed previously. Only results for the case of perfectly conducting patch have been reported in the open literature. In Section 2, the authors provide details of the application of the Galerkin's method in the Fourier transform domain to the analysis of high T_c superconducting microstrip antennas with air gaps. In Section 3, numerical results for the air gap tuning effect on the operating frequency and half power bandwidth of the high T_c superconducting microstrip antenna are presented. Finally, conclusions are summarized in Section 4.

Radiation Characteristics of a Wideband Triangular Antenna for Wireless Communications

Adel M. Abdin
Department of Communications, Faculty of Engineering, Shorouk Academy
Shorouk City, Cairo, Egypt

Abstract— In this paper a broadband microstrip triangular antenna with a slot fed by a microstrip transmission line is presented. It is suitable for ultra-wide band application. It is designed, fabricated, and measured. The characteristics of the antenna are optimized by testing the suitable dimension of the patch and the ground plane and the suitable dimension and position of the slot. Simulation and optimization are based on Zeland software. This is performed over the full range of frequencies (0–14) GHz, which is the limit of the Zeland software. The simulation is used to test the return loss, VSWR, input impedance, radiation pattern, and gain at different frequencies. The proposed antenna was fabricated on a dielectric FR4 (substrate thickness = 1.5 mm, $\varepsilon_r = 4.65$) and measured for return loss characteristic. The antenna has a bandwidth of 46% within 2:1 VSWR and operates in the (1.88–3.0) GHz frequency range. Range of antenna gain is between 2.2 dBi to 3.08 dBi which indicate that the proposed antenna can be used for various applications. It covering major wireless communication bands like GSM, AWS, WCDMA, UMTS, DSR, Wi. Bro, ISM application (Wi-Fi), Wi-max, Fixed microwave links DMB, and Onboard aircrafts internet based on the AMSS. The measured and simulated results are presented and discussed.

Characteristics of a Multi-bandwidth Gear Microstrip Antenna Using a Taper for Feeding

Adel M. Abdin
Dept. of Communications, Faculty of Engineering, Shorouk Academy
Shorouk City, Cairo, Egypt

Abstract— In this paper, a gear microstrip antenna (GMA) using a taper as a feeder is presented. Several techniques are demonstrated to overcome its inherent disadvantage of narrow bandwidth of microstrip antenna. For broadening the bandwidth, different configurations for the presented antenna using various materials are suggested. Partial ground with different dimensions and the GMA with a slot and without a slot are tested. Different substrates such as RT5880 substrate of thickness $h = 0.78\,\text{mm}$ and a relative permittivity $\varepsilon_r = 2.2$, FR4 substrate of $h = 1.5\,\text{mm}$ and ε_r =4.65 and RT/Duroid 6010 substrate of $h = 1.25\,\text{mm}$ and $\varepsilon_r = 10.5$ are also taken into account in the analysis. All these cases are analyzed using Zeland IE3D software and High Frequency Structure Simulator (HFSS) and the corresponding return loss are simulated. As much as 95%, 39.3%, 12.5%, 29.1%, 4%, and 2.5% SWR < 2 bandwidths are reported for the best case. Application of the GMA in modern wireless systems covering AWS, DCS, DECT, PCS, PHS, GSM, WCDMA, UMTS, DSR, Wi.Bro, ISM, DMB, C band and Ku band satellite, IMT2000, Wi-max, Wi-Fi, Fixed microwave links, DAB, and Bluetooth bands is widely demonstrated. The antenna comprises at six bands, from (1.6–4.5) GHz, (4.7–7) GHz, (7.5–8.5) GHz, (9.1–12.2) GHz, (13–13.5) GHz, and (19.5–20) GHz, having (2.9–4.5) dBi gain. This design has achieved a broad beam width, high average gain and low cross-polarization across its wide operating frequencies. The measured and simulated results are presented and discussed.

Design and Analysis of Coplanar-waveguide-fed Dual-band Antenna by FDTD

Hou Zhang and Jian Wang
Airforce Engineering University, Xi'an 710021, China

Abstract— In this paper, an improved FDTD using an adopting mode match method is employed to design and analyze a CPW-fed dual-band antenna. Compared to the traditional FDTD, the improved FDTD can decrease both memory requirements and computational time. Finally, a good agreement between calculated and measured results is presented by comparison.

Design of an Optimum Antenna System for Maximum Power Transfer Using Statistical Design of Experiment Approach

Arnab Roy, **Sushanta Paul**, **A. S. M. Shamsuzzaman**, **and Md Ishfaqur Raza**
ECE Department, East West University, Mohakhali, Dhaka-1212, Bangladesh

Abstract— For optimum design of the feed of an antenna, the location of the feed with respect to the antenna is critical. The location and design of the feed is a function of the antenna target frequency, material characteristics of the substrate, and the physical measures of the antenna. The objective is to match the impedance of the feed to the impedance at the feed point. In this paper the design of an antenna system is implemented using the design of experiment statistical approach. A micro strip patch antenna is used as a test case to illustrate the design methodology. All the parameters that define the antenna and the feed are taken into consideration in the experiment to ensure maximum power transfer from the feed to the antenna and minimize return loss. A screening experiment is run to characterize the parameters that affect the maximum power transfer. Later a custom design is presented using the screened transmission system input variables to enable maximize power transfer. The result of this process creates a simple empirical function to design an efficient antenna.

Renormalization Group Application to Multi-port Model for Studying Fractal-shaped Structures' Diffraction

T. BenSalah, C. L. Aguili, and T. Aguili
L. Syscom, ENIT, B. P. 37, Le Belvedere 1002, Tunis, Tunisia

Abstract— Fractal shaped structures are very complex to study particularly when not considering the very first iterations and more particularly for characterizing their EM properties. Even though, multi scale methods present interesting artifacts to help such characterization, they still lack rigorous results for infinite iterations. At their best they provide a convergence information about the structure.

This paper reports on the application of the renormalization group theory to the study of a fractal shaped structure's diffraction using the multi-port model proposed in the MS-MGEC, a MoM multi scale extension. Actually, the Surface Impedance Operator exposed in the latter method enables the formulation of expressions that lead to rigorous calculation of the stationary state of the studied system when the fractal iteration tends toward the infinity in an elegant manner. This corresponds to a multi-dimensional fixed point characterizing the invariance by renormalization of the structure regardless to fractal iteration.

As application we study a Cantor Iris structure placed into a rectangular waveguide and exposed to a modal excitation.

In this work, we show how to apply renormalization group theory to the multi-port model in such problem by presenting the different steps needed by the theory: decimation, scaling, introduction of effective parameters and validation of the invariance by renormalization which is ensured by a multi-dimensional fixed point.

REFERENCES

1. Wilson, K. G., "The renormalization group and critical phenomena," *Nobel Lecture*, 1982.
2. Wilson, K. G., "Renormalisation group and critical phenomenon: Renormalization group and Kadanoff scaling picture," *Phys. Rev. B*, Vol. 4, 3174–3183, 1971.
3. Fischer, M. E., "The renormalisation-group in the theory of critical behaviour," *Rev. Mod. Phys.*, Vol. 46, 597, 1974.
4. BenSalah, T. and T. Aguili, "Software implementation of a new multi-scale method for fractal-shaped structures' diffraction analysis", *PIERS Proceedings*, 836–840, Cambridge, USA, July 2–6, 2008.
5. Aguili, C. L., T. BenSalah, and T. Aguili, "Study of electromagnetic waves diffraction by bi-dimensional fractal structures using the renormalization method," *AEUE — International Journal of Electronics and Communications*, 2008, DOI: 10.1016/j.aeue.2008.05.013.
6. Collin, R. E., *Field Theory of Guided Waves*, IEEE Press, 1991.
7. Bajon, D. and H. Baudrand, "Equivalent circuit representation for integral formulations of electromagnetic problems," *Int. Journal of Num. Modeling*, 23–57, Vol. 15, 2002.

Input Impedance of Gap-coupled Circular Microstrip Antennas Loaded with Shorting Post

P. Kumar, **Vivek K. Dwivedi**, **G. Singh**, **and S. Bhooshan**

Department of Electronics and Communication Engineering
Jaypee University of Information Technology, Solan 173215, India

Abstract— Microstrip antennas are commonly used in aircraft, missile, satellite, wireless and mobile communication systems due to its low profile, simple and inexpensive to manufacture. The major disadvantages of the microstrip antennas are low efficiency and narrow bandwidth. The bandwidth of microstrip antenna can be increased using various techniques such as by loading a patch, by using a thicker substrate, by reducing the dielectric constant, by using gap-coupled multi-resonator. The problem with a thicker substrate is generation of spurious radiation and there are some practical problems in decreasing the dielectric constant [1–3]. The size of the microstrip antenna can be reduced by shorting the patch. In [4], circular microstrip antenna with dual frequency operation is designed by shorting the patch. The results are compared with the conventional circular microstrip antenna (without a shorting pin). In this paper, we have discussed the simulation results of the input impedance of the shorting posts loaded gap-coupled circular microstrip patch antenna at various gaps between adjacent edges. The simulation has been performed using the method-of-moment based commercially available software IE3D.

The geometry of proposed antenna is consists of two gap-coupled circular microstrip patches as shown in Fig. 1. The patch of radius '$r_1 = 15\,\text{mm}$' is feed patch and the patch of radius '$r_2 = 15$' is the parasitic patch. The parasitic patch is excited by the gap-coupling. The feed patch is shorted by a post of diameter 'p' as shown in Fig. 1. The height and permittivity of the substrate is '$h = 1.59\,\text{mm}$' and '$\varepsilon_r = 2.2$' respectively. The gap between the adjacent edges of the patches is 's'.

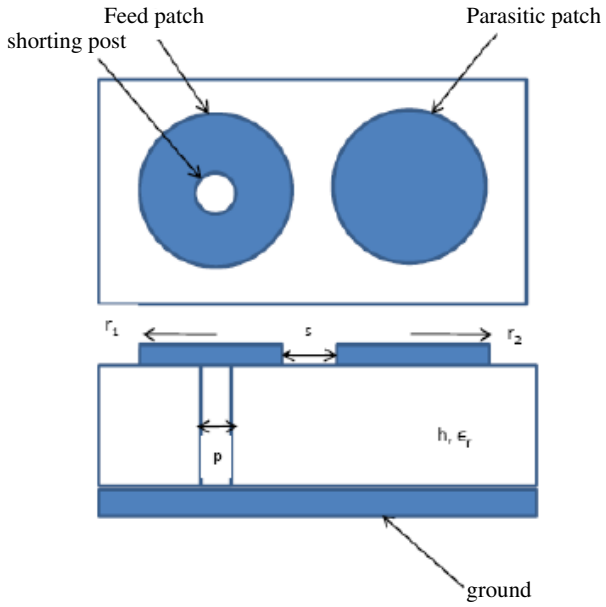

Figure 1: Geometry of gap-coupled microstrip antennas loaded with shorting post.

The input impedance of the antenna for different adjacent gaps distance as well as for different radius of shorting post for different modes is studied. The variation of real and imaginary part of the input impedance with gap between adjacent edges is shown in Fig. 2, which reveals that both these parts are shifted towards higher frequency as gap distance between adjacent edges increases. The variation of real and imaginary part of the input impedance with radius of shorting post is also studied. It shifted towards higher frequency and input impedance decreases as radius of shorting post increases. The variation of the real and imaginary part of the input impedance of

the antenna with feed location is also studied and it is seen, that the real and imaginary part of the input impedance increases when the feeding probe moves from center towards the edge of the patch.

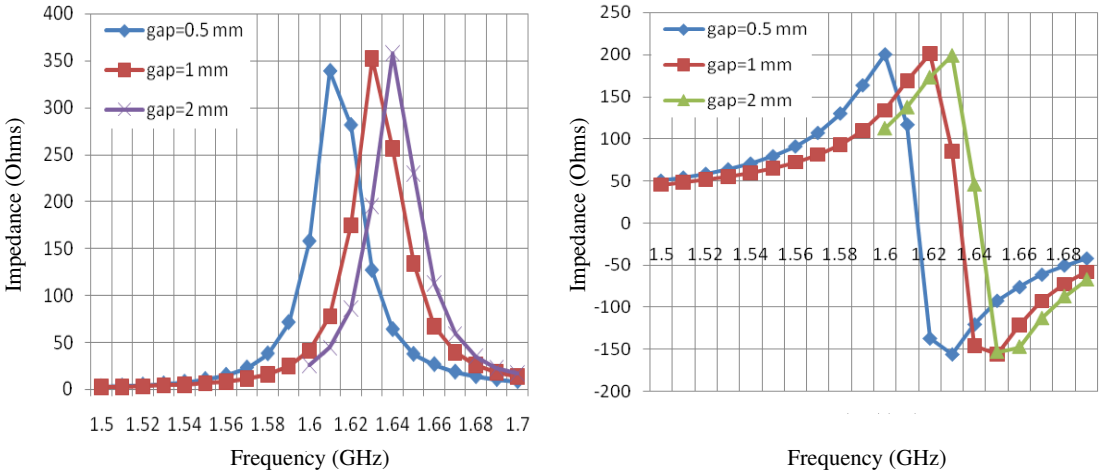

Figure 2: Variation of (a) real part, (b) imaginary part of the input impedance with gap between adjacent edges for TM_{01} modemode (pin radius = 0.5 mm).

REFERENCES

1. Kumar, P., T. Chakravarty, G. Singh, S. Bhooshan, S. K. Khah, and A. De, "Numerical computation of resonant frequency of gap coupled circular microstrip antennas," *Journal of Electromagnetic Waves and Applications*, Vol. 21, No. 10, 1303–1311, 2007.
2. Ray, K. P., S. Ghosh, and K. Nirmala, "Compact broadband gap coupled microstrip antennas," *IEEE Antennas and Propagation Society International Symposium*, 3719–3722, July 2006.
3. Tang, C. L., H.-T. Chen, and K.-L. Wong, "Small circular microstrip antenna with dual frequency operation," *Electronics Letters*, Vol. 33, No. 73, 1112–1113, 1997.
4. Wong, K. L. and W.-S. Chen, "Compact microstrip antenna with dual-frequency operation," *Electronics Letters*, Vol. 33, No. 8, 646–647, April 1997.

UWB Rectangular Ring Microstrip Antenna with Simple Capacitive Feed for Breast Cancer Detection

Sangam Kumar Singh and Arun Kumar Singh
Punjab Engineering College, Deemed University, Chandigarh 160012, U.T., India

Abstract— Breast cancer is a second leading cause of cancer in women today after lung cancer and is the most common cancer among women according to WHO. At present X-ray Mammography is approved technique for early breast cancer detection. But this technique have up to 20% false detection rate. There will be approximately 250,000 new cases of breast cancer in India by 2015. At present, India reports around 100,000 new incidence of breast cancer. We can eliminate this false detection using Microwave imaging. Microwave imaging is defined as "seeing" the internal structure of an object by means of electromagnetic fields at microwave frequencies (300 MHz–10 GHz).

Antenna is a key component in microwave imaging system. Required antenna should be ultra wideband, compact, planar, high HPBW. There are many type of antenna are designed which have wide bandwidth but at the expense of significant size. Also they are not planar. So antenna array will become complex and bulky when we use above mentioned antenna for example Unipolar and Antipodal Vivaldi antenna.

Microstrip antenna can become right candidate for Microwave imaging system. Because it is compact and planar but major drawback is its narrow bandwidth. But using different technique we can increase bandwidth up to 70%. First time in 2007 Aperture Coupled Stacked Patch Microstrip Antenna is designed with 77% impedance bandwidth at University of Bristol, UK for breast cancer detection [1]. But these configuration cause alignment issues while assembling and hence may increase the production cast. And Primary advantage of MSA lies in there eases of fabrication by standard lithographic techniques.

Single Layer Rectangular Microstrip Antennas with simple capacitive feed, offering an impedance bandwidth up to 50% is designed in IISc., Bangalore 2007 [2]. The proposed antenna is modification of above antenna. In this antenna, we replace rectangular patch with rectangular ring patch which increases impedance bandwidth more than 85% having resonance frequency 5.9 GHz due to inductive impedance match with some approximation. This wide impedance bandwidth is far greater than 77% recently reported in University of Bristol, UK for breast cancer detection.

REFERENCES

1. Nilavalan, R., I. J. Craddock, A. Preece, J. Leendertz, and R. Benjamin, "Wideband microstrip patch antenna design for breast cancer tumour detection," *IET Microwave Antenna Propagation*, Vol. 1, No. 2, 277–281, 2007.
2. Kasabegoudar, V. G., D. S. Upadhyay, and K. J. Vinoy, "Design studies of ultra-wideband microstrip antenna with a small capacitive feed," *Internation Journal of Antenna and Propagation*, Vol. 2007, 8, Article ID 67503, doi: 1155/2007/67503.

Multiband Rectangular Ring Microstrip Antenna for UWB Wireless Applications

Sangam Kumar Singh and Arun Kumar Singh
Punjab Engineering College, Deemed University, Chandigarh 160012, U.T., India

Abstract— In this paper, We have designed a Rectangular Ring Microstrip antenna for UWB (3.3 GHz–10.6 GHz) wireless applications. The beauty of this antenna is the use of single patch which makes it easy to fabricate consequently cost of antenna becomes cheaper. This antenna have three centre frequencies i.e., 4.49 GHz, 6.17 GHz and 9.64 GHz. The impedance bandwidth of this tri band antenna are 13.5%, 24.42% and 6% respectively. Return loss at all three centre frequency have less than −10 dB. Antenna efficiency achieved for this design is more than 95% at all centre frequencies. All simulations were carried out using IE3D v. 12 software, a Zeland Inc. Product, which is based on Method of Moment.

Session 4P6
Computational Techniques 2

Effective Electromagnetic Media for FDTD-PIC

Lars D. Ludeking and Andrew J. Woods
ATK-Mission Systems Group, Newington, Va 22122, USA

Abstract— Simulation and modelling using FDTD-PIC techniques requires the treatment and utilization of various electromagnetic media properties to provide high fidelity results. The various techniques available have practical limitations when employed in problems that include the modelling of ambient plasmas. The authors discuss some of the techniques and issues that must be overcome in obtaining robust simulations suitable for design and demonstration of useful physical principles.

Simulation is used to provide insight into physical processes and guide the design and development of a variety of technologies. Historically this approach has been applied in the domain of vacuum electronic devices, however, the methodology spans a much broader range of applications, which includes areas such as bio-electric effects, bio-medical, radar cross section, high power microwaves, and so forth.

The ATK software package known as the "Magic Tool Suite" is a widely used FDTD-PIC software suite. The basic approach for FDTD-PIC is well known and the literature contains the basic equations and descriptions for the solution of Maxwell's equations. This approach is very attractive because of its computational efficiency and relative ease of implementation.

Two of the principle challenges of any Maxwell solver however, lie in the termination of the simulation domain and the representation of complex media properties. Simple terminations such as the perfect conductor and periodic and mirror symmetries are readily treated. However, the open boundary termination is one which many researchers have devoted enormous amounts of energy in perfecting. The basic issue is the completion of the simulation domain with a one-sided wave equation. There are in fact two complementary aspects that are of value in Magic. These are the scattered wave component and the incident wave component. In addition there is the issue of modelling interior domains with permittivity and conductivity.

The simulation approach is widely used, and often misused. Novice users of this approach often fail to understand fundamental issues and constraints in the application of the various models and how they may interact. In this paper, the authors will address some of the FDTD-PIC constraints associated with the following algorithms:

- Matched Phase velocity method for bounding a domain and the introduction of electromagnetic pulse into the interior.
- The use of the CPML method and the caveats when applied to non-plasma free problems.
- The optimized "freespace" impedance matching method, or the "lazy mans version of PML". What are its advantages and disadvantages?
- Conductor surface loss models and the side effects. Practical remediation of the artefacts'.
- The use of interior electric and magnetic conductivity models for modelling of effective absorbers and mimicking FETs.

ACKNOWLEDGMENT

This material is based upon work supported by the Air Force Office of Scientific Research (AFOSR) under Contract No. FA9550-60-C-0148.

Numerical Analysis of Photonic Characteristics by a Multilayered Dielectric Deep Grating

Y. Okuno, **A. Matsushima**, **and T. Suyama**
Kumamoto University, Japan

Abstract— An effective computational method based on a conventional modal-expansion approach is presented for handling a multilayered dielectric grating whose profiles are strongly modulated. The groove depths can be the same as or a little more than the grating period. The materials can be dielectric or metal. In consideration of an application to a photonic crystal, we examine a characteristic of the multilayered dielectric grating. The method is based on Yasuura's modal expansion, which is known as a least-squares boundary residual method or a modified Rayleigh method. In the extended method, each layer is divided into shallow horizontal layers. The Floquet modal functions and approximate solutions are defined in each shallow layer, and the latter are matched with boundary conditions in the least-squares sense. A hugesized least squares problem that appears in finding the modal coefficients is solved by the QR decomposition accompanied by sequential accumulation. As numerical example, we calculate a diffractive characteristic by a multilayered deep dielectric grating and confirm that a common band gap occurs for both polarizations and all incident angles.

Introduction: A photonic crystal [1–3], which is composed by arraying periodically dielectric material having different permittivity, is receiving much attention nowadays. This type of crystal has a characteristic of what is called photonic band gap, which suppresses propagation in certain wavelength ranges dominated by crystal structure, and has many applications as devices for optical integrated circuits. Recent development of microfabrication technique makes it possible to produce deep gratings whose profile is strongly modulated [4].

From the viewpoint of numerical analysis, there are few examples which analyze diffraction characteristics of three-dimensional photonic crystals. The three-dimensional photonic crystal which we treat in the present paper is fabricated by laminating deep grating layers. To elucidate a characteristic of such photonic crystal, and to design a crystal having a desired gap, it is necessary to examine an interaction with structure (a laminate of doubly periodic deep gratings) and light (an electromagnetic wave). It is expected that the photonic characteristic is appeared clearly by a multilayered grating, and the polarization dependence is decreased by an introduction of twodimensional periodicity. We analyze the problem of plane wave diffraction by the multilayered deep grating, and confirm that a characteristic as photonic crystal is provided.

REFERENCES

1. Yablonovitch, E., "Inhibited spontaneous emission in solidstate physics and electronics," *Phys. Rev. Lett.*, Vol. 58, 2059–2062, 1987.
2. Ho, K. M., C. T. Chan, and C. M. Soukoulis, "Existence of a photonic gap in periodic dielectric structures," *Phys. Rev. Lett.*, Vol. 65, 3152–3155, 1990.
3. Villeneuve, P. and M. Piche, "Photonic band gaps in two dimensional square and hexagonal lattices," *Phys. Rev. B*, Vol. 46, 4969–4972, 1992.
4. Ohtsu, M., Y. Okuno, A. Matsushima, and T. Suyama, "A combination of up- and down-going floquet modal functions used to describe the field inside grooves of a deep grating," *Progress In Electromagnetics Research*, Vol. 64, 293–316, 2006.

New Method for an Analysis of Electromagnetic Wave Scattering Based on Sinc Function

Akira Komiyama
Osaka Electro-Communication University, Hatsu-cho Neyagawa-shi 572-8530, Japan

Abstract— In a two-dimensional problem the electric field E_y is expressed as

$$E_y(x,\, z) = \sum_{m=-\infty}^{\infty} E_y(mh,\, z) S(m,\, h)$$

where $S(m,\, h)$ is defined as

$$S(m,\, h) = \frac{\sin[(x - mh)\pi/h]}{(x - mh)\pi/h}$$

and is referred as the m-th Sinc function with step size h [1]. In a free space $E_y(mh,\, z)$ satisfies the following ordinary differential equation,

$$\frac{d^2 E_y(mh,\, z)}{dz^2} + \sum_{n=-\infty}^{\infty} M_{mm} E_y(nh,\, z) = 0$$

where $M_{mn} = k_0^2 \delta_{mn} - c_{mn}/2\pi h^2$ and $c_{mn} = (-1)^{m-n} 4\pi/(m-n)^2$. The solution is expressed as

$$E_y(mh,\, z) = \sum_{n=-\infty}^{\infty} a_n (f_n)_m e^{-j\sqrt{\lambda_n} z}$$

λ_n and f_n are the eigenvalue and the eigenvector of the matrix $M(= (M_{mn}))$, respectively. The coefficient a_n is determined from the boundary conditions.

E_y is expressed in terms of the Fourier integral,

$$E_y(x,\, z) = \frac{1}{2\pi} \int_{-\infty}^{\infty} A(p) e^{-jpx - j\sqrt{k_0^2 - p^2} z} dp$$

The spectrum function $A(p)$ is given by

$$A(p) = h \sum_{m=-\infty}^{\infty} E_y(mh,\, 0) e^{jmhp}, \quad |p| < \frac{\pi}{h}$$

Applying the saddle point method to the integral representation the far field is obtained.

This numerical method is applicable to a variety of scattering problems with plane boundaries.

REFERENCES

1. Stenger, F., *Numerical Methods Based on Sinc and Analytic Functions*, 91–97, Springer-Verlag, 1993.

Solving Guided Wave Modes in Plasmonic Crystals by Interfacial Operator and Coupling Interface Approach

Yu-Chen Shu[1, 4], **Chien C. Chang**[2, 4], **I-Liang Chern**[3, 4], **and Ying-Hong Liu**[1]

[1]Division of Mechanics, Research Center for Applied Sciences, Academia Sinica, Taipei 115, Taiwan, R.O.C.
[2]Institute of Applied Mechanics, National Taiwan University, Taipei 106, Taiwan, R.O.C.
[3]Department of Mathematics, National Taiwan University, Taipei 106, Taiwan, R.O.C.
[4]Taida Institute for Mathematical Sciences, Taipei 106, Taiwan, R.O.C.

Abstract— It has been difficult to solve eigenmodes of plasmonic crystals in two or three dimensions either analytically or numerically. In this study, we present an interfacial operator approach for solving guided wave modes of plasmonic crystals. They are formulated as an eigenvalue problem of the wavenumber along the axis of the crystal. In this formulation, the permittivity and permeability of the metallic component can be arbitrary functions of frequency. Moreover, a coupling interface method is introduced to facilitate accurate treatment of the interface conditions with an arbitrary shape between the metal and host materials. Numerical results are illustrated for different shapes of plasmonic crystals, layered, cylindracal and split-ring structures. The physical significance is discussed. Finally, it is demonstrated that the present method can resolve fine eigenmodes of the split-ring structure.

Extraction of Complex Permittivity of Multilayered Dielectric Sample Loaded in a Rectangular Waveguide

Uma Balaji
Electrical & Computer Engineering Department, California State University
Chico, CA 95929, USA

Abstract— Complex permittivity of materials loaded in the cross section of a rectangular waveguide can be determined from the S-parameter measurements of the discontinuity. An analytical or numerical electromagnetic tool is required to solve the scattering problem of dielectric loaded waveguide. Minimization of an error function is essential to extract the unknown complex permittivity of the material. The error function is a function of the calculated S-parameter from an estimated complex permittivity and the measured S-parameter of the discontinuity.

Mode matching technique is the numerical tool used in this paper to determine the S-parameter of the discontinuity of multilayered dielectric loaded in the rectangular cross-section of the waveguide. Minimization of the error function is performed using a practical Quasi-Newton algorithm. The novel contribution in this work is the approach used in the determination of S-parameters of the discontinuity particularly when the dielectric material is multilayered. The multiple discontinuities at small distances from each other at all layers of the dielectric are treated independently and then finally cascaded to determine the S-parameter of an empty waveguide loaded with the dielectric sample for a finite length.

The first step in the analysis is writing the fields on both sides of the discontinuity in terms of fundamental TE_{10} modes of incident and reflected waves. The magnitude of power carried by the modes in both sides of discontinuity is set to unity. The continuity conditions for the tangential components of electric and magnetic fields are imposed. Using the principle of orthogonality of modes, the equations of continuity conditions are rearranged to determine the scattering parameter at each layer of the discontinuity. It should be noted that each discontinuity is formed by two layers of differing relative permittivity. While analyzing the discontinuity at the interface of two layers it is assumed that the material is ideal. However since each layer is of finite length the S-parameter for the extended length of dielectric loaded waveguide is calculated considering the loss tangent and relative permittivity of the following layer. This process results in S-parameters of extended lengths of line available at all layers including the losses that take place in the loaded waveguide. In order to incorporate the fact that the last layer of the sample ends in an empty section of waveguide, the S-parameters of a discontinuity from the last layer of dielectric sample to an empty waveguide is calculated. These S-parameters are all cascaded according to the placement of each layer to obtain the theoretical S-parameter of the multilayered discontinuity. A two layered dielectric sample problem was investigated to test the algorithm. Analytically the unitary property of S-matrix was verified when the loss tangent of the material was set to zero. In order to test the inverse scattering problem, the theoretically determined S-parameter for a two layered dielectric sample was treated as measured S-parameter. Convergence to the actual value of complex permittivity was arrived in less than 15 iterations from the initial guess.

Determination of the complex permittivity of multilayered dielectric sample at all frequencies is very important in the design of microwave components. This problem has been studied in literature using several numerical techniques. This paper has approached the solution to this problem using mode matching technique.

Parallel Electric Field Integral Equation Solver for Arbitrary Shaped Conducting Bodies

Haythem H. Abdullah[1], **Jungsook Yang**[2],
Nader Bagherzadeh[2], **and Khalid F. Hussein**[1]
[1]Electronics Research Institute (ERI), Dokki, Cairo, Egypt
[2]University of California, Irvine, USA

Abstract— With the advent of high performance computing, electromagnetic researchers have been quick to take advantage of expanding capabilities with high performance techniques. Since the electromagnetic simulation of realistic problems, for example, computing radar cross section (RCS) of complex objects such as aircrafts is too heavy in computations because the long execution time and the heavy memory usage, the power of parallel processing is needed to increase the timing performance while reducing the memory consumption per node.

An appropriate method that can deal efficiently with the electromagnetic scattering problems from conducting surfaces is the moment method. In this analysis the electric field integral equation (EFIE) is used. Triangular patches are used to model the surface of the scatterer. This results in a very accurate geometrical modeling of the object. Triangular patches are best fitting for the curved shapes. A Rao, Wilton, and Glisson RWG basis function is used to represent the current distribution in two adjacent triangular patches sharing one common edge. Applying the moment method on the EFIE and using the testing function as the basis function results in a system of linear equations. This system of equation is solved for the unknown current distribution. In this paper, the optimum method for calculating the integrals on the surface of the scatterer is investigated. The analysis of both the Gauss Jordan Row Reduction method and the Conjugate Gradient method for solving the system of equations is applied.

Even with the optimization of the integration and the system solution, the running times on the order of hours, weeks, or longer are common when solving problems of realistic size. Some problems are too large to be solved due to the impractical computational time and memory constraints. The slow nature of the algorithm primarily results from the nested for-loops. Inside the nested loops double integrals is to be performed numerically. The computation of those double integrals uses other nested loops. To shorten the computational time, people acquire faster computers, lease time on supercomputers, to gain a parallel processing speed up. Other researchers have applied parallel processing to the 3D Finite Difference Time Domain (3DFDTD) method using a MeikoCS-2MPP (MassivelyCparallel processors) computer and the KSR- 1 "virtual shared computer". These computers are specially designed for parallel processing and have high speed data links between processors. These solutions are expensive and not accessible to many researchers.

In this work, a multiprocessor cluster system for EFIE solver is built over LANs to produce a large array of CPUs. This network solution has the advantages in that the high processing power enables computation times reduced and the computers can be used for other purposes when they are not used for simulating the code. In this paper a parallel processing algorithm is discussed in detail. The algorithm is generic and applicable to solve various scattering problems with arbitrary shaped bodies. For example it can be used for antenna analysis such as wire antennas (dipole, loop, helical, Yagi Uda, Log periodic antennas, etc.), reflector antennas with different types and conducting lens antennas. In addition, it can solve large scattering problems from aircrafts to mineral detection inside the earth. In this work, the parallel processing performance result obtained in the cluster system will be presented.

Improvement of Particle Swarm Optimization

K. Kawakami and Z. Meng
Department of Electrical Engineering, Fukuoka University, Japan

Abstract— There are cases when optimization is required in the field of electromagnetic engineering, such as optimizing design parameters, resolving a nonlinear inverse scattering problem as an optimization problem, and so on. Usually, an objective function has multiple local solutions due to the function complexity or errors in approximately calculation, and a global applicable optimization method is necessary. Particle swarm optimization (PSO) has achieved considerable success as a global optimization method with a wide range of applicability, requiring no prior information, being appropriate for diverse objective functions, and offering the ability of recovery even after trapping on a local solution. However, PSO has the following problems.

1. Difficult to use
   Several parameters are needed to control the algorithm. Unless these parameters are set appropriately, search efficiency drops significantly. There are, however, no clear rules for setting the parameters, and almost all users have considerable difficulty setting them without prior experience in parameter tuning.
2. Slow convergence
   Global optimization methods do not utilize differential information, so convergence is usually slower than that of the descent category optimization method.

In this paper, we introduce a new technique titled "Refresh Particle" and a hybridization with conjugate gradient method to PSO. The former charges power to inactive particle to improve recovery ability of particle population after trapping on a local solution, and as a result, the rule for setting parameters becomes clear and simple, and it is possible to keep high performance for diverse objective functions. On the other hand, the point of the latter is how to determine the changeover timing between the two methods. The convergence rate of PSO is not very important for the hybrid method. Some hints have been obtained from our numerical experiments.

An Improved Adaptive Finite Element Method for the Simulation of Electromagnetic Field

Zhanghong Tang[1], **Jiansheng Yuan**[2], **and Gai Tao**[1]

[1]College of Materials Science and Engineering
Beijing University of Technology, Beijing 100124, China
[2]Department of Electrical Engineering, Tsinghua University, Beijing 100084, China

Abstract— Adaptive finite element method is very popular in electromagnetic field computation nowadays since an accurate computation of the real engineering problems requires large number of unknowns, which cost large amount of computer resource. The adaptive finite element method in which a mesh is refined to improve a solution of the problem can significantly reduce the number of unknowns comparing to the traditional methods. Here mesh refinement is controlled and governed by the posteriori error estimation of the solution.

In general, the posteriori local and global error estimates are based on the Superconvergent Patch Recovery (SPR) technology. In this paper, a method for computation the error distribution over the solution and a remeshing strategy for construction of an optimal mesh based on the error distribution are studied and results show that this strategy can reduce the number of unknowns for many problems. However, further studies shows that for some large engineering problems, this remeshing strategy still generate too many elements.

In this paper, an improvement of this remeshing strategy is presented. The improved method introduced a new formula to estimate the global error after the refinement of every element. According to this method, the global error is kept watch on at any time and once it is satisfied for the given tolerance, the refinement is stopped at once and so the number of elements to be generated is optimal under the given accurate. Results show that the improved method can generate much less elements with more smoothly refined meshes. Fig. 1 shows a real two-dimensional electrostatic example. On the boundary Γ_1 and Γ_2 of Fig. 1(a), the Dirichlet boundary conditions are set: on Γ_1 the potential is 1 V and on Γ_2 the potential is 0 V. Figs. 1(b) and (c) show the results of adaptive generated meshes for the tolerance of 5% with the original remeshing strategy and the remeshing strategy presented in this paper. In Fig. 1(b), the total number of elements is 969 but in Fig. 1(c), the total number of elements is only 448.

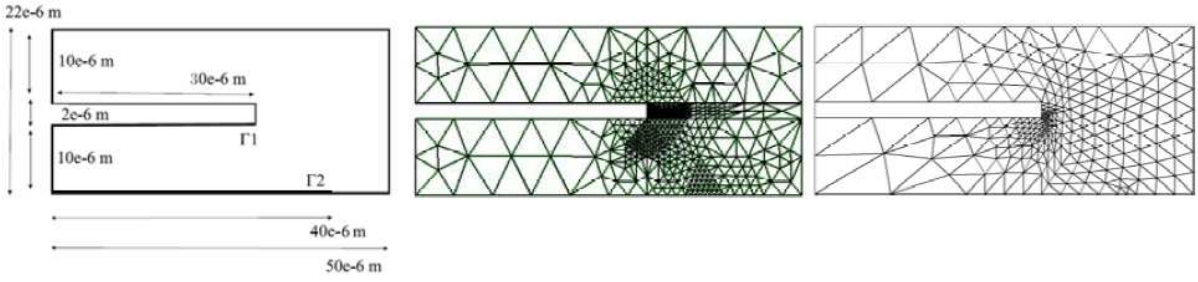

Figure 1: Adaptive refinement of a 2-D sample of electrostatic problem (a) Model size; (b) Adaptive refinement by original strategy; (c) Adaptive refinement by improved strategy.

A Domain Map Finite Element Method for Solving Open Boundary Electromagnetic Field Problem and Its Application

Zhanghong Tang[1], **Yueqin Dun**[2], **Jiansheng Yuan**[2], **and Gai Tao**[1]

[1]College of Materials Science and Engineering
Beijing University of Technology, Beijing 100124, China
[2]Department of Electrical Engineering, Tsinghua University, Beijing 100084, China

Abstract— There are many numerical methods to model the electrode-type resistivity tools of well logging, such as finite different method (FDM), finite element method (FEM) and numerical mode-matching method (NMM). Among these methods, the NMM method is most efficient because it can reduce the original higher dimensional layered problem to a series of lower dimensional problems, which is especially suitable to this kind of well-logging modeling. For example, a 3-D inhomogeneous horizontally-layered multiregion medium problem (as shown in Fig. 1) is reduced to two-dimensional problems, and the field in every layer is obtained by recursive formula.

In 3-D NMM method, the 2-D eigenvalue problems of all layers are solved at first, which can be converted to 2-D FEM problems. For the 3-D well-logging modeling, the mediums are horizontally-layered ground with different conductivities, which are open boundary field domains in the correspondent 2-D FEM problems. In general, the open boundary field domain is approximated by a large but limited disk and a boundary condition is applied to the disk boundary. This method needs large amount of computation for high accurate, since higher accurate needs larger domain, which needs more FEM nodes and elements.

In this paper, a domain map finite element method is introduced for open boundary field problems. This method converts the original infinite field domain into bounded field domain, which can save the memory and the CPU time greatly. This algorithm is successfully applied to the 3-D numerical mode matching method (NMM) for resistivity well-logging. Comparing with the original finite element method used in 3-D NMM for solving the well-logging problem, this new approach decreases the total number of nodal points to form the 2-D FEM matrices, which are the matrices of generalized matrix eigenvalue equation used in 3-D NMM. Further more, this new approach also changes the distribution of eigenvalues, which decreases the valid eigenvalues under the same truncation error. Results show that the new method is almost 7 times faster than the original one.

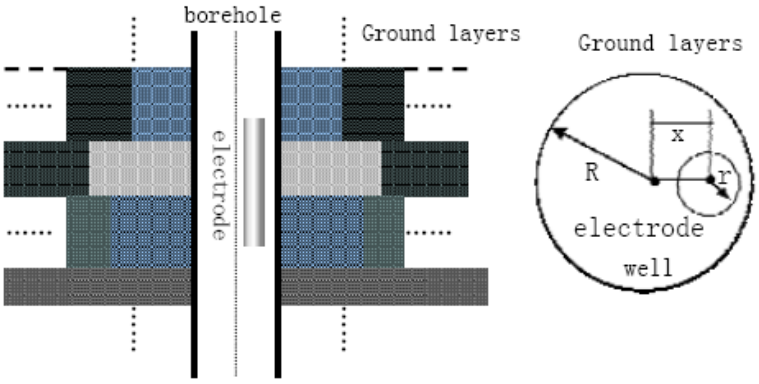

Figure 1: A geometry structure of resistivity well-logging (vertical well), (a) view from x-z plane, (b) view from x-y plane.

Nyström Method Solution for Electromagnetic Scattering by Three Dimensional Complex Material Bodies

M. S. Tong and W. C. Chew
University of Illinois at Urbana-Champaign, USA

Abstract— Nyström method was proposed by E. J. Nyström in 1928 and is an efficient numerical method for solving integral equations. The primary advantage of the Nyström method is that the integral operator is replaced with an appropriate quadrature rule when the operator is smooth and matrix entries can be generated by simply sampling integral kernels at quadrature points without involving numerical integration. In wave physics, the integral kernels are singular and a local correction scheme is required for solving integral equations. One has developed several local correction schemes, including our previous work, for electromagnetic (EM) applications.

Nyström method has received more and more attention in EM community in recent years. However, this method was mainly used to solve relatively simple problems in which perfectly electric conducting (PEC) objects are considered mostly and dielectric media are less involved. In this work, we apply this method to solve for electromagnetic scattering by relatively complicated structures with three-dimensional (3D) composite material bodies. The problem is usually formulated with surface integral equations (SIEs), including the electric field integral equation (EFIE), magnetic field integral equation (MFIE), combined field integral equation (CFIE), Poggio-Miller-Chang-Harrington-Wu-Tsai (PMCHWT) formulation and Müller formulation. These SIEs include both equivalent electric and magnetic currents as unknowns on the object surfaces.

Since CFIE, PMCHWT and Müller formulation have been demonstrated to be more stable and thus more widely used in the method of moments (MoM), we use Nyström method to solve EFIE and MFIE which are less solved in MoM. EFIE and MFIE in MoM solutions usually suffer from the basis problem in representing the magnetic current if the Rao-Wilton-Glisson (RWG) basis is used to represent the electric current. EFIE and MFIE are sensitive to the employed basis functions and the usual choices of the RWG, $\hat{n} \times$ RWG (where $\hat{n}$ denotes the unit normal vector at object surface) or dual basis in representing the magnetic current will have the instability, fictitious charge or high cost problems, respectively. Compared with MoM, Nyström method is simpler to implement and most importantly, it can fully get rid of basis problem. In addition, Nyström method has less requirements on geometrical meshes. The deficient meshes which are not allowed in MoM can also be utilized. Numerical examples show that the Nyström method based on our local correction scheme can produce stable and efficient solutions from the EFIE and MFIE even for those complicated composite structures and thus is a robust alternative numerical tool.

Scattering of Electromagnetic Waves by Slanted Dielectric Gratings Loaded with Two Adjacent Perfectly Conducting Strips

Tsuneki Yamasaki, **Ryosuke Ozaki**, **and Takashi Hinata**
Department of Electrical Engineering, College of Science and Technology
Nihon University, Japan

Abstract— Recently, many analytical and numerical methods which are applicable to the inhomogeneous dielectric gratings have been proposed such as optical fiber gratings, photonic bandgap crystals, frequency selective devices, and other applications by the development of manufacturing technology of optical devices. However, the theoretical and numerical studies have considered the periodic structures in which the material forming grating was either metallic or dielectric.

In this paper, we proposed a new method for the scattering of electromagnetic waves by slanted dielectric gratings loaded with two adjacent perfectly conducting strips using the combination of improved Fourier series expansion method and point matching method for TE waves.

In the slanted dielectric grating $S_2\,(0 < x < D)$, the permittivity profile $\varepsilon_2(x,\, z)$ is generally not separable with respect to the x and z variables. So main process of our methods are as follows: (1) The slanted layer is approximated by a transformation of coordinates system of modulated index profile with period $p' = p\cos(\varphi)$. (2) Taking new coordinate system, the electromagnetic fields are expanded appropriately by a finite Fourier series. (3) In the perfectly conducting strip and gap regions at C_1 (or $\overline{C_1}$) and C_2 (or $\overline{C_2}$) boundary, the electromagnetic fields are matched using an orthogonality relation which makes the matrix relation on both sides using point matching method. (4) Finally, all layers include the metallic regions are matched using appropriate boundary conditions to get the slanted dielectric gratings loaded with two adjacent perfectly conducting strips.

Numerical results are given for the transmitted scattered characteristics for the case of incident angle and frequency with $\delta[\varphi = \tan^{-1}(\delta/D)]$ for TE waves.

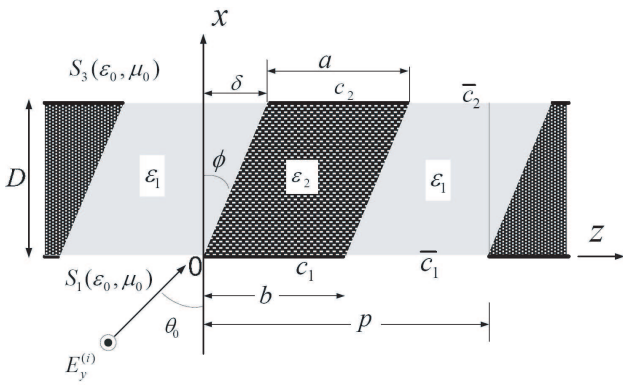

Figure 1: Structure of slanted dielectric gratings loaded with two adjacent Perfectly conducting strips.

Session 5A1
Optics and Photonics 2

Enhanced Transmission through 1D Slanted Subwavelength Slits Arrays in Metallic Films

Gérard Granet
LASMEA, UMR6602, 24 Av. des Landais 63177 Aubière, France

Abstract— Since the publication of a paper by Ebbesen et al. [1] many experimental and theoretical studies have been undertaken in order to determine the physical origin of the observed enhanced transmission through apertures in metallic films. It is now well known that plasmons and waveguide modes play a crucial rôle in the phenomena. This is the reason why modal methods are well suited to investigate the physics behind enhanced transmission. Here we are concerned with 1D slanted subwavelength slits arrays in metallic films (see Fig. 1). Our goal is to study the influence of the tilt angle of the slit. For example, Fig. 2 shows how the tilt angle affects the transmission spectrum.

We have implemented an original method that allows us to take rigorously into account the peculiar geometry of the slits: in the grating region, we used an inclined coordinate system (u, v, w) deduced from the cartesian coordinate system (x, y, z) by:

$$x = u + \tan(\phi)v \quad y = v \quad z = w$$

Thanks to this new coordinate system, the permittivity function depends only of the u variable which allows the grating region to be analyzed at once with a modal method. We choose the Parametric Fourier Modal Method [2] for its simplicity and its ability to give accurate results with a small number of Floquet harmonics.

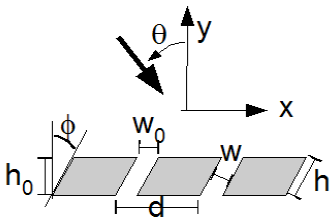

Figure 1: Slanted slits array in a metallic film.

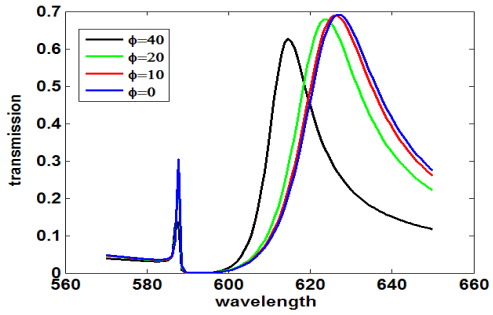

Figure 2: Transmission versus tilt angle. $h = 150\,\text{nm}$, $d = 500\,\text{nm}$, $w = 50\,\text{nm}$, $\theta = 10$.

REFERENCES

1. Ebbesen, T. W., H. J. Lezec, H. F. Gaemi, T. Thio, and P. A. Wolff, *Nature*, Vol. 391, 667, London, 1998.
2. Granet, G., *J. Opt. Am. A*, Vol. 16, 2510, 1999.

Study of Optical Propagation in Hybrid Periodic/Quasiregular Structures Based on Porous Silicon

José Escorcia-García[1] and Miguel E. Mora-Ramos[2]
[1]Centro de Investigación en Ingeniería y Ciencias Aplicadas
Universidad Autónoma del Estado de Morelos
Ave. Universidad 1001, Cuernavaca 62209, México
[2]Facultad de Ciencias, Universidad Autónoma del Estado de Morelos
Ave. Universidad 1001, Cuernavaca 62209, México

Abstract— In recent years, dielectric photonic band gap (PBG) structures have attracted great attention for their property to forbid the propagation of the light (at certain wavelengths) in and out the structure. This property can be used to confine, manipulate and guide photons, and hence make possible an expanded range of devices and applications. The simplest one dimensional PBG structure is the Bragg mirror (BG) which consists of alternating layers of high (nH) and low (nL) refractive indices, whose thicknesses satisfies the Bragg relation $2(n_H d_H + n_L d_L) = \lambda_m$. This structure is characterized by the presence on only one degenerate PBG in a period of the reciprocal space. On the contrary, multiple PBG are typical of aperiodic structures. Among these quasiregular structures we have the quasiperiodic Fibonacci (FN) structure, which is constructed by the pattern of the Fibonacci sequence given by the following addition rule $F_j = F_{j-2} + F_{j-1}$ and defining $F_1 = A$, $F_2 = AB$. This structure is classified as intermediate between periodic and aperiodic media. The optical properties of Bragg and Fibonacci structures have been extensively studied by different authors so far. However, there have been only very scarce studies on the resulting optical properties from the combination between periodic (BG) and quasiperiodic structure (FN), denominated hybrid structures [1, 2]. In this work we report the propagation of the light waves within the (BG-FN) hybrid structures and the appearance of photonic bandgaps in the reflectance spectrum (optical properties), which are studied theoretically with the use of oblique incidence transfer matrix technique. and experimentally studied. Some other quasiregular systems are also included as non-periodic elements in the calculation: The Thue-Morse, which is classified as a critical sequence and is generated by means of a two-letter alphabet with the substitution rule $A \rightarrow AB$; $B \rightarrow BA$. Additionally, we study the so-called Period Doubling, that classifies as an almost periodic structure and is based in a two-letter alphabet obeying the rule $A \rightarrow AB$; $B \rightarrow AA$. In all cases, the discussion is made regarding the possible application of these structure as photonic quasicrystals. For the simulation we have adopted the typical parameters of a Porous-Silicon dielectric multilayer, for the possibility of easy fabrication that the devices based on it exhibit.

REFERENCES

1. Maciá, E., *Phys. Rev. B*, Vol. 63, 205421, 2001.
2. Dong, J. W., P. Han, and H. Z. Wang, *Chin. Phys. Lett.*, Vol. 20, 1963–1965, 2003.

Magnetic Proximity Effect in Isolator Crystal Pairs

Yoav Linzon[1], **Marcello Ferrera**[1], **Luca Razzari**[1, 2], **Alain Pignolet**[1], **and Roberto Morandotti**[1]

[1]Universite du Quebec, Institute National de la Recherche Scientifique
Varennes, Quebec J3X 1S2, Canada
[2]Dipartimento di Elettronica, Universita di Pavia
via Ferrata 1, 27100 Pavia, Italy

Abstract— We experimentally studied the polarization dynamics (orientation and ellipticity) of near infrared light transmitted through magnetooptic Yttrium Iron Garnet isolator crystal pairs using a modified balanced detection scheme. When the pair separation is in the sub-millimeter range, we observed a proximity effect in which the saturation field is reduced by up to 20%. 1D calculations suggest that the proximity effect originates from magnetostatic interactions between the dipole moments of the isolator crystals, observed through the optical transmission polarization effects.

New Measuring Method of Examination of Planar Optical Waveguides

D. V. Svistunov

St.-Petersburg State Polytechnic University, Russia

Abstract— Parameters of the optical waveguide (WG) define the operating performances of the whole photonic device. In order to optimize these parameters, appropriate technology conditions should be chosen. Necessary works include preliminary computer simulation of the process, fabrication of trial samples and their examination.

Important part of examination of a planar optical WG is measurement of the WG mode spectrum. Usually this procedure is performed by well-known m-line spectroscopy technique. However, in cases of planar WG structures with thick cover layers or so-called buried graded-index WGs this method does not provide reliable measurements. Thick cover layers or large burying depths do not allow tunneling the modes to the external prism and forming corresponding spatial m-lines. In these cases, some modes (first of all, the lower-order modes) may be simply missed in examinations by m-line spectroscopy. The greater the burying depth the fewer number of modes can be measured by this method.

The report presents new measuring technique that is suitable for examination of planar WGs having arbitrary refractive index profiles including the noted ones. Both excitation and output of WG modes are performed at WG faces by the end-fire coupling method which allows reliable launching and output of the whole mode spectrum in any planar WG. The technique of mode index measurement is based on the registration of light beams radiated from the end face of a planar WG, with each beam corresponding to the individual mode. Modes of different orders demonstrate different refraction angles at the output face of WG if they are directed to this face under the same inclination angle. Measurement of these angles enables calculating the mode indices. The developed measuring technique was named the end-fire mode spectroscopy.

Furthermore, it is shown that the obtained output light pattern enables conducting direct measurement of the maximal refractive index in a graded-index WG, unlike conventional techniques that employ computing of this value basing on the set of measured mode indices. This feature could be very useful in the researches aimed at obtaining the WGs having certain pre-defined parameters, especially concerning fabrication of buried WGs.

The obtained results of comparative measurements performed by the end-fire mode spectroscopy and other methods prove the viability of the presented technique. Due to the used manner of launching and output of the modes, the end-fire mode spectroscopy allows characterization of arbitrary planar waveguides without any restrictions on burying depth and cover layer thickness.

Numerical Analysis of Polarization Gratings Using ADI-FDTD Method

Hong-Xing Zheng
Tianjin University of Technology and Education, China

Abstract— Polarization gratings (PGs) are generally described as periodic profiles of spatially varying optical anisotropy, which operate by locally modifying the polarization state of lightwave passing through them. The most studied PG profiles are continuous and transparent [1], which is classified into two types based on their local anisotropy: "circular PG" consisting of a spiraling, constant-magnitude, linear birefringence; and "linear PG" consisting of a varying-magnitude circular and linear birefringence. They manifest a unique combination of optical properties that can include 100% diffraction into a single order, diffracted orders with a fixed polarization state controlled by the PG profile, and efficiencies that are highly polarization sensitive. These make the PGs useful for numerous applications in a variety of fields, including polarimeters, displays, polarizing beam splitters, beam steering, and polarization multiplexers.

In this work, we present an extensive numerical analysis of the optical properties of PGs using the alternating- direction-implicit finite-difference time-domain (ADI-FDTD) method [2]. While concise analytic expressions for the optical properties of PGs have been derived using Jones calculus, these are limited by their assumptions to large grating periods, normal incidence, and infinite gratings. Furthermore, even the most unabridged coupled-wave analysis is limited to slowly varying envelopes, and has only been developed for pure volume holograms. Therefore, we aim to investigate three issues: First and most prominently, we seek to understand PG behavior as the grating period becomes comparable to the wavelength; second, we predict the angular response and the behavior of a finite grating; third, we confirm the paraxial analytic expressions. This work is the general numerical analysis of the PGs circular and linear, and presents their diffraction behavior on a fundamental level with as few assumptions as possible. Using our newly developed ADI-FDTD method for periodic anisotropic media, we found strong correspondence with the analytic expressions previously developed for "thin" PGs i.e., with small diffraction angles and normally incident illumination. A fundamental view at polarized wave behavior within PGs is presented using electricfield maps and animations. We explored the thin-thick grating regime transition, and identified as the most robust condition as opposed to Q-factor to delineate the grating regime. It is also apparent that materials with large linear birefringence are most likely to support a high diffraction efficiency and large diffraction angle simultaneously.

ACKNOWLEDGMENT

This work was supported by the National Natural Science Foundation of China Grant 60871026.

REFERENCES

1. Hasman, E., Z. Bomzon, A. Niv, G. Biener, and V. Kleiner, "Polarization beam-splitters and optical switches based on space-variant computer-generated subwavelength quasi-periodic structures," *Opt. Commun.*, Vol. 209, 45–54, 2002.
2. Namiki, T., "A new FDTD algorithm based on alternating-direction implicit method," *IEEE Trans. Microwave Theory Tech.*, Vol. 47, 2003–2007, 1999.

Investigation of Phononic Crystal Waveguide Using ADI-FDTD Method

Hong-Xing Zheng and Ying Liu
Tianjin University of Technology and Education, China

Abstract— The band structure of phononic crystals displays absolute gaps provided one imposes a large contrast between the elastic parameters and the mass density of the inclusions and of the array. Existence of absolute band gaps was predicted theoretically prior to being demonstrated experimentally in various phononic crystals constituted of solid components or mixed solid/fluid components. Recent studies have focused on transmission through perfect- or defect-containing waveguides [1]. The waveguide in phononic crystals is produced by removing or replacing the cylindrical inclusions along one or several rows of the array. The insertion of defects, such as cavities, inside or at the edge of a waveguide was shown to give rise to the filtering or to the rejection of selective frequencies in the guide's transmission spectrum. The ability to taylor the acoustic properties of phononic crystals and more specifically those of waveguides makes them particularly suitable for a wide range of applications from transducer technology to filtering and guidance of acoustic waves. In recent years, the finite difference time domain (FDTD) method has been extended to elastic waves [2]. This method solves the elastic wave equations by discretizing time and space and by replacing derivatives by finite differences.

In this approach, a class of two-dimensional (2D) phononic crystals which incorporate a tunable narrow pass band (NPB) in their gap has been investigated. These are constituted of a periodic repetition of hollow steel cylinders immersed in water. The concept of tunable NPB's from phononic crystals to waveguides is extended. Properties of a waveguide composed of a row of hollow cylinders in a 2D phononic crystal made of filled steel cylinders immersed in water are considered. The NPB frequency can be tuned by modifying the inner radius of the hollow cylinders. Using hollow cylinders with different inner radii, several NPB's and transmit along the guide acoustic waves at two or more selected frequencies have been created. Finally, the alternating direction implicit (ADI) FDTD approach is applied to calculating the transmission coefficient through finite thickness samples of phononic crystals. Mur's absorbing boundary condition is imposed at the free ends of the homogeneous regions. The calculations performed in this work are based on the ADI-FDTD method that has been proven to be an efficient method for obtaining both the transmission coefficient and the dispersion curves in phononic crystals.

ACKNOWLEDGMENT

This work was supported by the National Natural Science Foundation of China Grant 60871026.

REFERENCES

1. Vasseur, J. O., P. A. Deymier, B. Chenni, B. Djafari Rouhani, L. Dobrzynski, and D. Prevost, "Experimental and theoretical evidence for the existence of absolute acoustic band gaps in two-dimensional solid phononic crystals," *Phys. Rev. Lett.*, Vol. 86, 3012–3015, 2001.
2. Zheng, H. X., W. W. Huang, H. B. Xie, D. Y. Yu, and X. D. Chen, "Some problems of elastic waves simulation in time domain," *Journal of Tianjin University*, Vol. 40, 338–342, 2005 (in Chinese).

Electric Field Measurement Based on Optical Polarization-multiplexed Sensing Technique

Changsheng Li
School of Instrument Science and Optoelectronic Engineering
Beihang University, Beijing 100191, China

Abstract— Optical sensors for electromagnetic field measurement have potential applications in many fields such as researches on electromagnetic property of substance, electromagnetic compatibility, RF and microwave technology, space science and technology, high voltage test and electric power industry. Compared with conventional electrical and electronic sensors, optical sensors have advantages of high insulation, broadband frequency response, safety in use, small size and lower disturbance to measurand, etc. In order to perform optical measurement of electromagnetic field, polarimetric sensors utilize all kinds of electrooptic and magnetooptic effects in optical media, such as linear (Pockels) and quadratic (Kerr) electrooptic effects, electrogyration effect, Faraday effect and magnetooptic Kerr effects. The combing utilizations of these optical effects enable us to measure two- or three-dimensional electric and magnetic fields. For example, dual transverse Pockels effect, electrooptic Kerr effect and optical imaging technique have been used for two-dimensional electric field measurement.

This paper proposes two new polarimetric sensing schemes for electric field measurement. The first scheme is a two-dimensional electric field sensor based on dual transverse electrooptic Kerr effect and square wave modulation technique. The second scheme is a three-dimensional electric field sensor which simultaneously employs electrogyration effect and electrooptic Pockels or Kerr effect in some optical materials. Electrogyration effect can cause optical polarization rotation, and electrooptic Pockels or Kerr effect results in linear birefringence in optical material. If we set incident polarized light to be both time-division and polarization multiplexed, then three electric field components to be measured can be determined by polarization demultiplexing of the emerging light. The optical sensing element can be one crystal with both electrogyration and electrooptic effects, or composed of two cascaded crystals. The candidate materials for this optical sensing scheme are discussed.

REFERENCES

1. Hidaka, K., T. Kouno, and I. Hayashi, "Simultaneous measurement of two orthogonal components of electric field using a Pockels device," *Rev. Sci. Instrum.*, Vol. 60, No. 7, 1252–1257, 1989.
2. Zahn, M., "Optical, electrical and electromechanical measurement methodologies of field, charge and polarization in dielectrics," *IEEE Trans. Dielect. & Elect. Insul.*, Vol. 5, No. 5, 627–650, 1998.
3. Yariv, A. and P. Yeh, *Optical Waves in Crystals*, Wiley-Interscience, New York, 1984.
4. Vlokh, O. G., "Electrogyration properties of crystals," *Ferroelectrics*, Vol. 75, 119–137, 1987.
5. Li, C. S., "Stepped polarization states: Representation and its applications to optical sensing and measurement," *Opt. Commun.*, Vol. 281, 2033–2039, 2008.

Time-domain Analysis of Wideband Optical Pulse SHG in Layered Dispersive Material

M. A. Alsunaidi[1] **and F. S. Al-Hajiri**[2]
[1]King Fahd University of Petroleum & Minerals, Saudi Arabia
[2]King Faisal University, Saudi Arabia

Abstract— Time-domain analysis of Second Harmonic Generation (SHG) in modern optical devices provides an invaluable insight into the understanding and potential utilization of this phenomenon and wave-device interaction in general. For CW inputs or long pump pulses, it is quite sufficient to match the phase velocities of the propagating fundamental and second harmonic beams for optimum conversion. As the bandwidth of the pump (fundamental) pulse increases, the group velocity mismatch and wave packet spreading need to be taken into consideration. These effects become significant for pulse durations less than 100 femtoseconds. The earlier attempts to model and simulate pulsed SHG in second order materials involved 1-D approximations with high-order time derivatives and input depletion ignored to simplify the analysis. These attempts, in general, have ignored material dispersion. In this work, the analysis of ultrashort optical pulse propagation in dispersive second order nonlinear materials is introduced. The formulation of the problem involves incorporating the frequency-dependent material dispersion in the time-domain SHG model. For simulation purposes, explicit and uncoupled FDTD solution equations are obtained. The present model fully accounts for all temporal and spatial variations and takes the depletion of the input beam into consideration. The material is assumed to have the general Lorentzian dispersion relation of the form

$$\varepsilon_r(\omega) = \varepsilon_\infty + \frac{(\varepsilon_s - \varepsilon_\infty)\,\omega_o^2}{\omega_o^2 + 2j\omega\delta - (j\omega)^2}$$

where ε_s and ε_∞ are the static and optical values of the dielectric constant, respectively, ω_o is the material resonance frequency and δ is the damping factor. The frequency dependence in the dispersion relation is accommodated in the time domain model through an auxiliary differential equation relating the electric flux density to the field intensity. A symmetric AlGaAs-based dielectric slab waveguide is considered to test the proposed FDTD algorithm. It consists of a 0.44-μm thick guiding layer sandwiched between two 3-μm thick AlAs layers. The excitation field is a Gaussian-modulated CW signal at a fundamental wavelength of 1.064 μm. The transverse profile of the excitation corresponds to the first guided mode at the given operating frequency. Due to group velocity mismatch (GVM) phenomenon, the power exchange between the propagating input pulse and the generated second harmonic pulse diminishes along the propagation direction as shown in Figure 1. Eventually the two pulses seize to interact. This behaviour is very clearly exhibited as the pulse duration is made shorter. The power exchange process becomes similar to the CW case for longer pulses. The generated second harmonic pulse breaks up after propagating

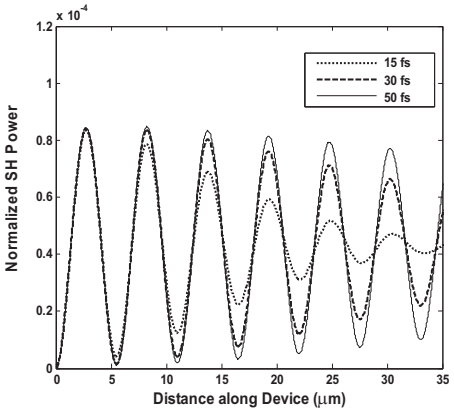

Figure 1: Normalized second harmonic power along the nonlinear, dispersive and lossless waveguide for different initial pulse waists.

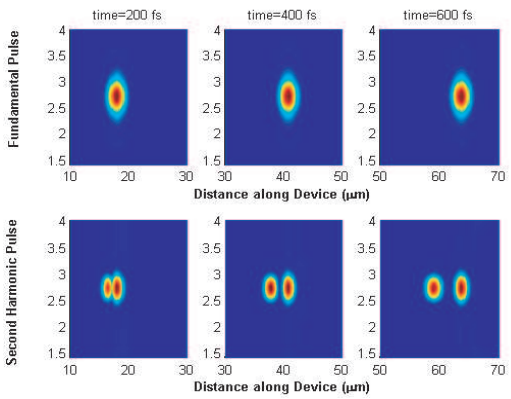

Figure 2: The fundamental and second harmonic fields inside the dispersive nonlinear waveguide. Initial pulse waist is 15 fs.

a curtain distance along the waveguide. The higher frequency components travel slower and lag the fundamental pulse. This process takes around 40 μm to complete for a 15 fs input pulse, as shown in Figure 2.

ACKNOWLEDGMENT

The authors would like to acknowledge the support of King Fahd University of Petroleum and Minerals.

Intense Terahertz Radiation from GaAs Photoconductive Antenna Array

Wei Shi, **Hong Xue**, **Xiangrong Ma**, **and Zhenzhen Zhang**
Department of Applied Physics, Xi'an University of Technology, Shaanxi 710048, China

Abstract— In this paper, we fabricated an intense photoconductive antenna array with eight antenna units. Each unit has separate electrodes and could be operated independently. The spacing between electrodes and the width of the electrodes are 150 μm and 10 μm, respectively. The substrate is commercial semi-insulating GaAs. The electrode pattern is made using a conventional photolithography technique. Ohmic contacts are obtained by using a standard mixture of Ni/Au-Ge/Au for the metallization and the thickness is 700 nm. The antenna array is mounted in an integrated circuit shell with ceramic substrate. Those antennas are tested by TDS-Z2 system made in Zomega Terahertz Corporation. A fiber laser (IMRA F-100) has been used in the system as the excitation source for the generation of THz radiation. The pump beam has a power of 90 mW, wavelength of 800 nm and the 1/e beam diameter on the emitter surface is about 20 μm, and so only one antenna unit is illuminated in our experiment. The field waveform is measured using an electrooptic sampling method employing a 1-mm-thick ZnTe crystal. To understand the behavior of interdigital antenna array, THz transmission through the ceramic substrate is measured. Only 23% of THz wave transmitted through the substrate. If a hole is drilled through the ceramic substrate to make THz wave go through, the THz amplitude of antenna unit will increase more than 4 times, and the THz amplitude from the antenna unit is 4/3 times larger than the THz amplitude from the stripline antenna at the same electrical field.

The Linear and Nonlinear Properties in Magnetic Plasmon Waveguide

S. M. Wang, **T. Li**, **H. Liu**, **F. M. Wang**, **and S. N. Zhu**
National Laboratory of Solid State Microstructures
Department of Physics, Nanjing University, China

Abstract— The subwavelength waveguide has attracted considerable attention in last few years. Several years ago, scientists in this field just focused on the system of coupled electric resonators, for example, the metallic nanoparticle chain. Recently, much attention has paid intensive attention on the subwavelength waveguide via coupling between magnetic resonators. The coupled magnetic resonance in the waveguide is called magnetic plasmon. In this work, the magnetic plasmon modes in the waveguide composed of nanosandwiches have been investigated through a Fourier Transformation method. The dispersion relationships of both the periodic and aperiodic cases can be observed directly from the Fourier Transformation maps of the magnetic field.

In the periodic case, the waveguide provides a band of extended magnetic plasmon mode below the light line, which can be used to guide electromagnetic field. Since the size of the period is much smaller than the wavelength, the waveguide can be considered as a one-dimensional effective medium. Then, we can further modify the waveguide by inserting the dielectrics into the waveguide to form a one-dimensional photonic-crystal-like system. The dispersion relation presents the correlated modification of some sub-band-gaps appearing. This property can be used to design the working frequencies of the waveguide. Moreover, after introducing nonlinearity to the system, the additional band edge can add the chance of the nonlinear enhancement.

In the aperiodic case, we focus on the graded waveguide, with the spacing between the nanosandwiches linearly increasing along the waveguide. The system can provide not only the extended magnetic plasmon modes for energy transfer, but also the special magnetic plasmon modes that only appear in the graded structures, magnetic plasmon gradon. The gradons have their special localization of the field in the waveguide. By using this property, one can design the graded nanosandwich waveguide to obtain a frequency selective switch to guide the field with different frequencies to different ports.

Beside the linear properties of the nanosandwich waveguide composed of metallic nanosandwiches, the nonlinear properties of the single nanosandwich and a chain of the nanosandwiches have also been investigated. For the middle layer owning the Kerr nonlinearity, the shift of the magnetic resonance frequency in single nanosandwich and the magnetic Plasmon frequency in the chain can be observed under different input field intensity. This property may have the potential application in making active nano-devices in the Integrate Optics.

Electromagnetic Radiation from Organic Light-emitting Diodes

A. Epstein, **N. Tessler**, **and P. D. Einziger**
Department of Electrical Engineering, Technion — Israel Institute of Technology
Haifa 32000, Israel

Abstract— The results to be presented are of an analytical model for the electromagnetic radiation emitted from a nanometric Organic Light-Emitting Diode (OLED) device [1, 2]. This is obtained via asymptotic evaluation of the resultant radiation integral in conjunction with coherence considerations, resulting in closed-form analytical expressions. These expressions can be most effectively utilized by engineers for improved design, as they enable the calculation of the device's physical parameters, such as electrical to optical conversion efficiency and emission angular distribution, as a function of the emitted photon frequencies. The resultant expressions are also useful for diode electrical analysis, as they relate between the electromagnetic source locations, that is, the recombination zone, and the device's optical properties. It is readily verified that in addition to the classical electromagnetic wave analysis, the device's physical characteristics, i.e., spatial and temporal coherence, have to be incorporated for a complete and meaningful analysis, as well as significant physical interpretation. This establishes the main contribution of our investigation, leading to analytical expressions which are well supported by both simulated and measured results.

It should be pointed out that the incorporation of both rigorous electromagnetic analysis and coherence effects is addressed in our report for the first time, to the best of our knowledge. This results in a precise model capable of repeating and interpreting experimental and simulated data [3, 4].

REFERENCES

1. Friend, R. H., R. W. Gymer, A. B. Holmes, J. H. Burroughes, R. N. Marks, C. Taliani, D. D. C. Bradley, D. A. Dos Santos, J. L. Brédas, M. Lögdlund, and W. R. Salaneck, "Electroluminescence in conjugated polymers," *Nature*, Vol. 397, 121–128, 1999.
2. Tessler, N., V. Medvedev, M. Kazes, S. H. Kan, and U. Banin, "Efficient near-infrared polymer nanocrystal light-emitting diodes," *Science*, Vol. 295, 1506–1508, 2002.
3. Celebi, K., T. D. Heidel, and M. A. Baldo, "Simplified calculation of dipole energy transport in a multilayer stack using dyadic Green's functions," *Opt. Express*, Vol. 15, No. 4, 1762–1772, 2007.
4. Chance, R. R., A. Prock, and R. Silbey, "Molecular fluorescence and energy transfer near interfaces," *Adv. Chem. Phys.*, Vol. 37, 1–65, John Wiley and Sons, New York, 1978.

Session 5A2
Recent Advances in Metamaterials and Invisibility Cloaking 2

Achieving Waveguide Connection with Left-handed Metamaterials

Jingjing Zhang[1], **Yu Luo**[1], **Hongsheng Chen**[1, 2], **Bae-Ian Wu**[2], **Lixin Ran**[1], **and Jin Au Kong**[1, 2]

[1]The Electromagnetics Academy at Zhejiang University, Zhejiang University
Hangzhou 310027, China
[2]Research Laboratory of Electronics, Massachusetts Institute of Technology
Cambridge, MA 02139, USA

Abstract— Coordinate transformation approach is applied to design a metamaterial coating, which can be used to realize waveguide connection. We use finite-element method to simulate the field distributions, showing that the proposed device can concentrate all the energy in the domain between the input and output waveguides into a small circular region. Since the electromagnetic wave cannot propagate along any other direction, totally transmission can be achieved from the input pot to the output pot even when the distance between the two waveguides is very long. The same device can also be used to realize waveguide bend, and further potential applications are discussed.

ACKNOWLEDGMENT

This work is sponsored by the Chinese National Science Foundation under Grant Nos. 60801005 and 60531020, the excellent doctoral thesis foundation of Zhejiang University (08009A), in part by the ONR under Contract No. N00014-06-1-0001, and the Department of the Air Force under Air Force Contract No. F19628-00-C-0002.

Electromagnetic Wave Manipulation by Layered Systems

Huanyang Chen and C. T. Chan
Department of Physics, Hong Kong University of Science and Technology
Clear Water Bay, Kowlong, Hong Kong, China

Abstract— We show that the optical properties of an oblique layered system with two kinds of isotropic materials can be described using the concept of transformation media as long as the thickness of the layers is much smaller than the wavelength. Once the connection with transformation media is established, we then show that oblique layered system can serve as a universal element to build a variety of interesting functional optical components such as wave splitters, wave combiners, one-dimensional cloaking devices and rotation cloak.

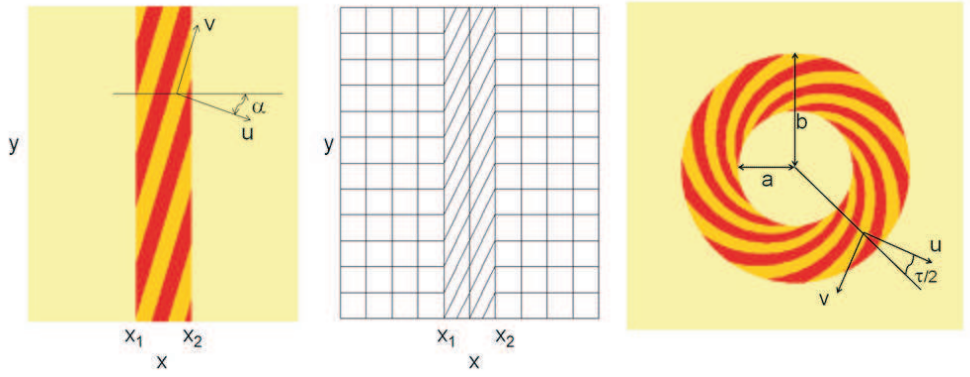

(a) (b) (c)

Figure 1: (a) The geometry of the oblique layered system with two materials. (b) The coordinate transformation to obtain the reflectionless wave shifter. (c) The geometry of the alternating layered system designed to produce the rotation cloaking effect.

REFERENCES

1. Chen, H. Y. and C. T. Chan, to appear in *Phys. Rev. B (2008)*, see also in the preprint: http://arxiv.org/abs/0805.1328.

Realization of Approximate Optical Cloaking Using Silicon Photonic Crystal Structures

D. Xiao and H. T. Johnson
Department of Mechanical Science and Engineering
University of Illinois at Urbana-Champaign, Urbana, Illinois 61801, USA

Abstract— In the last two years, new ideas have been proposed to realize an electromagnetic cloaking device [1–8]. Now it is theoretically possible to engineer a container that provides almost perfect invisibility based on a general recipe developed by Leonhardt [1] and following work by Pendry et al. [2]. Two-dimensional (2-D) cloaks at microwave frequencies have been experimentally realized using this index fitting method [3] and intensive research is being conducted to extend the design into the optical region. For example, optical cloaking has been designed based on the same idea [4].

However, analysis has shown that the cloaking design based on this idea is very sensitive to small perturbations [5]. Here we demonstrate the device sensitivity when the material loss is included. We assume that the cloaking device will have an effective refractive index that exactly follows the formalism proposed in Refs. 2, 3 and 6. Then we add a small effective conductivity of 500 S/m into such a perfectly designed system, with perfect matched layers (PMLs) surrounding a domain of $12 \times 9\,\mu m^2$. Finally we find that the transmitted power at the right boundary in this case is around 8% of the power one would measure in the absence of such a cloaking device with Gaussian beam incidence.

Here, we report on a simple axisymmetric PC structure that may be used to achieve an approximate cloaking effect. The structure is composed of concentric axisymmetric layers of silicon and air. The layered structure is divided into inner and outer parts. The outer part of the axisymmetric structure bends light via the anisotropy of the structure. To demonstrate this design, we consider a case of five layers with a radial period (i.e., the distance between two layers along the radial direction) of $a_1 = 0.06\,\mu m$ and a cylinder thickness $t_1 = 0.014\,\mu m$, for interaction with red light of wavelength $0.7\,\mu m$. H-polarized light is used in the cloaking design. For red light of $0.7\,\mu m$, the effective index can be calculated from the PBS using $n_{eff} = ck/\omega$ so that along the radial direction $n_r = 2.07$ and along the tangential direction $n_\theta = 1.13$. The essential feature for purposes of the design is that the outer part of the cloaking structure has a much larger effective index along the radial direction than along the tangential direction. The inner part of the anisotropic structure prevents light from penetrating the container, but it does permit light propagation tangentially. This part consists of layers with radial period $a_2 = 0.17\,\mu m$ and cylinder thickness of $t_2 = 0.03\,\mu m$. Light in the frequency of interest ($a_2/\lambda \approx 0.243$) is in the band gap along the radial direction, but in the first band along the tangential direction. The magnetic field distribution under the same Gaussian beam illumination shows an approximate cloaking effect when the light wavelength is between $0.65\,\mu m$ and $0.85\,\mu m$. The results are compared with the design using the index fitting method with an estimated effective conductivity of 500 S/m.

REFERENCES

1. Leonhardt, U., *Science*, Vol. 312, 17777, 2006.
2. Pendry, J. B., D. Schurig, and D. R. Smith, *Science*, Vol. 312, 1780, 2006.
3. Schurig, D., J. J. Mock, B. J. Justice, S. A. Cummer, J. B. Pendry, A. F. Starr, and D. R. Smith, *Science*, Vol. 314, 977, 2006.
4. Cai, W., U. K. Cahettiar, A. V. Kildishev, and V. M. Shalaev, *Nature Photonics*, Vol. 1, 224, 2007.
5. Ruan, Z., M. Yin, C. W. Neff, and M. Qiu, *Phys. Rev. Lett.*, Vol. 99, 113903, 2007.
6. Cummer, S. A., B. Popa, D. Schurig, D. R. Smith, and J. Pendry, *Phys. Rev. E*, Vol. 74, 036621, 2006.
7. Alu, A. and N. Engheta, *Phys. Rev. E*, Vol. 72, 016623, 2005.
8. Lezec, H. J., J. A. Dionne, and H. A. Atwater, *Science*, Vol. 316, 5823, 2007.

Medium Parameters and Electromagnetic Properties of Two-dimensional (2D) Cloaks with Arbitrary Geometries

Chao Li, **Kan Yao**, **and Fang Li**
Institute of Electronics, Chinese Academy of Sciences, Beijing 100190, China

Abstract— To reduce the electromagnetic (EM) scattering of objects has always been a subject of keen interest in microwave society. Recently, an intriguing idea was proposed for the design of invisible cloaks based on the form-invariant transformations of Maxwell's equations. The basic principle is to squeeze a volume in a virtual space into a shell in the physical space, which excluding EM waves in the concealment volume. Experimentally, an invisible cloak with simplified material parameters has been implemented with SRR structures at microwave regime. At optical wavelengths, a nonmagnetic cloak design has also been proposed that incorporates metallic nanowires. The possibility of the 'invisibility' was lately studied intensively with analytical and numerical methods. Up to now, most of the studies are focused on the spherical and cylindrical cloaks with rotational symmetry. Such symmetry may inevitably obscure some general physical mechanism. Latterly, cloaks with reduced symmetries, such as elliptic cylinders, eccentric elliptic cylinders and square cloaks were proposed. However, their transformation procedures are only suitable for design of cloaks with their individual shapes. In practice, it is desirable to have the shapes of cloaks be tailored similar as the objects to be concealed. This paper presents the design of 2D cloaks with arbitrary geometries. General expressions of the medium parameters are derived with their unique properties investigated. An irregular cloak is designed to show the flexibility of the method. Full-wave simulations with Huygens' Principle are applied to verify the invisibility of the cloak to external incident waves. The method and results in this Letter make an important step toward the design of cloaks with arbitrary shapes.

Cloak for Bianisotropic and Moving Media

Xiangxiang Cheng[1, 2], **Hongsheng Chen**[1, 2],
Bae-Ian Wu[3], **Lixin Ran**[1], **and Jin Au Kong**[1, 3]

[1]The Electromagnetics Academy at Zhejiang University, Zhejiang University
Hangzhou 310058, China
[2]Department of Information and Electronic Engineering, Zhejiang University
Hangzhou 310027, China
[3]Research Laboratory of Electronics, Massachusetts Institute of Technology
Cambridge, MA 02139, USA

Abstract— The study of cloaking when the background medium is bianisotropic or moving is very useful in practical situations. For example, we may want to conceal an object which is fixed in an environment with its background medium in constantly high-speed motion, such as a satellite in the windy aerosphere or a communication center in the flowing seawater, whose moving environment is not just vacuum. As long as the squared refractive index of the background medium is not equal to unity in its rest frame of reference, it becomes bianisotropic when viewed in the laboratory frame outside the moving environment [1]. If the speed of the moving medium could not be neglected, the effect of bianisotropy of the background medium should be taken into consideration in the cloak design.

First, the background medium possessing magnetoelectric coupling is considered. We present the calculation process of the electromagnetic material property tensors' transformation for the cloak in a bianisotropic background.

Since some bianisotropic medium can be generated by some uniaxial medium moving uniformly with the velocity $\bar{v}$ along a certain direction [1, 2], after the motion is taken into account for reconstructing the constitutive matrix, the medium appears to be bianisotropic to an observer in the laboratory frame, thus we can use exactly the same cloak transformation method as bianisotropic background for moving environment medium once its constitutive matrix has been transformed into the laboratory frame in advance. On the other hand, the cloak in the moving medium which has a complicated bianisotropy can also be described as a moving anisotropic medium with a velocity tensor.

REFERENCES

1. Kong, J. A., *Electromagnetic Waves Theory*, EMW Publishing, Cambridge, MA, USA, 2005.
2. Grzegorczyk, T. M. and J. A. Kong, *Phys. Rev. B*, Vol. 74, 033102, 2006.

Gaussian Beam Propagation in Chiral Nihility Media

Xiangxiang Cheng[1, 2], **Hongsheng Chen**[1, 2], **Bae-Ian Wu**[3], **and Jin Au Kong**[1, 3]

[1]The Electromagnetics Academy at Zhejiang University, Zhejiang University
Hangzhou 310058, China
[2]Department of Information and Electronic Engineering, Zhejiang University
Hangzhou 310027, China
[3]Research Laboratory of Electronics, Massachusetts Institute of Technology
Cambridge, MA 02139, USA

Abstract— Chiral nihility media are known to produce a backward wave as one of their both polarizations, yielding negative refractions at the interface of the chiral nihility medium and free space. In this paper, the analysis of chiral nihility effects are illustrated by showing the propagation of a Gaussian beam both reflected and refracted from an air-chiral interface and through layered chiral nihility media. The critical angle for total reflection and the index-matched total transmission in chiral half space are demonstrated as well as the wave splitting, wave widening, and a wave of standing phase in chiral nihility slabs.

Magnetic Plasmon Resonance at Optical Frequencies in a Slit-hole Resonator

Hui Liu, **Tao Li**, **Shu-Ming Wang**, **Zheng-Gao Dong**, **and Shi-Ning Zhu**
Department of Physics, Nanjing University, China

Abstract— In 1999, Pendry reported that a nonmagnetic metallic element, called as split ring resonator (SRR), with size below the diffraction limit, exhibits strong magnetic plasmon (MP) resonance and behaves like an effective negative permeability material. [1] An effective media made of SRRs and metallic lines can work as negative refraction materials. [2] Besides SRR, some new structures, such as nanorods [3], fish-nets [4], nano-sandwiches were invented to realize magnetic resonance at optical frequencies. Aside from the negative refraction, the application of MP has also been extended to cloaking materials [5], subwavelength waveguides [6] and polarization controllers [7, 8]. In this work, a novel design of magnetic resonator, slit-hole resonator (SHR) is proposed (Fig. 1(a)). It comprises of two parts: a nano-hole near the edge of a semi-infinite golden film and a slit linking the hole with the edge. The SHR can be seen as an equivalent LC circuit, with the nano-hole working as a conductor, and the slit working as a capacitor (Fig. 1(b)). Based on FDTD simulation results (Fig. 1(c)–(e)), we found that magnetic resonance can be realized at optical frequencies in SHR. The magnetic resonator SHR devised in this work may be used as a good "artificial atom" to constitute meta-materials and nanophotonic devices, such as negative refraction materials, cloaking materials, and superlens. The exploration of these applications is worthy of future research.

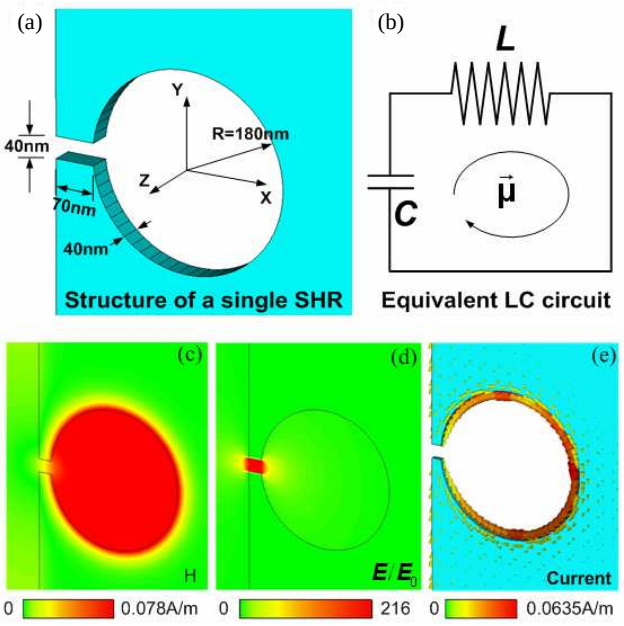

Figure 1: (a) Structure of a single SHR; (b) equivalent LC circuit of the single SHR; (c) magnetic field, (d) electric field and (e) induced current in a single SHR at magnetic resonance mode.

REFERENCES

1. Pendry, J. B., et al., *IEEE Trans. Microwave Theory Tech.*, Vol. 47, 2075, 1999.
2. Shelby, R. A., D. R. Smith, and S. Schultz, *Science*, Vol. 292, 77, 2001.
3. Shalaev, V. M., W. Cai, et al., *Opt. Lett.*, Vol. 30, 3356, 2005.
4. Zhang, S., W. Fan, et al., *Phys. Rev. Lett.*, Vol. 95, 137404, 2005.
5. Schurig, D., J. J. Mock, et al., *Science*, Vol. 314, 977, 2006.
6. Liu, H., D. A. Genov, et al., *Phys. Rev. Lett.*, Vol. 97, 243902, 2006.
7. Liu, H., D. A. Genov, et al., *Phys. Rev. B*, Vol. 76, 073101, 2007.
8. Li, T. Q., H. Liu, T. Li, et al., *Appl. Phys. Lett.*, Vol. 92, 131111, 2008.

Session 5A3
Rough Surface Scattering, Volume Scattering, and Electromagnetic Theory

Multilayer Structure with Gradient Periodicity in Absorption Application

Peiheng Zhou[1, 2], **Longjiang Deng**[1], **Bae-Ian Wu**[2], **and Jin Au Kong**[2]

[1]State Key Laboratory of Electronic Thinfilms and Integrated Devices
University of Electronic Since and Technology of China, Chengdu, China
[2]Research Laboratory of Electronics, Massachusetts Institute of Technology, Cambridge, MA, USA

Abstract— Multilayer structure with gradient periodicity at each layer is introduced in this work for absorbing material design. Based on the principle of coordinate transformation, the thickness of wedged-type absorber can be compressed by changing material's parameters while the electromagnetic properties of absorber remain the same. However, after the transformation, isotropic absorber becomes anisotropic and difficult to fabricate. With gradient periodicity, multilayer composed of four types of isotropic electromagnetic material, with an AB/CD structure, is designed to replace the anisotropic wedged-type absorber. Therefore, an effective approach to reduce absorber's thickness using isotropic material design is suggested. The effects of several crucial parameters on material design, e.g., volume fraction of components, layer number, and periodicities, are discussed in a practical design case.

Analysis of Scattering by Ocean-like Surfaces Using an Augmented SMCG Scheme with Curvilinear Modeling

S. W. Huang and M. Y. Xia
School of Electronics Engineering and Computer Science
Peking University, Beijing 100871, China

Abstract— Electromagnetic scattering from random rough surfaces has drawn a continuous attention for a couple of decades due to its broad applications, especially in microwave remote sensing such as ocean winds and soil moisture. Though there exist dozens of analytical models, their domains of validity are limited and largely uncertain. Rigorous numerical solution is becoming an essential tool to check the accuracy of the approximate models and provide valuable predictions for real-world applications. Rough surface scattering is a typical electrically large problem, and discretization of the governing surface integral equations would result in a large dense matrix system with millions of unknowns, which is solved by resorting to supercomputers in conjunction with advanced algorithms. One of the most efficient methods geared for this problem has been the sparse-matrix canonical-grid (SMCG) method, which exploits fast Fourier transforms (FFTs) to accelerate the repetitive matrix-vector multiplications in the iterative matrix equation solver. By virtue of the translational invariance of the Green's function, SMCG method is accomplished through approximating the Green's function as a truncated Taylor series and expressing the far interactions as a sum of partial matrices with block-Toeplitz structures. There are a single-level version and a multi-level version of the SMCG methods. For the single-level version that uses 2D FFT, the number of terms of the Taylor series expansion should be increased as the roughness of the simulated surfaces increases, which would render the version impractical because the deduction of the high-order derivatives of the Green's function and code implementation become prohibitively complicated. For the multi-level version that uses 3D FFT, the number of expansion levels should be increased with the roughness. However, this would badly lower the computing efficiency because the 3D FFTs need much more computer memory and the computation cannot be accelerated by invoking more available CPUs if the parallel FFTW (fastest Fourier transform in west) software is employed, which does not allow the number of CPUs to exceed each dimension of a 3D array.

To overcome the disadvantages of both the single-level and multi-level versions, a modified SMCG scheme that uses the Chebyshev polynomial approximation of the Green's function to replace the Taylor series expansion will be introduced in this work. Because the challenge of rough surface scattering simulation mainly arises from solving a large matrix system, to reduce the number of unknowns is highly desired. Compared with employing the planar triangular patch modeling and planar RWG basis functions (PRWG bases), adopting the quadratic curved triangular patch modeling and curvilinear RWG basis functions (CRWG bases) should be a viable measure, which permits us to extract results of same accuracy using much fewer unknowns. These two points are the motivations of the present paper. Numerical results for analyses of scattering from ocean-like surfaces will be provided to validate the approach and coeds.

Scattering from Random Stone Scatterers on Lunar Surface Using a Complex Image Technique

Hongxia Ye and Ya-Qiu Jin

Key Laboratory of Wave Scattering and Remote Sensing Information (MOE)
Fudan University, Shanghai 200433, China

Abstract— A complex image technique is developed for electromagnetic scattering from random stone scatterers on lunar surface. The stones are modeled as dielectric half-spheres randomly and sparsely distributed over a half-space of dielectric lunar media. To take account of interactions of random scatterers and underlying intersurface, the integral equations (IEs) is derived using Green's function of dielectric half-space, which is expressed by Sommerfeld spectral integral. The matrix pencil method is used to obtain the complex coefficients of Green's function. The spatial Green's function of dielectric half-space is obtained by making use of the spectral integration and Sommerfled identity. Using Monte-Carlo method to generate random stone scatterers in both location and size, electromagnetic scattering from composte stone scatterers and underlying interface is numerically calculated. Functional dependence on the parameters such as incident and scattering angles, dielectric properties of scatterers etc. are discussed. Applicability for multi-path propagation and communication above lunar surface is analyzed.

Modeling Rough Surface Effects in a Parallel Plate Waveguide

Ruihua Ding[1], **Leung Tsang**[1], **and Henning Braunisch**[2]

[1]Department of Electrical Engineering, University of Washington
Box 352500, Seattle, WA 98195, USA
[2]Components Research, Intel Corporation, Chandler, AZ 85226, USA

Abstract— An advanced parallel plate waveguide model with line source excitation is developed to address the rough surface effect on signal integrity in microelectronic systems. The metal and dielectric layers in printed circuit boards (PCBs) and package substrates are often roughened to improve adhesion between conductors and dielectrics. When the skin depth is comparable to the root mean square (RMS) height of the rough surface, the rough interface can have a significant effect on signal integrity. In this paper, the additional power loss due to the rough interface between the conducting and dielectric layers of a parallel plate waveguide is studied using the finite element method (FEM). The top plate of the waveguide is considered as a smooth, perfect electric conductor (PEC) and the bottom plate as a finite conductivity, rough surface characterized by a stationary random process. The excitation is performed by a line source outside the numerical modeling area. Modal basis functions are used in the input plane and the fields in the computational domain are solved by the FEM. Each modal basis function acts as excitation source for the numerical model and yields linear algebraic equations that are solved by direct sparse symmetric matrix inversion. Convergence and accuracy of the model are demonstrated by varying input parameters including evanescent modes, sampling points, and surface length. Simulation results show the power loss due to the rough surface as a function of surface parameters such as RMS height and correlation length. The simulation results are compared with the analytical results obtained by small perturbation method (SPM) and evaluation of a double Sommerfeld integral.

Fourth Order Moment Statistical Characteristic of the Laser Pulse Scattering on One-dimensional Random Rough Surface

Ming-Jun Wang[1, 2], **Zhen-Sen Wu**[2], **Ying-Le Li**[1], **and Geng Zhang**[2]

[1]Department of Physics, Xian Yang Normal College, Xianyang, Shaanxi 712000, China
[2]School of Science, Xidian University, Xi'an, Shaanxi 710071, China

Abstract— The fourth order moment statistical characteristic of the pulse wave scattering on one-dimensional random rough surfaces is investigated numerically and presented based on Kirchhoff's approximation in detail. As a special application, the fourth order moment (FOM) is simplified to get the two positions and two frequencies mutual correlation function of the pulse wave scattering on random rough surfaces. Which the distributions of FOM change with the coherence bandwidth frequency difference and scattering angles in different incidence angles, the mean of fluctuating heights and coherent length on the random rough surface is computed. The numerical results show that the mean of fluctuating heights and coherent length of random rough surfaces have an important effect on the value of the FOM. Generally, the largest scattering value and smallest coherence bandwidth of the FOM occur at the specular directions. That is to say, the FOM will have a lower coherent component and its distributions of scattering angles will be broadened in relation to the rugged surface. At same time, the FOM decreased rapidly as there was a bigger coherence bandwidth frequency difference.

ACKNOWLEDGMENT

Project supported by the National Natural Science Foundation of China (Grant No. 60801047, 60771038, 60741003) and the Natural Science Foundation of Shaanxi Province education office, China (Grant No. 08Jk480).

Electromagnetic Scattering of a Higher-order Hermite-Gaussian Beam Field by a Multi-layered Sphere

Hai-Ying Li and Zhen-Sen Wu
Science School, Xidian University, Xi'an 710071, China

Abstract— Electromagnetic scattering by particles is widely used in many experiments and other important environments. The scattering of a plane wave or Gaussian beam fields by a sphere or a circular cylinder has been analyzed by many researchers. The expressions of Gaussian beam are also discussed in detail, and the beam shape coefficients are well represented. It is shown that, under the paraxial approximation, the complex-source-point spherical wave becomes a Gaussian beam. Then, many scholars deal with the relationship between the complex-source-point and Hermite-Gaussian beam.

Based on the conclusion obtained above, scattering of a higher-order Hermite-Gaussian beam by a multi-layered sphere is described. In paraxial region, the incident higher-order Hermite-Gaussian beam field is expressed by the complex-source-point method, that is to say, the Hermite-Gaussian wave function is generated by assigning complex-source coordinates into multipole field expressions. The incident field, internal field and scattered field are expanded in terms of spherical vector wave functions. Using the orthogonal relationship of spherical vector wave functions, the beam shape coefficients of the incident beam are given. With boundary conditions on the surface of the sphere, scattering coefficients in the expression of scattered field are deduced. Results of numerical calculation of radar cross sections (RCS) are presented, and a comparison with those of incident plane wave is provided. The effects of the particle-parameters and beam-parameters on scattered field are involved. It can be concluded that the scattered field of higher-order beam is different from that of the basic mode field, and the forward RCS has a relation with the order of the Higer-order Hermite-Gaussian beam.

Two-dimensional Scattering by a Gyrotropic Elliptic Cylinder

Shi-Chun Mao, **Zhen-Sen Wu**, **and Li Yang**
School of Science, Xidian University, Xi'an 710071, China

Abstract— An exact solution to the two-dimensional electromagnetic scattering by an infinite gyrotropic elliptic cylinder is derived. The internal field in a gyrotropic elliptic cylinder is expressed as integral representations of plane waves with different wave numbers and different directions of propagation. Based on the classic eigenfunction expansion, the plane waves as well as the incident and scattered waves in the exterior regions are expanded in elliptic coordinates in terms of Mathieu functions. The unknown coefficients of these series expansion are determined by a set of simultaneous equations, which are determined by imposing appropriate boundary conditions. Electromagnetic scattering by a dielectric or a gyrotropic elliptic cylinder fails to satisfy the orthogonality properties at the interface. The elliptic cylinder harmonics inside the gyrotropic elliptic cylinder are different from those outside. Each expansion coefficient of the scattered and internal fields is coupled with every other expansion coefficients of the cylinder and those of the incident field. In order to solve the nonorthogonality properties of Mathieu functions at the interface between two different media, the series solution is truncated in a suitable fashion to obtain a finite matrix. The transmitted and scattered fields of the gyrotropic elliptic cylinder and radar cross sections per unit length are obtained. Only the case of transverse electric (TE) polarization is considered, while the similar formulation of transverse magnetic (TM) polarization can be obtained via duality. Some numerical results are presented finally. The result is in agreement with that available as expected when the elliptic cylinder degenerates to a gyrotropic circular one.

A New Matrix Splitting Scheme for Numerical Study of EM Scattering from Randomly Rough Surfaces

Yang Du and Bin Liu
The Electromagnetics Academy at Zhejiang University
Zhejiang University, Hangzhou 310027, China

Abstract— Among numerical approaches for analyzing electromagnetic scattering from 1D randomly rough surfaces, the physically based two grid (PBTG) method is one of the most popular due to its appealing low computational complexity in the order of NlogN, where N is the number of surface unknowns. Yet this approach breaks down if the strong interaction region has to be retained sufficiently large when the roughness is large. In other words, at large roughness PBTG either diverges or loses its advantage in terms of computational complexity. This difficult, however, can be overcome if the impedance matrix is split properly. One such splitting scheme is proposed in this paper and is validated by numerical examples for rms height as large as 4 wavelengths.

Computation of Multiple Scattering Effects in Volume Vegetation Modelling

V. Mouysset[1], **P. Borderies**[2], **X. Ferrieres**[2], **and P. A. Mazet**[1]

[1]Department of Information Treatment and Modelization, ONERA, Toulouse, France
[2]Department of Electromagnetism and Radar, ONERA, Toulouse, France

Abstract— A significant challenge in the numerical simulation of electromagnetic scattering of vegetation is to accurately render for coupling between multiple scatterers. In [1] we proposed a new decomposition method in sub-domains convenient to treat this problem in time domain. Principle of the method is to create separated domains Di and solve into each Di Maxwell equations by the most appropriate method, the various domains being updated at each time step by the contribution of all other domains by means of specific integral formulas. Main interest of this method in regard of other existing ones is inherent of its construction: the error of approximation introduced when replacing the complete Green formula by the proposed integral formula, and error of sampling reconstruction above the Huygens face of each domain Di are explicitly given in $O(\delta/d)$ where δ is an adaptive local parameter and d is geometrically linked to the studied scene. Moreover, it gives a straightforward strategy of parallelization. At last, as domains construction are independent, more appropriate orientations and sampling may be attributed to each domain.

In forests, branches have the shape of long and radially thin cylindrical geometries, and they present random angular and spatial distribution. Usually first order scattering models are considered for them, neglecting multiple mutual interactions. However, it is well known that multiple scattering plays a role overall in cross polarization and it is interesting to study its importance. Such modelling with classical FDTD would be in general very difficult. Indeed, the specific shape of the scatterers and their possible oblique orientation need a very fine sampling which is prohibitive when domain size becomes important. However, the proposed method permits to get rid out of these requirements.

Application is presented here for forest volume scattering in P band where branches are represented by elongated diectric cylinders with typical descriptive parameters and randomly distributed. The accuracy of the method as a function of the adaptative parameter (δ/d) is discussed and the benefits of the method exhibited; Then, coupling effects are discussed with results associated to Monte Carlo computations, with emphasis on cross polarization and extinction.

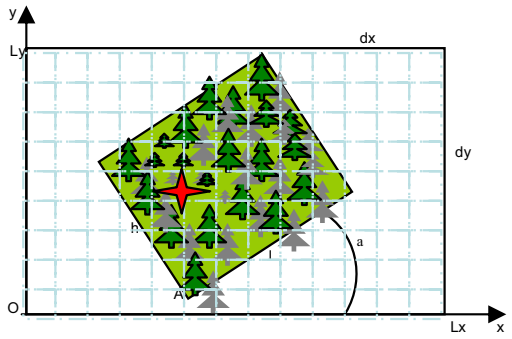

Figure 1: Scene and target location example.

REFERENCES

1. Mouysset, V., P. A. Mazet, and P. Borderies, "Effecient treatment of 3D time-domain electromagnetic scattering scenes by disjointing sub-domains and with consistent approximations," *Progress In Electromagnetics Research*, PIER 71, 41–57, 2007.

Session 5A4
Wireless Sensor Network and Environment Monitoring

Investigation of Novel Ultrasonic Positioning Method Installed in Sensor Network

Mitsutaka Hikita, **Yasushi Hiraizumi**, **Hiroaki Aoki**,
Junji Matsuda, **and Tomoaki Watanabe**
Faculty of Global Engineering, Kogakuin University, Shinjuku-ku, Tokyo 163-8677, Japan

Abstract—

Background and Motivation: A new concept called "Sensor Network" has been proposed with the development of mobile communications system such as cellular phone, radio LAN and Bluetooth. Signals from many sensor nodes spread in a wide area are gathered to a center node by technology similar to that in mobile communications. Sensor network enables home/office circumstance control, environment monitoring and protection based on the collected data. We proposed a novel ultrasonic positioning method which can be installed in sensor network. This method has also been investigated to be combined with 2.4-GHz ZigBee, which has been regulated by IEEE 802.15.4 [1] and ZigBee Alliance as wireless-communications medium for sensor network.

Statement of New Method: In the proposed method continuous-wave (CW) ultrasonic signals with a certain number of frequencies are transmitted and received among sensor nodes [2]. On the other hand, the conventional ultrasonic positioning method has used burst-type ultrasonic pulses which require very high-voltage handling capabilities for the transmitters and sophisticated signal-processing procedures for the receivers. In our method, frequency range of all transmitted CW signals is within a limited frequency bandwidth, which is determined by frequency characteristics of the transmitter and receiver ultrasonic transducers. The relative amplitude and phase between transmitted and received CW signal at each frequency are measured and sent to the center node via ZigBee. This procedure is repeated one after another at the above frequency range. The center node operates with different power supply and does not require low-power consumption, which can provide batch processing for all collected data. In the center node impulse responses between the transmitters and receivers are calculated using the received data and applying IFFT (Inverse Fast Fourier Transform) algorithm to them, which provides distance information from all reflected objects. The proposed positioning method can measure distances accurately with low-power consumption and its devices can be also included in sensor nodes which require a long-term and low-power operation.

Experimental Results: We made fundamental experiments to verify our idea. First we examined the conventional method, by sending burst pulses from a transmitter to a receiver apart from the transmitter with fixed distance. Experimental results show that sharp threshold characteristics can not be obtained by the conventional method. We applied the novel method to the same experimental setup by sending CW signals at dozens of frequencies. The results of IFFT procedure based on above data of the measured relative amplitudes and phases show that our method can achieve good threshold characteristics.

Conclusions: We proposed a novel ultrasonic positioning method which can measure distances from reflected objects accurately with low-power consumption. Experimental results confirmed the validity of our proposal. The sensor network including our positioning devices will be possibly applied to care for old people, prevention of crime and watch in hospitals.

REFERENCES

1. IEEE Standard 802.15.4: Wireless Medium Access Control (MAC) and Physical Layer (PHY) Specifications for Low Rate Wireless Personal Area Networks (LR-WPANs), 2003.
2. Japanese patent pending.

The Circuit Model of Built-up Areas

Giorgio Franceschetti[1] **and Sabatino Stornelli**[2]

[1]Università Federico II of Napoli, Italy
[2]Selex-Service Management, Roma, Italy

Abstract— Wireless propagation in built-up areas is a widely studied problem: electromagnetic solvers based on several ray-tracing techniques have been developed and are of common use; in addition, the statistical formulation of the signal propagation in the urban environment has lead to interesting results. However, the increasing demand of sensor networks, deployed at the street level, in the frame of the Homeland Security scenario, suggests development of a novel model of the urban tissue. As a matter of fact, the sensor net is deployed not only for collecting information to be transmitted to a central decision centre, but also for focusing interfering electromagnetic energy to a particular city spot, where temporary blackout of wireless communication is required. Accordingly, a description of the section of the city, where the net is present, as an equivalent planar circuit is highly desirable: each net node behaves as a transmitting/receiving point, localized in the network.

Use of this type of net is most likely to take place in downtown areas, where high-rise buildings and regular interception of streets are usually the rule. Accordingly, it is reasonable to model the streets as top-less rectangular waveguides, overmoded due to their dimension very large compared to the signal carrier wavelength, the carrier operating in the microwave regime. Similarly, the circuit equivalent of the street intersection is a microwave junction, to be modeled in terms of a scattering matrix.

The first step of the analysis is the modal expansion of the field inside the top-less rectangular waveguide. This is not a difficult issue, if the bottom and lateral walls of the waveguide are assumed to be perfectly conducting, and the transverse resonance condition is enforced along the vertical direction, by taking as equivalent load at the top of the guide the intrinsic impedance of free-space. The approximation involved in the perfectly conducting walls can be removed at a later stage of the analysis by implementing the usual perturbation techniques; and the approximation of the terminal load in the transverse resonance analysis can be improved, but is very reasonable in any case, due to the large aperture dimension. The real issue of the analysis is the exceedingly large number of propagating modes.

Although techniques are available to dominate this situation, a different approach is implemented: summation of modes with almost identical propagation constant along the street direction, this generating a set of supermodes; and subsequently choosing only those excited by the equivalent sources, set at prescribed locations in the equivalent guide. This procedure leads to a significantly smaller number of modes, thus allowing an easier evaluation of the scattering matrixes, representative of the equivalent junctions.

Results of above analysis is presented at the conference, together with experiments performed on a section of a city.

Study on Cross-layer Optimization in Wireless Sensor Networks with Energy Constrains

Guowei Fu[1], **Lu Rong**[2], **and Yang Du**[1]

[1]The Electromagnetics Academy at Zhejiang University
Zhejiang University, Hangzhou 310058, China
[2]Shanghai Research Center for Wireless Communications, Shanghai 200050, China

Abstract— In wireless sensor networks (WSN), nodes operate on batteries so that energy consumption must be minimized while satisfying given throughput and delay requirements. Cross-layer design in wireless sensor networks has been proposed to reduce the energy consumption. In this context, we consider the joint optimal design of the physical, medium access control (MAC), and routing layers to maximize the lifetime of energy-constrained WSNs.

The problem of computing lifetime-optimal routing flow, link adaptation, and link transmission powers for all active time slots is modeled as a non-linear optimization problem (to be exactly, a hybrid non-linear optimization problem for integer constrains involving), which is a challenging task. As the number of nodes increases, the variables and the constraints grow exponentially, and the computational complexity grows even faster. Constrained by computational complexity, previous work by other researchers mainly focused on no more than 4 nodes along a line (1-dimensional), so the advantages of cross-layer optimization cannot be fully explored and demonstrated. By solving the problem with effective models and numerical methods, we propose a detailed study on cross-layer optimization with up to 7 nodes in a line, and even up to 9 nodes in planar case (2-dimensional) to be more realistic. Numerical results show that optimal combination of multihop routing and variable-length TDMA schemes lead to significant energy savings in WSNs.

Positioning System for Wireless Sensor Networks with Location Fingerprinting

Di Cao, Hock Guan Goh, Kae Hsiang Kwong, Craig Michie, and Ivan Andonovic
Centre for Intelligent Dynamic Communications, Department of EEE
Royal College Building, 204 George Street, Glasgow, G1 1XW, United Kingdom

Abstract— Wireless sensor networks (WSN) are networks that deploy hundreds or thousands of wireless sensors in a pre-defined area that can communicate with each other to detect, for example the ambient environment. Each sensor is composed of the four basic elements: transmitting unit, processing unit, power unit and sensing unit. The main task of each sensor is to detect events, perform a restricted set of local data processing tasks and then transmit the data. This technology still in its early stage new researches are being conducted intensively in MAC protocols, network and routing layer, and adaptation into various domains applications. In this proposal, the focus is placed to investigate algorithms in mapping the location of sensor nodes. Knowing the location of the sensor node is critically important; the knowledge of the location of the sensor node that reported a detected event can reduce the time for assistants reaching to the outbreak point. This can potentially save life or can bring the outbreak event under control in shortest time.

As the sensor node's physical hardware is mainly comprises of low specification and low cost componentry to facilitate mass production hence affordable to be applied intensively in monitoring zone. This has created a tough challenge in mapping the locations of sensor nodes as the hardware can not provide precise timing in calculating time of flight of a packet which is an important parameter in estimating distance between transmitting node and receiving node. In general the sensor node is only equipped with a single antenna which has also rule out the possibility of using techniques rely on angle of arrival packet. Therefore, the research is limited to use the received signal strength as the main source in estimating the travelling distance for the received packet. This paper investigates positioning algorithms that based on received signal strength i.e., location fingerprinting. In positioning systems, location fingerprinting is also referred as pattern matching of radio signature. The advantages of using RF fingerprinting are it does not require any hardware modifications to the sensor node and in comparison to other algorithms it is immune environmental influences that caused signal attenuation such as multipath, fading, reflection, non line of sight, and etc.

This paper focuses on challenges that relate specifically to the location mapping of wireless sensor node including radio propagation of low specification WSN hardware, accuracy, operational range and impact of environmental factors. The optimized positioning system for WSN is documented, and results gained from experiment based on IEEE 802.15.4 WSN platform is provided.

Wireless Sensor Networks in Agriculture: Cattle Monitoring for Farming Industries

Kae Hsiang Kwong, **Tsung Ta Wu**, **Hock Guan Goh**, **Bruce Stephen**, **Michael Gilroy**, **Craig Michie**, **and Ivan Andonovic**
Centre for Intelligent Dynamic Communications, Department of Electronic and Electrical Engineering
University of Strathclyde, Glasgow, United Kingdom

Abstract— The newly emerged wireless sensor network (WSN) technology has spread rapidly into various multi-disciplinary. Agriculture and farming is one of the industries which have recently diverted their attention to WSN, seeking this cost effective technology to improve its production and enhance animal health care standard. This paper reports on the application of WSN technology to cattle health monitoring. By monitoring and understanding cattle's individual and herd behaviour, farmers can potentially identify the onset of illness, lameness or other conditions which might benefit from early intervention. The sensor node, which is small in size and low in power consumption, shows significant potential in this context. However, WSN solution faces with a number of significant technical challenges before it can be suitably and routinely applied. This paper thus focuses on challenges that closely relate to data transportation from cattle mounted sensory devices, comprises of data protocol, power consumption, mobility, operational range, data transmission volumes and herd size.

Challenges imposed from adaptation of WSN in agriculture and farming have been studied and evaluated. The main difficulty of adapting conventional WSN systems into cattle monitoring application is to support node's mobility that is caused by animal's movement. Although there have been diverse algorithms for data fusion and packet routing successfully applied in commercial product and a lot more being proposed by various researchers, majority of these schemes are only applicable to static sensor nodes. The key reason is most of the schemes are based on the assumption that the nodes will stay at a fixed position.

Animal movement and herd mobility have been studied with the use of GPS collars in our research. The results are related to the time any individual animal will spend in proximity to a base station. This study considerably embraced the impact it has on the targeted network performance. A novel Virtual Connection Routing Protocol (VCRP) is also proposed. VCRP is a light weight and agile routing algorithm that can satisfactorily support frequent animal movement. It allows a number of data transmission paths generated dynamically and enables sensory data to be relayed to centre management system. In terms of the radio channel itself, the presence of large numbers of cattle can seriously impact on the channel quality. The use of antennae diversity has been studied as a means of optimising access to a base station. We present the results from models and farm based trials.

Time Table Transfer Time Synchronization in Mobile Wireless Sensor Networks

Reza Khoshdelniat[1], **Moh Lim Sim**[1], **Hong Tat Ewe**[2], **and Tan Su Wei**[1]

[1]Faculty of Engineering, Multimedia University, Cyberjaya, Malaysia
[2]Faculty of Information and Communication Technology
Universiti Tunku Abdul Rahman, Malaysia

Abstract— The advance in technology has led us to find better and smaller means to monitor our environment and have a better control on our surrounding. The advances in technology especially in micro electro mechanical systems (MEMS), has led to the application of small sensor nodes and wireless sensor networks in the areas such as environment monitoring, smart offices, military applications, target tracking, and structural and seismic monitoring. Wireless sensor networks are composed of sensor nodes connected through wireless and multi hop communication among each other. These sensor nodes, due to their small size, have limitations on memory, computation power, and power supply. These limitations make it necessary to operate with power aware, low computation overhead, and low message overhead communication protocols for the sensor network.

In order to make these sensor nodes perform properly, in most applications, having accurate time synchronization among the nodes in the network would be crucial issue. Where ever the nodes need to determine the timing of the events, synchronization is an important part of sensor networks. Since all the clocks at the nodes do not work the same, there are time offset and clock drift among the nodes. The clock offset and clock drift between the nodes will cause the absolute timing of the events cannot be identified precisely.

In mobile sensor networks the condition for time synchronization is different from static networks. The movement of the nodes would have some advantages and some disadvantages. Most of the time synchronization protocols designed for static networks won't be applicable to mobile sensor networks. They would result in high convergence time and high message overhead which are not desirable in time synchronization. We have designed a new protocol for the time synchronization of mobile wireless sensor networks which would have a much better convergence time with good precision and good abilities to make the protocol attack resilient. Our protocol is named Time Table Transfer (TTT) time synchronization. The nodes would be using the round time trip method to calculate the time offset between themselves and the nodes they contact with. The time offsets associated with each node would be kept in the memory and upon communicating with a new node the time table would be transferred to the node. This method would be more reliable against attacks. Since the nodes would be receiving repeated time offsets of some nodes, and each node keeps the time offsets of other nodes, we would be able to implement the error detection techniques to find the false values sent by the attacker or a bad working node. This protocol would give partial synchronization to the network in each stage, which means each node would be able to communicate with the nodes around it or do a function because it is synchronized with a part of the sensors in the network. As the time passes the nodes would gain more timing information about the nodes in their network until each node has the clock offsets of all the other nodes in the network. Simulation of this protocol has been done on different situations, conditions and parameters such as different field sizes and number of nodes, and the results have been compared with other protocols such as RBS which show a better performance. A time synchronization protocol with good precision, low convergence time and reasonable message overhead which also is resilient to attacks is what we offer as a solution for time synchronization of mobile wireless sensor networks.

Performance Analysis of Unsaturated Slotted IEEE 802.15.4 with Downlink and Uplink Traffic

Wei Wang[1], **Lu Rong**[2], **and Yang Du**[1]

[1]The Electromagnetics Academy at Zhejiang University
Zhejiang University, Hangzhou 310058, China
[2]Shanghai Research Center for Wireless Communications, Shanghai 200050, China

Abstract— This paper is an extension of our previous work on modeling of unsaturated slotted IEEE 802.15.4 with uplink traffic to the analysis of both downlink and uplink traffics. We integrate these two transmission modes in one Markov chains model. The network operates in the beacon enabled mode, and we analyze the service time by means of the theory of M/G/1 queues. The effect of delay line is also considered. For the flows, it is assumed that the coordinator has Poisson flow to every node through indirect transmission and each node has Poisson flow to coordinator through direct transmission. Based on this model, for different Beacon Order (BO) and a wide range of traffic-load from 0.05 to 0.35, the normalized throughput, probability of collision, and service time are evaluated. The results are validated via Network Simulator (NS-2) simulations.

Separation of Detection Authorities (SDA) Approach for Misbehavior Detection in Wireless Ad Hoc Network

Zan Kai Chong[1], **Moh Lim Sim**[1], **Hong Tat Ewe**[2], **and Su Wei Tan**[1]

[1]Multimedia University, Malaysia
[2]Tunku Abdul Rahman University, Malaysia

Abstract— Wireless ad hoc network is a distributed wireless network without the presence of a physical network infrastructure. Having a limited wireless transmission range, all the nodes need to cooperate with each other during packet forwarding in order to maintain the connectivity. In addition, the lack of energy resources may cause a selfish node to drop legitimate packets which eventually disrupt the network performance. In fact, many detection protocols have been proposed to discourage such behaviour. However, the implemented penalization is ineffective as not all the surrounding nodes execute in the same manner. Moreover, most of them have neglected the existence of the malicious node that could inflict them directly and indirectly. In this paper, we present the separation of detection authorities (SDA) approach to detect and exclude the misbehaved nodes in the network. The SDA distributes the detection authorities to the reporter, investigation agents, and the central authority where each of them takes charge of different detection process. To ensure accuracy, only the central authority will report the result. Our evaluation demonstrated that SDA can detect misbehaved nodes in the network effectively.

Optimal Power Allocation Algorithm for AF BAT Relaying

Li Li and Yang Du
The Electromagnetics Academy at Zhejiang University
Zhejiang University, Hangzhou 310027, China

Abstract— The Amplifier-and-Forward (AF) Bi-directional Amplification of Throughput (BAT) relaying is one of the promising techniques to enhance the throughput of the relay-based bi-directional transmission. However, the AF BAT protocol only works effectively at symmetric channels in the bi-directional scenarios. In order to further enhance the system performance in various channel propagations, we study the optimal power allocation algorithm for the AF BAT protocol in this paper. The numerical results show that significant performance improvement is achieved for the AF BAT relaying after the power allocation algorithm is applied, especially for the transmission in asymmetric channels. Furthermore, compared with the DF BAT relaying, the AF BAT protocol with optimal power allocation achieves higher spectrum efficiency and is more robust to the various channel propagations.

Session 5A5a
Microwave Circuits and Systems

Generalization of the Full-wave Transmission Line Theory for Loaded Lines with Distributed Excitation

J. Nitsch[1], **S. Tkachenko**[1], **and F. Rachidi**[2]

[1]Otto-von-Guericke University Magdeburg, Germany
[2]Swiss Federal Institute of Technology Lausanne, Switzerland

Abstract— The necessity to investigate electromagnetic field coupling with multiconductor transmission lines of various kinds arises in different problems of electromagnetic compatibility. One can distinguish two main groups of such problems. The first one corresponds to the investigation of loaded transmission lines with lumped sources at one or two terminals. The knowledge of the corresponding solutions is necessary to investigate the energy or signal propagation along power lines, wiring structures in cars, printed circuits in computers, etc.. The second group of problems deals with the same transmission lines but with additional excitation by an electromagnetic field generated by an external source of different nature (i.e., lightning, intentional electromagnetic interferences, etc.).

For relatively low frequencies when the characteristic wavelength of electromagnetic field is much larger than the transversal section of the transmission line, both problems can be solved using the well-known transmission line (TL) approximation. However, the increase in the operating frequency of electronic products and the emergence of sources of disturbances with higher frequency (high power electromagnetic sources) content have led to a breakdown of the TL approximation's basic assumptions. To solve such full-wave problems usually different kind of pure numerical methods (like MOM) are used. However, numerical methods make it possible to obtain a solution only for specific configurations and cannot give much qualitative insight into mechanisms at work. Therefore, the generalization of the TL theory to take into account high frequency effects has emerged as an important topic of study in electromagnetic compatibility [1].

Two variants of full-wave transmission line theory (FWTL) were developed in [2–7]. First, a system of exact integro-differential equations for the current and potential on the boundary of the wire (Mixed Potential Integral Equation) describing the transmission line with lumped terminal excitations is reduced to a system of the TL-like linear differential equations of first order for the current and potential. As in classical TL theory, sources and loads are accounted for through the boundary conditions, and, the parameter matrix is length-dependent and is defined by the geometry of the line. However, the parameter matrix is complex valued and contains non-diagonal elements. For low frequencies, it turns into the usual anti-diagonal real matrix of the length-dependent per-unit length parameters (inductance and capacitance) for non-uniform transmission lines. The complex part of the parameter matrix and its diagonal elements are connected with the line radiation. A simple perturbation theory for the parameters, which is able to obtain them a priori, before solution of the MPIE, was proposed [5, 7].

In the second variant of FWTL, the current-charge pair of unknown functions was considered instead the pair current-potential [6]. Again, the system of integro-differential equations is reduced to an equivalent system of differential equations of first order. In this case, the second differential equation is the simple continuity equation for the pair current-charge. A connection between parameters in two variants of the theory was established.

The FWTL system with boundary conditions describes exactly the first group of TL problems (homogeneous problem) with terminal excitation (s) and load (s). To describe the second group of EMC problems, namely loaded transmission line with distributed excitations, one has to renormalize the sources by a quite complicated procedure, which contains integration with solutions of the homogeneous problem [3, 4, 6].

In the present paper, we propose another method of the solution of the inhomogeneous TL problem. The method is based on the following general theorem: the solution of the arbitrary linear integro-differential equation (in our case the electric field integro-differential equation of second order for the current) with n independent sources can be represented as a solution of a system of n different equations of first order for the current and $n-1$ auxiliary unknown functions. The corresponding matrix of this system can be constructed from the partial solutions for each of the affecting sources and their first derivatives and the sources of excitation. For the case of a homogeneous problem, when two independent terminal sources are present, we need one additional unknown function. For such a function, we can choose either potential or charge, and, of course, obtain two variants of FWTL.

For the inhomogeneous case, when we have three independent sources: two lumped sources at the terminals and distributed sources along the line, we need two auxiliary unknown functions, chosen to be the potential and charge. Thus we reduce the EFIE (or MPIE) for a loaded line excited by distributed sources into a system of three differential equations. The corresponding parameter matrix is complex-valued, length dependent and connected with radiation of the line. Unlike the parameter matrix of FWTL, the parameter matrix in the extended theory depends on the distributed exciting source. We have expressed it in an explicit form for two highly symmetrical configurations with known analytical solutions: an infinite horizontal wire and a semi-circular wire excited by a plane wave. To find this parameter matrix prior to the solution of the MPIE, a perturbation theory for parameters is proposed. Using this perturbation theory we have obtained an excellent agreement with pure numerical methods for several examples.

Finally, the extension of the proposed method to thick wires is discussed.

REFERENCES

1. Rachidi, F. and S. Tkachenko, *Electromagnetic Field Interaction with Transmission Lines: From Classical Theory to HF Radiation Effects*, WIT Press, 2008.
2. Haase, H. and J. Nitsch, "Full-wave transmission line theory (FWTLT) for the analysis of three-dimensional wire-like structures," *14th International Zurich Symposium and Technical Exhibition on Electromagnetic Compatibility*, 235–240, Zurich, Feb. 2001.
3. Haase, H., J. Nitsch, and T. Steinmetz, "Transmission-line super theory: A new approach to an effective calculation of electromagnetic interactions," *URSI Radio Science Bulletin*, Vol. 307, 33–60, Dec. 2003.
4. Haase, H., T. Steinmetz, and J. Nitsch, "New propagation models for electromagnetic waves along uniform and nonuniform cables," *IEEE Transactions on Electromagnetic Compatibility*, Vol. 46, No. 3, 345–352, Aug. 2004.
5. Nitsch, J. and S. V. Tkachenko, "Global and modal parameters in the generalized transmission line theory and their physical meaning," *Radio Science Bulletin*, Vol. 312, 21–31, Mar. 2005.
6. Haase, H., "Full-wave field interactions of nonuniform transmission lines," Otto-von-Guericke-Universität Magdeburg, Dissertation, 2005.
7. Nitsch, J. B. and S. V. Tkachenko, "Propagation of current waves along quasi-periodical thin-wire structures: Taking radiation losses into account," *URSI Radio Science Bulletin*, Vol. 322, 19–40, Sept. 2007.

A Multi-layer Microstrip Coupled-line Power Divider

Sheng-Jie You and Wen-Jiao Liao
The Department of Electrical Engineering
National Taiwan University of Science and Technology
43, Sec. 4, Keelung Rd., Taipei 106, Taiwan

Abstract— In this work, a power divider configuration made of overlapped coupled microstrip line is proposed. Unlike the conventional branch line power divider or the coupled-line power divider that runs two microstrip lines in parallel, this power division scheme is made of two overlapped microstrip lines running vertically in parallel. In order to increase the amount of coupling, two elliptical patches are added to the top and bottom traces of the coupled-line section as shown in Figure 1. By adjusting the sizes of the patches, a controllable power dividing ratio can be achieved.

The proposed configuration allows a larger range in its power dividing ratio and is therefore suitable for array antenna feeds with serially connected elements. The proposed power dividing scheme is also attractive in reducing power loss in the feeding network due to reduced number in power dividers and transmission line lengths.

Through simulations and measurements on prototypes, we found that this power divider scheme can achieve a power dividing ratio as high as 1 : 3.5. On the other hand, a power dividing ratio as small as 1 : 8 can also be implemented with this scheme. This wide range feature enables the proposed scheme as a complementary devise for the conventional branch line power divider. For example, if a 1 : 4 ratio is desired for a branch line with a 50 Ω input, the output line impedances would be 62.5 and 250 Ω, respectively. With the microstrip line configuration, the later one would result in an extremely narrow line width that is impractical to implement.

The proposed scheme can therefore be used with branch line power dividers to form a one-to-many power divider with outputs of equal amplitudes. Such a device is attractive for large array antenna design because the number of power dividers and the lengths of feed lines can be reduced to minimize lose. A one-tofour power divider is attempted in this work.

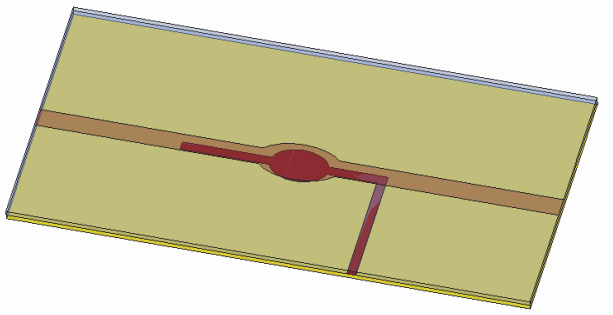

Figure 1: The proposed microstrip coupled-line power divider scheme..

ACKNOWLEDGMENT

This work is supported by the National Science Council of Taiwan [97-2221-E-011-021-].

A Compact and Low Loss V-band Lowpass Filter Using Coplanar Waveguide Structure

Hwann-Kaeo Chiou and I-Shan Chen
Department of Electrical Engineering, National Central University, Taiwan

Abstract— This paper presents a compact coplanar waveguide (CPW) low-pass filter (LPF) for V-band wireless personal area network (WPAN) communication systems. Fig. 1 schematically plots the equivalent circuit of the CPW LPF. The LPF is constructed by a series inductor at both ends with two shunted inductor-capacitor (LC) resonators at the center of the circuit. The fabricated chip is shown in Fig. 2. As can be seen, the series inductor can be realized as a series-short-stub in CPW line. The shunted series LC resonator is realized as a high impedance CPW line series with a low impednace CPW open stub. The full wave EM simulation was performed by Agilent Momentum^{TM} to predict the frequency response. The CPW LPF was implemented in WIN-semiconductor^{TM} 0.15 µm pHEMT technology. The measured result is shown in Fig. 3, the obtained insertion loss is small than 0.5 dB with a return loss better than 20 dB. The 3-dB bandwidth is from 0 to 70 GHz. A better than 20-dB rejection is obtained from 95 to 110 GHz. The measured frequency responses agree well with the simulated ones. The chip size is very compact of $0.4 \times 0.6\,\mathrm{mm}^2$.

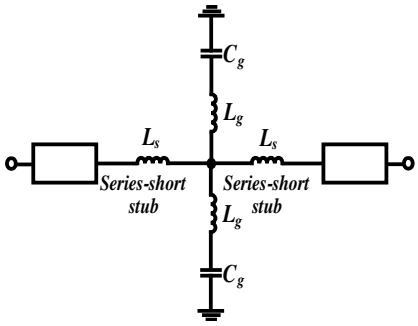

Figure 1.

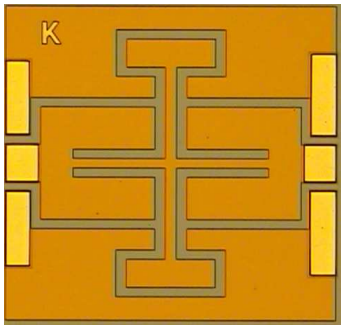

Figure 2.

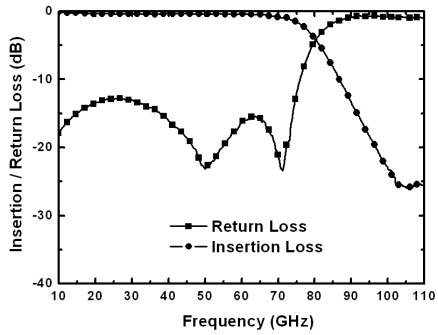

Figure 3.

Introduction to the System-level Susceptibility Assessments for HEMP and HPEM

Congguang Mao[1], **Hui Zhou**[1], **Jiwei Fu**[2], **Beiyun Sun**[1], **and Haitao Yu**[2]

[1]Northwest Institute of Nuclear Technology, Xi'an 710024, China
[2]Systems Engineering Division of CALT, Beijing 100076, China

Abstract— With the remarkable progress of the high-power electromagnetic (HPEM) source and antenna technologies, the susceptibility problem of the electronic systems and the infrastructures has abstracted increasing attentions. A special issue on HPEM and IEMI (intentional electromagnetic interferences) was published in IEEE transactions on EMC in August 2004. And a series of standards on HPEM and HEMP (high-altitude electromagnetic pulse) have been developed by the International Electrotechnical Commission (IEC). However, there are fewer open papers to systematically expound the problem of the system-level susceptibility assessments for HEMP and HPEM, which is believed to be the most complex and hardest task to fulfill of the HPEM problems. The relevant concepts of the system-level assessments and the relationships with the system-level analysis and design are clarified in this paper. The model based on the electromagnetic topology (EMT) is adopted to formulate the core contents of the assessment activities. The necessary parameters, their characteristics and corresponding testing types are presented and discussed in details. We believe that it is very significant and helpful to its reduction and solution in the first step to well illuminate the complicated systematic problem.

A Viewpoint of Time Variant Dielectric Effect in Vital Sign Detection Using Microwave Radar

Jingzhou Luo[1] **and Kemin Sheng**[2]

[1]Information Science and Engineering College
Zhejiang University, Hangzhou, Zhejiang, China
[2]Southwest Jiaotong University, Chengdu, China

Abstract—

Backgrounds and Purpose: Up to now, the main principle of microwave radar for vital sign detection is still based on Doppler theory, which states that when a human body is exposed under incidence of microwaves, the reflected signal will be phase modulated (PM) due to movements of respiration and heartbeat.

However, with further researches we find that there are some inconsistencies between the previous theory and experimental measurements. So, we show our considerations and give a hypothesis. Firstly, after a short review of Doppler radar theory we analyze two significant contradictions between this theory and measurement results. Then, we present a new theoretical hypothesis based on time variant dielectric effects in human body, which can explain the mechanism of vital sign detection more reasonably.

Main Problems We Pointed Out: When Doppler radar theory is using, we find two problems can be found: one is that the heartbeat and respiration baseband signals are inconsistent for measured data and theoretical analyzed results, and another is that the amplitude difference between heartbeat and respiration signals is unreasonable.

Our View Point: According to Bioelectronics, bioelectricity is an electrical phenomenon of organism. All of the movements of human body organs will result in a certain type of bioelectric effects, such as the heartbeat, the muscular contraction, the open of eyes, and the thinking in our brain etc. So the bioelectricity is generated and can be transmitted to outer skin through electric tissues and body fluid. In virtue of electromagnetic theory, the organic tissue of human body can be equivalent to time-varying dielectric coefficient $\varepsilon(t)$ and conductivity $\sigma(t)$, which carry the information of human body vital sign.

Based on this recognition, we derive an electromagnetic scattering surface integral expression. It can be illustrated as a simple amplitude modulation (AM) wave model in view of radar system. That is, when a high frequency electromagnetic wave is incident on the surface of a human body, $\varepsilon(t)$ and $\sigma(t)$ act as a function of modulation signal relative to the incident wave. According to Maxwell equation, the scattering wave has characteristics of an AM wave, then one can use an ordinary coherent demodulation technique to detect the vital sign information.

Conclusions: In this article the inconsistencies between Doppler radar theory for vital sign detection and known measurements are analyzed. A new mechanism and an AM-PM wave model for microwave radar vital sign detection based on time variant dielectric effect, which is essentially caused by bioelectrical phenomena are provided. The advantages of this model comparing with the traditional Doppler radar theory are also presented.

A Compact 5.8 GHz Rectifying Circuit Design and Experiments

Qijuan He, **Kama Huang**, **and Changjun Liu**
School of Electronics and Information Engineering, Sichuan University, Chengdu 610064, China

Abstract— A compact rectenna circuit at 5.8 GHz is presented. A matching inductor and two series diodes are introduced to the rectifying circuit so as to achieve well impedance matching. The circuit simulation and layout electromagnetic (EM) simulation are compared hereby to confirm this design. The layout EM simulation and circuit simulation are close to each other. There is a RF-DC conversion efficiency difference of about 3%–5% between them. The experiment DC output voltage of the rectifying circuit with this novel design achieves 9.80 V at a DC load 2000 Ohm, when the input RF power is at 20 dBm. The highest RF-DC conversion efficiency is 60%. The capacitors used in the rectifying circuit are also studied, and by adjusting their values, the RF-DC conversion efficiency at desired frequencies could be optimized.

Session 5A6a
State of the Art in Time Domain Methods

Parallelisation of Implicit Time Domain Methods: Progress with ADI-FDTD

Timothy D. Drysdale and Tomasz P. Stefanski
University of Glasgow, Glasgow G12 8LT, United Kingdom

Abstract— The parallelisation of implicit time domain solvers is essential for applications requiring large, highly over-sampled meshes that exceed the memory limitations of standalone workstations [1]. Prime application examples include large arrays of small antennas [2], and on-chip interconnects for state of the art integrated circuits (IC) [3]. The need for highly over sampled meshes in these applications can be illustrated by example. Current on-chip IC interconnect widths can be as low as 22 nm or less, yet cover an area $> 100\,(\mathrm{mm})^2$ and transmit signals with fundamental frequencies in the range DC-10 GHz. Typically, transient effects involving high frequencies are of the most interest, but even this can still require meshes with $\Delta x < (\lambda_0/10^6)$, i.e., four to five orders of magnitude smaller than for typical FDTD meshes (neglecting considerations relating to material properties). It is not practical to use explicit FDTD solvers for such meshes, even in parallel, because the Courant-Friedrichs-Lewy (CFL) stability criteria enforces a commensurate reduction in the time step size for numerical reasons. While implicit FDTD solvers, such as ADI-FDTD, offer freedom from the CFL stability criteria, it has been presumed that parallel implementations on all but the most specialised architectures [4] would be of little benefit due to the high communication overhead. However, we have been able to show that this is not the case [5].

In this Paper we will present an overview of our work to date on the parallelisation of implicit time domain methods, including parallel ADI-FDTD [1, 5] and parallel ADI-BOR-FDTD [6] on both symmetric multiprocessor (SMP) and distributed memory computer clusters (DMCC). We do not parallelise the tri-diagonal matrix solver itself, because each 2D matrix must have more than 4,000 (40,000) elements per direction before this becomes efficient for SMP (DMCC) machines. This requires 3D domains at are at or beyond current memory limits for state of the art machines. Instead, we employ domain decomposition and solve multiple, smaller, tri-diagonal matrix systems in parallel. Carefully organised data exchanges avoid unnecessary double-handling of data during communication, improving the parallel algorithm performance. We will describe our domain decomposition scheme, and show results for small and large domains, comparing parallel FDTD and parallel ADI-FDTD and parallel BOR-FDTD with parallel ADI-BOR-FDTD. We demonstrate efficient solutions of large full 3D meshes with 8 billion mesh cells for parallel ADI-FDTD. Since machines with SMP and DMCC architectures are widely available, our demonstration of parallel speed up represents an important step forward for the application of implicit time domain solvers for large, highly oversampled meshes with $\Delta x < 10^{-2}\lambda$. We expect that our parallelisation approach can be adopted for related implicit FDTD methods.

REFERENCES

1. Stefanski, T. P. and T. D. Drysdale, "Parallel implementation of the ADI-FDTD method," submitted to *Microwave and Optical Technology Letters*.
2. Yang, Y., et al., "Analysis of planar circuits using an unconditionally stable 3D ADI-FDTD method," *Microwave and Optical Technology Letters*, Vol. 46, 175–179, July 2005.
3. Choi, I.-J., et al., "ADI-FDTD for the modelling and simulation of VLSI interconnects," *Current Applied Physics*, Vol. 5, 356–364, May 2005.
4. Jordan, H., et al., "Experience with ADI-FDTD techniques on the cray MTA supercomputer," *Proc. SPIE*, Vol. 4528, 68–76, Aug. 2001.
5. Stefanski, T. P. and T. D. Drysdale, "Parallel implementation of ADI-FDTD on shared and distributed memory computers," *Proceedings of The Second European Conference on Antennas and Propagation*, Nov. 2007.
6. Stefanski, T. P. and T. D. Drysdale, "Parallel ADI-BOR-FDTD algorithm," accepted for publication in *IEEE Microwave and Wireless Components Letters*.

Fundamental Schemes for Implicit Finite-difference Time-domain Methods

Eng Leong Tan
School of EEE, Nanyang Technological University, Singapore

Abstract— This paper presents the recent progress in the unconditionally stable finite-difference time-domain (FDTD) methods for electromagnetics. Starting from the popular alternating-direction-implicit (ADI) FDTD method, the paper reviews the development of several other implicit schemes proposed recently including locally one-dimensional (LOD) FDTD, split-step (SS) FDTD and some variants of Crank-Nicolson-based FDTD schemes, e.g., Direct-Splitting (DS) FDTD, (conditionally stable) Cycle-Sweep-Uniform (CSU) FDTD, etc. The stability and accuracy of these implicit schemes are discussed. All these implicit schemes can be unified and made efficient via a family of fundamental schemes. The formulation of fundamental schemes is presented in terms of general matrix operator equations. This leads to novel efficient implementations of the implicit FDTD schemes using the most convenient forms with matrix-free right-hand sides. It is noted that all the new implicit schemes feature similar updating structures that are of fundamental nature in simplest forms with most concise right-hand sides. To give further insights into the significance of fundamental schemes, it is shown that the analyses can also be extended to many other schemes with distinctive splitting formulae. In particular, many classical implicit schemes employed previously for parabolic/elliptic problems may be extended and simplified for electromagnetic problems within the realm of fundamental schemes. Detailed algorithms are described for efficient implementation of some unconditionally stable FDTD methods based on the fundamental schemes, which involves fewer floating point operations and less memory access without additional memory arrays or for-loop counts. A comparative study of various implicit schemes in their original and new implementations is carried out, which includes comparison of their efficiency gains and computation costs. Some extensions of the fundamental schemes are discussed, including inhomogeneous equations and higher order accuracy in space/time, etc.

REFERENCES

1. Tan, E. L., "Fundamental schemes for efficient unconditionally stable implicit finite-difference time-domain methods," *IEEE Trans. Antennas Propag.*, Vol. 56, No. 1, 170–177, 2008.
2. Tan, E. L., "Efficient algorithms for Crank-Nicolson-based finite-difference time-domain methods," *IEEE Trans. Microw. Theory Tech.*, Vol. 56, No. 2, 408–413, 2008.
3. Tan, E. L., "Concise current source implementation for efficient 3-D ADI-FDTD method," *IEEE Microw. Wireless Compon. Lett.*, Vol. 17, No. 11, 748–750, 2007.
4. Tan, E. L., "Unconditionally stable LOD-FDTD method for 3-D Maxwell's equations," *IEEE Microw. Wireless Compon. Lett.*, Vol. 17, No. 2, 85–87, 2007.
5. Tan, E. L., "Efficient algorithm for the unconditionally stable 3-D ADI-FDTD method," *IEEE Microw. Wireless Compon. Lett.*, Vol. 17, No. 1, 7–9, 2007.
6. Fu, W. and E. L. Tan, "Development of split-step FDTD method with higher order spatial accuracy," *Electron. Lett.*, Vol. 40, No. 20, 1252–1254, 2004.
7. Tan, E. L. and D. Y. Heh, "ADI-FDTD method with fourth order accuracy in time," *IEEE Microw. Wireless Compon. Lett.*, Vol. 18, No. 5, 296–298, 2008.
8. Heh, D. Y. and E. L. Tan, "Split-step finite-difference time-domain method with fourth order accuracy in time," *Proc. Asia-Pacific Symp. Electromagn. Compat.*, 68–71, 2008.

New Strategies in DGTD-FDTD Hybridizations

S. Gonzalez Garcia, **M. Fernandez Pantoja**, **C. M. de Jong Van Coevorden**, **A. Rubio Bretones**, **and R. Gomez Martin**
University of Granada, Spain

Abstract— The Discontinuous Galerkin Time-Domain (DGTD) method is a promising alternative to the classical Finite Difference Time-Domain (FDTD) method to handle arbitrarily shaped geometries. DGTD takes advantage of a formulation very similar to that of the Finite Elements in Time Domain (FETD), but overcoming the fully implicit nature of FETD and significantly reducing its computer requirements.

The space is discretized in elements in the same way employed by Finite Elements, and Maxwell's curl equations are solved in time in an explicit manner, only needing the initial inversion of small matrices, whose size is the degree of approximation of the basis functions. For this reason, all the existing tools of geometrical modeling, employed by Finite Elements packages, can also be used by DGTD.

In this paper we present a method to hybridize the Discontinuous Galerkin Time Domain method (DGTD) with the classical Finite Difference Time Domain method (FDTD). This method maintains the generality of FDTD to treat the main part of a complex inhomogeneous problem, applying only DGTD for accurately taking into account the geometrical details of the objects which would not be properly treated with the usual staircased approximation of the classical FDTD.

Since the DGTD algorithm found using a 0th-order basis of functions in a cubic lattice, together with the LF scheme, is a classical nodal Finite Volume Time Domain (FVTD) algorithm, we devise a hybrid DGTD-FDTD new method inspired in previous hybridizations of FVTD-FDTD.

Open Issues in Unconditionally Stable Schemes

S. Gonzalez Garcia[1], **Fumie Costen**[2], **M. Fernandez Pantoja**[1], **Anthony Brown**[2], **and A. Rubio Bretones**[1]

[1]University of Granada, Spain
[2]University of Manchester, United Kingdom

Abstract— The classical Yee FDTD method has become a standard tool in computational electromagnetics. However, a major difficulty of FDTD is the long execution time needed to simulate problems with high spatial resolutions, since the time step is bounded by the minimum space step. The Alternating Direction Implicit ADI-FDTD method is an alternative to the explicit FDTD method theoretically overcoming this limitation.

However, severe drawbacks have been reported in the literature: accuracy losses, non-null divergence, negative group-velocity modes and asymmetrical propagation, which increase with the time-step. Hence its choice is actually limited by the accuracy required, rather than by the accurate modeling of the temporal variation of the fields.

Various alternatives have been proposed in order to overcome those limitations: modifications of the original ADI-FDTD, Locally One Dimensional schemes, Strang Splitting Schemes, etc.. A common starting point of many of these alternatives is the Crank-Nicolson FDTD, which implicitly solves Maxwell's equations in space without adding extra mathematical errors. However, not all of them are promising alternatives to ADI-FDTD, and some lack solid fundamental studies concerning their validity.

In this paper we review the state-of-the art of these alternatives and present a common framework to derive them. We demonstrate that most of them present the same limitations than the original ADI-FDTD: the truncation error depends on the time resolution of the spatial variations. As a conclusion, new strategies of research need to be developed starting from the original Crank-Nicolson scheme, from which all of them were inspired.

Session 5A6b
Computational Electromagnetics

Solving Electromagnetic Scattering from Dielectric-coated PEC Surfaces by Improved EFIE

Lijun Tian, **Jun Hu**, **Lin Lei**, **and Zaiping Nie**
School of Electronic Engineering, University of Electronic Science and Technology of China
Chengdu 610054, China

Abstract— The improved electric field integral equation (IEFIE) developed by us is extended to speed up solution of electromagnetic scattering from dielectric-coated PEC surfaces. Two different integral equation formulations are used for treatment of the structure with different coating thickness. For thin coating structure, a PEC-thin dielectric sheet model is applied. For thick coating structure, hybrid volume and surface integral equation is used. A well-conditioned improved EFIE operator is constructed by adding the principle value term of magnetic field integral equation operator into traditional electric field integral equation for PEC surface. Numerical results demonstrate the present method improves the computational efficiency of dielectric-coated PEC surfaces greatly.

Saving Memory with Vector Addition Theorem

Y. G. Liu and W. C. Chew
The University of Hong Kong, Pokfulam Road, Hong Kong, China

Abstract— In the low-frequency fast multipole algorithm (LF-FMA), instead of the traditional factorization of the scalar Green's function using scalar addition theorem, we adopt the vector addition theorem for the factorization of the dyadic Green's function to realize the memory savings. Recently, the factorization and the diagonalization of the dyadic Green's function is possible based entirely on the use of vector wave functions and vector addition theorem [1, 2]. In this work, we shall validate this factorization and diagonalization. This factorization can be used to develop a vector mixed-form fast multipole algorithm for the dyadic Green's function [3].

By using the new integral operator factorization with vector addition theorem and loop-tree basis, every element of the matrix resulting from applying the method of moments (MoM) to the electric field integral equation (EFIE) can be expressed by the radiation patterns, translator and receiving patterns. The storage of the radiation patterns and receiving patterns can be reduced by 25 percent compared with the one when the factorization of the scalar Green's function is used. In addition, since the elements of the new translator can be calculated on the fly from the elements of the translator given by the factorization of the scalar Green's function using scalar addition theorem, we need only to store the latter. Therefore the whole memory usage is reduced and the memory saving is important for the large-scale computation with finite computer resource.

REFERENCES

1. Chew, W. C., "Vector addition theorem and its diagonalization," *Comm. Comput. Phys.*, Vol. 3, No. 2, 330–341, Feb. 2008.
2. He, B. and W. C. Chew, "Diagonalizations of vector and tensor addition theorems," *Comm. Comput. Phys.*, Vol. 4, No. 4, 797–819, 2008.
3. Jiang, L. J. and W. C. Chew, "A mixed-form fast multipole algorithm," *IEEE Trans. Antennas Propag.*, Vol. 53, No. 12, 4145–4156, Dec. 2005.

Analysis of Tunneling and Growing Exponential in Double-negative Media Using ADI-FDTD Method

Hong-Xing Zheng
Tianjin University of Technology and Education, China

Abstract— Current interest in understanding the physics behind the anomalous properties of metamaterials is evident in the recent physics and engineering literature [1]. Artificial materials with ε-negative (ENG), μ-negative (MNG), and double-negative (DNG) media have been at the center of this attention, due to the anomalous phenomena theoretically predicted for their behavior. In particular, an ENG plasmonic medium exists naturally in the infrared and optical frequencies, such as noble metals below their plasma frequency and polar dielectrics, and it can be relatively easily synthesized at lower frequencies by embedding a regular lattice of thin metallic wires in a host medium. In analogy, an MNG material, such as a resonant ferromagnetic medium, may be synthesized by embedding resonant magnetic loops in a host medium, i.e., split-ring resonators, thereby providing the proper magnetic resonant polarizability in the desired frequency regime. These two techniques may be employed at the same frequency to obtain DNG materials within a given frequency range. In practice, the current technology for manufacturing DNG materials consists of stacking together electrically thin layers of ENG and MNG materials, whose collections may be regarded as a bulk DNG medium.

In the following, the physical mechanisms underlying the anomalous resonance between an ENG and an MNG planar layer have been investigated by using the alternating-direction-implicit finite-difference time-domain (ADI-FDTD) method. In particular, we study how a transient sinusoidal signal would interact with such a juxtaposed ENG-MNG pair, showing how the multiple reflections and transmissions at each interface can be designed to build up to the eventual resonant steady-state response of the pair. Pairing together planar material slabs with opposite signs for the real parts of their constitutive parameters has been shown to lead in the steady-state regime to interesting and unconventional properties that are not otherwise observable for single slabs, such as resonance, anomalous tunneling, transparency, and subwavelength imaging through the reconstruction of evanescent waves. Multiple reflections and transmissions at each interface are shown to build up to the eventual steady-state response of the pair, and during this process one can observe how the "growing exponential" phenomenon may actually occur inside this bilayer. As with any resonant phenomena, the time response of this effect depends on the Q-factor of the system, which is related to the geometrical and electrical parameters of the bilayer. Our ADI-FDTD results confirm the steady-state prediction of growing exponential behavior in the bilayer and the total resonant transmission through it. Consequently, the time delay is found to be, in general, a function of the thickness of the slabs and the possible losses in each slab.

ACKNOWLEDGMENT

This work was supported by the National Natural Science Foundation of China Grant 60871026.

REFERENCES

1. Ziolkowski, R. W. and E. Heyman, "Wave propagation in media having negative permittivity and permeability," *Phys. Rev. E*, Vol. 64, 056625, 2001.

An Improved GE's Method for Calculating Green's Functions in the Shielded Multilayered Structure

Huan Li, **Hao Gang Wang**, **and Hua Zhang**
The Electromagnetics Academy at Zhejiang University
Zhejiang University, Hangzhou 310027, China

Abstract— With some improvements, the discrete complex image method (DCIM) [1] can efficiently and accurately calculate the spatial domain Green's functions for multilayered structure in most conditions, but we find that it can not work well in the shielded structure, that is the first layer and the last layer are both perfect electric conductors (PECs), when ρ is larger than a certain value.

The Ge-Esselle's (GE's) method uses an analytical expression to evaluate the spatial domain Green's functions without extracting the quasi-static images and surface-wave poles (SWPs), but the results may not be expected.

In this paper, we do some improvements to make it much more robust and efficient for the shielded multilayered structure listed as below.

Step 1) Extraction of SWPs using a recursively contour integration method [3].

Step 2) Using a smoothing method to smooth the abrupt peak caused by the error locations of poles. An interpolation technique is applied to smooth the abrupt peaks, that is we use the points that their values are normal, to interpolate the points are abnormal.

Step 3) GPOF is applied to approximate the remaining spectral domain Green's functions along the path of the real axis of k_ρ plane instead of the rooftop shaped path suggested in their paper. We will find benefits in the following example.

A numerical example is given to verify that the improved GE's method can solve the shielded structure problem. We can see from Figure 1 that with the improvements, the GE's method and the numerical integration of SIs are coincide with each other perfectly.

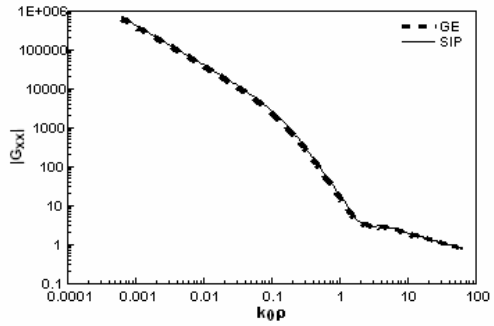

Figure 1: The coincidence of the improved GE's method and the integration of SIs.

ACKNOWLEDGMENT

This work is supported by the National Natural Science Foundation of China No. 60501017.

REFERENCES

1. Chow, Y. L., J. J. Yang, D. G. Fang, and G. E. Howard, "A closed-form spatial Green's function for the thick microstrip substrate," *IEEE Trans. Microwave Theory Tech.*, Vol. 39, 588–592, Mar. 1991.
2. Ge, Y. and K. P. Esselle, "A fast method of moments based on a new closed-form Green's function for microstrip structures," *IEEE Trans. Antennas Propagat.*, Vol. 50, 1556–1560, June 2002.
3. Ling, F., J. Liu, and J. M. Jin, "Efficient electromagnetic modeling of three-dimensional multilayer microstrip antennas and circuits," *IEEE Trans. Mircowave Theory Tech.*, Vol. 50, 1628–1635, June 2002.

Author Index